

GEOSYNTHETICS '89

FEBRUARY 21-23

TOWN & COUNTRY HOTEL, SAN DIEGO, CA

CONFERENCE PROCEEDINGS

Town & Country Hotel
San Diego, California
February 21-23, 1989

Volume 1

Sponsored by the Industrial Fabrics Association International under the auspices of the International Geotextile Society (IGS) and the North American Geosynthetics Society (NAGS) and with support of the American Society of Civil Engineers (ASCE).

GEOSYNTHETICS '89

FEBRUARY 21-23 TOWN & COUNTRY HOTEL, SAN DIEGO, CA

CONFERENCE PROCEEDINGS

Town & Country Hotel
San Diego, California
February 21-23, 1989

Volume 1

GEOSYNTHETICS '89 CONFERENCE

NORTH AMERICAN REGIONAL CONFERENCE

**SPONSORED BY:
THE INDUSTRIAL FABRICS
ASSOCIATION INTERNATIONAL**

**UNDER THE AUSPICES OF:
INTERNATIONAL GEOTEXTILE SOCIETY (IGS)
NORTH AMERICAN GEOSYNTHETICS SOCIETY (NAGS)**

**WITH THE SUPPORT OF:
AMERICAN SOCIETY OF CIVIL ENGINEERS (ASCE)
(THE COMMITTEE ON PLACEMENT AND IMPROVEMENT OF
SOILS)**

VOLUME 1

GEOSYNTHETICS '89 CONFERENCE

ORGANIZING COMMITTEE

CHAIRMAN

J. E. (TED) GAILER Chairman, Geotextile Division, IFAI; Organizing Committee Member, Geosynthetics '87.

COMMITTEE MEMBERS

JAY F. BEECH, Ph.D., P.E. Member, International Geotextile Society; Member, American Society of Civil Engineers.

R.G. (BOB) CARROLL, JR., P.E. Vice President, North American Geosynthetics Society; Member, Geotextile Division, IFAI; Member, Task Force 25.

LAURIE L. HONNIGFORD Staff Director of Geomembrane and Geotextile Divisions, IFAI.

JOSEPH D. LUNA Member, International Geotextile Society; Member, North American Geosynthetics Society; Member, ASTM D35 Committee on Geotextiles, Geomembranes and Related Products.

BILL NEAL Vice Chairman, Geomembrane Division, IFAI; Former Vice President, Society of Plastic Engineers.

IRAJ NOORANY, Ph.D. Professor, Civil Engineering, San Diego State University; Visiting Professor, University of California, San Diego; Recipient, Thomas A. Middlebrooks Award.

KERRY ROWE, Ph.D., P. Eng. Member, International Geotextile Society; Vice President, North American Geosynthetics Society; Editor, IGS News.

STEPHEN M. WARNER Executive Vice President, Industrial Fabrics Association International; Former Secretary General, American Society of Geosynthetics, (currently, North American Geosynthetics Society); Former Secretary General, 2nd International Conference on Geotextiles; Organizing Committee Member, Geosynthetics '87.

NEIL WILLIAMS, Ph.D., P.E. Member, Executive Committee ASTM D35; U.S. Delegate, International Standards Organization; Member, North American Geosynthetics Society; Member, American Society of Civil Engineers.

ADVISOR

JOSEPH E. FLUET, JR. P.E. President, North American Geosynthetics Society; Former Secretary/Treasurer, International Geotextile Society; Former Chairman, Geotextile Division, IFAI; Organizing Committee Member, 2nd International Conference on Geotextiles and 1st International Conference on Geomembranes; Former Committee Member Geotechnical Fabrics Conference '85; Chairman, Geosynthetics '87 Conference.

**These papers are published by:
Industrial Fabrics Association International
345 Cedar St., Suite 450
St. Paul, MN 55101
(612)222-2508
TWX: 910-563-3622
FAX: (612)222-8215**

Industrial Fabrics Association International

TABLE OF CONTENTS

TABLE OF CONTENTS

VOLUME 1

OPENING ADDRESS

Opening Address	1
GAILER, J.E. (Ted), Chairman, Organizing Committee, Geosynthetics '89 Conference	

SESSION 1A: LANDFILLS & LININGS SYSTEMS

Paradise Peak Tailings Impoundment Stage II Construction	5
A.A. McCREADY Harding Lawson Associates, U.S.A.	
The Use of Geosynthetics As Drainage Media at Solid Waste Landfills	10
C.M. LUNDELL, S.D. MENOFF Waste Management of North America, Inc., U.S.A.	
Rates of Leakage Through Landfill Liners	18
J.P. GIROUD, R. BONAPARTE, B.A. GROSS GeoServices, Inc., Consulting Engineers, U.S.A.	
Lined Cut and Fill Reservoirs in Israel- Forty Years of Development	30
P.I. MARCUS Mekorot Water Co., Ltd., Israel	
Stability Of Soil Layers On Geosynthetic Lining Systems	35
J.P. GIROUD, J.F. BEECH GeoServices, Inc., Consulting Engineers, U.S.A.	

SESSION 2A: QUALITY ASSURANCE AND SPECIFICATIONS

Stringent Construction Specifications and Quality Control Assure Maximum Liner Performance	47
T.N. DOBRAS, D.G. YACKO Harza Environmental Services, Inc., U.S.A.	

Design Methods and Construction Quality Assurance
For a Double Geocomposite Industrial Waste Landfill 58
M.J. MONTELEONE, G.J. DiPIPPO
AWARE Incorporated, U.S.A.

Inspection of HDPE Geomembrane Installations 70
G.R. KOERNER, Drexel University, U.S.A.
J.A. BOVE, Westinghouse Environmental Engineering, U.S.A.

The Benefits of Construction Quality Assurance of Lining
Systems Installation: Real or Perceived? 84
R.B. WALLACE
GeoServices, Inc., Consulting Engineers, U.S.A.

SESSION 3A AND 2B: DRAINAGE & WALLS

Design Of Verticle Drains Using The Hydraulic
Conductivity Ratio Analysis 95
S.M. LUETTICH, N.D. WILLIAMS
GeoServices Inc., Consulting Engineers, U.S.A.

Effectiveness of Tensile Reinforcement in Alleviating
Bridge Approach Settlement 104
T.H. WU, University of Colorado, U.S.A.
G.J. MONLEY, J.U. Lowney & Associates, U.S.A.

Parametric Study of Geosynthetic Reinforced
Retaining Walls Using the Displacement Method 112
J.P. GOURC, P.H. GOTTELAND, University of Grenoble, France
P. DELMAS, Laboratoire Central des Ponts et Chaussees, France

SESSION 5A: EMBANKMENTS

Consideration of Strain in the Design of Reinforced Embankments 124
R.K. ROWE, B.L.J. MYLLEVILLE
University of Western Ontario, Canada

Effect of Surface Crust on Reinforced Embankment 136
D.N. HUMPHREY
University of Maine, Orono, U.S.A.
R.D. HOLTZ
University of Washington, Seattle, U.S.A.

Design and Construction of Synthetic-Grid Reinforced Embankment over Soft Waste	148
M.F. HOULIHAN, W.K. RODGERS	
Law Environmental, U.S.A.	
G. WILLIBEY	
Nicolon Corporation, U.S.A.	
N.D. WILLIAMS	
GeoServices, Inc., Consulting Engineers, U.S.A.	
Case Study of a Geotextile Reinforced Levee on a Soft Clay Foundation	160
F.M. DUARTE, G.S. SATTERLEE	
U.S. Army Corps of Engineers, U.S.A.	
Design Methods For Reinforced Embankments On Soft Foundations	172
P.J. LANGSTON, N.D. WILLIAMS	
GeoServices, Inc., Consulting Engineers, U.S.A.	
Geotextile Assisted Soft Site Stabilization	184
J.N. PAULSON	
Exxon Chemical Co., U.S.A.	

SESSION 6A: FOUNDATIONS & RAILWAYS

A Functional Approach to the Design of Geotextiles	195
O. GICOT, Soltechnique, Fribourg, France	
J. PERFETTI, Rhone-Poulenc, Bezons, France	
J.M. RIGO, K. Smolders, University of Liege, Belgium	
C. LEGRAND, C.S.T.C. Belgium	
Foundation on Sand Underlain by Soft Clay with Geotextile at Sand-Clay Interface	203
B.M. DAS	
Southern Illinois University at Carbondale, U.S.A.	
A Comparison of Texturized and Non-Texturized GEOWEB-Reinforced Earth Slabs	215
V.A. GUIDO, J.P. SOBIECH	
The Cooper Union School of Engineering, U.S.A.	
S.N. CHRISTOU	
Kanika Construction Ltd., U.S.A.	

Finite Element Analysis of Footings on Geogrid-Reinforced Soil	231
--	-----

C.J. PORAN

University of North Carolina, Charlotte, U.S.A.

L.R. HERRMANN, K.M. ROMSTAD

University of California at Davis, U.S.A.

SESSION 7A: STEEP SLOPES

Reinforcement of an Earthen Buttress with a Polymer Geogrid	243
---	-----

D. CHU, I. POORMAND

Leighton & Associates, Inc., U.S.A.

Geogrid Steepened Slopes at Davis Creek Dam	255
---	-----

W.O. ENGEMOEN, P.J. HENSLEY

U.S. Bureau of Reclamation

Critical Failure Planes in Analysis of Reinforced Slopes	269
--	-----

R.R. BERG, V.E. CHOUERY-CURTIS, C.H. WATSON

Tensar Engineering, Inc., U.S.A.

Geosynthetically Reinforced Slopes: A New Procedure	279
---	-----

J.R. VERDUIN

Hart-Crowser, Inc., U.S.A.

R.D. HOLTZ

University of Washington, U.S.A.

A Test Embankment Reinforced by Four Types of Geosynthetics	291
---	-----

C.K. SU, N.N.S. CHOU

Colorado Department of Highways, U.S.A.

Volume 2

SESSION 1B: PAVEMENTS

The Use of Drainage Wicks for the Mitigation of Frost Effects on Existing Roadways	305
--	-----

R.A. D'ANDREA, J.D. SAGE

Worcester Polytechnic Institute, U.S.A.

A Study of Permanent Road Stabilization: Low-Cost Pavement Structures and Lightweight Geotextiles	316
---	-----

C.J. SPRAGUE, G. CICOFF

Hoechst Celanese Corporation, U.S.A.

Using Geosynthetics to Control Lateral Spreading of Pavements in Alaska--Preliminary Results	324
T.C. KINNEY, B.M. SAVAGE	
University of Alaska, Fairbanks, U.S.A.	
The Function of Geotextiles in Pavement Structures	334
J. PERFETTI, Rhone-Poulenc Fibres, France	
T. SANGSTER, Rhone-Poulenc Chemicals Ltd., United Kingdom	
The Influence of Nonwoven Geotextiles on the Compactability of the Fill Material	345
G. WERNER, S. RESL	
Polyfelt Ges.m.b.H., Linz/Austria	
R. MONTALVO	
Polyfelt Inc., U.S.A.	
Geotextiles and Geogrids: Cost Effective Alternate Materials for Pavement Design and Construction	353
P. ANDERSON, M. KILLEAVY	
Trow Geotechnical Ltd., Canada	

SESSION 3B: BEHAVIOR OF SOIL GEOSYNTHETIC SYSTEMS

Behavior of Soil-Geotextile Composites and its Application to Finite Element Analysis	365
T.H. WU	
University of Colorado at Denver, U.S.A.	
Stress-Deformation Response of Geotextile Reinforced Granular Structures	373
D.H. GRAY, M. KALDJIAN	
University of Michigan, U.S.A.	
C. WU	
Tamkang University, Taiwan	
Dynamic Behavior of Saturated Sand Reinforced with Geosynthetic Fibers	385
I. NOORANY	
San Diego State University, U.S.A.	
M. UZDAVINES	
Woodward-Clyde Consultants, U.S.A.	

SESSION 4B: TESTING - CHEMICAL

- Flex - An Expert System to Assess
Flexible Membrane Liner Materials 397
R.E. LANDRETH
U.S. Environmental Protection Agency, U.S.A.
- Polymers for Synthetic Lining Systems: Some Molecular
Structure-Property-Application Relationships 408
R.M. CHARRON
GeoSyntec, Inc., U.S.A.
- Microtome Sections for Examining Polyethylene
Geosynthetic Microstructures and Carbon Black Dispersion 421
I.D. PEGGS, R.M. CHARRON
GeoSyntec, Inc., U.S.A.
- Evaluation of the Effects of Waste Loads on Geocomposites
In Double-Lined Landfills and Surface Impoundments 433
G. YAZDANI, J. NORBERT
Poly-America, U.S.A.
- Evaluation Of HDPE Geomembrane Field Welding Techniques,
Need To Improve Reliability Of Quality Seams 443
A.L. ROLLIN, A. VIDOVIC
Ecole Polytechnique de Montreal, Canada
R. DENIS, M. MARCOTTE
Solmers International, Canada
- The Electrical Leak Location Method for Geomembrane Liners:
Development and Applications 456
G.T. DARILEK, D.L. LAINE, J.O. PARRA
Southwest Research Institute, U.S.A.
- Locating And Repairing Leaks In Landfill/Impoundment
Flexible Membrane Liners 467
R.E. LANDRETH
U.S. Environmental Protection Agency, U.S.A.
- Loading Point Puncturability Analysis of Geosynthetic Liner Materials . . 478
D.L. LAINE, M.P. MIKLAS, C.H. PARR
Southwest Research Institute, U.S.A.

SESSION 5B: TESTING - General

Shear Resistance Between Cohesive Soil and Geogrids	489
E.A. RICHARDS, J.D. SCOTT, L.W.M. BOBEY	
University of Alberta, Canada	
V. DIYALJEE	
Alberta Transportation and Utilities, Canada	
Evaluation Of The Degradation Of Geotextiles	501
J.R. MONTALVO	
Polyfelt, Inc., U.S.A.	
Microstructural Analysis Of The Durability of a Polypropylene Geotextile	513
L.G. TISINGER	
GeoSyntec, Inc., U.S.A.	
Analytic Behavior Of Geogrid Anchorage	525
R.M. KOERNER	
M.H. WAYNE	
Drexel University, U.S.A.	
R.G. CARROLL	
Tensar Corporation, U.S.A.	

CHAIRMAN'S OPENING REMARKS

Gailer, J.E.
Chairman, Organizing Committee
Geosynthetics '89 Conference

On behalf of the organizing committee; the sponsor of the conference, the Industrial Fabrics Association International, and the North American Geosynthetics Society; I would like to welcome you to San Diego and Geosynthetics '89.

It is my pleasure to introduce to you a very hard working group of people -- certainly for the last two years. They are the organizing committee for this North American Regional Conference on Geosynthetics.

- Dr. Jay Beech is a member of the International Geotextile Society (IGS) a member of the North American Geosynthetic Society (NAGS), and the American Society of Civil Engineers (ASCE).

Jay is chairman of the technical sub-committee for the conference and has done an outstanding job in selecting the over 50 technical papers.

- Mr. Bob Carroll is vice president of NAGS, an original member of the IFAI Geotextile Division, and active in ASTM. Bob is the liaison from the NAGS Board of Directors to the organizing committee.

- Mr. Joe Luna is a member of IGS, a member of NAGS, and ASTM D-35, the Committee on Geotextiles, Geomembranes and Related Products. Joe is responsible for the exhibits and meeting facilities for the Conference.

- Mr. Bill Neal is vice chairman of the IFAI Geomembrane Division, a member of IGS and a former vice president of the Society of Plastics Engineers. Bill is involved with financial matters for the conference.

- Dr. Iraj Noorany is a Professor of civil engineering at San Diego State University and a visiting professor at the University of California. He is the recipient of the Thomas A. Middlebrooks Award. Iraj has worked very hard to promote the Conference locally and with excellent results.

- Dr. Kerry Rowe is a professor at the University of Western Ontario on the faculty of Engineering Science. He is a member of IGS, vice president of NAGS and editor of the IGS News. Kerry has provided valuable assistance to the Technical Program sub-committee.

- Dr. Neil Williams is a member of the Executive Committee of ASTM D-35, a U.S. delegate to the International Standards Organization. He is also a member of NAGS, IGS and ASCE.

- Neil has worked hard as a member of the technical program sub-committee.

Geosynthetics '89 Conference
San Diego, USA

- Mr. Steve Warner is the executive vice president of the Industrial Fabrics Association International. He is former secretary general of the American Society of Geosynthetics (currently the North American Geosynthetics Society), former secretary general of the Second International Conference on Geotextiles, and a member of the organizing committee of Geosynthetics '87.

- Ms. Laurie Honnigford has been IFAI staff director for Geosynthetics '89 since August 7, 1988. She has done an excellent job in planning the conference details since taking over for Ms. Judy Dean.

Laurie is also general-secretary of NAGS, and IFAI Staff Director for both the Geotextile and Geomembrane Divisions.

- Mr. Joe Fluet is president of the North American Geosynthetic Society, former secretary-treasurer of IGS, former chairman of the Geotextile Division of IFAI, organizing committee member of the Second International Conference on Geotextiles and the First International Conference on Geomembranes, and a former committee member of the Geotechnical Fabrics Conference '85. Joe was organizing committee chairman of Geosynthetics '87 and serves as advisor to this organizing committee providing valuable direction and assistance.

I would like to take a moment to thank IFAI on behalf of the entire geosynthetics industry. They have been a driving force in our industry. The IFAI founded and sponsors the two major trade associations - the Geotextile Division and the Geomembrane Division. They also contracted to act as professional managers in support of NAGS. Most importantly, they have sponsored every major geosynthetics conference held in North America, including the Second International Conference on Geotextiles in 1982, the International Conference on Geomembranes in 1984, the 1985 Geotechnical Fabrics Conference, Geosynthetics '87, and now they bring us Geosynthetics '89. We as an industry are indebted to the IFAI.

Following the keynote address which is coming up shortly, there will be a panel discussion on the writing of geosynthetics specifications moderated by Joe Fluet. I know you will all find this very interesting and very appropriate at this stage of our industry's development.

Following the panel discussion, at 4:40 p.m. will be the General Assembly meeting of the North American Geosynthetic Society. And from 6:00 p.m. to 7:00 p.m. will be the reception.

Now, I am very proud to have the opportunity to introduce to you Dr. J. P. Giroud, the President of the International Geotextile Society. Dr. Giroud was educated in France where he earned both the professional and academic doctoral degree and worked as a professor, researcher, designer and consultant. He has authored a book and over 80 technical papers on geosynthetics, in addition to four books and more than 100 papers on other geotechnical engineering subjects. Dr. Giroud has developed many of the design methods used in geosynthetic engineering. He has taught many short courses on geosynthetics including three series of "Synthetic Liner" courses for the EPA. He has been active on committee work around the world including ASTM, RILEM and the French and Swiss National Committees. Dr. Giroud chaired the Second International Conference on Geotextiles, the International Conference on Geomembranes and the ISSMFE technical session at their last conference in San Francisco.

**Geosynthetics '89 Conference
San Diego, USA**

Dr. Giroud's keynote addresses at the Third International Conference on Geotextiles in Vienna in '86 and at Geosynthetics '87 in New Orleans were the highlight of the conferences. You now have the privilege of hearing perhaps the best known individual in our field.

SESSION 1A
LANDFILL & LINING SYSTEMS

1. The first part of the paper is devoted to a general discussion of the problem of the existence of a solution of the system of equations (1) for arbitrary values of the parameters α and β . It is shown that the system has a solution for arbitrary values of the parameters α and β if and only if the condition $\alpha + \beta = 1$ is satisfied.

2. In the second part of the paper the problem of the existence of a solution of the system of equations (1) for arbitrary values of the parameters α and β is solved. It is shown that the system has a solution for arbitrary values of the parameters α and β if and only if the condition $\alpha + \beta = 1$ is satisfied.

A.A. McCREADY
Harding Lawson Associates, U.S.A.

Paradise Peak Tailings Impoundment Stage II Construction

The Paradise Peak tailings impoundment was constructed by FMC Paradise Peak Corporation for retention of processed tailings and mill liquors from the gold processing facility located at Gabbs, Nevada. The first stage of impoundment construction was completed in 1986. It involved construction of an earth dam to form the impoundment area and approximately 110 acres of High Density Polyethylene (HDPE) liner. The upstream face of the dam was lined with 100-mil HDPE and the remainder of the impoundment area was lined with 60-mil HDPE. Special precautions were taken to prevent damage to the 60-mil HDPE which included a system of weighting the exposed liner to prevent uplift from wind and wave action. Since 100-mil HDPE is rarely affected by wind and wave action, no special precautions were taken to weight the liner on the upstream face of the dam.

After 2 years of operation, it has become necessary to design and construct Stage II of the impoundment. Stage II consists of raising the dam 40 feet using the downstream construction method as illustrated in Figure 1, preparing the subgrade, and lining the dam face and remaining impoundment area to the new operating elevation.

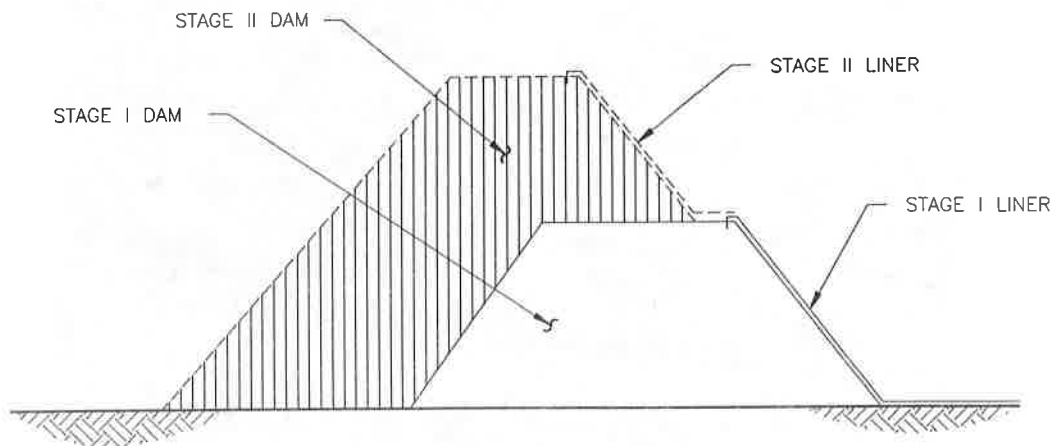


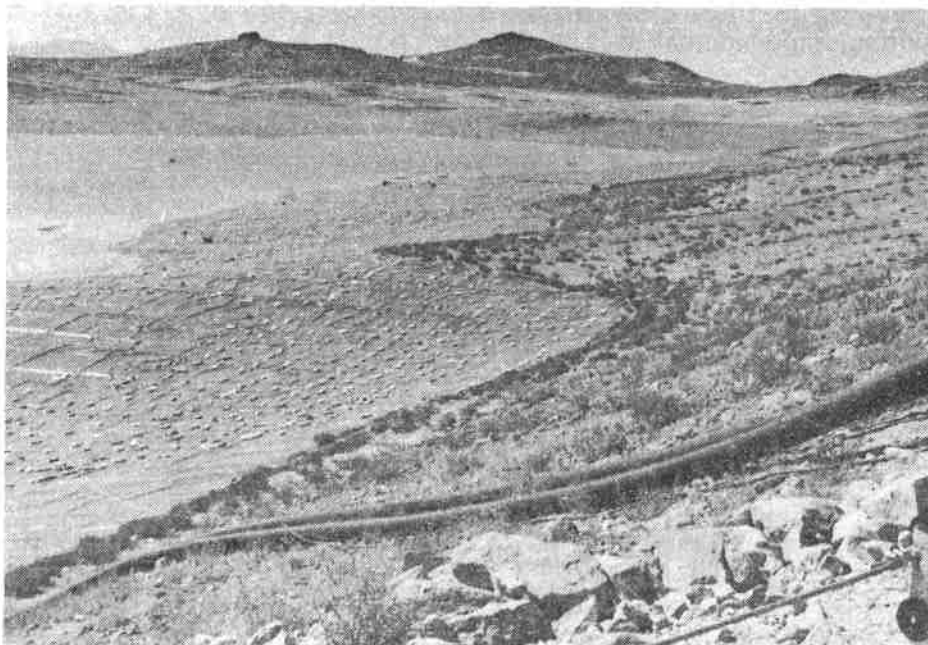
Figure 1
Downstream Staged Construction
5

Staged construction of lined impoundments requires special consideration throughout all design and construction stages. Paradise Peak Stage II expansion involved a number of problems requiring solutions.

- o Preparing the subgrade which included exposed coarse, angular rock and gravel particles, and outcrops of hard bedrock.
- o Constructing new subgrade without damaging the existing exposed liner,
- o Sealing new liner to the existing liner, and
- o Protecting the new and existing liners from damage caused by wind and wave action during operation.

Each of the problems listed will be described in detail along with the corrective design selected to mitigate the problem.

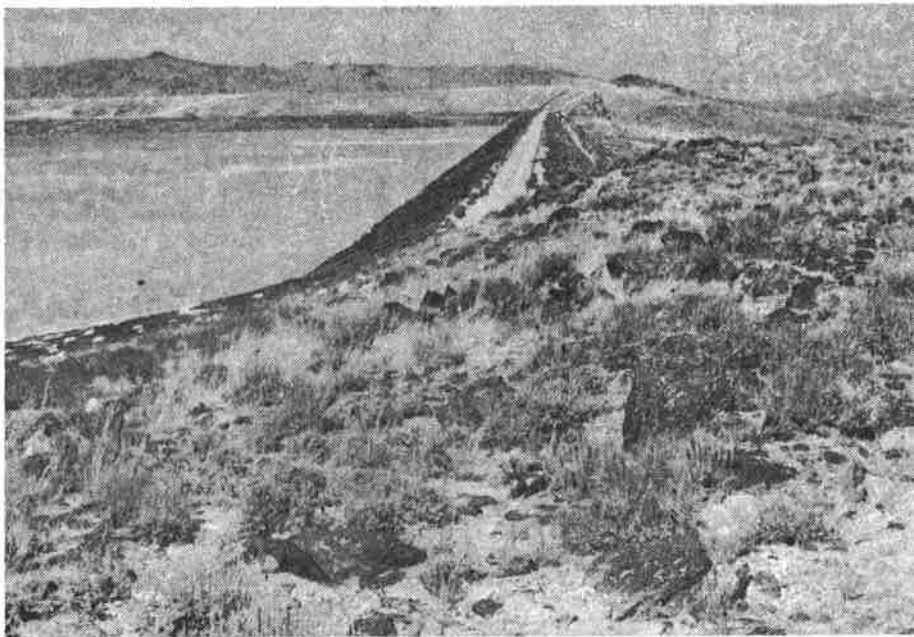
Prior to designing the Stage II expansion, a site visit was made to view the existing impoundment. Interviews were also conducted with operations personnel to review the impoundment's operating performance. As can be seen in Photograph 1, subgrade preparation and construction of the new liner without damaging the existing liner were primary concerns.



Photograph 1

SUBGRADE PREPARATION

Photograph 2 shows a close-up of the existing rocky and gravelly subgrade in the Stage II expansion area. The exposed angular particles would cause severe damage to either 60- or 100-mil HDPE if corrective measures were not taken. Because of the coarse and angular nature of the particles, geotextile cushioning alone was ruled out as a viable option. The preparation procedure that was most practical involved the following steps. The subgrade was scarified to a depth of 6 inches, raked using a 4-inch maximum size rock rake, compacted to 90 percent of ASTM 1557, and covered with a 6-inch-compacted-thickness layer of selected fine-grained soil. The final surface was prepared by rolling with a smooth drum roller.



Photograph 2

Portions of the subgrade were outcrops of bedrock. The outcrops were very hard and not rippable using standard construction equipment. Removal by blasting was considered; however, this method was not practical for removing the thin layer of rock necessary. Rather than blast and place a layer of fine-grained soils over the rock, it was decided that placement of select fine-grained soil over the outcrops would accomplish the same objective more economically. This procedure worked out well and provided satisfactory support for the 60-mil HDPE placed in these areas.

PROTECTION OF EXISTING LINER

During construction of the Stage II liner, it was necessary to provide protection for the existing exposed liner. Equipment and loose rock particles rolling downslope were primary considerations in providing protection. A simple but effective barrier of select fine-grained soil was designed and constructed around the perimeter of the Stage I liner to prevent equipment from inadvertently driving onto the liner and to prevent rocks, boulders, and other debris from rolling down onto the liner. The barrier was constructed of select soil windrowed just outside the existing liner. After rough grading of the Stage II subgrade, the windrow was bladed down to form the finished surface of the Stage II subgrade. Figure 2 is a cross section of the barrier.

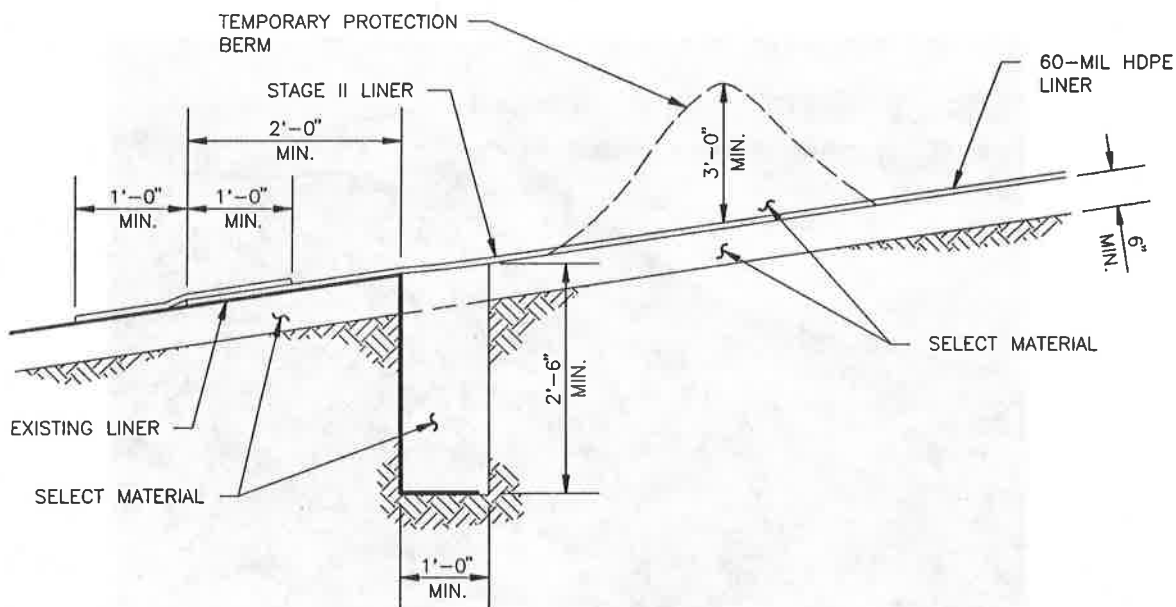
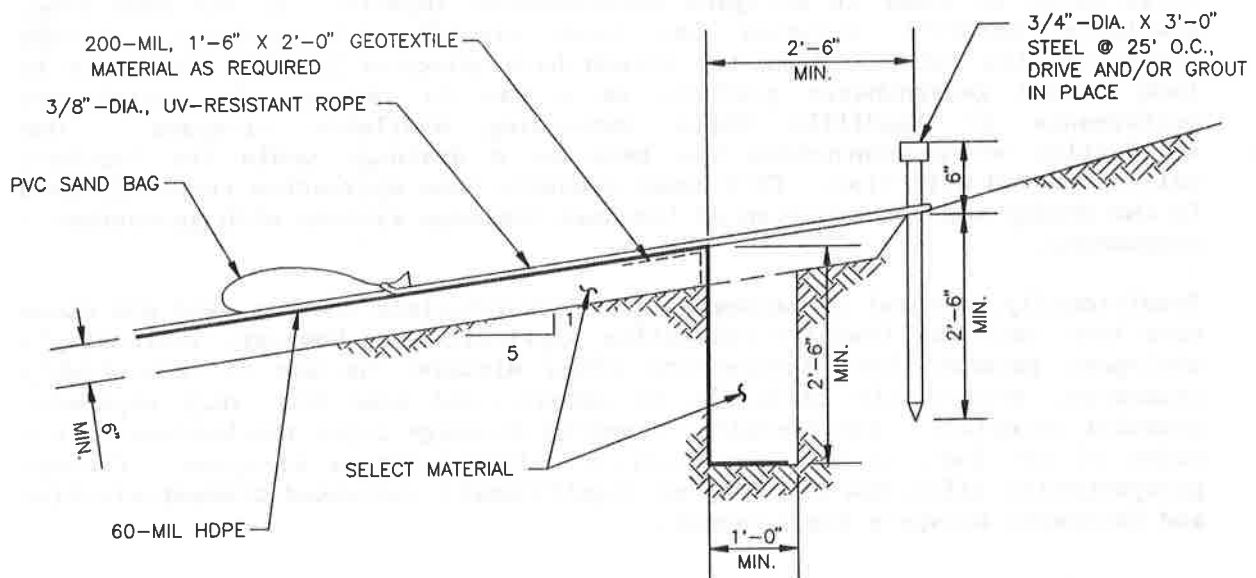


Figure 2
Protective Soil Berm and Old-to-New HDPE Weld

SEALING OLD AND NEW LINER

A key factor in the successful expansion of the impoundment was securely joining the old and new liners together to form a continuous, durable membrane. Because exposure to weather ages liner material, it was necessary to construct a good weld considering the aging of the existing liner. Testing of welds between old and new liner when joined with normal welding procedures indicated a slightly reduced strength compared to welds made with all new material. To compensate for this reduction in strength and to provide a backup seal, an additional cover strip as shown in Figure 2 was designed and constructed. The cover strip spanning the joint will protect the primary weld from weather and will add strength to the joint. Welding was accomplished using normal procedures. Field Quality Control (QC) and Quality Assurance (QA) test results indicated that the weld and cover strip met all specification requirements. The success of the joining system between the old and new liner



ted in October 1988.

C.M. LUNDELL, S.D. MENOFF

Waste Management of North America, Inc., U.S.A.

The Use of Geosynthetics As Drainage Media at Solid Waste Landfills

INTRODUCTION

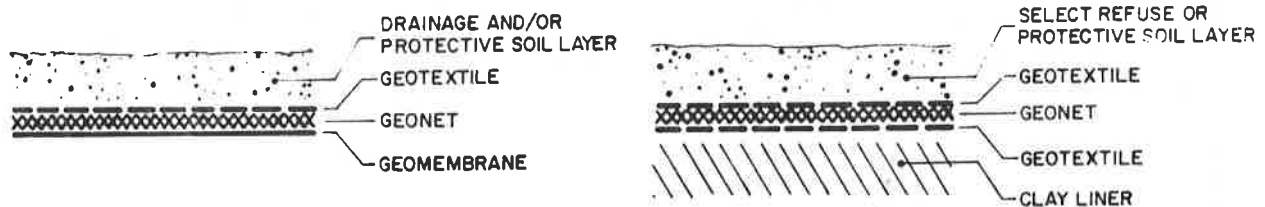
In recent years there has been an increasing emphasis on the implementation of technical improvements in the construction of containment facilities for solid waste in order to mitigate environmental impacts. At the same time, available landfill airspace has been significantly reduced, thereby increasing its value. These two trends have prompted landfill designers to look toward geosynthetic products as a way to improve the containment performance of landfills while increasing available airspace. One application of geosynthetics has been as a drainage media for leachate collection and detection. This paper presents some approaches currently used in the design and construction of leachate drainage systems with geosynthetic components.

Traditionally, natural or processed granular materials such as sand and stone have been used for leachate collection applications. However, increasingly stringent permeability requirements often dictate the use of more highly processed, potentially difficult to obtain, and sometimes very expensive granular materials. Additionally, required drainage layer thicknesses on the order of one foot or more may displace valuable refuse airspace. Certain geosynthetics offer the benefits of significantly increased transmissivities and decreased airspace displacement.

LANDFILL APPLICATIONS

Geotextiles and geonets have both been used as drainage media within landfills. However, the much higher transmissivities of geonets have made them the geosynthetic of choice in most instances. Geosynthetics can be used in primary and secondary leachate collection and detection systems with many different configurations. Some of the configurations which the authors have seen used or proposed are shown in Figure 1. Similar configurations are also used in final cover applications. However, because of the lower overburden pressures geotextiles can be substituted for geonets.

Primary Leachate Collection :



Secondary Leachate Collection :

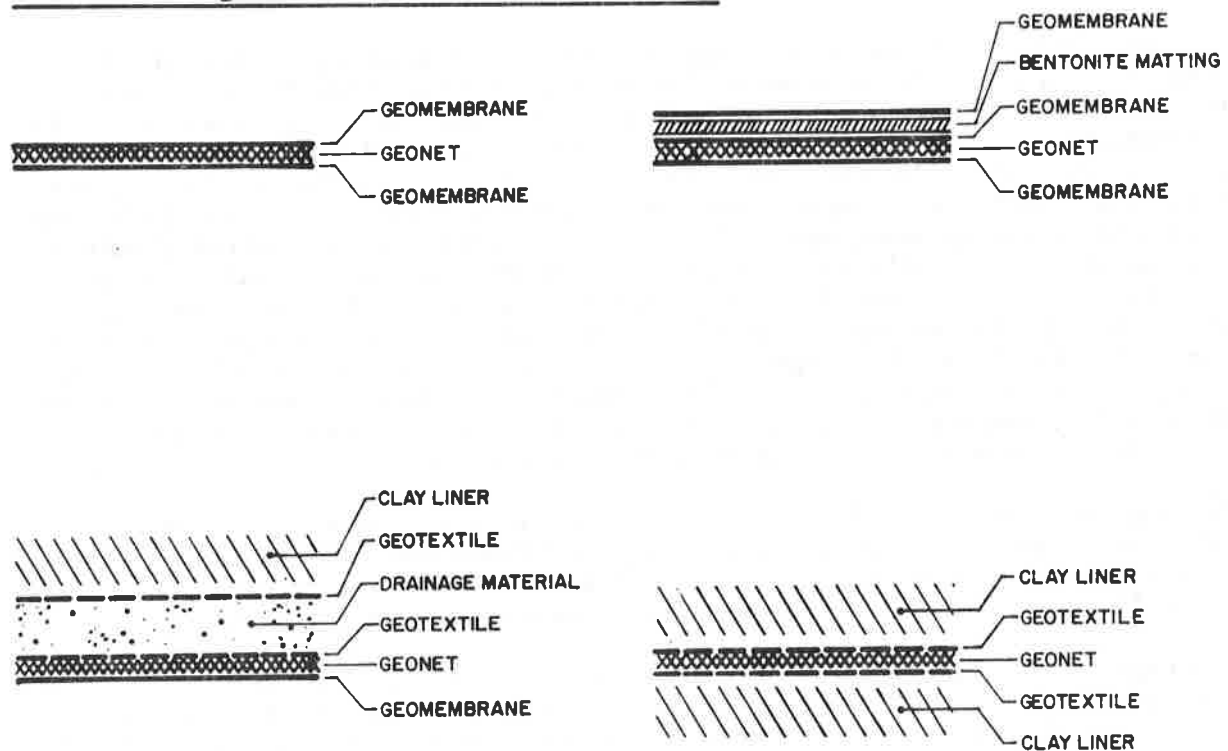


FIGURE 1. Geosynthetic drainage system configurations.

DESIGN CONSIDERATIONS

As mentioned above, geonet products have become the most commonly used geosynthetic for leachate collection. However, regardless of the material being considered, there are a number of issues which impact the design and construction of drainage systems which incorporate the geosynthetics. These design considerations include:

- Transmissivity
- Directional drainage characteristics
- Leachate compatibility
- Frictional characteristics
- Economics

Other considerations such as material availability and regulatory acceptability may also significantly impact the use of geosynthetics on a site specific basis.

Transmissivity

Any geosynthetic being considered for use as a drainage media should be subjected to carefully controlled laboratory testing (ASTM D4716) to measure the material's transmissivity and its response to overburden loading. Laboratory tests should carefully model the anticipated field conditions and include the materials which will be placed adjacent to the drainage layer, realistic overburden loads, and be conducted under range of hydraulic gradients (usually less than 1.0). The overburden loads applied should be increased incrementally to at least the maximum overburden load anticipated in the field. If possible, testing should be performed with applied overburden pressures which exceed the maximum anticipated pressures by at least 50% to check that significant transmissivity reduction will not take place if overloading does occur. Transmissivity reductions may be the result of material compression or, in the case of geonets, strand rollover or the intrusion of adjacent materials into the drainage channels.

The appropriate geosynthetics to be used in a drainage system should be selected in part, by comparing the required transmissivity to the available transmissivity and applying a factor of safety. Factors of safety used are generally greater than two but may vary depending on the application.

Drainage layer transmissivity variations are in part a function of the components of the drainage system and the materials immediately adjacent to it. Typical observed variations for drainage systems utilizing geonets are outlined in Table I. The transmissivity values shown are for extruded geonets approximately 0.2 inches thick. Typical reported values of geotextile transmissivity for planar flow are presented in Table II.

TABLE I Geonet Drainage System Transmissivities

<u>Drainage System Configuration</u>	<u>Typical Transmissivity @10,000psf, i=1.0</u>	<u>Granular Material Equivalency</u>
geomembrane geonet geomembrane	$1 \times 10^{-3} \text{ M}^2/\text{sec}$	12" @ $k=3 \times 10^{-1} \text{ cm/sec}$
soil** geotextile* geonet geomembrane	$5 \times 10^{-4} \text{ M}^2/\text{sec}$	12" @ $k=1.5 \times 10^{-1} \text{ cm/sec}$
soil** geotextile* geonet geotextile* soil**	$1 \times 10^{-4} \text{ M}^2/\text{sec}$	12" @ $k=3 \times 10^{-2} \text{ cm/sec}$

* Geotextiles are approximately 8 oz./square yard, nonwoven

** Cohesive soil

TABLE II Geotextile Planar Transmissivities

<u>Geotextile</u>	<u>Typical Transmissivity¹ @830psf</u>	<u>Granular Material Equivalency</u>
Woven - slit film	$1 \times 10^{-8} \text{ M}^2/\text{sec}$	12" @ $k=3 \times 10^{-6} \text{ cm/sec}$
Woven - monofilament	$3 \times 10^{-8} \text{ M}^2/\text{sec}$	12" @ $k=1 \times 10^{-5} \text{ cm/sec}$
Nonwoven - needled	$2 \times 10^{-6} \text{ M}^2/\text{sec}$	12" @ $k=7 \times 10^{-4} \text{ cm/sec}$

In general, only very thick nonwoven-needle-punch geotextiles have appreciable transmissivities. Even these are generally much less than those of geonets.

The transmissivity tests described above are generally performed at various load increments, with these loads being applied for a time duration ranging typically from less than one hour up to 24 hours. Limited testing has been performed on samples subjected to static loads with longer durations. Testing performed on geonet samples that have been loaded for a time period in excess of 600 days have shown only slight transmissivity reductions after one day. However, this data is available for only certain products and boundary conditions ^{2,3}. It is clear that additional testing is warranted.

Other factors which may impact the long term performance of the drainage media are its response to elevated temperatures and the potential for biological or mechanical clogging. Although field monitoring information suggests that these factors do not have major widespread impact on the drainage layer performance, these materials have been used for only a relatively short period of time in the field and additional testing and field monitoring is needed.

Directional Drainage Characteristics

Some geosynthetic drainage materials exhibit preferential drainage directions which should be taken into account during design and construction. Geotextiles do not generally exhibit significant transmissivity anisotropies. However, geonets may exhibit a wide range of directional drainage behavior. Some geonets have transmissivity anisotropies that are insignificant and require no special construction considerations. Other geonets have drainage preferences that are nearly unidirectional and the use of such products may require significant design consideration and careful construction control to be effective. In general, overall transmissivity behavior can be significantly effected by the orientation of the strands of polymer which make up the geonet.

Leachate Compatibility

If the landfill design and operation is effective, the geosynthetic drainage media will likely be subjected to leachate contact constantly for many years. It is therefore of critical importance that the drainage media be compatible with the anticipated leachate composition. The variation of leachate composition between solid waste landfills can be significant. Therefore, the drainage material should be constructed of a substance which is compatible with a wide range of possible leachate constituents. At the present time, high density polyethylene (HDPE) is widely regarded as the most compatible material available for use in this type of application. There are a number of geonet products which are composed of HDPE. HDPE geotextiles, however, are not readily available at this time in the United States.

Frictional Characteristics

During construction and operation of a landfill, the frictional characteristics of the various liner components may be of significant

importance. They may control the stability of the below grade slopes and the sequence of landfilling operations. Published data regarding frictional characteristics of various synthetic materials suggest that the geosynthetic interfaces tend to result in lower friction angles than do soil/geosynthetic interfaces, and, as a result, are generally the most critical interfaces to be evaluated during design. Geonets and geotextiles are often placed next to geomembranes, and these interfaces tend to have the lowest laboratory measured friction angles. Minimum friction angles on the order of 6° have been reported for geotextile/geomembrane interfaces.

Friction angles in the range of 15° to 17° have been reported for geonet/geomembrane interfaces⁴. It has been our experience that friction angles closer to those of geotextile/geomembrane interfaces can be measured in the laboratory for geonet/geomembrane interfaces. Therefore, the published numbers may be somewhat unconservative. In situations where the consequences of system failure are substantial, it is recommended that the lower friction angle values be used during design or that site specific laboratory evaluation of interface friction be performed. If laboratory tests are performed, care must be taken to minimize testing conditions (such as size and edge effects) which may result in the measurement of unrealistically high friction angles.

Economics

Prices for material and installation of geosynthetic drainage systems may range from approximately \$0.30 to over \$1.00 per square foot depending on the type of geosynthetic used and the components of the drainage system (i.e., the number of layers of geotextile and/or geonet) as well as general site specific considerations such as location, construction season, labor issues and other factors. The overall evaluation of the economic feasibility of the use of these materials should include consideration of the value of the available solid waste airspace retained as a result of the use of the geosynthetics.

CONSTRUCTION CONSIDERATIONS

The correct translation of design concepts to field construction is always important. However, it is extremely critical when geosynthetics are used. This is particularly true in a landfill setting. Quality control and quality assurance are integral parts of all geosynthetic installations.

Quality Control

Since the geosynthetic products to be used in the drainage system have been specified by the engineer based on laboratory testing, it is of utmost importance that the materials used in the construction of the landfill be the same as those tested in the laboratory. Therefore, since the critical properties of the geosynthetics being used can sometimes vary significantly even if manufacturing processes are varied only slightly, it is necessary

that good quality control be exercised during manufacturing of the geosynthetics. Samples should be taken on a regular basis during manufacturing (e.g. once every 50,000 ft²) and tested to evaluate pertinent geosynthetic characteristics. The manufacturer should maintain detailed quality control documentation and should provide certification of the quality of each roll of material produced.

It is advisable to use only thoroughly tested products from manufacturers who have a record of consistently producing a quality product and to carefully review their quality control procedures with them prior to running the product for a given site. Any producer who hesitates to fully cooperate with all quality control evaluation efforts or is unwilling to produce historical quality control records should be disqualified from consideration for the project.

Quality Assurance

During construction, a thorough quality assurance program is required in order to ensure that the geosynthetic installation conforms to the design intent. All construction should be overseen by a full-time quality assurance monitor who is familiar with geosynthetic installations and able to make decisions concerning the acceptability or unacceptability of materials and construction procedures. The construction quality assurance program should be supervised by a qualified professional engineer who should be required to certify all quality assurance documents and record drawings.

A detailed site specific quality assurance plan should be prepared and agreed to by all affected parties prior to commencing construction. Conformance testing should be performed on samples taken from rolls of geosynthetics delivered to the site. Samples should be taken at a pre-determined interval (e.g. one per 100,000 ft²) and the tests performed will depend on the type of geosynthetic being used.

Careful attention must be paid to any special installation requirements such as placement, orientation and joining techniques. In general, geotextiles should be sewn and geonets overlapped and tied. Geonet ties should not contain any metal, and should be of a contrasting color to the geonet to allow for easy inspection. Typically, geonets are overlapped a minimum of four inches and ties spaced on the order of five feet along slopes, two feet across slopes and six inches in anchor trenches. It is also important that the installation procedures (e.g., placing, cutting and joining) involved not be allowed to adversely affect the performance of adjacent materials, especially geomembranes.

All geosynthetics used for drainage applications should be clean and free of materials which might clog the drainage system during operation. The easiest way to ensure that only clean geonets and geotextiles are placed in the landfill is to store the drainage materials in a dry, covered area on site prior to installation. If this is not done, extensive cleaning may be required.

SUMMARY

The design and construction of drainage systems which incorporate geosynthetic components at solid waste landfills have been discussed in this paper. Since the use of geosynthetics in this type of application is relatively new, it is important that designs be based on carefully modeled laboratory testing and be checked with field observation and testing. Important design considerations include transmissivity, directional drainage, leachate compatibility, and frictional characteristics of the geosynthetics, along with economic feasibility. Some of these design properties are well known or can be measured during short term laboratory testing. The long term response of geosynthetic drainage materials to overburden loading, elevated temperature, and biological and chemical activity is not well documented. As a result, additional work in these areas is warranted. Careful quality control during manufacturing of the geosynthetic materials and full time quality assurance during construction are both critical to the successful performance of these types of drainage systems.

It is anticipated that in the future geosynthetics will find increased use as drainage media at solid waste landfills. This increased use will be driven by technical design considerations directed at minimizing environmental impacts and by economic and site life advantages. These geosynthetic materials can, in some cases, offer significant advantages to the use of granular materials in drainage layers. A geosynthetic drainage layer is not just a novel concept, but a practical and efficient application of technology to landfill construction. These types of products should be routinely considered during the conceptual design phase of all new landfill sites.

REFERENCES

1. Koerner, R.M. and Bove, J.A., "Lateral Drainage Designs Using Geotextiles and Geocomposites", Geotextile Testing and the Design Engineer, ASTM STP 952, 1987.
2. Slocumb, R.C., Demeny, D.D. and Christopher, B.R., "Creep Characteristics of Drainage Nets", Proceedings of the Ninth Annual Madison Waste Conference, Madison, Wisconsin, 1986.
3. Communication with George Zagorski of Fluid Systems, Inc.
4. Koerner, R.M., Designing With Geosynthetics, Prentice - Hall, Englewood Cliffs, New Jersey, 1986.

R. BONAPARTE

J.P. GIROUD

B.A. GROSS

GeoServices Inc., Consulting Engineers, U.S.A.

Rates of Leakage Through Landfill Liners

ABSTRACT

This paper describes methods for evaluating rates of leakage through landfill liners constructed with geomembranes. The paper addresses both geomembranes alone and geomembranes used in composite liners. Leakage through liners constructed with geomembranes can occur by fluid permeation through intact geomembranes and flow through geomembrane holes. Only leakage through geomembrane holes is considered in the paper. Leakage through a geomembrane hole is dependent on the hydraulic conductivities of the materials overlying and underlying the geomembrane. Three cases of leakage are considered: (i) leakage through geomembranes alone; (ii) leakage through composite liners; and (iii) leakage through geomembranes overlain by a drainage layer that impedes flow toward the geomembrane hole. A comparison of the leakage rates for these three cases shows that leakage through a hole in the geomembrane component of composite liner can be up to 100,000 times smaller than leakage through a hole in a geomembrane alone. It is also shown that the presence of sand overlying a geomembrane hole can reduce the rate of leakage through the hole by a factor of up to 50 compared to the case of a geomembrane alone.

INTRODUCTION

All hazardous waste landfills in the United States and an increasing number of municipal solid waste landfills are constructed with double liner systems. The lining systems of these landfills include the following four elements, from top to bottom: a leachate collection layer; a primary liner; a leakage detection and collection layer; and a secondary liner. In this paper, the leachate collection layer and the leakage detection and collection layer are generically called drainage layers.

This paper discusses the evaluation of the rate of leakage through the primary and secondary liners.

The primary or secondary liner can be a geomembrane or a composite liner, i.e., a liner composed of a geomembrane placed on a layer of low-permeability soil (i.e., a soil with a hydraulic conductivity less than 10^{-6} m/s (10^{-4} cm/s) and usually in the range of 10^{-8} to 10^{-10} m/s (10^{-6} to 10^{-8} cm/s)). Soil liners alone are not considered.

The leachate collection layer and the leakage detection and collection layer can be constructed with a variety of drainage materials. Some have high permeabilities, such as geonets and coarse gravels; some have medium permeabilities, such as sands and fine gravels. Typical hydraulic conductivities of drainage materials are: 10^{-1} to 1 m/s (10 to 100 cm/s) for coarse gravel; 10^{-1} m/s (10 cm/s) for geonets; 10^{-2} m/s (1 cm/s) for fine gravel; and 10^{-5} to 10^{-3} m/s (10^{-3} to 10^{-1} cm/s) for sand. The influence of the hydraulic conductivity of the drainage material on the leakage rate will be evaluated.

LEAKAGE MECHANISMS

There are essentially two mechanisms of leakage through geomembranes: fluid permeation through an intact geomembrane and flow through geomembrane holes.

Leakage due to permeation is not considered in this paper because, for landfills, leakage rates due to fluid permeation are usually much smaller than leakage rates due to flow through geomembrane holes. A review of this subject is presented in Giroud and Bonaparte (7).

Regarding leakage through geomembrane holes, several cases can be considered:

- If a geomembrane with a hole is overlain and underlain by high-permeability materials (such as geonet or coarse gravel), flow through the hole is not significantly impeded. Therefore, for this case, the flow of liquid can be considered as free flow through an orifice and the leakage rate is essentially governed by the size of the hole.
- If a geomembrane with a hole is placed on a layer of low-permeability soil (such as clay, silt, clayey soil, etc.) to form a composite liner, the low-permeability soil significantly impedes the flow of liquid through the hole, provided that the geomembrane is in close contact with the low-permeability soil.
- If a geomembrane with a hole, and placed on a high-permeability material, is overlain by a sand or a fine gravel, flow through the hole may be somewhat impeded, so that the rate of leakage through the hole is lower than in the case where the geomembrane is overlain or underlain by a high-permeability material, but higher than in the case where the geomembrane is placed on a low-permeability soil to form a composite liner.

These three cases will be discussed below, and equations to evaluate leakage rates will be presented.

RATE OF LEAKAGE DUE TO DEFECTS IN GEOMEMBRANES ALONE

In the context of this paper, a geomembrane alone is a geomembrane overlain and underlain by high-permeability materials (such as geonets or coarse gravels). In this case, unless the hole is a slit with a width less than the thickness of the geomembrane or a pinhole with a diameter less than the thickness of the geomembrane, Bernoulli's equation for free flow through an orifice can be used to evaluate the leakage rate (Giroud, 6):

$$Q = C_B a \sqrt{2gh}$$

(1)

where: Q = steady-state rate of leakage through one geomembrane hole; a = area of the hole in the geomembrane; g = acceleration of gravity; and h = head of liquid on top of the geomembrane. C_p is a dimensionless coefficient, valid for any Newtonian fluid, related to the shape of the edges of the aperture; for sharp edges, which is assumed to be the case for geomembrane holes, $C_p = 0.6$. Basic SI units are: Q (m^3/s), a (m^2), g (m/s^2), and h (m). As discussed subsequently, and shown in Figure 1, Equation 1 can be used if the soil underlying the geomembrane has a hydraulic conductivity greater than 10^{-3} m/s (10^{-1} cm/s) when the geomembrane hole area is 0.1 cm^2 (0.016 in^2) and greater than 10^{-2} m/s (1 cm/s) when the geomembrane hole area is 1 cm^2 (0.16 in^2).

RATE OF LEAKAGE THROUGH A COMPOSITE LINER

The mechanism of leakage through a composite liner with a hole in the geomembrane is as follows: the liquid first migrates through the hole in the geomembrane; the liquid may then travel laterally some distance in the space, if any, between the geomembrane and the low-permeability soil; finally, the liquid migrates into and eventually through the low-permeability soil.

There may be no space between the geomembrane and soil components of a composite liner if the geomembrane is sprayed directly onto the low-permeability soil layer. This technique is not very often used and, in the more usual case of a geomembrane manufactured in a plant, there will be some space between the geomembrane and soil components of a composite liner in almost all applications because:

- the geomembrane has wrinkles (note that geomembrane wrinkles may exist even under very high pressures as shown by Stone (10));
- there are clods or irregularities in the underlying soil surface; and/or
- even when the underlying soil surface is smooth, the geomembrane bridges small spaces between soil particles.

Laboratory test results discussed by Giroud and Bonaparte (7) seem to indicate that some lateral flow almost always occurs between the geomembrane and the underlying soil, even under laboratory test conditions where the geomembrane is placed as flat as possible on a soil layer that has a smooth surface.

In order to establish a method for evaluating the rate of leakage through composite liners with a hole in the geomembrane, Giroud and Bonaparte (7) have made a thorough review of the results of composite liner model tests conducted by Fukuoka (4, 5) and Brown et al. (1), and theoretical analyses carried out by Faure (2, 3), Sherard (9), Fukuoka (5), and Brown et al. (1). Giroud and Bonaparte (7) indicate that a key factor influencing the rate of leakage through a composite liner is the quality of contact between the geomembrane and low-permeability soil components of the composite liner. They ranked the experimental and theoretical results they reviewed as a function of the contact quality from a lower bound, corresponding to the theoretical case of perfect contact, to an upper bound, corresponding to no contact at all. They also proposed a method of interpolation between the various experimental and theoretical results. This method is described in detail in two publications [USEPA (11); Giroud and Bonaparte (7)]. Subsequently, Giroud et al. (8), using the proposed interpolation method, established the following empirical equations:

$$Q = 0.21 a^{0.1} h^{0.9} k_s^{0.74} \quad \text{for good contact} \quad (2)$$

$$Q = 1.15 a^{0.1} h^{0.9} k_s^{0.74} \quad \text{for poor contact} \quad (3)$$

where: Q = steady-state rate of leakage through one hole in the geomembrane component of a composite liner; a = area of the hole in the geomembrane; h = head of liquid on top of the geomembrane; and k_s = hydraulic conductivity of the low-permeability soil underlying the geomembrane. Equations 2 and 3 are not dimensionally homogeneous; they can only be used with the following units: $Q(\text{m}^3/\text{s})$, $a(\text{m}^2)$, $h(\text{m})$, and $k_s(\text{m}/\text{s})$.

The experimental data used to empirically establish Equations 2 and 3 suggest that the use of these equations should be restricted to cases where the hydraulic conductivity of the low-permeability soil is less than 10^{-6} m/s (10^{-4} cm/s). The theoretical analyses used to empirically establish Equations 2 and 3 also suggest that the use of these equations should be restricted to cases where the head of liquid on top of the geomembrane is less than the thickness of the low-permeability soil layer underlying the geomembrane. If this condition is fulfilled, the leakage rate does not significantly depend on the thickness of the low-permeability soil layer. This is why Equations 2 and 3 do not show a functional dependence of leakage rate on the thickness of the low-permeability soil layer.

The good and poor contact conditions are defined as follows:

- The good contact condition corresponds to a geomembrane installed with as few wrinkles as possible, on top of a low-permeability soil layer that has been adequately compacted and has a smooth surface.
- The poor contact condition corresponds to a geomembrane that has been installed with a certain number of wrinkles, and/or placed on a low-permeability soil that has not been well compacted and does not appear smooth.

These two contact conditions can be considered as typical field conditions. They are bounded by two extreme field conditions, the best case and the worst case, which can be defined as follows:

- In the best case: (i) the soil is well compacted, flat and smooth, has not been deformed by rutting due to construction equipment, and has no clods nor cracks; (ii) the geomembrane is flexible and has no wrinkles; and (iii) the geomembrane and soil are in close contact.
- In the worst case: (i) the soil is poorly compacted, has an irregular surface, and is cracked; and (ii) the geomembrane is stiff and exhibits a pattern of large, connected wrinkles.

RATE OF LEAKAGE THROUGH A GEOMEMBRANE overlain BY A DRAINAGE MATERIAL

As indicated above, high-permeability materials (such as geonets and coarse gravels) located above or below a geomembrane are not expected to significantly affect the flow of liquid through a hole in the geomembrane, and the flow rate is approximately the same as in the case of free flow through the hole. On the other hand, if a geomembrane resting on a high-permeability material (such as geonet or

coarse gravel) is overlain by a medium-permeability drainage material (such as sand or fine gravel), the flow toward the geomembrane hole is impeded by the drainage material, and the flow rate is less than in the case of free flow. A typical field situation is a geomembrane primary liner overlain by a sand leachate collection layer and underlain by a geonet leakage detection and collection layer.

In order to evaluate the leakage rate reduction due to the presence of the drainage material above the geomembrane, the following rationale has been used:

- When sand or fine gravel is placed above a geomembrane, excellent contact is expected between the sand or gravel and the geomembrane, because sand and gravel are cohesionless, and they follow the shape of the geomembrane, even if it exhibits wrinkles.
- However, even if the contact between a granular material and a flat boundary such as a geomembrane seems perfect, there is usually a preferential flow path in the granular material next to the boundary, because the porosity of a granular material in the vicinity of a flat boundary is usually greater than the porosity within the material.
- From the above, it appears that a lower bound solution for the leakage rate is provided by the equation for radial flow towards the geomembrane hole, since this equation corresponds approximately to the case of perfect contact without preferential flow, according to Giroud and Bonaparte (7).
- An obvious upper bound solution for the leakage rate is provided by Bernoulli's equation for free flow (Equation 1).
- Approximate theoretical evaluations of the rate of flow in the zone of greater porosity of the granular drainage material in the vicinity of the geomembrane were made by the authors. Using these approximate evaluations as a guide, several empirical approaches were attempted. It was found that a satisfactory approximate value for the leakage rate could be obtained by averaging the logarithms of the leakage rates obtained with the lower bound and upper bound solutions mentioned above.

The empirical equation thus obtained is:

$$Q = 3 a^{0.75} h^{0.75} k_d^{0.5} \quad (4)$$

where: Q = steady-state rate of leakage through one geomembrane hole; a = area of the hole in the geomembrane; h = head of liquid on top of the geomembrane; k_d = hydraulic conductivity of the drainage material overlying the geomembrane. Equation 4 is not dimensionally homogeneous; it can only be used with the following units: $Q(m^3/s)$, $a(m^2)$, $h(m)$, and $k_d(m/s)$.

Equation 4 is intended only for the case of granular drainage materials and, therefore, should only be used when the hydraulic conductivity of the drainage layer material is greater than $10^{-6} m/s$ ($10^{-4} cm/s$). Also, some of the analyses used to establish Equation 4 suggest that use of the equation should be limited to cases where the head of liquid on top of the geomembrane, h , is less than the thickness of the drainage layer; this condition is usually fulfilled in the case of landfills.

COMPARISON OF LEAKAGE RATES

Two tables were established to compare leakage rates through a geomembrane alone, a composite liner, and a geomembrane overlain by a drainage layer.

Equations 1 and 2 were used to establish Table 1, which compares the rates of leakage through a hole in the geomembrane component of a composite liner with those through a hole in a geomembrane alone, i.e., a geomembrane overlain and underlain by high-permeability materials (such as geonets or coarse gravels). This table was established assuming that the head of liquid above the geomembrane hole is constant (i.e., that there is no drawdown of liquid over the hole). This table shows that there is great benefit in using composite liners. For example, in the case of a small hole (i.e., $0.1 \text{ cm}^2 = 0.016 \text{ in}^2$), it appears that the ratio between the rates of leakage through a hole in geomembrane alone and a composite liner are, for the case of "good contact", in the following ranges:

- 25,000 to 60,000 if $k_s = 10^{-10} \text{ m/s}$ (10^{-8} cm/s)
- 5,000 to 10,000 if $k_s = 10^{-9} \text{ m/s}$ (10^{-7} cm/s)
- 800 to 2,000 if $k_s = 10^{-8} \text{ m/s}$ (10^{-6} cm/s)
- 150 to 400 if $k_s = 10^{-7} \text{ m/s}$ (10^{-5} cm/s)
- 30 to 70 if $k_s = 10^{-6} \text{ m/s}$ (10^{-4} cm/s),

where k_s is the hydraulic conductivity of the low-permeability soil component of the composite liner. In each range, the lower value is for a head of liquid on top of the geomembrane of 0.1 m (4 in.) and the higher value is for 0.01 m (0.4 in.). The beneficial effect of the composite liner is slightly greater if the hole size is greater than the considered 0.1 cm^2 (0.016 in^2).

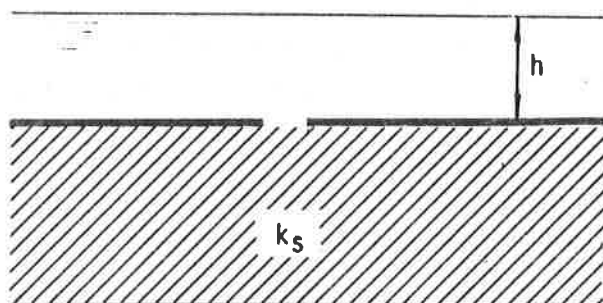
Equations 1 and 4 were used to establish Table 2, which compares the rates of leakage through a hole in: (i) a geomembrane overlain by a sand or fine gravel and underlain by a high-permeability material such as a geonet or coarse gravel; and (ii) a geomembrane alone, i.e., a geomembrane overlain and underlain by high-permeability materials. This table shows that the drainage material overlying the geomembrane can have a significant influence on the rate of leakage through a hole in the geomembrane. For example, in the case of a small hole (e.g., $0.1 \text{ cm}^2 = 0.016 \text{ in}^2$), it appears that the ratios between the rates of leakage through a hole in a geomembrane alone and a hole in a geomembrane overlain by a sand or fine gravel are in the following ranges:

- 30 to 50 if $k_d = 10^{-5} \text{ m/s}$ (10^{-3} cm/s)
- 10 to 15 if $k_d = 10^{-4} \text{ m/s}$ (10^{-2} cm/s)
- 3 to 5 if $k_d = 10^{-3} \text{ m/s}$ (10^{-1} cm/s),

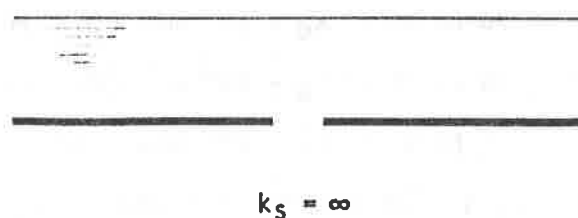
where k_d is the hydraulic conductivity of the drainage layer material overlying the geomembrane. In each range, the lower value is for a head of liquid on top of the geomembrane of 0.1 m (4 in.) and the higher value is for 0.01 m (0.4 in.). The effect of drainage materials having a hydraulic conductivity equal to or greater than 10^{-2} m/s (1 cm/s) is negligible.

Table 1. *Ratio of Leakage Rates Between Composite Liner and Geomembrane Alone.* This table was obtained by dividing Equation 2 (composite liner with good contact) by Equation 1 (geomembrane alone, i.e., geomembrane overlain and underlain by a high-permeability material).

Hole Size	Hydraulic Conductivity of Low-Permeability Soil, k_s m/s (cm/s)	Depth of Liquid, h (m (in.))			
		0.001 (0.04)	0.01 (0.4)	0.1 (4)	0.3 (12)
1 cm ² (0.16 in ²)	10 ⁻¹⁰ (10 ⁻⁸)	7.9 x 10 ⁻⁷	2.0 x 10 ⁻⁶	5.0 x 10 ⁻⁶	7.7 x 10 ⁻⁶
	10 ⁻⁹ (10 ⁻⁷)	4.3 x 10 ⁻⁶	1.1 x 10 ⁻⁵	2.7 x 10 ⁻⁵	4.3 x 10 ⁻⁵
	10 ⁻⁸ (10 ⁻⁶)	2.4 x 10 ⁻⁵	6.0 x 10 ⁻⁵	1.5 x 10 ⁻⁴	2.3 x 10 ⁻⁴
	10 ⁻⁷ (10 ⁻⁵)	1.3 x 10 ⁻⁴	3.3 x 10 ⁻⁴	8.3 x 10 ⁻⁴	1.3 x 10 ⁻³
	10 ⁻⁶ (10 ⁻⁴)	7.2 x 10 ⁻⁴	1.8 x 10 ⁻³	4.6 x 10 ⁻³	7.1 x 10 ⁻³
0.1 cm ² (0.016 in ²)	10 ⁻¹⁰ (10 ⁻⁸)	6.3 x 10 ⁻⁶	1.6 x 10 ⁻⁵	4.0 x 10 ⁻⁵	6.1 x 10 ⁻⁵
	10 ⁻⁹ (10 ⁻⁷)	3.4 x 10 ⁻⁵	8.7 x 10 ⁻⁵	2.2 x 10 ⁻⁴	3.4 x 10 ⁻⁴
	10 ⁻⁸ (10 ⁻⁶)	1.9 x 10 ⁻⁵	4.8 x 10 ⁻⁴	1.2 x 10 ⁻³	1.9 x 10 ⁻³
	10 ⁻⁷ (10 ⁻⁵)	1.0 x 10 ⁻³	2.6 x 10 ⁻³	6.6 x 10 ⁻³	1.0 x 10 ⁻²
	10 ⁻⁶ (10 ⁻⁴)	5.7 x 10 ⁻³	1.4 x 10 ⁻²	3.6 x 10 ⁻²	5.6 x 10 ⁻²
Ratio of Leakage Rates Between Composite Liner and Geomembrane Alone					



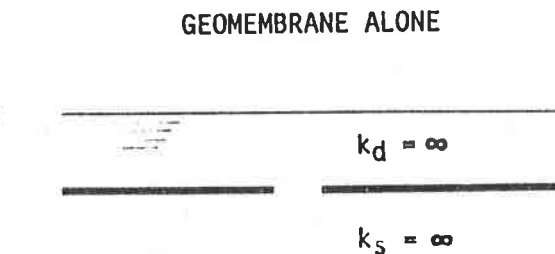
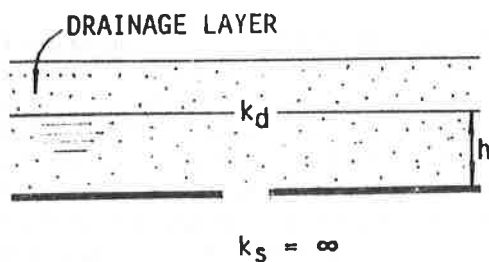
COMPOSITE LINER



GEOMEMBRANE ALONE

Table 2. *Effect on Leakage Rate of the Drainage Layer Overlying the Geomembrane.*
This table was obtained by dividing Equation 4 by Equation 1.

Hole Size	Hydraulic Conductivity of Drainage Material, k_d m/s (cm/s)	Depth of Leachate, h (m (in.))			
		0.001 (0.04)	0.01 (0.4)	0.1 (4)	0.3 (12)
1 cm ² (0.16 in ²)	10 ⁻⁵ (10 ⁻³)	0.006	0.012	0.021	0.027
	10 ⁻⁴ (10 ⁻²)	0.021	0.037	0.065	0.085
	10 ⁻³ (10 ⁻¹)	0.065	0.115	0.205	0.270
	10 ⁻² (1)	0.205	0.365	0.649	0.855
	10 ⁻¹ (10)	0.649	>1	>1	>1
	1 (100)	>1	>1	>1	>1
1 cm ² (0.016 in ²)	10 ⁻⁵ (10 ⁻³)	0.012	0.021	0.037	0.048
	10 ⁻⁴ (10 ⁻²)	0.037	0.065	0.115	0.152
	10 ⁻³ (10 ⁻¹)	0.115	0.205	0.365	0.481
	10 ⁻² (1)	0.365	0.649	>1	>1
	10 ⁻¹ (10)	>1	>1	>1	>1
	1 (100)	>1	>1	>1	>1
Ratio of Leakage Rates Between Geomembrane Overlain by a Drainage Material and Geomembrane Alone					



It therefore appears that placing soil below or above a geomembrane significantly decreases the leakage rate through a hole in the geomembrane. However, the two beneficial effects should not be added to each other. For example, if a geomembrane is underlain by clay and overlain by sand, the beneficial effect of the sand cannot be added to the beneficial effect of the clay. The rationale is as follows: the hydraulic conductivity of clay is much lower than that of sand and, therefore, it controls the velocity of liquid flow through the geomembrane hole; the presence of sand does not have any noticeable influence on flow velocity and, consequently, on leakage rate.

RATE OF LEAKAGE THROUGH A QUASI-COMPOSITE LINER

There are many practical situations where clay or clayey soils are not available to construct a composite liner and where a geomembrane is placed on a layer of sandy or silty soil (either the natural subgrade or a compacted layer of bedding soil) with a hydraulic conductivity in the range of 10^{-6} - 10^{-4} m/s (10^{-4} - 10^{-2} cm/s). Although this is not as good as a composite liner where the low-permeability soil component has a hydraulic conductivity less than 10^{-6} m/s (10^{-4} cm/s), the presence of the sandy or silty soil under the geomembrane is likely to decrease the leakage rate through a geomembrane hole compared to the case of a geomembrane placed on a highly pervious soil. The association of a geomembrane and a medium-permeability soil can be called a quasi-composite liner.

At the present time, to the best of our knowledge, there is no method to evaluate the rate of leakage through a quasi-composite liner due to a hole in the geomembrane. Equations 2 and 3 are valid only if the soil component of the composite liner has a hydraulic conductivity less than 10^{-6} m/s (10^{-4} cm/s). If Equation 2 or 3 are used with a value of the hydraulic conductivity greater than 10^{-6} m/s (10^{-4} cm/s), the equations overestimate the leakage rate because they exaggerate the influence of lateral flow between the geomembrane and soil. (Lateral flow is expected to be very small when the soil underlying the geomembrane does not have a low hydraulic conductivity.)

Another approach to calculating the leakage rate through a hole in the geomembrane component of a quasi-composite liner would be to use Equation 4, which was developed to evaluate the effect of the overlying material, with k_s substituted for k_d . This would tend to underestimate the leakage rate because Equation 4 was established assuming excellent contact between the overlying granular material and the geomembrane, while the contact quality may not be as good when the granular soil is below the geomembrane.

It may therefore be concluded that Equation 2 provides an upper bound solution and Equation 4 (with k_s instead of k_d) a lower bound solution for the case of a quasi-composite liner.

It is interesting to use both equations to determine the hydraulic conductivity of the underlying soil for which the leakage rate is the same as in the case of free flow (Equation 1). For a 0.1 cm^2 (0.016 in^2) hole, this occurs at k_s approximately equal to 10^{-4} m/s (10^{-2} cm/s) with Equation 2, and k_s approximately equal to 10^{-2} m/s (1 cm/s) with Equation 4. By interpolating between these two values, it can arbitrarily be concluded that free flow occurs when the hydraulic conductivity of the material underlying the geomembrane is on the order of 10^{-3} m/s (10^{-1} cm/s) or greater. This value is consistent with the results of some tests by Brown et al. (1).

To evaluate the beneficial effect of a quasi-composite liner between $k_s = 10^{-6}$ m/s (10^{-4} cm/s) and $k_s = 10^{-3}$ m/s (10^{-1} cm/s), interpolation on a logarithmic scale is suggested, as shown in Figure 1. This figure also illustrates the beneficial effect of composite and quasi-composite liners in the case of a geomembrane hole with an area of 1 cm^2 (0.16 in^2).

For practical applications, Figure 1 can be used for a rapid evaluation of the beneficial effect of a composite liner, whether it is a true composite liner ($k_s < 10^{-6}$ m/s (10^{-4} cm/s)) or a quasi-composite liner ($k_s \geq 10^{-6}$ m/s (10^{-4} cm/s)). Figure 1 is based on good contact between the geomembrane and soil components of the composite liner.

RELATIONSHIP BETWEEN LEAKAGE AND LEACHATE GENERATION

The above discussion on the effect of the drainage material overlying the geomembrane on the rate of leakage through a hole in a geomembrane liner could lead to the belief that it is preferable to use sand rather than a more permeable material such as geonet or gravel to construct leachate collection layers. For equal heads of leachate on the geomembrane, the rate of leakage through the primary liner is indeed smaller if the leachate collection layer material is sand rather than gravel, because sand will impede the flow of leachate towards the geomembrane hole, thereby reducing the leakage rate as compared to the case where the leachate collection layer material has a higher permeability than sand. However, such a comparison is not correct because, for a constant rate of leachate generation, the larger the hydraulic conductivity of the leachate collection layer material, the smaller the leachate head on the geomembrane. Therefore, to make a fair comparison between leachate collection layer materials regarding their influence on leakage rate, it is necessary to consider a given rate of leachate generation instead of a given head of leachate on the geomembrane. The authors are currently investigating the combined influence of drainage layer permeability and leachate generation rate on leakage rates through geomembrane holes.

LIMITATIONS

The methods of evaluating rates of leakage through geomembrane holes presented above are based on theoretical analyses and a limited number of laboratory tests. These methods still need to be compared to leakage rates measured in additional laboratory tests and in actual landfills that have reliable leakage detection and collection systems. To date, only very limited data are available and interpretation is always difficult because: (i) the sizes of geomembrane defects are not known; (ii) liquid heads acting on the primary liners are not known; and (iii) many landfills have liquids in their leakage detection and collection layers from sources other than leakage through the primary liner. Therefore, in the present state of knowledge, the above methods should be used with caution and only by experienced engineers.

CONCLUSIONS

This paper has described methods for evaluating rates of leakage through landfill liners constructed with geomembranes. The methods were applied to both geomembranes alone and to composite liners comprised of a geomembrane upper component and a soil lower component. Comparisons of the results of the evaluations demonstrates the effectiveness of composite liners. Table 1 shows that leakage rates through a geomembrane hole are significantly reduced by placing

RATIO BETWEEN LEAKAGE RATES THROUGH GEOMEMBRANE ALONE AND COMPOSITE LINER

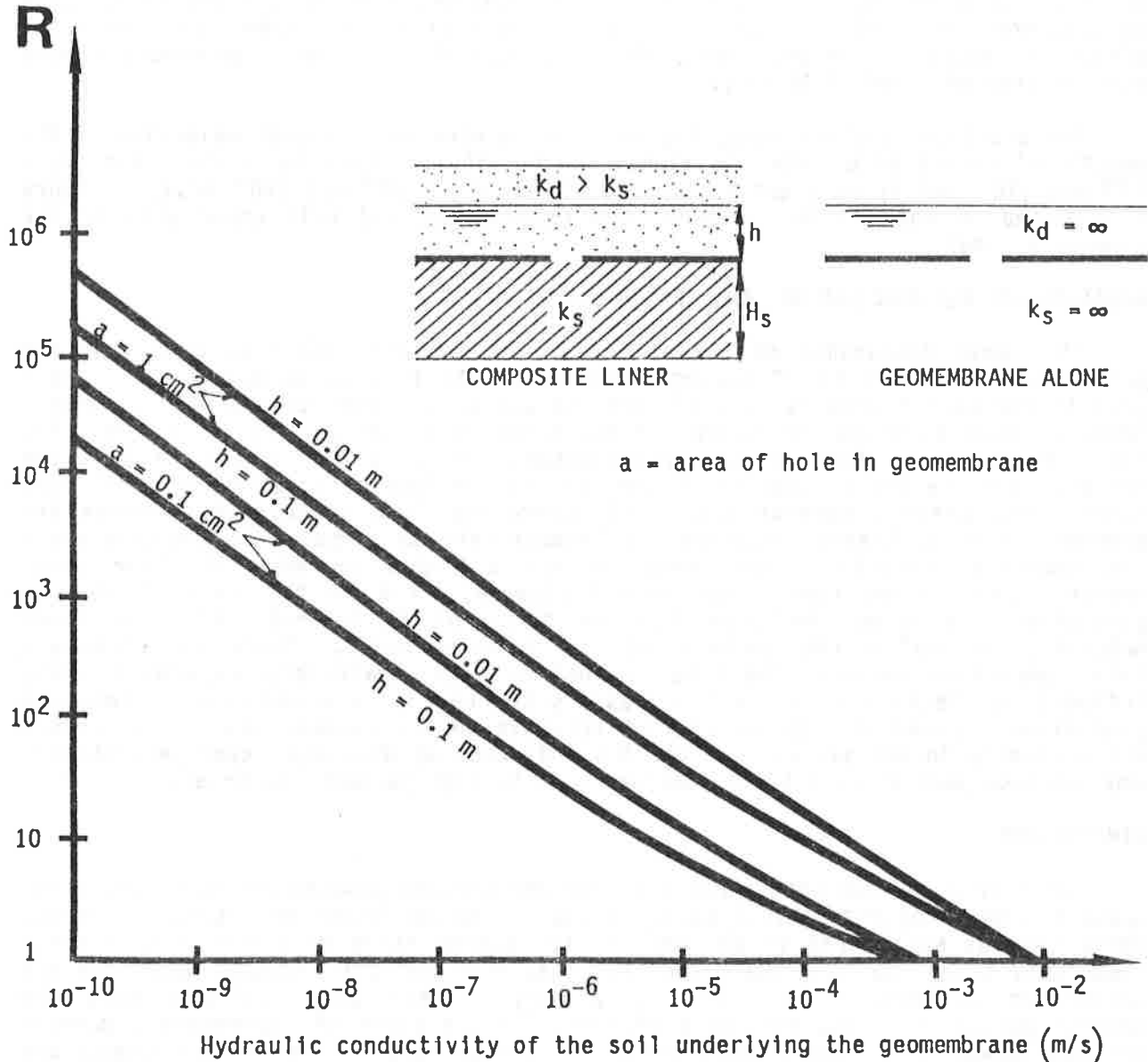


Figure 1. *Effectiveness of a Composite Liner.* This figure gives the ratio, R , between the leakage rates (due to a geomembrane hole) through a geomembrane alone and through a composite liner, as a function of the hydraulic conductivity, k_s , of the soil component of the composite liner. The portions of the curves for $k_s < 10^{-6}$ m/s (10^{-4} cm/s) were established by dividing Equation 1 by Equation 2. The portions of the curves for $k_s > 10^{-6}$ m/s were obtained by interpolation between the portions of the curves for $k_s < 10^{-6}$ m/s and the value of k_s for which free flow is expected. The curves are independent of the thickness, H_s , of the soil layer if $h < H_s$.

a layer of low-permeability soil under the geomembrane. The paper also demonstrates (Table 2) that, for a given head on top of a geomembrane, the presence of a layer of sandy or silty soil on top of or beneath the geomembrane significantly impedes the flow rate through a hole in the geomembrane.

The leakage rate evaluations have been combined into a chart (Figure 1) that can be used with Equation 1 to estimate leakage rates through geomembrane holes when the liquid head acting on top of the geomembrane is known or can be estimated. This chart can be used for practical applications in conjunction with guidelines provided by Giroud and Bonaparte (7) on the sizes and frequencies of geomembrane holes that could be encountered in the field.

REFERENCES

- (1) Brown, K.W., Thomas, J.C., Lyhon, R.L., Jayawickrama P., and Bahrt, S.C., "Quantification of Leak Rates Through Holes in Landfill Liners", USEPA Report CR 810940, Cincinnati, USA, 1987, 147 p.
- (2) Faure, Y.H., "Nappes Etanches: Debit et Forme de l'Ecoulement en Cas de Fuite", Thesis, University of Grenoble, France, Dec 1979, 263 p. (in French)
- (3) Faure, Y.H., "Design of Drain Beneath Geomembranes: Discharge Estimation and Flow Patterns in Case of Leak", Proceedings of the International Conference on Geomembranes, Vol. 2, Denver, USA, Jun 1984, pp. 463-468.
- (4) Fukuoka, M., "Outline of Large Scale Model Test on Waterproof Membrane", Unpublished Report, Japan, May 1985, 24 p.
- (5) Fukuoka, M., "Large Scale Permeability Tests for Geomembrane-Subgrade System", Proceedings of the Third International Conference on Geotextiles, Vol. 3, Vienna, Austria, Apr 1986, pp. 917-922.
- (6) Giroud, J.P., "Impermeability: The Myth and a Rational Approach", Proceedings of the International Conference on Geomembranes, Vol. 1, Denver, USA, Jun 1984, pp. 157-162.
- (7) Giroud, J.P. and Bonaparte, R., "Leakage Through Liners Constructed with Geomembranes", accepted for publication by Geotextiles and Geomembranes, 1989.
- (8) Giroud, J.P., Khatami, A., and Badu-Tweneboah, K., "Evaluation of the Rate of Leakage Through Composite Liners", (to be published), 1989.
- (9) Sherard, J.L., "The Upstream Zone in Concrete-Face Rockfill Dams", Proceedings of a Symposium on Concrete Face Rockfill Dams - Design, Construction, and Performance, Sponsored by the Geotechnical Engineering Division of the American Society of Civil Engineers, J. Barry Cooke and James L. Sherard, Eds., Detroit, USA, Oct 1985, pp. 618-641.
- (10) Stone, J.L., "Leakage Monitoring of the Geomembrane Liner for Proton Decay Experiment", Proceedings of the International Conference on Geomembranes, Vol. 2, Denver, USA, Jun 1984, pp. 475-480.
- (11) USEPA, "Background Document: Proposed Liner and Leak Detection Rule", EPA/530-SW-87-015, Prepared by GeoServices Inc., May 1987, 526 p.

P.I. MARCUS

Mekorot Water Co., Ltd., Israel

Lined Cut and Fill Reservoirs in Israel-Forty Years of Development

SUMMARY

This paper reviews the development in Israel of exposed lined, uncovered reservoirs of the cut and fill type from the early 'fifties to the present time.

Design parameters and operation and maintenance issues are presented for reservoirs ranging in capacity from 20,000 to 200,000 cu.m. and lined with reinforced shotcrete or geomembranes. The paper focuses on the major maintenance problem encountered in these reservoirs, namely the periodic cleaning of organic and inorganic deposits from their banks and bottom.

The geomembrane lined reservoirs are provided with reinforced concrete tracks to permit travel of mechanical tools on their bottom, thus facilitating the cleaning process. These tracks increase both, initial investment and maintenance expenditures, making the geomembrane lining less competitive to other lining materials.

The paper presents the conclusions of recent studies performed in Israel on the development of mechanical tools for cleaning geomembrane lined reservoirs. These studies proved that appropriate mechanical tools can travel over geomembrane linings without damage to lining or subgrade. The use of these mechanical tools makes the cleaning process safer and more efficient and avoids the necessity for reinforced concrete tracks. The conclusions of these studies are fundamental in the present policy of planning and design of exposed lined, uncovered, cut & fill reservoirs.

INTRODUCTION

This paper refers to reservoirs of the cut and fill type serving for short-time (weekly) regulation within the national and regional domestic and irrigation water supply networks in Israel.

The reservoirs range in capacity from 20,000 to 200,000 cu.m. Depth of water is from 3 to 8 m while the area of wetting in the larger reservoirs may amount to a few hectares. All the reservoirs are uncovered and, in order to reduce seepage losses to a minimum, are lined.

RESERVOIRS CONSTRUCTED IN THE 'FIFTIES & 'SIXTIES

Design Parameters

These reservoirs are of circular or rectangular shape, with an inner bank inclination of 3:1 (horizontal:vertical). The bottom has a uniform slope of about 1% towards the lowest part, where the inlet-outlet pipe is located. No drainage facilities are provided, and the only means of dewatering the reservoirs is via the inlet-outlet pipe.

The reservoirs are uncovered and concrete lined. The lining consists of 5 cm thick shotcrete reinforced with iron mesh comprising 5 mm dia. bars, 15 cm apart. The lining is without exception applied directly over the subgrade (natural ground or compacted fill). Construction joints, at intervals of about 10 m, are filled with a bituminous mastic.

Operation and Maintenance Problems

In their thirty years of existence, the reservoirs have posed no major O&M problems, apart from their cleaning. Cleaning of the reservoirs is necessary at least once a year since inorganic materials (silt and sand) together with materials of organic origin (mainly algae) deposit on banks and bottom. The deposits must be removed for both sanitary reasons (in domestic water supply networks) and to prevent clogging of sprinklers and drippers in irrigation water supply networks.

In the past two decades, certain species of fish have been introduced to consume the suspended materials depositing on the banks and bottom of reservoirs. Although successful, the "fish treatment" is not able to fully replace mechanical cleaning, and the latter must still be performed, although less frequently than in the absence of the "fish treatment".

Mechanical cleaning of a reservoir is time consuming, costly and hazardous. The reservoir is first dewatered, following which the banks are manually hosed and scrubbed. A slurry is formed, part of which flows toward the bottom and part of which is pushed down manually. The work on the slippery inclined banks is difficult, and the workers must pay great attention to their own safety.

Cleaning of the reservoir bottom is performed in a similar manner to that of the the banks, i.e. by manual hosing and scrubbing. Materials deposited on the bottom, together with the slurry obtained from cleaning of the banks, are pushed manually toward the lowest part of the reservoir. In some cases, this operation is assisted by a tractor lowered by cables along the banks; the tractor is equipped with a special "rubber bulldozer" for impelling the slurry without dammaging the concrete lining. The slurry, which accumulates in the lowest part of the reservoir, is generally evacuated by means of mud or concrete pumps. As no synchronization can be achieved between the processes of cleaning, pushing along the bottom and pumping out, cleaning of reservoir bottoms is both difficult and inefficient.

RESERVOIRS CONSTRUCTED IN THE LATE 'SEVENTIES AND EARLY 'EIGHTIES

Developments in geosynthetics have made available two-dimensional, continuous, flexible materials (geomembranes) which can compete with concrete for seepage control, and often require a considerably lower investment. Cut and fill reservoirs constructed in Israel since late 'seventies are geomembrane lined.

Design Parameters

The geomembrane lined reservoirs are generally of rectangular shape, and, with respect to earthworks, have similar design parameters to the concrete lined ones: an inner bank slope of 3:1 (see Fig. 1).

—The geomembrane, like the concrete, is applied directly over the cut or filled subgrade. Some reservoirs have a geomembrane lining laid over a 15-20 cm layer of fine granular material in order to prevent possible leakage through the lining from reaching the banks.

Some appurtenances, which do not exist in the concrete lined reservoirs, have also been introduced. These comprise:

- a drainage pipe, with its inlet at a lower level than the invert of the inlet-outlet pipe, for gravitational conveyance of the slurry resulting from the cleaning process.
- steeper bottom inclination (2%-4%) to facilitate manual pushing of the slurry during cleaning.
- a concrete canal connecting the inner toes of the banks across the reservoir bottom in order to collect the slurry and allow its mechanical pushing toward the drainage pipe inlet located midway along the canal length. Access to the canal from the service road is via concrete strips cast on gentler slopes (4.5:1) on the banks.

Operation and Maintenance Problems

Operation records of exposed geomembrane lined reservoirs within the national and regional domestic and irrigation water supply networks in Israel are relatively short, the first such reservoir having been commissioned only some seven years ago.

The main problem encountered in all these reservoirs is geomembrane failure at connections to structures (see Fig. 1, Section b-b). Almost all the failures experienced have been caused by subgrade settlement near joints between the two very different construction materials: the rigid three-dimensional concrete and the flexible two-dimensional geomembrane. In the light of this, therefore, it was concluded that when planning and designing geomembrane lined reservoirs, the contact area between rigid structures and geomembranes should be reduced to a minimum, and, where such contact cannot be avoided, sound and stable subgrade should be provided.

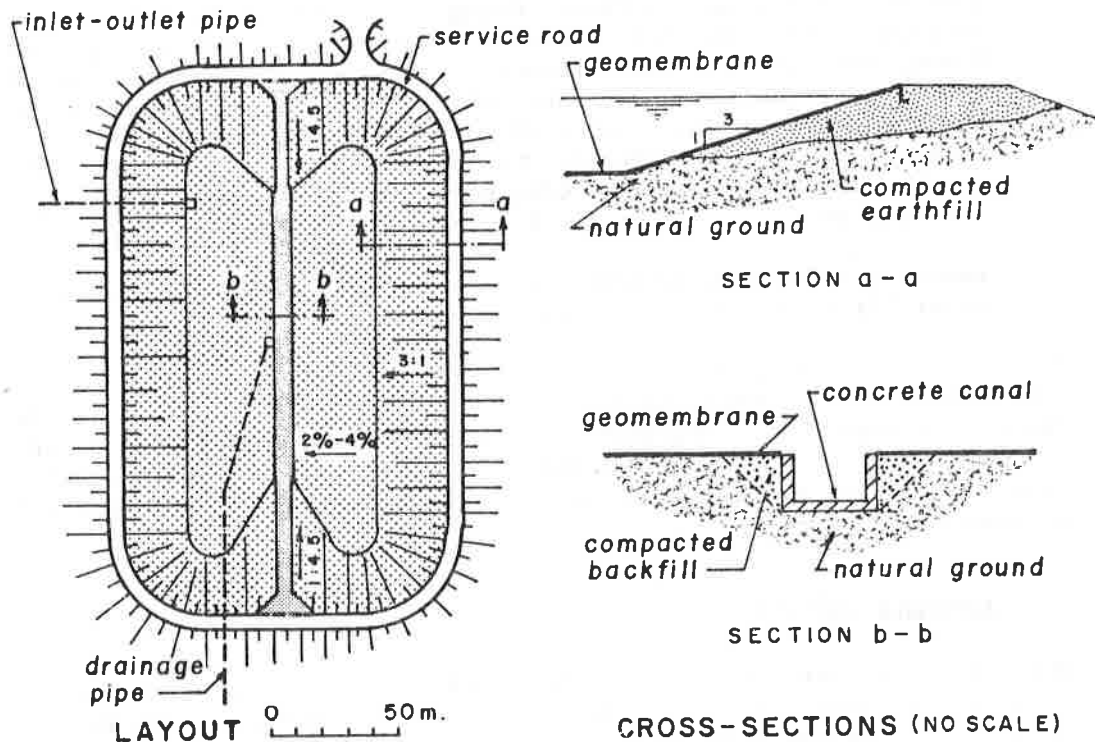


Fig. 1: Cut and fill reservoir, 100,000 cu.m capacity

**PRESENT POLICY REGARDING PLANNING OF CUT AND FILL RESERVOIRS
WITH EXPOSED LINING**

The advantages of geomembranes over concrete (low cost, short construction time) are negated by the cost of the concrete canal necessary for reservoir cleaning as well as the costs of repair at the contact areas.

No technical means for economically avoiding the need to clean the reservoirs are at present available. Efforts are therefore being directed toward improving cleaning efficiency. Studies were initiated in 1987 to try to understand the behaviour of slurry during the cleaning process and to develop mechanical tools able to perform cleaning in a more efficient and safer manner. Although these studies are still under way, certain conclusions reached to date have already had a serious impact on the planning of cut and fill reservoirs with exposed lining. These are principally as follows:

- four-wheel tractors, up to 1.5 tons in weight and with suitable tires having an air pressure of about 3-4 p.s.i., can move over geomembrane linings without damaging either the linings or the subgrade. The tractors encounter no problems when moving over clean, wet or dry geomembrane, or geomembrane lining covered with dry deposits. They are stable in their movement on the reservoir bottom and banks (3:1 slope) in any direction: along contour lines, perpendicular to contour lines or obliquely. The tractors can develop a working power of 35% of their own weight - estimated to be sufficient for the cleaning process.
- reservoirs lined by geomembranes do not in fact need a concrete canal for cleaning or any other purpose.

Present policy in planning cut and fill reservoirs is therefore to continue to use geomembranes for lining, wherever possible. The reservoirs would be constructed without the concrete canal and appurtenances, making the geomembrane lining more competitive with other materials from the point of view of both initial investment and maintenance costs.

ACKNOWLEDGEMENTS

The author wishes to express his gratitude to S. Kantor, Chief Engineer of Mekorot Water Co. Ltd., for his constant encouragement of efforts to improve the efficiency of reservoir cleaning, and for granting permission to publish this work. Appreciation is also extended to E. Zehavi, Consulting Engineer, for his work in developing mechanical tools for efficient cleaning of reservoirs.

J.P. GIROUD

J.F. BEECH

GeoServices Inc., Consulting Engineers, U.S.A.

Stability Of Soil Layers On Geosynthetic Lining Systems

ABSTRACT

Geosynthetic lining systems comprised of several layers of geomembranes, geonets, and geotextiles are commonly used in waste disposal facilities. Geosynthetics are sensitive to shocks and/or ultraviolet light. Consequently, geosynthetic lining systems are usually covered with a soil layer. Interface friction angles between adjacent geosynthetics or between soil and geosynthetic can be low, thereby creating a potential slip surface which may cause instability of the soil layer. This paper presents a method to evaluate the stability of soil layers overlying geosynthetic lining systems on slopes. The method is illustrated with a design example.

INTRODUCTION

Background

Lining systems, including geosynthetics, are used to line municipal waste landfills, hazardous waste landfills, and liquid containment facilities. This paper is restricted to landfills, which essentially contain solid material.

Two lining systems are typically used in landfills for leachate control, as shown in Figure 1:

- *Containment Lining System.* The containment lining system is used to line the ground and the dikes, in order to prevent infiltration of leachate into the ground.
- *Cap Lining System.* The cap lining system is used to cover the waste at closure of the landfill, in order to prevent precipitation from entering the waste, thereby minimizing the long-term generation of leachate.

Stability is primarily an issue on the steeper portions of the containment and cap lining systems where the slopes often range between 4H:1V (14°) and 2.5H:1V (22°). Geosynthetics routinely incorporated in lining systems include: geomembrane liners, geonet drainage layers, and geotextile filters. Typical cross-sections of lining systems on slopes are shown in Figure 2. The lining systems illustrated in Figure 2 are covered with a soil layer because geosynthetics are sensitive to shocks and/or ultraviolet light. Interface friction angles between geosynthetics or between soils

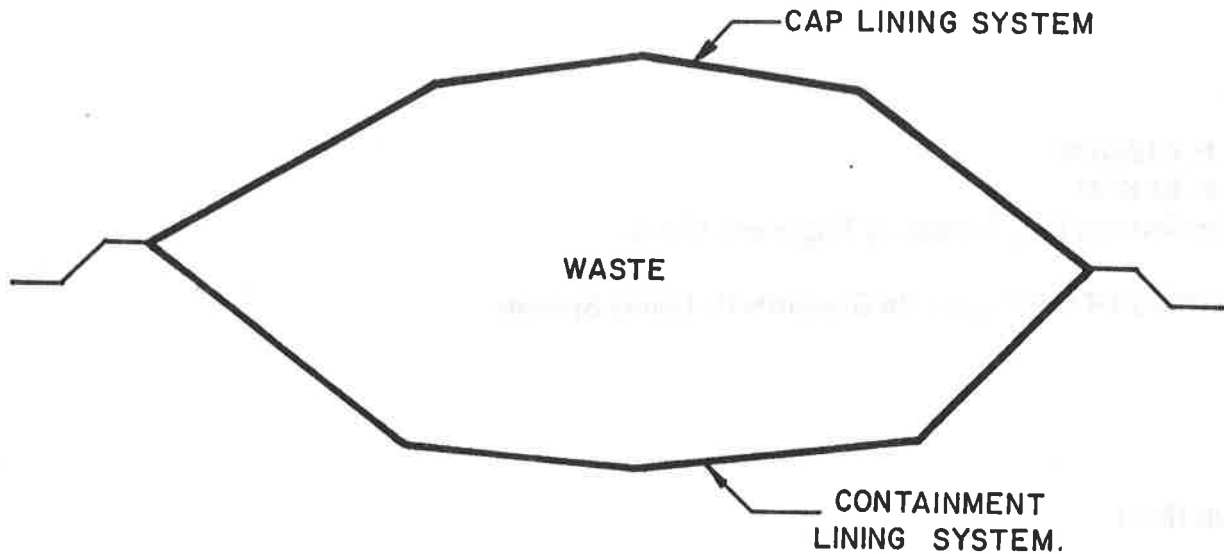


Figure 1. *Schematic Cross Section of a Landfill.*

and geosynthetics typically range from 10° to 25° . Some of these friction angles are smaller than the slope angles mentioned above. Slip planes can develop along interfaces with a friction angle less than the slope angle. The presence of a slip plane can cause instability of the lining system. Therefore, in landfill design, it is necessary to carefully address the stability of soil layers overlying geosynthetic lining systems.

Slope Stability Concept

A simplistic approach is to consider the slope to be infinite. In this case, the soil cover is stable if the following condition is met:

$$\beta \leq \phi_i \quad (\text{Equation 1})$$

where: β = slope angle; and ϕ_i = minimum interface friction angle.

For example, consider the cross-section shown in Figure 2b, with the following typical interface friction angles between each layer: (i) soil cover - geotextile interface, $\phi_i = 32^\circ$; (ii) geotextile filter - geonet drainage layer interface, $\phi_i = 28^\circ$; (iii) geonet drainage layer - geomembrane liner interface, $\phi_i = 16^\circ$; and (iv) geomembrane liner - subgrade interface, $\phi_i = 21^\circ$.

With the infinite slope assumption, the soil cover, the geotextile, and the geonet would slide as a block along the geonet-geomembrane interface if the slope angle is greater than 16° . In reality, slopes are not infinite and the above lining system could be stable on a slope steeper than 16° . Two reasons for a finite slope to be more stable than an infinite slope are:

- **Geosynthetic anchorage at the crest.** The geosynthetics that comprise the lining system are anchored at the crest of the slope. As slippage along the critical geosynthetic interface occurs, tensile forces are generated in the geosynthetics above the critical interface. These tensile forces contribute to the stability of the potential sliding block.

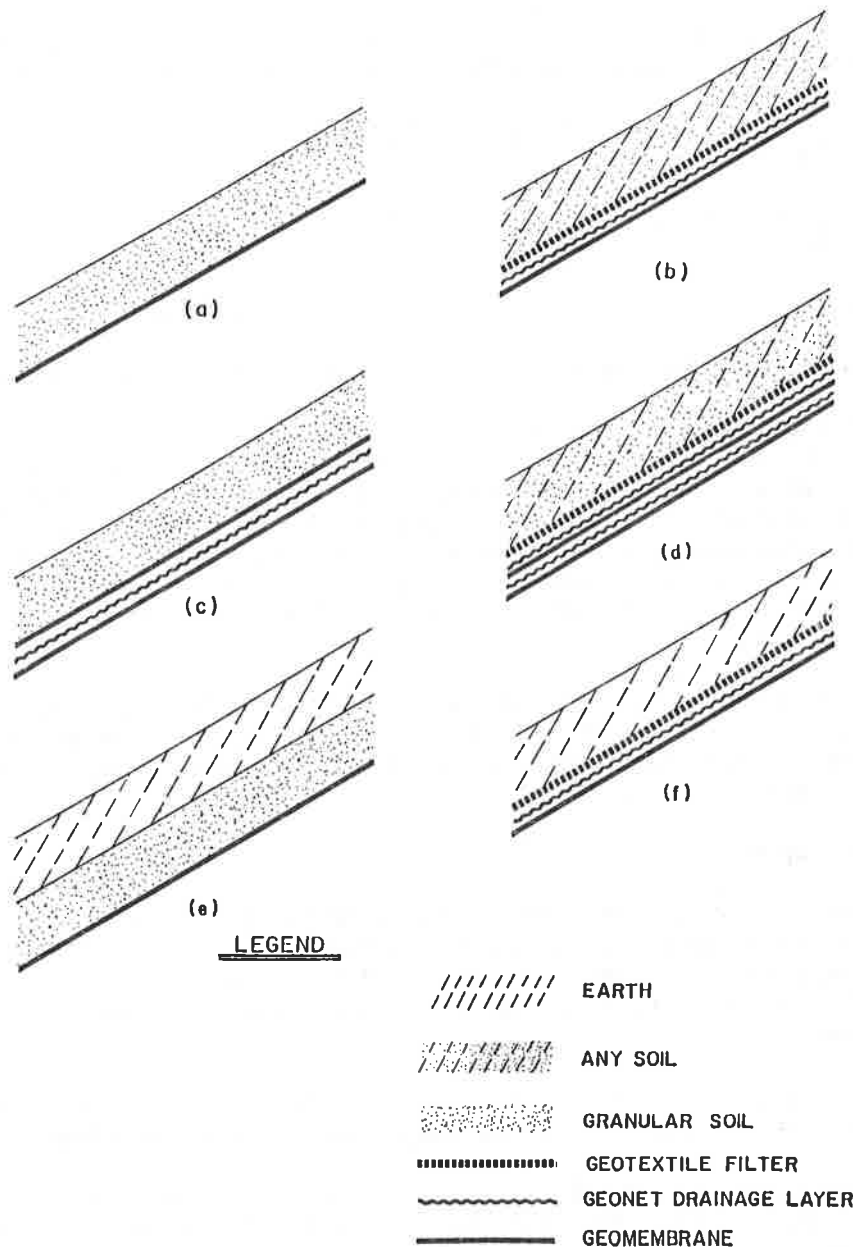


Figure 2. Examples of Lining Systems: (a) containment single liner with a granular layer used as a leachate collection layer and protective soil cover; (b) containment single liner with a geonet leachate collection layer, a geotextile filler and a protective soil cover; (c) containment double liner with a geonet leakage collection layer and protective soil cover; (d) containment double liner with a geonet leakage collection layer, a geonet leachate collection layer, a geotextile filler, and a protective soil cover; (e) cap single liner with a layer of topsoil to grow vegetation and a granular drainage layer; and (f) cap single liner with a layer of topsoil to grow vegetation, a geotextile filler, and a geonet drainage layer.

- *Soil buttress at the toe.* The soil cover, at its toe, rests on a firm foundation. As slippage along the critical interface occurs, downward movement of the soil cover is buttressed by the firm foundation. This "toe buttressing effect" contributes to the stability of the soil layer.

The three factors contributing to the lining's stability are schematically shown in Figure 3 and act as follows:

- the geosynthetic tension, α , resulting from *crest anchorage*, acts at the top of the slope, at point A;
- the *shear resistance developed along the interface*, S_i , acts along AB; and
- the *toe buttressing effect*, S_s , results from the soil strength along BC.

Geosynthetics used in lining systems (geomembranes, geonets, and geotextiles) usually have a low modulus and, therefore, they cannot provide any significant tension, α , at an acceptable strain (such as 2 percent). Consequently, tension in the lining system geosynthetics will be neglected in this study. However, significant tension can be provided if one or more layers of geosynthetic reinforcement are placed in the soil cover. Geogrids are typically used in this application (Figure 4). In order to be effective, the geogrid reinforcement must be firmly anchored at the crest of the slope (Figure 5).

The contribution of the soil shear strength to the stability ("toe buttressing effect") is quite significant. Typically, a soil cover can be stable on a slope several degrees steeper than the minimum interface friction angle because of the toe buttressing effect.

Scope of this Paper

The purpose of this paper is to present a method to evaluate the stability of soil layers resting on a geosynthetic lining system on a slope. The method takes into account geosynthetic tension, interface friction resistance, and toe buttressing effect. It is important to note that pore water pressures are not considered in the method. Therefore:

- The method presented in this paper is not applicable to liquid containment facilities, especially those subjected to rapid drawdown.
- In the case of waste disposal facilities, for which the method is intended, it is assumed that the soil cover is perfectly drained. The soil cover would become unstable if the soil is not permeable enough, or if the drainage layer located between the soil cover and the geomembrane does not have enough transmissivity, to prevent pore pressure buildup in or under the soil cover.

Also, the method presented in this paper does not consider erosion problems.

LINING SYSTEM STABILITY ANALYSIS

Limitations and Assumptions

The method presented in this section is valid only if the soil layer overlying the geosynthetic lining system:

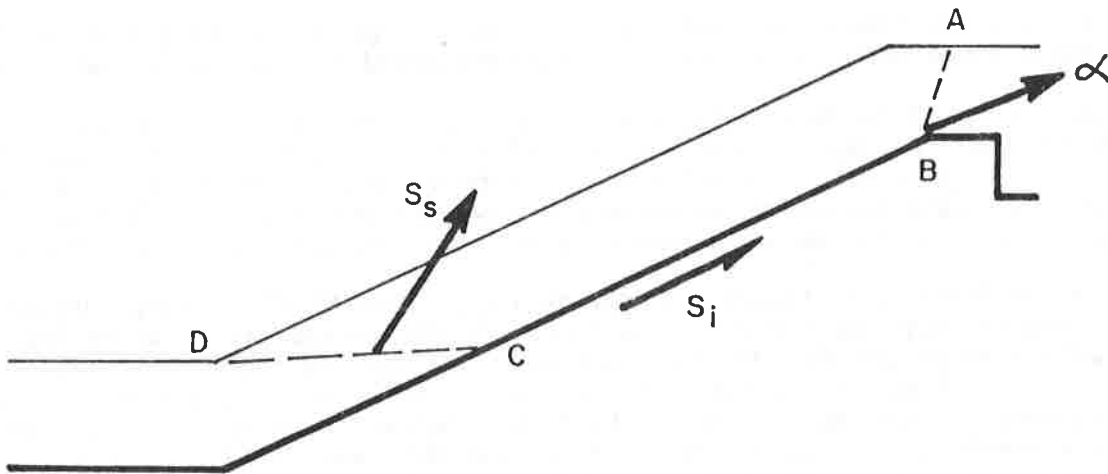


Figure 3. *Potential Slip Surface.* The forces contributing to the stability are schematically represented as follows: α = tension in the geosynthetics located above the slip surface; S_i = shear force along the minimum friction interface; and S_s = soil shear strength.

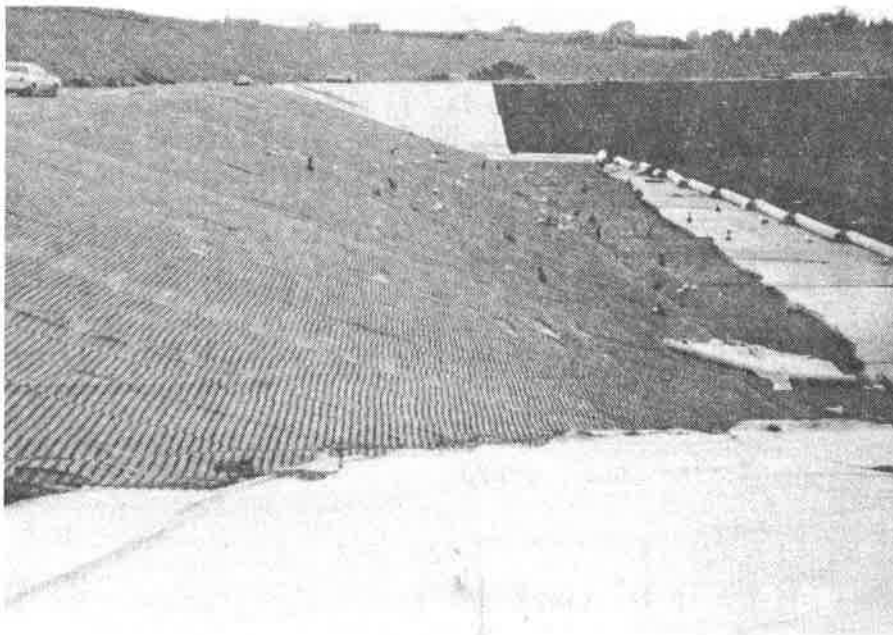


Figure 4. *Geogrid Reinforcement for a Soil Cover.* In this project, only one layer of geogrid reinforcement was used. It was placed right on top of the geotextile filter.

- has a uniform thickness; and
- is comprised of a cohesionless soil.

The latter assumption corresponds to: (i) granular soils; and (ii) fine-grained soils in the drained state, which is typically considered for long-term stability.

Two cases can be considered: (i) the case of a partial soil cover, i.e., a cover at a certain stage during its construction (Figure 6a); and (ii) the case of a complete cover (Figure 6b). The relevant parameters are defined in Figure 6. The slip surface for these two cases are assumed to have the geometry shown in Figures 6a 6b, respectively. The following comments can be made regarding the slip surface:

- In the first case (Figure 6a), the entire portion AB of the slip surface is along the minimum friction interface. In the second case (Figure 6b), we will also assume that the friction angle is equal to the minimum friction interface from A through B. This is conservative because the friction angle is greater than the minimum friction angle between A and A'. In most cases, the length AA' is small compared to AB and the approximation is good. As a result of this assumption, the same equations will be applicable to the partial and the complete soil cover.
- The portion BC of the slip surface has been arbitrarily chosen to be horizontal, and a parametric study not presented here has shown that this assumption is acceptable for cohesionless soils or drained cohesive soils.

As a result of the above assumptions, the problem reduces itself to the analysis of the stability of the wedge ABC shown in Figure 7a.

Method of Analysis

The classical two-part wedge analysis is used. This consists of assuming that the entire sliding wedge, ABCD, shown in Figure 7a, is comprised of two parts: ABB'D and BCB'. The separation between the two parts, BB', is assumed to be vertical, and P is the force transmitted across the separation between the two parts. The force P is assumed to be parallel to the slope.

The polygons of forces per unit widths are shown in Figure 7b. Polygon 1 is related to part 1 of the wedge (BCB') and polygon 2 to part 2 (ABB'D). In order to trace the polygons, it is necessary to determine the weights per unit width, W_1^* and W_2^* , of the two parts of the wedge, which can be done using the following equations (Figure 7c):

$$W_1^* = \frac{\gamma_c T_c^2}{2 \sin \beta \cos \beta} = \frac{\gamma_c T_c^2}{\sin 2\beta} \quad (\text{Equation 2})$$

$$W_2^* = \frac{\gamma_c T_c}{\sin \beta} \left[H - \frac{T_c}{2 \cos \beta} \right] = \frac{\gamma_c T_c^2}{\sin 2\beta} \left[\frac{2H \cos \beta}{T_c} - 1 \right] \quad (\text{Equation 3})$$

where: γ_c = unit weight of the soil; T_c = thickness of the soil cover; H = height of the slope; and β = slope angle. Basic SI units are W_1^* (kN/m), W_2^* (kN/m), γ_c (kN/m³), T_c (m), H (m), and β (degrees); β is dimensionless.

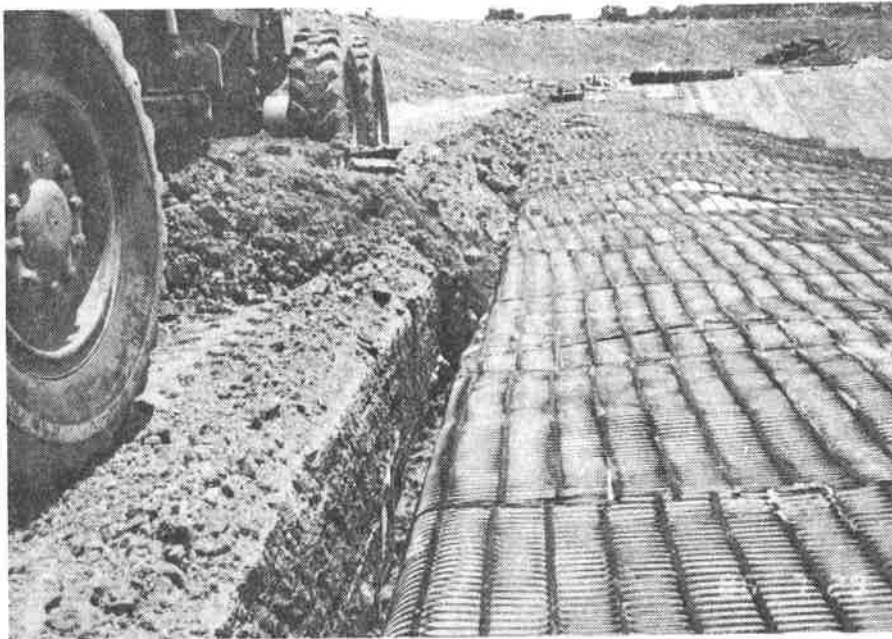


Figure 5. *Anchorage of the Geogrid.* In this project, the geogrid was placed in the same anchor trench as the lining system.

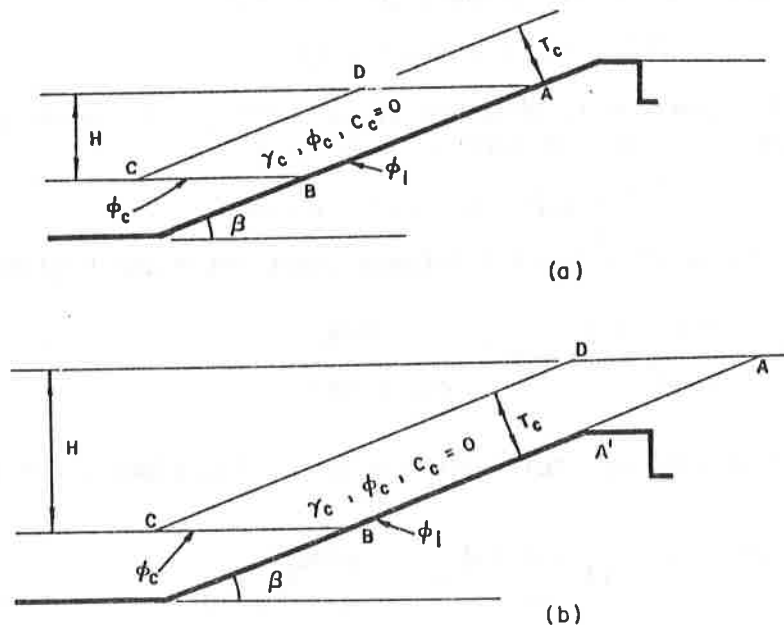


Figure 6. *Geometry of the Soil Cover for the Simplified Method:* (a) partial soil cover; and (b) complete soil cover. The relevant parameters are: H = height of the slope; β = slope angle; T_c = soil cover thickness; γ_c = unit weight of soil; ϕ_c = friction angle of soil; ϕ_i = minimum interface friction angle in the lining system. The cohesion of the soil is assumed to be zero ($c_c = 0$).

Polygon 1 is traced first. When polygon 2 is traced, it appears that the required geosynthetic tension, α , is either positive (as shown in Figure 7b), or negative. Therefore, two cases must be considered:

- If the required geosynthetic tension, α , is positive, one or more geosynthetic reinforcement layers are required to carry this tension, because, as indicated previously, the geosynthetics used in lining systems are usually unable to withstand significant tensions.
- If the required geosynthetic tension, α , is negative, the soil cover is stable without any reinforcement.

Equations

The proposed method can be used graphically as explained above or can be expressed analytically as indicated below.

The magnitudes of the friction forces per unit width F_1^* and F_2^* are not known, but their directions are known (Figure 7). Therefore, F_1^* and F_2^* can be eliminated by projections perpendicular to their directions.

The following equation is obtained by projecting the forces per unit width of polygon 1 in Figure 7 on a line perpendicular to F_1^* :

$$W_1^* \sin \phi_c = P \cos(\beta + \phi_c) \quad (\text{Equation 4})$$

The following equation is obtained by projecting the forces per unit width of polygon 2 in Figure 7 on a line perpendicular to F_2^* :

$$W_2^* \sin(\beta - \phi_i) = (P + \alpha) \cos \phi_i \quad (\text{Equation 5})$$

Eliminating the unknown force P between Equations 4 and 5 gives:

$$\alpha = W_2^* \frac{\sin(\beta - \phi_i)}{\cos \phi_i} - W_1^* \frac{\sin \phi_c}{\cos(\beta + \phi_c)} \quad (\text{Equation 6})$$

Replacing W_1^* and W_2^* by their values given by Equations 2 and 3 results in:

$$\alpha = \frac{\gamma_c T_c^2}{\sin 2\beta} \left[\left(\frac{2H \cos \beta}{T_c} - 1 \right) \frac{\sin(\beta - \phi_i)}{\cos \phi_i} - \frac{\sin \phi_c}{\cos(\beta + \phi_c)} \right] \quad (\text{Equation 7})$$

This equation shows that there is no need for geosynthetic reinforcement (i.e., $\alpha = 0$) if:

$$H \leq H_{\max} \quad (\text{Equation 8})$$

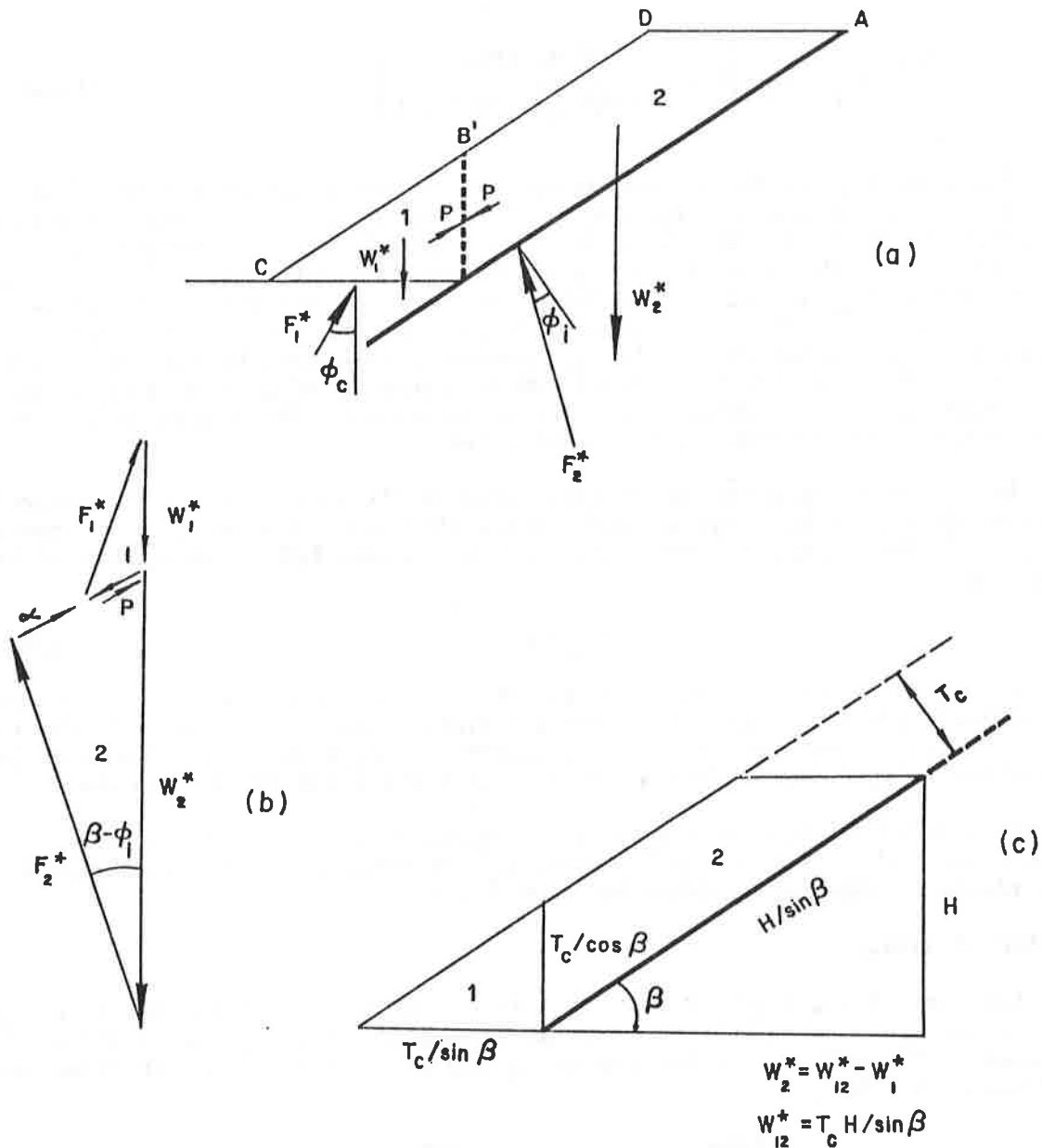


Figure 7. *Simplified Method:* (a) two-part wedge; (b) force-per-unit-width polygons; and (c) weight calculations. The forces per unit width are as follows: W_1^* = weight of part 1 per unit width perpendicular to the plane of the figure; W_2^* = weight of part 2 per unit width perpendicular to the plane of the figure; P = force per unit width transmitted between the two wedges; F_1^* = force per unit width due to soil friction; F_2^* = force per unit width due to interface friction within the geosynthetic lining system or between the lining system and the soil; and α = tension in the geosynthetics located above the slip surface, including geosynthetic reinforcement layers, if any. Note: The simplified method is valid only in the case of a soil cover with a uniform thickness, constructed with a cohesionless material.

where H_{\max} is given by:

$$\frac{H_{\max}}{T_c} = \frac{1}{2 \cos \beta} \left(1 + \frac{\sin \phi_c \cos \phi_i}{\cos(\beta + \phi_c) \sin(\beta - \phi_i)} \right) \quad (\text{Equation 9})$$

Equation 9 gives the maximum height for a soil cover with a given thickness on a given slope, without reinforcement. Equation 9 can be used only if the interface friction angle, ϕ_i , is less than the slope angle β . If ϕ_i is greater than β , H_{\max} is infinite, i.e., the slope is stable regardless of its height. If the height of the slope exceeds H_{\max} , the soil cover can be reinforced by a geogrid anchored at the crest of the slope. The tension that must be provided by the reinforcement is given in Equation 7. The selected geogrid must provide the required tension at a small strain, typically 2%. A greater strain would cause unacceptable elongation of the geosynthetics located above the critical interface. Therefore, only high modulus geosynthetics can be used in this application.

An alternate solution can be considered in the case of waste containment lining systems (i.e., in the case of soil covers that will be eventually in contact with waste). In this case, the soil cover can be constructed in increments of height H_i given by:

$$H_i = H_{\max} - s \quad (\text{Equation 10})$$

where: H_{\max} = maximum height of an unreinforced soil cover in the considered conditions, given by Equation 9; and s = minimum step between top of soil cover and waste level to ensure that the lining system is always protected from waste placement operations (Figure 8). (Typical values for s are 0.5 m (20 in.) or more.)

This solution is viable only if the waste is properly placed and compacted to ensure the stability of the soil cover, and the temporarily exposed geosynthetics are not adversely impacted by exposure to sunlight.

Factor of Safety

Equations 6 and 9 do not include a factor of safety. A factor of safety can be determined by using mobilized friction angles, ϕ_{cm} and ϕ_{im} , in Equations 6 and 9, instead of the actual friction angles, ϕ_c and ϕ_i . The mobilized friction angles are defined as follows:

$$\tan \phi_{cm} = \frac{\tan \phi_c}{FS} \quad \text{and} \quad \tan \phi_{im} = \frac{\tan \phi_i}{FS} \quad (\text{Equation 11})$$

where: FS = factor of safety.

DESIGN EXAMPLE

A geosynthetic lining system is comprised from top to bottom of: (i) a protective soil cover; (ii) a geotextile filter; (iii) a geonet drainage layer; and (iv) a geomembrane (Figure 2b). The minimum interface friction angle, $\phi_i = 16^\circ$, is between

the geonet and the geomembrane. The slope is 9 m (30 ft) high and the slope angle is defined by: $\tan\beta = 0.4 = 1V:2.5H$ (i.e., $\beta = 21.8^\circ$). The material available for constructing the soil cover is a sand with a friction angle of 30° and a unit weight, $\gamma_c = 19.5 \text{ kN/m}^3$ (124.5 pcf). Thicknesses of 0.3 m (1 ft) and 0.45 m (1.5 ft) are considered. Is it necessary to reinforce this soil cover? What is the influence of soil cover thickness on stability?

First, the maximum height of the soil cover without reinforcement can be determined using Equation 9 as follows:

$$\frac{H_{\max}}{T_c} = \frac{1}{2 \cos 21.8^\circ} \left[1 + \frac{\sin 30^\circ \cos 16^\circ}{\cos (21.8^\circ + 30^\circ) \sin (21.8^\circ - 16^\circ)} \right]$$

$$H_{\max} = 4.68 T_c$$

$$\text{Hence: } H_{\max} = 2.11 \text{ m (84 in.) if } T_c = 0.45 \text{ m (18 in.)}$$

$$H_{\max} = 1.4 \text{ m (56 in.) if } T_c = 0.30 \text{ m (12 in.)}$$

Both values of H_{\max} are less than 9 m (30 ft). Therefore, either the soil cover is constructed in increments alternating with waste placement (as shown in Figure 8), or the soil cover is reinforced (as shown in Figure 4).

If the soil cover is constructed in increments, a soil cover thickness of 0.45 m (18 in.) will be preferred to a thickness of 0.3 m (12 in.). The latter would lead to very small increments, as shown above, which would be impractical. (The fact that a thicker soil cover is more stable is not surprising; the stability of a very thick soil cover would be essentially governed by toe buttressing and the influence of the interface shear resistance would be negligible.)

If the soil cover is reinforced, the required tension to be provided by the reinforcement geosynthetic can be determined using Equation 8 as follows, for a soil cover thickness of 0.45 m (18 in.):

$$\alpha = \frac{19.5 \times 0.45^2}{\sin 43.6^\circ} \left[\left(\frac{(2 \times 9 \times \cos 21.8^\circ)}{0.45} - 1 \right) \frac{\sin (21.8^\circ - 16^\circ)}{\cos 16^\circ} - \frac{\sin 30^\circ}{\cos (21.8^\circ + 30^\circ)} \right]$$

$$\alpha = 17.1 \text{ kN/m}^2 \text{ (1164 lb/ft)}$$

Similar calculations for a soil cover thickness of 0.3 m (12 in.) give:

$$\alpha = 12.6 \text{ kN/m}^2 \text{ (864 lb/ft)}$$

If reinforcement is provided by a typical high-modulus geogrid capable of providing a tension of 13 kN/m (891 lb/ft) at a 2% strain, it appears that two layers are required if the soil cover thickness is 0.45 m (18 in.) while only one layer is sufficient if the soil thickness is 0.3 m (12 in.). Therefore, if the soil reinforcement option is selected, a 0.3 m (12 in.) thickness will be preferred to a 0.45 m (18 in.) thickness.

It should be noted that, if the geosynthetic reinforcement exhibits a strain of, say, 1%, the two geosynthetic components of the lining system located above the slip surface, i.e., the geotextile and the geonet, will also exhibit a 1% strain. Their tension will contribute to the stability of the soil cover, however by a negligible amount. If reinforcement is used in a cohesionless soil layer, then it is necessary to verify that the stresses normal to the reinforcement are large enough to ensure shear stress transfer between the soil and the reinforcement.

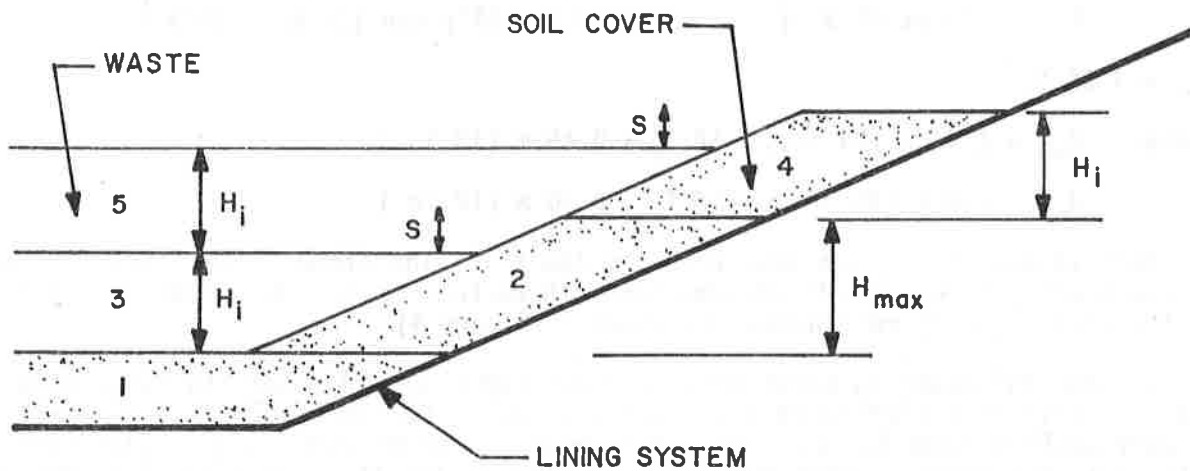


Figure 8. *Incremental Construction of the Soil Cover.* Placement stages are numbered sequentially from 1 through 5. Cover placement stages (2, 4, etc.) alternate with waste placement stages (3, 5, etc.). The maximum increment height, H_{max} , beyond which the soil cover becomes unstable, is used only for the first soil cover increment. Subsequent soil cover or waste increments are equal to $H_i = H_{max} - s$. The resulting steps s between soil cover and waste ensures that the lining system is always protected from waste placement operations.

SUMMARY

Placement of a protective soil cover over a geosynthetic lining system can lead to instability. To deal with this potential problem, a lining system stability method which accounts for geosynthetic anchorage, interface sliding resistance and buttressing at the toe of the slope was presented. The method can be used to determine the maximum height to which an unreinforced protective soil cover can be placed. If the design slope height is greater than the maximum slope, then it is necessary to anchor the protective soil cover with geosynthetic reinforcement or place the soil cover incrementally. The presented method can be used to calculate the required reinforcement tension or the increment height. It was demonstrated using an example, that a thin protective soil cover is preferred when reinforcing the protective cover, while a thick protective cover is preferred for incremental placement.

SESSION 2A
QUALITY ASSURANCE & SPECIFICATIONS



T.N. DOBRAS

D.G. YACKO

Harza Environmental Services, Inc., U.S.A.

Stringent Construction Specifications and Quality Control Assure Maximum Liner Performance

SUMMARY

In 1987 Peoria Disposal Company (PDC) of Peoria, Illinois, received the first RCRA Part B Permit awarded in Illinois, and only the fifth nationwide for the construction and operation of a new hazardous waste landfill. The relatively early acceptance of the design by both the United States and Illinois Environmental Protection Agencies is a true testimony to the philosophies of both PDC and their permitting, design and construction consultant, Harza Environmental Services, Inc. of Chicago, Illinois, to meet or exceed the EPA's Minimum Technological Requirements. The design of the 42 acre landfill addition included extensive use of high density polyethylene (HDPE) liners, and other geosynthetic materials such as drain net and filter fabric. Construction of Trench C-1, the first of 5 eight-acre landfill cells, began in June 1987 and was fully operational in the summer of 1988. This paper attempts to put into perspective the reasons why strict construction specifications and quality control/quality assurance programs are absolutely essential in assuring landfill liner integrity. The old adage "if anything can go wrong, it will" is certainly true in liner construction.

DESCRIPTION OF LINER SYSTEM

Trench C-1 is the first PDC landfill cell constructed under the tough new RCRA guidelines. It measures approximately 830' x 365' with a vertical height ranging from 20' to 50'. Interior side slopes are 3H:1V, and the bottom of the landfill is sloped between 3% and 5% towards the leachate collection manholes. The bottom composite liner consists of 3 feet of compacted clay having a coefficient of permeability of 1×10^{-7} cm/sec and 80 mil HDPE liner placed on top of the clay. HDPE drain net is used above the bottom liner for leak collection. The 80 mil HDPE primary liner directly overlies the secondary drain net. The primary leachate collection system consists of an additional HDPE drain net layer covered by 100 mil non-woven polypropylene geotextile on the sideslopes, with a 50 mil HDPE temporary protective cover added for UV protection and runoff control. The primary leachate collection system on the trench bottom consists of 12" of granular drain material having a transmissivity of approximately 1×10^{-1} cm/sec, overlain by a protective 6" layer of finer granular material. Figure 1 illustrates the liner/leachate collection systems on the slope and bottom of the landfill.

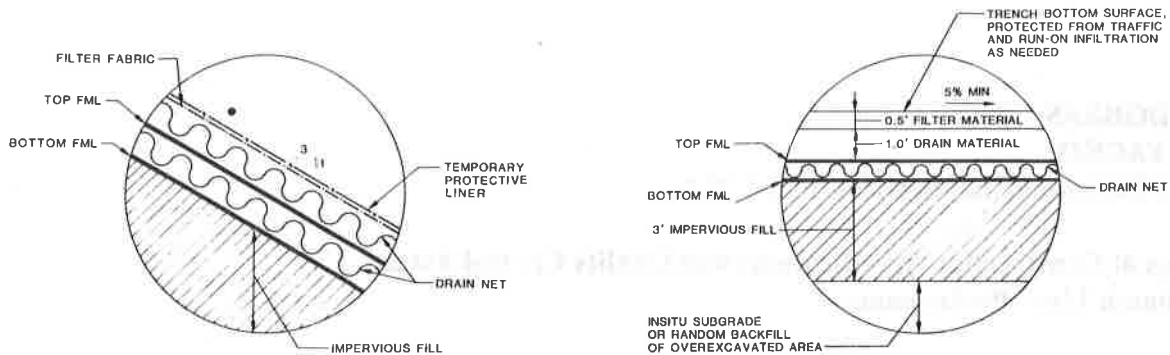


Figure 1. Liner and leachate collection on the landfill slope (left) and bottom (right).

An array of five 4" diameter slotted HDPE collection pipes in both the secondary and primary leachate collection systems transport the leachate to the respective secondary and primary concrete sump manholes. The center three sets of pipes are connected to concrete cleanout manholes at the upstream end of the landfill.

All concrete manholes have a four foot inner diameter, and are lined outside with 80 mil HDPE. The two leachate collection manholes are lined with HDPE both on the interior and exterior walls.

The secondary leachate collection system is totally enclosed by a welded seal between the primary and secondary liners at the anchor trench. Figure 2 shows the landfill near the end of secondary liner installation.

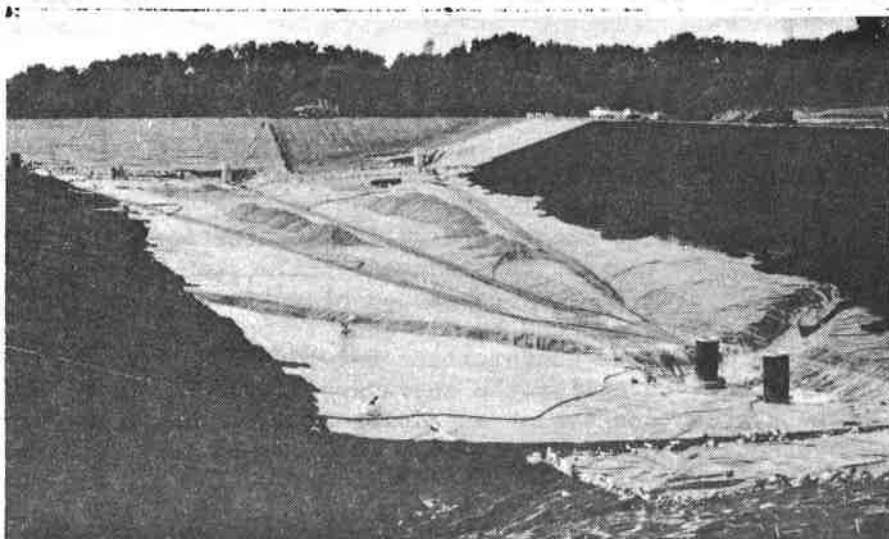


Figure 2. Construction of the secondary liner and leak collection/detection system.

WHAT IS UNIQUE ABOUT THIS LINER DESIGN?

Totally Enclosed Secondary Collection System

One of the unique features of this landfill design is the total encapsulation of the entire secondary leachate collection system. This required welding the primary and secondary liners together in the anchor trench, making it impossible for any water to enter the secondary leak collection/detection system except via leaks in the primary liner. Without this seal there is a very real possibility for rainwater to enter the system through saturation of insufficiently compacted anchor trench backfill. This concept of closing-off the secondary system sounds simple enough, but unless comprehensive pre-construction plans and schedules are developed, significant delays and problems will likely result.

Material Testing Program

Material property and testing requirements assured that we would be receiving only top quality materials, with test results generated both in-house by the Manufacturer and independently documenting 100% compliance with our specified design requirements.

EPT 90/90 Compatibility Test. Every synthetic material used on the project, including the 80 mil HDPE liner, the HDPE drain net, the polypropylene geotextile and the HDPE collection pipes, underwent EPT 90/90 (120 day) compatibility testing performed by an independent laboratory using PDC's leachate. The results of the testing were analyzed by Harza, and all the materials selected were found to be compatible with PDC's waste.

Fingerprint and Property Testing of Shipped Liner. Samples from every one of the 40 rolls of liner shipped to the site were sent to an independent laboratory for "fingerprint testing" of liner properties. A total of 9 property tests were performed, including thickness, density, tensile strengths at yield and break, elongations at yield and break, puncture resistance, tear resistance and carbon content. Each property had a specific allowable range of values permitted in the technical specification portion of PDC's RCRA Permit.

Transmissivity Testing of Drain Net. A key component of the overall design was the hydraulic transmissivity of the drain net. Through a series of detailed calculations based on a 25₂ year, 24-hour storm, the design requirements dictated a transmissivity of 0.0006 m²/sec under a normal load of 10,000 psf with the drain net sandwiched between the specified liner and filter fabric. The detrimental effect of material creep on long-term transmissivity was recognized, and we therefore required the specified minimum transmissivity be maintained after 60 days of continuous testing.

A few manufacturers had trouble complying with this requirement. Although the transmissivity would exceed the specified requirements initially, ultimately material creep and the resulting reduction in material thickness caused the transmissivity to decrease to a level less than the minimum requirement.

Liner Installation Quality Control Criteria

Weld Strength. The most important criteria for ensuring the integrity of a liner seam is the strength in peel and shear, provided film tear bond (FTB) is the failure made during the test. Visual criteria alone are insufficient to properly evaluate weld integrity because they do not necessarily demonstrate alterations caused by the heat of welding to the liner material adjacent to seams. Therefore, a minimum allowable strength value in both peel and shear was established to provide a quantitative evaluation of both the seams and the seaming operation. The strength requirement was established in accordance with NSF Standard 54, which shows, although inconsistently, a minimum allowable HDPE yield strength between 1750 psi and 1800 psi depending on liner thickness. The more conservative, 1800 psi value was selected as the governing criteria. We believe that this value acknowledges that there will be a certain reduction in liner strength at seam locations due to sheet crystallization or the effects of imperfect field conditions, since the actual yield strength of HDPE sheet generally ranges from 2500 to 3000 psi, numbers which were verified by our own field and laboratory testing. The 1800 psi value therefore, allows for a strength reduction of at least 28%.

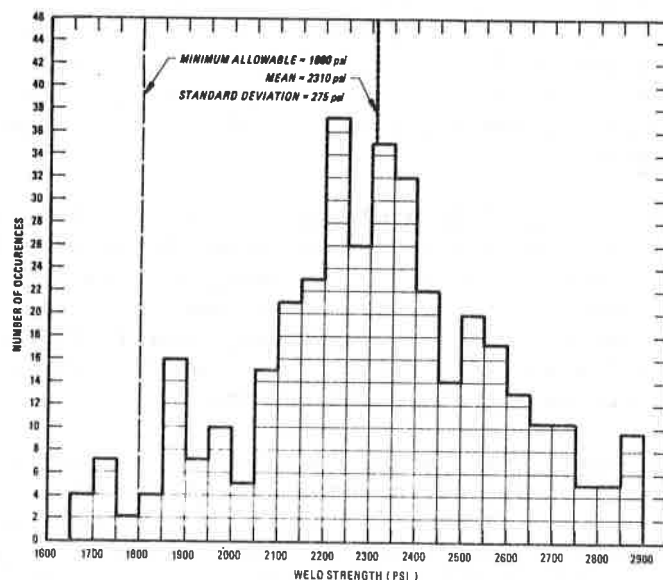


Figure 3. Weld strength histogram (Aug. 1987 - Feb. 1988).

One question has been raised as to whether the peel test itself is causing the sheet to behave in a different manner than an unwelded liner specimen undergoing a tensile test because of possible applied bending moments. It is questionable whether this is true and at the time of this writing the authors know of no quantitative measure of this effect. Many weld samples tested during Trench C-1 construction resulted in peel strengths very close to the measured liner yield strength. In fact, we attribute most of the lower strength values to poor workmanship, environmental conditions, and faulty or poorly adjusted equipment.

Much has been learned during the 9 months of continuous construction through all types of environmental conditions (ambient temperatures during construction ranged from 100° to -10°F) including the fact that the welding process is subject to a wide variability. The histogram in Figure 3, which was based on over 400 field and laboratory peel tests performed on actual seams, illustrates this variability. The mean for this particular project and welding process (extrusion welding either between the sheets or on the top surface) is a comfortable 2300 psi, but the range of 1250 from 1650 to 2900 psi causes concern. The variations observed provide excellent justification for the quantitative strength requirement. In addition, the mean of 2300 psi tells us that the 1800 psi minimum criteria is reasonable and achievable and allows for statistical variations inherent in any process, yet maintains a sufficient level of control over the system quality. The values at the upper-end of this range almost exactly correlate to the actual sheet strength at yield, contradicting the belief widespread throughout the industry that the peel strength must always be significantly less than the yield tensile strength of the sheet because of behavioral differences during testing.

Additional Quality Control Criteria. The specified quality control program was comprehensive and strictly adhered to. Details of the quality control protocols applied are discussed below.

1. Each welding technician performed two 5' long test welds per day. Five weld specimens were cut and tested on-site in a portable tensiometer. Each of the five had to pass the criteria listed below. If any of the five specimens failed any of the criteria, the welding equipment parameters were adjusted and the test weld was redone.
 - a) The peel strength had to be at least 1800 psi. A micrometer was used to accurately measure sample width and sheet thickness. After about six weeks of construction, we were able to predict with surprising accuracy the weld strength based on the visual results observed. We therefore felt we could reduce quantitative measurement to only one specimen per test weld for documentation purposes. Five additional specimens were tested qualitatively using a hand held field peel tester. This change in procedure significantly reduced the time required to complete test welds because of the time-consuming nature of the tensiometer test.
 - b) The sheet must fail before the weld and must exhibit elongation and ductility upon failure. Sheet cracking and weld shearing were usually an indication of sheet crystallization, and grounds for weld rejection.
 - c) A maximum of 1/8" of weld peel was acceptable, anything more rejected.

Geosynthetics '89 Conference
San Diego, USA

2. A 1' x 2' in-place weld quality assurance (QA) sample was cut every 500' of seam, and half of the sample was tested for both peel and tensile strength in the field and the other half similarly tested at the liner contractor's laboratory. A total of 10 peel specimens and 10 tensile specimens were tested for each QA sample and all 20 had to exceed the three criteria previously stated or the seam was repaired.
3. Weld samples measuring 1" x 6" were cut from in-place liner at the discretion of either the liner contractor's Quality Control Inspector or Harza's Quality Assurance Officer, and tested in peel. These samples were normally taken every 200' of seam, two per shift, or at any location where seam quality was suspect.
4. Every seam was 100% impact tested and vacuum box tested.
5. Every penetration through the liner (manholes and pipes) was double protected utilizing either a combination of stainless steel battens and neoprene gaskets, with HDPE covering the batten strips, or welded HDPE skirts over the previously welded penetration. Penetration welds were found to be extremely difficult to perform and effectively vacuum box test. Quality control relied heavily upon visual inspection, impact testing, and adequate test welds. The double protection served to minimize the potential for leaks.

Quality Control Procedures

We were able to develop a set of specific procedures and responsibilities in order to best ensure and document that the quality requirements were met. The program required a full-time Quality Control Inspector from the lining contractor and a full-time Resident Quality Assurance Officer from Harza, each keeping independent records and each independently signing-off every liner panel and seam. Seam quality control tracking was especially confusing with seams being impact and vacuum box tested simultaneously, and each repair or patch requiring additional inspection and testing. Therefore, it was imperative that accurate and up-to-date records documenting the sequence of QC events and location of all repairs be maintained. To aid this process, repair locations were marked directly on the liner in different colors of paint or with different nomenclature to differentiate one repair type from another and facilitate inspection. We also found it helpful to have the impact and vacuum box test QC personnel put his signature directly on the liner as satisfactory testing was completed on repairs. The complexity of the liner system and the extent of seaming is indicated in the primary system as-built drawing shown in Figure 4.

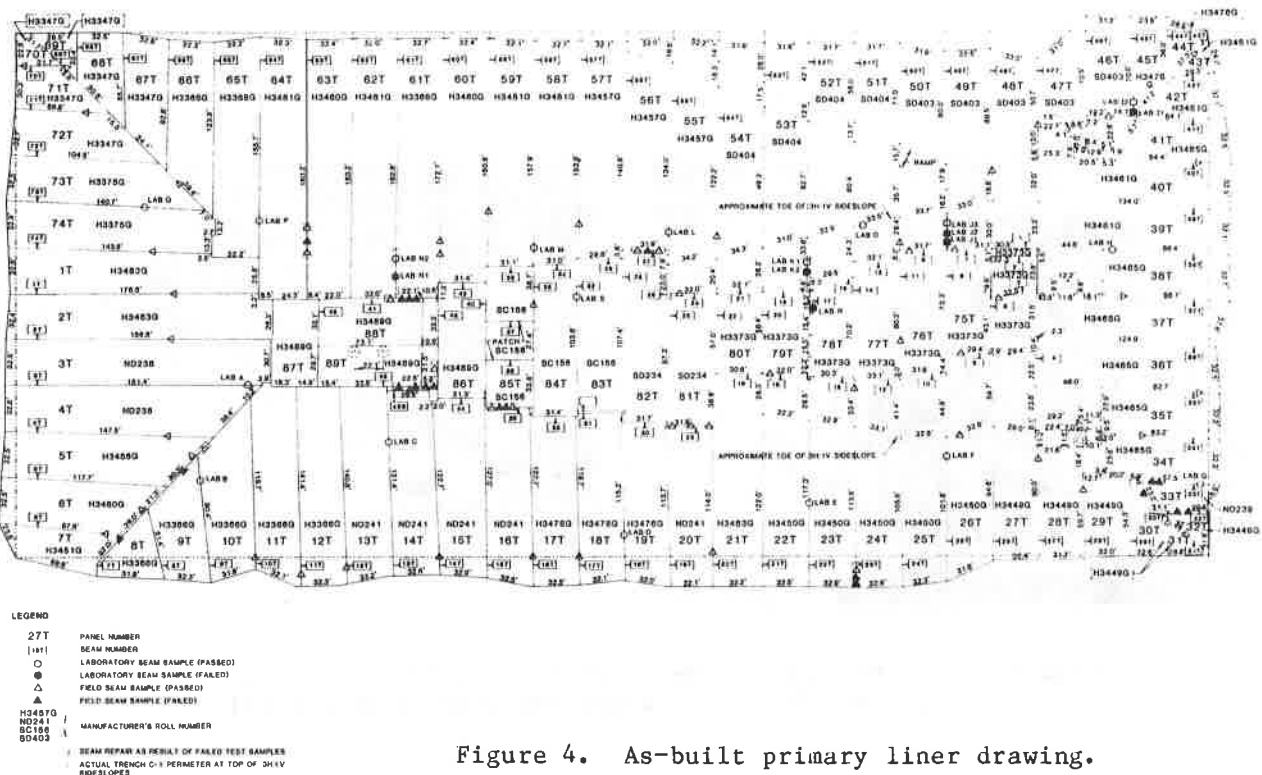


Figure 4. As-built primary liner drawing.

SPECIAL QUALITY CONTROL MEASURES FOR PROBLEMS ENCOUNTERED DURING CONSTRUCTION

Anchor Trench

Because of the requirement to completely weld the primary liner to the secondary liner, it was initially agreed upon to allow the anchor trench to be left open during liner placement. It was anticipated that the secondary liner could be held in place with sandbags, and the welding done directly in the anchor trench. The sandbags, however, proved inadequate. The resulting slippage created both a large wrinkle at the landfill toe and insufficient liner in the anchor trench (Figure 5). Because pulling the liner system back up the slope was infeasible, the excess material at the toe was cut and removed, and additional liner was spliced at the top of the panels to ensure that the liner extended to the back of the anchor trench. Mud and water accumulation in the anchor trench prevented the welding from being accomplished in the trench. As a result the secondary liner had to be pulled out of the trench, held in place to prevent further slippage, and welded to the primary liner on the top of the berm (Figure 6). Additional comprehensive QC/QA efforts were required because of the additional seaming. Significantly increased labor and inspection manhours resulted to assure a properly constructed anchor trench liner system and backfill.

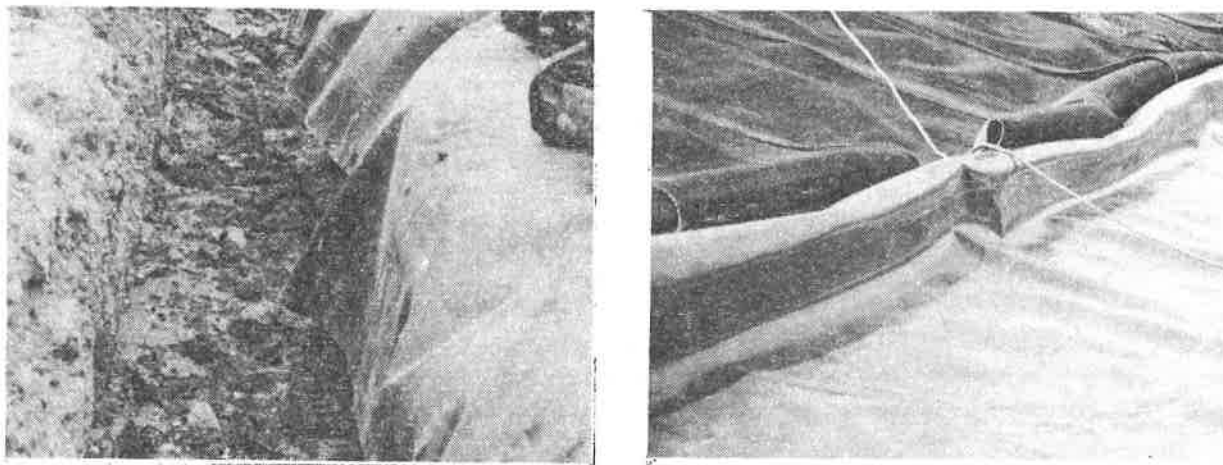


Figure 5. Liner slipped downslope causing shortage in anchor trench (left) and excessive wrinkle at toe (right).



Figure 6. Pulling liner out of anchor trench to weld primary and secondary liners together.

Based upon our experiences, certain guidelines for anchor trench work were established.

1. As much as is reasonably possible, the anchor trench should not be left open for even a short period of time.
2. A minimum of 1' of compacted backfill should be placed directly over each layer of geosynthetic material installed.
3. The anchor trench excavation should not proceed more than one day ahead of liner placement and the backfilling operation should take place daily, if at all possible.
4. If welding of the primary liner to the secondary liner is a requirement, the best approach would be to use slightly longer panels to allow the welding to take place on top of the trench. The cost of the additional material will be more than offset by the manhour savings during construction. It is estimated that the problems associated with the anchor trench as described above required an additional 50 man-days over that budgeted by the liner contractor.

Driving on the Liner

Despite claims by liner contractors that driving on HDPE liner with rubber-tired vehicles will not affect liner integrity, we experienced quite a different result. Our design called for granular drain material in the secondary collection pipe trenches. To transport and place this drain material over previously installed secondary liner, a small, rubber-tired front-end loader was used. The liner was severely creased when the loader drove over small wrinkles in the sheet (Figures 7 & 8). These wrinkles were due to the thermal expansion of the material, and are a normal occurrence during HDPE liner installation. We also noted numerous scratches and small punctures caused by the loader bucket. Because of the extent of damage, corrective action required that nearly 30,000 square feet of damaged liner be replaced.

Contraction of Sheet

HDPE has a high coefficient of thermal expansion and contraction, and exhibits significant, dimensional changes overnight or even over a few hours if the temperature changes rapidly. The resultant liner "trampeling" at any corner or grade change requires that sufficient excess material be provided to allow for thermal contraction. Careful inspection during the coolest part of the day was necessary in order to locate those areas where insufficient liner length was provided. The situation was remediated by cutting problem areas to allow the contracted liner to conform to the lines and grades, and capping the area with additional liner of sufficient dimension.

Construction Over the Liner

Any construction activity over the liner must be continuously observed by a quality control inspector. The most careful equipment operator has occasional accidents. Any damage or operation which endangers the liner needs to be identified, and remedial or corrective actions taken immediately.



Figure 7. Front-end loader used to transport drain material to secondary leak detection pipe trenches.

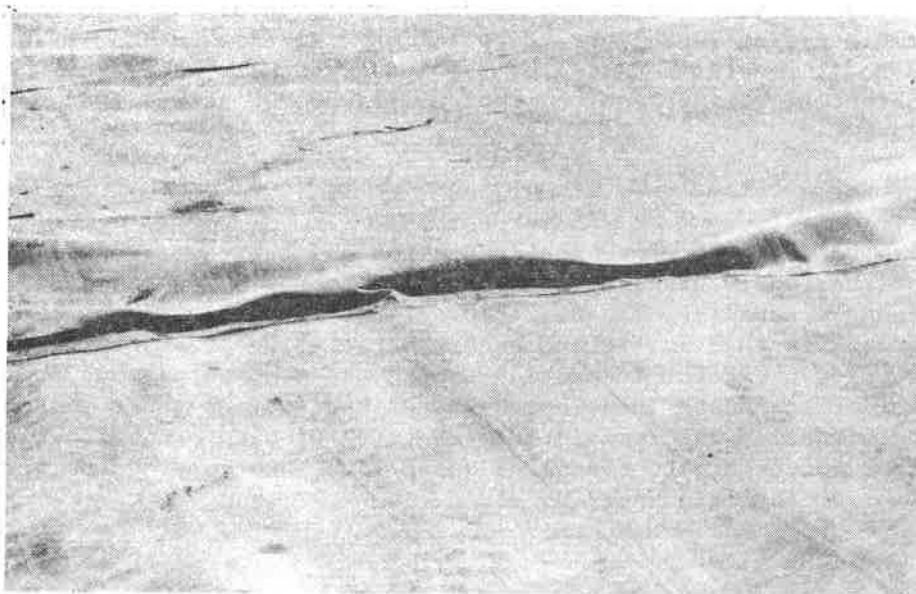


Figure 8. Creases caused by front-end loader driving over wrinkles.

HYDROSTATIC FLOOD TEST OF SUMP AREA

In any landfill, the sump area is the most critical and requires the most attention, care during construction, and built-in safety measures; and the area where leachate is most likely to pond to the EPA maximum allowable head of one foot for short periods of time following the design storm. Even small perforations in the liner can pass a significant quantity of water under hydrostatic pressure. As a check of the sump area liner integrity after all construction had been completed, PDC agreed to perform a hydrostatic flood test within the sump area, which measured approximately 90' x 30'. The purpose of the flood test was to determine whether or not there was communication between the primary and secondary systems. The test took 3 days, and involved monitoring various hydrostatic levels in the primary leachate collection system while pumping from the secondary system manhole. The various levels in the primary system represented different concentric areas of concern around the sump area. A biodegradable dye was also introduced into the primary manhole to allow visual inspection of any direct communication to the secondary manhole.

By the end of the test it was concluded that there was communication between the secondary and primary systems. The apparent leak in the sump was most likely the result of construction damage which may have occurred during unsupervised placement of drain and filter materials. The leakage problem was corrected by capping the entire sump area primary liner. Since this cap has been completed, flow into the secondary manhole has steadily decreased and there is apparently no further communication between the manholes. PDC received an operating permit from the Illinois EPA in May 1988, and are currently disposing of waste in Trench C-1.

CONCLUSION

A stringent specification and a strict quality control/quality assurance program are required during the installation of flexible membrane liners to ensure the material and seams have the properties and characteristics intended in the design. Without continuous on-site quality control and quality assurance monitoring throughout the construction period many of the installation problems discussed above would have gone undetected and/or unrepaired, which could have resulted in significant regulatory implications and cost to PDC if discovered after placing the landfill in operation.

M.J. MONTELEONE

G.J. DiPIPPO

AWARE Incorporated, U.S.A.

**Design Methods and Construction Quality Assurance For a Double
Geocomposite Industrial Waste Landfill**

INTRODUCTION

This paper will present design and construction quality control methods utilized for the construction of an industrial non-hazardous waste sludge landfill. The paper will discuss topics pertaining to geotechnical and geosynthetic composite design issues such as foundation design, side slope stability, liner thickness, leak detection/collection flow rates and general construction quality assurance techniques employed during construction of the lower system. Lastly, the paper will highlight areas of particular difficulty encountered during the design and construction phases of this project.

SITE DESCRIPTION AND BACKGROUND

The site is situated on the seaward edge of the Atlantic Coastal Plain in southern New Jersey and is underlain by alternating layers of sand, gravel and clay. The geology beneath the site consists of layers of unconsolidated sands, silts, and clays.

Local site geology at the landfill is similar to that described for the overall site with the exception of a low permeability clay lense approximately twenty-five feet beneath the landfill which supports a seasonally fluctuating perched water table. The terrain at the landfill is relatively flat at an elevation of approximately 56 feet above sea level, with the perched water table at an elevation of 29 feet. As a result, the majority of the waste, when placed, will be aboveground. Only wastewater treatment plant sludge (WTPS), classified by NJDEP as I.D. 27, is permitted to be disposed of within the landfill facility. This paper will present the recent design and construction of the third cell (Cell No. 3 of) this seven cell facility.

A double geocomposite liner system comprised of synthetic and compacted earthen materials was selected based on current technology and NJDEP solid waste regulations. This paper will focus on the geosynthetic and geotechnical design considerations and construction intricacies associated with a liner system of this type.

FOUNDATION DESIGN

At the outset of the project a geotechnical investigation was performed to determine the underlying soil strata thickness, profile and engineering properties. With this information in hand a stability, settlement and bearing capacity analysis of the in-situ material could be performed for the intended base grade geometry. The landfill was designed to be constructed within the in-situ sand layer above the clay. Since the landfill is essentially an above ground facility the base grade was relatively shallow with its deepest slope length to be not greater than sixty feet. The construction and material restrictions of the primary geocomposite system dictated that the slopes should be no steeper than 3H:1V.

A slope stability analysis was performed on the open cut earthwork excavation of the base grades. A computer version of the simplified Bishop Method was used to model and analyze the intended base grade configuration. Using the data obtained from the field investigation, the computer model yielded a minimum factor of safety against side slope failure of 2.1. The foundation base grades were then analyzed for settlement and bearing capacity. From the field investigation it was determined that the in-situ sand would have a minor role in the estimated base grade settlements and that the clay would control settlement of the landfill foundation. Using Terzaghi's Time Dependent Consolidation Equation, the foundation settlement was computed to be on the order of .5 feet, a nominal amount, which could be easily designed for in the liner system. The landfill bottom was designed at a grade of 3% to control head buildup in the collection system, as well as allowing for the computed settlements to be taken up within the liner system without reducing the minimum drainage slopes to less than 2% as required by the NJDEP solid waste regulations.

Lastly, the ultimate bearing capacity for the landfill foundation was computed using Meyerhof's Bearing Capacity equation with shape factors, assuring a 25' x 550' rectangular foundation print. The factor of safety against bearing capacity failure, as expected, was quite high at 18.9. As part of routine base grade preparation, the foundation area was proof rolled prior to construction of the liner system. This final proof roll would take out any of the remaining immediate settlement within the upper foot of sand base grades.

GEOSYNTHETIC COMPOSITE LINER DESIGN

The liner system for this facility was designed as a double geocomposite liner system as shown in Figure 1. The system is comprised of secondary and primary geocomposite liner system, which combined high density polyethylene (HDPE) and compacted clay with a maximum permeability of 1×10^{-7} cm/sec. While both liners had slightly different construction and design requirements, a common design approach was utilized which focused on designing each component of the synthetic system by function. The "design by function" approach analyzes and designs each component of the system based on its final end use function. This method, unlike designing by cost or specification, relies primarily on traditional geotechnical design concepts modified to incorporate the various physical and mechanical properties of the synthetic materials within each of the component systems.

SECONDARY GEOCOMPOSITE LINER SYSTEM

The secondary geocomposite liner system is comprised of a compacted clay and geosynthetic composite system. The secondary clay layer within this system consists of a minimum of three (3) feet of compacted clay with a maximum hydraulic conductivity of 1×10^{-7} cm/sec. The secondary geosynthetic liner system consists of a high density polyethylene (HDPE) geomembrane, a high capacity drainage net (geonet) and a geotextile. Collectively these components, combined with the three (3) feet of clay, comprise the secondary liner and leak detection system for the landfill. This section will discuss the design of the geosynthetic components of the secondary liner system.

The secondary geomembrane's physical, mechanical and chemical properties were determined by an evaluation of the functions for which the liner system was to perform. The geomembrane's primary function was two-fold. First, to be chemically compatible with the expected leachate within the leak detection system, and second, to provide a relatively impermeable barrier. Based on leachate composition from existing cells, high density polyethylene (HDPE) was chosen as the polymer of preference for its relative inertness to a variety of chemical environments.

To establish that commercially available HDPE roll goods were capable of withstanding exposures to the leachate anticipated to be generated within the landfill, EPA 9090 tests were performed on HDPE samples from two geomembrane manufacturers. The liner samples were exposed to a synthesized leachate, which was approved by NJDEP prior to testing. The samples were exposed for a maximum of 120 days and tested at 30-day intervals. Samples were incubated at temperatures of 23°C and 50°C during these exposure periods. These tests indicated that materials submitted by both manufacturers exhibited little variation in both physical and mechanical properties when exposed to the leachate.

The liner thickness for the secondary geomembrane was determined considering localized and differential settlements of the secondary clay layer. Using an analytical approach presented by Koerner⁽²⁾, which considers a localized protrusion or soft spot within the clay layer, the following equation of equilibrium was used:

$$t = \frac{q(x)}{\cos B(O_y)} (\tan S_u + S_l) \quad (1)$$

where,

- q = overburden normal pressure
- x = overburden immobilization
- B = angle of deformation
- O_y = liner yield stress
- S_u = shear force above liner
- S_l = shear force below liner

Both static and dynamic loading conditions were evaluated using equation (1). The static loads are representative of the long-term loading conditions that the geomembrane liner will experience upon final closure. The dynamic loads imposed on the geomembrane will occur as a result of placement and compaction of the primary clay layer (i.e. sheepsfoot rollers and dozers). A static load of 4000 psf yielded a liner thickness of 22 mils, while a dynamic load of 9500 psf yielded a thickness of 50 mils. It should be noted that this analysis assumed that pressure from the heaviest piece of construction equipment would be transmitted directly to the geomembrane. This would not be the situation during construction. As a result, the estimated liner thickness is overly conservative. However, in an effort to account for unexpected loads (i.e. due to installation or transportation), a F.S. of approximately 1.5 was applied to the dynamic liner thickness which yielded a total liner thickness of approximately 80 mils.

The next design consideration was the anchor trench for the geosynthetics. The critical aspects of the anchor trench design were the runout length at the crest of the slope, depth of the trench and finally the trench width. Currently, there are two methods available to determine the trench dimensions. The first method, an analytical procedure presented by Koerner⁽²⁾, analyzes the pressure distributions above the liner runout and within the anchor trench. The second method available simply uses the industry standard for anchor trenches which requires a geomembrane runout length of not less than three feet, a trench depth of two feet, and a trench width of one foot. Both methods were evaluated, with the most conservative method adopted.

Upon completion of the analytical method, it was determined that with a trench depth of two feet, a runout length of 0.64 feet is required for a factor of safety of 1. Comparing the industry standard with the computed value, it was determined that the standard detail was at least four times more conservative than the analytical approach. Since the anchor trench detail is a crucial element in the landfill design, it was decided that the conservative, industry's standard detail, would be utilized for the anchor trench design.

The final design consideration for the secondary geomembrane liner was the side slope stability of the secondary clay layer beneath the secondary geomembrane liner. The analysis used to determine the stability of the three-foot clay layer found on in-situ sand material, was the Simplified Bishop Method. The slope stability concern of the three-foot clay layer was the possibility of sloughing of the clay after the geomembrane is placed, which could rupture and/or tear the geomembrane on the side slope. From this analysis, it was determined that a deep seated toe failure possesses the lowest factor of safety of 4.5. A factor of safety less than 1.5 was considered to be unacceptable. From this result, it is quite apparent that sloughing of the secondary clay layer was remote.

The last major design concern was that of the leak detection system design. The secondary leak detection system must be capable of providing a transmissivity of 3.28×10^{-4} ft/sec. This is based on regulations established by NJDEP which require a leak detection system to have one foot of clean washed sand with a minimum hydraulic permeability of 1×10^{-2} cm/sec. In an effort to utilize the landfill volume more efficiently, and to promote quick efficient drainage to the

Geosynthetics '89 Conference
San Diego, USA

sumps, it was decided to investigate the practical use of high drainage capacity polyethylene netting material (more commonly known as a geonet) to transmit flow within the leak detection layer. The advantages of a geonet vs. sand are as follows:

- o The polyethylene geonet possesses the same chemical compatibility as that of the geomembrane.
- o Since most geonets are approximately 0.25" in thickness, the landfill volume increases by one foot over the surface area of the landfill.
- o In general, these materials are capable of transmitting twenty times the transmissivity of one foot of sand.
- o The time required for a leak to be detected in the sump is on the order of days as opposed to several months for sand.
- o Its ease of construction far surpasses that of sand. In addition, there is less chance to damage the underlying geomembrane.
- o Side slope installation is relatively effortless.
- o The material cost of the geonet is approximately 70% less than sand.

The disadvantages associated with utilizing geonets are as follows:

- o In general, this component of the side slope system will be in direct contact with the geomembrane. As a result, this geonet/geomembrane interface will possess the lowest friction angle of the geocomposite system. This low friction angle plays a significant role in the stability of the geocomposite liner system above the secondary liner.
- o The geonet material has little tensile strength. As a result, the material cannot be expected to support much of the load distribution within the geosynthetic composite.
- o The geonet by virtue of the open nature of its structure, also allows for two potential clogging problems. The first source being the restriction of flow in the geonet via deformation of geotextiles into the pore structure of the geonet. As will be discussed in the sections to follow, this may be accounted for in the design parameters. The second source of clogging is from clay fines passing through the geotextile. This problem however can be minimized during the filter criteria selection of the geotextile.

The primary function of the geonet is flow capacity. Two elements must be considered in determining the required geonet flow capacity. The first element is that of being able to handle anticipated flow through the primary liner system, which in theory is negligible. However, there will be minor amounts of water within the primary clay which will be expelled during consolidation of the clay liner. It has been estimated by others on past projects that this amount may be on the order of 70 gal/month (0.001 gal/min). The flow capacity of the geonet may be estimated utilizing available transmissivity data from manufacturers and Darcy's equation. From the available literature a 0.25" geonet is capable of transmitting 0.11 gal/min/ft. However, the literature assumes rigid upper and lower boundaries around the geonet. Since this is not the case with the intended liner system, some type of flow reduction factor was required to more accurately represent the actual transmissivity of the geonet. This data was presented by Giroud⁽⁷⁾ for various boundary conditions. The reduction factor for a system with a rigid geomembrane lower boundary and a flexible geotextile upper boundary was 5.0. Using a minimum hydraulic gradient of 2.6%, the total flow capacity of the

geonet is 0.45 gal/min. This result indicates that one layer of 0.25 inch geonet is capable of delivering 19,000 gal/month-ump. It may therefore be considered that the flow capacity of the geonet is more than adequate to handle the anticipated flow requirements.

The second element in determining the required flow capacity of the geonet was to satisfying NJDEP solid waste regulations which require a minimum transmissivity of 3.28×10^{-4} ft²/sec. As previously stated, transmissivity data for geonets at various overburden stresses may be obtained from manufacturers' literature. Given an estimated landfill overburden stress of 3,000 psf, the geonet transmissivity for a 0.25" thick net would be 1×10^{-2} ft²/sec. Comparing this value with the NJDEP minimum transmissivity of 3.28×10^{-4} ft²/sec indicates that the geonet is capable of transmitting thirty (30) times the amount of flow required.

This result, however, is misleading since the upper boundary of the geosynthetic composite is a geotextile overlain by clay and not another geomembrane. As discussed previously, a reduction factor of 5 must be applied to the transmissivity of the geonet. This reduction factor is required since the geotextile will have a tendency to block the pore structure of the geonet, thus reducing the flow capacity. As a result, the estimated geonet transmissivity is capable of transmitting 6 times the amount of flow required within the regulations.

The second function of the geonet is to provide rapid leak detection of leachate to the sump areas. The time required for a leak to be detected at the sump was computed by Darcy's equation as follows:

$$\begin{aligned} Q &= kiA & (2) \\ T &= \frac{NL}{ki} & (3) \end{aligned}$$

time to detect leak

where:

- N = porosity of geonet = 0.80
- L = maximum length of drainage path = 360'
- i = hydraulic gradient (slope) = 2.6%
- k = permeability of geonet = 0.5 ft/sec

Applying a reduction factor of 5 to the permeability of the geonet yields a leak detection time of approximately one day. If sand were used, the detection time would be approximately 150 days. It should be noted that the detection time is sensitive to the slope of the detection layer. For this reason, no area within the landfill has a slope less than 3%, to allow for settlement and consolidation of the secondary clay layer.

PRIMARY GEOCOMPOSITE LINER SYSTEM

The primary geocomposite for the Cell 3 liner system is comprised of a clay and geomembrane composite. The primary clay layer has a minimum thickness of two (2) feet with the upper 6" compacted to a maximum hydraulic conductivity of 1×10^{-7} cm/sec. The primary geomembrane consists of a high density polyethylene (HDPE) membrane possessing a thickness of 80 mils (.08 inches).

Geosynthetics '89 Conference
San Diego, USA

The major difference between the secondary clay layer and the primary clay layer is that the primary clay is constructed in a different sequence due to inherent construction restrictions associated with compacting earthen materials over geosynthetics. The concern was for the integrity of the secondary geosynthetic liner system while placement and compaction of the primary clay layer proceeded. Given this construction consideration, it was recommended by NJDEP that only the upper six (6) inches of the two foot primary clay layer be compacted to a minimum hydraulic conductivity of 1×10^{-7} cm/sec. Construction of the primary clay layer in this manner will preserve the integrity of the secondary geosynthetic liner system and provide a hydraulic barrier to leachate which may penetrate the primary geomembrane. Although the lower eighteen inches of the primary clay layer will be lower in density permeability, the minimum loss in structural stability and permeability is insignificant when compared to the potential damage to the secondary liner system.

The most critical aspect of the primary geosynthetic liner system design was the side slope stability of the primary clay and operations layer above the primary geosynthetic liner system. As may be seen in Figure 1, the side slope composite configuration is complex due to the number of layers within the system. Since each layer within the system possesses a different friction angle with its adjacent material, the problem becomes a matter of determining the actual friction angles at the interface of each adjacent component of the geocomposite liner system. These values may be obtained from published laboratory data available within current literature. However, if values are not available for a given soil to synthetic or synthetic to synthetic system, the values may be determined experimentally in the laboratory by using a modified direct shear test.

As discussed in the previous section, the possibility of the secondary clay layer sloughing and jeopardizing the integrity of the liner was an issue which was analyzed using the Simplified Bishop Method. However, in the case of the primary geocomposite liner, sloughing of the primary clay layer is also of concern, but the mechanism by which the failure could occur is somewhat different. The primary clay layer, on the side slope, rests on the secondary leachate detection system which is comprised of a non-woven geotextile and geonet, which in turn is underlain by the secondary geomembrane liner. A problem arises since the geonet and geomembrane are both made of high density polyethylene (HDPE) which exhibits a low friction angle of 16° . The slip plane with the lowest friction angle exists between the geonet and geomembrane. This interface is the weakest plane in the geocomposite liner system. Two analytical methods are available to investigate the stability of the primary clay layer after construction. The first method is an infinite slope analysis which simplifies the system by considering the situation as a classical sliding block problem. The following equation was used to compute the factor of safety against sliding.

$$F.S. = \frac{\tan S}{\tan B} \quad (4)$$

where:

- S = friction angle between the geonet and geomembrane 16°
- B = angle of slope (3H:IV) 18.4°

The factor of safety was computed to be .86 which is less than 1.0. This result indicates that the primary clay layer is unstable once construction is completed. There are two crucial elements not taken into account in this analysis. The first element is the buttress effect that the soil wedge at the toe of the slope (referred to as the neutral block), has on the structural stability of the clay layer to support the weight of the active block. The second element neglected in this analysis was the strength mobilized by forces within the anchor trench to resist pullout. Therefore, a more rigorous form of analysis is required in order to analyze this slope configuration. The Sliding Wedge Analysis was employed, which enabled the investigation of the neutral block's ability to buttress the primary clay layer. In addition, pore water uplift pressures and tension cracks were incorporated into the analysis. The analysis indicated that a minimum safety factor would be realized by a slope configuration described as a "neutral block", with uplift pressures. This safety factor was 6.7.

It should be noted that at the present time there is no published procedure for determining the beneficial effects derived from the anchor trench, therefore, it was not incorporated in the stability analysis. It is apparent from the table that the additional stability derived from the anchor trench system is not required, since the clay layer demonstrated its stability without the presence of the anchor trench. For an additional factor of safety, a geogrid was designed to be placed on top of the non-woven geotextile to allow a portion of the load from the primary clay and operations layer to be transferred from the secondary liner and leak detection system to the anchor trench, much in the same manner that a column in a building transfers its load to a foundation. In addition, the geogrid aided during the construction of the primary clay layer on the 3H:IV side slopes by presenting a surface with a much higher friction angle.

The last system of the primary geocomposite layer to be designed was the primary leachate collection system. The design of the primary leachate collection system was divided into three components. The first component of the system was to determine the required thickness of the drainage layer. The second component involved determining the required transmissivity of this layer. The last component of the primary leachate collection system to be designed was a geotextile separation layer between the collection sand layer and the operational sand layer. The primary function of this geotextile is to allow liquid to pass while keeping the collection layer free of fines and material which may jeopardize the integrity of the collection system.

The required collection layer thickness was computed using the equations presented below:

$$H_{\max} = L ([e/k + \tan^2 B]^{1/2} - \tan B) \quad (5)$$

$$T_{\max} = H_{\max} (\cos B) \quad (6)$$

where:

- L = maximum drainage path length
- e = estimate of uniform precipitation
- k = permeability of drainage layer
- B = slope of drainage layer
- H_{\max} = maximum water height thickness
- T_{\max} = required thickness of collection layer
(in any consistent set of units)

For small values of slope angle, the cosine of B approaches unity, therefore, $T_{max} = H_{max}$. Typically in this type of design the precipitation estimate and permeability of the drainage layer are determined by regulations or local weather conditions. Therefore, the drainage path length and slope may be adjusted to optimize the landfill volume and hydraulic performance of the leachate collection system. Given the economics involved with the design and construction of landfills, it is critical that the landfill geometry utilize as much of the available space to maximize the final closure volume of the cell. The maximum volume for this cell yielded a maximum drainage path length of 350 feet at a maximum slope of 3%. The analysis was first performed assuming a clean washed sand was used with a permeability of 1×10^{-2} cm/sec. The uniform precipitation for the site was determined to be 1.28 inch/day. With these data in hand the maximum collection layer thickness was determined to be 13.6 feet. This result demonstrates that a sand drainage layer is not capable of handling the expected flows from a 7-day, 10-year storm during operation. Since the precipitation rate and cell geometry is fixed, the only variable that may be varied is the soil permeability. While this is theoretically possible, it is from a practical view not economical. Therefore, synthetic drainage materials were reviewed to determine their applicability to this layer. The type of drainage media selected was a geonet. This type of material, due to its open net structure (porosity of .80), will allow for a high flow capacity. Using Darcy's equation and the analysis used to determine the leak detection flow capacity, it was calculated that the geonet could provide a transmissivity of 1×10^{-2} ft²/sec. The minimum transmissivity required by NJDEP regulations is 4.49×10^3 ft²/sec. The required value versus the estimated transmissivity of the geonet yield a factor of safety of 2.4 which is more than sufficient for this system. Two feet of clean sand washed sand was included in the collection layer to perform primarily as an operational layer for which construction vehicles may be operated without damaging the primary geosynthetic system.

The last component of the collection layer system to be designed was a filter fabric to protect the integrity of the geonet from the operational sand. Using Giroud's filter criteria for relative densities greater than 80%, required an apparent opening size (AOS) of the filter fabric to be greater than No. 20 sieve size. With these data in hand the manufacturers literature may be reviewed to determine the suitability of available geotextiles. This geotextile will be required to withstand construction loads and static earth loads imposed during the installation of the operational sand layer on the side slopes. The stability wedge analysis and a modification of the anchor trench analysis were utilized to determine the required tensile strength of the geotextile. A geotextile with a wide width tensile strength of 180 lbs. was required. Given the required AOS and tensile strength, a 4 ounce non-woven geotextile was chosen to satisfy these requirements.

CONSTRUCTION QUALITY ASSURANCE

In an effort to establish that the construction specifications and drawings were executed in a manner consistent with the design intent, a construction quality assurance (CQA) plan was developed for the owner by the design engineer. The program encompassed various phases of liner construction which included clay

compaction, operational sand installation, geosynthetic installation and sump installations. This section will focus on that portion of the CQA plan which monitored the geosynthetic installation.

The CQA plan developed for each of the geosynthetic components had the same objectives to obtain; however, the method by which those objectives were achieved varied according to the function of the synthetic type. The objectives of the geosynthetic CQA plan were as follows:

- o Inspection of the geosynthetics upon delivery of the site for any physical damages or material substitution.
- o Conformance testing of on site geosynthetics for compliance with minimum physical and mechanical properties. This was to be performed prior to installation of the materials.
- o Construction observation of the geosynthetic installation.
- o Preservation of all installed geosynthetic components during succeeding earthwork or synthetic installations.

In general, a visual inspection of delivered rolls of geomembranes, geotextiles, geonets and geogrids was performed upon arrival on site for damage to rolls during loading or unloading. In addition, geotextiles were inspected to establish that they were properly wrapped in plastic to protect the roll goods from U.V. degradation and inclement weather. Lastly, the geosynthetic rolls were visually verified to confirm that the material submitted by the contractor to the engineer was delivered to the site.

Upon completion of visual inspections, samples from geomembranes, geotextiles, geonets and geogrids were obtained and forwarded to the geosynthetic testing laboratory for representative physical and mechanical testing of the delivered materials to indicate conformance with the technical specifications. The sample frequency for conformance testing was approximately one out of three rolls for geomembranes, and one out of ten rolls for all other geosynthetics.

The geomembrane installation was observed during all phases of construction. For this project, all field seams were welded using a double track hot wedge fusion system. This type of welding system created an annular space between the two welded tracks which was then pressurized with air to verify seam continuity. This type of testing provided information as to a seams ability to maintain a seal under a pressurized condition. If a loss in pressure during the test was detected, the seam was retested until the discontinuity was localized. The area was then repaired with an extrusion welded patch. It should be noted that in using double track welding systems for HDPE, a certain percentage of the seams for the job will be extrusion welded, typically about 10 to 15 percent. Extrusion welded seams were all vacuum tested to establish the continuity of the weld.

Lastly, the mechanical strength of the field seams was evaluated by obtaining a sample from a field seam and forwarding the sample to the geosynthetic laboratory. When performing this phase of the CQA plan, time was essential. Further work by the contractor would be potentially impacted by not being able to continue with succeeding layers of geonet and/or geotextiles. Samples were air shipped next day

Geosynthetics '89 Conference
San Diego, USA

delivery and tested the same day, with laboratory results verbally confirmed on the telephone. This allowed for field samples to be tested and evaluated within 24 hours. A seam failing mechanically in shear or peel was required to be reconstructed.

The geotextile installation was observed during each phase of construction. The primary construction item of concern during the geotextile installation was field sewing of rolls. Sewn seams were visually inspected for skips and discontinuities in the seam. If factory seams were present they were visually inspected as well. The geonets were inspected for dust or debris which might hamper their performance as a drainage layer. The geogrids were visually inspected for cuts or tears to the fabric structure. Since the primary function of the geogrid was in a load bearing capacity, it was essential that the materials were installed in good condition.

All geosynthetics were inspected for distress or damage during succeeding geosynthetic or earthwork operations. Of special concern was the installation of the primary clay layer which required heavy construction vehicles such as sheepfoot rollers and dozers to operate over two feet or less of clay material. This problem was minimized by requiring that the clay be placed and compacted on a minimum eighteen inch lift. By constructing in this manner and sequence, protection of the integrity of the primary geocomposite system was maintained while still achieving 6 to 8 inches of compacted clay at a maximum hydraulic conductivity of 1×10^{-7} cm/sec., and thus meeting NJDEP regulations.

CONCLUSIONS

The design and construction of this double geocomposite liner system illustrated the need to incorporate "design by function" within geosynthetic systems. Upon the successful completion of this project it is clear that geosynthetic components must be evaluated and selected based on function. It is clear that the proper material design and selection will provide a properly functioning geocomposite liner system. A construction quality assurance plan is essential to a high quality installation of geosynthetics. As with the quality assurance of any type of construction project, the successful implementation of the CQA plan will in large determine the success or failure of the geosynthetic system.

REFERENCES

- (1) Juang, Y.H., Stability Analysis of Earth Slopes, Van Nostrand, 1983.
- (2) Koerner, R.M., Designing with Geosynthetics, Prentice-Hall, 1986.
- (3) Das, B.M., Advanced Soil Mechanics, Hemisphere Publishing, 1983.
- (4) Bowles, J.E., Foundation Analysis and Design, McGraw-Hill, 1982.
- (5) Hook, E., Rock Slope Engineering, The Institution of Mining & Metallurgy, London, 1981.
- (6) Martin, J.P., Koener, R.M., and Whitty, J.E., Experimental Friction Evaluation of Slippage between Geomembranes, Geotextiles and Soils, Proc. Int. Conf. Geomembranes, Denver, Colo., June 20-24, 1984, IFAI Publ., Vol. 1, PP. 191-196.
- (7) Giroud, J.P., Geotextiles and Geomembranes - Definitions, Properties and Design, Industrial Fabrics Association International, 1984.
- (8) Giroud, J.P., and Fluet, J., Course Notes for a Seminar in Geomembranes, presented at Lehigh University, November 1986.

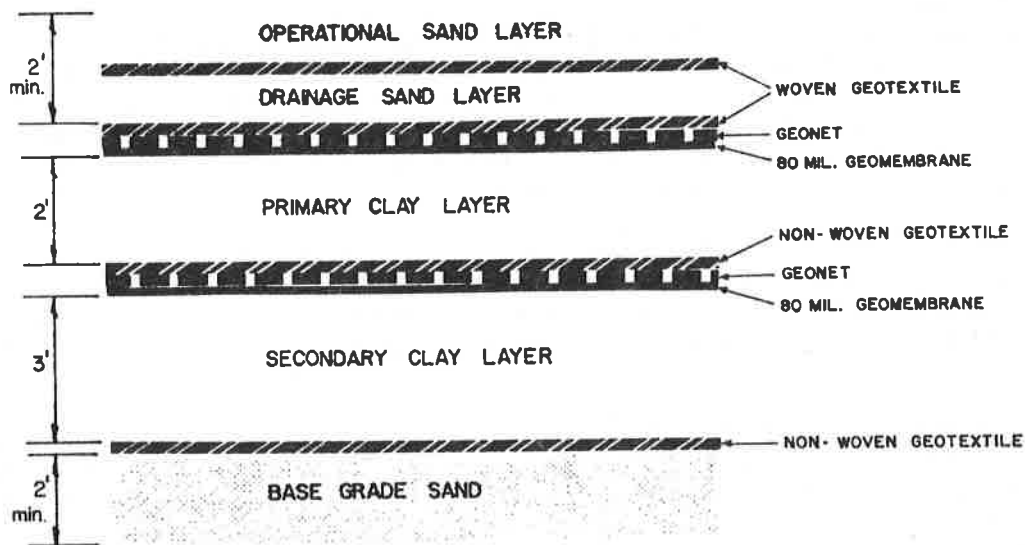


Figure 1: Typical Landfill Liner and Sideslope Details.

G.R. KOERNER

Drexel University, U.S.A.

J.A. BOVE

Westinghouse Environmental Engineering, U.S.A.

Inspection of HDPE Geomembrane Installations

ABSTRACT

This paper outlines what is felt to be the proper sequence of events leading up to a successful installation using high density polyethylene (HDPE) geomembranes. The paper offers numerous suggestions which might circumvent routine problems with HDPE installations for both hazardous and nonhazardous facilities. Resources for this paper include a comprehensive review of the literature, manufacturers information and field experience from several sites.

INTRODUCTION

Over the course of the last ten years an increased use of high density polyethylene (HDPE) for landfills, waste piles, tailings facilities, and surface impoundments has occurred. This is due in large part to the November 8, 1984 Resource Conservation and Recovery Act (RCRA) which was amended by the Hazardous and Solid Waste Amendments (HSWA) [1]. Among the provisions that went into effect were minimum technological requirements (MTR) for hazardous waste land disposal facilities. HSWA requires that all new facilities must be lined with flexible membrane liners (FML's) called in this paper geomembranes. This legislation created an opening for a large market for geomembranes which has grown over the intervening years.

In addition to geomembranes on the bottom and sides of the facilities, regulations were passed mandating that all completed landfills must be covered. Although this market has not been the primary target of HDPE geomembrane manufacturers, it is also possible to use HDPE for such applications.

As one of a variety of geomembrane types, HDPE's growing popularity is due to its outstanding performance in the EPA's 9090 chemical resistance test. Other factors such as good mechanical properties are an added bonus for HDPE. However, the material is not without its shortcomings. Both positive and negative features will be presented in this paper.

As a resin for a large number of applications, HDPE has a sizable market in the USA. In 1987 there was an estimated 100 million kilograms of resin produced of which approximately 2% was used for geomembrane production. As a whole HDPE geomembranes represent a 100 million dollar a year industry in North America [2].

The purpose of this paper is to present an overview of HDPE production and installation, and to point out the sequence of events which lead to a successful installation.

OVERVIEW OF HDPE

Geomembranes are relatively impermeable polymeric sheets used to control liquid and/or vapor migration. In general, polyethylene geomembranes have an equivalent Darcian permeability coefficient of approximately 1×10^{-14} cm/sec, as measured by a water vapor transmission test [3]. This polymer is characterized as a semicrystalline thermoplastic and is grouped by ASTM in density brackets as follows: high density (HDPE) is from 0.965 to 0.941, medium density (MDPE) is from 0.940 to 0.926 and low density (LDPE) is from 0.925 to 0.910 gm/cm³. Most commercially available sheet is in the upper range of MDPE and only by including carbon black does it fall within the HDPE range. In keeping with current industrial practice, however, we will refer to the material as HDPE.

Additives are typically compounded with the polymer to improve the physical and long term characteristics of HDPE. Protection from ultraviolet (UV) degradation is provided by adding carbon black. Most commercial HDPE geomembranes consists of 90-95% polymer, 0-5% additives, 2-5% carbon black and about 1% antidegradants [4]. The additives are also called processing aids. They are proprietary within the resin supplier and sheet manufacturer's community.

HDPE sheet is manufactured by three uniquely different processes. The first method utilizes a flat mouth extruder, see Figure 1. Resin pellets are introduced into the feed hopper, melted and mixed in the barrel of the extruder, and then squeezed out of a flat mouth die. The sheet is eventually rolled up after it has passed through downstream equipment such as monitoring and control systems. The current maximum width sheet that is produced by this process is approximately three meters. The sheet is generally of high quality and can be made very long. Because of the relatively narrow width, panels are typically constructed in the factory by welding a series of sheets together.

The second process for making HDPE sheets utilizes an oscillating feed outlet and stainless steel indexing drum. As shown in Figure 2, the extruder produces the hot melt. The melt is dispensed in 40 cm ribbons back and forth above the drum while it incrementally advances. The sheet is then calendered between counter-rotating rollers to insure good adhesion between the individual ribbons. The geomembrane sheet from this process is typically ten meters wide. However, thickness control of the process is difficult (due in part to factory seams every 40 cm), and it also has a tendency to bloom (a white residue on the bottom of the sheet is indicative of blooming). This process is best suited for the thicker range of applications, e.g., greater than 1.5 mm.

The third method to make HDPE sheet is with a cylindrically blown film extruder as depicted in Figure 3. Basically the polymer melt is forced through two concentric rings. Internal air pressure forces the "bubble" to expand into a controlled diameter as it is raised vertically 15 m to 30 m in height. Thickness is also controlled in the same manner. The tube of HDPE is then drawn upward, bent over nip rolls, cut on one side, unfolded and then rolled up on a take-up roll. This take up process can be seen in the blow-up sketch of Figure 3. Sheets as wide as 14 m have been produced using this process. The only drawback with this method is that it induces two longitudinal folds in the geomembrane sheet which are only partially removed during take-up and storage.

CONSTRUCTION QUALITY CONTROL AND ASSURANCE

Construction quality control (CQC) and construction quality assurance (CQA) may be defined as follows [5];

CQC - Those actions which provide a means to measure and regulate the characteristics of an item or service to contractual and regulatory requirements.

CQA - A planned and systematic pattern of all means and actions designed to provide adequate confidence that items or services meet contractual end requirements and will perform satisfactorily in service.

In the context of geomembrane-lined facilities, CQC refers to those actions taken by the manufacturer and/or installer to ensure that their methods, materials and workmanship are accurate and correct, and meet the requirements of regulations, plans and specifications [5].

CQA on the other hand, refers to the means and actions employed by the owner through the designer and/or quality assurance team to assure conformity of the design, production and installation with the quality assurance plan, as well as drawings and specifications. "Third party construction quality assurance" refers to quality assurance team which is independent of the designer, manufacturer, fabricator, installer or owner [5].

An EPA technical guidance document entitled "Construction Quality Assurance for Hazardous Waste Land Disposal Facilities," has been released which describes a typical CQA plan. This is required reading for those involved with geomembrane installations [6].

INTERPARTY COMMUNICATION

Like all construction projects there are many parties involved with a geomembrane installation. A successful project requires the interaction between the design engineer, manufacturer, fabricator, installation contractor, inspectors, owner/operator and CQA team.

In regard to the effectiveness of the CQA component of the project, it is most effective if all parties involved are fully informed of the conditions under which they will work. This means that the manufacturer, fabricator and installer should be informed by the bid document that a CQA plan will be in effect by an independent third party.

CQA programs should cover every component or operation during construction, and should be extremely careful regarding the following points, each of which will be further described.

- (a) Qualification and certification of the companies and their employees
- (b) Certification and Testing
- (c) Final documentation and warranty

(a) Qualification and Certification of the Companies and their Employees

It is important to insure that the geomembrane manufacturer has previously demonstrated its ability to produce HDPE geomembrane for containment purposes. One typically requires a minimum total of produced sheet to insure that such experience is evidenced. References should be requested and checked.

In the same vein, it is important that one is dealing with skilled labor. In short, you do not want field personnel learning how to weld HDPE on your job. Therefore, insist that a superintendent is on site and that a designated foreman will continuously work with each seaming crew. The superintendent ideally should have at least two years of experience, while the foreman should have at least one year. It is not unusual to insist that all installation personnel submit resumes.

(b) Certification and Testing

HDPE resin is generally delivered to a liner manufacturer in pellet form. From a non-polymer chemist's point of view, there are two significant properties which give one a good idea of the index characteristics of HDPE resin. These properties are density (ASTM D1505) and melt index (ASTM D1238).

The density of HDPE is related to the degree of crystallinity. The higher the density, the more crystalline the material. In turn, the higher the crystallinity the better the chemical resistance of the geomembrane to harsh chemical leachates. However, there is a functional limit to the density of HDPE. If the density (crystallinity) is too great, the geomembrane sheet becomes difficult to seam and even becomes "brittle". It should be noted that the density of carbon black is approximately 1.95 g/cc where the density of HDPE resin is approximately 0.94 g/cc. Therefore a different criteria is warranted when testing the density of the resin versus the geomembrane sheet.

The second property used to characterize HDPE is the melt index. The lower the melt index, the higher the molecular weight. High molecular weight indicates long polymeric chains which correspond to HDPE sheet with good physical, mechanical and chemical properties [7].

Before the sheet is sent to the job site, a number of tests should be performed to insure its integrity. Table 1 presents a comprehensive testing program and suggests target values for a 2 mm HDPE sheet. This thickness sheet has been used in a number of hazardous waste landfill sites. It is recognized, however, that the EPA regulations state minimum values of 0.8 mm to 1.2 mm depending on cover placement. Table 1 represents only a partial list of geomembrane tests. Obviously, the nature of one's project will govern the extent of testing. Table 1 is divided into three sections. Section "A" is a list of the resin tests, Section "B" a list of sheet tests, and Section "C" is a list of seam tests. All of these properties should be evaluated by the design engineer on a site specific basis. The designer must rank the importance of each property and select a set of minimum criteria for the candidate geomembrane.

It is important that each roll of geomembrane sheet is identified with sufficient information. The following identification, after Schmidt [8], is

Table 1 - Typical Properties of 80 mil HDPE Geomembrane

Property (units)	Testing Frequency (1)	Test Method	Typical Min/Max Values
(a) Resin Tests			
Density, excluding carbon black (g/cc)	every other roll	ASTM D1505 Density ASTM D792, Method A-1	0.93
Melt Index (g/10 min)	one per lot or batch (railcar)	ASTM D1238, condition 190/2.16 kg	0.2
Carbon Black Content (%)	every other roll	ASTM D1603	2.00-2.50
Carbon Black Dispersion (Grade)	every other roll	ASTM D3015	(2)
(b) Sheet Tests			
Thickness (mils)	each roll	ASTM D751	2 mm (\pm 0.2 mm)
Minimum Tensile Properties, each direction	as per ASTM D4354	ASTM D638, type IV, dumb-bell @ 2 ipm	
1. Tensile Stress @ Yield (MPa)		ASTM D638, speed 4	15
2. Tensile Stress @ Break (MPa)	test in each		21
3. Elongation @ Yield (%)	principal sheet		10
4. Elongation @ Break (%)	direction		600
5. Modulus of Elasticity (MPa)		ASTM D882	621
Tear Resistance Initiation (N)	as per ASTM D4354	ASTM D1004, die C	67
Brittleness Temperature (°C)	one per lot	ASTM D746, procedure B	-40°C no break
Volatile Loss (%)	one per lot	ASTM D1203, Method A	0.1
Dimensional Stability, each direction (% change maximum)	one per lot (not required for caps)	ASTM D1204, 212°F, 1 hr	+/- 2
Environmental Stress Crack (minimum hours)	one per lot	ASTM D1693, Condition C	0 failures @ 1000 hrs
Impact Resistance (J)	five per lot	Proposed ASTM	95

Table 1 - Typical Properties of 80 mil HDPE Geomembrane (continued)

(b) Sheet Tests (continued)			
Water Absorption (% Weight change/4 days)	one per lot	ASTM D570	0.1 max
Moisture Content (%)	one per lot	ASTM D570	< 0.1
Low Temperature Brittleness (°C)	five per lot	ASTM D746 Procedure B	- 75
Puncture Resistance (N)	five per lot	ASTM D4833	1,300
Ozone Resistance	one per lot	ASTM D1149 7 days 100 mPa, 40°C Magnification	No cracks 7 x
Moisture Vapor Transmission (gm/m ² · day)	one per lot	ASTM E96	0.02
Thermal Stability Oxidative Induction Time (OIT) (minutes, minimum)	one per lot	ASTM D3895 130°C, 800 psi O ₂	2000
Chemical Compatibility (%)	one set per lot	EPA 9090	-10
Hyd: --- Resistance (MPa) (Biaxial Test)	as per ASTM D4354	ASTM D751, Method A procedure 1	4.5
Creep Test	one per lot	Proposed ASTM	@ 60% Y stress strain = 10%
Direct Shear Friction	3 points per critical condition site specific		Proposed ASTM
(c) Seam Tests			
Environmental Stress Rupture	five per facility	As per ASTM D2552	No failures 1,000 hrs.
Bonded Seam Strength, Shear (KN/m)	start-up welds and random samples	ASTM D3083	30
Bonded Seam Strength, Peel (KN/m)	start-up welds and random samples	ASTM D413	24
Peel Adhesion	start-up welds and random samples	ASTM D413	Film Tear Bond
Nondestructive Seam Evaluation			
Ultrasonic Shadow Method	100% of field seams	GRI # GMI-86	All 100% compliance
Pulse Echo Technique		ASTM D4437	" "
Vacuum Box Technique		ASTM D4437	" "
Pressure Testing Technique		NSC Test	" "
Air Lance Technique		ASTM D443	" "

**Geosynthetics '89 Conference
San Diego, USA**

recommended for each roll; name of manufacturer/ fabricator, product type, product thickness, manufacturers batch code, date of manufacture, physical dimensions (i.e. length and width), panel number per design layout pattern, and direction for unrolling panel.

It has been stated by many, that the overall integrity of the facility lies in the quality of the field seams. By far, this factor is the weak link in most projects and should be scrutinized closely. The most important factor in good seaming is compatibility between the sheet material and the seaming technique (or material). There exists a window in which a good seam can occur. It is the job of the installer to find this window and stay within its boundaries.

HDPE sheet may be joined by one of five methods. Each method is listed in Table 2. The table indicates the seam types, typical joining systems used to make the seams and typical cross section configurations of the seams produced by their respective methods. Each installer has the option of using any of the seaming methods listed in Table 2. It is the responsibility initially of the designer and of the CQA inspector during installation to check the integrity of the seam and conclude that it will perform adequately.

Field quality assurance testing of geomembranes involves both destructive and nondestructive testing of the seams made in the field. Destructive testing of the field seams is done on a periodic basis whereas nondestructive testing is performed on 100% of the seams. Destructive test samples are of two varieties. The first is called a start-up seam. It is not a seam to be used at the actual facility, rather it is a seam which is prepared on a scrap piece of geomembrane specifically for checking if the installers procedure is correct. The frequency of these start-up tests is typically at the beginning of each shift or whenever the welder is turned off and then put back into service. Destructive testing of the actual FML seam occurs every 150 to 300 meters of seam and on a judgemental basis if the seam is suspect in any way.

Currently there are two types of mechanical tests performed on specimens cut from a field seam. The actions of shear and peel tests are shown in Figure 4. Conventional acceptance criteria states that the seam strength in shear should equal that of the parent material [9]. Through past experience, it is believed that a reasonable criteria for a passing peel test is the witnessing of a film tear bond (FTB) and a strength of 80% of the parent material. The general consensus is that the shear test reveals the strength of the parent material, while the peel test is a good indicator of the strength of the seam.

As for nondestructive tests, Table 3 yields an overview of testing methods available to the third party CQA personnel.[1] It should be noted that 100% of the facility must be tested via one of these nondestructive tests.

Prior to embarking on a project, it is important to make a decision on response to noncompliance of test data. Outliers are not uncommon. Problem areas are remedied by one of three methods. The three methods are a) to patch, ("cap strip") b) to grind and reweld, c) or to cut out the seam, slide the two sheets together and then reweld. Cutting out and then patching imperfections is felt to be the best remedial solution. Grinding and rewelding is not recommended for many installations.

Table 2 - Field Seaming Technique for HDPE Geomembranes

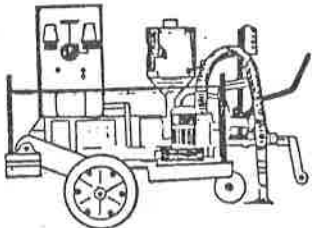
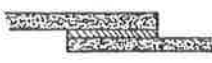
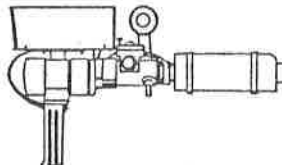


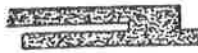
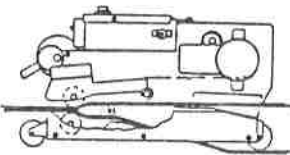


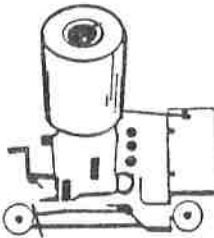

Seaming Technique	Equipment Used	Configuration of Seam	Speed	Comments
FLAT EXTRUSION			150 m/Hr	<ul style="list-style-type: none"> - Good on long flat surfaces - Highly automated machine - Difficult for side slopes - Cannot be used for close details - Pellet fed
FILLET EXTRUSION			30 m/Hr	<ul style="list-style-type: none"> - Upper and lower sheets must be roughened - Upper sheet must be beveled - Height and location of bead important to seam quality - Can be rod or pellet fed - May be equipped with an air heater/blower to preheat the sheet - Routinely used for difficult details
HOT AIR			150 m/Hr	<ul style="list-style-type: none"> - For HDPE, used only to tack weld - Hand held and automated devices are available - Air temperature fluctuates greatly - No extrudate added
HOT WEDGE		 	100 m/Hr	<ul style="list-style-type: none"> - Single and double track devices are available (Double track device patented) - Built in nondestructive test - Cannot be used for detailing - Temperature control is critical - No extrudate added - Consistency of "squeeze out" is a good indication of seam quality
ULTRASONIC			100 m/Hr	<ul style="list-style-type: none"> - New Technique for geomembranes - Sparse experience in the field - Capable of full automation - No extrudate added

Table 3 - Overview of Nondestructive Geomembrane Seam Tests
after Koerner and Richardson (1987)

Nondestructive Test Method	Primary User			General Comments					
	Contractor	Design Engineer Inspector	Third Party Inspector	Cost of Equipment	Speed of Tests	Cost of Tests	Type of Result	Recording Method	Operator Dependency
1. air lance	yes	-	-	\$200	fast	nil	yes-no	manual	v. high
2. mechanical point (pick) stress	yes	-	-	nil	fast	nil	yes-no	manual	v. high
3. vacuum chamber (negative pressure)	yes	yes	-	\$1,000	slow	v. high	yes-no	manual	high
4. dual seam (positive pressure)	yes	yes	-	\$200	fast	mod.	yes-no	manual	low
5. ultrasonic pulse echo	-	yes	yes	\$5,000	mod.	high	yes-no	automatic	moderate
6. ultrasonic impedance	-	yes	yes	\$7,000	mod.	high	qualitative	automatic	unknown
7. ultrasonic shadow	-	yes	yes	\$5,000	mod.	high	qualitative	automatic	low

(c) Documentation

Prior to geomembrane shipment, a set of field drawings showing the geomembrane panel layout should be submitted to the design engineer by the installation contractor. The layout plan should indicate the location of all field seams and details of all geomembrane anchorages. In the same vein, an as-built set of plans should be submitted after the project has been completed. A daily field record shall be maintained by the CQA team of the actual placement of each panel, noting the condition of the subgrade, weather, welding parameters, and the locations of the specimens taken for testing.

The most comprehensive part of the final CQA/CQC report is the section containing the test results. All results for the resin, sheet, subgrade and seams must be presented. It goes without saying that all results should meet or exceed the target values of the specification.

The final section of the CQC document is the warranty. Basically it should state that the geomembrane contractor shall guarantee the integrity of the installed geomembrane for its intended use against material or installation defects. The warranty should provide for the total and complete repair and/or replacement of any defects or defective areas of the installation.

SOME POTENTIAL PROBLEMS

The ability of a geomembrane to resist puncture and tear during installation and operation is dependent on the subgrade on which it is placed. Puncture of the liner generally occurs in an unseen manner when full weight of the landfill is placed above it. It is most prone to happen from sharp object located in the upper portion of the subgrade. This can occur in a proof-rolled subgrade by sliding the liner panels into position for seaming and thereby roughening the subgrade. It can be shown in biaxial tests that even small scratches or imperfections significantly reduce the mechanical characteristics of HDPE. Therefore the subgrade must be free of all sharp objects, and the geomembrane must be handled carefully.

Rain causes problems during installation. All surface water runoff must be kept away from unseamed areas and from beneath the geomembranes. This can be accomplished by shingling the panels such that they overlap from high elevations to low elevations. Placing the panels in this manner involves additional work since each lower sheet must be tucked under the upper sheet. However, the long term benefits are often substantial. Any water found beneath the geomembrane must be removed and the affected underlying subgrade (depending on its type) must be replaced or repaired.

Under no circumstances shall vehicular traffic be allowed on the geomembrane. Any material exposed to such conditions should be removed and replaced.

The geomembrane should be installed so as to eliminate "trampolining" at the toe of the slopes. The geomembrane must not bridge abrupt changes in grade at any temperature. Trampolining may be eliminated by seaming at ambient temperatures between 5 and 20°C. If above 20°C, adequate slack must be left in the panels to accomodate shrinkage during cooler temperature periods.

**Geosynthetics '89 Conference
San Diego, USA**

Environmental Stress Cracking (ESC) is a phenomenon that has been identified by the gas-pipe, geomembrane and other industries using high density polyethylene in engineering applications. ESC is a brittle-type crack growth that results in material rupture at a tensile stress less than the short term tensile strength. For geomembranes, ESC may initiate at surface notches along seams and propagate through the material due to stress cycling from, for instance, daily changes in ambient temperatures. In general, excessive grinding, abrasion or overheating of the geomembrane during installation must be avoided to assure long term performance.

Geomembranes are typically shipped to the job site in rolls on flat bed trucks. HDPE should never be folded under any condition. If it arrives on site folded in any way, it is not acceptable. The best method to unload rolls is with canvas slings wrapped around the rolls or with inserts placed within the internal core. Any time that the rolls are slid or dragged invites problems. If there are signs of abrasions and scuffs it is not uncommon to request that the contractor discard the first few raps of the roll. This will insure that the sheet is of first quality.

Rolls of geomembrane must be stored off the ground and in a secure area that protects the panels from damage by man or animals, or contamination by dirt, dust or water.

Unrolling the sheet requires considerable effort. After the sheet has been deployed it is clamped (typically with wide mouth Vice-Grips® or sheet metal clamps) and maneuvered into final position. The labor force used to position the panels are typically hired on a local basis. In most cases they have never seen a HDPE liner. They have no respect for it and treat it as if it were steel. With such a large inexperienced work force, the inspector must constantly watch for dropped tools, scuff marks from shoes (it is a good idea to suggest the wearing of sneakers), trash, and accidental liquid spills. It is best to keep people off the liner after it has been deployed and seamed.

As the panels are being deployed and subsequently seamed, it is important to weigh them down so they do not blow away in the wind. Sand bags (recommended) or tires are typically utilized for this purpose. Sand bags may cause problems because they often are filled with gravel and not sand. When the bags rip open, the gravel must be swept off the geomembrane to insure that it does not puncture it in the future. Tire may fill with water over time which may interfere with the seaming process.

From Table 2 it is obvious that there are many options available for field seaming HDPE geomembranes. The best way to find out the idiosyncrasies of each technique is to experience welding first hand. It is surprising how receptive the installation personnel are to letting the inspectors operate the equipment on a test strip. The following items will then become apparent:

- adjusting the temperature and speed setting is a delicate balance,
- assuring that the area to be welded is clean and dry is necessary,
- assuming and maintaining proper positioning on the seam for the entire length of the weld run is difficult, and
- never force the welding machine to go faster than its predetermined and acceptable speed

Particular care must be taken when forming connections or detailing. Areas such as sumps, weirs, inlet and outlet pipes are often difficult to seal due to their complexity. It is very important that the CQA inspector closely monitors these areas because they are often prone to problems.

SUMMARY AND CONCLUSIONS

This paper has briefly presented many aspects of the HDPE installation. We have investigated the production of HDPE geomembrane from resin and focused in on its inevitable deployment in a facility. In conclusion it must be mentioned that the success of any given installation depends primarily on the installing personnel. Installers generally follows applicable industry recommendations. Typically, considerable effort is made on the part of all parties to cooperate and produce a successful end product. However, the severity and complexity of these installations must not be overlooked. It is imperative that everyone involved tolerates nothing less than perfection.

REFERENCES

1. Richardson, G. N. and R. M. Koerner (1986), "Geosynthetic Design Guidance for Hazardous Waste Landfill Cells and Surface Impoundments," EPA Contract No. 68-03-3338.
2. Koerner, R. M. (1988), "An Overview of Geomembranes in North America," RILEM Committee TC-107, Montreal, Canada.
3. Koerner, R. M. (1986), Designing with Geosynthetics, Prentice-Hall, Inc., Englewood Cliffs, NJ.
4. Haxo, H. E. (1983), "Analysis and Fingerprinting of Unexposed and Exposed Polymeric Membrane Liners," Proc. 9th Annual Research Symposium, Land Disposal of Hazardous Waste, EPA-600/9-83-018.
5. Giroud, J. P. and J. E. Fluet, Jr. (1985), "Quality Assurance of Geomembrane Lined Containment Facilities," Jour. of Geot tiles and Geomembranes.
6. Herrmann, J. G. (1986), "Construction Quality Assurance for Hazardous Waste Land Disposal Facilities," EPA Technical Guidance Document OSWER Report No. EPA/530-SW-86-031.
7. Cadwallader, M. W. (1986), "Chemical Compatibility Considerations for HDPE Liners in Waste Containment," American Institute of Chemical Engineers National Meeting, Boston, MA.
8. Schmidt, R. K. (1983), "Specifications and Construction Methods for Flexible Membrane Liners in Hazardous Waste Containment," Technical Report no. 102, Gundle Lining Systems, Inc., Houston, TX.
9. Peggs, I. D. and D. Little (1985), "The Effectiveness of Peel and Shear Tests in Evaluating HDPE Geomembrane Seams," Second Canadian Symposium on Geotextiles and Geomembranes, Edmonton, Alberta.
10. Birley, A. E., et al. (1988), Plastics Materials Properties and Applications, 2nd Edition, Chapman and Hall, New York, NY.

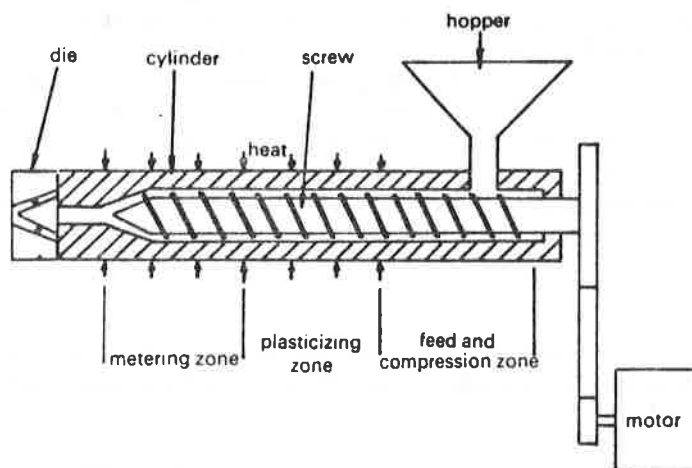


Figure 1. Flat Mouth Extruder [10]

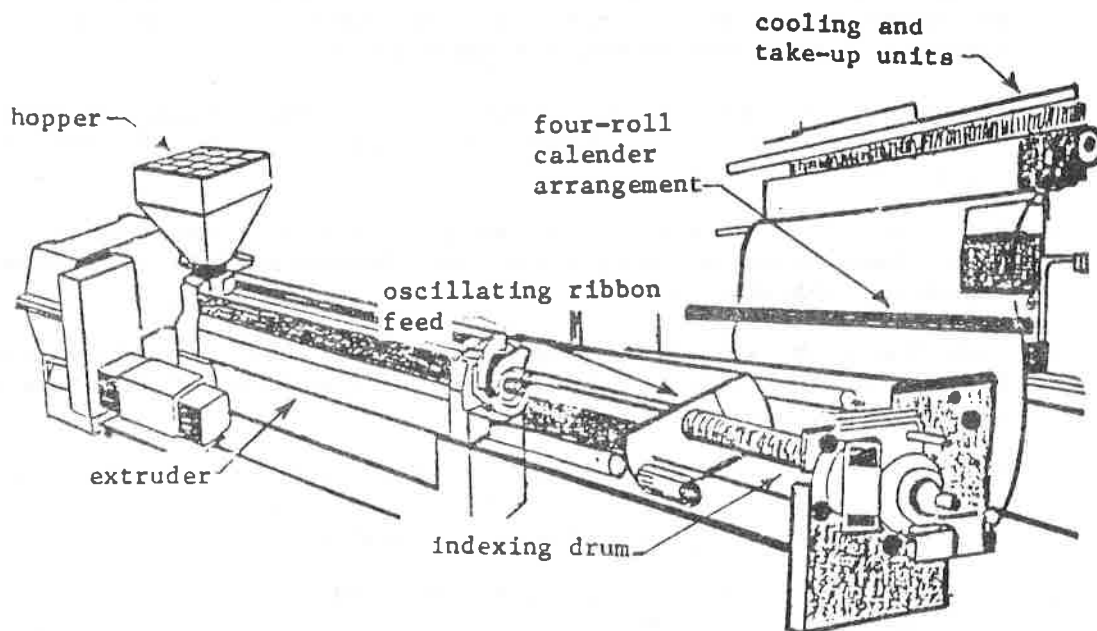


Figure 2. Extruder, Ribbon Spreader, and Take-up Roll

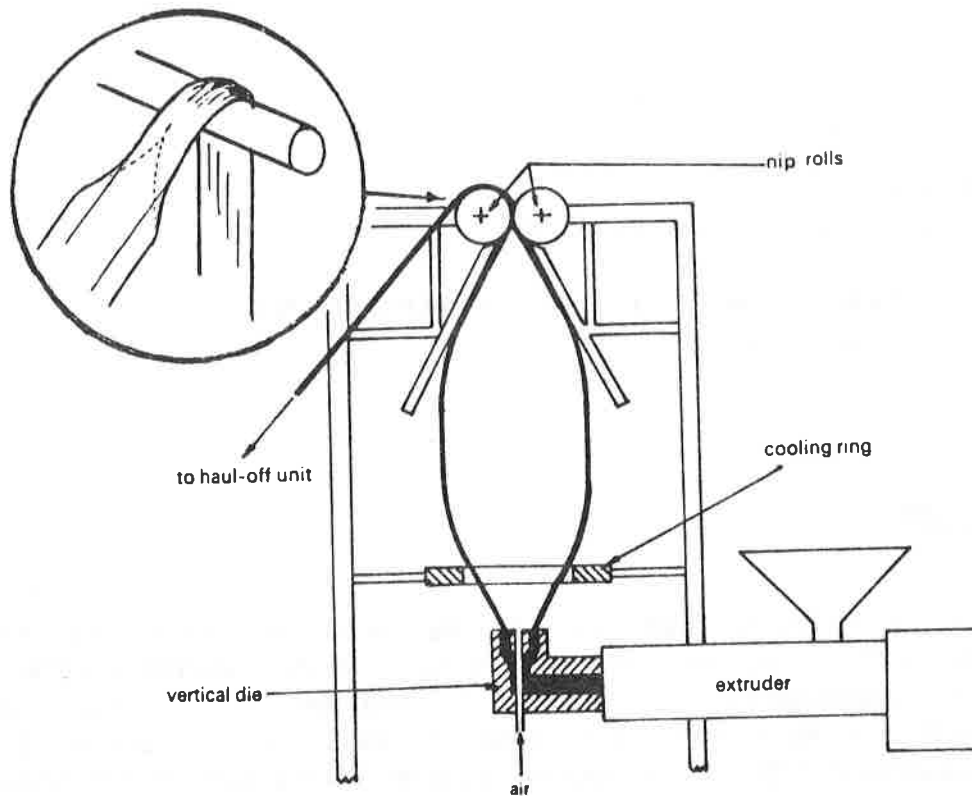


Figure 3. Blown Film Process [10]

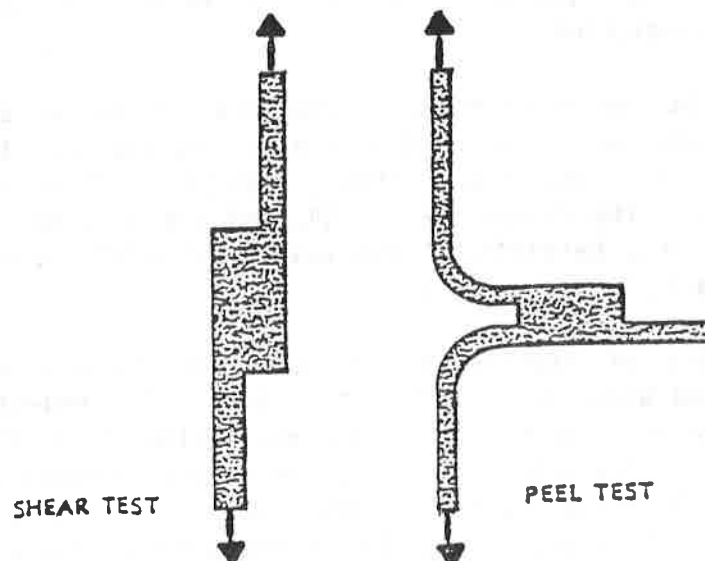


Figure 4. Peel and Shear Seam Strength Tests

R.B. WALLACE

GeoServices Inc., Consulting Engineers, U.S.A.

**The Benefits of Construction Quality Assurance of Lining Systems
Installation: Real or Perceived?**

INTRODUCTION

Four years have now elapsed since the Resource Conservation and Recovery Act (RCRA) was modified by the Hazardous and Solid Waste Amendments (HSWA) [1]. One particular consequence of that legislation was the introduction of the requirement for much more formalized and detailed programs of Construction Quality Assurance (CQA) of the installation of lining systems for hazardous waste disposal facilities than had previously existed. Many private operators of non-hazardous waste and other storage facilities have electively mandated comprehensive CQA programs for their new facilities as well. There is also now an increasing trend in State Environmental Regulatory Agencies toward the requirement for the provision of CQA of the construction of facilities permitted under their jurisdiction.

CQA has now become a permanent component of installation operations for geosynthetic and geosynthetic/soil lining systems for a growing variety of project types. Much has been written on CQA [2,3,4,5] with particular regard to the need for CQA, the components of CQA, and the "how to" of CQA. In addition, for four years the benefits of CQA have been avidly touted in publications, courses, seminars, and other fora.

With four years of experience providing CQA in accordance with the RCRA regulations, and under less stringent criteria for non-hazardous sites, it is appropriate now to conduct an objective evaluation of the CQA programs, and look at the benefits. Are they real, or do we simply perceive or presume that there are benefits? It is my belief that these benefits are very real, and in fact we can try to quantify them, through the examination of the consequences of a poor installation. This paper investigates these questions, and provides at least partial answers, based on the experiences of the writer's firm, during the provision of CQA services for over 7 000 000 m² (75,000,000 ft²) of geosynthetics in lining systems.

PURPOSE

The writer has been responsible for almost fifty CQA programs conducted to standards equivalent to those required by the HSWA. Based on this experience, it is possible to examine the circumstances and provisions of these CQA programs, and make some observations related to the benefits which were derived from them.

First, it is necessary to identify the potential benefits of a CQA program for the installation of a geosynthetic lining system. These benefits can be shown to include:

- higher quality construction;
- fewer problems during and subsequent to construction;
- facilitated investigation and remediation of problems that do occur after commencement of operations;
- potential lower cost; and
- better protection of human health and the environment.

The cost of a CQA program is relatively modest (typically 10 to 15 per cent of the cost of the lining system) compared to the costs of post-construction repairs, delays in permitting or commencement of operations, or future litigation. Nevertheless, the benefits of CQA can be seen to be much greater than their costs, even if all they provide is a higher confidence level that the incidence of future problems will be reduced.

THE BENEFITS OF CQA

The benefits of CQA are real, although they can be both tangible and intangible. The benefit of finding a major flaw when it can be easily repaired may, in addition, be quantifiable relative to the cost that would have been incurred after the fact.

The principal benefit of a thoroughly documented CQA program is that the quality of construction is generally superior to that of an installation constructed without third party CQA. One of the objectives of the program is to ensure that the systems are installed in a manner that meets the design criteria and assumptions. If the facility has been designed with the assumption that it will perform within the design requirements if properly constructed, then it is a

purpose of the CQA program to ensure that this occurs. It is impossible to say with certainty whether a given flaw or damaged location requiring repair that was detected by the CQA personnel would not have otherwise been detected and repaired. Based on the experience gained from over fifty CQA programs, however, it seems that it can be positively stated that flaws or damage will always be detected by knowledgeable CQA, over and above those detected by the installer. No system is truly fail-safe, but it should follow that a more secure system will result in this case.

Another benefit of CQA is the incidence of fewer problems during construction. Qualified CQA personnel, familiar with the requirements for the successful installation of geosynthetic components of lining systems are involved, can frequently spot potential problems which have otherwise gone undetected, and inform the installer in advance of their becoming real problems.

The incidence of problems can also be decreased due to human nature, in that the mere presence of the CQA monitoring personnel will often tend to draw a greater degree of diligence and attention to detail in the installer's on-site personnel. The degree of care and attention is further developed when the CQA monitors are seen to be knowledgeable in their duties. If the CQA monitors are not totally familiar with the various installation activities and the recognition of problems, the process can break down. In those cases, even poor workmanship may not be detectable.

The incidence of problems after construction is much more critical, in that the flaws or damage that are encountered during the construction program can be relatively easily fixed. Once the cover materials have been placed over the lining system and operations have been under way for some time, the cost and physical effort required to correct a problem can be overwhelming.

A remedial investigation of problems (e.g., detected leakage in excessive quantities) can be facilitated due to a well documented, thorough program of CQA providing the complete knowledge of the locations of all seams, repairs, and any problems that may have occurred during the installation. If, therefore, it is necessary to exhume an area after completion due to a detected leak, a detailed knowledge of the seaming, testing, and repair history of that location can allow easy cross-checking of the related areas prepared in the same manner. In the absence of these data, the remedial measures cannot easily be extrapolated to similar areas, and either wholesale excavation becomes necessary, or the assumption that the only leak has been detected may be made, which will seldom be the case.

The quality assurance of any product has a price, whether it be a manufacturing operation, production process, or construction of a waste disposal facility. In manufacturing, for example, the cost of this quality assurance is normally determined through statistical and risk analyses, whereby the cost of the service

can be optimized by comparison with the cost of waste and the incidence of flawed products. In such a case, the penalty for doing too little QA can be monetary loss only. In the case of a regulated waste disposal facility, the consequences are not only much more severe, but are usually not identified until later, at which point the cost of remediation is considerably higher. A CQA program for a double liner system, including leachate collection and removal (LCRS) and leakage detection, collection, and removal (LDCRS) systems will cost between 8 and 20 per cent of the cost of the entire system, varying from project to project for a variety of reasons (nature of the facility, degree of regulatory control, etc.).

Public Law 98-616, known as the Hazardous and Solid Waste Amendments of 1984, had as its stated objective, that it shall be "the national policy of the United States" to reduce or eliminate hazardous wastes, but in any event, for wastes that are generated, "to minimize the present and future threat to human health and the environment" [6]. Any program which shares this objective is a worthwhile venture. By virtue of the stated benefits of a CQA program outlined above and elsewhere, any actions taken by designers, owners, operators, and constructors of waste facilities in support of this policy are directed to the public good.

FAILURES IN THE ABSENCE OF A CQA PROGRAM

The writer and his colleagues have had the opportunity of investigating a wide variety of failures involving lining systems. These failures have ranged from the detection of higher than expected levels of leakage through the upper liner, to total lack of containment and escape of the leachate or impounded materials to the adjacent environment.

An overwhelming majority of the failures that have been investigated were of facilities for which no proper program of CQA was incorporated into the installation. By the use of the word "proper", it is intended that a complete, thorough program of CQA shall consist of both the monitoring of all of the critical activities of the installer (e.g., seaming, nondestructive testing), as well as the detailed documentation of those activities. A "proper" CQA program must, therefore, incorporate both of these basic components of CQA. Very often, while investigating failures or problems with lining systems, we have been assured by the owner that a very comprehensive CQA program was included. Unfortunately, in most cases of this type, there was no documentation of the installation. The value of the CQA program was therefore negligible, because the information that would have been of assistance was not available when it was needed.

In general, most failures of lining systems and/or associated drainage and leak detection systems which have been investigated are attributable to either poor

design or poor construction. The former could be mitigated in many cases by the provision of design peer review, either internally, or preferably by a "peer" consultant experienced in that area. This clearly represents a form of the quality assurance of design not dissimilar to CQA. It appears to be a difficult decision on the part of a designer, however, as seeking out-of-house peer review can be viewed as being tantamount to an admission of a lack of confidence or uncertainty in the design. On the other hand, if design peer review was standard practice, there almost certainly would be fewer failures. It may be that in the future such design reviews could be commissioned by the owners to provide their another form of quality assurance.

Poor construction practice as a cause of failures should not exist if there were a CQA program. Nevertheless, even when CQA programs have been conducted, there have been failures. In the majority of cases, review of the CQA documentation during the remedial investigation revealed either that this documentation was deficient, or in some cases that it was non-existent. No program of CQA is absolute, however. Sometimes, circumstances are such that not every activity of the installer can be fully monitored and documented, and in those cases, the CQA personnel can only verify that the methods and procedures generally conformed to the plans, specifications, and good construction practice. In those cases, individual activities can only be monitored within the constraints of the number of CQA personnel. That is usually sufficient to determine the degree of care and workmanship being exhibited by the installer.

In at least two programs with which the writer is familiar, problems were detected after commencement of operations, for a project on which a good program of CQA had been applied. The detailed construction monitoring records greatly facilitated the remedial measures, and in fact in one case allowed no interruption in operations, a paramount consideration on the part of the facility owner or operator, due to the significant monetary consequences of shutdowns of any duration. The locations and reasons for the leaks were very quickly determined (in both cases, leaks occurred in corner seam locations which could not, and therefore had not been nondestructively tested during installation). The review of the CQA documentation allowed the engineer to determine that fact, and allowed the repairs to be expedited without delays. It also allowed the owner to remain confident in the integrity of the system, due to the good results obtained in the remainder of the facility, which had undergone complete testing and surveillance.

Other situations have arisen in which we have been able to review the installation of lining systems on non-regulated facilities for which no CQA program was required or provided. Occasional visits have allowed us to observe instances of accumulated potential problems which would normally be detected in a CQA program. These include severe bridging at the toe of slopes, which could result in overstressing or rupture of the geomembrane upon loading, or to long

term distress due to the formation of localized crazes or cracks at the stress concentration locations. Similarly, the lack of trial seams to determine the quality of the seaming equipment settings in a given shift or on a given day can allow the installation of large quantities of production seams, which may not be sampled and destructively tested. (It should be noted that nondestructive test methods (i.e., vacuum testing, pressure testing, and spark testing) are totally qualitative tests of the seam continuity - they do not provide any indication of the strength of the seam, which must be determined by destructive testing.) Inadequate seams in these areas could go undetected. This could be one of the greatest contributors to seam failures in facilities constructed without a CQA program.

In general, a high quality CQA program is the best insurance that a facility operator can invest in, with regard to obtaining a high confidence level in the quality of the system. This is true for any lining system, whether prepared for a RCRA-regulated facility or not. If the objective of any system is containment, a CQA program will be beneficial in assuring the highest quality containment possible for that design.

QUANTIFYING THE BENEFITS OF CQA

It is difficult to quantify the benefits of a CQA program, because it is impossible to say that a flaw or failure encountered after the start of operations would have been intercepted if a CQA program had been provided. Similarly, we cannot say that there will be no failures if CQA is provided. We do, however, know that the overwhelming majority of flaws or damage in a lining system will be detected and repaired while installation is still ongoing, if a high quality CQA program is provided. The cost of the repair of a hole during installation is infinitesimal compared to the cost of repair after start of operations. After this startup, there are costs associated with the specific mobilization of the repair crew, the cost of shutdown if necessary, and the significant cost of lost revenue in the case of a revenue-producing facility, such as a landfill.

In 1986, an attempt was made by the writer's firm to quantify the non-monetary benefit of CQA by conducting an evaluation of the proportion of repairs required that were identified by the CQA personnel rather than the installer. To do so, the CQA monitoring staff waited until after the contractor had completed an area, including the marking of any flaws, defects, damage, or inadequate seams, before they proceeded with their walkover evaluation.

The results are presented in Table 1. Acceptance of these data without qualification, however, would be misrepresentative. Although the CQA personnel waited until after the installer had walked the area, having identified many

TABLE 1 PROPORTION OF REPAIRS IDENTIFIED BY CQA ON AN HDPE GEOMEMBRANE							
	NUMBER OF PANELS	AREA	NUMBER OF REPAIRS			NUMBER OF REPAIRS IDENTIFIED BY CQA	CQA PROPORTION
			EXTRUSION	PATCH	TOTAL		
PANEL REPAIRS	112	593,000 S.F.	98	58	156	116	74.4 %
	TOTAL SEAM LENGTH	TOTAL REPAIRS	NUMBER OF REPAIRS IDENTIFIED BY CQA			CQA PROPORTION	
SEAM REPAIRS	26,833 FT.	696	229			32.9 %	
PROPORTION OF ALL REPAIRS DETECTED BY CQA = 40.5 %							

locations requiring repair and making those repairs, it is not fair to say that all of those locations subsequently marked by CQA would not eventually have been detected prior to turnover. As a result, in the absence of CQA, we can assume that perhaps as much as 50 per cent of the additional locations would eventually have been repaired. Even so, that would still leave in the order of 150 to 170 locations which were determined by CQA to require repair of some form that would not have been remedied. If only ten per cent of those resulted in leaks, that is 15 to 17 leaks. The design of leak detection systems normally presumes in the order of three to four "holes" per acre, which can represent leaks [7], or for this site, about 50 total holes, even assuming high quality CQA. These 15 to 17 estimated additional flaws would therefore result in 30 per cent more "holes" than assumed for the design of a leak detection system. In this specific example, the system was only a single liner, and so expected containment loss would have been at least 30 per cent higher if the CQA was not provided, and that is giving the installer credit for returning to a given area and finding many more repairs than on the initial examination.

This example in no way constitutes anything approaching data on which other than very basic conclusions can be drawn. Circumstances have not allowed us to repeat this test on other projects with the same confidence in our control conditions.

In general, however, it is our practice to allow the installer to mark locations for repair in advance of the CQA personnel. In those cases, it is our observation that anywhere from 30 per cent to 70 per cent of the total repair locations are noted by the CQA personnel. This does consistently show, however, that there are a significant number of repairs detected by the CQA personnel on every project, over and above those detected by the installer.

It is understandable that CQA personnel would find additional needed repairs. This is at least in part due to the role emphasis of the CQA personnel (i.e., to ensure conformance with the plans and specifications, and to look for potential problems) versus the role emphasis of the installer's personnel (i.e., to place, seam, and test the geomembrane). The focus of the installer's attention to geomembrane seams is shown from the data on Table 1, in that almost 70 per cent of the repairs required on seams were identified by the installer, as opposed to 25 per cent of the panel repairs.

In general, therefore, it is possible to make the claim with reasonable certainty that a much higher proportion of all potential flaws and damage to the geomembrane will be detected and repaired when a CQA program is provided than if not. The example shows one particular situation in which some quantification of the benefit is possible, although this cannot reliably be extrapolated to monetary terms. It is believed that this does demonstrate that tangible benefits exist for the provision of CQA.

CONCLUSIONS

The performance of a program of CQA during the installation of geosynthetic lining systems would not be justifiable unless there was some perceived benefit. In most cases, this perceived benefit is a better job: fewer repairs required due to better workmanship; repair of flaws or damage that may otherwise have gone undetected; reduced incidence of post-construction repairs; and, implicitly, reduced leakage through the primary liner to the LDCRS.

At least some of these perceived benefits are real. The experience with the provision of CQA services for over 7 million square meters (75 million square feet) of geosynthetics, on which this paper is based, shows that at least, higher quality construction is obtained. All factors in a project interrelate, however. Good CQA programs cannot mitigate poor design, and a large number of failures that have occurred have still been attributable to poor design. Each of the components of a project must be optimized, in order to attain the design objectives of safety and containment.

REFERENCES

1. Public Law 98-616 - November 8, 1984.
2. Giroud, J.P. and Fluet, J.E., Jr., "Quality Assurance of Geosynthetic Lining Systems", Geotextiles and Geomembranes, Vol. 3, No. 4, 1986, pp. 249 - 286.
3. Fluet, J.E., Jr., "Geosynthetic Lining Systems and Quality Assurance - State of Practice and State of the Art", Geosynthetics '87, Vol. 2, New Orleans, Feb 1987, pp. 530-541.
4. Wallace, R.B. and Steinle, E.R., "Construction Quality Assurance of Geosynthetics Installations", 40th Canadian Geotechnical Conference, Regina, Oct 1987, pp. 365-373.
5. Wallace, R.B., "Construction Quality Assurance of Lining System Installations", Geotechnical News, March, 1988.
6. Public Law 98-616 - November 8, 1984, Sec. 101,b,1.
7. USEPA, "Background Document: Proposed Liner and Leak Detection Rule", EPA/530-SW-87-015, Prepared by GeoServices Inc., May 1987, 526 p.

Figures: In general, as many of the CQA operations as possible should be monitored and documented. These include: deployment; measurement of critical dimensions; grinding and seaming; nondestructive testing; and sampling for destructive testing.



Figure 1: deployment



Figure 2: measurement of anchor
trench dimensions

Figure 3: measurement of material
overlap

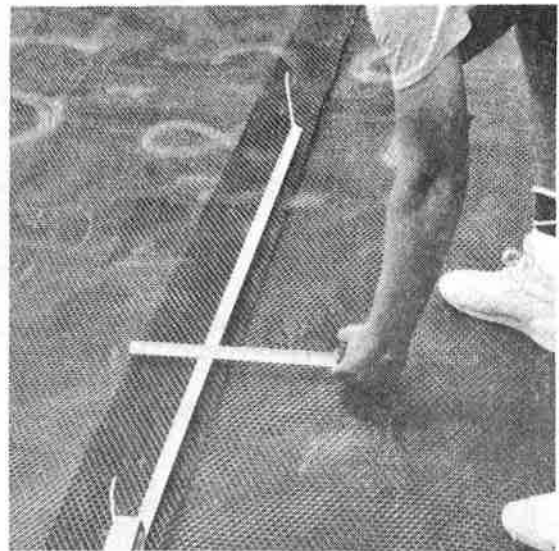


Figure 4: measurement of geomembrane
thickness

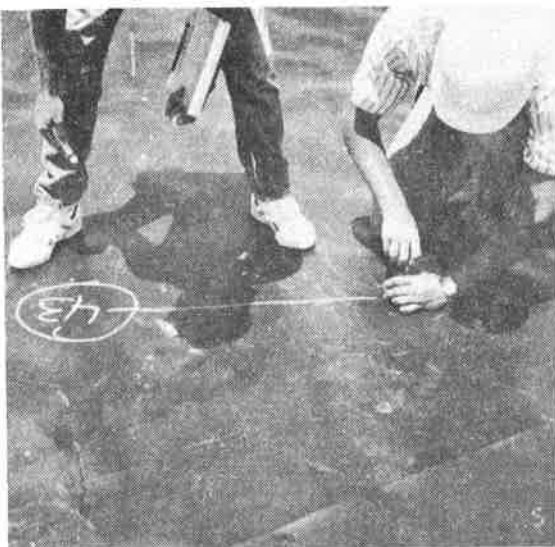




Figure 5: grinding and seaming



Figure 6: nondestructive testing



Figure 7: sampling for destructive
testing

SESSIONS 3A & 2B
DRAINAGE & WALLS



S.M. LUETTICH

N.D. WILLIAMS

GeoServices Inc., Consulting Engineers, U.S.A.

Design Of Vertical Drains Using The Hydraulic Conductivity Ratio Analysis

ABSTRACT

Subsurface drainage systems in civil engineering structures are often constructed using geotextile filters. This paper introduces the Hydraulic Conductivity Ratio (HCR) analysis as a method of evaluating geotextile filter performance in this application, and the HCR test as a means of quantitatively measuring impedance of flow across the filter. A step-by-step procedure is presented which addresses the design of geotextile filters in vertical drainage systems using the HCR analysis.

1. INTRODUCTION

Geotextiles are widely used in subsurface drains in conjunction with conventional sand and gravel drainage media and synthetic drainage products. A properly designed geotextile serves two primary functions in the drainage system: (i) the geotextile retains fine-grained soil particles; and (ii) the geotextile promotes development of a filter layer within the adjacent soil which, in turn, serves as the long-term filter for the drainage system.

When fine-grained soils are placed against a geotextile and a hydraulic gradient is applied across the soil/geotextile interface, a large velocity gradient may develop. As water exits from the soil into the free draining geotextile, the velocity of the water increases, often causing soil particles at the soil/geotextile interface to dislodge and move with the flow. Movement of soil particles adjacent to the geotextile filter can manifest itself in one of three ways.

- *Piping.* Small soil particles may migrate through the geotextile into the drainage media. A small amount of piping may be desirable to form a stabilized filter layer adjacent to the geotextile. Continued piping of silt and clay particles, however, is undesirable since excessive loss of fines through the geotextile filter may result in instability of the adjacent soil, may create preferential flow paths which could lead to the formation of large voids in the soil, or may result in the accumulation of fines in other components of the drainage system causing a reduction in flow capacity. For the purpose of this paper, piping will refer to continuous loss of fine-grained soil particles through the geotextile.

- *Clogging.* Small and intermediate soil particles may become entrapped physically or electrostatically within the fibers of the geotextile. When a sufficient number of soil particles become entrapped in the geotextile to impede flow from the soil into the drainage media, the geotextile becomes clogged and the overall flow capacity of the drainage system is diminished.
- *Blinding.* A transitional filter may develop in the soil at the soil/geotextile interface. The transitional filter, or filter layer, develops from successive filtration of fine-grained soil particles along the side of the geotextile exposed to the soil [Lawson, 1982]. The formation of the filter layer eventually results in a stabilized reduced flow capacity across the soil/geotextile interface. The stabilized flow is usually reduced from the initial flow across the interface when blinding occurs. The magnitude of this reduction, however, is a function of many parameters, including soil particle-size distribution, flow conditions, and field stresses.

In a typical drainage system such as a vertical wall drain, all three types of particle movement may occur simultaneously. Initially, piping often occurs as fine-grained soil particles adjacent to the geotextile migrate through the geotextile and into the drainage system. However, as soil particles are restrained by the geotextile, successive filtration of soil particles occurs, resulting in the formation of a stable filter layer, which causes the piping to stop. As a result, the effluent from a drainage system is typically turbid immediately after placement of the drain. However, within a relatively short period of time, the effluent from the drain should become clear, indicating the filter layer has formed. If the effluent does not become clear, it is an indication that continued piping is occurring through the geotextile.

The reduction in flow across the soil/geotextile interface, resulting from clogging and/or blinding, is often the limiting component of the drainage system. Therefore, the influence of the filter layer must be accommodated in the design process. The influence of the filter layer, and the propensity for blinding and clogging of geotextiles can be measured in a Hydraulic Conductivity Ratio (HCR) test, which is discussed in Section 2. A design method for geotextile filter layers in vertical wall drains which incorporates the HCR analysis is presented and discussed in Section 3. The conclusions are presented in Section 4.

2. THE HCR TEST

The hydraulic conductivity ratio (HCR) test is performed in a triaxial permeability device under conditions designed to simulate field conditions. The soil sample is prepared using standard laboratory or field sampling techniques that are designed to simulate field placement or in-situ conditions. The state of stress, stress history, void ratio, soil structure, and flow conditions in the soil and geotextile are carefully controlled throughout the test. Since the soil sample may be fully saturated and the triaxial permeability device used in the HCR analysis provides control of the flow direction and hydraulic gradient, the primary variables affecting the filtration characteristics and flow properties of geotextile/soil composites are either controlled or measured during the HCR analysis [Abouzakhm, 1986].

The specimen is constructed in the triaxial device such that the soil to be tested is overlain by the candidate geotextile filter, as shown in Figure 1. The hydraulic conductivity of the parent soil, k_s , is initially measured by permeating a relatively small amount (approximately one pore volume) of liquid through the specimen. The flow

during the measurement of k_s is directed from the top of the sample to the bottom (i.e., through the geotextile, then the soil). The flow direction is then reversed such that the permeant flows through the soil first, then across the soil/geotextile interface, and through the geotextile. The hydraulic conductivity of the soil/geotextile composite is defined as k_{sg} . As the permeant flows from the soil across the soil/geotextile interface, soil particles may be dislodged resulting in piping, clogging or blinding. If blinding occurs, the hydraulic conductivity, k_{sg} , typically decreases until an equilibrium condition is achieved. The HCR may then be defined as the ratio of the stabilized value of k_{sg} to the hydraulic conductivity of the soil, k_s .

$$HCR = \frac{k_{sg}}{k_s} \quad (1)$$

Results of the HCR test (i.e., k_s , k_{sg} , and HCR) are typically presented as a function of the flow volume permeated through the specimen. The volume is expressed in terms of pore volumes, PV. One pore volume is equivalent to the volume of voids within the specimen when the HCR test is initiated. Figure 2 shows idealized results of HCR analyses for four different geotextiles against the same soil. The horizontal portion of each curve for flow volumes of less than one PV is the hydraulic conductivity of the soil, k_s . After one pore volume of flow, the flow direction was reversed. The hydraulic conductivity across the soil/geotextile interface, k_{sg} , then decreased as a function of the flow volume for geotextiles A, B, and C, and increased slightly for geotextile D. The HCRs for geotextiles A, B, C, and D in Figure 2 are 0.75, 0.40, 0.10 and 1.0, respectively.

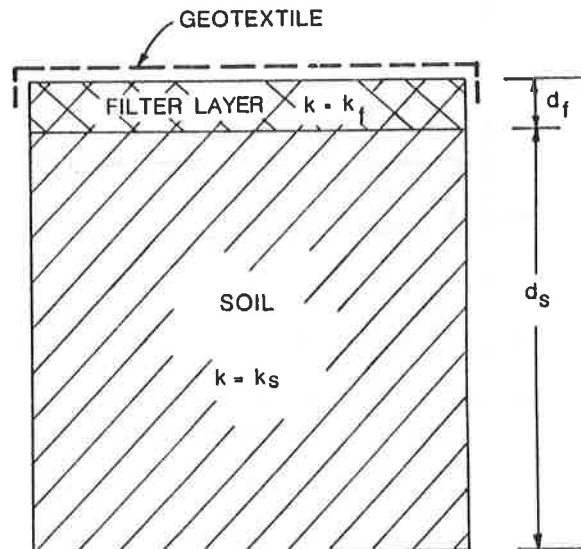


FIGURE 1
HCR TEST SPECIMEN

The quantity of fine-grained soil particles passing through the geotextile into the effluent is observed by visual inspection. If the effluent remains cloudy after more than one or two PVs have passed across the soil/geotextile interface, it is considered that piping is occurring through the geotextile. Piping is often manifest by an increase in HCR with flow volume, and a high HCR value (sometimes greater than 1.0). In general, for soil/geotextile combinations that do not show evidence of piping, higher HCR values indicate greater flow capacities of the filter system.

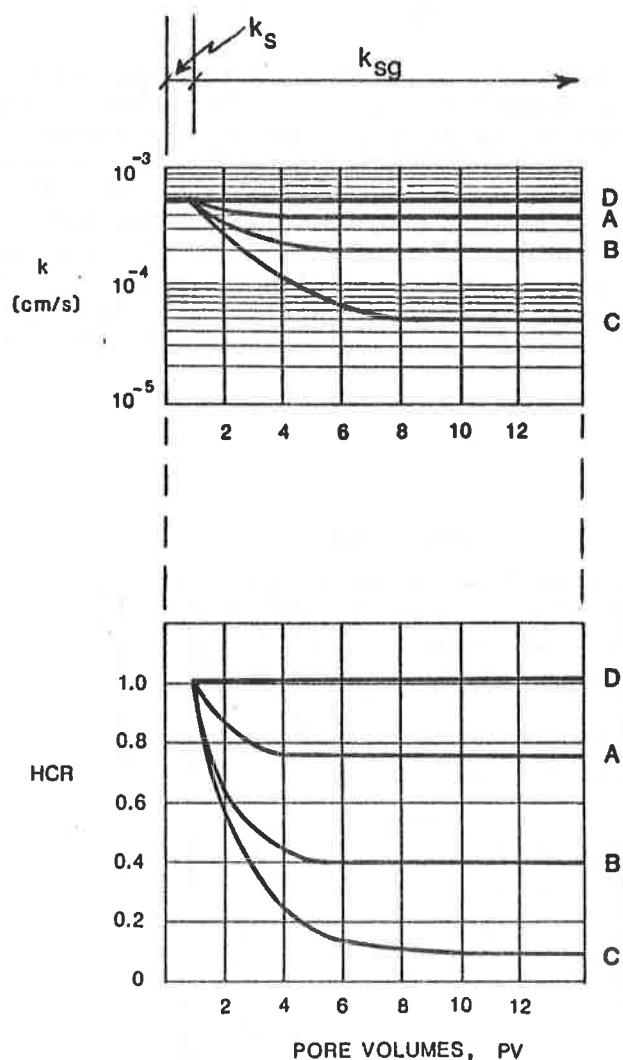


FIGURE 2
GRAPHICAL RESULTS OF HCR TEST

3. HCR-BASED DRAINAGE ANALYSIS

Design Methodology

The HCR test has been presented as a means of determining which of the three types of particle movement is governing the filter behavior. If continued piping or continued clogging of a considered filter material is observed, the material is judged to be inadequate and other materials should be considered. Piping is of particular concern in structures where catastrophic failure may result from excessive loss of the soil structure, or in drainage systems that may clog with the fines passing through the filter.

When a stabilized filter layer forms, however, the interaction between the soil and the geotextile may be the controlling factor in the evaluation of the flow capacity of a drainage system. Therefore, the design process should incorporate the flow impedance resulting from the formation of a stable filter layer. A design methodology is proposed which utilizes the results of HCR tests to evaluate the impact of soil/geotextile interaction on the flow capacity of the drainage system. This design methodology is presented in a step-by-step manner for conditions similar to the vertical wall drain shown in Figure 3. Each component of the design process is derived and discussed below.

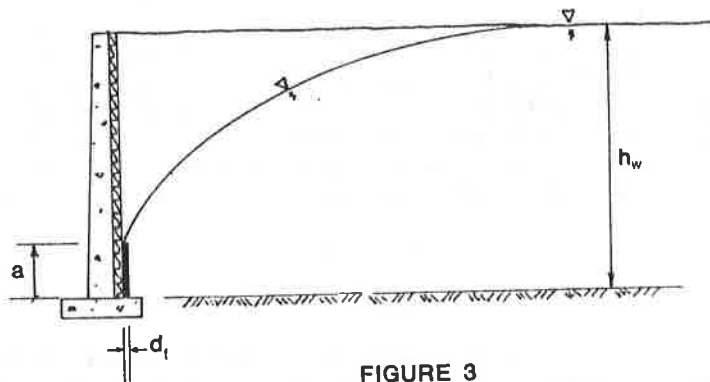


FIGURE 3
DRAWDOWN PROFILE - VERTICAL WALL DRAIN

Step 1: Determine Field Conditions

The primary components of the field monitoring program are an assessment of wall geometry, a site boring program to assess soil lithology and obtain soil samples for laboratory testing, a hydrogeologic assessment, a laboratory testing program and a preliminary analysis of vertical and horizontal stress distributions adjacent to the proposed wall.

The purpose of the laboratory testing program is to evaluate soil properties (typically the backfill material) that are used in the design of the wall drainage system. The tests that would typically be performed include grain-size distribution analyses, hydraulic conductivity tests, Atterberg limits, and compaction (Proctor) tests.

The hydrogeologic assessment would include an evaluation of site ground-water depths, flow directions and flow velocities. This assessment is typically made based on ground-water elevations in borings and data obtained from a literature review. In some cases it may be necessary to install piezometers and monitor ground-water elevations over a period of time.

Step 2: Select Candidate Drainage and Filter Materials

Candidate drainage and filter materials are often selected based on experience with installations similar to the proposed use. For preliminary selection of candidate drainage media, index and design properties such as the hydraulic transmissivity, compressive strength and creep characteristics of the drainage media are considered. For preliminary selection of filter media, the opening characteristics of the filter media relative to the soil particle-size distribution is considered. For geotextile filters, the Apparent Opening Size (AOS) is often provided by the manufacturer for this purpose. Several selection methods have been developed in recent years which relate AOS to the soil particle distribution for the purpose of preliminary filter performance evaluation. Other factors which should be considered in the preliminary selection process of geotextile filters are geotextile construction survivability and geotextile durability.

Step 3: HCR Analysis

The HCR of the candidate geotextile(s) should be evaluated for the proposed soil backfill in the range of stresses and boundary conditions anticipated in the field. The potential for soil particle movement, as described previously, should be evaluated.

If the HCR analysis indicates a stable filter layer has formed, the average hydraulic conductivity of the filter layer may be evaluated. The primary assumptions required to evaluate the hydraulic conductivity of the filter layer are: (i) Darcy's equation is valid; (ii) the principle of flow continuity between layers applies; (iii) the thickness of the filter layer is constant once equilibrium conditions have been reached. Based on these assumptions, the average hydraulic conductivity of the filter layer may be computed as follows:

$$k_f = \frac{d_f k_s (\text{HCR})}{d_f + d_s (1 - \text{HCR})} \quad (2)$$

where: d_f = the thickness of the filter layer; d_s = the thickness (height) of the soil sample; k_s = the hydraulic conductivity of the soil; and k_f = the average hydraulic conductivity of the filter layer. Based on numerous HCR analyses, the thickness of the filter layer may be assumed to be in the range of 0.04 to 0.4 in. (1 to 10 mm). For the analyses presented in this paper, the thickness of the filter layer is assumed to be 0.125 in. (3 mm).

Step 4: Evaluate Drawdown and Seepage Rate

The drawdown of the water table in the soil backfill adjacent to the vertical drainage system is evaluated for steady-state conditions. This analysis is based on the following assumptions:

- homogenous, isotropic backfill with horizontal impermeable boundary at the elevation of the base of the wall;
- Darcy's Equation is valid;
- there is sufficient recharge to maintain the original water table elevation at a lateral distance of 1.5 times the height of the ground water;
- the flow capacity of the drainage system is greater than the seepage rate from the soil into the drain; and
- a stable filter layer develops at the soil/geotextile interface.

The drawdown for $HCR = 1.0$ (i.e., zero impedance) steady-state conditions may be evaluated by a graphical solution (flow net) or numerical methods (finite element analysis). From these analyses, an approximate closed-form solution has been developed for steady-state drawdown conditions and $HCR = 1.0$:

$$a_o = \frac{\sqrt{(1.5h_w)^2 + 4h_w^2 (1 + 0.9h_w)} - 1.5 h_w}{2 (1 + 0.9 h_w)} \quad (3)$$

where: a_o = the steady-state height of water (measured in feet) adjacent to the wall when $k_f/k_s = 1.0$ (i.e., $HCR = 1.0$ conditions); and h_w = the original maximum height of ground water measured in feet from the bottom of the vertical drainage layer.

Equilibrium conditions existing after a stable filter layer forms may be evaluated using numerical methods, or, alternatively, when the HCR value is greater than approximately 0.2, the drawdown may be estimated based on the following equation:

$$a = a_o [1.75 - 0.75 (HCR)] \quad (4)$$

where: a = the height of water adjacent to the wall after the stable filter layer is formed. The HCR must be greater than or equal to 0.2 for Equation 4 to give sufficiently accurate results.

The relationship between a/a_o and the HCR is shown in Figure 4. As shown in the figure, when the HCR is less than 0.2, the ratio of a/a_o increases dramatically. Therefore, the HCR value should be greater than about 0.2 when used in vertical drainage design. This corresponds to a k_s/k_f ratio of about 100.

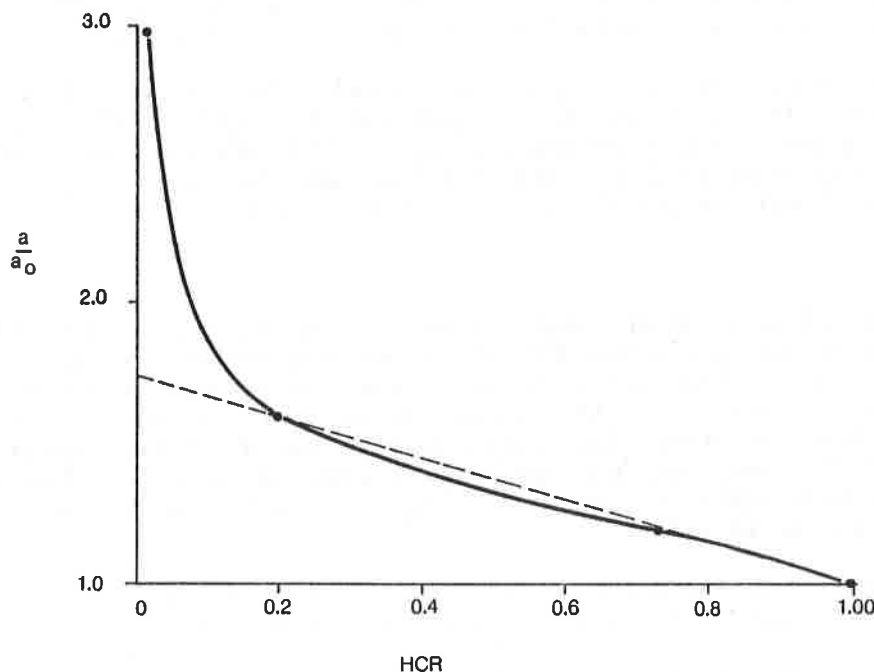


FIGURE 4
RELATIONSHIP OF a/a_o TO HCR

The steady-state seepage rate from the soil, through the filter layer, into the drainage system may be estimated using flow nets, numerical analysis, or it may be calculated based on a number of simplifying assumptions. For the latter case, the primary assumptions are as follows:

- the gradient in the filter layer at the ground-water surface is 1.0;
- the flow into the filter layer is horizontal; and
- the maximum gradient at the base of the wall is $i_{\max} = \left[\frac{a}{d_f} - \frac{a_o}{d_f} \right]$

Based on these assumptions, the seepage rate may be approximated using the following equation:

$$q_s = \frac{a k_f}{2d_f} (a - a_o + d_f) \quad (5)$$

where: q_s = steady-state seepage rate through the filter layer into the drain.

Step 5: Evaluate Flow Capacity of Drain

The in-plane flow capacity of a planar synthetic drainage composite is measured in a transmissivity analysis. The flow capacity of the drain is primarily a function of the boundary conditions, maximum confining stress (at the base of the wall) and the hydraulic gradient ($i = 1$ for a vertical wall). The boundary conditions, confining stress and hydraulic gradient used in the transmissivity analysis must be similar to field conditions in order to measure the flow capacity of the drain.

The safety factor for flow capacity may be defined as the ratio of the in-plane flow capacity of the drain to the steady-state seepage rate through the filter layer into the drain. The anticipated steady-state seepage rate into the drain may be calculated using Equation 5. The recommended safety factor for flow capacity should be greater than 2.5 for noncritical applications and 10 for critical applications.

4. SUMMARY

The performance of vertical drainage systems is affected by the interaction between the backfill soil and the geotextile filter. As water migrates from the soil into the geotextile, the velocity of the water increases, causing movement of the soil particles near the interface. Three types of particle movement may occur: (i) piping; (ii) clogging; and/or (iii) blinding. Typically a combination of all three occurs, however, ultimately most filter behavior is governed by only one of the types of movement. The HCR test has been presented as a means of distinguishing which type of particle movement is governing the filter behavior.

Optimum performance of the drainage system occurs when initial piping of some fine-grained particles through the geotextile occurs shortly after the drain is constructed. As the initial piping occurs, a stable filter layer forms in the soil against the geotextile. This filter layer successively filters the soil particles and causes the piping to stop. This process is necessary for the long-term performance of the drainage system. However, the resulting hydraulic conductivity of the filter layer influences the performance of the drainage system, and is therefore a necessary component of the design of the drainage system.

The HCR analysis has been used to evaluate the effects of soil/geotextile interaction and to assess its impact on the flow across the interface. If HCR analyses are performed with site soils and geotextiles under boundary conditions which simulate field conditions, HCR analyses can be used to estimate the hydraulic conductivity and thickness of the filter layer.

A design methodology for vertical drains is presented which incorporates the results of the HCR analyses. Based on the proposed methodology, a drainage system may be selected which meets or exceeds the flow requirements and limits the hydrostatic pressure against the adjacent wall or structure.

5. REFERENCES

Abouzakhm, M.A., "Permittivity of Geotextile/Soil Composites", M.Sc. Special Research Problem, School of Civil Engineering, Georgia Institute of Technology, Atlanta, GA, 1986.

Calhoun, C.C., Jr., "Development of Design Criteria and Acceptance Specifications for Plastic Filter Cloths", Technical Report S-72-7, U.S. Army Waterways Experimental Station, Vicksburg, MS, 1972.

Giroud, J.P., "Filter Criteria for Geotextiles", Proceedings, Second International Conference on Geotextiles, Vol. 1, Las Vegas, NV, 1982, pp. 103-108.

Lawson, C.R., "Filter Criteria for Geotextiles: Relevance and Use", Journal of Geotechnical Engineering Division, Proceedings of the American Society of Civil Engineers, Vol. 108, 1982, pp. 1300-1317.

Richardson, G.N. and Koerner, R.M., "Geosynthetic Design Guidance for Hazardous Waste Landfill Cells and Surface Impoundments", Office of Research and Development, U.S. Environmental Protection Agency, Cincinnati, OH, 1987.

T.H. WU

University of Colorado, U.S.A.

G.J. MONLEY

J.U. Lowney & Associates, U.S.A.

Effectiveness of Tensile Reinforcement in Alleviating Bridge Approach Settlement

ABSTRACT

It had been reported that the inclusion of tensile reinforcement in the approach fill behind bridge abutments reduced backfill settlement, hence alleviated the "bump" otherwise often experienced at both ends of the bridge. This study was undertaken to investigate, by the finite element method, the effectiveness of emplacing tensile reinforcement in the backfill to reduce approach settlement. The analytical procedure employed in this study was verified by comparing analytical results with the measured response of a large-scale geogrid-reinforced bridge abutment test, which had probably the best data available to-date. Using the validated procedure, a parametric study was conducted to examine the effectiveness of using tensile reinforcement to alleviate backfill settlement under different backfill, foundation and reinforcement conditions. The results of the analysis were discussed.

INTRODUCTION

Excessive differential settlement often occurs between bridge abutments and the approach backfill, especially where foundation conditions are poor. Several factors, often acting together, contribute to the differential settlement. Three of the most important factors are: (1) weak foundation soils which settle significantly after construction of the embankment -- a factor that is especially important where the bridge abutment is more strongly supported by a pile foundation; (2) inadequate compaction of the backfill, due in part to the inherent difficulty in compacting available backfill material and in part to the restrictions imposed by the bridge structure; and (3) poor drainage of the approach backfill.

Approach settlement can range from a few inches to a couple of feet and progress throughout the lifetime of the structure. Because of this, rough and sometimes hazardous driving conditions are created by the resultant abrupt step ("bump") at both ends of the bridge, and alleviating this problem after it has developed often requires ongoing and expensive maintenance such as mudjacking and resurfacing.

Over the years, several methods have been attempted to prevent the "bump" from developing. Two most common methods are: (1) placement of a rigid reinforced concrete slab behind the bridge abutment to spread out the differential settlement

over a wider area, and (2) use of a highly granular fill or pulverized fuel ash that will experience negligible settlement after placement and is often used in combination with the approach slab. Although Method (1), the approach slab, has been found to be beneficial in many cases, where differential settlement is substantial the use of approach slabs has only been partially successful and in some cases can aggravate the problem (4). On the other hand, finding high-grade material in the near vicinity that can be economically retrieved and transported to the project site can be a major problem with Method (2).

Since 1983, the Wyoming Highway Department has built or retrofitted over 38 bridges using geotextiles to reinforce the approach backfill. Multiple layers of geotextile material are placed within the backfill and folded at the sides to form geotextile facings adjacent to the abutment and wingwalls. Price and Sherman (5) reported that, by using a geotextile having a moderately high modulus and low elongation to break, a stiffer soil mass was created which could distribute traffic loads over a wider area and thus alleviated settlement from occurring within the reinforced section. It had been further reported that, since their installment, no repairs had been made to bridges using reinforcing resulting from differential settlement.

This study was undertaken in order to gain a better understanding of the effectiveness of tensile reinforcement in alleviating approach settlement. Two excellent large-scale tests of bridge abutments with and without tensile reinforcement were investigated and used to establish validity of a finite element analytical model. The analytical model was then used to conduct a parametric study to examine the effectiveness of using tensile reinforcement for alleviating approach settlement under different foundations, backfills and tensile reinforcements.

LARGE-SCALE TEST

Two excellent large-scale tests were conducted by the Civil Engineering Research Institute, Japanese Ministry of Construction to determine the ability of high strength geogrid reinforcement to alleviate differential settlement between the abutment and backfill (3). A diagrammatic representation of the test is presented in Figure 1 in which the abutment is restrained from moving with respect to the backfill, thus simulating an abutment founded on a very firm foundation.

A description of the test, paraphrased from Japanese, is reported below. To simulate the prototype, a large bin was constructed 14 m in length, 2.6 m in height and 1.0 m in width and the sidings were built of clear plexiglass to observe the soil-structure interactive behavior throughout the test. The abutment itself was modeled after one in the field and the backfill stood 1.45 m in height and extended 10.0 m in length behind the abutment. Five layers of geogrid were placed in the backfill with one end of each layer securely fixed to the abutment wall. As shown, the layers of reinforcement were spaced 0.2 m apart and extended back 4.0 m from the abutment. The properties of the backfill soil and geogrid reinforcement are presented in Table 1. To activate settlement of the backfill, a 0.2 m thick layer of soluble ammonium sulphate was placed between the bottom of the backfill and brick base. After backfilling was completed this layer was dissolved, thus simulating settlement due to a weaker shallow foundation.

Two tests were conducted: one in which only soil occupied the backfill and one in which five layers of geogrid were included in the backfill. After the

completion of each test, observations were made as to the magnitude and profile of surface settlement and the development of cracks and voids in the backfill.

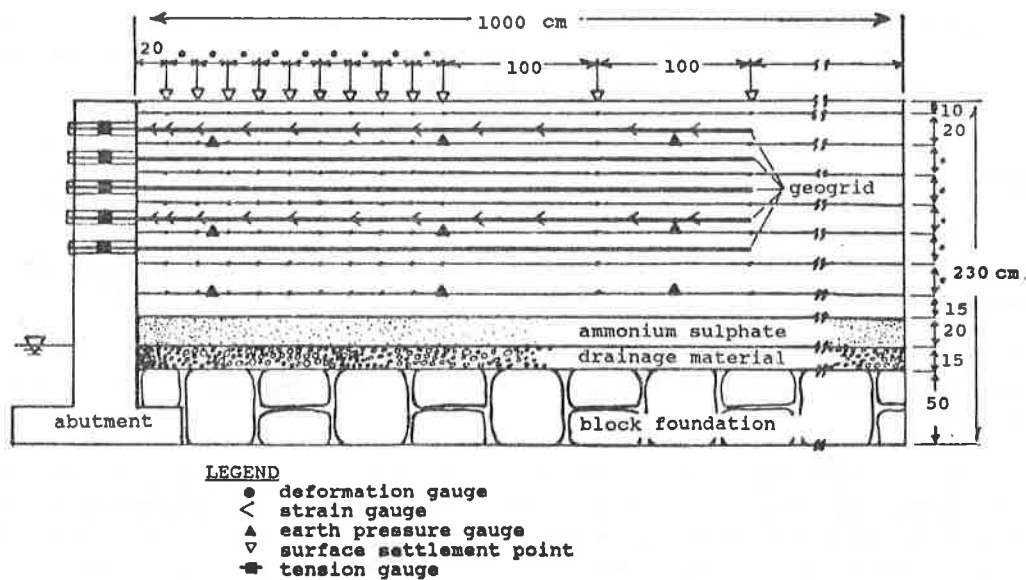


Figure 1. Diagrammatic Representation of Kutara's Large-Scale Test (3).

Table 1. Material Parameters of Soil and Geogrid in Kutara's Test (3).

Soil

<u>Parameter</u>	<u>Symbol</u>	<u>Value</u>
unit weight (tf/m ³)	γ	1.6
cohesion (tf/m ²)	c	2.0
internal friction angle	ϕ	29.0
Poisson's Ratio	ν	0.4
Young's Modulus (tf/m ²)	E	800
Soil classification		SM
gravel (%)		0.0
sand (%)		50.1
silt (%)		31.9
clay (%)		18.0

Geogrid

<u>Parameter</u>	<u>Symbol</u>	<u>Value</u>
weight (gf/m ²)		938
spacing (mm.)		22 x 111
area (m ²)	A	0.000297
tensile strength (kgm/m)	σ_t	8000
rupture strain (%)		12.0
40% of rupture strain (%)		3.0
Young's modules tf/m ²)	E	400000.0

Where no reinforcement was used, 0.17 m to 0.18 m of fairly uniform settlement occurred due to 0.2 m of the induced settlement at the base, and frictional resistance activated between the backfill and abutment did not alleviate the development of an abrupt step occurring at the abutment face. In the test in which geogrid was emplaced, a negligible amount of settlement occurred at the abutment face and fairly smooth, gradual settlement occurred moving back from the abutment, eventually reaching 0.2 m of settlement approximately 1.0 m behind the abutment, thus alleviating the "bump." However, large cracks and voids were also described, especially in the region of gradual settlement adjacent to the abutment, reportedly caused by the redistribution of settlement that was prevented from occurring at the backfill-abutment interface.

The analytical model used in this investigation incorporated quadrilateral elements with Duncan-Chang hyperbolic model (1) to simulate the nonlinear, stress-dependent stress-strain behavior of soil; and one-dimensional bar elements with linear elastic constitutive law to simulate the reinforcement behavior. Figure 2 depicts the finite element discretization of the large-scale test. Sequential construction operation was simulated. After backfilling to the top of the abutment, 0.2 m of the settlement was induced by artificially applying a uniform load to the nodes at the bottom of soil layer 1 (refer to Figure 2) in order to simulate the test condition.

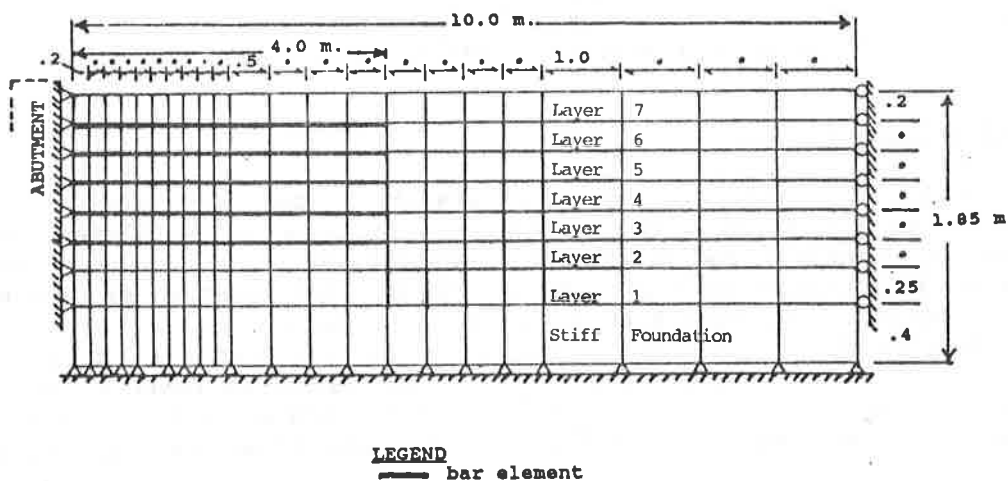


Figure 2. Finite Element Discretization of Kutara's Test.

The settlement profile obtained from the analysis in comparison with measured settlement is presented in Figure 3. It shows that the analytical model provided a very good simulation of the settlement occurring in the test. The analysis indicated large localized zones of tension and shear yielding and is attributed to the developments of large voids and cracks in the geogrid-reinforced backfill as observed in the test. Yielding in the soil mass likely developed because foundation settlement occurred in one load increment after construction to simulate rapid foundation settlement in the test, and this did not allow for the redistribution of induced stresses in the backfill which would likely occur under more gradual settlement conditions.

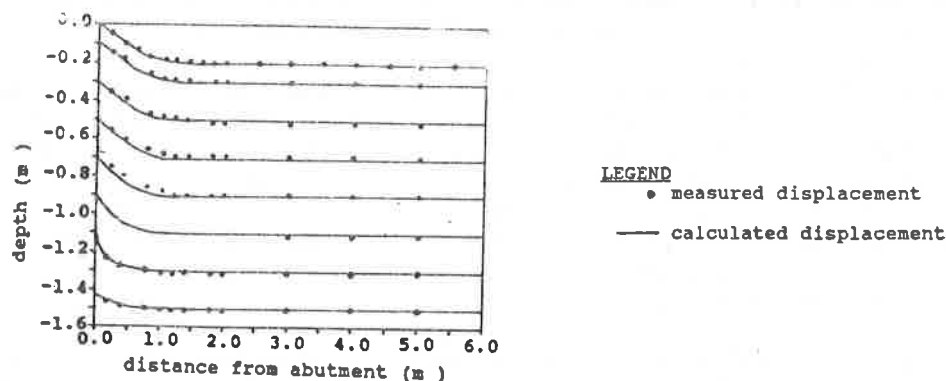


Figure 3. Comparison of Calculated versus Measured Displacement in the Backfill

Although the results of the large-scale test clearly show that the "bump" can be alleviated by attaching geogrid reinforcement to the abutment wall, no further study was performed to examine the effect of additional loading (traffic loads, for instance) on the approach settlement due to the existence of cracks and voids beneath the geogrid layers. It is therefore difficult to assess the effectiveness of the geogrid reinforcement under service conditions.

PARAMETRIC STUDY

Using the analytical model, a parametric study was conducted to examine the effectiveness of tensile reinforcement in alleviating settlement under changing foundation, backfill and reinforcement conditions. The analysis incorporated the geometry illustrated in Figure 4, a typical configuration of a geotextile-reinforced abutment constructed on a cut slope. The finite element mesh employed for this study is shown in Figure 5, and parameters representing a range of foundation, backfill and reinforcement conditions are presented in Table 2 and 3. To examine the effects of surcharge loading due to traffic and other loads, a uniform 49 kN/m² pressure load was applied to the top of the backfill at the completion of backfilling.

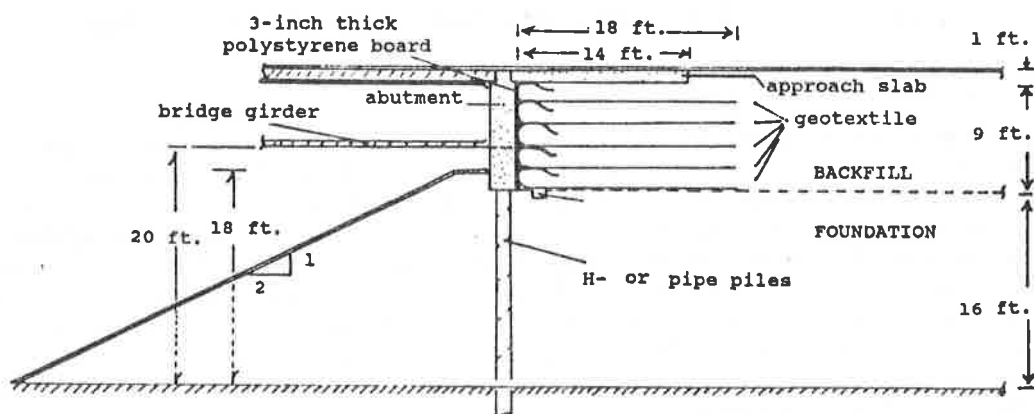


Figure 4. A Typical Geotextile-Reinforced Bridge Abutment.

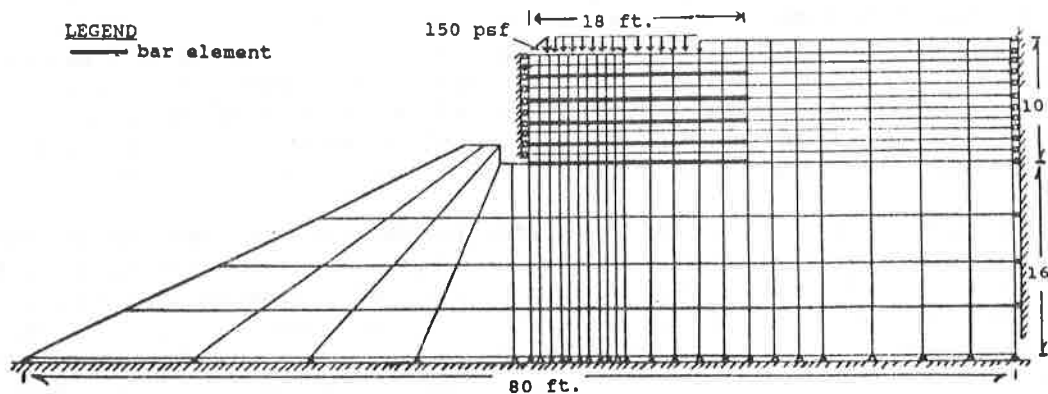


Figure 5. Finite Element Discretization of the Geotextile-Reinforced Bridge Abutment.

Table 2. Duncan-Chang Parameters Representative of Varying Foundation and Backfill Conditions.

	Condition	Unified Soil Classif.	RC*	m (tf/m^3)	ϕ	C (tf/m^2)	K	n	R_f	G	F	d
Backfill	1	GP	95	2.00	36	0.24	300	0.40	0.7	0.30	0.0	0.0
	2	SP	90	1.92	32	0.24	300	0.25	0.7	0.30	0.0	0.0
Foundation	1	CL	--	1.92	32	4.88	150	0.45	0.7	0.30	0.0	0.0
	2	CL	--	1.84	30	2.44	120	0.45	0.7	0.30	0.0	0.0

* RC = relative compaction (Standard AASHTO)

Table 3. Structural Element Parameters Representative of Varying Tensile Reinforcement Behavior

Type	Secant modulus (tf/m^2)	Area (m^2)	thickness (m)
Trevira 1127 Non-woven Geotextile	** 547	0.00097	0.0032
Geogrid	386,660	0.00116	0.0038

** Secant modulus for Trevira 1127 at 2% strain and 2.80 tf/m^2 overburden pressure

Initially, the abutment-embankment was analyzed using backfill and foundation parameters corresponding to Condition 1 shown in Table 2, and by comparing settlement when geotextile reinforcement was included in the backfill to that when no reinforcement was emplaced. In each case, a uniform surcharge pressure was applied at the end of construction. The analysis indicated that emplacing multiple layers of reinforcing in the backfill did not measurably reduce the amount of settlement caused by the weight of the soil or due to surcharge loading. Likewise, distribution of stresses and overall stability of the backfill was not noticeably affected.

To further substantiate these findings, three more conditions were analyzed. First, a weaker backfill material was simulated using backfill parameters corresponding to Condition 2 in Table 2 while foundation parameters corresponding to Condition 1 and emplacement of geotextile reinforcing was maintained. Next, weaker

foundation conditions corresponding to Condition 2 were used while backfill parameters for Condition 1 and geotextile reinforcing were maintained. Third, a stronger geogrid was simulated using parameters presented in Table 3 was considered while both backfill and reinforcement parameters for Condition 1 were used. In each case, a uniform pressure load was applied at the end of construction. Again, the analysis showed that the inclusion of reinforcement did not markedly alleviate settlement from occurring in the backfill behind the bridge abutment.

The reason why is believed to be due to the boundary conditions inherent in the embankment-abutment system. Figure 6 depicts the resulting soil movement vectors when backfill and foundation parameters corresponding to Condition 1 were used without the inclusion of the geotextile reinforcement. A lateral component of soil movement can be seen in the foundation in the direction of the cut-slope. In contrast, the backfill soil shows nearly exclusive vertical soil movement, caused primarily by the lateral restraints imposed by the abutment. Tensile reinforcements such as geotextiles add increased strength to a soil by restraining soil deformation, through frictional and passive resistance, parallel to the plane that the reinforcement is emplaced. Because the reinforcement was placed laterally whereas a negligible amount of lateral soil movement occurred, the analysis indicates that the tensile resistance of the reinforcing was not activated in any measurable capacity.

These findings are also supported by the results of a recent study conducted at Purdue University (2) in which the behavior of reinforcements placed in embankments (which have less inherent lateral restraint than the backfill placed behind bridge abutments) of different geometries were analyzed. The study indicated that while the use of reinforcements can effectively reduce shear and lateral strains and increase embankment stability, they have little effect on alleviating vertical settlement.

CONCLUDING REMARKS

- (1) The results of this study clearly indicated that, under similar compaction efforts and boundary restraints, settlement of the backfill is not alleviated by the inclusion of soil reinforcement. Due to the boundary restraints inherent in the abutment structure, the backfill

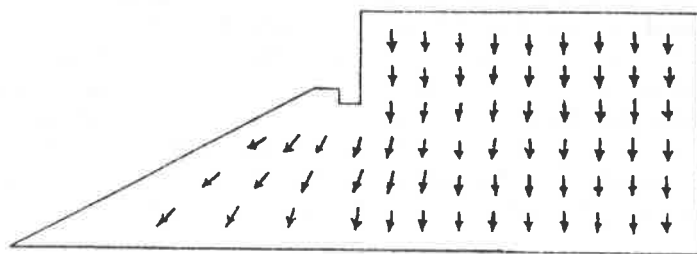


Figure 6. Displacement Vectors in the Backfill and Foundation, Condition 1, unreinforced.

tends to move vertically downward and the amount of lateral soil deformation needed to mobilize the tensile resistance of the reinforcing is negligible.

- (2) By attaching the reinforcement to abutment wall, the differential settlement can be spread over a wider area, thus alleviates the "bump." The voids occurred beneath the attached-end of the reinforcement, however, may produce ill effects under service conditions.
- (3) The apparent success reported by the Wyoming Highway Department is speculated by the authors as a result of the improved backfill stiffness due to inclusion of geotextile as a compaction aid. Further research is continuing at the University of Colorado at Denver to investigate this mechanism. Presently the Wyoming Highway Department is conducting full-scale tests to measure the effectiveness of geosynthetic reinforcement and similar plans are underway in Colorado.

REFERENCES

- (1) Duncan, J.M., and Chang, C.Y. (1970). "Nonlinear Analysis of Stress and Strain in Soils," Journal of the Soil Mechanics and Foundations Division, ASCE, Vol. 96, SM5, September, pp. 1629-1654.
- (2) Humphrey, D.N. (1986). "Design of Reinforced Embankments." Joint Highway Research Project, Report No. JHRP-86/16, Final Report, Purdue University, October.
- (3) Kutara, K., Gomado, M., Takeuchi, T., and Maeda, S. (1985). "Use of Geotextiles as a Countermeasure for Differential Settlement in Road Embankments." Soils and Foundations, Vol. 33, No. 5, pp. 27-32 (in Japanese).
- (4) Monley, G.J., "An Investigation of the Effectiveness of Tensile Reinforcement in Alleviating Approach Fill Settlement Behind Bridge Abutment," M.S. Thesis, Department of Civil Engineering, University of Colorado at Denver, December 1987.
- (5) Price, J.T. and Sherman, W.F. (1986). "Geotextiles Eliminate Approach Slab Settlement." Public Works, January, pp. 58-59.

J.P. GOURC

P.H. GOTTELAND

University of Grenoble, France

P. DELMAS

Laboratoire Central des Ponts et Chaussées, France

Parametric Study of Geosynthetic Reinforced Retaining Walls Using the Displacement Method

SUMMARY

For two years now, the "Displacement Method" has been widely used in France for the design of geosynthetic-reinforced retaining walls with a vertical or sloping facing. Compared with the more conventional limiting equilibrium methods, the displacement method has the notable advantage of making allowance for the tensile modulus of the geosynthetic sheet, the soil-geosynthetic sheet interaction conditions and different construction conditions (fixing the geosynthetic material to the facing, for example). The following article explains the method and gives details of a particular application.

The "Displacement Method" is a design method for reinforced soil retaining blocks. The method is based on the limiting equilibrium principle for the soil and on the principle of local equilibrium for each geosynthetic sheet. These two aspects of the method will be described first before illustrating a concrete example.

1. LIMITING EQUILIBRIUM OF THE SOIL RETAINING BLOCK

The conventional method consists in assuming that the block of active soil is in limiting equilibrium. This soil block is separated from the rest of the soil massif by a slip line. Along this slip line, the soil satisfies Coulomb's law:

$$(a) \quad \tau_{pc} = \frac{\tau_p}{F_s} = \frac{c + \sigma_z \tan \phi}{F_s} = c_c + \sigma_z \tan \phi_c$$

τ_p is the maximum shear stress and τ_{pc} is the limit value required to obtain limiting equilibrium of the active soil block along the slip line. F_s is the safety factor of the soil in shear.

Numerous methods based on the slope stability study are available. They differ by the shape of the slip line and by the equilibrium equations used. The most widely used for reinforced soil massifs is the "two-block method" which was presented elsewhere (3). The slip line is a broken line but, unfortunately, this method is not statically acceptable as it does not satisfy the equilibrium of moments. In (4), the results obtained were compared with those from the displacement method.

Bishop's simplified method is a slice method widely-used for slope stability calculations. Unfortunately, this method is again statically unacceptable and the slip line has got to be circular.

Consequently, the perturbation method (6) had to be chosen. This is a statically acceptable slices method (the static equilibrium equations are established for each slice) where the slip line is assumed to have any shape. The fundamental hypothesis relates to the distribution of forces normal to the slice base (figure 1 - (5)):

(b) $N_i = N_{i0} \cdot (\lambda + \mu \cdot \tan \gamma_i)$

(c) with $N_{i0} = (W_i - S_{iz}) \cdot \cos \gamma_i + S_{ix} \cdot \sin \gamma_i$

λ and μ are parameters determined by the calculation.

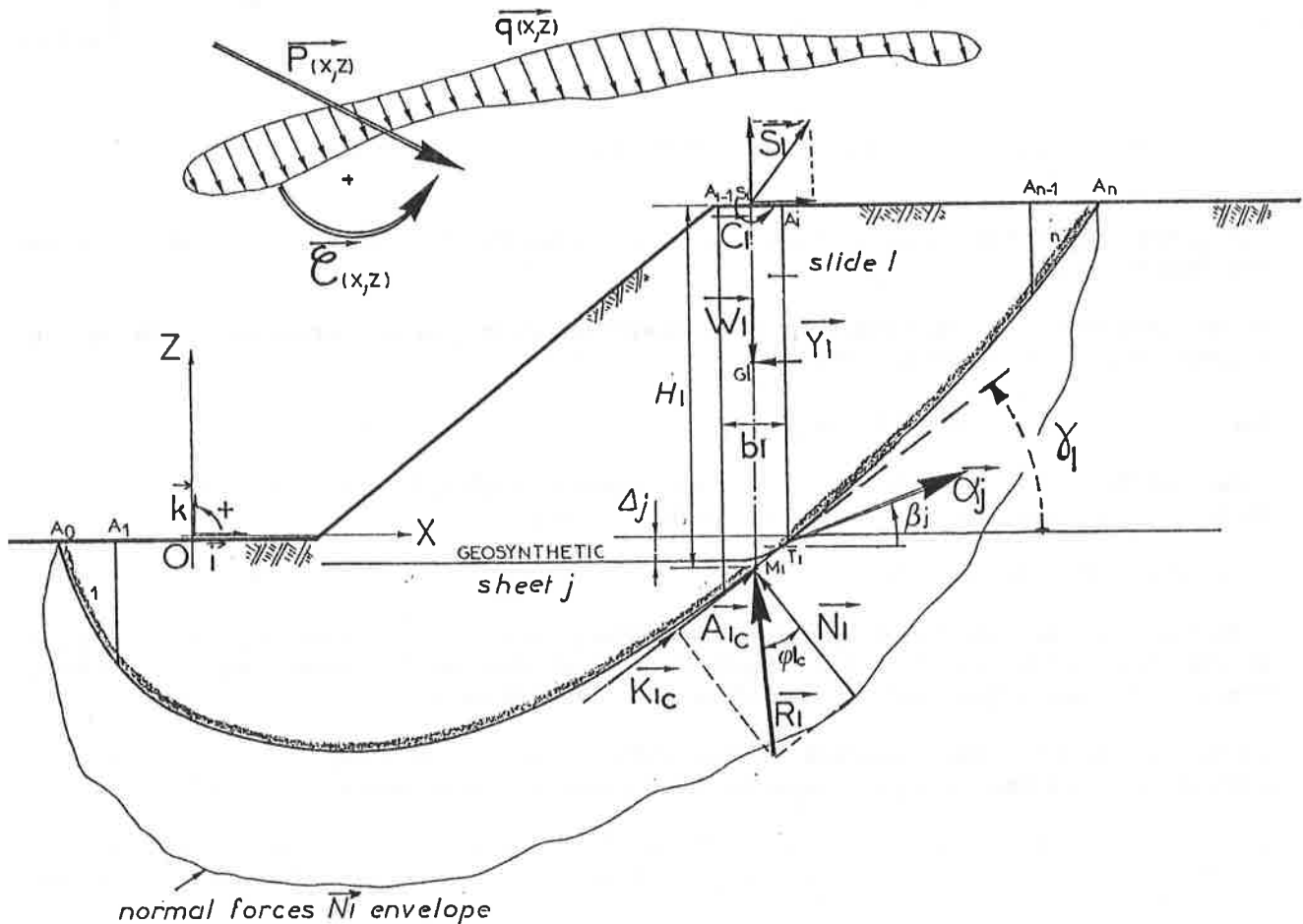


Figure 1 : Use of Slices Method for reinforced soil mass

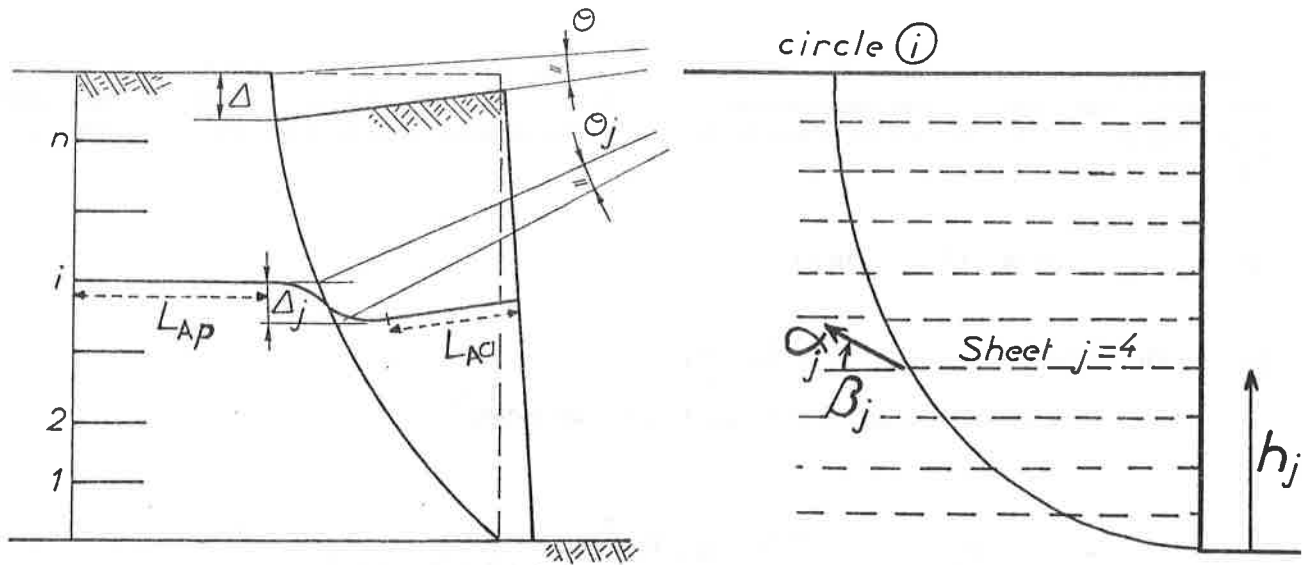


Figure 2 : "Displacement Method" - Proposed mechanism

The system of equilibrium equations is solved in order to obtain (F_{so}, λ, μ) , where F_{so} is the safety factor on non-reinforced soil.

In the case reinforced soil, the tensile force in the geosynthetic sheet j at the intersection with the slip line, is α_j inclined at β_j . N_{lo} is therefore replaced by N_{lr} :

$$(d) \quad N_l = N_{lr} = N_{lo} + \alpha_j \cdot \sin(\gamma_l + \beta_j)$$

Values for (F_{sr}, λ', μ') are obtained by the separate determination of (α_j, β_j) . For a fixed slip line ($F_{so} < 1.5$), the limiting equilibrium with reinforcement is obtained when $F_{sr} = 1.5$.

2. SLIDING BLOCK KINEMATICS

In the rest of the study which follows, consideration will be given only to circular slip lines: circles centred on the free surface of the top of the slope (Figure 2), although other slip line shapes could be considered, especially the lines merging with the geosynthetic sheet at the bottom.

Let the active block be subject to a rotation: in that which follows, a constant rotation $\theta_j = \theta$ will be assumed, acting along the slip line, although a progressive failure movement can be taken into account (1).

In this overall movement, each reinforcement sheet is subjected to shear - flexion forces at the intersection with the slip line and comes under tension (α_j, β_j) through its anchorages in the soil (L_{Aa} in the active zone, L_{Ap} in the passive zone).

3. PULL-OUT BEHAVIOUR OF AN ANCHORED GEOSYNTHETIC SHEET

The soil-geosynthetic sheet interaction behaviour can be assessed by means of friction tests. This behaviour will be characterised by τ_p (equation (a)) and by u_p relative soil-geosynthetic sheet displacement required to

reach $\tau = \tau_p$. A large number of friction tests have been carried out, leading to the proposed simplified relation in figure 3. The following equation is also proposed:

$$(e) \quad u_p = u_{p0} + u_{p1} \cdot \sigma_z / (1 + \xi_1 \cdot \sigma_z)$$

In that which follows, the value of u_p will be assumed to be constant with σ_z .

The behaviour of the geosynthetic sheet under tensile stress will be characterised by its tensile modulus J :

$$(f) \quad \alpha = J \cdot \epsilon \quad \text{with } \alpha \leq \alpha_1$$

where ϵ is the elongation and α_1 the intrinsic tensile stress (maximum permissible).

The theoretical behaviour of a geosynthetic sheet anchored over a length L_A can be obtained from knowledge of the behavioural laws under friction and tensile forces (3). Let u_A be the displacement of the anchorage head for a tensile force α_A . Figure 4-a represents the behaviour of a sheet with free-end in G ($\alpha_G = 0$) and figure 4-b the behaviour of a sheet fixed to the facing in G ($u_G = 0$). For the example in Section 6, this corresponds respectively to passive and active zone anchorage.

L_A and J have a proportionally much greater effect than u_p .

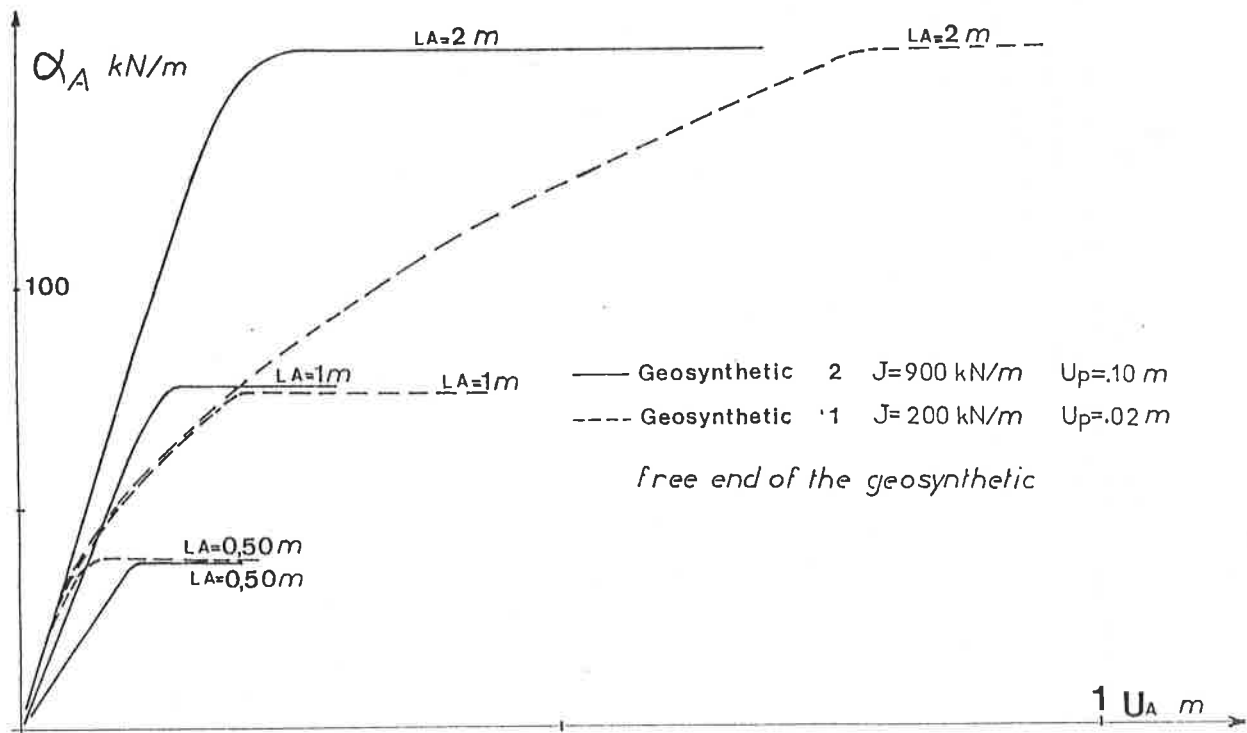


Figure 4a : Pull out
behaviour of a
geosynthetic
sheet - free end-

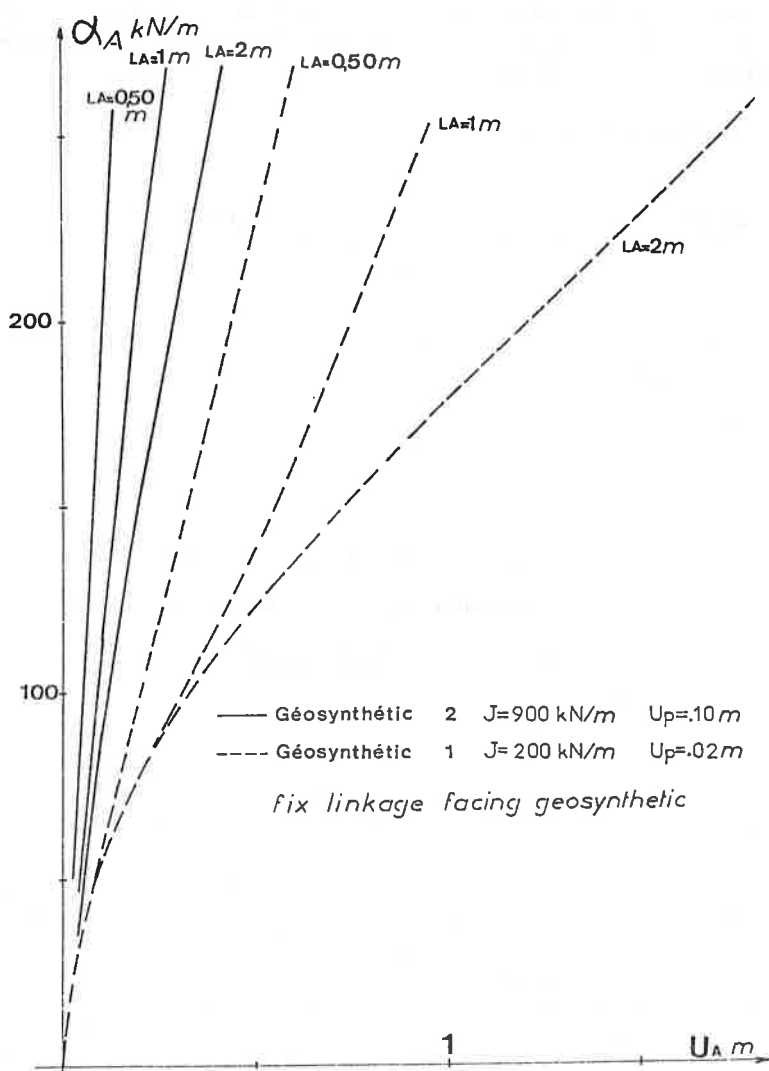
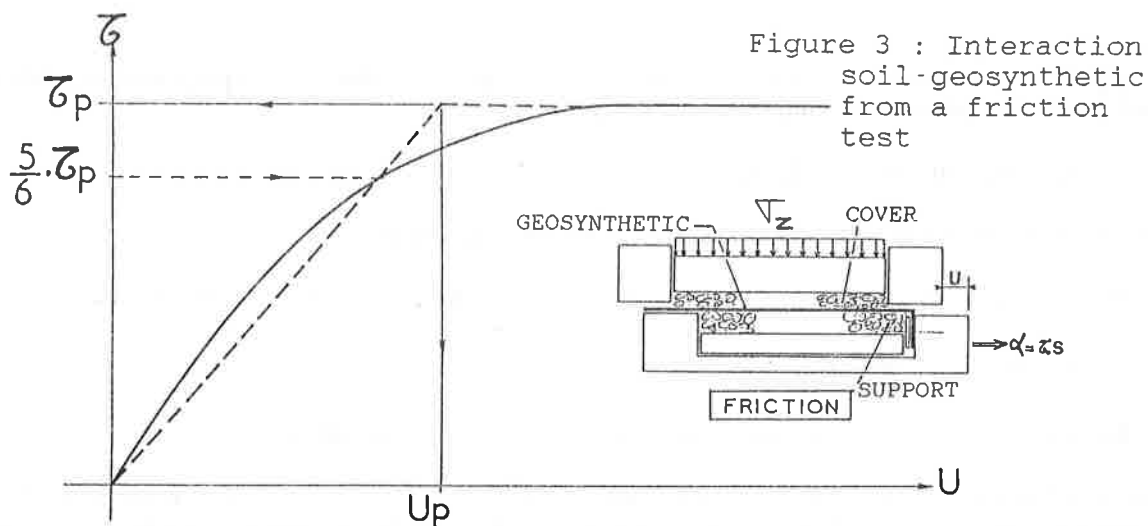


Figure 4b : Pull out behaviour of a geosynthetic sheet - fix linkage facing geosynthetic

4. SHEAR - FLEXION BEHAVIOUR OF A GEOSYNTHETIC SHEET

In the vicinity of the slip line, the sheet has a convex membrane shape. It was shown in (2) how the membrane sheet deformation could be estimated on the basis of Δ_j (figure 2), the active $[\alpha_j = f(u_{Aj}^a)]$ and passive $[\alpha_j = g(u_{Aj}^p)]$ anchorage boundary conditions, the tensile modulus J , and the stiffness modulus, K_s .

Figure 5 shows the influence of soil stiffness K_s on the equilibrium shape for the particular case of the Kingston experimental wall (Canada) (3), with all other parameters remaining the same. Unfortunately, for a structural works project, K_s will often be difficult to estimate. Faced with this difficulty, the *Laboratoire Central des Ponts et Chaussées* (LCPC) (1) proposed a simplified mechanism (cf. figure 6). In that which follows, a distinction will be made between the "MEMBRANE" program, used essentially for research and taking into account sheet membrane flexion (IRIGM), and the "CARTAGE" program ($\beta_j = 0$), widely used by the LCPC for design work.

5. DISPLACEMENT METHOD CALCULATION PROCEDURE

Consider a fixed slip line for which $F_s = F_{s0} < 1.5$ for $\Delta = 0$. The limiting equilibrium will be reached for a value of $F_s = F_{sr} = 1.5$ by mobilisation of reinforcement sheets ($\Delta > 0$).

For a vertical slip Δ_j , the equilibrium tensile force α_j between the anchorage zones and the shear - flexion zone is obtained. For the anchorage zone:

$$(g) \quad u_{Aj}^a = v(\alpha_j, L_{Aj}^a, u_{Gj} \text{ or } \alpha_{Gj} = 0)$$

$$(g') \quad u_{Aj}^p = v(\alpha_j, L_{Aj}^p, \alpha_{Gj} = 0)$$

In addition, it will be checked that:

$$(h) \quad \alpha_j < (\alpha_j^{\max} \text{ anchorage}) \text{ and } \sum \alpha_j < \frac{2}{3} \cdot \sum (\alpha_j^{\max} \text{ anchorage})$$

For the shear - flexion zone: the tension is constant in the shear - flexion zone and equal to the tensile force at the anchorage head.

$$(i) \quad \text{"MEMBRANE" program} \quad \Delta_j = f(K_s, \alpha_j, \beta_j, u_{Aj}^a, u_{Aj}^p)$$

$$(j) \quad \text{"CARTAGE" program} \quad \Delta_j = (u_{Aj}^a + u_{Aj}^p) \cdot \sin \gamma_1 \quad \text{and } \beta_j = 0$$

The procedure consists in increasing $\Delta_j = \Delta$ by small increments. α_j (and β_j for the Membrane program) increases with Δ . The limiting equilibrium is obtained when $F_s = F_{sr} = 1.5$.

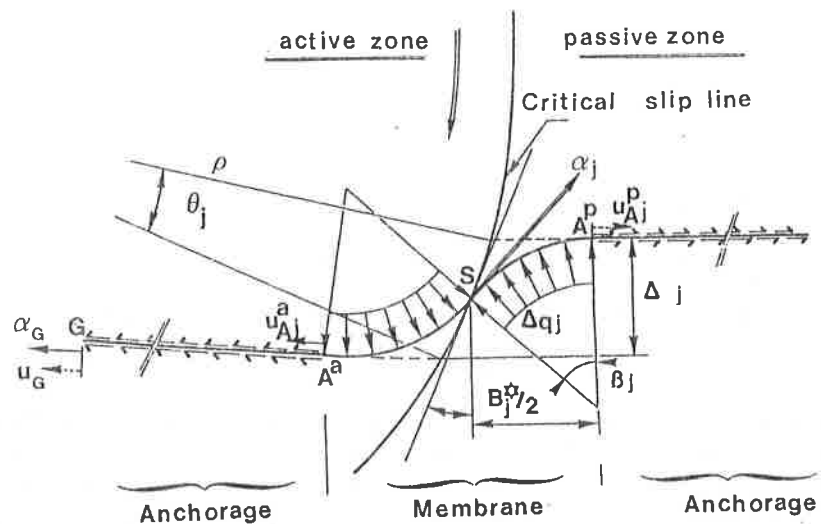
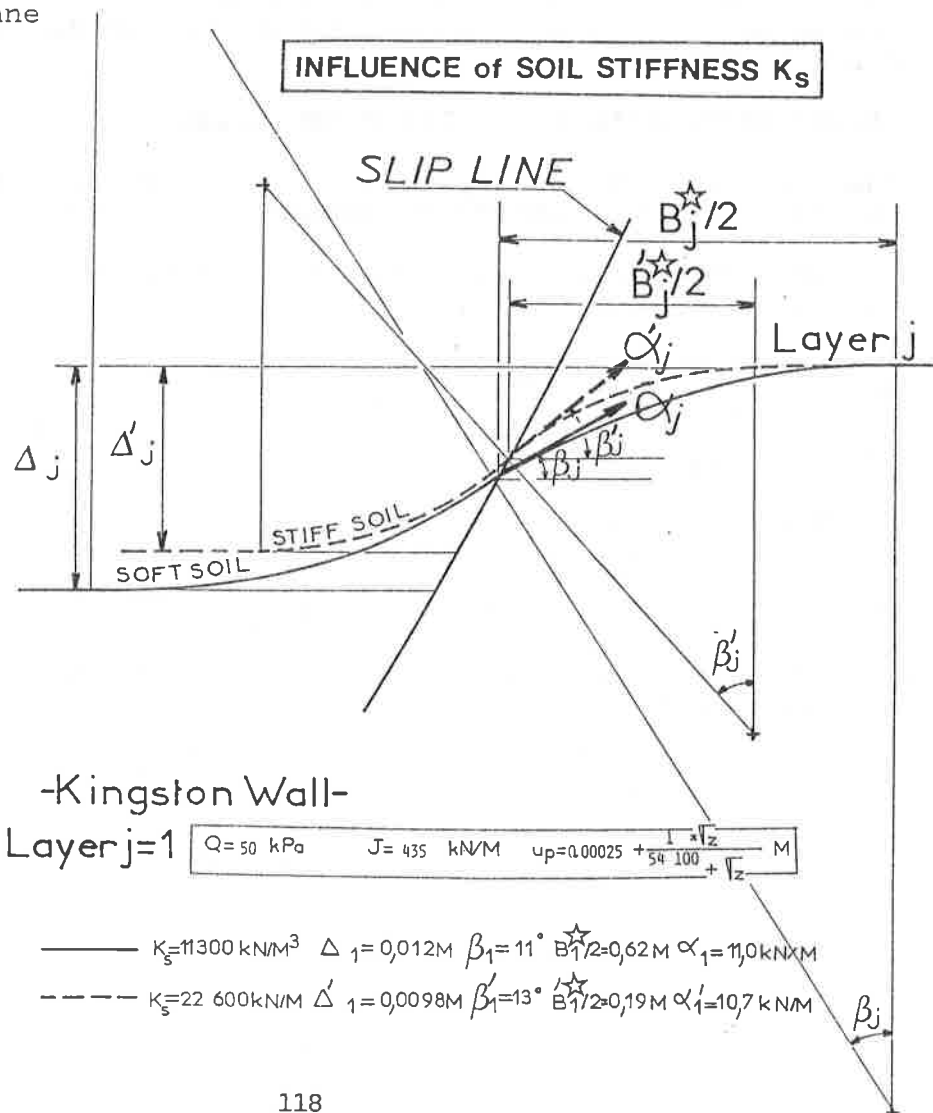


Figure 5 : Influence
of soil stiffness
on the membrane
behaviour of
geosynthetic
(Program
"MEMBRANE")



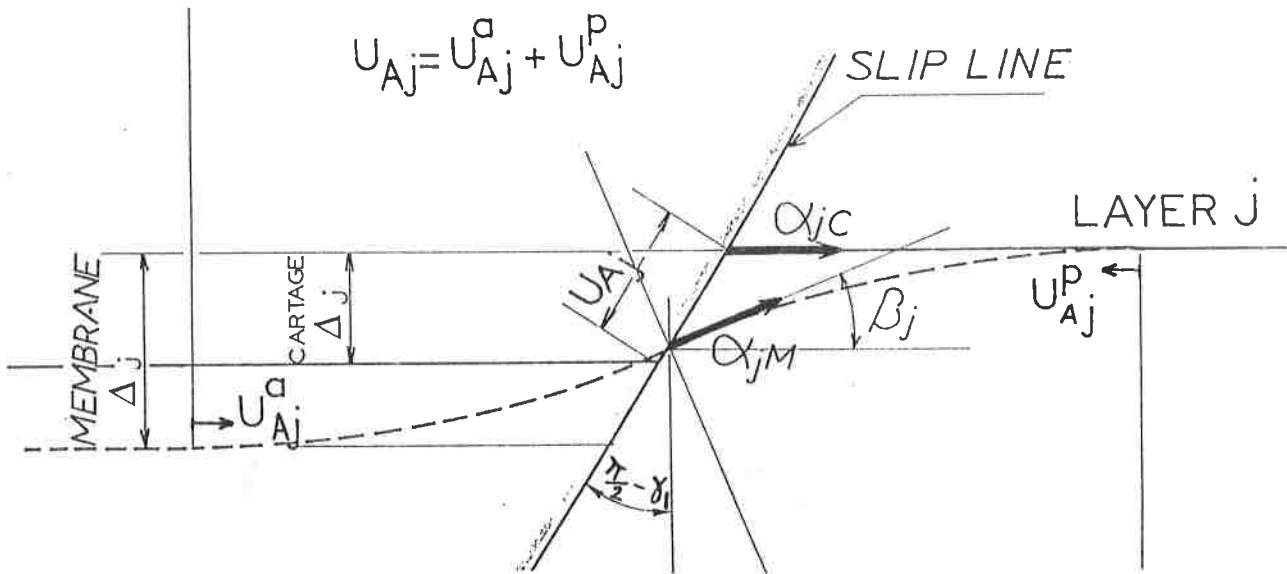


Figure 6 : Different assumptions for "MEMBRANE" and "CARTAGE" programs

α_{jM} , α_{jC} tensile forces for MEMBRANE and CARTAGE programs

6. APPLICATION OF THE DISPLACEMENT METHOD

The displacement method is applied to a vertical facing massif, of height $h = 6$ m, made of soil reinforced with 11 sheets of geosynthetic material (cf. figure 7) fixed to the facing ($u_{Gj} = 0$). The length L of the sheets is variable. The intrinsic tension (maximum permissible) will be chosen greater than the maximum mobilised tension according to the equilibrium calculation.

$$(k) \quad \alpha_{\max} \leq \alpha_i$$

Figure 7 (CARTAGE) shows the monitored procedure: by modifying the slip line (in this case 6 circles $i = 1$ to 6), a variation in equilibrium α_j and Δ values is obtained. It is found that the maxima of Δ and $(\max \alpha_j)$ are generally obtained for the same slip line (here, the critical circle, $i = 4$).

The α_j distributions obtained, compatible with slip kinematics, are considered to be much more realistic than those obtained from a trapezoidal distribution of soil thrust for example (Reinforced Earth Method) (7).

Figure 8 shows that the Membrane Program gives higher Δ values than those with Cartage, for realistic K_s values. However, the tensile forces α_j remain within the same order of magnitude ($\beta_j > 0$ leads to a reduction in α_j).

Figure 9 shows that charts can be obtained from $\alpha_{\max} = \max_i (\max_j \alpha_j)$ and from $\Delta_{\max} = \max_i \Delta$. Compared to traditional methods, a double design criterion can be used.

$$(k) \quad \alpha_{\max} \leq \alpha_i$$

$$(l) \quad \Delta_{\max} \leq \Delta_{\text{permissible}}$$

A typical chart was presented in (4), where the relationships $\alpha_{\max} = c(L, J)$ and $\Delta_{\max} = d(L, J)$ are obtained for several J values. By respecting the criteria (k) and (l), a family (α_i, J) of suitable geosynthetic sheets for the structure is obtained.

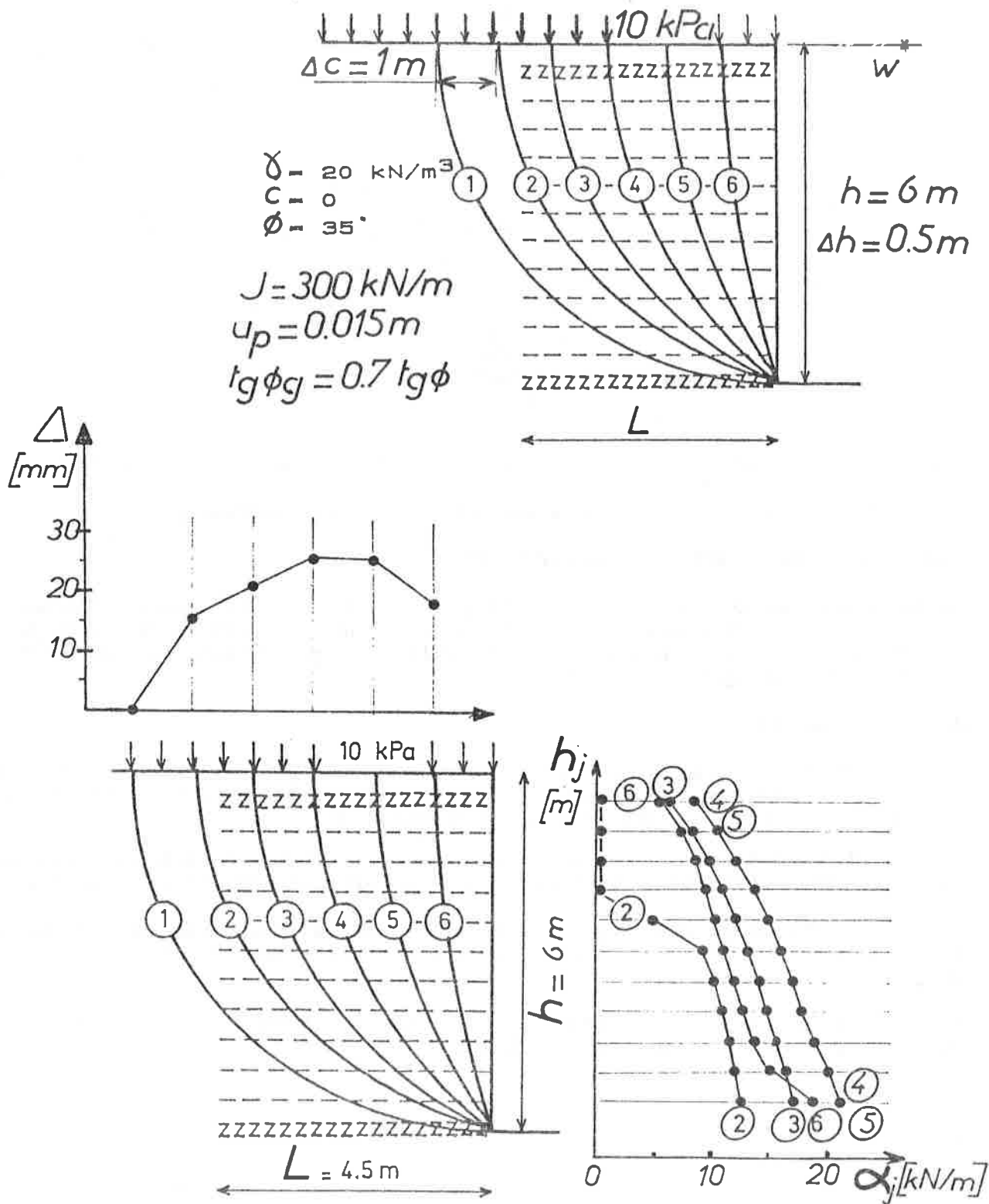


Figure 7 : "CARTAGE" Program - Influence of the slip line

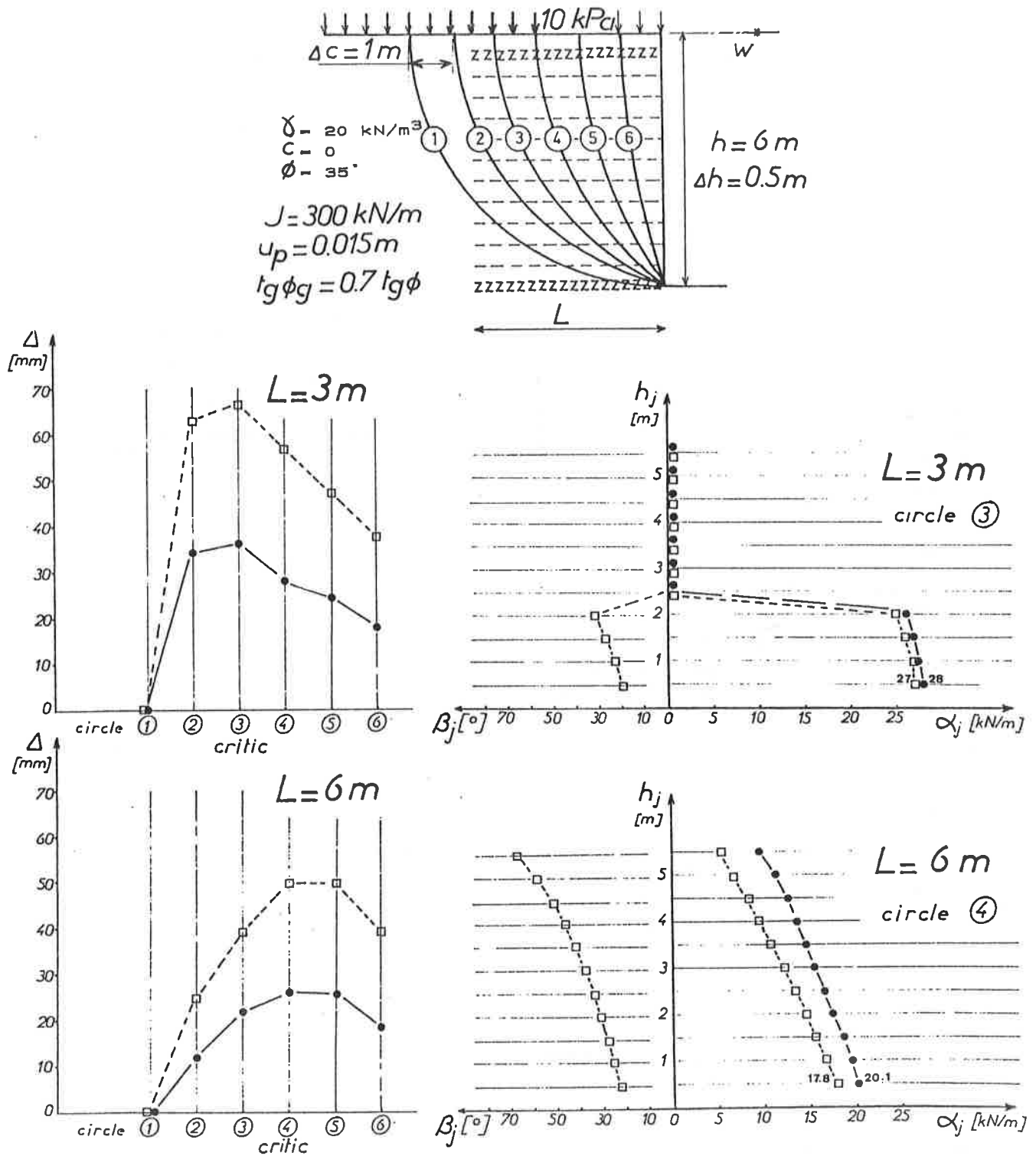


Figure 8 : Comparison "MEMBRANE" - "CARTAGE" for 2 widths L of the retaining wall

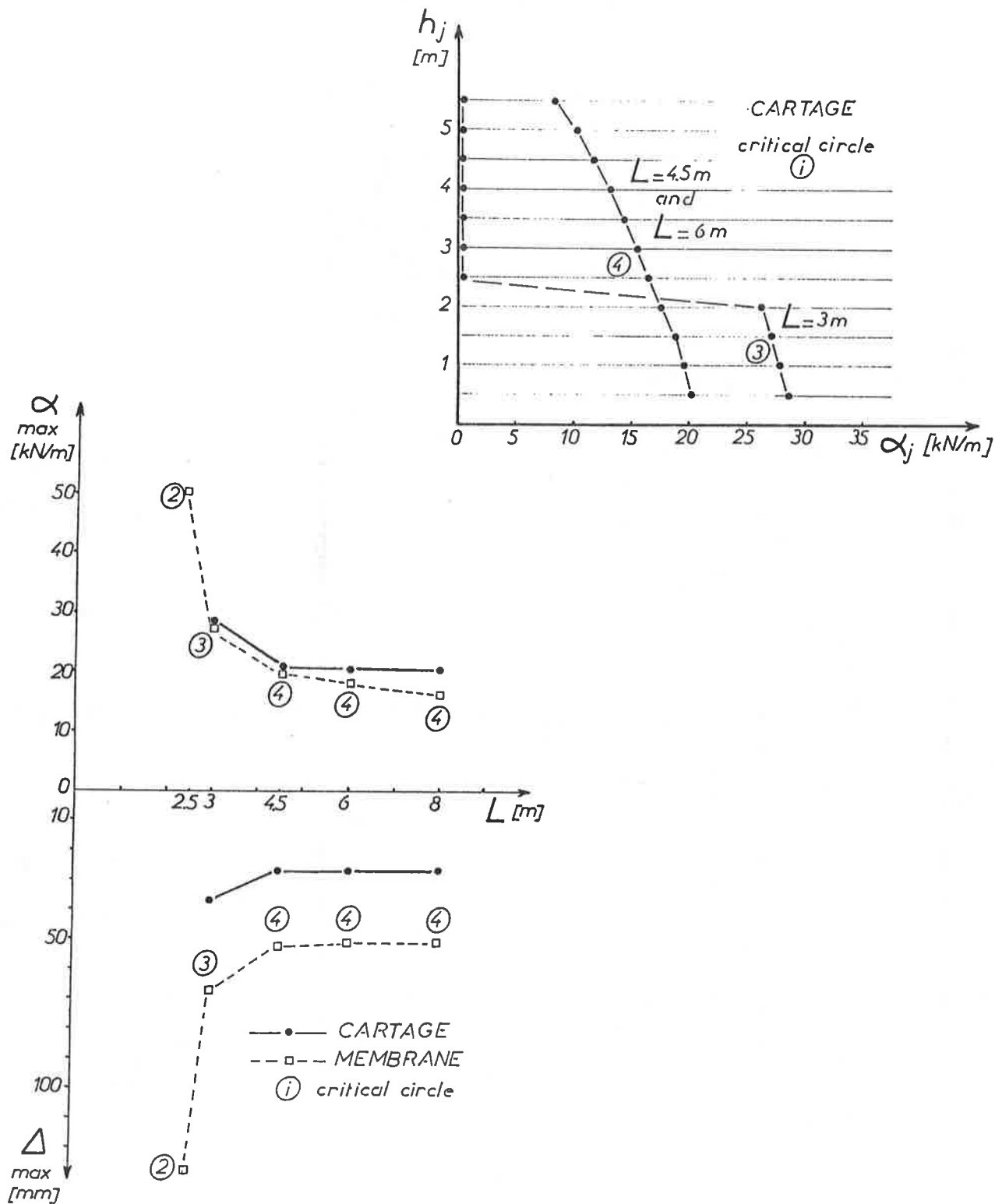


Figure 9 : Model of chart, to design soil reinforced retaining wall

REFERENCES :

- (1) Delmas, Ph., Berche, J.C., Gourc, J.P., "Le dimensionnement des ouvrages renforcés par géotextile : programme CARTAGE", Bulletin de Liaison des Laboratoires des Ponts et Chaussées, Paris, 1986, n° 142.
- (2) Gourc, J.P., Ratel, A., Delmas, Ph., "Design of fabric retaining walls : the Displacements Methods", Proceedings of Third International Conference on Geotextiles and Geomembranes, Vienne, Austria, 1986.
- (3) Gourc, J.P., Ratel, A., Gotteland, Ph., "Design of reinforced soil retaining walls : Analysis and Comparison of existing methods and proposal for a new approach", The Application of Polymeric Reinforcement in soil Retaining Structures, Nato Asi Series - Applied Sciences - Vol 147 - 1988.
- (4) Gourc, J.P., Gotteland, Ph., Delmas, Ph., "Design of geosynthetic retaining walls : Displacements Method and Two-Blocks Method. Comparison and Charts", Proceedings of International Geotechnical Symposium on Theory and Practice of Earth Reinforcement, Fukuoka Kyushu, Japan, 1988.
- (5) Ratel, A., "Modelisation d'un sol renforcé par géosynthétique. Application de la Méthode en Déplacements", Thesis Dr Ing. IRIGM, University of Grenoble 1, France, 1987.
- (6) Raulin, P., Rouqués, G., Toubol, A., "Calcul de la Stabilité des pentes en rupture non circulaire", Rapport de Recherche des Laboratoires des Ponts et Chaussées, Paris, 1974, n°36.
- (7) Schlosser, F., Long, N.T., "Recent Results in French Research on Reinforced Earth", Journal of the Construction Division, ASCE, Vol 100, N° 003, Sept 1974.

SESSION 5A
EMBANKMENTS

1. The first step is to identify the problem or question that needs to be answered.

2. The second step is to gather relevant information and data.

3. The third step is to analyze the information and data to identify patterns and trends.

4. The fourth step is to develop a hypothesis or theory based on the analysis.

5. The fifth step is to test the hypothesis or theory through experiments or observations.

6. The sixth step is to evaluate the results of the tests and draw conclusions.

7. The seventh step is to communicate the findings to others.

R.K. ROWE

B.L.J. MYLLEVILLE

University of Western Ontario, Canada

Consideration of Strain in the Design of Reinforced Embankments

ABSTRACT

An examination of the development of shear strain in soft clay foundations underlying geotextile reinforced embankments is presented. It is shown that the shear strain response of the foundation is significantly affected by the reinforcing fabric modulus and the foundation soil modulus. Results are presented at various stages of loading which demonstrate the formation of a band of maximum shear strain as the reinforced embankment approaches failure and ultimate collapse. Implications with regard to strain softening soils are briefly discussed.

INTRODUCTION

In recent years, research has been undertaken to establish the potential benefits of using geotextile reinforcement to improve the performance of embankments on poor foundations and to develop design methods (eg. (1), (2), (3), (4) and (5)). Recognizing that geotextile reinforcement may improve embankment performance is only one step. There is also a need to investigate the response of the underlying soft foundation and establish the extent to which various factors affect that response.

The purpose of this paper is to discuss some finite element results which illustrate the shear strain response of the foundation soil due to loads imposed by geotextile reinforced embankments. The effects of various factors such as the modulus of fabric and foundation on the development of shear strain in the foundation will also be discussed. Due to space limitations, it will only be possible to present a few results for the case of a granular reinforced embankment with a crest width of 18 m and 2:1 side slopes. The foundation is assumed to have an undrained strength and modulus profile which increase linearly with depth.

DETAILS OF THE NUMERICAL ANALYSIS

The results reported in this paper were obtained using a small strain elastoplastic finite element program. The specific formulation adopted assumes a Mohr-Coulomb failure criterion together with a flow rule of the form proposed by Davis (eg. (6)). Utilizing a finite element mesh with 4247 degrees of freedom, embankments were "constructed" by turning on gravity within rows of elements. This involved up to 14 lifts and a total of up to 250 load steps. Comparison of results

with benchmark solutions suggests that the collapse height obtained with this mesh is accurate to within 7% of plasticity solutions.

Embankments with a crest width of 18 m and side slopes of 2 to 1 were constructed on 15 m deep soft clay deposits. The clay foundation was in turn assumed to be underlain by a rigid base.

In general, the most critical stage when constructing embankments on soft clay foundations corresponds to that at the end of construction. As a result, the undrained shear strength, $c_u(\phi=0)$ and undrained modulus E_u (taking Poisson's ratio to be 0.48) were used to predict the short term behaviour of embankments constructed on relatively soft cohesive soils. The finite element results presented herein are for the case of a soft clay deposit with strength and modulus which increase linearly with depth from some surface value. Strength profiles of this type are commonly encountered in soft, normally or slightly overconsolidated clays. Two values of the ratio of undrained modulus to undrained strength (E_u/c_u) were considered, namely, $E_u/c_u = 125$ and $E_u/c_u = 500$. The clay foundation was assumed to have a unit weight, γ , of 16.5 kN/m^3 and a coefficient of earth pressure at rest, K'_0 , of 0.60.

The embankment fill was assumed to have a stress-dependent Young's modulus based on Janbu's equation, where the fill modulus is a function of minor principal stress. The parameters used for the granular fill were $\phi = 32^\circ$, $\gamma = 20 \text{ kN/m}^3$ and $\nu = 0.35$.

The geotextile was assumed to be located within the embankment fill at a distance of 375 mm above the clay-fill interface, thus allowing for a 375 mm granular working mat. The fill-geotextile interface friction angle was taken to be 32° . The analyses allowed for slip at the clay-fill interface below the reinforced embankment as well as slip at the fill-geotextile interface. In some of the cases considered, a 0.75 m thick granular pad extended up to 4.4 m from the toe of the slope shown in the figures. This fill had no significant effect on the general observations to be made, although it does have a small effect on local strain and stability.

DEVELOPMENT OF SHEAR STRAIN IN THE FOUNDATION DURING LOADING

Figures 1 through 3 show contours of maximum shear strain at various stages in the "construction" of an 18 m wide (crest width) embankment on a soft clay deposit. The deposit has a nominal (unfactored) undrained shear strength, c_{u0} of 15 kPa at the surface of the deposit and a rate of increase in strength with depth, ρ_c , of 2 kPa/m. The analyses were performed with a factor of 1.3 applied to the foundation strength parameters, (i.e. $c_{u0}^* = 15/1.3 = 11.54 \text{ kPa}$ and $\rho_c^* = 2/1.3 = 1.54 \text{ kPa/m}$). Unless otherwise noted, the ratio of undrained modulus to undrained strength (E_u/c_u) adopted for the clay foundation was 125 and geotextile modulus, J , was 4000 kN/m .

For purposes of further discussion, shear strain, γ , in the clay foundation is defined as the maximum or engineering shear strain (eg. (7)).

Figure 1 shows the contours of maximum shear strain in the clay foundation for a height of fill equal to 5.2 m. The maximum shear strain experienced by the underlying soil is approximately 6% and occurs below the centreline of the embankment. At this point the maximum strain in the fabric is 1.7%.

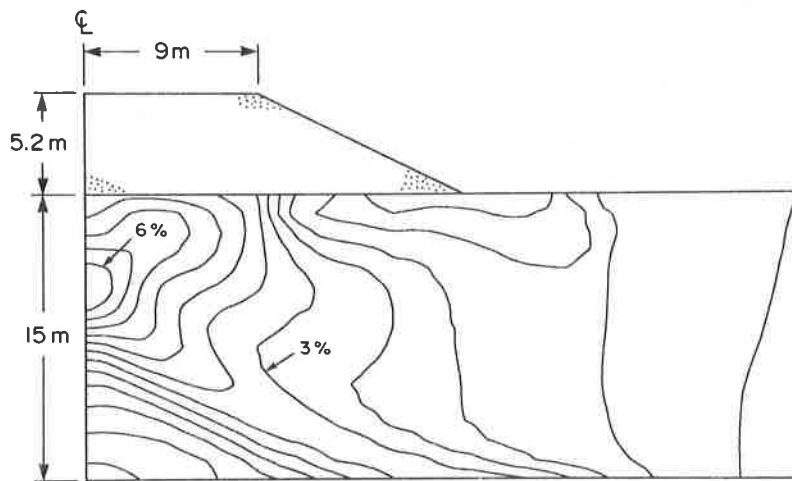


Figure 1. Shear strain contours at 5.2 m fill thickness: factored parameters c_{u0}^* , ρ_c^* , $E_u/c_u = 125$ and $J = 4000$ kN/m (0.5% contour interval)

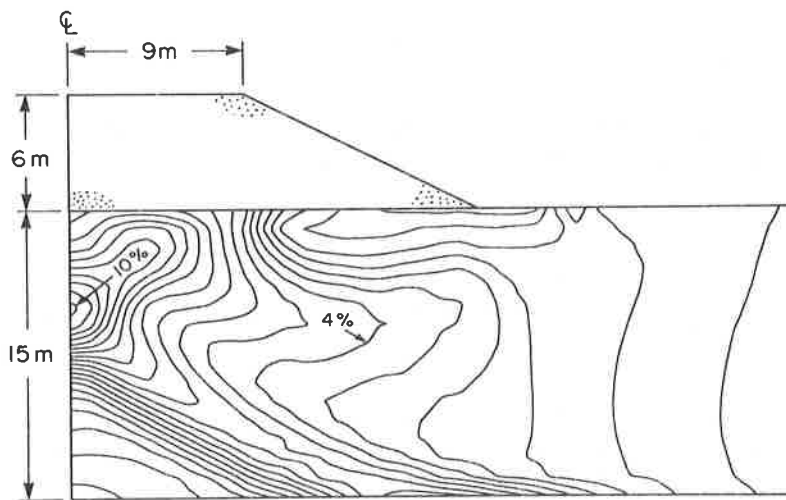


Figure 2. Shear strain contours at 6 m fill thickness: factored parameters c_{u0}^* , ρ_c^* , $E_u/c_u = 125$ and $J = 4000$ kN/m (0.5% contour interval)

The contours of shear strain at a fill height of 6 m are plotted in Figure 2 with the maximum being in the order of 10%. Once again, the maximum shear strain experienced by the clay foundation occurs under the centreline of the embankment. The maximum strain in the fabric has increased to 2.5%. What is interesting to note from Figure 2 is that under the shoulder of the embankment one can see the beginning of the formation of what turns out to be (in Fig. 3) a band of maximum shearing strain in the clay foundation.

For purposes of further discussion, a reinforced embankment will be deemed to have failed at a fill height where the increment in vertical displacement is equal

to or exceeds the increment in fill thickness just added. Thus, the addition of more fill will not result in a net increase in embankment height. (For a detailed discussion regarding the failure and collapse of geotextile reinforced embankments, see Rowe and Soderman, i.e. (8) and (9).)

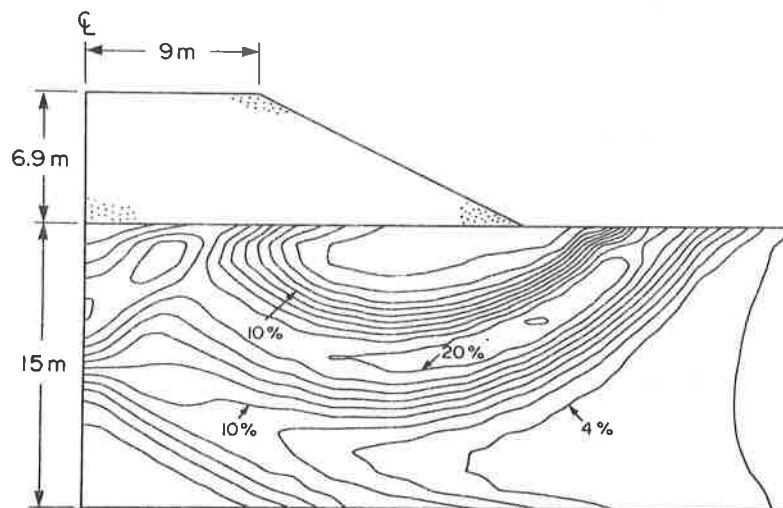


Figure 3. Shear strain contours at failure (6.9 m): factored parameters c_{uo}^* , ρ_c^* , $E_u/c_u = 125$ and $J = 4000$ kN/m (2% contour interval)

Figure 3 shows the shear strain contours plotted at a 2% interval, at the failure height of 6.9 m for this reinforced embankment. It can be seen that a band of maximum shear strain has now developed in the clay foundation with a maximum value of about 23%. At failure, the maximum strain in the geotextile is approximately 7%.

As might be expected, the foregoing results demonstrate that the shear strain in the soil increases with increasing embankment height. What is less obvious is the fact that even with a high modulus reinforcement, there can be significant shear strains developed in the foundation and that these shear strains may be much greater than the maximum tensile strain developed in the reinforcing geotextile. For example, at a height of 5.2 m (see Fig. 1), there is an extensive region of the soil where the shear strain is between 3% and 6%, even though the maximum fabric strain is only 1.7%. For an elasto-perfectly plastic soil (i.e. where there is no strain softening), the failure height of 6.9 m is well below the plasticity collapse height, however the engineering shear strains in the foundation are of the order of 18% or higher along the potential failure surface despite the fact that the maximum fabric strain is only about 7%. These results indicate that considerable caution is required in projecting the likely strains that will develop in the foundation based on an allowable or expected strain in the geotextile reinforcement.

For a given geometry and strength profile, the relationship between strain in the geotextile and shear strain in the foundation will depend on a number of factors such as the modulus of the foundation soil, the load level and the modulus of the fabric. The effect of soil modulus will be discussed in subsequent sections. Space does not permit the presentation of many results for different fabric mo-

duli, however it is noted that for a given embankment height, the shear strains in the foundation are greater for fabric moduli less than the value of $J = 4000 \text{ kN/m}$ adopted for Figures 1-3. On the other hand, it is also found that the failure height (and consequently the allowable design height) can increase with increasing fabric modulus. For these situations, one can compare the shear strains in the foundation obtained at an allowable height corresponding to a factor of safety of 1.3 (based on peak shear strength) and it is found that the engineering shear strain in the foundation under working conditions increases with increasing modulus of the fabric. Thus, for an elasto-plastic soil and a given factor of safety increasing the modulus of the fabric may increase the allowable design height, but the engineering shear strain will also increase with the increased embankment height. This increase in engineering shear strain may pose a problem for strain softening soils since the increase in shear strain will lead to additional loss of shear strength. Hence, it may not be possible to realize the same improvement in performance by increasing geotextile modulus as is possible for perfectly plastic soils.

BAND OF MAXIMUM SHEAR STRAIN AND POST FAILURE RESPONSE

The numerical analysis indicates that as one approaches failure, and ultimately collapse, a band of maximum shear strain develops in the clay foundation. This band of maximum shear strain is, in essence, the location through which the failure mechanism passes, as can be illustrated by comparing the strain contours shown in Figure 3 with the velocity field at failure shown in Figure 4. The arrows in the velocity field indicate the direction and relative magnitude of soil movement at failure of the reinforced embankment system. Here, a surface which encompasses the region of major movement in the clay foundation, as indicated by the velocity field, also corresponds to the location of the band of maximum shear strain shown in Figure 3.

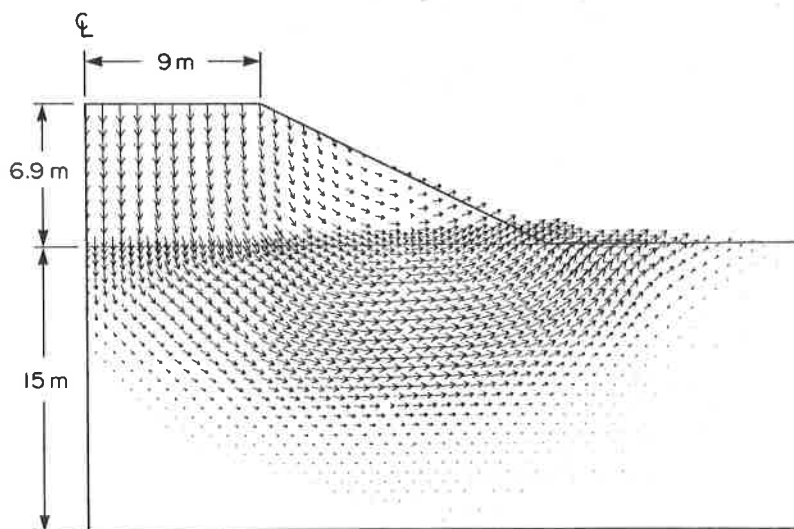


Figure 4. Velocity field at failure (6.9 m): factored parameters
 $c_{u0}^*, \rho_c^*, E_u/c_u = 125$ and $J = 4000 \text{ kN/m}$

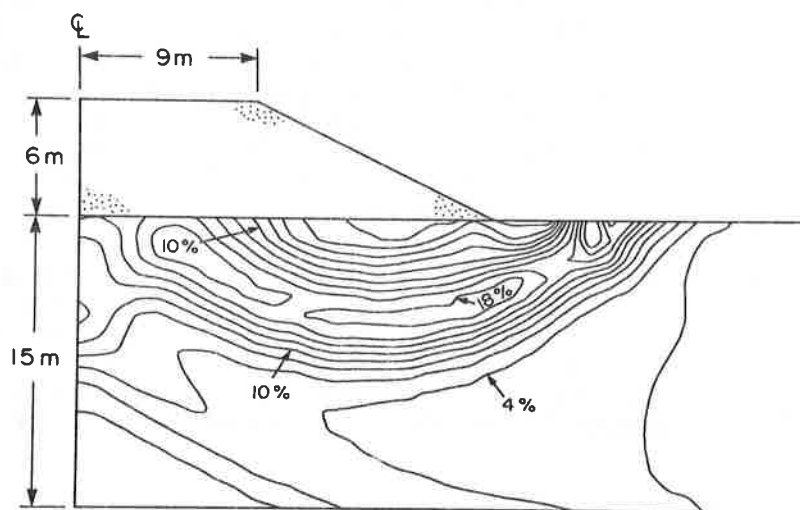


Figure 5. Shear strain contours at 6 m fill thickness: factored parameters c_{u0}^* , ρ_c^* , $E_u/c_u = 125$ and $J = 1000$ kN/m (2% contour interval)

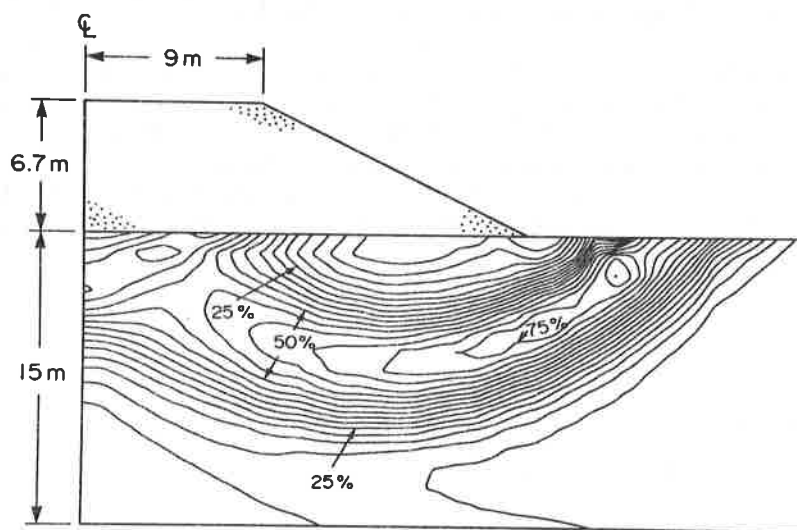


Figure 6. Shear strain contours at 6.7 m fill thickness (i.e. post failure): factored parameters c_{u0}^* , ρ_c^* , $E_u/c_u = 125$ and $J = 1000$ kN/m (5% contour interval)

The strain contour shown in Figures 1-3 were obtained for a fabric modulus, $J = 4000$ kN/m. Figures 5 and 6 show strain contours obtained for the same foundation properties but a fabric modulus of $J = 1000$ kN/m.

Firstly, a comparison of Figures 2 and 5 shows that at an embankment height of 6 m the shear strains developed in the soil for $J = 1000$ kN/m (Fig. 5) are much larger than the strains obtained for $J = 4000$ kN/m (Fig. 2). In fact, for $J = 1000$ kN/m, the fill height of 6 m corresponds to the failure height. Comparison of Figures 3 and 6 also shows the benefit of geotextile modulus for an elastic-

perfectly plastic soil. With $J = 4000 \text{ kN/m}$, the strains in the foundation at failure (6.9 m, see Fig. 3) are substantially less than the strains developed at a height of 6.7 m for $J = 1000 \text{ kN/m}$ (Fig. 6).

As noted by Rowe and Soderman (8), (9), failure of a reinforced embankment may be deemed to have occurred when the addition of more fill does not increase the net embankment height above original ground level, however the plasticity collapse "height" (i.e. the maximum thickness of fill which can be added before "collapse" occurs) may be considerably greater than the failure height. Figure 5 shows the strains at failure (6 m) and Figure 6 shows the strains which result from increasing the fill thickness to 6.7 m. Comparing Figures 5 and 6, it can be seen that there has been a substantial increase in shear strain due to the additional 0.7 m of fill. This comparison clearly shows that even though from the strict standpoint of plasticity the embankment may not have collapsed, it most certainly has failed at a height of 6 m and the post failure response involves excessive straining of the foundation.

If the 6.7 m embankment has failed, but not collapsed (where collapse involves indeterminant strains and deformations), how is the increased fill height being supported? In part, the additional fill (beyond the failure height) is being supported by the increased strain and force in the fabric. However, this additional fill results in a change in the location of the zone of maximum shearing, which is forced deeper into the foundation soil. Since the soil's strength increases with depth, this then supports a higher embankment height. The movement of the zone of intense shearing is evident from Figures 5 and 6. In Figure 5 ($h = 6 \text{ m}$), the band of intense shearing extends to a depth of approximately 5 m below the surface of the clay foundation. In Figure 6 ($h = 6.7 \text{ m}$), the band of intense shearing extends to a depth of approximately 6.6 m. Thus, the post failure response of the embankment involves movement of the potential shear plane deeper into the foundation material. This can happen for a perfectly plastic soil, however if the soil exhibits any measure of strain softening then localization will occur along the original plane of intense shearing (eg. as shown in Figure 5). One would not expect that the shear plane could subsequently move deeper as was seen in Figure 6 and consequently one would expect that collapse would occur at an embankment height very similar to the failure height (i.e. the response would be far more brittle). Clearly, more research is required to identify the effects of strain softening on the performance of reinforced embankments.

WORKING STRESS CONDITIONS AND THE EFFECT OF FOUNDATION MODULUS

To provide an indication of the shear strains which might be expected in the clay foundation beneath the embankment at working stress levels, analyses were performed with nominal (unfactored) parameters. The results presented in Figures 7 and 8 are for a clay foundation with a nominal undrained shear strength at the surface $c_{u0} = 15 \text{ kPa}$ and a rate of increase in strength with depth of $\rho_c = 2 \text{ kPa/m}$. Thus, the "design" height for a factor of safety of 1.3 corresponds to the failure heights obtained using factored parameters as reported in the previous section.

In both cases the embankment was reinforced with a geotextile having a modulus $J = 1000 \text{ kN/m}$. The primary difference in the two analyses is the ratio of the undrained modulus, E_u , to the undrained strength, c_u , in the clay foundation (E_u/c_u). For an E_u/c_u ratio equal to 125 and an allowable working height of 6 m (based on analyses performed using factored parameters, see Fig. 5), finite

element analyses suggest that the clay foundation should experience a maximum shear strain of about 5% under working conditions, as shown in Figure 7. Under these conditions, the corresponding strain in the geotextile is approximately 2.1%. Increasing the stiffness of the foundation four-fold (i.e. $E_u/c_u = 500$) has significantly reduced the shear strains experienced by the underlying clay foundation for the same allowable working height. The maximum shear strain in the underlying clay is about 1.3% (Figure 8), with the corresponding strain in the geotextile equal to about 0.6%. The four-fold increase in foundation stiffness from $E_u/c_u = 125$ to $E_u/c_u = 500$ has resulted in a reduction in foundation soil shear strain and fabric strain of almost a factor of four.

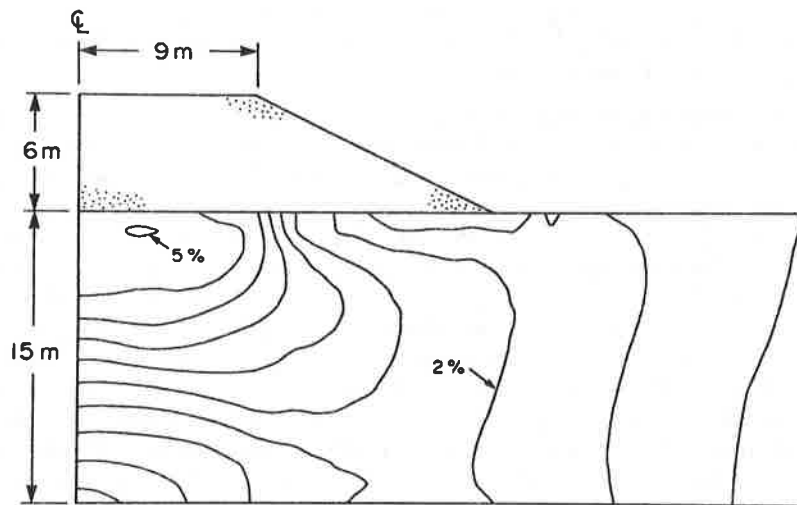


Figure 7. Shear strain contours under working conditions: nominal parameters, c_{u0} , ρ_c , $E_u/c_u = 125$ and $J = 1000$ kN/m (0.5% contour interval)

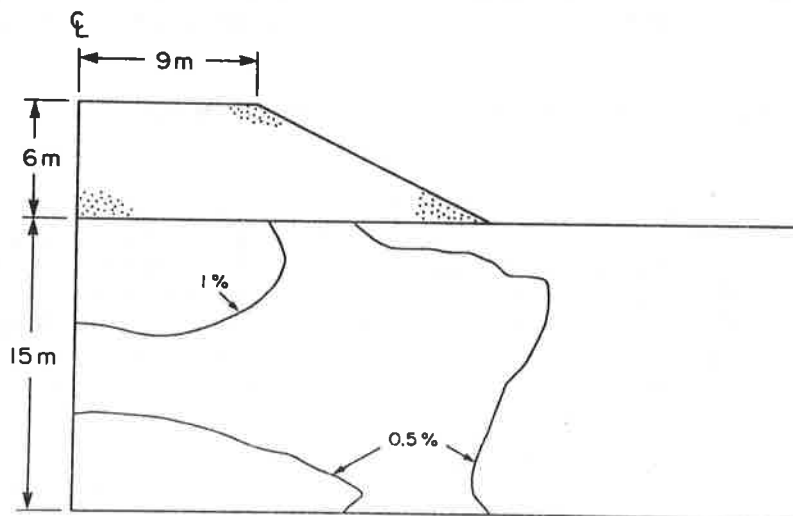


Figure 8. Shear strain contours under working conditions: nominal parameters, c_{u0} , ρ_c , $E_u/c_u = 500$ and $J = 1000$ kN/m (0.5% contour interval)

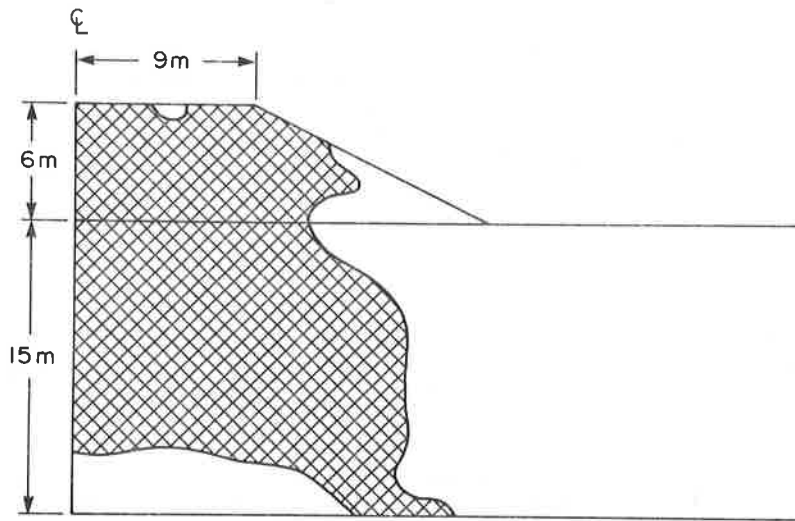


Figure 9. Plastic region under working conditions: nominal parameters, c_{u0} , ρ_c , $E_u/c_u = 125$ and $J = 1000 \text{ kN/m}$

Figure 9 shows the plastic region corresponding to the allowable working height for $E_u/c_u = 125$. The cross-hatched area indicates the zone of soil which has reached its shear strength. Clearly, the embankment is still quite stable under working conditions, since the zone of plastic soil is contained by a large mass of elastic soil. The only significant difference between this plastic region and that obtained for $E_u/c_u = 500$ was that for $E_u/c_u = 500$; there was less plasticity in the embankment fill. This is due to the fact that a stiffer foundation resulted in smaller deformations in the embankment fill at this load level and hence less soil plasticity occurred.

Thus, under working load conditions (with a factor of safety of 1.3), the strains in the geotextile and the shear strains in the underlying foundation are strongly influenced by the undrained modulus of the underlying soil. However, for smaller factors of safety, plastic strain begins to dominate over elastic strains and the failure height of this embankment is essentially independent of the modulus of the foundation material.

It is of some interest to compare the results from the finite element analysis with what might have been expected using conventional limit equilibrium design methods for this particular case. As the basis of comparison, the "allowable height" was determined using factored parameters $c_{u0}^* = c_{u0}/1.3$ and $\rho_c^* = \rho_c/1.3$

($c_{u0} = 15 \text{ kPa}$, $\rho_c = 2 \text{ kPa/m}$) and a fabric modulus of 1000 kN/m . Based on the finite element calculation, the failure height for the factored parameters was 6 m and the strain in the fabric was about 8% (for both $E_u/c_u = 125$ and 500). Using a conventional limit equilibrium analysis and allowable fabric strains of 2% and 5% , the corresponding "failure heights" were 4.8 and 5.1 m respectively. This suggests that for this specific case and a perfectly plastic soil, the conventional approach is conservative if a limiting strain of either 2% or 5% is specified.

The "failure heights of the embankment" deduced using factored parameters correspond to the working or design height for the nominal parameters. Table 1 summarizes the strains determined from finite element analyses for working condi-

tions where the allowable height of 6 m was deduced from the finite element analysis as well as allowable heights of 4.8 and 5.1 m which were deduced from a limit equilibrium analysis using 2% and 5% "allowable" strains as previously discussed. Results are given for values of E_u/c_u of 125 and 500. These ranges are considered to bracket the ratio of E_u/c_u expected for most soft soils (eg. see (10)).

TABLE 1 Summary of Calculated Maximum Strain in the Geotextile and Foundation Under "Working" Conditions - $c_{u0} = 15$ kPa, $\rho_c = 2$ kPa/m

Fill Thickness (m)	Modulus Ratio			
	$E_u/c_u = 125$		$E_u/c_u = 500$	
	Maximum Fabric Strain (%)	Maximum Shear Strain in Foundation (%)	Maximum Fabric Strain (%)	Maximum Shear Strain in Foundation (%)
Allowable Heights				
4.8* ($\epsilon_f=2\%$)	1.2	3.3	0.3	0.9
5.1* ($\epsilon_f=5\%$)	1.4	3.8	0.4	1.1
Allowable Height				
6.0	2.1	5.0	0.6	1.3
Height Exceeding Allowable				
6.5	2.6	6.3	0.7	1.7
6.8	3.1	7.3	1.7	4.9

* Calculated from limit equilibrium using factored parameters and an allowable strain, at limiting equilibrium, of ϵ_f .

At an embankment height of 6 m, the strain developed in the fabric is quite small and ranges between 0.6 and 2.1% depending upon the ratio of E_u/c_u . The embankment height 4.8 m was based on an allowable fabric strain of 2% using factored parameters and the calculated strain range of 0.3 to 1.2% obtained using the nominal parameters at this design height is less than the 2% assumed at "failure", however the engineering shear strain varied from 0.9 to 3.3% depending on E_u/c_u .

The embankment height of 5.1 m was based on an allowable fabric strain of 5% and it can be seen that the calculated maximum fabric strain at this height ranged between 0.4 and 1.4% (i.e. they are well below the "allowable" strain of 5%).

Thus, provided that the initial estimate of shear strength (i.e. the nominal parameters) was either accurate or conservative then, for this case, a design based on a limit equilibrium calculation using an allowable strain of either 2% or 5% would perform quite satisfactorily for a perfectly plastic or strain hardening soil.

An examination of the engineering shear strains tabulated in Table 1 indicates that at the 6 m design height based on the finite element calculations, the maximum shear strain in the foundation is sensitive to the modulus ratio and varied between 1.3 and 5%. As the embankment height is increased from 6 to 6.8 m, there is a rapid growth in the plastic region in the underlying soil and as the plastic strains begin to dominate over the elastic strains, the effect of the ratio E_u/c_u becomes less significant. Thus, at a height of 6.8 m, the maximum engineering shear strain in the foundation ranged from 4.9 to 7.3%. If the soil is perfectly plastic or work hardening, then these maximum shear strains may not be of concern. However, if the foundation material is strain softening then there is considerable cause for concern, since one would normally expect considerable strength loss in the soil at shear strains approaching 5%. It is also noted that the stiffer soil profile ($E_u/c_u = 500$) exhibits a much more brittle behaviour than the soil profile with $E_u/c_u = 125$ even for a perfectly plastic material. While the soil is largely elastic, the strains for $E_u/c_u = 500$ are quite small however they increase rapidly once the plastic region becomes extensive. Thus, the presence of small strains and good performance at a given height does not necessarily imply that more fill can be added without significant change in embankment performance. For example, with $E_u/c_u = 500$, increasing the height by 5% from 6.5 m to 6.8 m more than doubled the calculated maximum strain in the geotextile and increased the maximum shear strain in the foundation by a factor of 2.9.

It is noted that if no limit is placed on allowable strain in the reinforcement, limit equilibrium would indicate that the allowable height could be at least 7.1 m (based on factored parameters and a factor of safety of 1.3).

CONCLUSIONS

Some results obtained from a study of the effects of geotextile and foundation soil moduli on the shear strain response of a soft foundation underlying a geotextile reinforced embankment have been presented. It has been shown how the shear strain field beneath a geotextile reinforced embankment changes during loading. At load levels well below "failure", the maximum shear strain experienced by the underlying clay foundation is located below the centre of the embankment. As loading continues to failure and ultimately collapse, a band of maximum shear strain develops which coincides with the potential shear plane defining a failure mechanism. Post failure response of the embankment involves movement of the potential shear plane deeper into the foundation soil. Implications with regards to strain softening soils were briefly discussed.

In general, the shear strain in the foundation soil increases with increasing embankment height. Analyses have shown that at a given load level prior to failure and for geotextile moduli less than $J = 4000$ kN/m, increasing fabric modulus tends to decrease foundation soil shear strain. However, for an elastoplastic soil and a given factor of safety, increasing the modulus of the fabric may increase the allowable design height but the engineering shear strain will also increase with increased embankment height.

For any given geometry and strength profile, the relationship between strain in the geotextile and shear strain in the foundation will depend on a number of factors. These factors include foundation soil modulus, reinforcing fabric modulus and load level.

Geosynthetics '89 Conference
San Diego, USA

Considerable caution should be exercised when projecting the likely strains that will develop in the foundation soil based on an allowable or expected strain in the geotextile. Even with high modulus geotextile there can be significant shear strains developed in the foundation soil. Shear strains may be much greater than the maximum tensile strain developed in the reinforcing geotextile. This suggests that considerable caution should be adopted in using conventional limit equilibrium calculations to estimate stability if the foundation material exhibits strain softening.

ACKNOWLEDGEMENTS

The work described in this paper forms part of a general programme of research into reinforced soil funded by the Natural Science and Engineering Research Council of Canada under Grant No. A1007.

REFERENCES

- (1) Rowe, R.K. and Soderman, K.L., "An Approximate Method for Estimating the Stability of Geotextile-Reinforced Embankments," Canadian Geotechnical Journal, Vol. 22, No. 3, 1985, p.p. 392-398.
- (2) Rowe, R.K. and Soderman, K.L., "Reinforced Embankments on Very Poor Foundations," International Journal for Geotextiles and Geomembranes, Vol. 4, No. 1, 1986, p.p. 65-81.
- (3) Fowler, J., "Theoretical Design Considerations for Fabric Reinforced Embankments," Proceedings, 2nd International Conference on Geotextiles, Las Vegas, Vol. 2, 1982, p.p. 665-670.
- (4) Jewell, R.A., "A Limit Equilibrium Design Method for Reinforced Embankments on Soft Foundations," Proceedings, 2nd International Conference on Geotextiles, Las Vegas, Vol. 2, 1982, p.p. 671-676.
- (5) Boutrup, E. and Holtz, R.D., "Analysis of Embankments on Soft Ground Reinforced With Geotextiles," Proceedings, 8th European Conference on Soil Mechanics and Foundation Engineering, Helsinki, Vol. 2, 1983, p.p. 469-472.
- (6) Davis, E.H., "Theories of Plasticity and Failure of Soil Masses," In: Soil Mechanics - Selected Topics, Ch. 6, Ed. by I.K. Lee, Butterworths, London, 1968.
- (7) Poulos, H.G. and Davis, E.H., Elastic Solutions for Soil and Rock Mechanics, John Wiley Inc., New York, 1974.
- (8) Rowe, R.K. and Soderman, K.L., "Reinforcement of Embankments on Soils Whose Strength Increases With Depth," Proceedings of Geosynthetics '87 Conference, New Orleans, U.S.A., p.p. 266-277.
- (9) Rowe, R.K. and Soderman, K.L., "Stabilization of Very Soft Soils Using High Strength Geosynthetics: The Role of Finite Element Analyses," International Journal for Geotextiles and Geomembranes (to appear Vol. 6, No. 1, 1988).
- (10) Duncan, J.M. and Buchigani, A.L., "An Engineering Manual for Settlement Studies," Geotechnical Engineering Report, Dept. of Civil Engineering, University of California at Berkeley, 94 p.

D.N. HUMPHREY

University of Maine, Orono, U.S.A.

R.D. HOLTZ

University of Washington, Seattle, U.S.A.

Effect of Surface Crust on Reinforced Embankment

ABSTRACT

Reinforced embankments are often constructed on soft clay deposits which are overlain by a thin surface crust. This paper uses a finite element analysis with a cap type soil model to show that the properties and thickness of this crust are dominant factors affecting reinforced embankment behavior. It is shown that crust strength has the greatest influence on the increase in embankment height made possible by reinforcement. Crust thickness and compressibility are also important factors. The analyses show that reinforcement is effective for reinforcing embankments constructed on foundations with pockets of weak soil in an otherwise strong crust.

INTRODUCTION

Geosynthetic reinforcement is commonly used to increase the stability of embankments founded on soft clays. Soft clays often are overlain by a thin surface crust with higher strength and lower compressibility than the underlying soil. The strength and deformation properties of the crust have a significant influence on the design of reinforced embankments (2). This was evidenced by two geogrid reinforced embankments constructed to failure on Champlain Clay near St. Alban, Quebec. It was concluded that crust strength was the most important factor controlling the observed failure heights(1). A previous study by the authors (2) showed that crust strength was more important than overall foundation thickness, compressibility of foundation soil, embankment width, and embankment side slope in determining reinforced embankment behavior.

This paper will show the importance of the surface crust on the behavior of reinforced embankments. The effect of crust strength, thickness, and stiffness on deformations, failure height, and reinforcing force are presented. The influence of overall foundation thickness and embankment width is discussed. In addition, the effect of pockets of weak soil in an otherwise strong crust is examined. This study is an extension of work presented in (2).

A finite element analysis technique was used. Soil behavior was represented by a cap type work hardening soil model. A brief description of the model and analysis procedure is given in the next section. Further details are given in (2,6). Procedures to determine the model parameters from readily available soil test results are given in (3). Model parameters for a wide variety of clayey soils is given in (4).

ANALYSIS PROCEDURE

The effect of reinforcement on embankment behavior was studied using a plane strain finite element program PS-NFAP. The cap soil model was implemented in the program by McCarron (6). Program operation is described in (5). There are main-frame and PC versions of the program. Most of the analyses for this study were performed using the PC version operating on a 12 Mhz AT-compatible computer. Typical solution times ranged between 30 minutes and 2 hours.

Foundation soil behavior was represented by an elastic-plastic model with a strain hardening cap. The main features of the cap model are outlined in the next section. Further details are given in (2,6). The procedure used to represent embankment and reinforcement behavior is described in the subsequent section. Eight node isoparametric quadrilateral elements were used for both the embankment and foundation.

Cap Soil Model

The form of the cap model used in this paper has a cone shaped Drucker-Prager ultimate failure surface and an elliptical work hardening cap (Fig. 1). They are expressed in terms of effective stresses by the first invariant of the stress tensor I'_1 and the second invariant of the stress deviator tensor J_2 . Compressive stresses and strains are taken as negative. The ultimate failure surface has a slope α and an intercept with the $J_2^{1/2}$ axis of κ (Fig. 1). The equation of this surface is

$$\alpha I'_1 + J_2^{1/2} - \kappa = 0 \quad (1)$$

The cap intersects the I'_1 axis at x and the ultimate failure surface at coordinates $[l, (x-l)/R]$ (Fig. 1). The aspect ratio R is the ratio of the major and minor radii. The cap's shape is described by the equation of an ellipse

$$(I'_1 - l)^2 + R^2 J_2 - (x - l)^2 = 0 \quad (2)$$

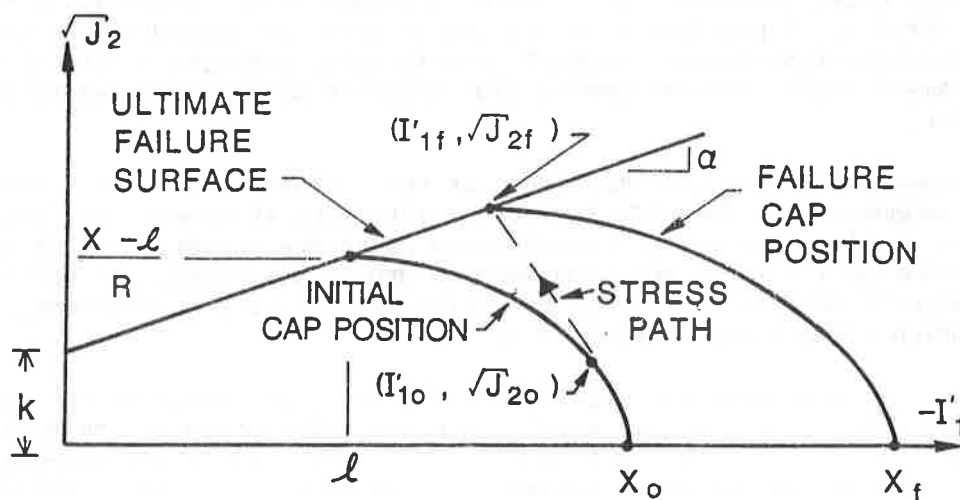


Fig. 1 Cap model in $I'_1 - J_2^{1/2}$ space.

The position of the cap is coupled to the plastic volumetric strain ϵ_V^p by the relation

$$\epsilon_V^p = W[\exp(Dx) - 1] \quad (3)$$

where W and D are curve fitting parameters. A normal flow rule is assumed. For overconsolidated soils the initial position of the cap is fixed by the undrained shear strength (2).

Elastic behavior is governed by the bulk (K) and shear (G) moduli which are given by

$$K = K_1 A_p [I_1' / (3A_p)]^{K_2} \quad ; \quad G = G_2 + G_1 K \quad (4)$$

where K_1 , K_2 , G_1 , and G_2 are fitting parameters; A_p is atmospheric pressure and has the same units as the moduli. A small minimum value of the bulk modulus K_{min} was specified to avoid numerical difficulties. For undrained loading the condition of no volume change is obtained by adding the apparent stiffness of the pore fluid-solid particle system to the stiffness of the soil skeleton (6).

A loading increment can produce one of the following types of strain response depending on where the state of stress plots in stress space (Fig. 1). (1.) For states of stress within the region bounded by the cap and ultimate failure surface the response is elastic. The initial state of stress for overconsolidated soils plot in this region; thus, their initial response is elastic. (2.) For states of stress on the cap or on the ultimate failure surface the response is elastic plus plastic. The initial state of stress for normally consolidated soils plot on the cap. (3.) For states of stress at the intersection of the cap and ultimate failure surface the response is plastic. Soils that have reached their ultimate shear strength plot at this point and exhibit perfectly plastic behavior.

Representation of Embankment and Reinforcement Behavior

The stress-strain behavior of the embankment fill was taken to be elastic-plastic with an ultimate failure surface of the Drucker-Prager type (2). A typical lift by lift embankment construction sequence was simulated using an incremental loading technique (6). Buoyant unit weight was used for fill that settled below the ground water table which was taken to be at the original ground surface.

The reinforcement was modeled with 2 or 3 node one-dimensional truss elements which supported only axial tensile loads. No slip was allowed at the soil-reinforcement interfaces. This is reasonable provided the interface shear strength equals or exceeds the soil shear strength. One measure of the benefit provided by the reinforcement is the relative increase in embankment height defined as the percent increase in height of the reinforced embankment over the unreinforced embankment compared at the lesser of the two horizontal deformations at failure. This definition is used throughout the remainder of this paper.

CASES ANALYZED

The cases analyzed had the basic geometry shown in Fig. 2. The embankment had 2h:1v side slopes. Two embankment base widths were considered: 27.4 m (90 ft) and

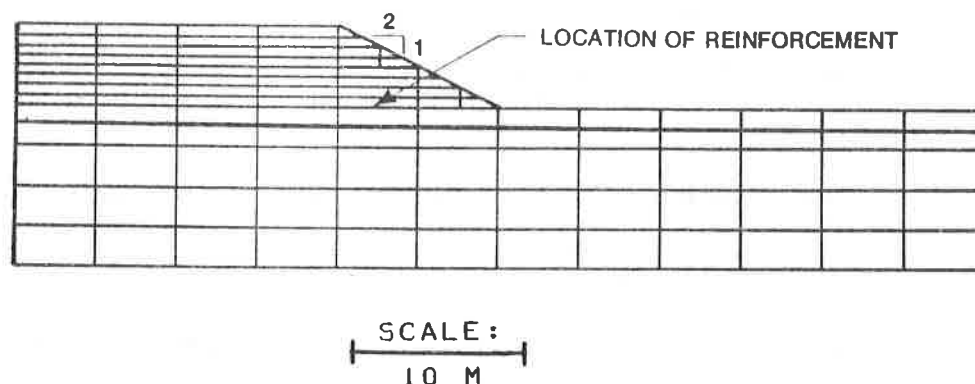


Fig. 2 Problem geometry and typical finite element mesh.

54.9 m (180 ft). The overall foundation thickness was generally 9.1 m (30 ft) but a thickness of 4.6 m (15 ft) was used for a few cases. Surface crust thicknesses of 0 m (no crust), 1.1 m (3.75 ft), and 2.3 m (7.5 ft) were analyzed. The soil underlying the crust was taken to be normally consolidated. The reinforcement was located at the base of the embankment and had a modulus of 880 kN/m (5000 lb/in) which represents a strong, high modulus geotextile or geogrid. A typical finite element mesh is shown in Fig. 2. The problem geometry is symmetric about the embankment centerline; thus, only half of the embankment and foundation was modeled.

The embankment fill was granular. Its effective friction angle was $\phi' = 32^\circ$ which corresponds to $\alpha = 0.17$ for plane strain conditions (2,3). A small cohesion intercept of 0.005 kPa was used to avoid numerical difficulties. The bulk modulus fitting parameters were chosen to match nonlinear stress strain parameters given by (7). $K_1 = 190$ and $K_2 = 0.65$ provided a reasonable fit. A_1 was 101.3 kPa. A minimum bulk modulus of 1 kPa (20 psf) was specified. Poisson's ratio was taken to be 0.35 resulting in $G_1 = 0.33$ and $G_2 = 0.0$. The fill had a unit weight of 19.6 kN/m^3 (125 pcf).

The normally consolidated foundation soil had the properties given in Table 1. The corresponding cap parameters were determined using the procedures given in (2,3) and are summarized in Table 2.

The surface crust was taken to be overconsolidated. It had the same properties as the normally consolidated foundation soil (Table 1) except as noted below. Two undrained shear strengths of the crust were considered: 12 kPa (250 psf; strong crust) and 6 kPa (125 psf; weak crust). The cap parameters for the crust were determined using the procedures given in (2,3) and are summarized in Table 2. In addition, the effect of a more compressible crust was examined by performing analyses with $K_1 = 49.0$ and 26.1. These had the effect of reducing the bulk and shear moduli of the crust by roughly 1/2 for $K_1 = 49.0$ and 1/4 for $K_1 = 26.1$.

BEHAVIOR OF REINFORCED EMBANKMENTS

The results of a finite element study of the influence of the crust on the behavior of reinforced and unreinforced embankments are presented in this section. First, the behavior of an embankment with a 54.9 m base width constructed on a

Table 1. Foundation soil properties.

$\phi' = 28^\circ$	$c'_r = 0.04$
$c' = 0.0$	$e_o = 0.7$
$s_u/\sigma'_{vo} = 0.32$	$w' = 0.3$
$C_c = 0.25$	$\gamma_{sat} = 18.1 \text{ kN/m}^3$

Table 2. Cap parameters for foundation soil.

Parameter	Normally consolidated	Strong crust	Weak crust
α	0.183	0.16	0.17
κ	0.005 kPa	0.005 kPa	0.005 kPa
K_1	98.0	98.0	98.0
K_2	1.0	1.0	1.0
K_{min}	48 kPa	48 kPa	48 kPa
A_p	101.3 kPa	101.3 kPa	101.3 kPa
G_1	0.46	0.46	0.46
G_2	0.0	0.0	0.0
Dx_o	-0.996	-0.996	-0.996
x_o	n.a.	-1.75	-0.83
W	0.146	0.146	0.146
R	0.75	0.75	0.75
K_o	0.47	1.0	0.6

foundation with an overall thickness of 9.1 m and a 2.3 m thick weak crust is examined in detail. This will show the effect of reinforcement on the deformations and induced stresses. Then, the effects of crust strength, thickness and compressibility will be examined individually. Finally, the influence of a pocket of weak soil in an otherwise strong crust will be presented.

Comparison of Reinforced and Unreinforced Embankment Behavior

A detailed examination is presented of the behavior of reinforced and unreinforced embankments with a 54.9-m base width constructed on a foundation with an overall thickness of 9.1 m and a 2.3-m thick weak crust. Horizontal displacement at the embankment toe versus embankment height for reinforced and unreinforced embankments is shown in Fig. 3. The embankment height was taken to be the distance from the low point on the after settlement embankment crest to the original ground surface. It can be seen that the reinforcement increased the height at failure and reduced horizontal displacement at the toe. For both embankments the rate of displacement increased as the height increased. The height at failure was 2.5 m for the reinforced embankment compared to 2.2 m for the unreinforced embankment. The relative increase in height (defined above) made possible by the reinforcement was

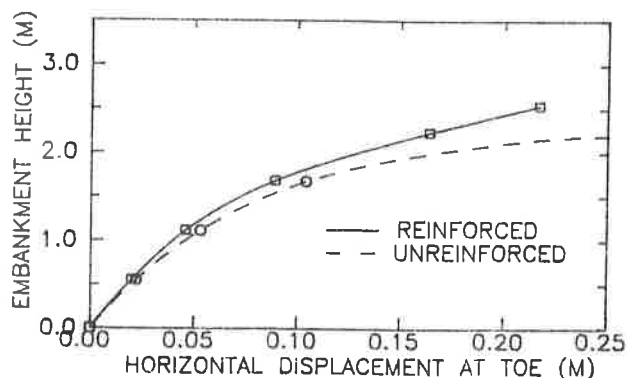


Fig. 3 Horizontal displacement at toe, 54.9-m wide embankment, 9.1-m thick foundation, 2.3-m thick weak crust.

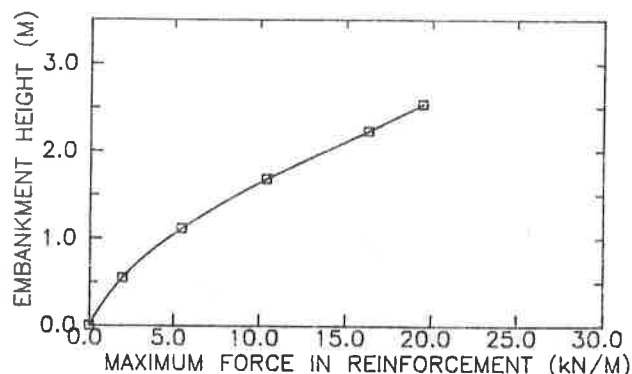


Fig. 4 Maximum force in reinforcement, 54.9-m wide embankment, 9.1-m thick foundation, 2.3-m thick weak crust.

22%. The maximum force in the reinforcement versus embankment height is shown in Fig. 4. The force at failure was 19 kN/m.

Horizontal displacements along several vertical sections in the foundation for an embankment height of 2.2 m are shown in Fig. 5. The largest displacements occur in the upper 3 m at the sections beneath the slope (23 m from centerline) and at the toe (27 m from centerline). Reinforcement clearly reduces deformations in this region but has a much smaller effect at other sections and at greater depths. Thus, the largest displacements and the greatest effect of the reinforcement occurs primarily in the crust.

The change in shear stress in the foundation caused by the reinforcement was examined by comparing the $J_2^{1/2}$ in reinforced and unreinforced embankments at a height of 2.2 m. The change in $J_2^{1/2}$ caused by reinforcement is shown in Fig. 6. The largest reduction in $J_2^{1/2}$ occurred beneath and beyond the toe in the upper 1 m of the crust. Again, the reinforcement has the largest influence in the crust. Further discussion of the effect of reinforcement on stresses and displacements is given in (2).

Effect of Crust Strength

Displacements at the toe of reinforced and unreinforced embankments on foundations with strong, weak, and no crust are compared in Fig. 7 for the 54.9-m wide embankment on a foundation with an overall thickness of 9.1 m and a 2.3-m thick crust. Crust strength is seen to have a large effect on displacements and height at failure. Similar behavior occurred for other combinations of embankment width, foundation thickness, and crust thickness.

The relative increases in height made possible by reinforcement are compared for 5 combinations of geometry in Table 2. Reinforcement clearly becomes more effective as the crust strength decreases. For the strong, weak, and no crust cases the range in relative increase in height was 5-11%, 13-22%, and 60%-72%, respectively. Thus, the relative increases for each crust strength fall in a limited

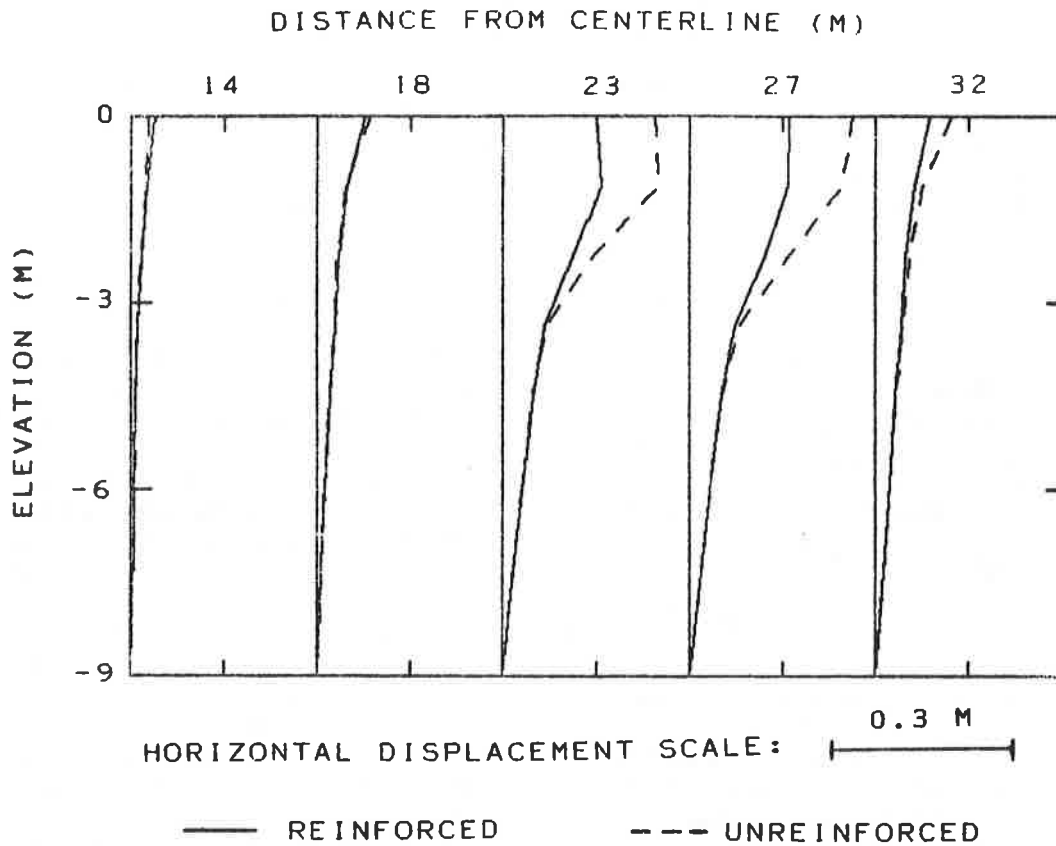


Fig. 5 Comparison of horizontal displacement profiles, 54.9-m wide embankment, 9.1-m thick foundation, 2.3-m thick weak crust.

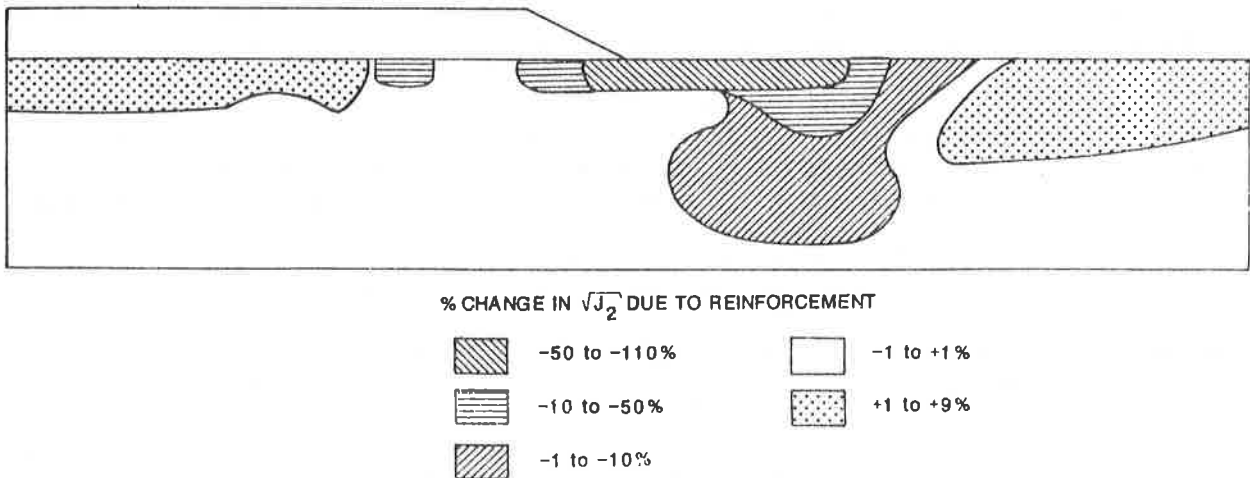


Fig. 6 Change in $J_2^{1/2}$ in foundation due to reinforcement for, 54.9-m wide embankment, 9.1-m thick foundation, 2.3-m thick weak crust.

Table 3. Effect of crust strength on relative increase in height made possible by reinforcement.

Embankment base width (m)	54.9	54.9	54.9	27.4	27.4
Foundation thickness (m)	4.6	9.1	9.1	9.1	9.1
Crust thickness (m)	2.3	2.3	1.1	2.3	1.1
Crust strength:	Strong	5%	6%	9%	11%
	Weak	15%	22%	17%	13%
	None	60%	72%	72%	70%

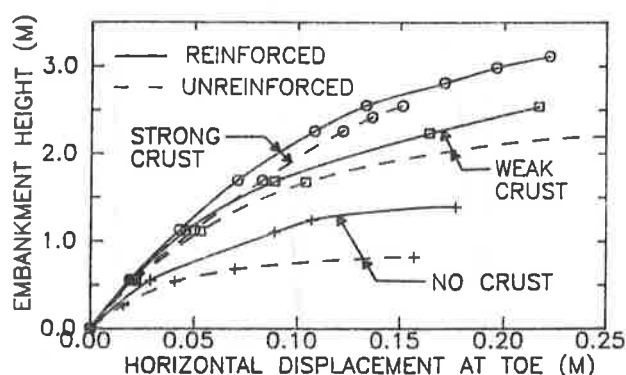


Fig. 7. Effect of crust strength on horizontal displacement at toe, 54.9-m wide embankment, 9.1-m thick foundation, 2.3-m thick crust.

range even though 5 combinations of base width, foundation thickness, and crust thickness were examined.

Crust strength also has a large effect on failure height of reinforced and unreinforced embankments as shown in Table 4. Failure height is plotted versus crust strength for 2.3-m and 1.1-m thick crusts in Fig. 8. For the no crust cases the failure height was plotted at an undrained shear strength of 3 kPa which is the average value of the upper 2.3 m of the normally consolidated foundation soil. It is seen that the influence of embankment width and overall foundation thickness is small compared to the effect of crust strength.

The maximum force in the reinforcement is plotted versus embankment height in Fig. 9 for the 54.9-m wide embankment on a foundation with a 9.1 m overall thickness and a 2.3-m thick crust. For a given embankment height the reinforcing force increases as the crust strength decreases. The maximum force in the reinforcement at failure for 5 combinations of geometry and the strong, weak, and no crust cases is given in Table 5. The reinforcing force at failure ranged from 14 to 33 kN/m. There is no discernable relationship between the reinforcing force at failure and

Table 4. Effect of crust strength on height at failure for reinforced and unreinforced embankments.

Embankment base width (m)	54.9	54.9	54.9	27.4	27.4
Foundation thickness (m)	4.6	9.1	9.1	9.1	9.1
Crust thickness (m)	2.3	2.3	1.1	2.3	1.1
Crust strength:	Strong	3.1/2.9*	3.1/2.5	2.1/2.0	3.2/2.8
	Weak	2.6/2.0	2.5/2.2	2.0/1.6	2.5/2.2
	None	1.4/0.9	1.4/0.8	1.4/0.8	1.3/0.8

*Height of reinforced/unreinforced embankment at failure (m)

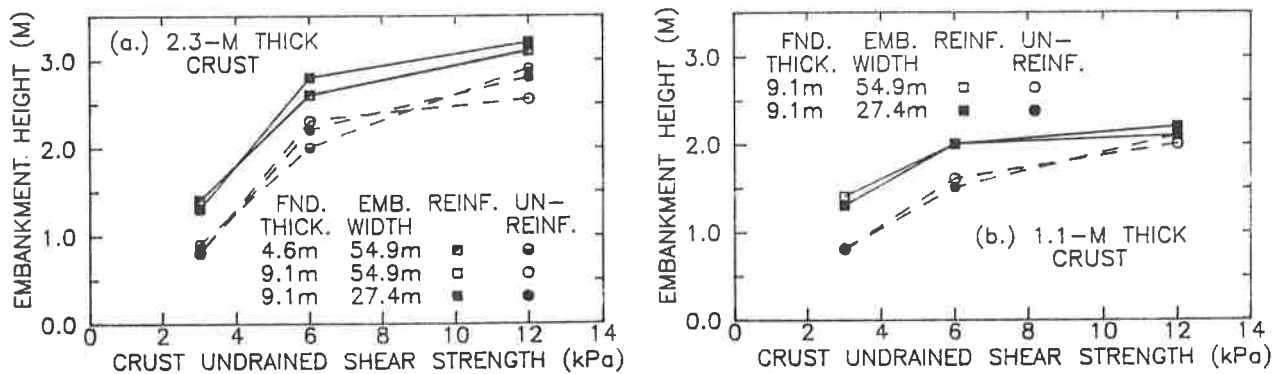


Fig. 8 Embankment height at failure versus undrained shear strength of crust.

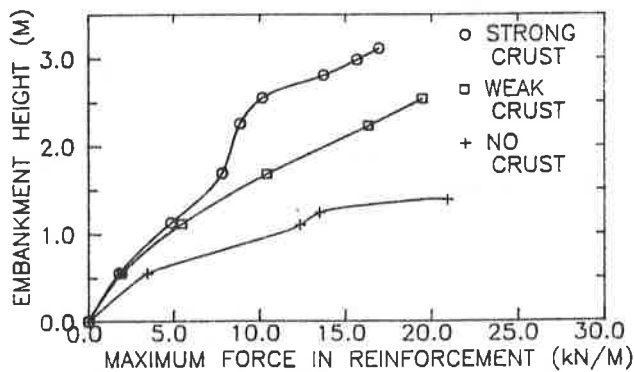


Fig. 9. Effect of crust strength on maximum force in reinforcement, 54.9-m wide embankment, 9.1-m thick foundation, 2.3-m thick crust.

crust strength. One reason is that the computed force is very sensitive to the exact point where the FE solution fails to converge.

Effect of Crust Thickness

Displacements at the toe of reinforced and unreinforced embankments on foundations with 2.3 and 1.1-m thick strong crusts as well as no crust are compared in Fig. 10 for the 54.9-m wide embankment on a 9.1-m thick foundation. Similar behavior occurred for the 27.4-m wide embankment and weak crust cases. Examination of Table 3 shows that crust thickness of 2.3 m or 1.1 m have only a small influence on the

relative increase in height made possible by reinforcement. However, there is a large relative increase for the no crust cases. Table 4 and Fig. 10 show that the failure height decreases as the crust thickness decreases.

The maximum force in the reinforcement at failure is plotted versus embankment height for embankments with a 54.9-m base width on a foundation with a 9.1-m overall thickness, and 2.3 and 1.1-m thick strong crusts as well as no crust in Fig. 11. It is seen that for a given embankment height the reinforcing force increases as the

Table 5. Effect of crust strength on maximum force in the reinforcement at failure.

Embankment base width (m)	54.9	54.9	54.9	27.4	27.4
Foundation thickness (m)	4.6	9.1	9.1	9.1	9.1
Crust thickness (m)	2.3	2.3	1.1	2.3	1.1
Crust strength:					
Strong	19 kN/m	17	14	22	26
Weak	23	19	17	33	17
None	15	21	21	15	15

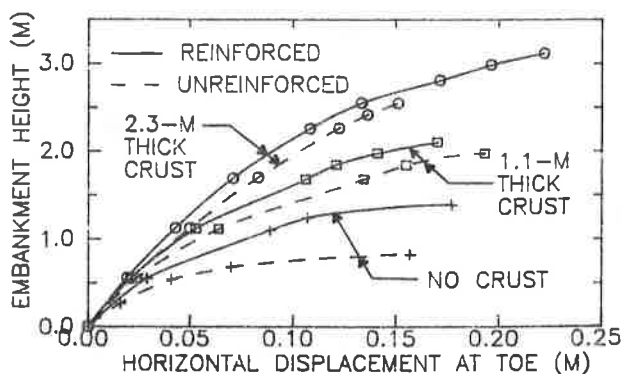


Fig. 10 Effect of crust thickness on horizontal displacement at toe, 54.9-m wide embankment, 9.1-m thick foundation, weak crust.

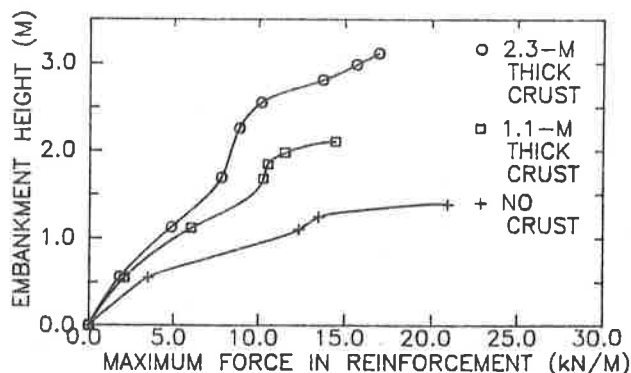


Fig. 11 Effect of crust thickness on maximum force in reinforcement, 54.9-m wide embankment, 9.1-m thick foundation, 2.3-m thick weak crust.

crust thickness decreases. However, there is no discernible relationship between maximum reinforcing force at failure and crust thickness.

Effect of Crust Compressibility

The effect of crust compressibility was examined for a 54.9-m wide embankment on a foundation with a 9.1-m overall thickness and a 2.3-m thick strong crust. This was done by performing analyses with three values of the cap modulus parameter $K_1 = 98.0$, 49.0, and 26.1. This had the effect of varying the bulk and shear moduli with lower values as K_1 decreased. The resulting displacements at the toe for reinforced and unreinforced embankments are shown in Fig. 12. The displacements increase and the failure height decreases as K_1 decreases. The relative increase in failure height due to reinforcement was 6% for $K_1 = 98.0$, 16% for $K_1 = 49.0$, and 30% for $K_1 = 26.1$. Thus, the reinforcement becomes more effective as the compressibility of the crust increases. For a given embankment height the reinforcing force was found to increase as K_1 decreases. The maximum reinforcing force at failure was between

16 and 17 kN/m for all three values of K_1 .

Effect of Weak Pocket

The influence of a pocket of weak, normally consolidated soil in an otherwise strong crust was investigated. An embankment with a 27.4-m base width on a foundation with an overall thickness of 9.1-m and a 2.3-m thick strong crust was used for this analysis. Two positions of the weak pocket were considered, one at the embankment toe and one beneath the embankment slope, as shown in Fig. 13. The displacement at the embankment toe for the weak pocket

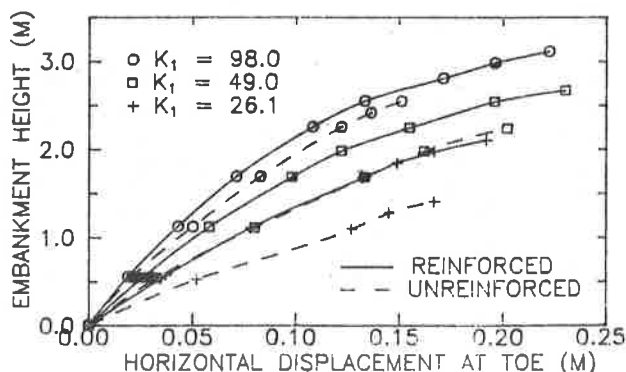


Fig. 12. Effect of crust stiffness on horizontal displacement at toe, 54.9-m wide embankment, 9.1-m thick foundation, 2.3-m thick strong crust.

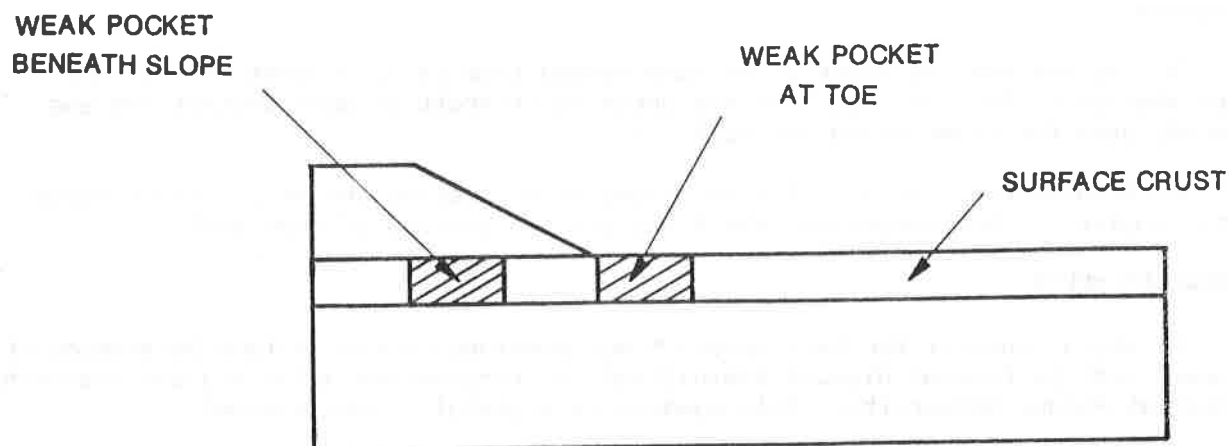


Fig. 13 Location of weak pockets.

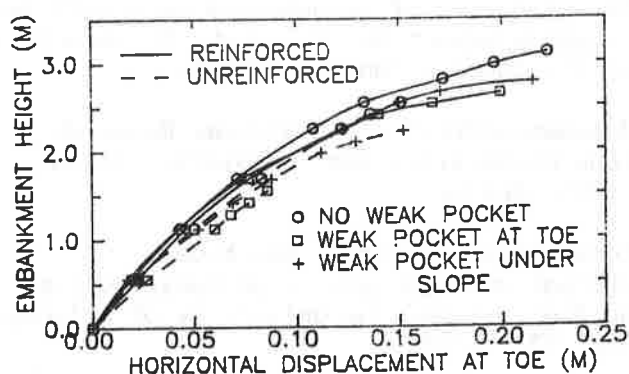


Fig. 14 Effect of weak pocket on horizontal displacement at toe. 24.7-m wide embankment, 9.1-m thick foundation, 2.3-m thick strong crust.

in both positions, as well as a case with no weak pocket for comparison, is shown versus embankment height in Fig. 14. The reinforcement significantly reduces displacement. The relative increase in height due to reinforcement was 17% for the weak pocket at the toe and 16% for the weak pocket beneath the slope. This is compared to 11% for a strong crust with no weak pocket. Thus, reinforcement is an effective means to reinforce foundations that may contain pockets of weak soil. The maximum force in the reinforcement at failure was 20 kN/m for the weak pocket at the toe and 24 kN/m for the weak pocket beneath the slope.

CONCLUSIONS

Based on this study the following conclusions are made:

1. The properties and thickness of the crust are a very important factor in the behavior of reinforced embankments.
2. The reinforcement has the greatest effect on reducing displacements and shear stresses in the upper portion of the foundation where the crust generally occurs.
3. The relative increase in embankment height made possible by reinforcement increases as the crust strength decreases and as the crust compressibility increases; however, the effect of crust thickness is small.

Geosynthetics '89 Conference
San Diego, USA

4. For a given embankment height the maximum force in the reinforcement increases as the crust strength decreases, thickness decreases, and compressibility increases.

5. The reinforcing force at failure ranged from 14 to 33 kN/m for all the cases analyzed. This is less than the breaking strength of most geotextiles and geogrids used for reinforcing applications.

6. Reinforcement is an effective means of increasing the stability of embankments constructed on foundations which may contain pockets of weak soil.

ACKNOWLEDGEMENTS

Financial support for this research was provided by the Indiana Department of Highways and the Federal Highway Administration, through the Joint Highway Research Project at Purdue University. This support is gratefully acknowledged.

REFERENCES

- (1) Busbridge, J.R., Chan, P., Milligan, V., La Rochelle, P.R. and Lefebvre, L.D., "The effect of geogrid reinforcement on the stability of embankments on a soft sensitive Champlain Clay deposit," Transport Canada Report No. TP 6308E, Transportation Development Center, National Research Council, Quebec, Canada, 277 pp.
- (2) Humphrey, D.N., "Design of reinforced embankments," Joint Highway Research Project, School of Civil Engineering, Purdue University, West Lafayette, Indiana, Report No. FHWA/IN/JHRP-86/16, December, 1986, 423 pp.
- (3) Humphrey, D.N. and Holtz, R.D., "A Procedure to Determine Cap Model Parameters," Proceedings of the Second International Conference on Constitutive Laws for Engineering Materials: Theory and Application, The University of Arizona, Tucson, Arizona, January, 1987, Vol. II, pp. 1225-1232.
- (4) Humphrey, D.N. and Holtz, R.D., "Cap Parameters for Clayey Soils," Proceedings of the Sixth International Conference on Numerical Methods in Geomechanics, Innsbruck, Austria, April, 1988, Vol. I, pp. 441-446.
- (5) Humphrey, D.N., McCarron, W.O., Holtz, R.D., and Chen, W.F., "Finite element analysis of plane strain problems with PS-NFAP and the cap model -- User's manual," Joint Highway Research Project, School of Civil Engineering, Purdue University, West Lafayette, Indiana, Report No. FHWA/IN/JHRP-86/17, December, 1986, 184 pp.
- (6) McCarron, W.O., "Soil plasticity and finite element applications," Ph.D. Thesis, Purdue University, West Lafayette, Indiana, 1985, 265 pp.
- (7) Rowe, R.K., MacLean, M.D. and Soderman, K.L., "Analysis of a geotextile-reinforced embankment constructed on peat," Canadian Geotechnical Journal, Vol. 21, No. 3, August, 1984, pp. 563-576.

M.F. HOULIHAN, W.K. RODGERS

Law Environmental, U.S.A.

G. WILLIBEY

Nicolon Corporation, U.S.A.

N.D. WILLIAMS

GeoServices Inc., Consulting Engineers, U.S.A.

Design and Construction of Synthetic-Grid Reinforced Embankment over Soft Waste

Abstract

Law Environmental, Inc. and Nicolon, Inc. designed a synthetic-grid reinforced diversion ditch embankment over a soft waste foundation to divert potential run-on around a regulated unit and to an adjacent river. The embankment is approximately 3.7 meters (12 feet) high at the crest and 9 meters (30 feet) wide at the base, and was built on a foundation of soda ash waste with a typical average shear strength of 5 kPa (250 psf) and typical pH in the range of 10.5 to 12.5. One section of the embankment was instrumented with two lines of instruments to monitor deformations in the structure so that the performance of the embankment could be evaluated using actual field data. Geosynthetics were also used to line the diversion ditch on top of the embankment and for separation between a drainage layer and fine-grained fill material.

This paper presents the design procedure followed in producing the original design for this project, including the development of a high-strength base reinforcement material, and an evaluation of the embankment stability. The construction of the dike is discussed, and the results of a limited field instrumentation program and the conclusions drawn from these results are presented. Finally, conclusions and recommendations for work on similar facilities are presented.

1.0 Introduction

Geosynthetics have been in use in civil engineering applications for several decades, so much so that there are now many "common" uses of geosynthetics. These uses have included pond and landfill linings using geomembranes, slope and foundation reinforcement using geogrids, and filtration and separation functions using geotextiles. These uses of engineering fabrics, which were revolutionary and innovative a short time ago, are commonplace today. However, innovative applications continue to evolve, particularly in designs for hazardous waste-related applications.

The hazardous waste industry and the geosynthetic industry uniquely complement each other for several reasons. The use of geosynthetics in designs involving hazardous waste allows the owner and designer a greater degree of flexibility in problems associated with these types of projects. These problems may involve chemical compatibility of materials, handling of waste material during construction, and exposure of personnel and equipment during construction. The use of geosynthetics may also allow the designer to

Geosynthetics '89 Conference
San Diego, USA

minimize or avoid the high costs associated with handling and exposure to waste. In addition to these general considerations, other complications may arise in dealing with hazardous waste due to governmental regulations regarding these products. These regulations are extensive and strictly enforced in the United States. One project recently completed at a hazardous waste site incorporated geosynthetics in many different functions to minimize the inherent problems associated with work involving hazardous materials.

2.0 Background

The site is a former industrial waste unit which is located in a mountainous region of the eastern United States. Past waste disposal practices at the operating facility resulted in formation of a waste "pond" having dimensions of approximately 282,000 square meters (70 acres) surface area and 20 meters (65 feet) deep. The unit is bounded on one side by a steep mountain slope and on the other side by a river. A plan view locating these features is shown in Figure 1. One of the environmental concerns associated with the site involves the leaching of hazardous constituents from the facility into the adjacent river due to excessive run-on to the pond from the surrounding drainage basin.

In order to minimize run-on from the adjacent mountain slope, the owner constructed a 610-meter (2000 foot) long diversion ditch around the facility, adjacent to the hillside, in 1983. The location of this ditch is shown in Figure 1. However, in 1986, the structure was observed to have failed in several locations along its alignment, and there was concern that run-on would enter the waste "pond". An investigation by Law Environmental indicated that the structure had failed due to a combination of factors, including poorly compacted fill material, surface infiltration through the ditch (due to adverse grades and a rough, porous channel surface), subsurface seepage, and low foundation strength. Using the methods described in Section 4, the existing structure was determined to have a calculated factor of safety against slope stability failure of 0.9. The factors contributing to failure and the computed critical failure surface are illustrated in Figure 2.

3.0 Remedial Alternative Selection

The remedial alternative selection process involved identifying performance and design criteria, identifying and evaluating the alternatives, and choosing an alternative for implementation.

The performance and design criteria used to compare, evaluate and select the preferred remedial alternative were identified based on economic and regulatory considerations. First, the alternative had to provide sufficient capacity to handle a 100-year flood. Second, the preferred solution would be required to allow the embankment to accommodate minor settlement and differential settlement with minimal maintenance. Third, the preferred solution would be able to be constructed using conventional earthwork methods, minimizing the risk of exposure to hazardous materials by personnel or equipment, and having a minimum factor of safety for slope stability of 1.4. Finally, the remedial alternative should be cost effective.

Several alternatives were identified to re-establish run-on control at the facility. Alternatives included (1) diversion of run-on at the roadway uphill of the facility (see Figure 1), (2) resurfacing of the existing ditch

to prevent surface infiltration, and (3) reconstruction of the diversion ditch along its existing alignment. The first two alternatives were eliminated because they either did not provide the necessary degree of minimization of run-on or provide long-term survivability of the structure.

Two concepts for implementation of the third alternative included (1) replacing the soft waste beneath the diversion ditch embankment with structural fill or (2) reconstructing the diversion ditch over the soft waste. The first concept was eliminated due to anticipated complications concerning handling the waste and the cost associated with excavating the waste and replacing with structural fill (approximately \$100,000). Therefore, the chosen remedial alternative involved excavation and reconstruction of the severely distressed sections of the embankment along its existing alignment and surface retreatment of the more stable sections of the embankment to re-establish flow in the ditch channel.

4.0 Embankment Design

4.1 Design Considerations

Several factors affected the selection of a final design cross-section for the reconstructed sections, including the strength of the waste and fill materials, the final height of the embankment, hydraulic flow, and seepage control considerations.

The strengths of the waste and backfill materials were evaluated by performing triaxial shear strength tests on undisturbed (waste) or remolded (backfill) samples of the material obtained from the site. The results of the laboratory testing program are summarized in Table 1. As shown in the table, the existing embankment fill material was generally a low plasticity silty, clayey sand, and the waste material beneath the fill was a highly plastic silt. During the field investigation, the waste was observed to vary in granular consistency from location to location, and in some areas the waste was observed to have some pozzolanic properties. In other areas the waste was observed to contain voids. The pozzolanic properties may have been the reason for the high cohesion displayed by the waste during triaxial testing. A lower, presumably more representative, value of strength was used in the design stability analyses. Also, the phreatic surface was observed to be near the surface of the soft waste. The embankment fill displayed some low Standard Penetration Resistance values ($N < 10$) in some locations, indicating variable levels of compaction.

The final height of the embankment was chosen based on the hydraulic requirements of the diversion ditch. The hydraulic design was required to carry the 100-year, 24-hour flood run-off from the adjacent area. The resulting ditch required to carry this flow was approximately 6 to 10 meters (20 to 32 feet) wide at the top and 0.9 to 1.8 meters (3 to 6 feet) deep. Constrained to a mild 0.5 percent final grade along the ditch invert, the resulting height of the embankment was approximately 3.7 meters (12.0 feet).

The drainage control features associated with preventing surface infiltration and controlling subsurface seepage did not significantly affect the stability of the embankment, but did represent another area where geosynthetics were used in this project. Geosynthetics were included in the final cross-section to provide separation, filtration, protection, and

low hydraulic conductivity. The several different geosynthetics used are indicated on the as-built cross section in Figure 3.

4.2 Detailed Analysis

After selecting a preferred cross-section, the embankment was analyzed using several methods to determine the amount, if any, of reinforcement required to construct the embankment as planned. The embankment was analyzed for failure against bearing capacity, slope stability, block sliding, and plastic failure. A finite element analysis was also performed. The analytical methods and results are described below. Figure 4 shows a diagram of each method of analysis for reference. The results of the analyses are summarized on Table 2.

Bearing Capacity: Bearing capacity of the existing embankment was evaluated using classical bearing capacity theory. The embankment was modeled as an eccentrically-loaded footing over the waste, with an additional lateral load due to the active pressure of the adjacent embankment section over the rock hillside. Under the existing conditions, the embankment had a calculated factor of safety against bearing capacity failure of 1.6. Therefore, it was concluded that bearing capacity was not the critical mode of failure. The design cross-section was also analyzed against bearing capacity failure, giving a calculated factor of safety of 1.8. Assuming that reinforcement could be installed to balance the lateral load (thereby eliminating the effects of the lateral load on the analysis), the design cross-section had a calculated factor of safety of 2.6.

Slope Stability: The embankment was evaluated for slope stability using two different computer programs, STABGM and PCSTABL5. STABGM is a limit-equilibrium slope stability program which uses Bishop's Modified Method to compute the factor of safety as a ratio of the moments resisting failure to the moments inducing failures. The effect of reinforcement is included by calculating the resisting moment afforded by the reinforcement, taken as the design strength per foot of the reinforcement times the moment arm. PCSTABL5 is also a limit equilibrium program, but uses the Janbu method to calculate the factor of safety as the ratio of resisting to driving moments. The performance criteria for the project called for a minimum factor of safety for slope stability of 1.4.

The existing embankment was evaluated for slope stability using both programs. The calculated factors of safety were 0.9 by both STABGM and PCSTABL. Thus, it was concluded that the probable mode of failure was a circular shear failure caused by the weak foundation (this conclusion was supported by the presence of tension cracks at the top of the existing ditch). STABGM was used to back-calculate the strength of reinforcement needed to provide a computed factor of safety of 1.4 for the design slope of 1.5:1. Calculations indicated that a tensile strength of approximately 175 KN/meter (12,000 pounds per linear foot) was required to provide a computed factor of safety of 1.4. However, analyses indicated that if the reinforcement force were not mobilized at the rock/soil interface, then the critical failure circle would pass through that point; the calculated factor of safety of the design cross section under this condition would be approximately 1.0. Therefore, the reinforcement force was modeled as being fully mobilized at the rock/soil interface.

Finally, the embankment was evaluated using drained, (effective stress) material strength parameters and no reinforcement to evaluate the long term stability of the structure. This analysis provided for failure (degradation) of the reinforcement over the long-term (30 years) design life of the facility. Under these conditions, the calculated factor of safety was an acceptable 1.3.

Block Sliding: The design embankment was evaluated to determine the calculated factor of safety against block sliding along the rock interface and along the surface of the weak waste material using the computer program PLSTABL5. The embankment over the waste was assumed to act as the central block, with the active block defined as the portion over the rock. The effects of reinforcement were not considered in the analysis. The resulting factor of safety against block sliding was computed to be 1.8.

Finite Element Analysis: The computer program SSTIPN (Soil-Structure Interaction Program), developed Ozawa (1973), Kulhawy, Duncan, and Seed (1969), and Wong (1976), was used to evaluate the stresses, strains and displacements within the completed structure. The program incorporated a nonlinear, stress-dependent "hyperbolic" model for the constitutive stress-strain relationship of the soils and waste materials. Also, internal forces and displacements were calculated for structural elements, in this case, the base reinforcement layer. The possible reinforcing effects of other layers of geosynthetics (separating geotextiles, etc.) were ignored. Input parameters for the model were determined based on the results of triaxial shear strength tests of the embankment soil and waste materials, and physical characteristics of candidate reinforcement materials. The properties of the thin gravel drainage layer were estimated from published values for similar materials.

The results of the analysis indicated that for the unreinforced embankment, settlement would be approximately 5 cm (2 inches), that several elements in the waste material approached failure, and that potentially significant differential settlement could occur along the embankment foundation. The reinforced embankment, however, had a calculated settlement of approximately 3 cm (1.2 inches), had few elements approaching failure, and showed minimal differential settlement along the embankment foundation. Although apparently small, differential settlements of this magnitude could cause ponding and adverse grades in the channel of the ditch, and were to be minimized. Stress in the reinforcement was calculated to be approximately 137 KN/m (9400 pounds per linear foot). Figure 5a shows the elements which approach failure in the unreinforced case; Figure 5b shows the elements which approach failure in the reinforced case. The deformed shape of the foundation is illustrated in Figure 6 and discussed in Section 6.

Plastic Failure Analysis: Plasticity theory as presented by Linn (1967) was used to evaluate the safety of the proposed design under plastic failure conditions. A significant assumption in the analyses stated that the active pressure wedge over the rock produces a lateral force on the embankment which is resisted totally by either the weak waste material (unreinforced case) or the reinforcement (reinforced case), and that this is the reinforcement's only effect on stability. This assumption required that the reinforcement be anchored to the rock hillside during construction. The plastic failure analysis was not used as a design analysis but rather to provide insight into understanding the likely failure mechanisms and to bound the range of acceptable solutions to the problem.

The analyses indicated that a "safe", statically admissible stress field (lower bound) existed for an unreinforced embankment of less than 2.9 meters (9.4 feet) height and for a reinforced embankment of less than 3.9 meters (12.8 feet) height. Also, a kinimatically admissible failure surface (upper bound) was determined to exist for an unreinforced embankment of greater than 4.3 meters (14.0 feet) height and for a reinforced embankment of greater than 5.9 meters (19.2 feet) height. Thus, the plasticity analysis indicated that the design height of 3.7 (12.1 feet) meters was less than the "safe" reinforced height of 3.9 meters. By comparison, analyses indicated that the existing failed section height of 3.6 meters (11.8 feet) was greater than the safe, lower-bound calculated height of 2.7 meters (9.0 feet).

4.3 Selection of Reinforcement

Having calculated the required reinforcement force needed to provide stability, the type of reinforcement was chosen. The type of reinforcement was selected based on stress-strain characteristics, creep characteristics, and chemical compatibility of each of the candidate materials. These considerations, along with damage to the geogrid during construction, were used to determine the required wide-width tensile strength of the fabric. However, no single-layer geosynthetic having the required tensile strength was available from geosynthetic manufacturers. The use of multiple layers of geosynthetics was not considered to be desirable because the structure was relatively short, and numerical analyses indicated that only the lower layer of reinforcement typically mobilizes the full design strength. Therefore, a high strength and high modulus woven geogrid was selected.

The stress-strain characteristics of the reinforcement were chosen to match, as closely as possible, the stress-strain properties of the soil and waste materials. Candidate materials included steel, polyester, polypropylene and nylon, which were chosen because of their availability. The stress-strain properties vary significantly between the extensible polymer materials and the relatively inextensible steel; the polymers attain their maximum strength at between 5 and 25 percent elongation, and steel at approximately 0.2 percent elongation. Thus, the polymer materials have a greater degree of strain-compatibility with the soil and waste, which attain their maximum undrained shear strengths at 3 to 5 percent strain, than the steel, and so steel was eliminated as a candidate reinforcement material. The creep characteristics of the materials were compared based on manufacturer-supplied data of raw polymer material. Extrapolating the data one logarithmic cycle beyond the test duration, the effects of creep on the elastic modulus of the material were observed to be minimal beyond a period of approximately sixteen years. However, polyester was observed to retain a much greater percent of its strength after this period than either nylon or polypropylene. Also, polyester had significantly greater tensile strength characteristics than either nylon or polypropylene. Therefore, polyester was chosen as the preferred reinforcement material. Since polyester is not generally compatible with some of the waste constituents, a coating of PVC was specified for the geogrid. PVC was chosen also because its elastic modulus is lower than that of polyester, and therefore would stay continuous over the ployester at the anticipated strains.

To insure long-term performance of the geogrid, several strength reduction factors were specified, which required that the geogrid be

manufactured with a significantly higher tensile strength than that required in the design. Factors of 0.5 for creep, and 0.9 for construction survivability were selected to account for deviations in the expected performance of the geogrid from the performance during wide-width tensile strength testing, resulting in a specified wide-width tensile strength of the geogrid of approximately 330 KN/meter (23,000 pounds per linear foot). The final material had a wide-width tensile strength of approximately 350 KN/m (24,000 pounds per linear foot), and the PVC coating stayed continuous over the polyester during wide-width testing, even at relatively large strains.

5.0 Construction

The embankment was constructed using conventional construction equipment and methods. To provide access by construction equipment, the contractor initially constructed a road adjacent to the future toe of the embankment by pushing this existing embankment material out onto the waste pond. A medium-strength, woven geotextile was used for base reinforcement of the road. The road was eventually left in place after construction of the embankment. After construction of the access road, the sections of the embankment which were to be completely rebuilt were excavated down to the waste material level. A polypropylene separating geotextile was then placed over the waste, followed by 8 to 12 inches (20 to 30 cm) of washed gravel. The geotextile was placed in such a way as to minimize contact of personnel or equipment with the waste. The details of the constructed cross-section are shown in Figure 3.

The high strength reinforcing geogrid was then placed on the gravel layer. To simplify installation, all seams were sewn in the factory. Field installation was directed by Nicolon's representative, using the contractor's crews. Installation of the geogrid took about one to two hours. In order to provide anchorage of the geogrid to the rock hillside, a critical feature based on the results of the detailed analyses, the geogrid was placed up the slope for a distance of five feet, which exceeds the expected bond length of the gravel/reinforcement interface. After placing the remaining 6 to 8 inches (15 to 20 cm) of gravel over the geogrid, the front end of the reinforcement was wrapped over the gravel drainage layer to retain the gravel during the remainder of construction.

After placement of the gravel drainage layer and associated geosynthetics, the soil embankment was constructed using conventional methods. The geosynthetic and gravel layers provided a firm foundation on which to compact the backfill soils, which were placed in thin lifts and compacted using a sheepsfoot roller to 95 percent of ASTM D-698 Standard Proctor maximum dry density. Following construction of the embankment, a surface treatment of protecting geotextile, HDPE, and grout blanket was placed in the ditch invert to promote surface drainage and to minimize surface infiltration. These materials are identified on the as-built cross-section shown on Figure 3.

6.0 Instrumentation

In order to estimate the actual mobilized tensile force in the reinforcement, two lines of instruments were placed in one section of the embankment. The purpose of the instrumentation was to provide verification of the design, rather than for research; therefore, a durable, dependable, and relatively inexpensive system was chosen for instrumentation. Horizontal

inclinometers were installed directly above the reinforcement in order to indirectly obtain a deformed shape of the reinforcement and allow calculation of the local in-situ strain. From this, the approximate stress in the geogrid was determined based on the results of the wide-width tensile test. For a more exact determination of in-situ stress, strain gauges, extensimeters, or other direct measuring devices for direct measurement of stress and strain should be used.

The results of the reading of one of the inclinometers is shown on Figure 6. The figure shows that the structure has deformed slightly, as predicted, and that the location of maximum stress in the reinforcement is adjacent to the rock face. The deformation shown is generally consistent with the results of the finite element program; deviations from the predicted deformation are likely the result of nonhomogeneity of the waste, the existence of the access road adjacent to the toe of the embankment, and the significantly higher strength of the actual reinforcement than the strength specified in the analysis. Based on the deformed shape of the reinforcement, indirectly measured by the inclinometer, a maximum strain of approximately 2 percent has occurred near the rock face, and the corresponding stress is approximately 135 KN/M (9000 pounds per linear foot). Therefore, the fabric is likely performing at a stress level somewhat below the design specifications, but consistent with the levels predicted by the finite element analysis. This difference in stress levels is to be expected, since the design specifications incorporated a relatively high factor of safety. The instrumentation results also indicate that the reinforcement closer to the face of the embankment is experiencing lower levels of strain than the reinforcement near the rock face, which is consistent with the results of the finite element and other analyses.

7.0 Conclusions and Recommendations

This case history demonstrates that innovative solutions involving the development of specialty geosynthetics may be a considered option in approaching challenging design situations, and that the innovative solutions may prove to be functionally and economically more attractive than conventional engineering solutions. Based on the design requirements, the selected remedial alternative, and the results of detailed design and limited instrumentation results, it is concluded that the selected alternative provided the desired degree of long term survivability, minimization of required maintenance, and flexibility, all of which were identified as important factors during alternative selection.

The results of the detailed analysis and limited field monitoring support the selection of the specific components of the final design cross-section. The field instrumentation, although limited in scope, has provided useful information regarding the working stresses in the fabric and deformation of the base of the fill. The results of the detailed analysis satisfactorily predicted the response of the waste and the reinforcement under the load of the reconstructed embankment. However, of the analyses performed, only the bearing capacity and slope stability analyses (and possibly the deformational analysis) would likely be required to evaluate the suitability of a design for most projects. The selected solution also provided the least expensive of the several solutions proposed. Therefore, the use of geosynthetics in this project benefited the client with respect to function, ease of implementation, and cost.

References:

- Chen, W. F. and Baladi, G.Y., "Soil Plasticity: Theory and Implementation", Vol. 38 of Developments in Geotechnical Engineering: Elsevier Press, London England, 1985.
- Duncan, J. M. and Wong, K.S., "STABGM: A Computer Program for Slope Stability", Virginia Tech, 1984.
- Dickens, J., Duncan, J.M., et.al., "SSTIPN-Soil Structure Interaction Finite Element Program", University of California at Berkeley, 1976.
- Jewell, R.A., "A Limit Equilibrium Design Method for Reinforced Embankments Over Soft Soils", Proc. 2nd Int'l Conf. on Geotextiles, Vol. III, pp. 671-676.
- Linn, W.D.L., "Applications of Limit Plasticity in Soil Mechanics", Journal of the Soil Mechanics and Foundations Division, ASCE, September 1967, pp. 101-120.
- Terzaghi, K., "Theoretical Soil Mechanics", John Wiley and Sons, New York, 1943.

TABLE 1
SUMMARY OF LABORATORY TEST RESULTS

MATERIAL TYPE	BORING NO.	SAMPLE TYPE	SAMPLE DEPTH (FT.)	U.S.C.S. GROUP SYMBOL		GRAIN SIZE DISTRIBUTION (%)			ATTBERG LIMITS %			NATURAL MOISTURE %	SHEAR STRENGTH	
													TOTAL	EFFECTIVE
						GRAVEL	SAND	FINES	L.L.	P.L.	P.I.		ϕ (°) C (PSF)	ϕ (°) C (PSF)
Road Embankment Fill	B-2	SS	4 - 5.5	GM		53	33	14						
	B-2	SS	14 - 15.5	SC		36	38	26						
	B-2	SS	24 - 25.5	SC		27	34	39						
	B-8	SS	6.5 - 8	CL		1	24	75	30	23	7	14		
	B-8	SS	14 - 15.5	CL		0	9	91	44	25	19	14		
Ditch Fill	B-4	UD	3 - 5	SC - SM		18	24	46	38	25	13	20	28 200	37 100
	B-5	SS	1.5 - 3	CL		13	28	59	39	23	16	19		
	B-10	SS	1.5 - 3	CL		3	39	58	30	21	9	28		
	B-11	SS	4 - 5.5	SC		18	46	36	38	21	17	15		
Waste	B-6	UD	11 - 13	MH		0	23	77	106	82	24	156		
	D-10	UD	14 - 16						128	83	45	273	12 500	53 0

NOTES : (1) U. S. C. S. = UNIFIED SOIL CLASSIFICATION SYSTEM
 (2) L.L. = LIQUID LIMIT
 (3) P.L. = PLASTIC LIMIT
 (4) P.I. = PLASTICITY INDEX
 (5) ϕ = SHEAR FRICTION ANGLE OF RESISTANCE
 (6) C = COHESION
 (7) SS = SPLIT SPOON
 (8) UD = UNDISTURBED

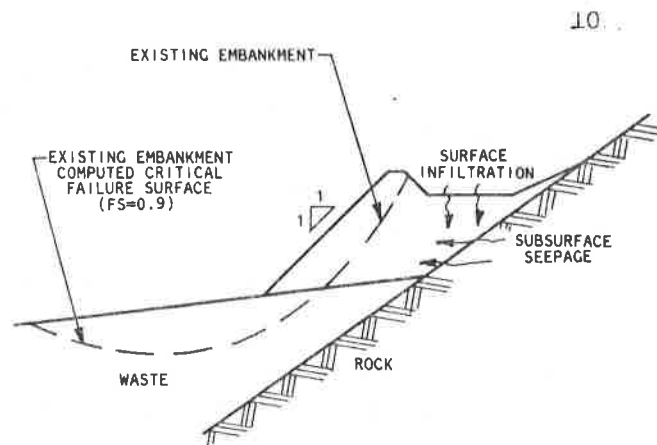
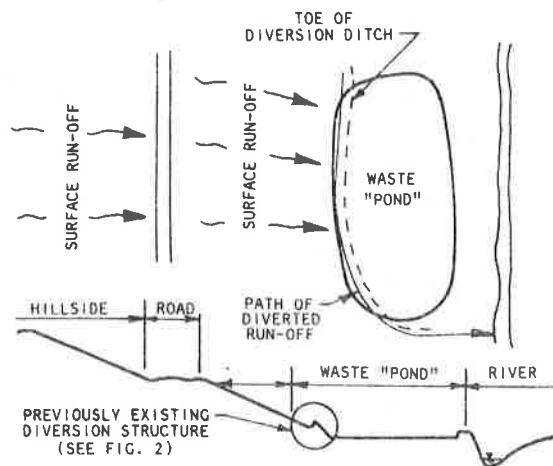


FIGURE 1 - PLAN & PROFILE OF PROJECT AREA

FIGURE 2 - FACTORS CONTRIBUTING TO FAILURE OF EXISTING EMBANKMENT

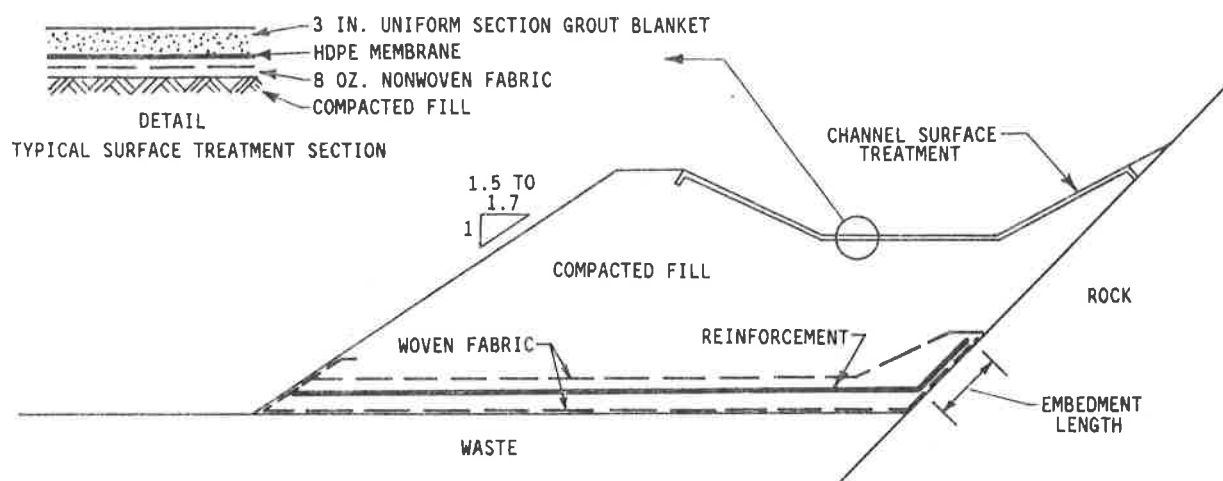


FIGURE 3 - AS-CONSTRUCTED SECTION DETAIL

TABLE 2

Summary of Embankment Analysis Results

Analysis Method	Results	
	Unreinforced	Reinforced
Bearing Capacity	FS = 1.8	FS = 2.6
Circular-Arc Slope Stability	FS = 1.0	FS = 1.4
Block-Sliding Slope Stability	FS = 1.8	---
Finite Element	Settlement = 5 cm	Settlement = 2 cm
Plasticity - Lower bound	Emb. height = 2.9 m	Emb. height = 3.9 m
Plasticity - Upper bound	Emb. height = 4.3	Emb. height = 5.9 m

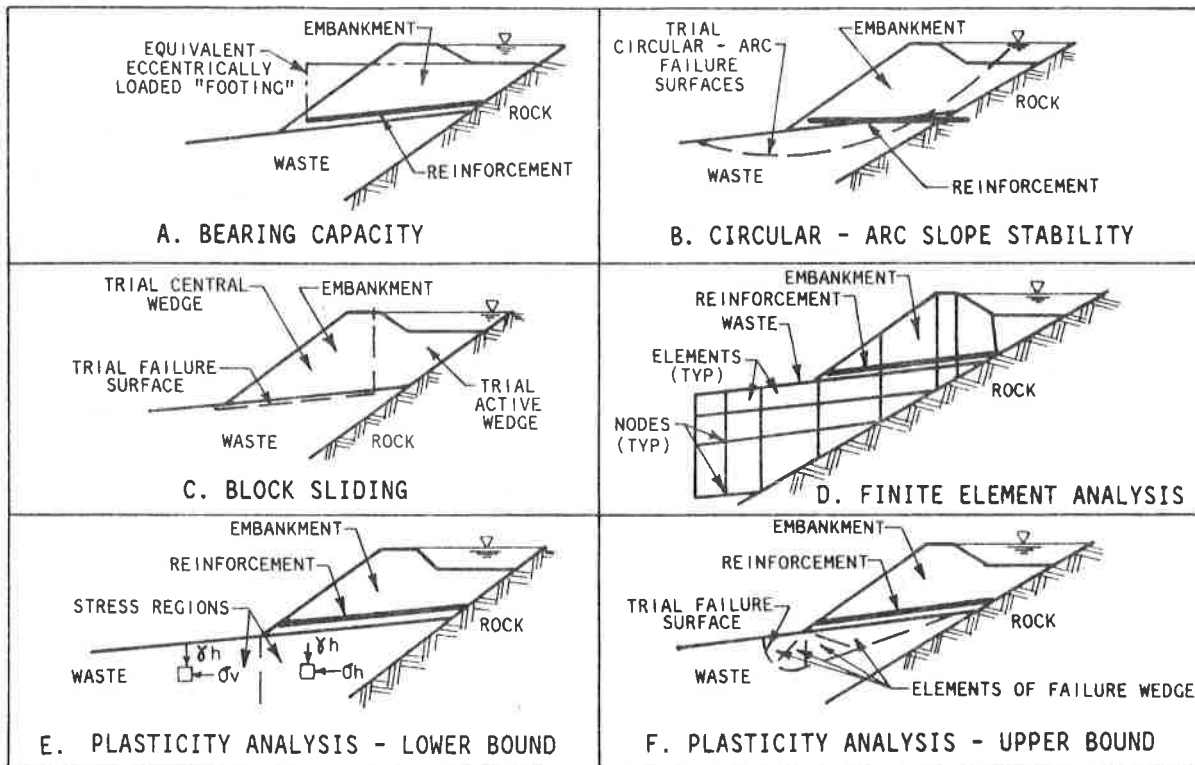


FIGURE 4 - ILLUSTRATIONS OF ANALYSIS METHODS

KEY:

- ELEMENTS FAILING
- ELEMENTS EXPERIENCING 90% OR GREATER OF CRITICAL STRESS LEVEL
- ELEMENTS EXPERIENCING LESS THAN 90% OF CRITICAL STRESS LEVEL

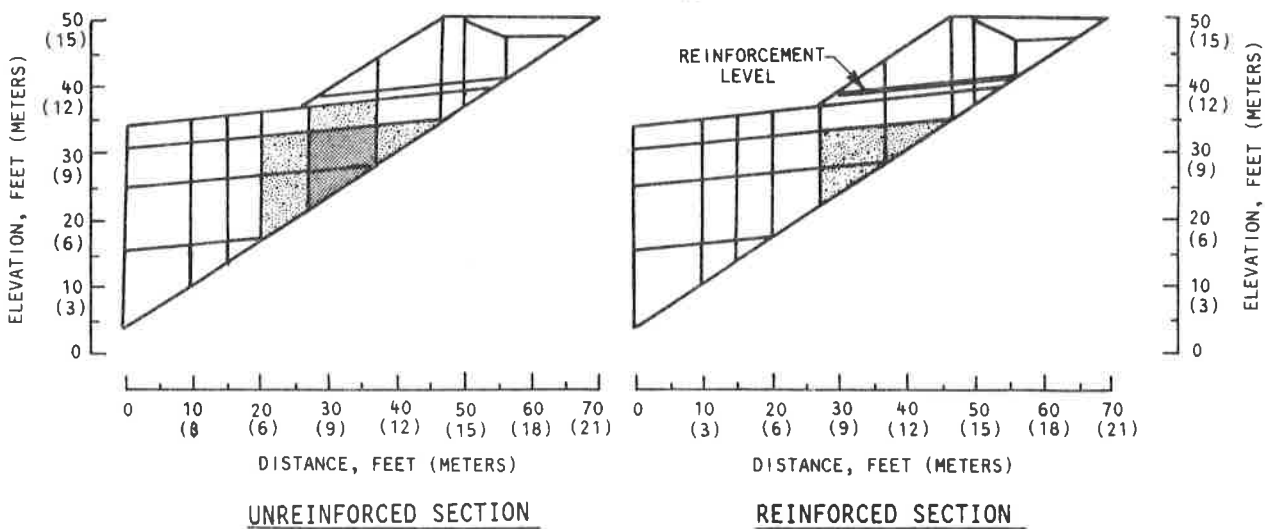


FIGURE 5 - RESULTS OF FINITE - ELEMENT ANALYSIS

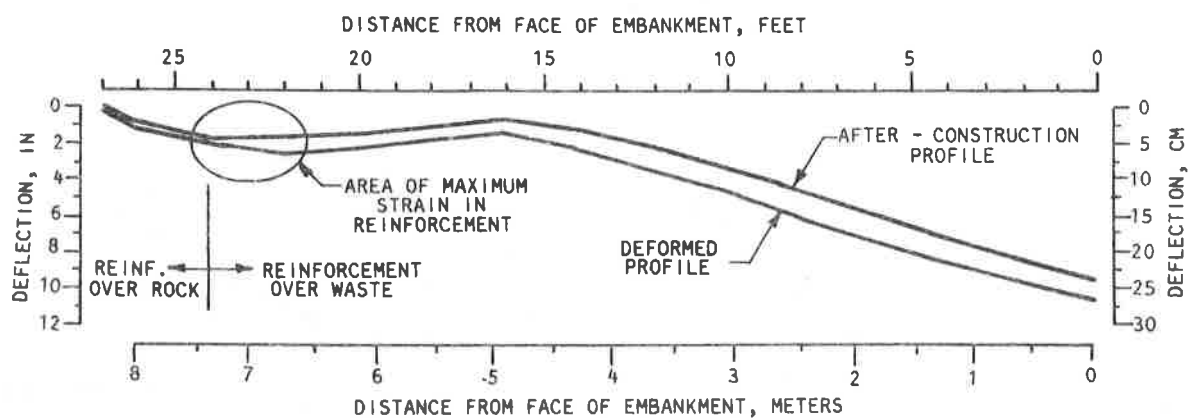


FIGURE 6 - RESULTS OF INSTRUMENTATION

F.M. DUARTE
G.S. SATTERLEE
U.S. Army Corps of Engineers, U.S.A.

Case Study of a Geotextile Reinforced Levee on a Soft Clay Foundation

ABSTRACT

This paper presents the results of a levee test section that was reinforced by a single layer of high strength polyester geotextile. Strain gages were attached to the geotextile to measure the strain in the geotextile during and after construction. Settlement plates, piezometers, and inclinometers measured the deformation and performance of the composite structure. Geotextile tensile requirements were computed using the Spencer and Bishop circular arc methods, and the wedge method of slope stability analysis. The tensile values from the limit equilibrium slope stability analysis are compared to the tensile values recorded by the strain gages attached to the geotextile, to evaluate how accurately the theoretical values compare with the field data.

INTRODUCTION

Geotechnical engineers are often faced with the challenge of constructing a structure on a very soft foundation, or enlarging an existing structure. When the desired factor of safety for rotational stability can not be achieved, alternatives for building the structure on the existing alignment are generally expensive, and a new alignment is usually selected. In southern Louisiana, the two most commonly used methods to construct over very soft soils is to build on piles, or remove the soft organic material and replace it with sand or shell. Both alternatives are very costly, require specialized equipment, and are also very time consuming. With the development of high strength geotextiles a new alternative has been introduced.

This paper presents the results of a 152.4 meter long levee test section in which a high strength polyester geotextile (297.7 kN/m at 5% strain) was used to reinforce a levee enlargement. The project is located in the southeastern portion of the State of Louisiana, in lower Plaquemines Parish (county), between the towns of Nairn and Empire.

An aerial view of the site is presented in Figure 1.



Figure 1. Aerial view of construction site.

The people who live on the very narrow strip of land between the Mississippi River and the bays that lead to the Gulf of Mexico are protected from river floods and hurricane surges by the levee systems. The test section was constructed on the hurricane protection levee.

Currently, the crown of the existing levee is at approximate elevation 2.29 meters National Geodetic Vertical Datum (N.G.V.D.). It has to be raised to an elevation of 4.42 meters to provide protection against a 100-year storm, and also to compensate for foundation settlement. Stability analysis of the existing levee indicates that the factor of safety is approximately 1.1. Raising the crown elevation to 4.42 meters, with the required side slopes, results in a factor of safety of 0.8 for a slide into the drainage canal, and a factor of safety of 0.85 for a slide towards the gulf. Stability berms cannot be constructed to improve the stability of the section because the canal is too close to the existing levee.

Construction without a reinforcing geotextile requires moving the centerline of the levee approximately 36.6 meters towards the gulf and excavating a 3 meter deep trench to remove the highly compressive organic material. A hydraulic dredge would be used to pump sand into the trench, and after allowing the sand to drain, several clay pumpings would be required to bring the section to design grade. This type of construction is estimated to cost \$85,000,000, covers 4000 acres of marsh, and take 13 years to construct 13 miles of levee.

The primary objective of the study is to determine if a single layer of high strength geotextile can be used effectively to reinforce the section so that the present levee can be enlarged on the existing alignment. Other items of interest are the strains in the reinforcing geotextile and the deformations and performance of the composite section.

DESIGN SECTION

The levee was enlarged by holding the landward existing levee toe and raising the levee towards the gulfside, thus resulting in a 6.1 meters gulward shift of the present baseline. The top 0.9 meters of the existing levee were degraded to establish a flat wide platform to work from, but more importantly to provide more anchorage by placing the geotextile deeper into the section. The high strength geotextile was placed on the degraded levee portion, down the existing levee slope, over the marsh grass, and submerged in the ponded areas. Both ends of the geotextile were folded back to form anchors to provide additional resistance to pull-out. Sand was placed over the fabric to a maximum height of 1.2 meters, and clay was placed above the sand to design grade. The final section has a 2.44 meter crown width, a protected side slope of 1V on 3H, and a marsh side slope of 1V on 4H. Refer to Figure 7 for more details.

INSTRUMENTATION

Several lines of instruments were placed perpendicular to the levee centerline to measure the performance of the test section during and after construction. Instruments consist of strain gages, settlement plates, piezometers, and inclinometers. This report focuses mainly on strain gage and inclinometer data. The strain gages provide feed back on the tensile demand on the geotextile, and the inclinometers provide information on the lateral deformations. Both are essential in determining the potential failure plane and the magnitude of the resistance required to balance the driving force and increase the factor of safety.

STRAIN GAGES

Strain gages were placed at three locations approximately 30.5 meters apart. Two of the locations contained displacement transducers that were manufactured at the Waterways Experiment Station (WES), and the third location contained foil gages. A schematic of the foil gage layout is presented in Figure 2. Most gages were placed perpendicular to the levee centerline to determine the maximum tensile demand on the fabric. The data obtained from the WES gages is inconclusive and erratic, and therefore is not presented. Data from the foil gages appears to yield good values, but unfortunately, the foil gages were only placed in a limited area over the marsh. The foil gage readings were normalized to an initial reading of 0.9 to facilitate comparisons among the gage plots. This value is convenient because one third of the gages which are perpendicular to the centerline had this value for their initial reading prior to fill placement. This offset value is approximately the same as that obtained from the laboratory tests that were performed at Drexel University, and shown on Figure 5. The strain measured by the foil gages increases towards the marsh, with the furthest marshward gages showing a strain of 3.5%, indicating that the greatest tensile demand on the geotextile is at or beyond this location. Strain gage plots showing the strain at selected locations on the instrumented geotextile panel are presented in Figure 3.

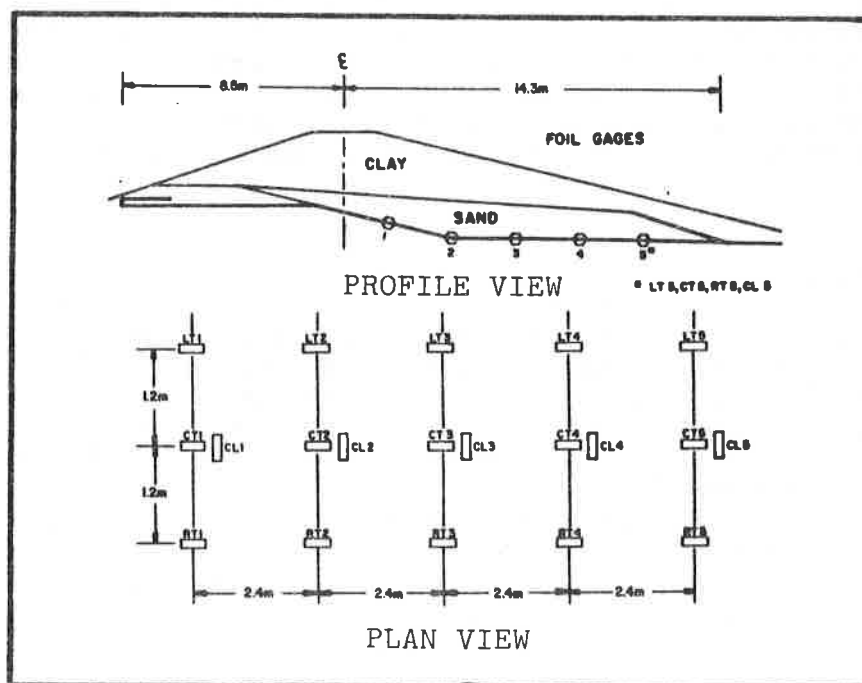


Figure 2. Strain gage locations

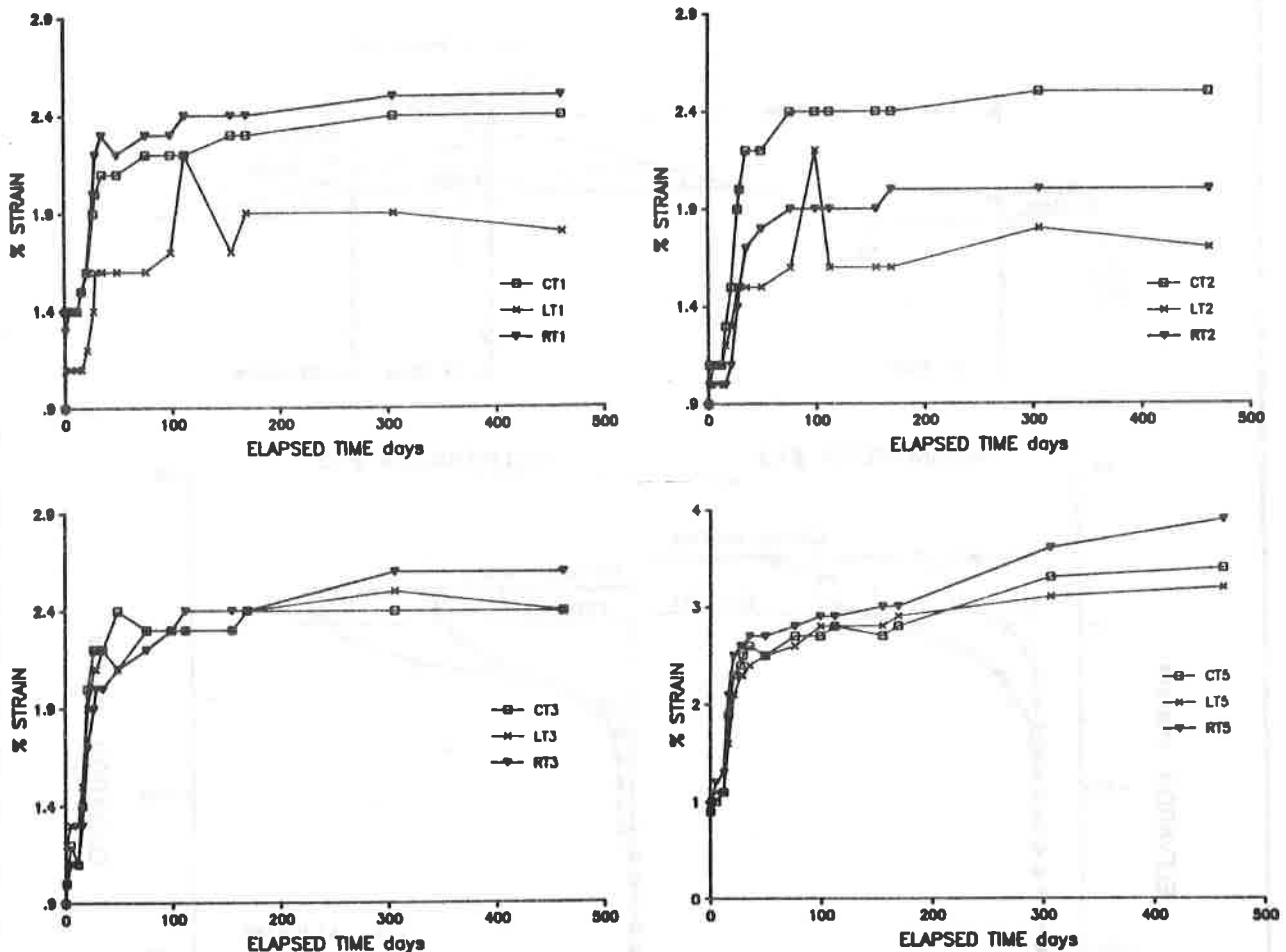


Figure 3. Strain gages plots.

INCLINOMETERS

Inclinometers were placed at two levee stations approximately 30.5 meters apart. Three inclinometers were placed at each station. Figure 4 presents the inclinometer layout and deflections for the station containing inclinometers 11, 13, and 15. Inclinometer 11 was placed next to the existing canal to monitor the ground movement toward the canal. Inclinometer 13 is at a distance of 1.7 meters gulfward of the new levee centerline, and inclinometer 15 is at a distance of 9 meters. The inclinometers close to the center of the slope experienced the largest gulfward movement, approximately 35.6 cm. at inclinometer number 15. Inclinometers adjacent to the crown, also experienced significant movement towards the gulf, approximately 30.5 cm. at inclinometer number 13. No apparent movement was recorded by the instruments next to the canal. Maximum movement occurred above approximate elevation -3.4m. This information was used to establish the critical elevation for the gulfside slope stability analysis.

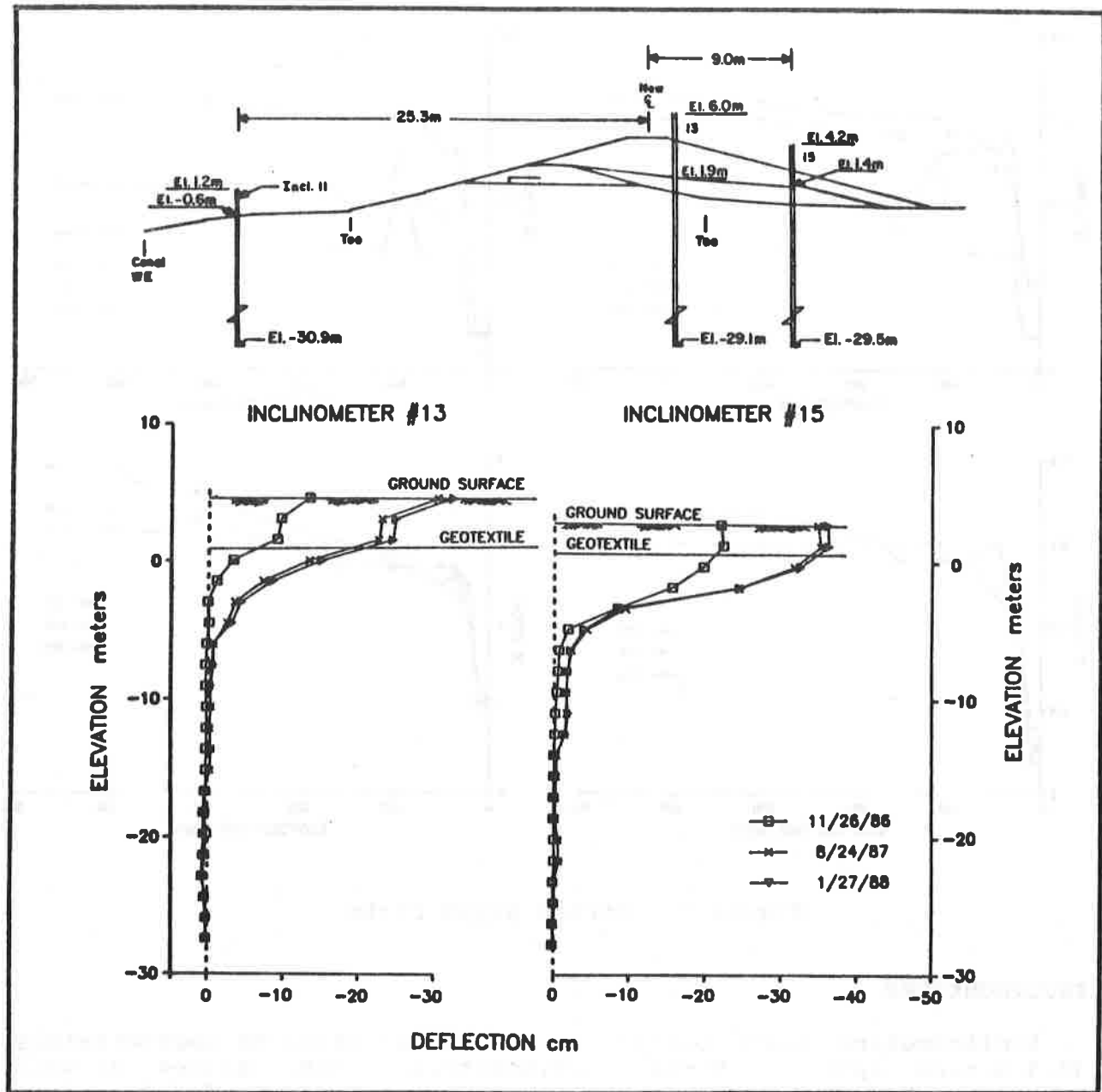


Figure 4. Inclinator locations and gulfward movement

SETTLEMENT

Settlement plates were installed on top of the reinforcing geotextile at distances of 1.5 and 7.6 meters on the gulfside of the new crown centerline. Consolidation was relatively fast and constant during the first month after construction, but slowed down thereafter. Four hundred days after construction, the settlements were 0.62 and 0.78 meters, respectively. Consolidation is still progressing at a very slow rate.

PIEZOMETERS

Piezometers were installed under the gulfside edge of the new levee crown at elevations -1.5, -3.3, -6.3, and -9.2 meters to monitor the pore pressure in the foundation. Pore pressures peaked at the end of construction and rapidly dissipated to a residual value above the initial readings. The maximum pore pressures were 1.6, 3.0, 0.8, and 2.3 meters, respectively.

GEOTEXTILE PROPERTIES

Laboratory results of the polyester geotextile test specimen indicate that the fabric has a tensile strength of 297.7 kN/m at 5% strain, an ultimate strength of 665.4 kN/m, a friction angle of 30 degrees when pulled over a silty soil and 14 degrees against a marshy organic clay with very high water content. The strains in this paragraph were measured by a linear voltage displacement transducer (LVDT).

SLOPE STABILITY ANALYSES

Before the test section was constructed, stability analyses were performed using the wedge method of analysis to determine the geotextile tensile strength that was required to resist the unbalanced forces and increase the factor of safety to 1.3. Based on the design parameters, x-section, and stratification that was available, the most critical failure mode was towards the canal, at an elevation of -12 meters. A geotextile with a tensile strength of 297.7 kN/m at 5% strain was chosen. The factors of safety presented in the introduction are also based on the same set of analyses. The analyses presented in this paper include the data that was obtained from the test section, which resulted in slightly different design parameters, x-section, and stratification than had been used in the previous analyses. Review of the test data reveals that the critical failure surface is towards the gulf at an elevation of -3.4 meters.

Stability analyses, using the latest information, were conducted to compare the tensile values that are obtained by the wedge method (1) and circular arc methods, and to determine how accurately these theoretical values compare to the values measured by the strain gages. Safety factors were computed for the unreinforced and geotextile reinforced sections using the Wedge method, and the Spencer (1967) and Simplified Bishop (1955) methods from the UTEXAS (2) slope stability program.

WEDGE ANALYSIS

Stability analyses were performed for a failure surface at elevation -3.4 meters, the elevation above which maximum movement was indicated by the slope inclinometers, to determine the geotextile tensile strength required to increase the factor of safety to 1.0. A geotextile with a tensile strength of 117 kN/m is required. Geotextile tensile requirements were computed using the following equation:

$$\begin{aligned} T &= F.S. (D) - R \\ D &= D_a - D_p \text{ (active \& passive driving forces)} \\ R &= R_a + R_b + R_p \text{ (resisting forces)} \\ F.S. &= \text{required factor of safety} \\ T &= \text{Tensile requirement in the geotextile kN/m} \end{aligned}$$

CIRCULAR ARC ANALYSES

Circular arc analyses were used to compute the safety factors of the same section that was analyzed by the Wedge Method. Results for the unreinforced section are presented in Figure 6. Analyses for the reinforced section are presented in Figure 7. A geotextile with a tensile strength of 96.3 kN/m is required to increase the factor of safety to one, for a failure surface at elevation -3.4 meters. This tensile value and the tensile value obtained by the wedge analysis will be compared to the tensile demand measured by the foil gages.

STRAIN GAGE ANALYSIS

Samples of the polyester geotextile were recovered from the field and instrumented with foil strain gages for tensile/strain tests (3). Each specimen contained a foil gage and an LVDT measuring device side by side to compare the strain measured by each instrument. It is necessary to establish a relationship between stress versus strain for the foil gages, because this relationship can be used to convert the strain that is measured by the foil gage in the field to a tensile force. The tensile force from the stability analysis is compared to the tensile force from the foil gages to determine how accurately the analysis predicts geotextile tensile demand. The largest strains were recorded by the gages furthest gulfward (CT 5, LT 5, RT 5). The average last reading for these gages is 3.5% strain which corresponds to an average tensile demand of 57.6 kN/m in Figure 5. The tensile demand measured by the foil gages that are attached to the geotextile is significantly less than the tensile values computed by the wedge or circular arc slope stability methods. The tensile value computed by the wedge analysis is 2.03 times that measured by the foil gages. For the circular arc analysis, the value is 1.67 times larger than the measured value.

Inspection of Figure 5 shows that the tensile values obtained by the circular arc and wedge analysis correspond to 4.5% and 5% strain.

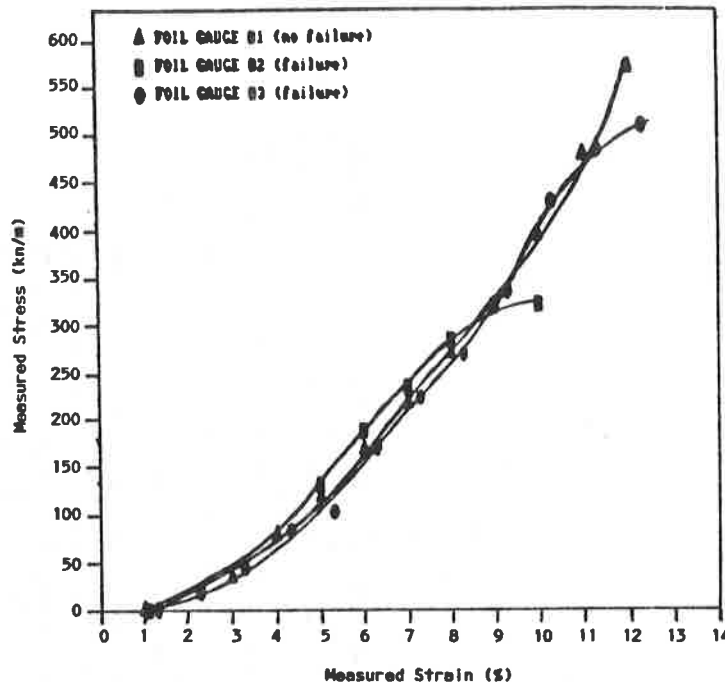


Figure 5. Stress versus strain of the three foil gages

CONCLUSIONS

Results of the test section clearly show that a geotextile reinforced levee is a viable alternative to increase the flood protection. The test section was completed over two years ago, and since then all of the instruments have been monitored extensively to determine the performance of the composite section. All of the data to date indicates that the section is working better than had been anticipated, especially since the field geotextile strains are lower than the computed values from limit equilibrium analysis. There is no evidence of cracks or any signs of unacceptable stress in the test section. Lateral deformations, measured by the inclinometers, have stopped for all practical purposes. Strain gage readings peaked during August 1987 and there has been no increase since then.

Circular arc slope stability analysis, for a factor of safety of one, require a geotextile with a tensile strength of 96.3 kN/m. The wedge method of slope stability requires a tensile strength of 117.0 kN/m, for the same factor of safety. Maximum tensile demand was

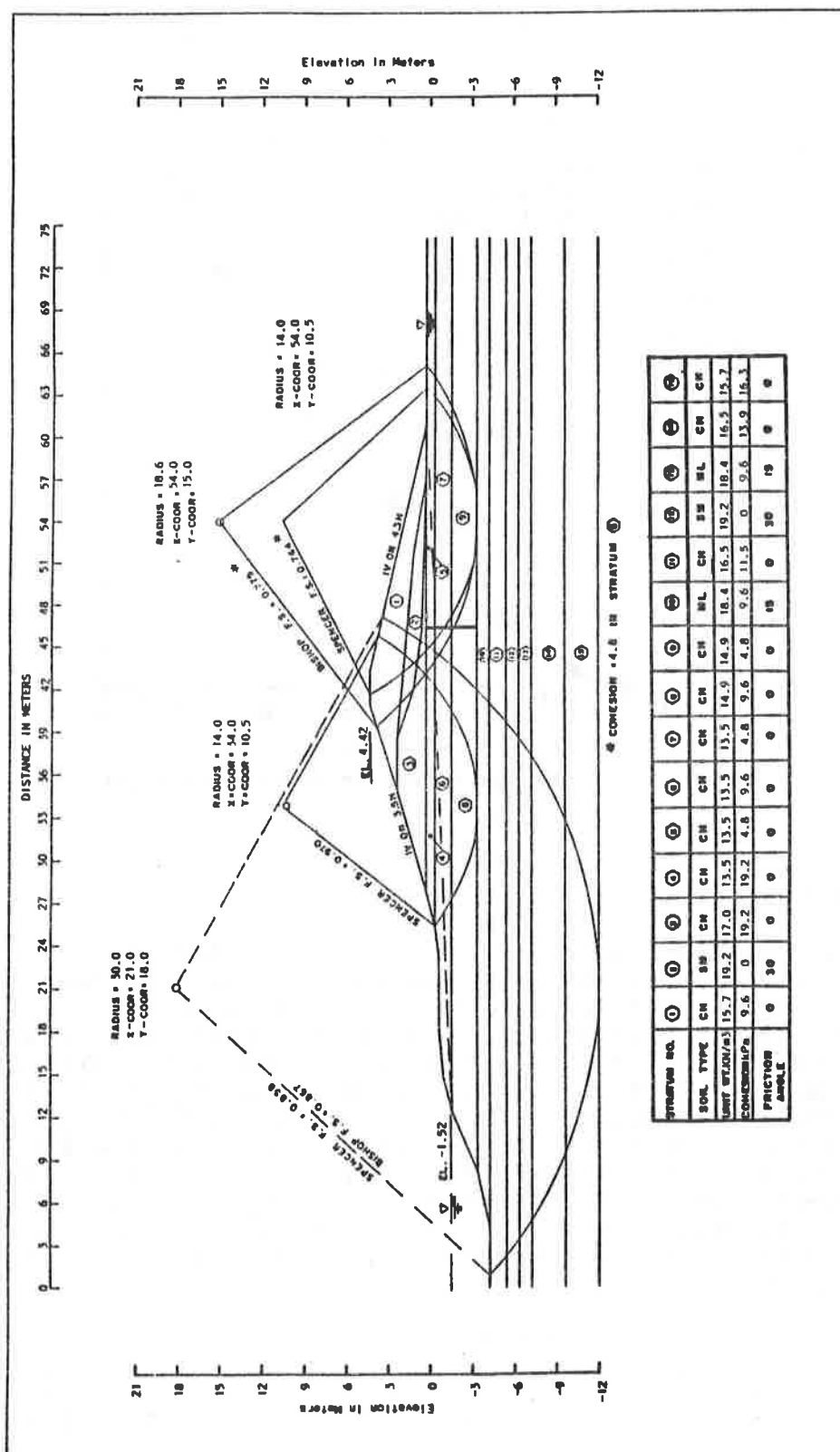


Figure 6. Circular arc analysis for the unreinforced section.

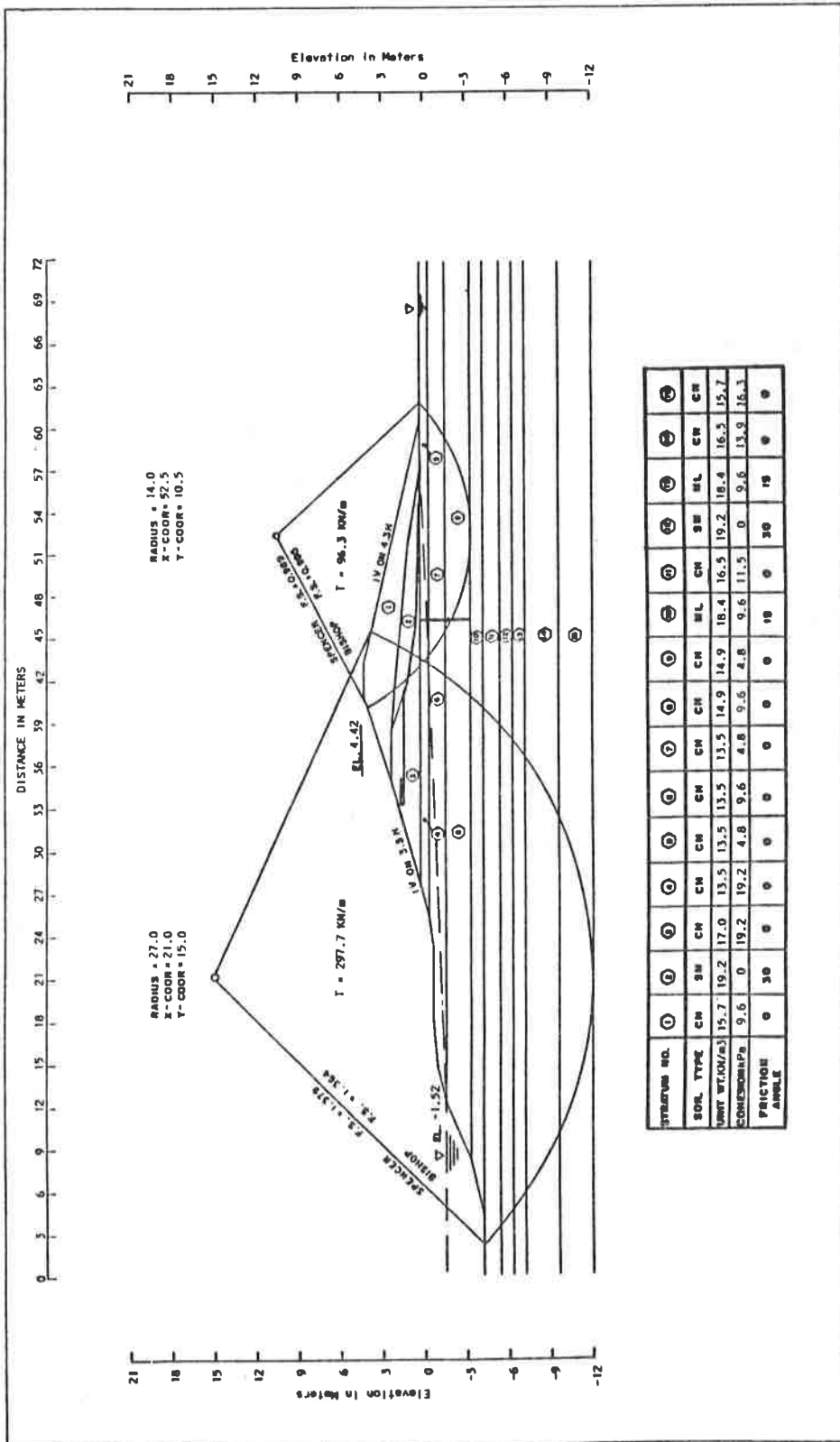


Figure 7. Circular arc analysis for the reinforced section.

recorded by the gages furthest gulfside. A tensile demand of 57.6 kN/m was measured. Both stability methods gave conservative results, with the wedge analysis yielding a F.S. = 2.03 when compared to the demand measured by the foil gages. It should be noted that the zone of maximum tension was not at the circle/soil interface, but far from it, close to the toe of the new levee. This may suggest that a failure mechanism other than the circular arc is at work. Even if this is so, the current methods of stability analyses are requiring tensile strengths that are on the safe side. This is acceptable until the mechanics of the composite section can be better understood and the analysis can be refined to yield more accurate and economical designs.

The geotextile reinforced levee alternative will reduce the estimated construction cost for the 13 miles of levee from \$85 million to \$54.2 million; construction time from 13 years to 6 years; and marsh destruction from 4000 acres to 100 acres. Residents will also benefit from lower flood insurance premiums during the reduced construction time. After the levee is complete, the first floor of residential and commercial buildings will not have to be constructed 4.3 meters above the ground surface, as is presently required to prevent damages from flooding.

REFERENCES

(1). Caver, W. W., "Slope Stability in Soft Layered Soil Systems", Master of Science Degree, Oklahoma State University, May 1973.

(2). Edris, E. V. Jr., "UTEXAS 2 Slope - Stability Package, Volume 1, User's Manual," Department of The Army Waterways Experiment Station, Corps of Engineers, I. R. GL-87-1, August 1987.

(3). Koerner, R. M., "Comparative Strain Evaluation of the Nicolon 0-2 Geotextile Using LVDT and Foil Strain Gauges", Drexel University, April 1987.

P.J. LANGSTON
N.D. WILLIAMS

GeoServices Inc., Consulting Engineers, U.S.A.

Design Methods For Reinforced Embankments On Soft Foundations

ABSTRACT

Embankments constructed on soft foundations may be designed with geosynthetic tensile reinforcement to increase stability. This paper presents a five-step, systematic approach for the evaluation of reinforced embankment stability. Each of the five steps addresses a different failure mechanism. When more than one method is available to analyze a particular failure mechanism, the methods are compared and recommendations are made.

INTRODUCTION

An embankment constructed on a soft foundation may be designed with a layer of tensile reinforcement at its base to reduce lateral displacements and improve the overall stability of the embankment. The design of the embankment must be established to determine the reinforcement properties required for adequate performance and safety. A systematic design approach should be followed to evaluate embankment stability with respect to the internal and external failure mechanisms shown in Figure 1 [Koerner, 1987]. One systematic approach is to divide the design into five steps:

- 1) A bearing capacity analysis to evaluate the limits of the embankment geometry. Unfortunately, conventional bearing capacity analyses neglect the effects of the reinforcement and the lateral interface shear stress resisting deformation. Therefore, conventional analyses will be conservative and modified methods of analysis will provide a more realistic estimate of capacity.
- 2) A slope stability analysis to evaluate the location of the surface of maximum shear stress in both the embankment and the foundation soils. The effect of the reinforcement may be handled in several different ways.
- 3) A deformation analysis to estimate the elongation of the reinforcement. The results from this analysis are used to estimate the required modulus of the reinforcement, the strains in the reinforcement, and the anchorage requirements.
- 4) An anchorage length evaluation to estimate the distribution of tensile force in the reinforcement along its length.
- 5) A base sliding evaluation to estimate the required interface shear strength between the embankment and the reinforcement.

This paper presents a discussion of this five step approach to the design of embankments constructed over soft foundations. The design approach focuses on the use of geosynthetic reinforcement, though the same general approach could be used with other reinforcing materials.

BEARING CAPACITY

As stated previously, conventional bearing capacity analyses may be used to evaluate the ability of the foundation soils to support the entire embankment. Conventional analyses typically neglect the effects of the embankment side slopes, mobilized reinforcement tension, mobilized shear stresses at the embankment-foundation interface, and the deformation of the foundation soil as the embankment is constructed. The bearing capacity of an unreinforced embankment may be evaluated using the following equation [Bowles, 1988]:

$$q_a = q_u / F_{BC} = [c N_c + q N_q + (\gamma B N_\gamma)/2] / F_{BC} \quad (1)$$

where: q_a = allowable foundation bearing capacity (γH_a); H_a = allowable embankment height; γ = effective unit weight of the foundation soil; q_u = ultimate foundation bearing capacity; F_{BC} = factor of safety against bearing capacity failure; c = the undrained shear strength of the foundation soil; N_c , N_q , N_γ = bearing capacity factors; q = surcharge stress due to embankment fill; and B = foundation width.

Bearing capacity factors developed by Meyerhof, Hansen, and Vesic can be used with Equation 1 [Bowles, 1988]. Additionally, bearing capacity factors such as those developed by Mandel and Salencon [1967] can be used to account for increasing shear strength with depth and/or layered soil conditions.

For embankments constructed over soft, cohesive foundations where short-term (i.e., undrained) loading is the considered failure mode, Equation 1 may be reduced to:

$$q_a = c N_c / F_{BC} \quad (2)$$

Evaluation of the bearing capacity using Equation 2 may yield a factor of safety less than 1.0 for a reinforced embankment, even though test results or finite element analyses demonstrate stability. Based on finite element solutions, Rowe and Soderman [1987] developed a slightly different bearing capacity analysis that includes the effects of the average height of the embankment and the influence of the side slopes. In this analysis, the embankment is assumed to act as a rigid footing with the fill essentially held together by the reinforcement. Rowe and Soderman also suggests using data which reflect undrained strength increasing with depth.

For their analysis, Rowe and Soderman define an equivalent width, b , of the embankment in order to use plasticity solutions for a rigid footing. The pressure at the edge of a rigid footing, as evaluated from plasticity theory, is $(2 + \pi)c$. Assuming that the effective width extends between points on the embankment where the overburden pressure, γh , equals $(2 + \pi)c$, the following equations can be evaluated:

$$h = (2 + \pi)c / \gamma \quad (3)$$

$$\text{and,} \quad b = B + 2n(H - h) \quad (4)$$

where terms are denoted in Figure 2.

From Figure 2, the triangular edge of the embankment is assumed to provide a surcharge which tends to increase the footing stability. The surcharge pressure, q_s , is assumed to be distributed over a distance x from the edge of the footing. It is assumed that x is approximately equal to either the depth, d , at which the pressure is dissipated or the depth, D , of the deposit, whichever is smaller.

Figure 3 can be used to determine the depth, d , at which the pressure is dissipated. The figure can also be used for soils whose undrained strength is relatively constant with depth or increases with depth. The assumed surcharge pressure, q_s , acting over the distance x can be calculated by:

$$q_s = \gamma h^2 / 2x \quad \text{for } x > nh, \quad (5)$$

$$\text{and, } q_s = (2nh - x)\gamma h / 2nh \quad \text{for } x \leq nh, \quad (6)$$

The ultimate bearing capacity of a rigid footing, q_u' , of width, b , is calculated using:

$$q_u' = c N_c + q_s \quad (7)$$

The average applied pressure, q_a' , due to the embankment over the width, b , is calculated using:

$$q_a' = \gamma [BH + n(H^2 - h^2)] / b \quad (8)$$

The maximum possible factor of safety for a given geometry is evaluated using:

$$F_{BC}' = q_u' / q_a' \quad (9)$$

According to Rowe and Soderman [1987], when $q_u' / q_a' = 1.0$, collapse is considered to be imminent.

The allowable height can be increased by building the embankment in stages and allowing time between each stage for the foundation soil to consolidate and gain strength. If the hydraulic conductivity of the soil is low, vertical drains may be placed in the subgrade to accelerate consolidation.

Comparison of Bearing Capacity Analyses

Consider the embankment in Figure 4. In this example, the desired height is known and the factor of safety is calculated for various side slope conditions. In Table I, the effect of varying the side slope geometry is explored using both a conventional bearing capacity analysis (Equation 2) and Rowe and Soderman's analysis (Equations 7 to 9). Additionally, the factor of safety is calculated for two other arbitrary cases: (i) the actual embankment height and the assumed surcharge given by Equation 5 or 6 (i.e., $F_{BC}'' = q_u' / q_a'$); and (ii) the average embankment and no surcharge (i.e., $F_{BC}''' = q_u / q_a'$). As illustrated in Table I, the improvement in the factor of safety using Rowe and Soderman's analysis is primarily due to the stabilizing effect of the surcharge. At this time, there is little field or experimental data on the bearing capacities of reinforced embankments. Therefore, it may be prudent to be conservative and consider the Rowe and Soderman analysis an upper bound solution. For design, it is suggested that the improvement in the factor of safety due to the use of the average height of the embankment be ignored and that F_{BC}'' be used (rather than F_{BC}').

Table I. Comparison of Factor of Safety for Bearing Capacity

Side Slope	Conventional			Rowe and Soderman			Modified FS	
	q_u	q_a	F_{BC}	q_u'	q_a'	F_{BC}'	F_{BC}''	F_{BC}'''
3:1	809	1200	0.67	1180	1090	1.08	0.98	0.74
4:1	846	1200	0.70	1372	1075	1.23	1.14	0.79
5:1	884	1200	0.73	1415	1063	1.33	1.18	0.83
6:1	921	1200	0.77	1493	1055	1.42	1.24	0.87
7:1	959	1200	0.80	1559	1048	1.49	1.30	0.92

SLOPE STABILITY

The reinforcement force needed to increase the factor of safety against slip surface failure through the embankment and foundation can be approximated using limit equilibrium analyses, plasticity analyses, or finite element analyses. Currently, the most widely used technique is the limit equilibrium approach, modified to account for the tensile force in the reinforcement. This section addresses only limit equilibrium analyses.

When an embankment is constructed on a soft foundation, the reinforcement is usually placed at the interface of the embankment and the foundation. In the limit equilibrium analysis, the reinforcement is treated as an independent free-body tensile force. Assumptions with regard to the orientation and magnitude of the reinforcement force at the slip surface are required. Almost all reinforcement is placed horizontally. Most analysis methods incorporate the assumption that this orientation does not change during or after construction. There is currently some debate, however, as to whether the reinforcing force should be assumed to be horizontal or at some intermediate angle [Collins, 1987]. The horizontal orientation provides the most conservative results.

Overview of Limit Equilibrium Analyses

There are several available limit equilibrium methods for slope stability analysis. These methods differ in the number of equilibrium equations satisfied and the assumptions made. Assumptions are necessary because the number of available independent equilibrium equations is smaller than the number of unknowns.

This section provides a comparison of several of the more commonly used limit equilibrium analyses methods, including the Ordinary Method of Slices [Fellenius, 1936], Bishop's Modified method [Bishop, 1955], Janbu's method [Janbu, 1954], Spencer's method [Spencer, 1967], and the Log Spiral method [Taylor, 1937, and Haug and Avery, 1976]. all modified for inclusion of tensile reinforcement. In addition, Jewell's design method [Jewell, 1980] which was specifically developed for reinforced embankments, is also compared.

General Comparison of Limit Equilibrium Methods

The limit equilibrium methods for slope stability analysis have four common characteristics [Duncan, 1980]:

- 1) They all use the same definition of the factor of safety, F : $F = \frac{\text{soil shear strength along a considered slip surface}}{\text{shear stress required for equilibrium along the same slip surface}}$.

- 2) They all assume that the stress-strain characteristics of the soil used in the slope are non-brittle, and that the mobilized shear stress is the same along the entire slip surface.
- 3) They all use some or all of the independent equilibrium equations to calculate the shear stresses and normal stresses on the slip surface. The normal stresses are, in turn, used to calculate the distribution of soil shear strengths along the failure surface.
- 4) Since the number of equilibrium equations is smaller than the number of unknowns, all the methods make assumptions in order to solve the equations.

A summary of the equilibrium equations satisfied by each method of analysis and the assumptions significant to each method are provided in Tables II and III respectively. Most of the limit equilibrium methods divide the analysis into a number of vertical slices bounded by the slip surface, as illustrated in Figure 5. These methods allow determination of non-linear slip surfaces and conditions where soil properties and pore pressures vary along the slip surface.

Reinforcement

The limit equilibrium methods described above must be modified to account for the presence of reinforcement (with the exception of Jewell's method). In the analysis, the assumption is made that the reinforcement layer provides an additional restoring moment $M_R = T \cdot y_R$, where T is the mobilized reinforcement force at the intersection of the slip surface and the reinforcement, and y_R is the vertical distance between the center of rotation for the considered slip surface and the reinforcement, assuming the reinforcement has a horizontal orientation. The overall moment equilibrium equation for the factor of safety of a reinforced embankment becomes:

$$F = \frac{\text{moments resisting failure} + \sum T \cdot y_R}{\text{moments inducing failure}} \quad (10)$$

Table II. Characteristics of Equilibrium Methods
[after Duncan and Wright, 1980, with modification]

Procedure	Equilibrium Conditions Satisfied				Equations and Unknowns*	Shape of Slip Surface
	overall moment	slice moment	vert. force	horiz. force		
Ordinary Method	yes	no	no	no	1	circular
Bishop's Modif.	yes	no	yes	no	$N + 1$	circular
Janbu's	yes	yes	yes	yes	3N	any
Spencer's	yes	yes	yes	yes	3N	circular
Log Spiral	yes	N/A	yes	yes	3	log spiral
Jewell's	yes	no	yes	no	$N + 1$	circular

* N = number of slices

Table III. Assumptions in Equilibrium Methods [after Johnson, 1974, with modification]

<u>Procedure</u>	<u>Assumptions Employed</u>
Ordinary Method	Resultant of side forces is parallel to base of each slice.
Bishop's Modified Method	Resultant of side forces is horizontal (no vertical side forces).
Janbu's Generalized Method	Location of side force resultants on sides of slice is assumed but can be varied.
Spencer's Method	Side forces are parallel.
Log Spiral Method	Shape of the slip surface is a logarithmic spiral.
Jewell's Method	Uses slip circle analysis to determine reinforcement force and compare to available force for compatibility.

Comparison of Limit Equilibrium Analyses with Base Reinforcement

A number of comparative analyses have been made for unreinforced embankments to evaluate the differences in the minimum factors of safety calculated by the different methods [Duncan, 1980, and Fredlund, 1977]. One problem in rigorously comparing the methods over a wide range of conditions is that a large number of parameters are involved including the embankment geometry, the values of the strength parameters (c and ϕ), the unit weight of the soil, and the pore water conditions.

In order to compare the limit equilibrium methods for the application considered in this paper, a sample problem was analyzed using each of the methods. The same soil properties and embankment geometry shown in Figure 6 were used with each method. For simplicity, a constant undrained shear strength with depth was assumed for the foundation soil. Computer generated solutions were used when available to search for the critical failure surface. Based on that critical surface, the effect on the factor of safety of a layer of geosynthetic reinforcement with a horizontal orientation and a mobilized reinforcement force of 12,000 lb/ft was evaluated. The results of these analyses are presented in Table IV.

Table IV. Comparison of Factors of Safety
Based on Various Methods of Slope Stability Analysis

Method of Analysis	Unreinforced Factor of Safety		Mobilized Reinforcement Force (lb/ft)	Reinforced Factor of Safety
	Computer	Hand		
Ordinary Method	0.86	*	12,000	1.27
Bishop's Modified	0.90	0.90	12,000	1.30
Janbu's Rigorous	0.84	0.84	12,000	1.26
Spencer's	0.90	0.93	12,000	1.34
Log Spiral	*	0.90	12,000	1.30
Jewell's	*	*	12,000	1.30

* Data not available.

The conclusions reached from inspection of Table IV are essentially no different than those from previous investigations of unreinforced embankments. The factors of safety calculated by the various methods are only different by a few percent. Duncan [1980] and Fredlund [1977] both determined that the methods which evaluate a factor of safety based on moment equilibrium (i.e., Ordinary, Bishop's, Spencer's, Janbu's, Log Spiral, Jewell's) are less sensitive to the side force distribution than the methods that evaluate the factor of safety only with respect to force equilibrium (infinite slope or wedge analysis).

DEFORMATION ANALYSIS

For a given reinforcement, the mobilized reinforcement tension is a function of the strain in the reinforcement and the reinforcement modulus. The larger the strain the higher the tensile force. However, if too much deformation is allowed, the embankment can develop cracks and the reinforcement may no longer be able to tie the structure together, thereby reducing stability. Therefore, "relatively high" modulus values are desirable in the reinforcement of embankments over soft soils.

Strains may be induced in the reinforcement as a result of [Bonaparte et al., 1987]:

- 1) Placement of reinforcement and fill;
- 2) Undrained settlement of the foundation soil during and just after construction;
- 3) Localized elongation of the reinforcement at the embankment foundation interface due to the development of a slip surface at the end of construction or after a period of undrained creep; and
- 4) Consolidation settlement of the foundation soils.

According to Bonaparte et al. [1987], for high modulus reinforcement placed with proper construction procedures, the tensile strain due to installation and fill placement should be no more than 1 to 2 percent. The tensile strains induced in the reinforcement as a result of settlement during construction have been determined by finite element analysis to be on the order of 1 to 8 percent depending on the embankment height, soil and reinforcement properties, and soil/reinforcement interaction. The strain generated by the slip surface formation is typically neglected since the desired modulus should be high enough to prevent this from occurring. Finally, strains induced by consolidation are usually disregarded because soil consolidation is usually relatively uniform and does not cause large lateral movement. As consolidation progresses, the soil strength increases, thereby reducing the need for the reinforcement [Bonaparte et al., 1987]. Based on these considerations and available information from recent projects, Bonaparte and Christopher [1987] recommended the following tensile strains, ϵ_{\max} , for selecting reinforcement tensions for limit equilibrium analyses: highly sensitive or brittle clays, $\epsilon_{\max} = 2$ to 3 percent; medium- to low- sensitivity clays, $\epsilon_{\max} = 4$ to 6 percent; and nonsensitive and plastic clays, $\epsilon_{\max} = 10$ percent. For a required mobilized reinforcement tension, T , and value for ϵ_{\max} , the required reinforcement tensile modulus is given by:

$$E = T / \epsilon_{\max} \quad (11)$$

where: T = the required mobilized reinforcement tension in units of force per unit width obtained from the limit equilibrium analysis; E = the required reinforcement secant tensile modulus given in units of force per unit width of reinforcement; and ϵ_{\max}

is as recommended above. The maximum reinforcement strain for design, ϵ_{\max} , is also affected by the strain limits required to prevent creep rupture of the reinforcement. Although a discussion of creep rupture is beyond the scope of this paper, it should be evaluated as part of design.

ANCHORAGE LENGTH AND DESIGN TENSILE STRENGTH

The assumed stress distribution in the reinforcement varies from zero at the toe of the embankment to the design tensile stress, α_D , at a distance, l , from the toe of the slope, as shown in Figure 7. The anchorage length, l , is a function of the overburden pressure, interface shear strength between the embankment and reinforcement, interface shear strength between the subgrade and reinforcement, and the side slope of the embankment. The anchorage length may be computed as follows:

$$l = \frac{\alpha_D}{(a + \sigma_v \tan \delta)} \quad (12)$$

where: α_D = reinforcement design tension (which incorporates a factor of safety); a = the adhesion between the reinforcement and subgrade; σ_v = the maximum overburden stress (γH); γ = the unit weight of the embankment soil; H = the height of the crest of the embankment; and δ is the interface friction between the embankment and the reinforcement.

If the embedment length, calculated from Equation 12, is less than sH , where s is the side slope as denoted in Figure 7, then the embedment length may be computed as follows:

$$l = \frac{-a + \sqrt{a^2 + 4\alpha_D s^{-1} \gamma \tan \delta}}{2 s^{-1} \gamma \tan \delta} \quad (13)$$

If the embedment length, calculated from Equation 12 is greater than $b/2$, then the embedment is $b/2$, and the reinforcement design tension may be computed as follows:

$$\alpha_D = b/2 [a + \sigma_v \tan \delta] \quad (14)$$

where: b = the base width of the embankment as shown in Figure 7.

The adhesion, a , and interface friction angle, δ , can be measured in direct shear or pullout tests. The boundary conditions in the tests should simulate field conditions to the extent possible. That is, the subgrade and embankment soils should be placed in the test apparatus at the same water content and density that are anticipated in the field and the test should be performed at a confining stress and rate of deformation representative of field conditions.

BASE SLIDING

Lateral spreading or sliding of the embankment relative to the reinforcement may occur if there is insufficient shear strength mobilized between the embankment and the reinforcement as shown in Figure 1(c). The factor of safety against lateral spreading may be computed by dividing the shear force resisting failure, S , by the active force inducing failure, P_a . The factor of safety reduces to:

$$F_{BS} = \frac{(2x + sH)\tan\delta_b}{HK_a} \quad (15)$$

where: x = the horizontal distance along the crest of the embankment to the point of sliding, as denoted in Figure 7; H = the height of the crest of the embankment; s = side slope as denoted in Figure 7; δ_b the interface friction angle for base sliding; and $K_a = \tan^2(45^\circ - \phi/2)$. The critical value of x can be determined by manipulation of the equation assuming a factor of safety equal to 1.0.

$$x = H \left[\frac{K_a}{2\tan\delta_b} - \frac{s}{2} \right] \quad (16)$$

If the value of x , computed by Equation 16, is less than 0.0, then $x = 0.0$ should be used in Equation 15 to calculate the factor of safety. The interface friction angle, δ_b , used in Equations 15 and 16, is the interface friction angle for base sliding. This value should be measured in a direct shear test which properly models the boundary conditions above and below the base reinforcement. If direct shear data are not available, the interface friction angle for base sliding between cohesionless soils and geotextiles may be conservatively assumed to be approximately equal to 0.80.

OTHER DESIGN CONSIDERATIONS

In addition to the analyses for bearing capacity, slope stability, deformation, anchorage length, and lateral spreading, several other design consideration may need to be considered.

Effects of Consolidation

As an embankment is constructed, excess pore-water pressures develop in the foundation soil. The shear strength of the subgrade soil increases with time as the excess pore pressures dissipate and the soil consolidates. The rate of increase of the soil shear strength may be evaluated using consolidated undrained triaxial shear tests.

The rate of consolidation of the foundation soil may be increased through the use of sand columns or wick drains. Sand columns or wick drains decrease the length of the drainage path, thus allowing excess pore-water pressures to dissipate more rapidly. Analytical or numerical (i.e., finite element or finite difference) analyses may be used to evaluate the rate of excess pore pressure dissipation and the rate of increase of the shear strength.

Minor Principal Stress

In linear embankment construction, the major principal stress in the geosynthetic is assumed to act in the direction parallel to the embankment cross-section and the minor principal stress is assumed to act parallel to the center-line of the embankment. However, during construction significant stresses may be induced in the minor principal stress direction. For this reason, Koerner [1987] recommends the assumption that the minor principal stress is 50% of the major principal stress unless construction can be controlled adequately to allow for smaller values. In addition at the ends of the embankment, the minor principal stress may be equal to the major principal stress.

Effects of Seams and Holes

Seams are one of the most critical components in geosynthetic reinforcement. They are required primarily to provide uniform stress transfer from one piece of material to another. The method used to join the adjacent pieces of geosynthetic affects the performance of the entire assembly. Seams may be constructed by mechanical, physical, or chemical means. Mechanical joining includes using pins, staples, and sewing. Physical means include welding or heat seaming. Chemical bonding of materials can be achieved with adhesives [Ko, 1987].

Sewing is the most commonly used method for seaming geotextiles used in embankment construction, while mechanical joining is most commonly used with geogrids. According to Ko [1987], the strength of seams formed by sewing depends on four factors: 1) stitch geometry; 2) seam geometry; 3) sewing thread material and structural geometry; and 4) geotextile material and construction. The geotextile specification should define these four factors.

The loss in strength of the geosynthetic due to holes in the material must also be assessed. Holes may be caused by the installation of wick drains or monitoring devices, or they may result from accidents during construction. The loss in strength due to holes has been assessed experimentally by Koerner [1987]. The data demonstrates that while the geosynthetic strength decreases almost linearly (within +9% to -4%) with hole size, the seam strength loss is considerably higher. The designer must estimate the size, spacing, and number of holes to predict the total anticipated strength reduction. If drains are to be installed the number of holes can be estimated within reason.

CONCLUSIONS

The five step approach outlined in the previous sections encompasses the minimum requirements for the design of a reinforced embankment over a soft foundation. By approaching the design in a systematic and logical manner, geosynthetic performance properties can be determined for inclusion in the project specifications.

REFERENCES

1. Bishop, A.W. (1955), "The Use of the Slip Surface in the Stability Analysis of Slopes", Geotechnique, Vol. 5, No.1, pp. 7-17.
2. Bonaparte, R., and Christopher, B.R. (1987), "Design and Construction of Reinforced Embankments Over Weak Foundations", Proc. Symposium on Reinforced Layered Systems, Transportation Research Board Meeting, January, 1987.
3. Bonaparte, R., Holtz, R.D., and Giroud, J.P. (1987) "Soil Reinforcement Design Using Geotextiles and Geogrids," Geotextile Testing and Design Engineer, ASTM STP 952, J.E. Fluett, Jr., Ed., American Society for Testing and Materials, Philadelphia, pp. 69-116.
4. Bowles, J.E. (1988), Foundation Analysis and Design, McGraw Hill Book Company, New York, pp. 171-316.
5. Carpenter, J.R. (1986), STABL5/PC STABL5 User Manual, Joint Highway Research Project JHRP - 85 - 17.
6. Chen, W. (1975), Limit Analysis and Soil Plasticity, Elsevier Scientific Publishing Company, New York.
7. Chen, W. (1973), "Bearing Capacity Determination by Limit Analysis", Proc. ASCE, Vol. 99, No. SM6, pp.433-440.
8. Christopher, B.R. and Holtz, R.D. (1985), Geotextile Engineering Manual, Federal Highway Administration, Washington, D.C.
9. Collins, S.A. (1987), "Reinforcement of Embankment Over Soft Foundation: Design Steps", Short Course Soil Reinforcement: Mechanics and Design, Georgia Institute of Technology and University of Oxford, Atlanta, Georgia.
10. Dawson, A.W. (1972), "LEASE II - A Computerized System for the Analysis of Slope Stability", C.E. Thesis, Department of Civil Engineering, M.I.T.
11. Duncan, J.M. and Wright, S.G. (1980), "The Accuracy of Equilibrium Methods of Slope Stability Analysis", In: S.L. Koh (editor), Mechanisms of Landslides and Slope Stability, Engineering Geology, No. 16, pp. 5-17.

12. Duncan, J.M. and Wong, K.S. (1984), STABGM : A Computer Program for Slope Stability Analysis With Circular Slip Surfaces and Geogrid Reinforcement, Microcomputer Version, The Tensar Corporation User's Manual.
13. Fellenius, W. (1936), "Calculation of the Stability of Earth Dams", Proceedings of the Second Conference on Large Dams, Vol. 4, pp. 445-463.
14. Fowler, J. (1982), "Theoretical Design Considerations for Fabric Reinforced Embankments", Proceedings of the Second International Conference on Geotextiles, 4C, Las Vegas, Nevada, pp. 665-670.
15. Fowler, J. (1981), Design, Construction, and Analysis of Fabric Reinforced Embankment Test Section at Pinto Pass, Mobile, Alabama, Technical Report EL-81-7, USAE WES, Vicksburg, Mississippi.
16. Fowler, J. and Koerner, R.M. (1987), "Stabilization of Very Soft Soils Using Geosynthetics", Geosynthetics '87 Conference Proceedings, Industrial Fabrics Association International, St. Paul, MN., pp. 289-299.
17. Fredlund, D.G. and Krahn, J. (1977), "Comparison of Slope Stability Methods of Analysis", Canadian Geotechnical Journal, Vol. 14, pp.429 - 439.
18. Huang, Yang H. (1983), Stability Analysis of Earth Slopes, Van Nostrand Reinhold Company, New York.
19. Huang, Yang H. (1976), "Stability of Slopes by Logarithmic Spiral Method", Proc. of ASCE, Vol.102, No. GT1, pp.41-49.
20. Janbu, N. (1954), "Stability Analysis of Slopes With Dimensionless Parameters", Harvard Soil Mechanics Series, No. 46.
21. Jewell, R.A. (1980), "A Limit Equilibrium Design Method for Reinforced Embankments on Soft Foundations", Proceedings of the Second International Conference on Geotextiles, Las Vegas, Vol. 3, pp. 671-676.
22. Johnson, S.J. (1974), "Analysis and Design Relating to Embankments", Analysis and Design in Geotechnical Engineering, Vol. 2, ASCE, pp. 1-48.
23. Ko, F. (1987), "Seaming and Joining Methods", Proceedings 1st GRI Seminar, Philadelphia, PA., pp.88-103.
24. Koerner, R.M. and Hwu, B.L. and Wayne, M.H. (1987), "Soft Soil Stabilization Designs Using Geosynthetics", Proceedings 1st GRI Seminar, Philadelphia, PA., pp. 26-57.
25. Koerner, R.M. (1980), "Stress-Strain-Time Behavior of Geotextiles in Universal Tension", Proceedings Symposium on Geotextiles, ASCE, Portland, Oregon, pp.31-52.
26. Mandel, J. and Saleon, J. (1967), "Force portante d'un sol sur assise rigide: Etude theorique", Geotechnique, Vol. 22, No. 1, 1967, pp. 79-93.
27. Mitchell, J.K. (1976), Fundamentals of Soil Behavior, J. Wiley and Sons, Inc., N.Y.
28. Rowe, R.K. and Soderman, K.L. (1987), "Stabilization of Very Soft Soils Using High Strength Geosynthetics: The Role of Finite Element Analyses", Proceedings 1st GRI Seminar, Philadelphia, PA., pp. 58-87.
29. Spencer, E. (1967), "A Method of Analysis of the Stability of Embankments Assuming Parallel Inter-Slice Forces", Geotechnique, Vol. 17, pp. 11-26.

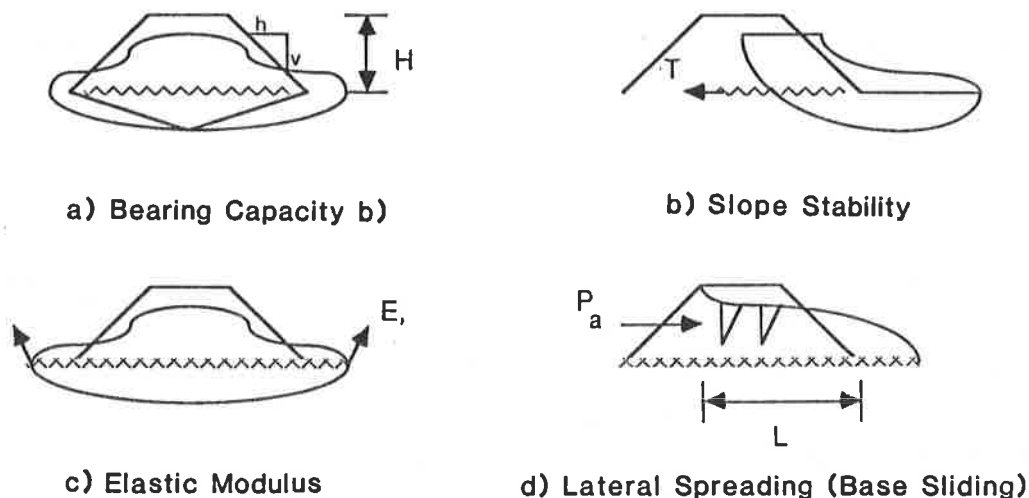


Figure 1. Failure Mechanisms To Be Analyzed In The Design Of Reinforced Embankments (After Fowler and Koerner, 1987).

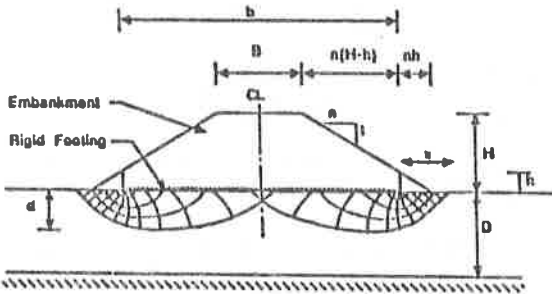


Figure 2. Definition of Variables Used in Rowe's Analysis of Bearing Capacity (After Rowe, 1987).

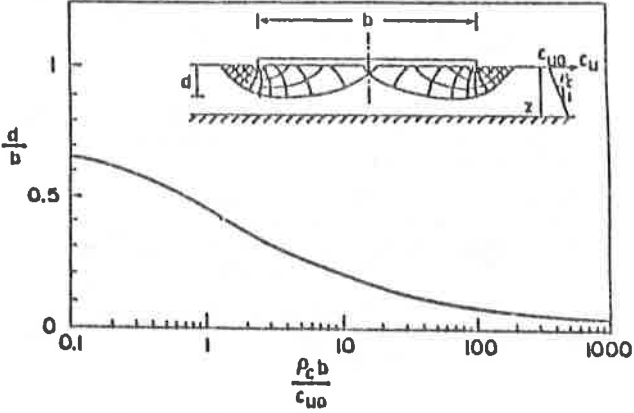


Figure 3. Effect of Non-Homogeneity on Depth of the Failure Zone Beneath a Rough Rigid Footing (Rowe, 1987).

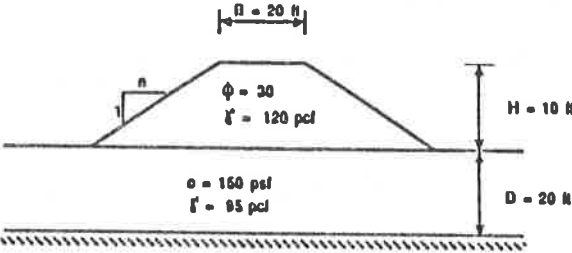


Figure 4. Example Problem: Bearing Capacity Analysis

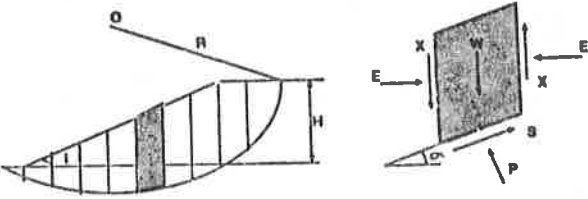


Figure 5. Typical Forces on a Slice

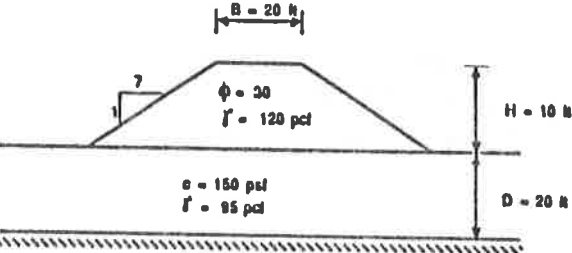


Figure 6. Example Problem: Slope Stability Analysis

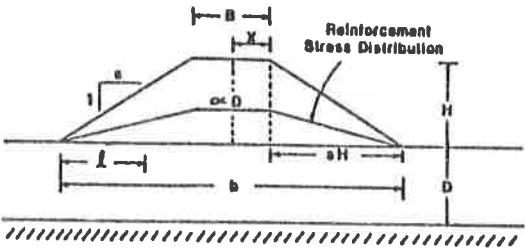


Figure 7. Reinforcement Stress Distribution

J.N. PAULSON
Exxon Chemical Co., U.S.A.

Geotextile Assisted Soft Site Stabilization

INTRODUCTION

Land with poor soil subgrade conditions is becoming increasingly more valuable as cities develop and expand. Property once bypassed by developers because of soft soil conditions is now in the center of town, making it much more valuable.

As well, spoil areas used to contain dredged river silts are beginning to fill up, resulting in the need to find some means of closure and use by the city or local government. This land can be turned into a park, recreational area or developed in some way for the public good.

Finally industry is capping old waste and storage ponds and basins. In some instances the company no longer wishes to maintain a waste storage facility on its premises. Others are to comply with regulation governing disposal of waste materials.

The condition common to all these situations is the very soft nature of the soil deposit, and the consequent difficulty in placing any type of fill on top of these sites. The use of geotextile reinforcement is a relatively new and successful way to facilitate site closures. Their use has resulted in site cappings that would have been difficult or impossible to accomplish with conventional civil engineering means.

ANALYSIS AND DESIGN APPROACH

Use of geotextiles for soft soil site closures requires evaluation of 4 key areas:

- Geotechnical - underlying soil strength/bearing capacity
- Loading - applied loads/stresses
- Geosynthetic - geotextile requirements and selection
- Construction - installation and filling procedures

Each will be discussed individually, followed by a review of their interrelationships.

Geotechnical

Bearing capacity can be determined using the following equation.

$$q_{ult} = C_u * N_c + q * N_q +$$

Where: C = soil cohesion (psf)

N_c = bearing capacity factor (dimensionless)

q = surcharge

N_q = Bearing capacity factor

For cohesive soils with $\phi = 0$, this equation reduces to:

$$q_{ult} = C_u * N_c$$

Where:

$$N_c = 5.14 \text{ square footing} \\ = 5.7 \text{ strip footing}$$

The appropriate bearing capacity factor to use is dependent upon the method of filling, and the construction equipment used. If the soil cover is placed in strips or fingers, the strip footing best approximates the loads induced by the fill and equipment. If the fill is spread by heavyweight equipment uniformly over the fill a square footing approach, simulating the bulldozer may be more applicable.

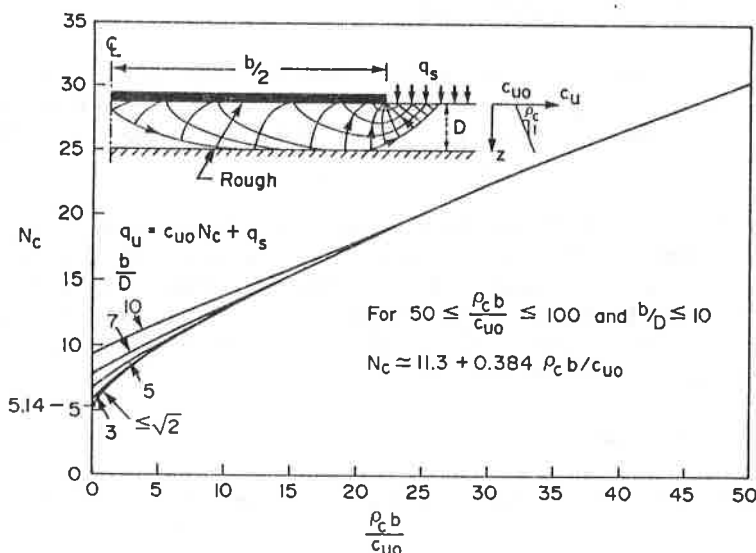


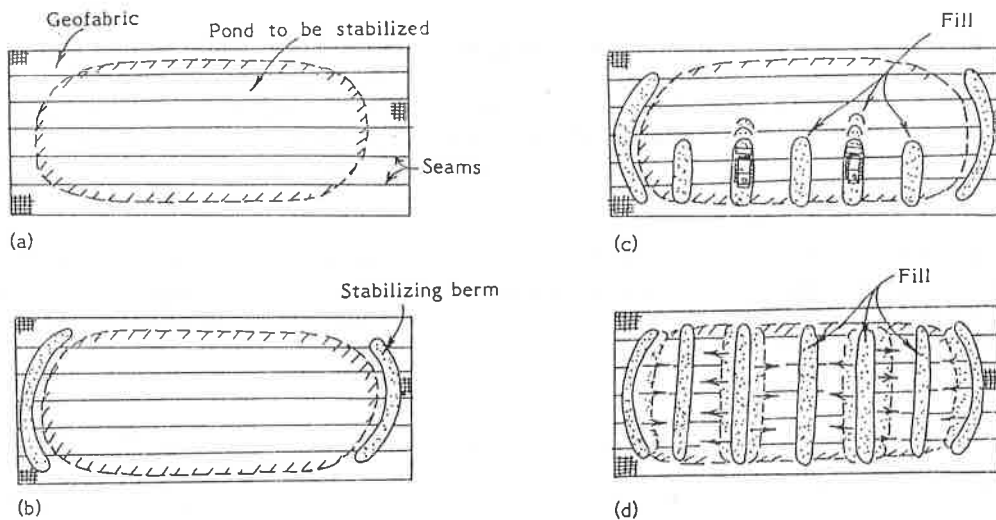
Figure 1

Fig. 5. Bearing capacity factor for non-homogeneous soil (synthesized from results by Davis and Booker,³⁵ and Matar and Salencon.³⁶ FROM ROWE (1)

Rowe (1) looked at the effect of tensile strength and modulus on stability of embankments constructed on soft soils. He reported an increase in the net fill height as the geosynthetic modulus increased, approaching the perfectly rigid case depicted above.

These factors assume a reinforced fill at the surface and no increase in cohesion with depth, which is the case when soft, unconsolidated silts, dredge spoils or tailings are the foundation soils. If the subgrade strength increases with depth or there is a finite depth to the soil deposit, figure 1 can be used to determine increase in N_c . Note that figure 1 is the upper limit in bearing capacity, assuming a rigid geotextile reinforced fill.

All this assumes that the soil undrained shear strength is known. One of the most difficult aspects of this type of geotechnical problem is determining that strength. If tube samples are obtainable, care must be used to limit disturbance to the sample from transportation and handling. Extremely soft soils will not hold their shape when the sample is removed from the sampling tube. In-situ testing is best suited for this soil type, usually vane shear testing. These results should be corrected (3&4).



Proposed construction method. (a) Placement of geofabric; (b) placing of stabilizing berms; (c) placement of fill; (d) widening of berms

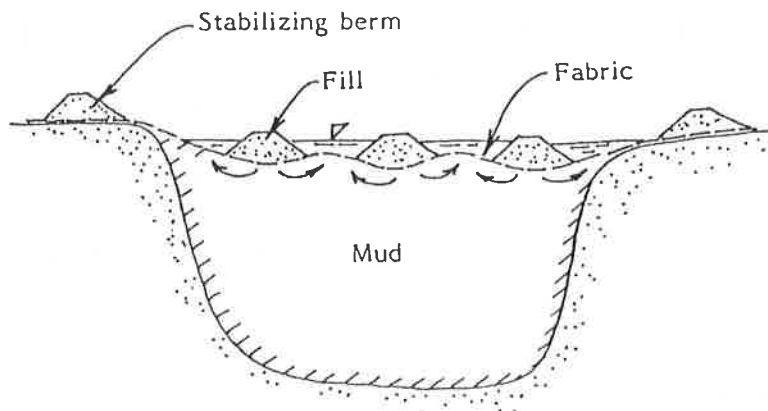


Fig. 2. Stabilization of very soft clay (mud) with geofabric. Broms (2)

One design procedure (Brohms,2) takes into account subgrade strength, geosynthetic strength, modulus and installation and fill placement procedures. By inducing an undulating shape during fill placement the geosynthetic is stressed, purposely redistributing fill loads. This procedure is directed at fills of large aerial extents where edge fixity (anchorage) can be assured and the fabric possesses a tensile modulus sufficient to redistribute the soil loads and confinement conditions. This "finger" approach can be used with success in filling soft areas where the bearing capacity is limited or questionable. The load redistribution is similar to the tensioned membrane approach for geotextile reinforced haul roads.

Applied loading

Placement of fills over soft sites induces both a live load and a dead load on the foundation soils. Each is critical and both are interrelated. Figure 3 shows the load induced by the fill (dead load) and by low ground pressure equipment (live load). The combined or resultant curve is also shown. Note the minimal pressure at a depth of 1.5 feet. For comparison both 4 psi and 8 psi contact pressure have been plotted.

Usually low ground pressure equipment (LGP) is used for placement of the first lift. It is important to evaluate contact pressure for the equipment used. If pads are attached to the tracks, with the load not properly centered, a nonuniform contact pressure results.

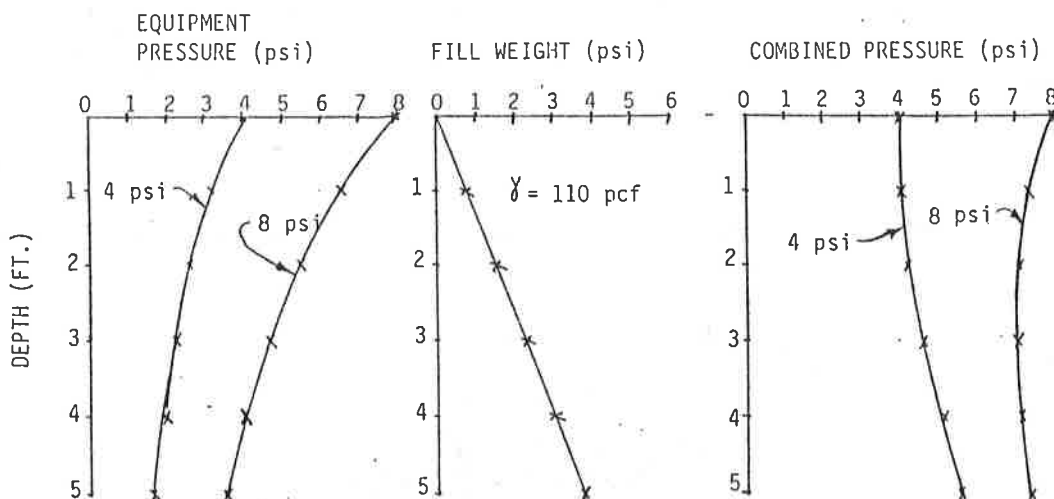


FIGURE 3. VERTICAL PRESSURE VS. DEPTH
(ASSUMES 62° LOAD DISTRIBUTION (1:2) WITH EQUIPMENT LOADS OVER
A 10 X 10 FT. AREA)

Geosynthetic requirements

Two geotextile functions required for this type application are:

- 1) Separation, and 2) Reinforcement.

Separation

Separation is required to prevent intermixing of the fill and the foundation soils. In this function construction survivability becomes important. The Task Force 25 interim recommendations for high and very high survivability site conditions (6) may be used as minimal guidelines for survivability. Although not finalized as of this date they are a good general indicator of minimum physical properties.

<u>SURVIVABILITY CATEGORY</u>	<u>GRAB</u>	<u>BURST</u>	<u>PUNCTURE</u>	<u>TRAPEZOID TEAR</u>
HIGH	180 LBS	290 PSI	75 LBS	50 LBS
VERY HIGH	270 LBS	430 PSI	110 LBS	75 LBS

To this must be added any additional requirements related to the project conditions, dependent upon the secondary functions the fabric may be asked to provide. Filtration is sometimes considered in fills over soft ground, where drainage up thru the fabric is anticipated. In that event fabric permittivity, opening size, flow capacity may also be specified.

Reinforcement

Geosynthetic reinforcement can add stability to fill lift heights by increasing edge of fill stability and as a tensioned membrane to increase ultimate bearing capacity. Critical geosynthetic reinforcement properties are tensile strength and tensile modulus. Wide-width strip tensile testing (ASTM D 4595) should be specified, with the complete stress-strain curve defined. For extremely soft sites fabric stiffness (vs drapability) can improve installation ease. Geotextile seam strength must be specified, requiring prior submittal of factory and field seams for verification testing .

Additional physical properties which may be considered are creep and durability. Geotextile creep can be critical if long term loading is anticipated on the geosynthetic. However, in many closure situations, the stresses are relatively short term, in that once the site is covered and final graded, most of the reinforcement needs have been met.

Durability is a second consideration, one that can be important in closures of chemical ponds. This should be investigated if aggressive chemicals are anticipated in an impoundment, or if very high (or low) Ph conditions are present. Exposure testing is useful for evaluating the resistivity of the geosynthetic.

Construction

Construction with geotextile fabrics is comprised of several steps, all important to the finished project.

Fabrication is the combining of individual rolls of fabric to make up a full sheet. The standard loom widths of 12ft-17ft necessitate seaming in order to transfer load between adjacent sheets and assure reinforcement and separation integrity. Seam strengths must be specified using wide strip tensile test methods in order to relate seam strength to fabric strength. Overlapping of geotextiles to provide reinforcement is ineffective and not recommended.

Seaming is accomplished with both factory and field sewing. Factory sewing is typically the combining of 2,3, or 4 rolls prior to shipment to the field. Notable exceptions are found in the literature (5) where gigantic rolls were factory sewn, rolled onto a large cylinder, then barged to the site and installed.

Field sewing requires experience. One approach is to fabricate at one end of the area to be covered and accordion sew a sufficient number of rolls to make up the completed sheet. Figure 4 shows this method.

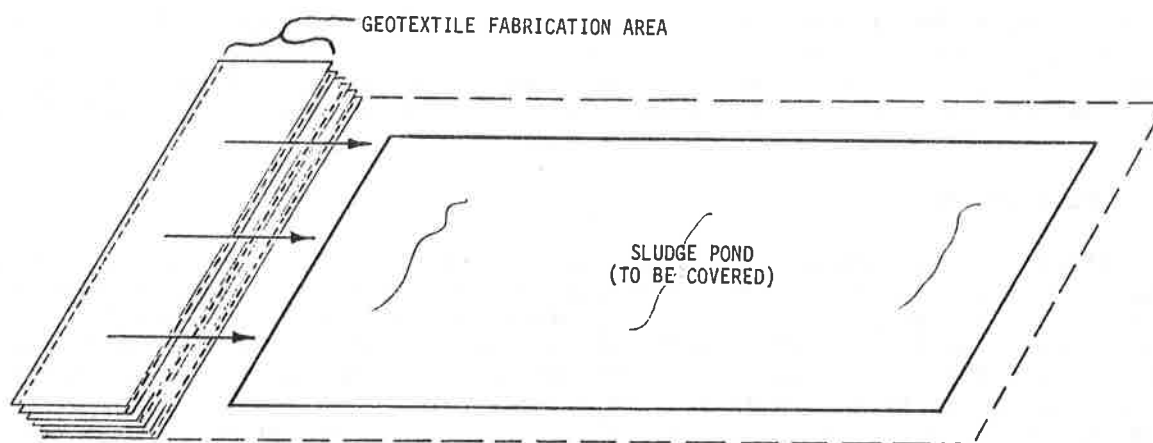


FIGURE 4. TYPICAL GEOTEXTILE CLOSURE PROJECT LAYOUT

Installation can be simple or difficult, depending on fabrication techniques and site conditions. Polypropylene geotextiles can be easily installed on a water filled pond by floating the fabricated sheet across (Gs .94). Polyester fabrics will sink if not installed quickly (Gs 1.03).

Localized stresses induced by pulling at selected points can result in tearing of the reinforcement during installation. More pull points are preferred (100' spacing, maximum) providing better control over the process. Installation should be avoided on very windy days.

Fill Placement is a critical step in the geotextile assisted soft site stabilization process. The first or initial lift requires the most care and attention. This is the time when overstressing of the subgrade soil is most likely. Lightweight equipment (<6psi), uniform thin lifts and ordered placement are the keys to a successful project.

The placement procedures outlined in Broms(2) are effective on very soft sites and large aerial extents to develop fabric tension and load redistribution. Other approaches are used when roadways of limited width are being constructed. (6)

In summary, the importance of a good site investigation to determine the soft soil properties cannot be overestimated. One case history to follow was less than successful because the soft soils or sludges to be covered was not investigated thoroughly enough.

Soil and equipment loading is important part in the closure success. Low ground pressure equipment will reduce the applied loads.

Geosynthetic specifications must take into account the strength properties sufficient to withstand installation as well as subsequent soil loading. Durability and longevity required of the geosynthetic may or may not be critical.

Most important in soft site closure success is the method of installation. This will affect the applied loads and the durability or survivability requirements for the fabric.

COMPLETED PROJECTS

Three projects will be described below, each with its own unique characteristics.

Bentonite sludge pond closure

The Wyoming Department of Environmental Quality required that an obsolete bentonite tailings pond be closed. Subgrade soils, composed of bentonite mine tailings, were estimated to have shear strengths of less than 100psf. The site had a small amount of standing water at one edge. Pond dimensions were 225 feet by 400 feet.

The engineer specified a geotextile with a seam strength of 300 lbs per inch wide width tensile strength. As well, an 18 inch wood chip cover was specified to be placed before any soil fill. This reduced the contact pressure at the fabric soil interface from the four psi equipment load to approximately 3 psi.

The geotextile was fabricated on one edge of the pond and consisted of 38 12.5ft wide rolls each 200 feet long accordion sewn. One interesting construction development was the effect the cold temperatures had on the sewing operation. The polypropylene geotextile supplied became very stiff at low temperatures which slowed the sewing operation down considerably on cold days.

An anchor trench was required to be cut around the perimeter, the geotextile anchored and the anchorage covered with three feet of soil before closure could proceed. The wood chips were installed using a highway snow blower, followed by placement of the first 18 inch soil lift. Fill was placed from all four sides toward the center. Because of the compression of the wood chips the size and shape of the mud wave, if present at all, could not be determined. After the second 18 inch soil layer was placed, fill trucks were driving directly over the pond with no difficulty.

Chemical Sludge Pond Closure

A chemical waste sludge pond was to be covered in the northeast. The aroma, unsightly nature and the fact that the pond was filled to capacity necessitated a closure plan.

Site investigations were quite difficult, but an estimate of the sludge was made, with strengths ranging from 0 to 50 psf. The pond had approximately 18 inches of standing water, and contained remnants from an old plastic liner placed there some years before in an attempt to reduce the smell. Pond dimensions were 450 ft wide and 600 ft long, running South to North.

A geotextile reinforced solution was specified and a geotextile with over 400 lbs per inch wide width tensile strength selected. Seam strengths tested indicated a seam strength of approximately 300 lb per inch.



FIGURE 5. VIEW OF THE SITE SHOWING GEOTEXTILE BUBBLE

Field sewing commenced at the south edge with factory supplied rolls 12.5ft wide and 440 ft long. Cables were attached to the fabric at three points using a C clamp type 4x4 type arrangement and the completed panel was dragged across from south to north.

During the pull debris from the old plastic liner became caught on the geotextile, resulting in increased drag on the fabric, resulting in some rips and tears. As well the sludge possessed an adhesive quality that further increased the resistance to fabric movement. After several repositions of pull points the pond was eventually covered. Patches the full width of the pond were installed over the torn areas, and the placement of two feet of anchorage fill around the perimeter begun.

Soil placed around the perimeter to allow access onto the pond sunk down to the dike level, with no visible increase in support noted. Fill placement resulted in displacement of the sludge, ending in large bubbles or waves of liquid underneath the geotextile. Although a tightly stressed fabric resulted, no fill could be placed successfully on top of the fabric.

Discussions with plant engineers revealed the sludge to have a "quick clay" nature to it, where although it appeared to possess shear strength, once stressed the strength disappeared. In essence the result was not unlike trying to put a soil cap onto a waterbed.

The project was then covered with lightweight straw fill in an attempt to traverse the site.

Dredge Silt Pond Cap

A dredge spoil lagoon in the Tidewater area was filled and required closure. The city elected to cap the site using geotextile reinforcement and turn it into a recreation area for the local residents. Although irregular in shape, the dimensions were 2000 feet long and 300-500 wide. The soil within the pond was thought to have been deposited over the past 10-20 years, and to have reached some degree of consolidation and strength gain. Still, soil shear strengths were estimated at less than 100psf.

First attempts at closure resulted in about 75% of the site being capped. The remaining 25% was rebid as a different contract. Problems with geotextile seam strength during the first installation resulted in close attention being paid to the field sewing operation.



FIGURE 6. FABRICATED GEOTEXTILE PANEL BEING PULLED ACROSS SOFT AREA

The geotextile selected was a stitchbonded composite, a very stiff material which possessed a minimum wide width tensile strength of 440 (warp) by 400 (fill) lbs. per inch. Seams were sewn using Kevlar thread, two stitch lines in a "j" seam. Tested seam strengths were in excess of 300 lbs. per inch. Rolls shipped to the project site were of varying lengths, allowing the contractor to construct a custom pattern panel to fit the irregular shape of the area to be capped. Sewing of the 18000 SY panel required about one week.

Installation was accomplished early in the morning before winds picked up, using four cranes lifting the geotextile at equally spaced intervals. Placement took about 20 minutes once everything was ready. The stretching and smoothing out of wrinkles required another 2 hours. The fill was then brought onto the site and placement commenced, from the two sides toward the center, which was the weakest soil area.

The filling procedure outlined by Broms (2) was used with such success. This "fingers of fill" placement approach resulted in an increase in the stability of the filled areas, expediting fill placement.

CONCLUSIONS

Geotextiles can be beneficial in the closures of soft sites. The success depends on a reasonable assessment of the subgrade shear strength, with fill height and placement determined so as not to exceed the ultimate bearing capacity. When insufficient bearing capacity is available, a procedure utilizing a forced undulating shape can be implemented, with selection of the appropriate geotextile strength and modulus coupled with the fill placement approach.

Fabrication of the panels requires preplanning to order proper length rolls, and to specify factory sewing. Field sewing is subject to the elements, with cold and wet conditions hampering sewing progress. Installation is a critical part of the construction process, with the potential to damage the fabric if proper techniques are not utilized.

Fill placement, especially for the first few lifts, should be performed using lightweight, low ground pressure equipment to reduce the load at the fabric/subgrade interface. Light weight fill is sometimes used to reduce the soil surcharge loads.

The geotextiles used in these projects were stitchbonded composites, manufactured by Exxon Chemical Company.

REFERENCES

1. Rowe, R.K. and Soderman, K.L., 1987, "Stabilization of Very Soft Soils Using High Strength Geosynthetics: The Role of Finite Element Analyses". Geotextiles and Geomembranes, Vol. 6, Nos. 1-3, PP. 53-80.
2. Broms, B.B., 1987, "Stabilization of Very Soft Clay Using Geofabric". Geotextiles and Geomembranes, Vol. 5, No. 1, PP. 17-28.
3. Ladd, C.C., et al, 1977, "Stress-Deformation and Strength Characteristics. State-of-Art-Report", 9th ICS MFE, Vol. 2, PP. 421-494.
4. Bjerrum, L., 1972, "Embankments on Soft Ground", 5th FSC, ASCE, Vol..2, PP. 1-54.
5. Heerten, G., 1984, "Geotextiles in Coastal Engineering - 25 Years Experience". Geotextiles and Geomembranes, Vol. 1, No. 2, PP. 119-141.
6. Christopher, B.R., Holtz, R.D. and Dimaggio, J.A., Geotextile Engineering Manual, U.S. D.O.T. FHWA Contract No. DTFH 61-80-C-00094, 1984.

SESSION 6A
FOUNDATIONS & RAILWAYS



O. GICOT

Soltechnique, Fribourg, France

J. PERFETTI

Rhone-Poulenc, Bezons, France

J.M. RIGO

K. Smolders, University of Liege, Belgium

C. LEGRAND

C.S.T.C. Belgium

A Functional Approach to the Design of Geotextiles

Summary

The number of application including the use of geotextiles is important and still increasing. However, the existing design methods are not applicable to all cases, but are rather limited to well specified fields. To fill up this gap, an approach of designing geotextiles by functions is proposed. It first concerns a quantitative procedure which leads to the choice of the best appropriate family of geotextiles for a given application. This functional approach is then extended in order to try to quantify the required characteristics of the geotextile and to be able to choose the appropriate geotextile. Finally, this approach should consider all aspects of the design of a geotextile (function, installation, long term behaviour, economy, ...) and thus become what could be called a global procedure for designing geotextiles.

1. INTRODUCTION

The design of civil engineering structures is often complex, particularly in the case of new techniques such as geotextiles.

Objective design rules for geotextiles are practically non-existent; for in most cases they are influenced by their promoter.

- * In his instructions for use, a geotextile manufacturer tends to promote the properties and characteristics of his own product, an often minimises those of his competitors.
- * A consulting engineer justifies his calculations by reference to traditional theories which are often ill-adapted to a new technique.
- * The client proposes design methods which give precedence mainly to the safety of the structure, and consequently the geotextile is over-designed.
- * The contractor is chiefly concerned with the economic aspect, with the result that the geotextile may be under-designed.

To avoid the user having to interpret the various design methods himself, a simple, global approach is proposed here, that enables the design rules of geotextiles to be justified objectively.

2. EXISTING CONCEPTS FOR DESIGNING GEOTEXTILES

2.1. Analytical method

This type of design rests on laws of behaviour and interaction established in the laboratory and which are based on simplifying assumptions. The surrounding medium is assumed to be homogeneous, and all the parameters introduced into the model calculus are representative of a continuous medium.

In order to remain realistic, the model has to be adjusted and the limits of its validity must be defined.

It should be noted that in an analytic approach, the aspects of installation and long term behaviour are considered only in terms of arbitrarily defined factors of safety.

2.2. Empirical method

The empirical method is based essentially on experience, which, if it is to be applicable to all cases, must embrace a large number of representative results. The normative approach is derived from such a method.

It should be pointed out that standards or specifications of use are applicable in a context which takes local traditions and particularities into account. It is therefore always risky to simply transpose standards or specifications.

2.3. Pragmatic method

Pragmatism is based on general observation in the broadest sense, taking both technical and economic aspects into account. This approach is close to the functional concept which shall be presented here.

The recommendations and directives for use are issued from such an approach. The purpose of recommendations is to reveal all the major or secondary parameters which may have an effect on the design and to express how they may vary. They tell the engineer what appears to be the best line to follow, in order to solve his particular problem.

3. THE FUNCTIONAL APPROACH

3.1. Principle of the approach

To arrive at a generally applicable approach, the various major or secondary parameters must be related together and their interactions established. Therefore, the extent and limits of a "Geotextile/Structure" system, has to be defined. This system is then divided into two subsystems, in order to evaluate :

- on one hand the characteristics specific to the geotextile;
- on the other hand the characteristics required by the type of application.

The only way of establishing and combining the two subsystems is via the functions of geotextiles, namely drainage, separation, filtration, reinforcement, protection, containment, ...

The evaluation of the functional requirements of the application of the geotextile in a structure, compared with the functional potentiality of the different families of geotextiles available on the market, makes it possible to arrive at an optimal structural design.

3.2. The qualitative approach (1)

In an initial stage, the functional potentiality of the geotextile is defined (drain, filter, etc.). After identifying the characteristics of the geotextile, it is possible to establish a relationship between these ones and the functions and subsequently a hierarchy (Table I of figure 1).

In a second stage, the functional requirements specific to a given application in a structure are defined. These requirements will differ according to the application.

These functions are then hierarchized in terms of their degree of importance. 100 % is assigned to the principal function or functions. (Table II of figure 1).

In a third stage, the combination of the two preceding tables (table III of figure 1), taking into account the importance of the functions and assigning a weighting factor to the characteristics related to the functions (a to g in table I of figure 1), makes it possible to determine, in graphic form, the profile of the optimal characteristics of the geotextile for the given application. (Table IV of figure 1).

This profile may then be compared to the corresponding profile of the various families of geotextiles (woven, nonwoven, grids), from which the best appropriate family can be chosen for the given application.

3.3. The quantitative approach

The quantitative approach has as objective the determination of the required characteristics of the geotextile (it means then not only for a family of geotextiles and not any more in form of a profile as previously) for a given application. It tries to translate the existing experience in order to quantify the characteristics of the geotextile.

A first approach of this design method has been carried out for site roads. A study of the existing documents lead to discern six different cases frequently encountered on sites. The features of these cases are detailed in figure 2 (cases I to VI).

A requirement level for the geotextile has been associated to each of the six cases. These requirements increase from case I to case VI. They are the expression of the level of sollicitation, that the geotextile has to sustain.

On one hand, a ponderation similar to the one used for the qualitative approach has been defined for the six cases. This ponderation expresses the level of performance required from each function of the geotextile. The combination of the importance of the functions and of the importance of the characteristics related to the functions allows to define a resulting functional weight factor for the application.

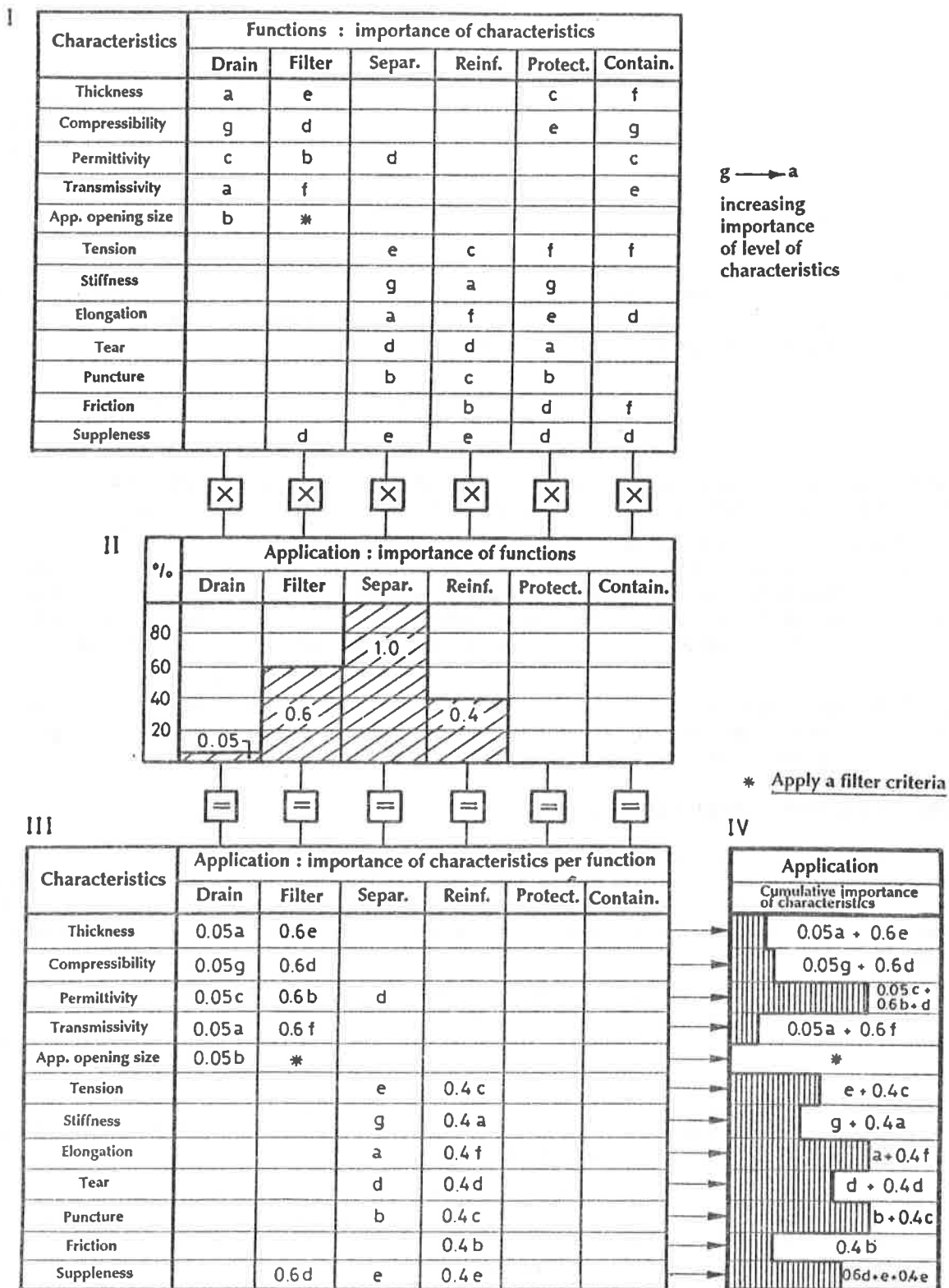


Figure 1. The quantitative approach to the design of geotextiles by functions.

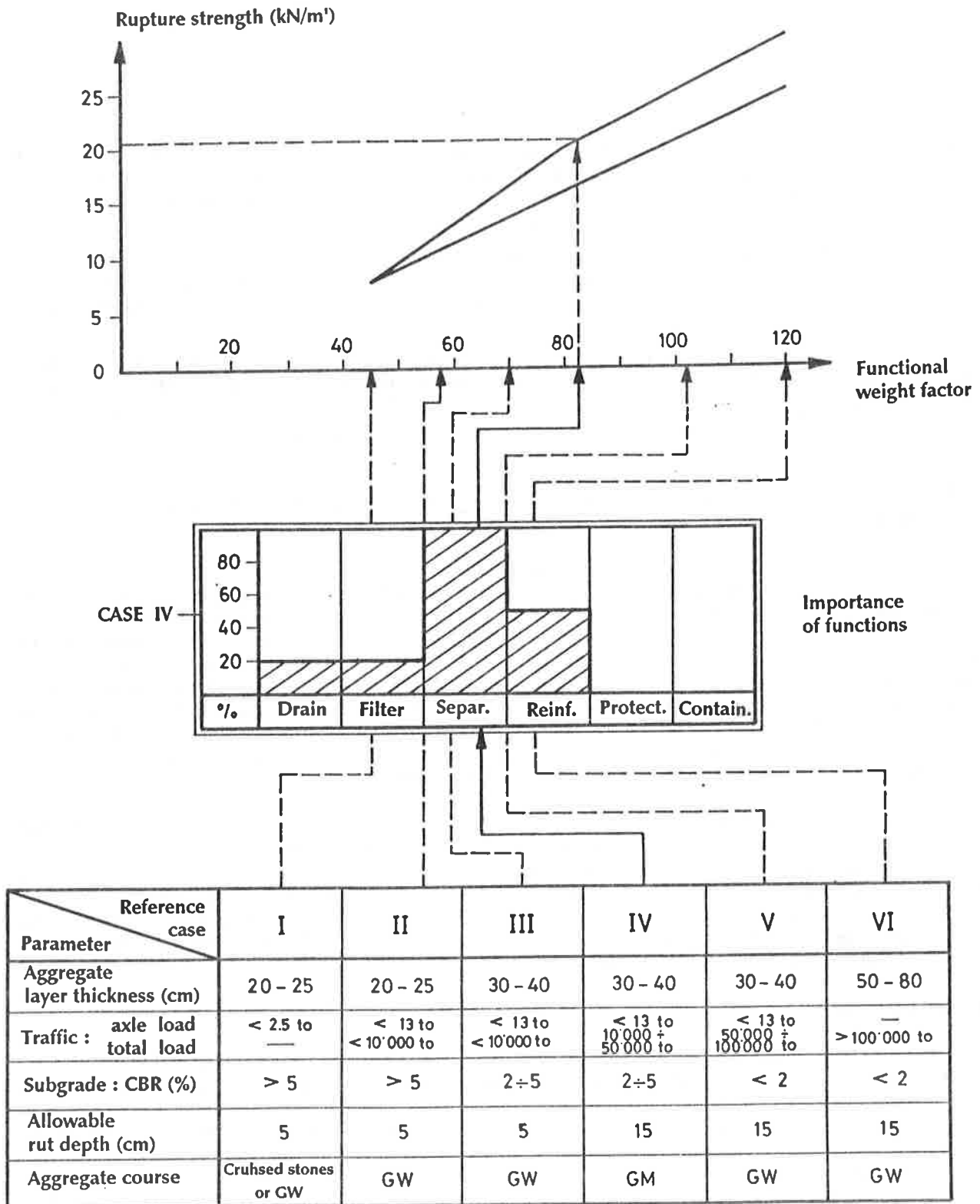


Figure 2. From the qualitative to the quantitative approach to the design of geotextiles by functions.
Example : site roads.

On the other hand, the six cases have been analysed through the recommendations of the French Committee on Geotextiles and Geomembranes (C.F.G.G.) (2) and the recommendations of the Swiss Association of Geotextile Professionals (A.S.P.G.) (3). This study permitted to refine the required characteristics of the geotextile (rupture strength, elongation, permeability,...).

Finally, a diagram was drawn, which associates the qualitative to the quantitative approach as can be seen on figure 2. At each case I to VI is associated a functional weight factor to which corresponds a required value for a given characteristic of the geotextile (i.e. rupture strength).

The user has to situate his application in comparison with the six reference cases. He thereby fixes the importance level of the different functions and gets consequently the required characteristics of the geotextile. Figure 2 shows that for a site road corresponding to case IV, the rupture strength recommended by the C.F.G.G. will be of about 20 kN/m.

3.4. The global approach to the design of geotextiles by functions and the involved parameters

The final goal of a design approach as presented in the preceeding chapters is to have at disposal a design method, which not only takes into account the functional parameters, but also other parameters, in other words to become a global design method. It is indeed not conceivable to develop a rigorous method (it means where all parameters could be calculated), which considers parameters as various as the ones involved in the choice of a geotextile. Then, the functional approach represents, in its extension, an interesting solution, as it may consider quantitative as well as qualitative criteria in the determination of the required characteristics of the geotextile in its application. The requirements related to the long term behaviour of the geotextile may also be considered.

Figure 3 shows how the various parameters can be taken into account in the global approach. As can be seen, the choice of the appropriate geotextile passes on one hand through the setting up or the application of qualitative and quantitative criteria and by requirements related to the raw material or the manufactured product. On the other hand, standards or specifications (that might be revealed as being too conservative or too restrictive by such a global procedure), as well as the economical parameters, act as "filters".

4. CONCLUSION

Up to now, the methods of designing geotextiles applied to well specified fields. It has been tried to develop a functional approach being first qualitative, and then quantitative in order to be able to choose among the various families and products the best appropriate geotextile for a given application. In its extension, this approach may allow to consider not only the functional parameters, but also other parameters involved in the design of geotextiles in a structure.

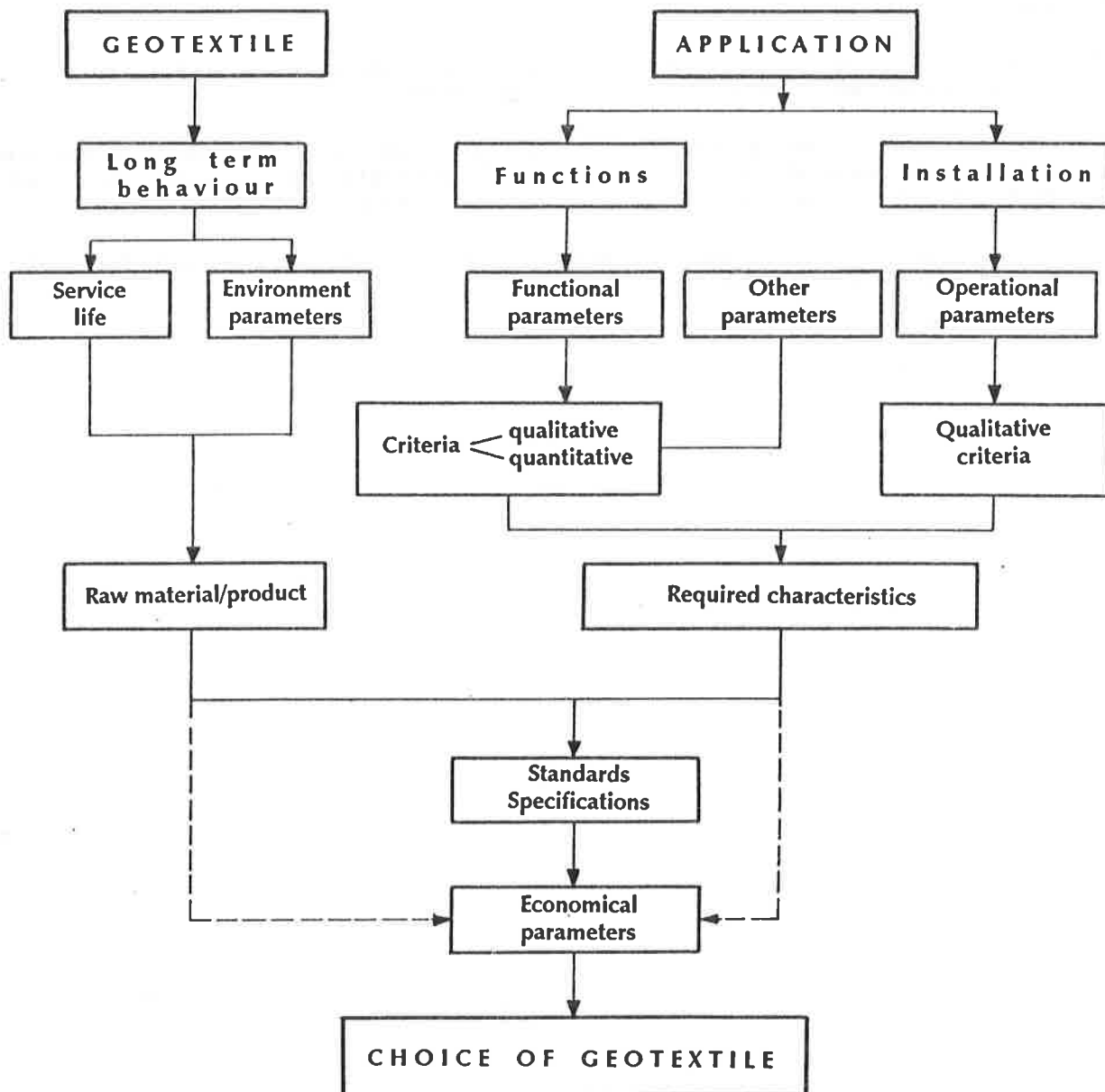


Figure 3. The parameters in the global approach to the design of geotextiles by functions.

Bibliography

- (1) Gicot, O. and Perfetti, J. : "Les géotextiles : guide de l'utilisateur", Fribourg, Suisse and Bezons, France, December 1987.
- (2) Comité français des géotextiles et des géomembranes, "Recommandations pour l'emploi des géotextiles dans les voies de circulation provisoire, les voies à faible trafic et les couches de forme", Paris, France, February 1981.
- (3) Association suisse des professionnels de géotextiles, "Le manuel des géotextiles", St-Gallen, Switzerland, July 1985.

B.M. DAS

Southern Illinois University at Carbondale, U.S.A.

Foundation on Sand Underlain by Soft Clay with Geotextile at Sand-Clay Interface

SUMMARY

Laboratory model test results for the ultimate bearing capacity of *strip* and *square* shallow foundations supported by a compact sand layer underlain by a soft clay with and without a geotextile at the sand-clay interface have been presented. The bearing capacity increase due to the use of a geotextile at the interface has been expressed in terms of nondimensional bearing capacity ratio.

INTRODUCTION

Shallow foundations constructed over soft clay soil possess low ultimate and allowable bearing capacities and experience large elastic settlement. One method of improving the load-bearing capacity and reducing the settlement of the foundation is to use a compact granular fill material over the soft clay. Relatively few studies, theoretical and/or experimental, are presently available in literature relating to the estimation of the ultimate bearing capacity of shallow foundations on a compact sand layer overlain by a soft clay at a shallow depth. Of those available, the work of Meyerhof and Hanna (8) appears to be the most rational one.

During the last fifteen years several studies relating to the estimation of the ultimate bearing capacity of shallow foundations supported by soils with reinforcements have been published. Biquet and Lee (2) and Fragaszy and Lawton (5) used multilayers of household aluminum foil as reinforcement in sand for determination of the bearing capacity of model strip foundations. Akinmusuru and Akinbolande (1) used multilayers of rope in sand under square foundations for their laboratory model tests. Guido *et al.* (6) have published the results of their model tests for bearing capacity of square foundations supported on sand with multilayer geogrid reinforcement. Ingold and Miller (7) studied the behavior of strip footings in clay with geogrid reinforcement. Based on the above studies, it appears that the beneficial effects in the performance of a shallow foundation on a compact sand layer underlain by a soft clay can be further improved by inclusion of a layer of geotextile at the sand-clay interface as shown in Fig. 1.

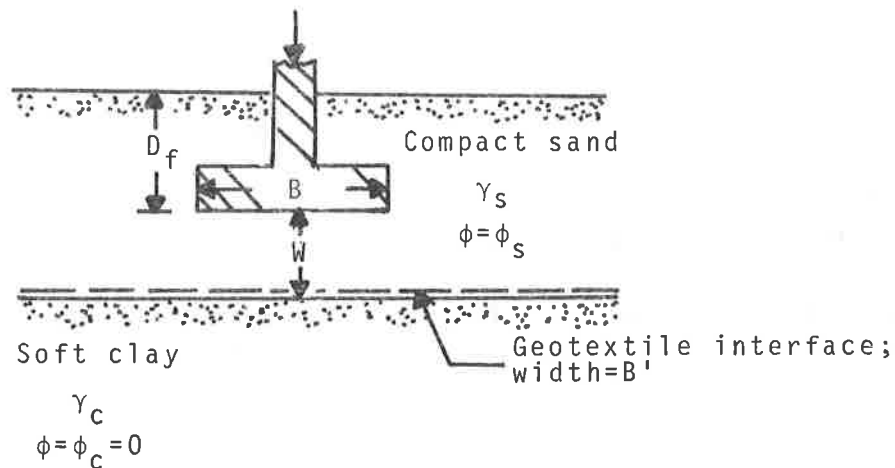


Fig. 1. Foundation on a compact sand layer underlain by a soft clay with geotextile at the sand-clay interface

The purpose of the present paper is to present some recent laboratory model test results for a *strip* and a *square* foundation on a sand layer overlain by a soft clay with and without the inclusion of a geotextile at the sand-clay interface. For comparison purposes, it appears necessary to present a brief overview of the ultimate bearing capacity relationship as obtained by Meyerhof and Hanna (8) for foundations on layered soil without the use of geotextile at the sand-clay interface. This is done in the following section.

BEARING CAPACITY THEORY--COMPACT SAND UNDERLAIN BY SOFT CLAY WITHOUT GEOTEXTILE INTERFACE

Figure 2 shows the basic assumptions of failure surface in soil as suggested by Meyerhof and Hanna (8). When the distance H between the

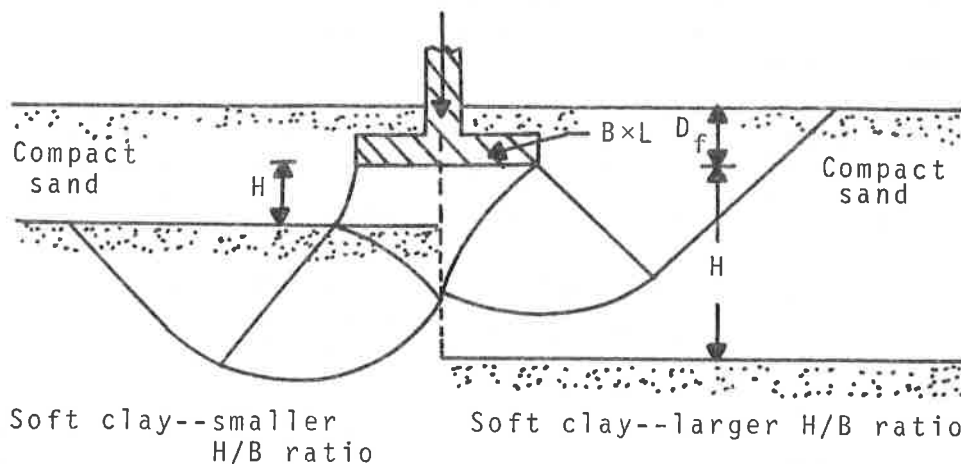


Fig. 2. Failure mode in soil under a foundation at ultimate load

bottom of the foundation and the sand-clay interface is relatively small compared to the foundation width B, failure will take place by punching in the sand layer followed by a general shear failure in the underlying clay layer as shown in the left-hand side of Fig. 2. For larger H/B ratios the failure surface in soil will be entirely contained in the sand layer as shown in the right-hand side of Fig. 2. According to Meyerhof and Hanna (8) for rectangular foundations

$$q_u = (1 + 0.2 \frac{B}{L}) c_u N_c(\phi=0) + (1 + \frac{B}{L}) \gamma_s H^2 (1 + \frac{2D_f}{H}) K_s (\frac{\tan \phi_s}{B}) + \gamma_s D_f \leq q_s \quad (1)$$

where q_u =ultimate bearing capacity; B=foundation width; L=foundation length; c_u =undrained cohesion of clay layer; $N_c(\phi=0)$ =bearing capacity factor for clay with $\phi=0$ (undrained condition)=5.14; γ_s =unit weight of sand; D_f =depth of embedment of the foundation; K_s =punching shear coefficient; ϕ_s =friction angle of sand; and q_s =ultimate bearing capacity when H/B is relatively large (i.e. when the failure surface is entirely located in sand as shown in the right-hand side of Fig. 2), which can be expressed as

$$q_s = \frac{1}{2} (1 - 0.4 \frac{B}{L}) \gamma_s B N_{\gamma(s)} + \gamma_s D_f N_{q(s)} \quad (2)$$

where $N_{\gamma(s)}$ and $N_{q(s)}$ are the bearing capacity factors which correspond to the soil friction angle ϕ_s .

The punching shear coefficient K_s is a function of ϕ_s and the ratio of $[c_u N_c(\phi=0)]/[0.5 \gamma_s N_{\gamma(s)}]$. For *strip* foundations B/L=0, so

$$q_u = 5.14 c_u + \gamma_s H^2 (1 + \frac{2D_f}{H}) K_s (\frac{\tan \phi_s}{B}) + \gamma_s D_f \leq 0.5 \gamma_s B N_{\gamma(s)} + \gamma_s D_f N_{q(s)} \quad (3)$$

Similarly, for *square* foundations B/L=1, and

$$q_u = 6.168 c_u + 2 \gamma_s H^2 (1 + \frac{2D_f}{H}) K_s (\frac{\tan \phi_s}{B}) + \gamma_s D_f \leq 0.5 \gamma_s B N_{\gamma(s)} + \gamma_s D_f N_{q(s)} \quad (4)$$

LABORATORY MODEL TESTS

The model foundation used for the laboratory tests had dimensions of 76.2 mm × 304.8 mm (for *strip* foundation tests) and 76.2 mm × 76.2 mm (for *square* foundation tests). Thus the width B of each foundation was kept at 76.2 mm. These model foundations were made from an aluminum plate 9.53 mm thick.

The tests on the *strip* foundation were conducted in a box measuring 915 mm (length) × 304.8 mm (width) × 762 mm (height), and the *square* foundation was tested in a box measuring 915 mm (length) × 915 mm (width) × 762 mm (height). The sides of the box were heavily braced to avoid lateral yielding.

A polypropylene needlepunched nonwoven geotextile was used for the present tests. According to the manufacturer's data, the average grab tensile strength, grab elongation, burst strength, trapezoidal tear strength, and puncture resistance were, respectively, 534 N, 50%, 1448 kN/m², 200 N, and 289 N.

The sand used for the model tests had 98% passing No. 10 U.S. sieve, 72% passing No. 40 U.S. sieve, and 0% passing No. 200 U.S. sieve. The clay used for the tests had 61% passing No. 200 U.S. sieve, with a liquid limit of 34% and a plasticity index of 21%. The pulverized clay soil was mixed with the required amount of water and stored in several sealed plastic bags in a moist curing room before use.

For conducting a test, the moist clay soil was compacted in the test box in 50.8 to 76.2 mm layers up to the desired height and unit weight using a flat-bottomed rammer. After compaction, if required, the geotextile was placed over the compacted clay layer. Sand was then poured into the box and compacted in 25.4 to 50.8 mm layers. At the end of sand compaction, the model foundation was placed centrally in the box. Load on the model foundation was applied by a hydraulic jack. The settlement of the foundation was measured by a dial gauge. Schematic diagrams of the test arrangements are shown in Fig. 3. The sequence of the model tests and the numerical values of the average soil parameters are given in Table 1. Results of some of the tests reported herein on *strip* foundations are also available in the works of Das (4).

MODEL TEST RESULTS

Figure 4 shows typical load per unit area on the foundation (q) vs. displacement plots obtained from Test Series 2. The ultimate bearing capacity (q_u) is determined from the load-displacement diagrams in the manner described by Vesic (9). The ultimate loads are also shown in Fig. 4. The load-displacement diagrams for all test series showed a similar configuration.

Figure 5 shows the plot of q_u vs. H/B for Test Series 1 and 2 in which a geotextile was not used at the interface of the sand-clay layer. As expected for each test series the q_u value increased with H/B up to a maximum value and remained constant thereafter beyond $(H/B) \geq (H/B)_{cr}$ at which q_u becomes equal to q_s . Also plotted in this figure is theoretical variation of q_u as predicted by the Meyerhof and Hanna theory (8). In predicting the theoretical variation, the values of the bearing capacity factors $N_q(s)$ and $N_\gamma(s)$ proposed by Caquot and Kerisel (3) have been used. The agreement between the theory and experiment is relatively good.

The ultimate bearing capacity q_u obtained from Test Series 3 and 4 are shown in Fig. 6 as a function of H/B . These tests were conducted with a geotextile at the sand-clay interface. For any given test series, the magnitude of q_u increases with H/B up to a maximum value, and with further increase of H/B it reduces to a relatively constant value. The interpretation of the ultimate bearing capacity obtained from Test Series 1 and 3 and 2 and 4 can be done in the following manner

$$q_u = q_1 + q_2 + q_3$$

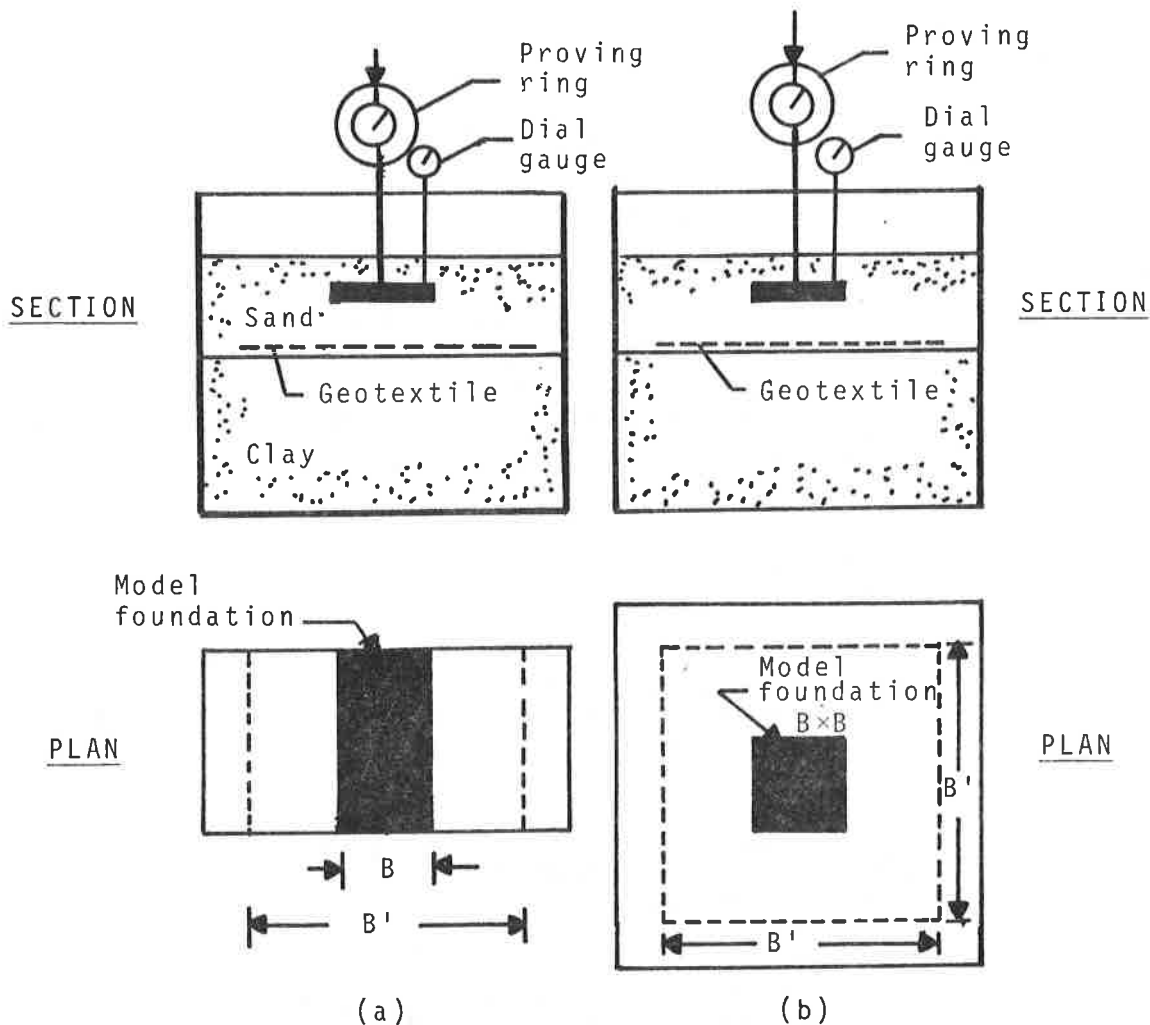


Fig. 3. Schematic diagram of laboratory test arrangement

where q_u =ultimate bearing capacity with geotextile interface at a given H/B value; q_1 =ultimate bearing capacity at $H/B=0$; q_2 =increase of ultimate bearing capacity due to the sand layer of thickness H only; q_3 =increase of ultimate bearing capacity due only to the inclusion of the geotextile.

The explanations of q_u , q_1 , q_2 , and q_3 are schematically shown in Fig. 7. Equation (5) can be written in a nondimensional form of bearing capacity ratio (2) as

$$BCR = \frac{q_u}{q_1} = 1 + \Delta(BCR)_S + \Delta(BCR)_G \quad (6)$$

where BCR =bearing capacity ratio; $\Delta(BCR)_S$ =contribution of the sand layer of thickness H to the bearing capacity ratio; and $\Delta(BCR)_G$ =contribution of the geotextile to the bearing capacity ratio.

TABLE 1
SEQUENCE OF MODEL TESTS AND AVERAGE SOIL PARAMETERS

TEST SEQUENCE	
Test series	Test details
1	<i>Strip</i> foundation tests <i>without</i> geotextile at sand-clay interface. $D_f/B=0.5$; $H/B=0, 0.25, 0.5, 1.0, 1.5, 2.0, 2.5$ and 3.0 .
2	<i>Square</i> foundation tests <i>without</i> geotextile at sand-clay interface. $D_f/B=0.5$; $H/B=0, 0.25, 0.5, 0.75, 1.0, 1.5$ and 2.0 .
3	<i>Strip</i> foundation tests <i>with</i> geotextile at sand-clay interface. $D_f/B=0.5$; $H/B=0.25, 0.5, 0.75, 1.0, 1.25, 1.5, 2.0, 2.5$ and 3.0 ; $B'/B=10$
4	<i>Square</i> foundation tests <i>with</i> geotextile at sand-clay interface. $D_f/B=0.5$; $H/B=0.2, 0.4, 0.6, 0.75, 1.0, 1.5$ and 2.0 . $B'/B=10$.
5	<i>Strip</i> foundation tests <i>with</i> geotextile at sand-clay interface. $D_f/B=0.5$; $H/B=0.75$; $B'/B=2, 3, 4, 5, 6$ and 8 .
6	<i>Square</i> foundation tests <i>with</i> geotextile at sand-clay interface. $D_f/B=0.5$; $H/B=0.6$; $B'/B=2, 3, 4, 6$ and 8 .

NOTE: B' =width of geotextile

AVERAGE SOIL PARAMETERS

CLAY: Moist unit weight, $\gamma_c=20.12 \text{ kN/m}^3$; $c_u=14 \text{ kN/m}^2$ (from undrained triaxial test); moisture content =21%; degree of saturation=95%

SAND: Unit weight, $\gamma_s=17.01 \text{ kN/m}^3$; $\phi_s=43.5^\circ$ (determined from direct shear tests)

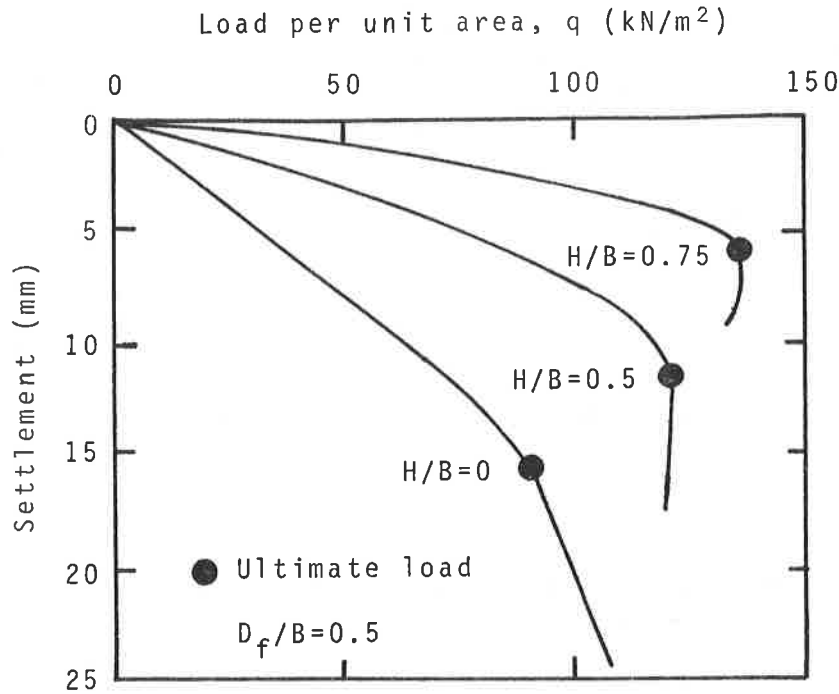


Fig. 4. Typical load per unit area vs. settlement diagram--Test Series 2

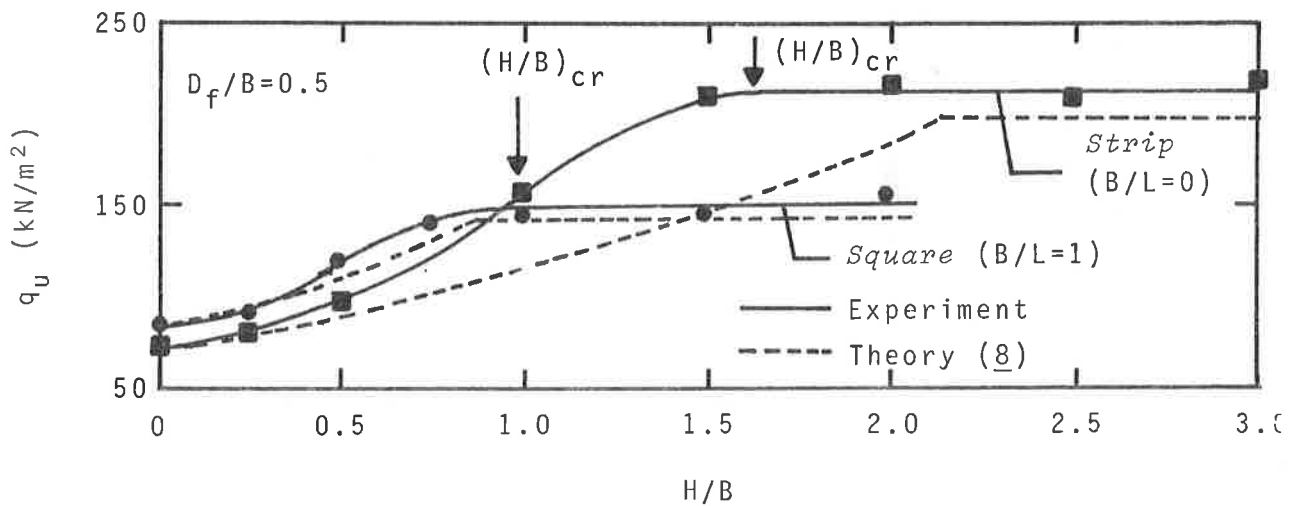


Fig. 5. Variation of ultimate bearing capacity with H/B for *strip* and *square* foundations (Test Series 1 and 2) without inclusion of geotextile at sand-clay interface

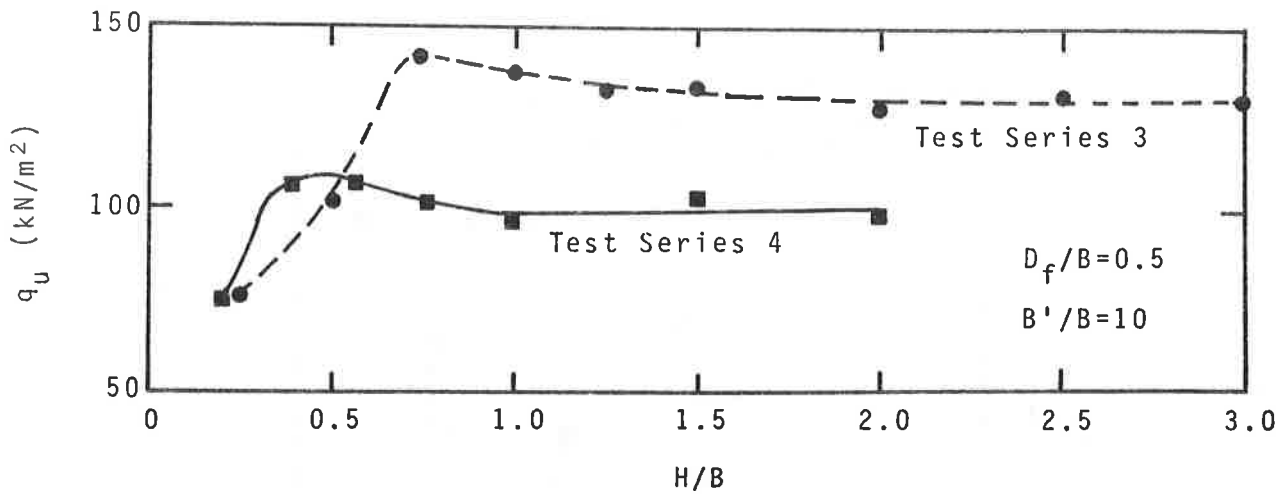


Fig. 6. Ultimate bearing capacity obtained from Test Series 3 and 4

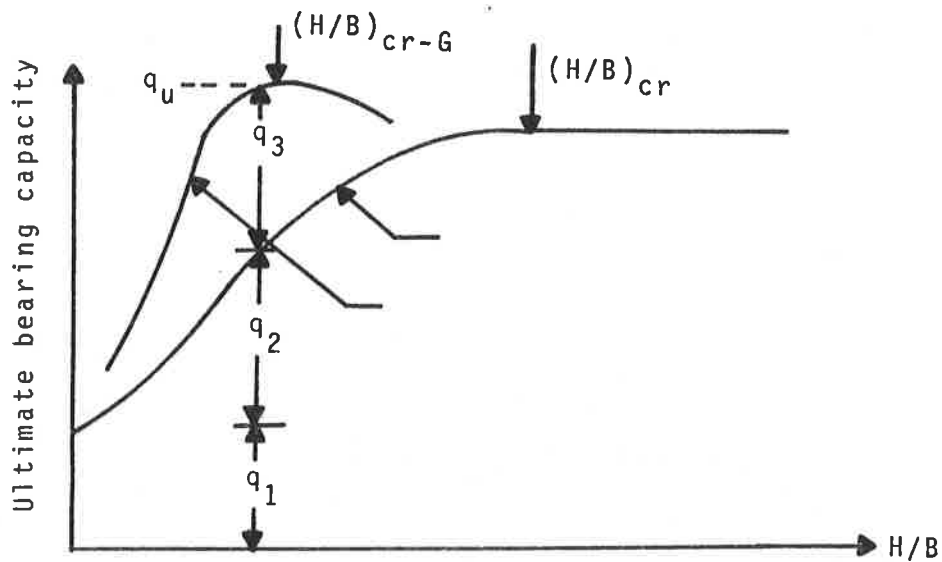


Fig. 7. Explanation of notations given in Eq. (5)

Using Eq. (6) and the average experimental plots shown in Figs. 5 and 6, the variations of $\Delta(\text{BCR})_S$ and $\Delta(\text{BCR})_G$ have been calculated and are shown in Fig. 8(a) and (b). From this figure it may be seen that $\Delta(\text{BCR})_G$ (i.e. the influence of the geotextile on the ultimate bearing capacity) becomes practically equal to zero at $H/B=1.5$ for *strip* foundations and at $H/B=1$ for *square* foundations.

Figure 9 shows the variation of $\text{BCR}=1+\Delta(\text{BCR})_S$ and $\text{BCR}=1+\Delta(\text{BCR})_S+\Delta(\text{BCR})_G$

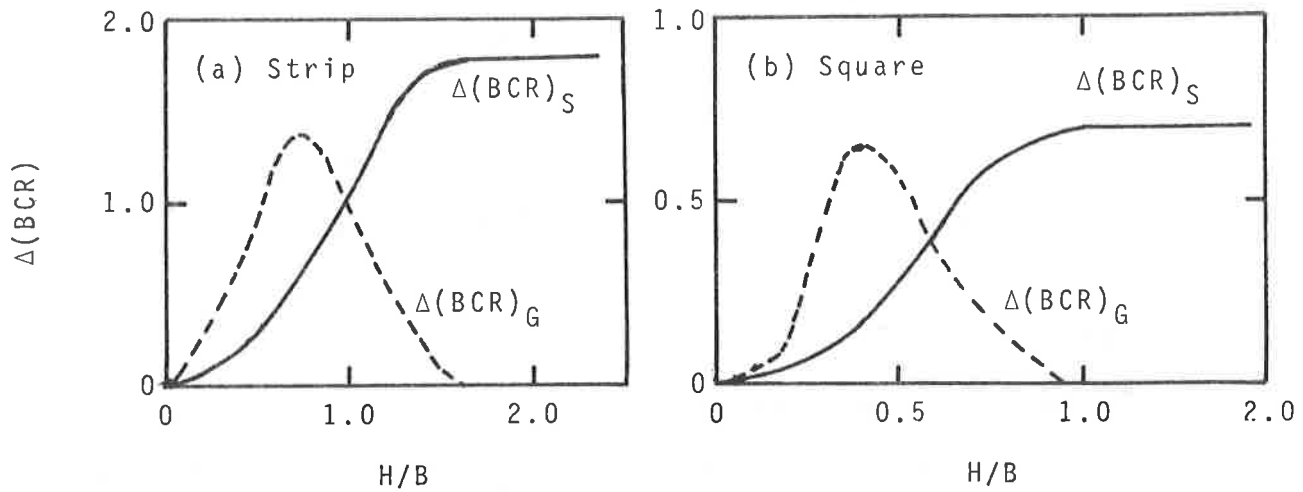


Fig. 8. Variation of $\Delta(\text{BCR})_S$ and $\Delta(\text{BCR})_G$ for: (a) *Strip* foundation; (b) *square* foundation

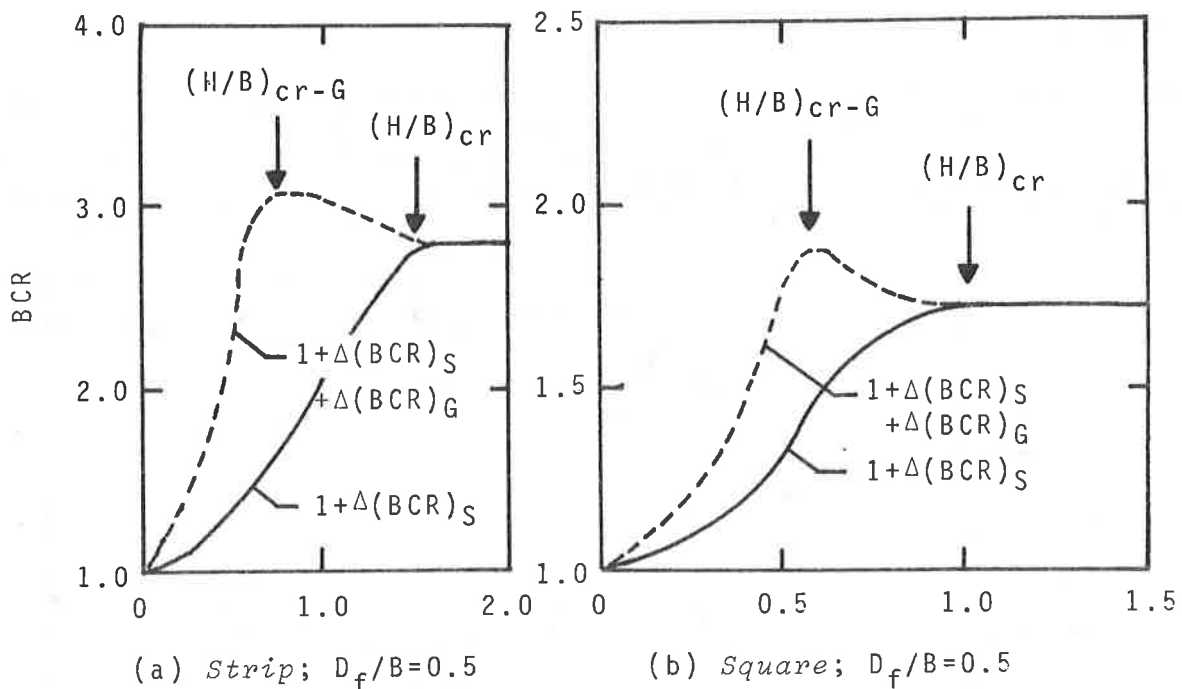


Fig. 9. Variation of bearing capacity ratio with and without geotextile at sand-clay interface (Test Series 1, 2, 3 and 4)

based on the average experimental plots given in Figs. 5 and 6. From this figure, the following observations can be made:

1. For *strip* foundations, the ratio of the maximum bearing capacity ratio with geotextile at the interface to that without geotextile can be given as

$$\frac{(BCR)_{\max\text{-with geotextile}}}{(BCR)_{\max\text{-without geotextile}}} = \frac{[1+\Delta(BCR)_S+\Delta(BCR)_G]_{\max}}{[1+\Delta(BCR)_S]_{\max}} \approx 1.08$$

2. For *square* foundations

$$\frac{(BCR)_{\max\text{-with geotextile}}}{(BCR)_{\max\text{-without geotextile}}} \approx 1.24$$

3. The maximum value of $(BCR)_{\max}$ with geotextile at the interface occurs at $H/B=(H/B)_{cr-G}$, and the maximum value of $(BCR)_{\max}$ without geotextile use occurs at $H/B=(H/B)_{cr}$. The ratio of $(H/B)_{cr-G}/(H/B)_{cr}$ is about 2 for *strip* and *square* foundations.
4. The magnitude of $(H/B)_{cr-G}$ decreases from about 0.75 for *strip* foundations to about 0.5 for *square* foundations.

OPTIMUM WIDTH OF GEOTEXTILE

Test Series 5 and 6 were conducted to determine the optimum width B' of the geotextile. Results of these tests are shown in Fig. 10. From these results it can be seen that, for a given foundation, the magnitude of q_u increases with B'/B up to a maximum value and remains practically constant thereafter. The minimum value of B'/B at which the

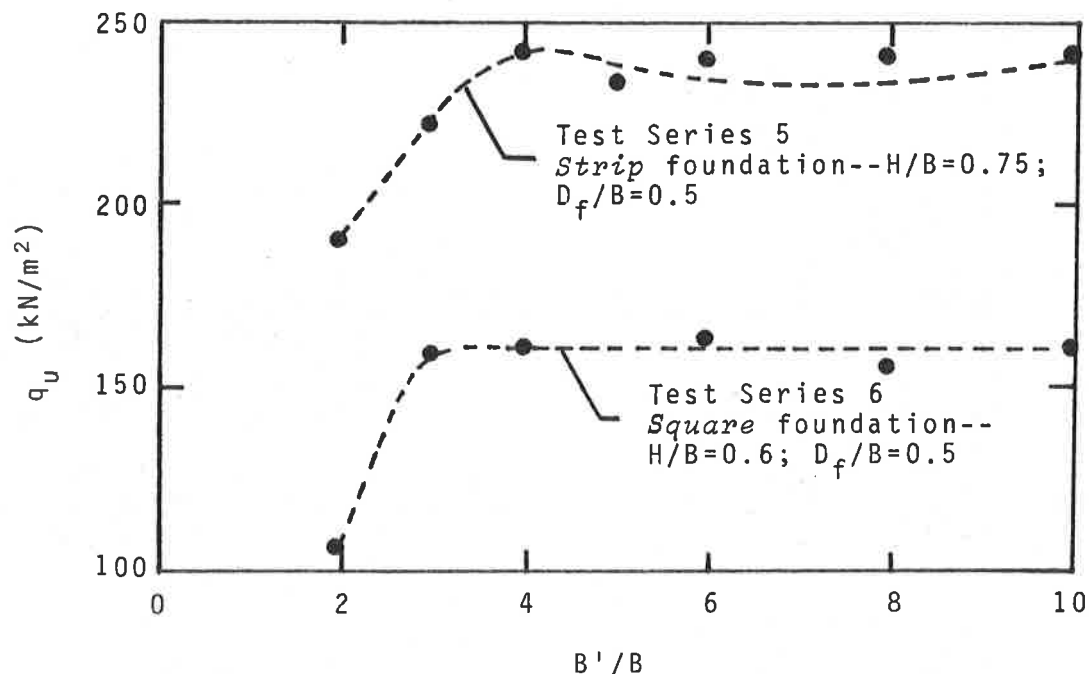


Fig. 10. Variation of q_u vs. B'/B (Test Series 5 and 6)

maximum value of q_u is derived is equal to about 3 for *square* foundations and about 4 for *strip* foundations.

CONCLUSIONS

A number of laboratory model test results for the bearing capacity of *strip* and *square* foundations on a compact sand layer underlain by a soft clay layer have been presented. Based on these tests, the following conclusions can be drawn:

1. The maximum bearing capacity ratio of a foundation increases with the use of geotextile at the sand-clay interface. For the present tests, the increase is about 24% for *square* foundations and it decreases to about 8% for *strip* foundations.
2. With the use of geotextile, the critical value of the H/B ratio at which the maximum bearing capacity ratio occurs is about 0.75 for *strip* foundations and about 0.5 for *square* foundations. These values of H/B are about half of those obtained when a geotextile was not used at the interface.
3. The optimum width of the geotextile layer for deriving the maximum possible bearing capacity ratio is about 4B for *strip* foundations and 3B for *square* foundations.
4. The increase of the bearing capacity ratio obtained by using a geotextile at the sand-clay interface may also be a function of the tensile strength of the geotextile itself. For the present tests only one type of geotextile was used; hence, further tests are required to develop a parametric model.

REFERENCES

1. Akinmusuru, J.O. and Akinbolande, J.A., "Stability of Loaded Footings on Reinforced Soil," Journal of Geotechnical Engineering, ASCE, Vol. 107, No. GT6, 1981, p.p. 819-827.
2. Binquet, J. and Lee, K.L., "Bearing Capacity Tests on Reinforced Earth Slabs," Journal of the Geotechnical Engineering Division, ASCE, Vol. 101, No. GT12, 1975, p.p. 1241-1255.
3. Caquot, A. and Kerisel, J., "Sur le Terms de Surface dans le Calcul des Fondations en Milieu Pulverulent," Proceedings, III International Conference on Soil Mechanics and Foundation Engineering, Vol. 1, 1953, p.p. 336-337.
4. Das, B.M., "Shallow Foundation on Sand Underlain by Soft Clay with Geotextile Interface," Geosynthetics, Ed. R.D. Holtz, ASCE Geotechnical Special Publication No. 18, 1988, p.p. 112-126.
5. Fragaszy, R.J. and Lawton, E., "Bearing Capacity of Reinforced Sand Subgrades," Journal of the Geotechnical Engineering Division, ASCE, Vol. 110, No. GT10, 1984, p.p. 1500-1507.
6. Guido, V.A., Chang, D.K. and Sweeney, M.A., "Comparison of Geogrid and Geotextile Reinforced Earth Slabs," Canadian Geotechnical Journal, Vol. 23, No. 4, 1986, p.p. 435-440.
7. Ingold, T.S. and Miller, K.S., "Analytical and Laboratory Investigations of Reinforced Clay," Proceedings, Second International Conference on Geotextiles, Vol. 3, 1982, p.p. 587-592.
8. Meyerhof, G.G. and Hanna, A.M., "Ultimate Bearing Capacity of

Geosynthetics '89 Conference
San Diego, USA

- Foundations on Layered Soil Under Inclined Load," Canadian Geotechnical Journal, Vol. 15, No. 4, 1978, p.p. 565-572.
9. Vesic, A.S., "Analysis of Ultimate Loads on Shallow Foundations," Journal of the Soil Mechanics and Foundations Division, ASCE, Vol. 99, No. SM1, 1973, p.p. 45-73.

V.A. GUIDO, J.P. SOBIECH

The Cooper Union School of Engineering, U.S.A.

S.N. CHRISTOU

Kanika Construction Ltd., U.S.A.

A Comparison of Texturized and Non-Texturized GEOWEB-Reinforced Earth Slabs

SYNOPSIS

GEOWEB-reinforcement is a three-dimensional grid (cell) confinement system; where grid confinement decreases lateral movement of the soil particles when loaded, thus increasing both stability and load carrying ability of low quality soils, e.g., loose sands and clay backfill material. A comparison of the results of laboratory model plate loading tests using both untexturized and texturized GEOWEB-reinforcement is presented herein. The model plate loading tests were used to study the load bearing capacity and settlement characteristics of GEOWEB-reinforced earth slabs. Five parameters were investigated: texturization of the GEOWEB material, expressed in terms of the root-mean-square (RMS), the number of layers of GEOWEB-reinforcement, the depth below the plate to the top of the first layer of GEOWEB-reinforcement, the size of the GEOWEB-reinforcement, and the relative density of the soil. For all parameters investigated the texturized GEOWEB-reinforcement performed substantially better than the untexturized GEOWEB-reinforcement, always yielding higher load bearing capacities and lower settlements than those for the earth slab reinforced with untexturized GEOWEB material. In general, the maximum load bearing capacity increases (180%) and settlement reductions (87%), due to the placement of GEOWEB-reinforcement in the earth slab, occurred with the texturized GEOWEB material. The maximum increase in load bearing capacity and reduction in settlement due to texturization of the GEOWEB material were 130% and 42%, respectively.

GEOWEB GRID CONFINEMENT SYSTEM

At present, the GEOWEB grid (cell) confinement system is manufactured with an untexturized GEOWEB material. As will be reported herein, texturization is a definite improvement that should be considered. After extensive testing at the U.S. Army Engineer Waterways Experiment Station (WES) Vicksburg, MI, it was found that axisymmetric cell shapes worked best while plastic materials proved to be durable, inexpensive and easy to handle. This testing also determined that the ratio of the

cell width, B_1 , to the cell depth, h was an important parameter, with an optimum value of approximately 1.0.

GEOWEBS are lightweight grids (cells) made from high density polyethylene strips having dimensions of 11 ft. (3.4m)x8 in. (23 cm)x0.05 in (1.3 mm), connected by ultrasonic welds at 13 in. (33 cm) spacings. Each unexpanded grid section is 5 in. (13 cm.) thick and expands to form a honeycomb arrangement of 561 cells covering an area of 8 ft. (2.5 m)x20 ft. (6m). See Fig. 1 and Table I for typical dimensions and structural properties of the aforementioned GEOWEBS.

The GEOWEB grid (cell) confinement system not only increases the load bearing capacity of the soil but also substantially reduces the settlement. This is accomplished by the confinement of the failure wedges, which would be developed in an unreinforced soil, from displacing laterally and outward. In addition, the frictional interlock between the infill material and the cell walls allows the load to be distributed or shared with adjacent cells. Therefore, it would seem to be apparent that an improvement in the frictional resistance between the cell wall material and the infill material would yield higher load bearing capacities and lower settlements of the GEOWEB-reinforced earth slab. This improved frictional resistance would take the form of texturization of the GEOWEB material.

TABLE I
GEOWEB STRUCTURAL PROPERTIES

	English System	SI System
1. Expanded Dimension	8 ft.x 20 ft.x8 in.	2.5m x6m x23cm
2. Collapsed Dimension	11 ft.x 5 in.x8 in.	3.4m x13cm x23cm
3. Panel Thickness Nominal	0.047 in.	0.119cm
4. Weight	5.7 lb/yd ²	30.3N/m ²
5. Cell Area	41 in. ²	265 cm ²
6. Cell Seam Node Pitch	13 in.	33 cm
7. Welds/Seam	7	7
8. Seams Tensile Peel Strength	150 lbs.	667N
9. Installation Temperature Range	-16 ⁰ F to 110 ⁰ F	-27 ⁰ C to 43 ⁰ C

Polymer Material: High Density Polyethylene
Color: Black
Carbon Black Content: 2%
Chemical Resistance: Superior

FIXED SHEAR BOX TESTS

The data presented in Figs. 3 and 4 are the results of a series of 60 fixed shear box tests and a series of 22 triaxial compression tests. The triaxial compression tests were performed to determine the angle of internal friction of soil on soil, ϕ , at different relative densities. The fixed shear box tests were performed to determine the angle of friction, δ , between the GEOWEB material (untexturized or texturized) and the soil. Of the 60 fixed shear box tests 38 were performed with texturized GEOWEB material and the remaining 22 were performed with untexturized GEOWEB material.

The soil used in the fixed shear box tests was the same soil used in the model plate loading tests. This soil was a narrowly graded sand (SP) whose properties are found in Table II. The GEOWEB material is texturized by an embossing process when the material is extruded. This embossing process will generate a surface pattern. Lay is the term used to designate the direction of the predominant surface pattern produced by the embossing process. For the GEOWEB material this is either the Transverse Direction (TD) or Machine Direction (MD). Roughness refers to the finely spaced surface irregularities. It results from embossing operations and is measured by the heights of the irregularities with respect to an average line, see Fig. 2. These measurements usually are expressed in microinches (μin). To define the surface roughness or texture of the GEOWEB material either the arithmetical average (AA) or root-mean-square (RMS) can be used:

$$AA = \frac{y_1 + y_2 + y_3 + \dots + y_n}{n} \quad (1)$$

where y is a vertical distance from the center line and n is the total number of vertical measurements taken within a specified cutoff distance, and

$$RMS = \sqrt{\sum y^2 / n} \quad (2)$$

RMS will be used to determine the surface roughness of the GEOWEB material. Three textures were used for the fixed shear box tests: No Texture, Medium Texture, and Coarse Texture, see Table III for their RMS values.

A square split shear box 4 in. (10.2 cm.) wide and 2 in. (5cm) deep was used. The GEOWEB material, attached to a wooden block, was placed in the lower half of the box. The range of normal stresses used were from 1 tsf (96kPa) to 3 tsf (287kPa) while the relative densities ranged from 23% to 84%. Where relative density, D_r , is defined as

$$Dr = \frac{1/\gamma_{dmin} - 1/\gamma_d}{1/\gamma_{dmin} - 1/\gamma_{dmax}} \times 100\% \quad (3)$$

A displacement rate of 0.0007 in/sec (17.8 μ m/s) was used.

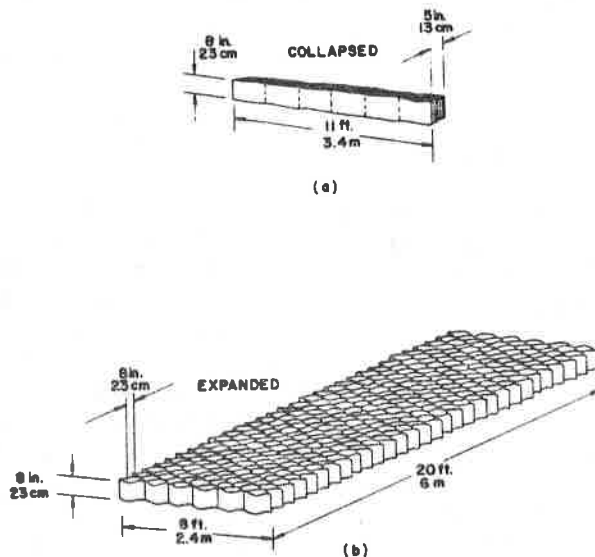


FIG. 1 GEOWEB GRID CONFINENT SYSTEM
(a) COLLAPSED AND (b) EXPANDED

TABLE II
PROPERTIES OF THE SAND USED IN MODEL TESTS

Uniformity Coefficient, C_u	1.90
Coefficient of Concavity, C_c	1.23
Effective Size, D_{10} , mm	0.086
Specific Gravity	2.66
Minimum Dry Unit Weight, γ_{dmin} , kN/m^3	13.10
Maximum Dry Unit Weight, γ_{dmax} , kN/m^3	15.65

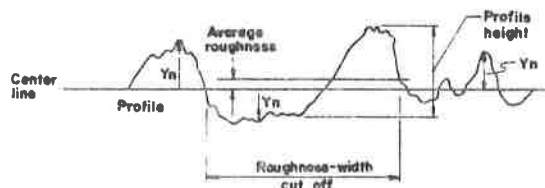


FIG. 2 SCHEMATIC OF SURFACE PROFILE AS PRODUCED BY A STYLUS DEVICE SHOWING SOME TYPICAL Y_n VALUES WITH RESPECT TO THE CENTER LINE

TABLE III

RMS VALUES FOR THE GEOWEB MATERIAL
USED IN THE FIXED SHEAR BOX TESTS

TEXTURE	ROOT-MEAN-SQUARE (RMS) *	
	TRANSVERSE DIRECTION	MACHINE DIRECTION
NONE	9-12	13-15
MEDIUM	130-150	120-135
COARSE	500-600	500-600

* Measurements in microinches

Shown in Fig. 3 is the relationship between relative density, peak angle of friction between soil and GEOWEB material and RMS. Both the medium and coarse texturizing patterns, Figs. 3(c) and (d) give friction angles substantially larger than the untexturized GEOWEB material, Fig. 3(b), on the order of 50% to 55%. Except at very low values of relative density (0% to 35%), the medium texture yields larger friction angles than the coarse texture. A possible explanation for this is the relationship between the depth of the roughness pattern and the grain size of the soil being reinforced. The depth of the roughness pattern for the coarse texture is 4 to 5 times that of the medium texture. For the narrowly graded fine sand used, some of the soil grains may be embedding themselves into the coarse texture pattern. This in turn would not be causing the soil to shear directly against the texturized GEOWEB material but against a composite sand-texturized GEOWEB surface, Fig. 3 (d). This would reduce the friction angle to a value between that obtained from soil on texturized GEOWEB material Fig. 3(c), and of soil on soil, Fig. 3(a).

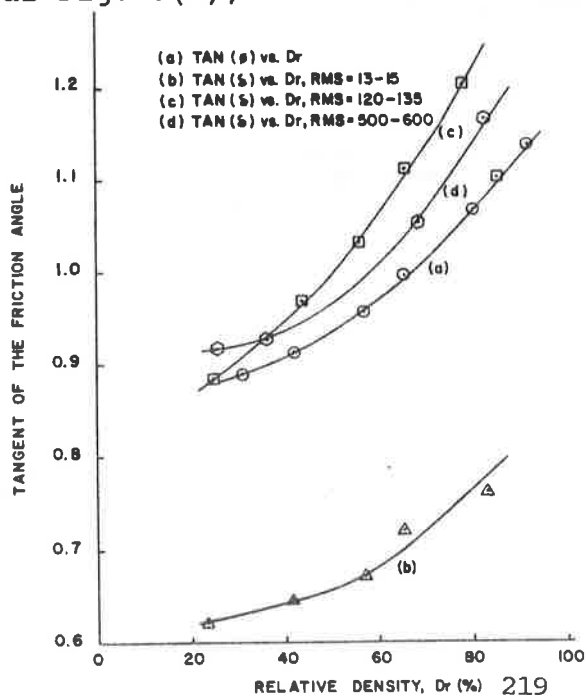


FIG. 3 VARIATION OF TAN(ϕ) AND TAN(δ) WITH Dr.

In Fig. 4 is shown the relationship between the relative density, RMS, and efficiency. Martin et al (6) defined efficiency, E, as

$$E = \frac{\text{TAN}(\delta)}{\text{TAN}(\phi)} \quad (4)$$

The untexturized GEOWEB material has efficiency values ranging from 0.6 to 0.7 for relative densities ranging from 55% to 85%. Whereas, the medium and coarsely texturized GEOWEB materials have efficiencies ranging from 1.1 to 1.2 and 1.05 to 1.15, respectively, for the same range of relative densities. This substantiates that texturizing of the GEOWEB material has distinct benefits.

From the curves in Fig. 4 it would appear that for the range of relative densities, considered in the model plate loading tests, the maximum friction angle (for the sand used) would be for the medium texture. For these reasons the medium texture pattern was chosen to be used for the GEOWEBs for the model plate loading tests. The RMS values in the machine direction are quoted in all subsequent results since this is the direction most frequently cited. Further research is needed to develop a parameter relating depth of texturizing pattern to soil grain sizes.

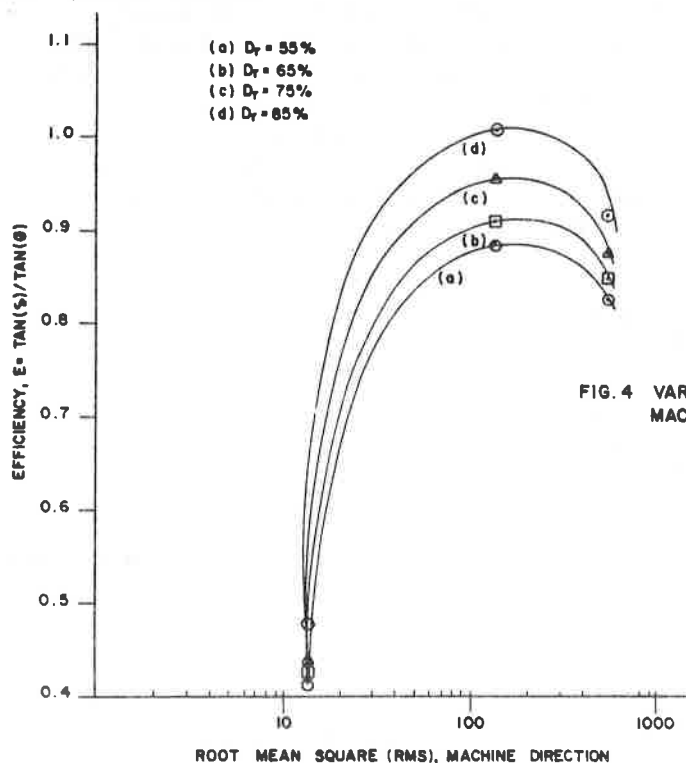


FIG. 4 VARIATION OF EFFICIENCY WITH ROOT MEAN SQUARE (RMS) MACHINE DIRECTION

MODEL PLATE LOADING TESTS

The material presented herein is the result of 73 model plate loading tests; 41 of which were performed with an untexturized GEOWEB material, and 32 of which were performed with the GEOWEB material having medium texturization.

LABORATORY MODEL

The tests were performed in a square stiffened wooden box, 48 in. (1.22m) wide and 36 in. (0.92m) deep. The soil used was the same as used in the fixed shear box tests- a narrowly graded sand (SP), see Table II for properties of the sand. Depending on the relative density, the sand was placed in 1 in. (2.54cm) to 3 in. (7.6cm) lifts. In all but 18 tests the relative density was 55%. Since the GEOWEB grid confinement system works very well with poor quality soils, the use of a 55% relative density for the sand dramatically demonstrated the benefits to be derived from the GEOWEB. Subsequent tests, where the relative density was varied, illustrated that the benefits to be gained at higher relative densities were very small, see Fig. 9.

The GEOWEBS used in the model plate loading tests did not have the dimensions indicated in Table I. The box used to perform the plate loading tests was too small to accomodate such large grids. A scaled-down version of the GEOWEB was used, retaining the cell width to cell depth ratio of 1.0 which had been found to be optimum by other investigators. Instead of the cell having a depth of 8 in. (20.3 cm) a depth of 2 in. (5.1 cm) was used. In addition, the size of the collapsed GEOWEB was such that when expanded it would yield the desired size to be tested in multiples of the width of the loading plate. It was felt that the particle size of the sand used and the scaled-down grid size would be compatible, producing minimal modeling effects on the results. The GEOWEB was stretched on a wooden frame, specially made for a specific width size of GEOWEB. This frame was subsequently removed when sand was placed inside the GEOWEB cells. Since the GEOWEBS used were 2 in. (5.1 cm) deep, enough sand was placed in the model, with the use of a mechanical drum dumper, to completely fill the cells and the annulus of space between the walls of the box and the GEOWEB reinforcement. Depending on the desired relative density, the sand could have required vibration.

The sand was loaded at its surface through a square plate with a 12 in. (30.5 cm) width. The loading plate consisted of 0.75 in. (1.9cm) exterior grade plywood stiffened by 2 - 0.3125 in. (8 mm) aluminum plates; one above and the other below the plywood. A static load was applied to the plate by a 25 ton (223 kN) capacity hydraulic cylinder and hand pump. The load applied in small increments, was recorded on a 10 ton (89 kN) capacity load ring, and the resulting displacements recorded by four dial gages placed at the four corners of the plate. These dial gages had a 2 in. (5.1 cm) capacity with a 0.001 in. (25 μ m) sensitivity. The GEOWEBS used were such that when expanded they were square in plan area and were placed concentrically under the square loading plate. No GEOWEB grid confinement system was used more than once to insure that no damaged reinforcement was used. The geometry of the test model is shown in Fig. 5.

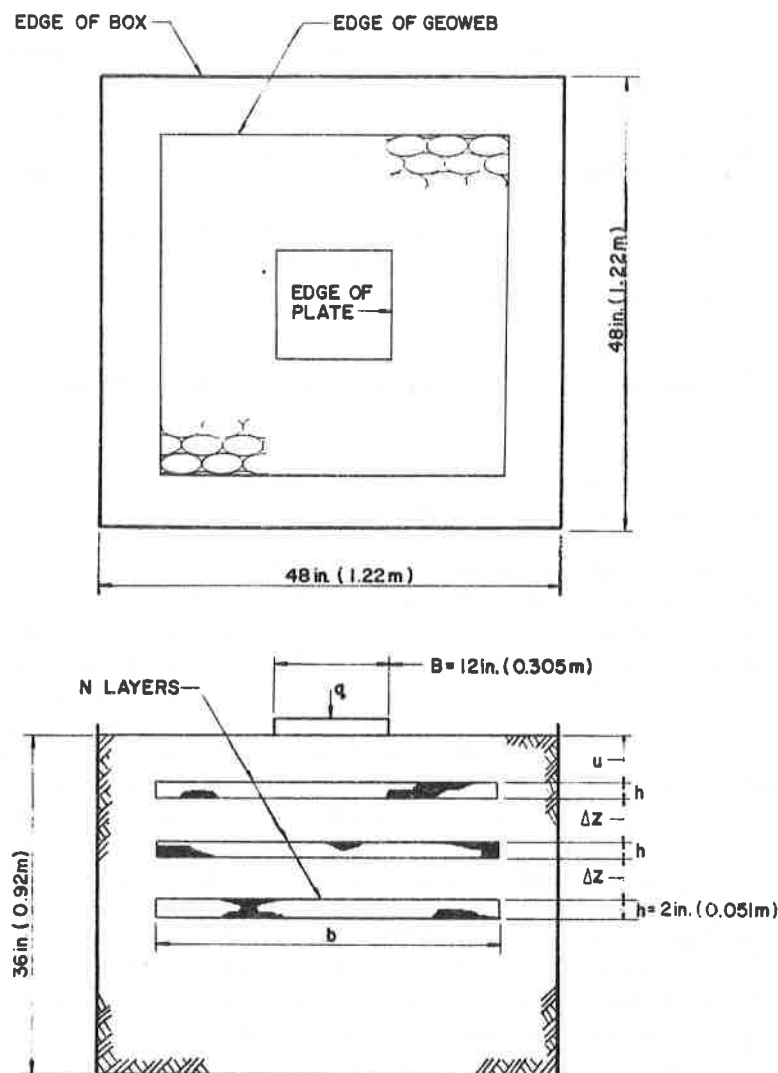


FIG. 5 GEOMETRY OF TEST MODEL.

TEST RESULTS

The effect of four parameters on the bearing capacity and settlement characteristics of either untexturized or texturized GEOWEB-reinforced earth slabs were investigated. They were:

- 1) Number of layers of GEOWEB-reinforcement, N .
- 2) Depth below the plate to the top of the first layer of GEOWEB-reinforcement, u , expressed in dimensionless form as u/B where B is the width of the plate.
- 3) Width size, b , of a square area of expanded GEOWEB-reinforcement expressed in dimensionless form as b/B , the width ratio.
- 4) Relative density of the sand, D_r .

For convenience in expressing and comparing test data, the bearing capacity ratio (BCR) and settlement reduction factor (SRF) will be used:

$$\text{BCR} = q_r/q_o \quad (5)$$

and

$$\text{SRF} = (s/B)_r / (s/B)_o \quad (6)$$

where q_o is the ultimate bearing pressure for the unreinforced sand at a specific settlement ratio, s/B and q_r is the bearing pressure of the GEOWEB-reinforced sand at a settlement ratio corresponding to the settlement ratio at the ultimate bearing pressure for the unreinforced sand. For the unreinforced case at a relative density of 55%, the load-settlement curve approached a vertical asymptote at a value of the settlement ratio, s/B of 0.07. Failure was defined at this value of s/B , since an increase in settlement was not accompanied by as large a percent increase in load. $(s/B)_o$ is the settlement ratio for the unreinforced sand corresponding to a specific ultimate bearing pressure, q and $(s/B)_r$ is the settlement ratio for the GEOWEB-reinforced sand at a bearing pressure corresponding to the ultimate bearing pressure of the unreinforced sand.

1. Number of Layers of GEOWEB-Reinforcement

Fig. 6 shows the variation of BCR and SRF with the number of layers of GEOWEB-reinforcement.

In Figs. 6(a) and (b) both the untexturized and medium texturized GEOWEBs show an increase in load bearing capacity with the number of layers of GEOWEB-reinforcement. The untexturized GEOWEB yields a substantial increase (25%) in the load bearing capacity with only one layer of GEOWEB-reinforcement approaching optimum values at approximately $N=4$. For the medium texturized GEOWEB, initially for one layer of GEOWEB-reinforcement, there is little difference between the BCR values for the untexturized and texturized GEOWEBs, however, as the number of GEOWEB-reinforcing layers increases, texturization yields substantial increases in the bearing capacity (140% at $N=4$ - an 84% increase over the untexturized GEOWEB). In addition, the BCR values for the medium texturized GEOWEB are not approaching an optimum at $N=4$, they are still increasing.

In Figs. 6(c) and (d) both the untexturized and medium texturized GEOWEBs show a decrease in the settlement with the number of layers of GEOWEB-reinforcement. In addition, both texturizations reach maximum settlement reductions at approximately $N=4$. The maximum settlement reduction is 45% for the untexturized GEOWEB and 74% for the medium texturized GEOWEB. There is an additional 29% decrease in the settlement due to the texturizing.

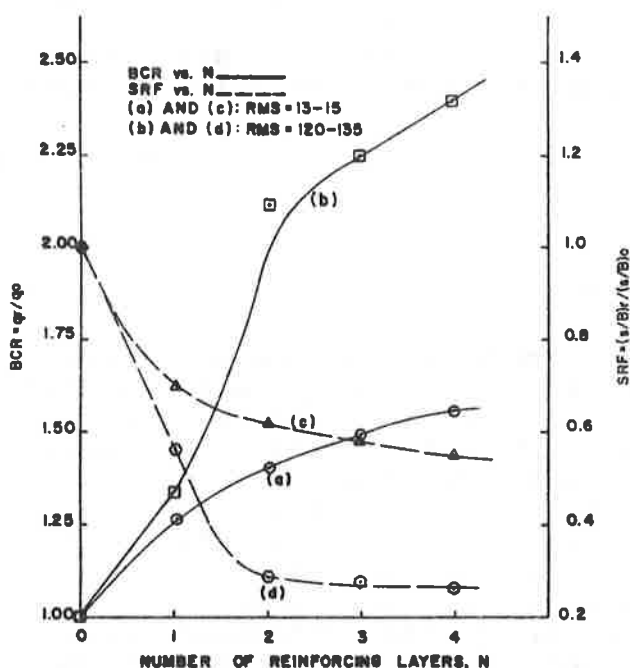


FIG. 6 VARIATION OF BCR AND SRF WITH THE NUMBER OF LAYERS, $u/B=0.50$, $z/B=0.25$, $b/B=2.0$ AND $D_r=55\%$

2.) Depth to the Top of the First Layer of GEOWEB-Reinforcement

In Fig. 7 is shown the variation of BCR and SRF with the depth to the top of the first layer of GEOWEB-reinforcement, u/B .

Figs. 7 (a) and (b) show that for both the untexturized and medium texturized GEOWEBs an increase in the load bearing capacity occurs as the depth to the top of the first layer of GEOWEB-reinforcement decreases. Similar results have been observed by Akinmusuru and Akinbolade (1), and Guido et al (4) and (5) for different reinforcing materials. For the untexturized GEOWEB, at a u/B value of approximately 1.0, the BCR indicates the GEOWEB reinforced soil is behaving essentially as if it were unreinforced; whereas for the medium texturized GEOWEB the same phenomenon occurs at a slightly deeper depth (u/B of 1.25). At the shallowest depth tested ($u/B=0.25$), the texturized GEOWEB produced an 89% increase in the load bearing capacity over the unreinforced capacity, while the untexturized GEOWEB only produced a 57% increase in the load bearing capacity. At all values of u/B the texturized GEOWEB performed better than the untexturized GEOWEB.

From Figs. 7(c) and (d) it can be seen that as the depth to the top of the first layer of GEOWEB-reinforcement decreases the settlement decreases. This trend is applicable to both the untexturized and medium texturized GEOWEB, however, the settlement reduction is more for the medium texturized GEOWEB. At a u/B value of 0.25, the settlement reduces 46% for the untexturized GEOWEB from that of the unreinforced earth slab, whereas, the settlement reduction is 75% for the medium texturized GEOWEB an additional 29% due to texturization.

Therefore, when u/B is sufficiently large the GEOWEB-reinforcement does not interfere with the formation of the failure planes and a shear failure of the sand occurs above the top of the uppermost layer of GEOWEB-reinforcement. The GEOWEB-reinforcement acts as a rigid boundary preventing the shear zone to penetrate it. This is one of the three failure modes of reinforced earth slabs described by Binquet and Lee (2).

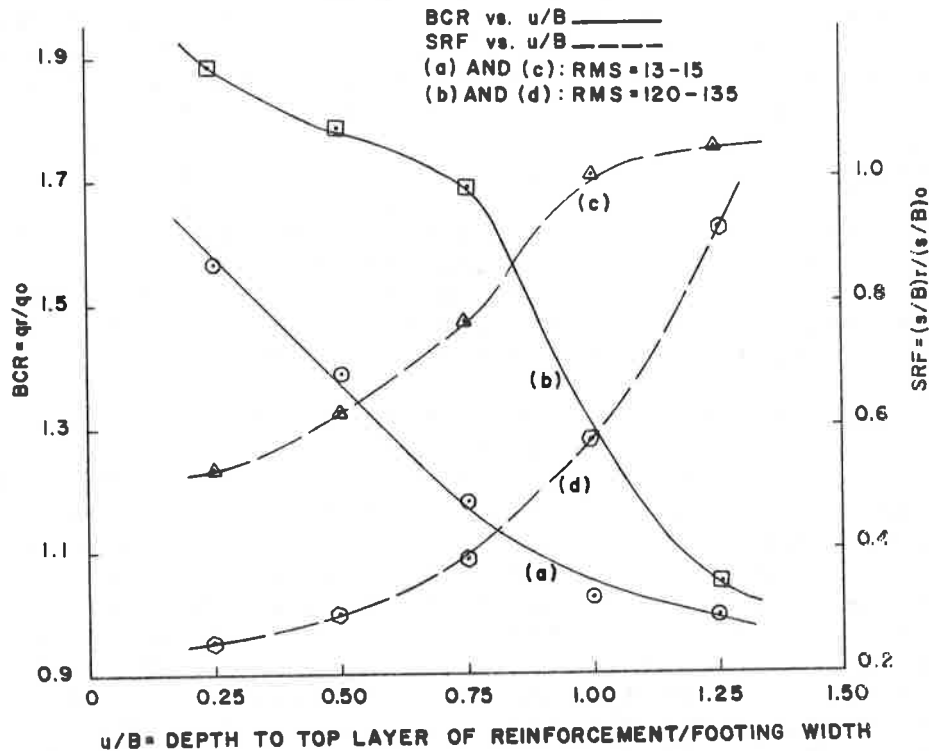


FIG. 7 VARIATION OF BCR AND SRF WITH DEPTH TO TOP LAYER
 $\Delta Z/B = 0.25$, $N = 2$, $b/B = 2.0$ AND $D_r = 55\%$.

3.) Width Size of a Square Area of Expanded GEOWEB-Reinforcement

Fig. 8 shows the variation of BCR and SRF with the width size of a square area of expanded GEOWEB-reinforcement, b/B .

From Figs. 8(a) and (b) it can be seen for both the untexturized and medium texturized GEOWEB that as b/B increases, the load bearing capacity also increases. Similar results have been observed by Fragaszy and Lawton (3), and Guido et al (4) and (5) for different reinforcing materials. This increase is more modest for the untexturized GEOWEB, reaching a maximum value of 50% at approximately b/B of 2.0. This indicates that to have an expanded GEOWEB of square area with a width larger than 2.0 times the width of the footing would be ineffective. The grid confinement system functions with the grid cells sustaining the imposed load. As the

untexturized GEOWEB-reinforcement falls farther and farther outside the stress boundaries developed within the earth slab, the cells outside the stress boundaries sustain less and less of the load, with the majority of the load being carried by the cells within the stress boundaries.

The increase in load bearing capacity of the medium texturized GEOWEB is substantially greater than either that of the unreinforced earth slab or the untexturized GEOWEB-reinforced earth slab. At b/B of 3.0 the BCR is continuing to increase and the increase in load bearing capacity is 188% more than the unreinforced earth slab and 132% more than the untexturized GEOWEB-reinforced earth slab. Because of the increased friction angle, between the cell wall material and infill material, of the medium texturized GEOWEB over the untexturized GEOWEB, the load can be distributed better between adjacent cells. Therefore, the cells outside the stress boundaries sustain more of the load when the frictional resistance of the cell wall material is increased, and the optimum width of a square area of expanded GEOWEB material increases.

Figs. 8(c) and (d) show that the settlement decreases as b/B increases, for both the untexturized and medium texturized GEOWEBs. For the untexturized GEOWEB an optimum reduction in the settlement occurs at approximately b/B of 2.5, whereas, the settlement reduction is continuing to increase at b/B of 3.0 for the medium texturized GEOWEB. The settlement reduction is larger for the texturized GEOWEB than the untexturized GEOWEB for all values of b/B considered. At b/B of 3.0 the reduction in settlement for the untexturized GEOWEB-reinforced earth slab is 46% less than that of the unreinforced earth slab, while the settlement reduction for the medium texturized GEOWEB-reinforced earth slab is 88% - an additional reduction of 42%.

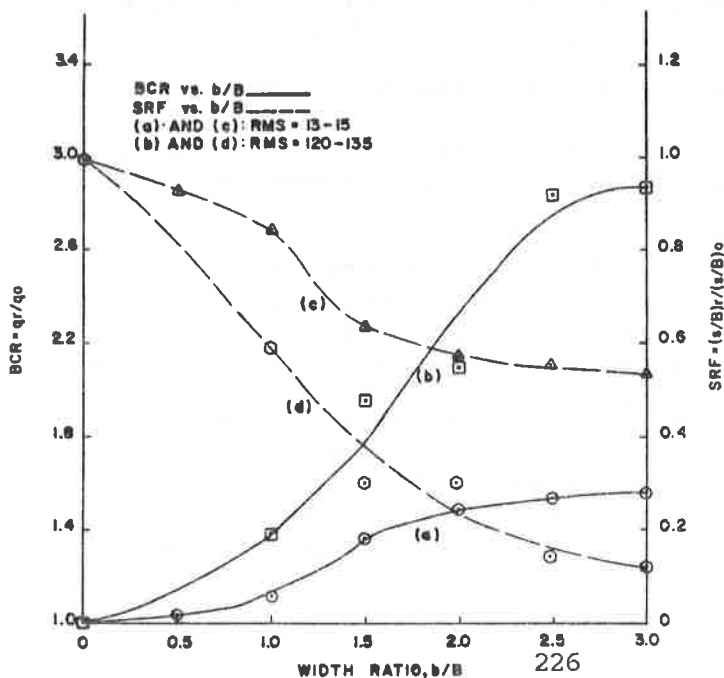


FIG. 8 VARIATION OF BCR AND SRF WITH WIDTH RATIO, $U/B = 0.5$, $\Delta Z/B = 0.25$, $N = 3$ AND $D_r = 55\%$.

4.) Relative Density of the Sand

Fig. 9 shows the variation of BCR and SRF with the relative density of the sand.

Figs. 9(a) and (b) indicate that as the relative density increases the increase in the load bearing capacity of the GEOWEB-reinforced earth slab over that of the unreinforced earth slab diminishes. This is true for both the untexturized and medium texturized GEOWEBs. Up to a relative density of 80% the medium texturized GEOWEB yields larger load bearing capacities than the untexturized GEOWEB, after which the untexturized GEOWEB yields slightly higher values of approximately 5%. It is evident that as the relative density increases the percent gain in the load bearing capacity is substantially greater for the unreinforced sand than for either the untexturized or medium texturized GEOWEB-reinforced sand. The untexturized and medium texturized GEOWEB-reinforced sand at a relative density of 55% show an increase in the load bearing capacity of approximately 80% and 108%, respectively, from that of the unreinforced sand, whereas, at a relative density of 85% the untexturized and medium texturized GEOWEB-reinforced sand show an increase of approximately 5% and 0%, respectively, from that of the unreinforced sand. This indicates that for poorer quality soils tremendous benefits can be had from the inclusion of untexturized or texturized GEOWEB-reinforcement, whereas, for better quality soils the benefits may only be marginal. At lower relative densities the GEOWEB grid confinement system helped the earth slab to be more rigid than the unreinforced case, therefore, preventing lateral and outward displacement of the sand. This in turn leads to higher load bearing capacity for the GEOWEB-reinforced earth slab versus the unreinforced earth slab. For higher relative densities the GEOWEB grid confinement system did not rigidify the earth slab substantially more than the already rigid unreinforced case, therefore, yielding essentially the same load bearing capacities for the reinforced and unreinforced cases.

From Figs. 9(c) and (d) it can be seen that as the relative density increases the percent decrease in settlement of the GEOWEB-reinforced earth slab versus that of the unreinforced earth slab diminishes. This is true for both the untexturized and medium texturized GEOWEBs, with the medium texturized GEOWEB yielding larger settlement reductions than the untexturized GEOWEB up to a relative density of approximately 80% after which the untexturized GEOWEB has slightly smaller settlements of approximately 5%. The untexturized and medium texturized GEOWEB-reinforced sand at a relative density of 55% show a decrease in the settlement of approximately 53% and 70%, respectively, from that of the unreinforced sand, whereas, at a relative density of 85% the untexturized and medium texturized GEOWEB-reinforced sand show a decrease in the settlement of approximately 5% and 0%, respectively, from that of the unreinforced sand.

CONCLUSIONS

The test results have shown that the insertion of GEOWEB-reinforcement into an earth slab can substantially increase its load bearing capacity and decrease its settlement from those of an unreinforced earth slab. Albeit the plate loading tests were performed on a sand subgrade, 80% of them were on a loose to medium density sand ($D_r = 55\%$) indicating similar trends should be expected for silty and clay-type soils (although extensive testing with these soils must be conducted before more definitive statements regarding them can be made). An extrapolation of the results presented herein, which are for a sand fill over a sand subgrade, is not warranted at this time to a sand fill over a clay subgrade until a more indepth study of the results is made.

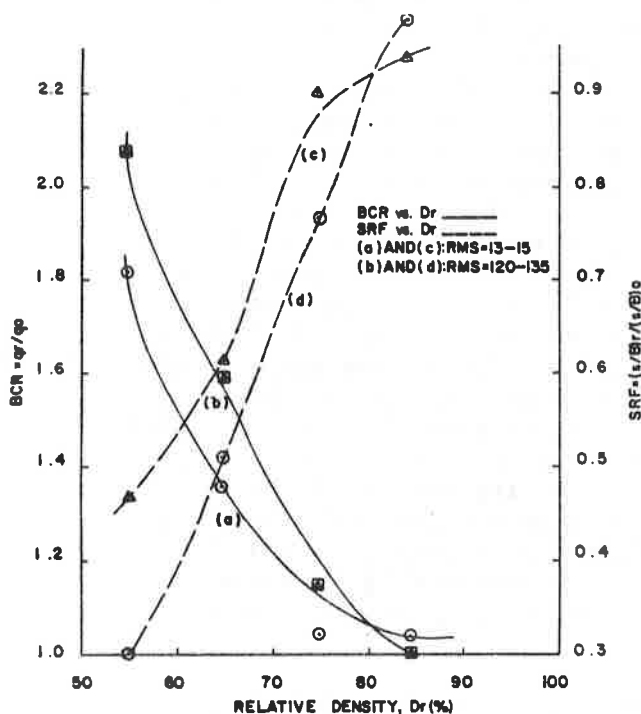


FIG. 9 VARIATION OF BCR AND SRF WITH RELATIVE DENSITY, $u/B=0.25, \Delta Z/B=0.25, N=3$ AND $b/B=2$.

By using a texturizing pattern on the surface of the GEOWEB cell material the benefits can be doubled or tripled. The test results presented for the untexturized GEOWEB grid (cell) confinement system illustrate the benefits derived from using the GEOWEBs was mainly due to lateral confinement of the soil, whereas, the increased benefits due to texturizing of the GEOWEB material are due mainly to the increased frictional resistance between the texturized cell wall material and the infill material.

Two practical applications of GEOWEB-reinforcement are below shallow foundations and in pavement bases and/or sub-bases. For both situations if the in-situ soil is of inferior quality and suitable good quality backfill material is either not available or economically not viable, the use of GEOWEB-reinforcement with the in-situ soil will yield a satisfactory

solution. The soil can be placed in the cells at low relative density yielding large increases in the load bearing capacity and large decreases in the settlement. Even the presence of a texturized GEOWEB at high relative densities will not yield substantial benefits to the reinforced soil. One for one, the presence of GEOWEB below a footing provides little improvement when compared with the situation where the same amount of well-compacted backfill is placed with no GEOWEB. The advantage of using GEOWEB (especially one which is texturized) below the footing occurs when an inferior grade backfill material is to be used (such as poor quality in-situ soil) instead of quality backfill material and comparable improvements are obtained at much reduced construction costs. When GEOWEBs are placed in a pavement base and/or sub-base the thickness of that layer will be reduced, with the texturized GEOWEB layer of a lesser thickness than an untexturized GEOWEB layer.

For practical reasons, such as footing pit excavations, it may not be feasible to use a GEOWEB which expands to a square area of a very large width. In addition, it may not be feasible to use a large number of GEOWEB layers because of the limitations on the depth of excavation. Therefore, to attain the same increase in the load bearing capacity and decrease in settlement that a large number of layers and a large width of untexturized GEOWEB would yield, a lesser number of layers and a smaller width of a texturized GEOWEB can be used.

As was indicated above, at the present time a texturized GEOWEB grid (cell) confinement system is not manufactured, only an untexturized system is available. From the results of the research performed by the authors and presented herein it is evident that texturizing of the GEOWEB material as it is extruded is extremely beneficial. The embossing process should not substantially effect the cost of a texturized versus untexturized GEOWEB. Additional research is required to determine the best embossing patterns to be used with different ranges of grain sizes. At the present time research is being conducted on the effect of different texturizations on the adhesion of clay-type soils.

REFERENCES

- (1) Akinmusuru, J.O. and Akinbolade, J. A., "Stability of Loaded Footings on Reinforced Soil", ASCE Journal of Geotechnical Engineering, 1981, 107 (GT6) p.p. 819-827.
- (2) Binquet, J. and Lee K.L., "Bearing Capacity Analysis of Reinforced Earth Slabs", ASCE Journal of Geotechnical Engineering, 1975, 101 (GT12) p.p. 1257-1276.
- (3) Fragaszy, R. J. and Lawton, E., "Bearing Capacity of Reinforced Sand Subgrades", ASCE Journal of Geotechnical Engineering, 1984, 110 (GT10), p.p. 1500-1507.
- (4) Guido, V.A., Biesiadecki, G. L. and Sullivan, M.J., "Bearing Capacity of Geotextile Reinforced Foundations", Proceedings of Eleventh International Conference on Soil Mechanics and Foundation Engineering, San Francisco, 1985, Vol.

**Geosynthetics '89 Conference
San Diego, USA**

3, p.p. 1777- 1780.

(5) Guido, V. A., Knueppel, J. D. and Sweeney M.A. "Plate Loading Tests on Geogrid-Reinforced Earth Slabs", Proceedings of the Geosynthetics '87 Conference, New Orleans, 1987, Vol. 1, p.p. 216-225.

(6) Martin, J.P., Koerner, R.M. and Whitty, J. E., "Experimental Friction Evaluation of Slippage Between Geomembranes, Geotextiles and Soils", Proceedings of the International Conference on Geomembranes, Denver, 1984, Vol. 1, pp. 191-196.

C.J. PORAN

University of North Carolina, Charlotte, U.S.A.

L.R. HERRMANN

K.M. ROMSTAD

University of California at Davis, U.S.A.

Finite Element Analysis of Footings on Geogrid-Reinforced Soil

ABSTRACT

It is common practice to construct footings on a layer of granular soil placed over soft subgrade. With the advent of geosynthetics in recent years new techniques for improvement of such footings have been introduced. Among these methods, the inclusion of one or several geogrid layers with high tensile modulus and strength to reinforce the granular base have been very effective in increasing load bearing capacity and reducing settlements. However, the existing simplified methods for calculating bearing capacity of such footings are approximate and it is almost impossible to estimate footing settlement. In many cases footing settlement is the governing design criteria, and therefore granular layer thickness and footing size should be determined based on allowable settlement, especially with geogrid reinforcement. This paper presents an alternative design procedure based on finite element analysis which includes a visco-plastic model for soils and special visco-elastic membrane elements to model geogrid behavior. The proposed design procedure for continuous and axisymmetrical footing may be especially beneficial in cases where small settlements are allowed.

INTRODUCTION

In recent years much attention has been devoted to polymer geosynthetics applications for the reinforcement of granular fill overlaying soft clay subgrade. Such systems are presently used to construct unpaved roads, and areas which may support heavy loads such as industrial equipment and oil drilling platforms. Generally, for the design of such systems, the required thickness of the granular fill is determined based on the footing size or the loaded area. The fill is designed sufficiently thick to provide an operating surface on which footing loads may be carried without causing excessive subgrade settlements and failure.

Most analytical procedures for unreinforced systems assume some form of stress distribution within the granular fill. Usually, failure is

defined when the reduced stresses at the soft clay interface equals the bearing capacity of the clay which is based on limit state classical solutions with certain modifications. These modifications account for factors such as: difference in stiffness between the granular fill and the soft clay (Hanna and Meyerhof, 1980); loss of confinement at the interface due to the lateral deformations of the granular fill which reduces the bearing capacity as described by Bender et al. (1978), Giroud et al. (1981, 1984), Poran (1985) and others; and, the shear stresses at the clay interface which increase lateral deformation and reduce the bearing capacity (Love et al., 1987).

To improve such systems, a layer of geosynthetic fabric or geogrid is placed at the base of the granular fill. The geosynthetic improves the bearing capacity and reduces footing settlement due to the reinforcing effect, and provides separation between the selected granular fill and the soft subgrade soil. This practice offers cost savings by reducing the required thickness of the granular fill with respect to a comparable unreinforced system. However, as most researchers acknowledge, the mechanism of such system is complex. Many investigators including Bender et al. (1978), Giroud et al. (1981, 1984), and Poran (1985) suggested simplified design procedures. Some of these earlier procedures are based on simplified deformation mechanism where geotextiles, with relatively low tensile stiffness, are significantly deformed, and the load carrying improvement is attributed primarily to the membrane effect as shown in Figure 1.

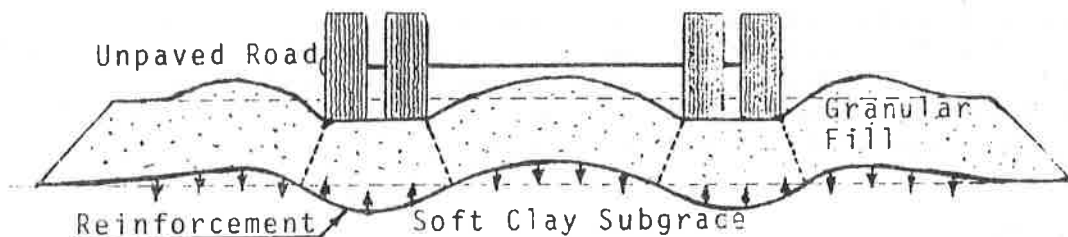


Figure 1. Membrane Effect with Geotextile.
After Love et al. (1987)

These methods have been adequate for design of unpaved roads with low traffic volume where large ruttings may be acceptable. Later methods, most of which are empirical, have provided satisfactory results for certain soil and reinforcement properties as described by Poran (1985). Love et al. (1987) suggested a more comprehensive model based on principles of plasticity where the failure mechanism also addresses the effect of the shear stresses at the clay-granular fill interface.

Generally, only limited deformations are acceptable for many footings and loaded areas. Therefore, at present, stiffer geosynthetics are used for these systems and the deformations are significantly reduced

due to the added reinforcing effect. For these systems with limited deformations, the membrane effect becomes insignificant.

As previously indicated, geotextile reinforcement of such system also provides separation between the soft subgrade and the granular fill. The improvement of system performance due to separation is of particular importance in unpaved roads and other traveled areas with many loading cycles. Stiff reinforcement geogrids, which are commonly used at present, form an interlock with the granular soil which also provide some degree of separation. Most investigators acknowledge that it is difficult to quantify the benefit of separation. The subjects of unpaved roads applications and separation effects are not included in this paper.

The paper presents an alternative design procedure for footings and loaded areas, based on finite element analysis. The procedure is especially beneficial for working stress analysis when the allowable settlements are small relatively to the footing width.

The finite element code and material models used for the analysis are discussed as follows.

THE FINITE ELEMENT MODEL

An analytical model of the behavior of geogrid reinforced was developed by Herrmann et al. (1983). It was used by Poran (1985) and Poran et al. (1986) to model the behavior of such systems and has shown good correlation between the analytical results and experimental observations. This paper includes the results of a parametric study conducted by Poran (1985) using the original model for plane strain analysis of spread footings on granular fill overlaying soft clay subgrade with and without geogrid reinforcement. Several recent modifications of the model are also discussed.

In general there are two fundamental approaches to the finite element analysis of reinforced soil systems; discrete and composite. In a discrete analysis the detailed geometry of each and every component of the heterogeneous system is modeled by an assemblage of appropriate kinds of finite elements; nonlinear-inelastic continuum elements to represent the soil and membrane or bending elements to represent the reinforcement. In addition a special bond element is needed to link the reinforcement to the soil in order to model possible slippage of the reinforcement relative to the soil. In a composite analysis the reinforcing members and the matrix soil are in sense viewed as distributed uniformly and simultaneously over the body so that the reinforced mass can be modeled as an equivalent orthotropic homogeneous continuum. The orthotropic properties of the equivalent continuum are selected so as to capture the composite nature of the reinforced system.

For any given reinforced soil configuration the choice between a discrete and composite analysis is for the most part dictated by the

number of reinforcing members present. When the number is small a discrete analysis is feasible and usually desirable. However, when the number is large, such as in the case of geogrid reinforcement discussed in this paper, a composite analysis is usually preferable because a discrete analysis may not be feasible from computational cost standpoint.

The finite element model code SAC-2 developed by Herrmann et al. (1983) was modified to account for the special characteristics of the analysis of footings placed on a reinforced granular base overlaying soft clay. A semi-discrete model was used for this study and is discussed as follows.

Model for Clay and Granular Fill

The elastoplastic "bounding surface" formulation by Dafalias et al. (1982) was implemented in the SAC-2 finite element code. In this finite element model numerical analysis concepts are used to express the rate-dependent processes governing the consolidation phenomenon and the inelastic stress strain behavior for soils in incremental form.

The comprehensive finite element analysis is based upon a variational statement of these incremental equations. The clay model is almost identical to the model used for the granular fill. The only difference is that the sand model uses a single ellipsoidal bounding surface, whereas the clay uses a surface formed by two different ellipses with a hyperbolic curve in between. This finite element model is able to include consolidation and loading rate effects (including cyclic loading) as necessary. Recent modifications of the code by Herrmann et al. (1985 and 1987) include an addition of viscoplasticity terms to the "bounding surface" formulation and improved numerical technique to enable faster convergence and larger stress increment during the analysis.

The Geogrid Model

In order to include the effects of the geogrid reinforcement a "composite" layer model was adopted and involved the "overlay" of two sets of elements. The layer of "mesh elements" at the grid level has the same properties as the surrounding granular soil, and is overlaid by a special beam-membrane type four node element with large deformation capabilities. The "composite layer" provides both the flexural stiffness of the reinforcement including large displacement effects to capture the possible local membrane effects, and the unique "platform-like" behavior of the granular soil compacted into the openings of the reinforcing grid. This model was used by Poran (1985) for plane strain analysis and the results correlated well with model tests.

At present a new geogrid model is used for this type of analysis, as indicated by Poran et al. (1986). This new model was incorporated into the SAC-2 code and used for two-dimensional (2-D) analysis. It differs from the original beam-membrane model in that the geogrid is

modeled using two node membrane elements which include the effects of large deformations. However, the results of a parametric study reported in this paper are based on the original model. Obviously, any number of geogrid layers placed within the granular fill may be incorporated into the finite element model.

Computer Codes

Three computer codes are usually incorporated in a typical analysis, as follows:

- **EVALS:** Material model calibration code developed by Herrmann et al. (1983) and Kaliakin (1985) which is used to evaluate the properties of the granular fill and the subgrade soils. The code is used to evaluate the effects of certain parameters of the "bounding surface" soil model on the shear strength and stress-strain relationship of the soils by comparing predicted results to results of triaxial tests performed on the actual soils, or to obtain desired shear strength values for other typical soils such as those used in the parametric study discussed in this paper.

- **SAC-2:** A comprehensive 2-D finite element code modified to incorporate the reinforced soil model discussed previously is used for the analysis of both reinforced and unreinforced systems. This FORTRAN code is relatively large and most analyses reported in the literature were conducted on a DEC VAX-11/780 computers with the VMS operating system. However, a smaller version of the program is currently being implemented on an upgraded personal computer system.

- **POST:** An interactive post processor developed especially for plotting the results of this type of analysis as reported by Poran (1985). This FORTRAN code is designed for the DEC VAX-11/780 computer with the VMS operating system and linked with the DI-3000 plot package. It is capable of plotting deformed shapes of the mesh, and stress and strain contours and arrows.

PARAMETRIC STUDY

Analytical results using this finite element model correlated well with test results (Poran, 1985) and an example parametric study was conducted. The goal of this parametric study was to establish the load-displacement behavior of strip footings (plane strain 2-D analysis) over a range of parameter values in order to develop design charts. The analysis was conducted both for immediate settlements, where the clay is in undrained condition, and for long term settlements which are time dependent due to the consolidation of the clay. However, due to space limitations, the results presented in this paper include only the immediate footing settlement. The parametric study is described in the following section.

Model Parameters

The model parameters used to characterize the different materials are described as follows:

- **Clay Subgrade:** The study was restricted to soft clays, thus the undrained shear strength of the clay was limited to what is considered as the lower range for in situ clay deposits. Undrained cohesion values used for the analysis were 7.7, 15.3 and 30.6 KPa. Based on these values the appropriate parameters were selected for the "bounding surface" model after calibration with the EVALS program.

- **Granular Fill:** Two types of granular fill materials were used in this parametric study; dense sand with an internal angle of friction $\phi = 47^\circ$; and loose sand with $\phi = 37^\circ$. The calibration process included correlating the selected "bounding surface" parameters to actual results of triaxial compression tests performed on well graded sandy soil typically used for such granular fills.

- **Reinforcing Geogrid:** The SS-1 polymer geogrid manufactured by the Tensar Corporation was used for the parametric study since it was also used by Poran et al. (1987) in his experimental work. Obviously, any other geogrid may be incorporated into the analysis using similar procedure. The Tensar SS-1 Geogrid has orthotropic force-deformation properties. For a plane strain analysis it is necessary to adopt a set of 2-D properties for the geogrid. Plate bearing test results (Poran, 1985) indicated only small discrepancies between the force-deformation profile and geogrid strains in the two orthotropic directions. Also, several 2-D finite element analyses were conducted using the different orthotropic properties for the longitudinal and transverse directions of the Tensar SS-1 geogrid and property values which were the average of the two directions. The load deformation results were essentially identical, and, therefore, an average set of properties was selected to characterize the geogrid for this 2-D analysis. As previously mentioned the properties of the beam-membrane element are linear elastic. Since the actual load deformation curves of the geogrid are nonlinear, the tensile modulus was evaluated at 2% tensile strains (Poran, 1985) which is the recommended working range for this grid (Tensar, 1984), and, as indicated by Poran et al. (1987), was the peak tensile strain recorded in his plate bearing tests.

In the current version of SAC-2 the geogrid is modeled as a linear viscoelastic membrane element with large deformation capabilities and in order to account for the nonlinear characteristics a trial and error analysis is performed to identify the prevailing stress level for a given loading condition.

Dimensions

Two values of base thickness (H) were selected for this example parametric study; 20 and 40 cm. Footing width (B) was varied for H/B ratios of 0.4 to 2 for the different analyses. Many researchers

concluded that for $(H/B) > 2$ bearing capacity failure may be controlled by the granular fill alone, and the geogrid reinforcement, when placed at the clay-granular fill interface, would have insignificant effect.

The finite element meshes for this study were selected following preliminary experimentation with several mesh sizes and number of elements. The mesh size was determined by Poran (1985) based on the principles of soil plasticity. A typical mesh is shown in Figure 2.

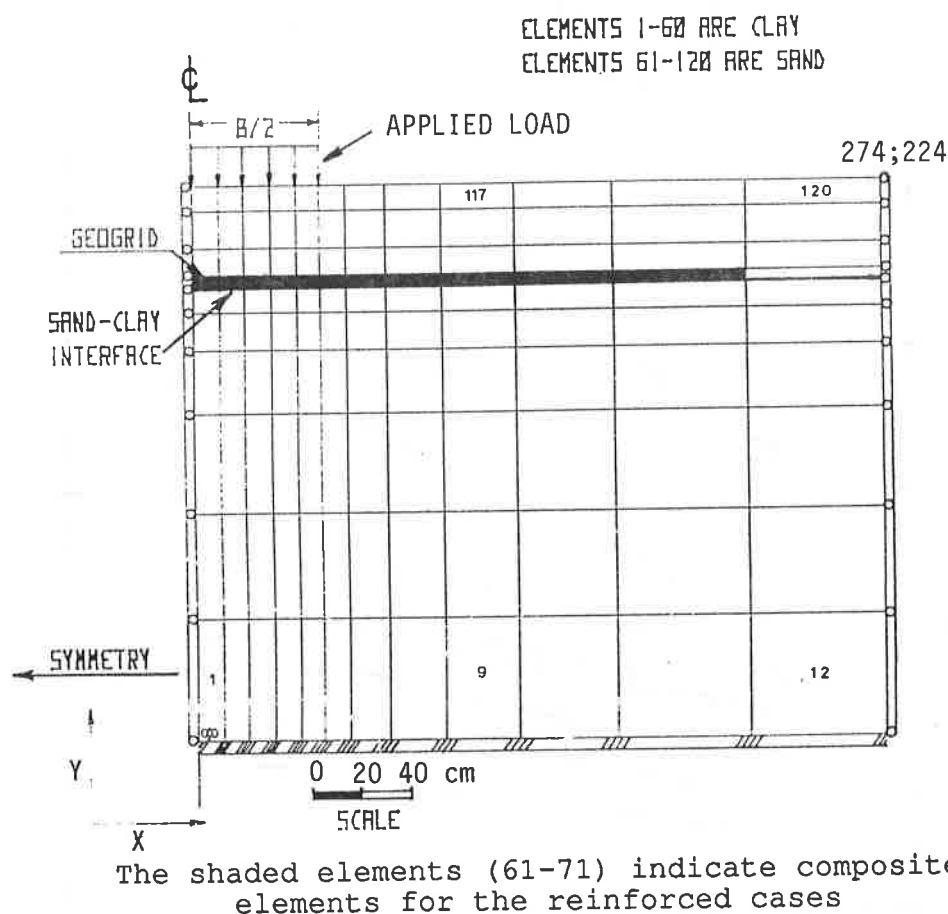


Figure 2. Finite Element Mesh for the 2-D Parametric Study

Results

The results from this parametric study were compiled and analyzed for immediate footing settlement (S) of 2.5 cm, i.e. undrained conditions for the clay, and plotted in charts shown in Figures 3 and 4. These charts may be applied to estimate footing size for a limited settlement of 2.5 cm for a system where footing load, soil properties, and thickness of granular fill are given, without and with Tensar SS-1 geogrid reinforcement.

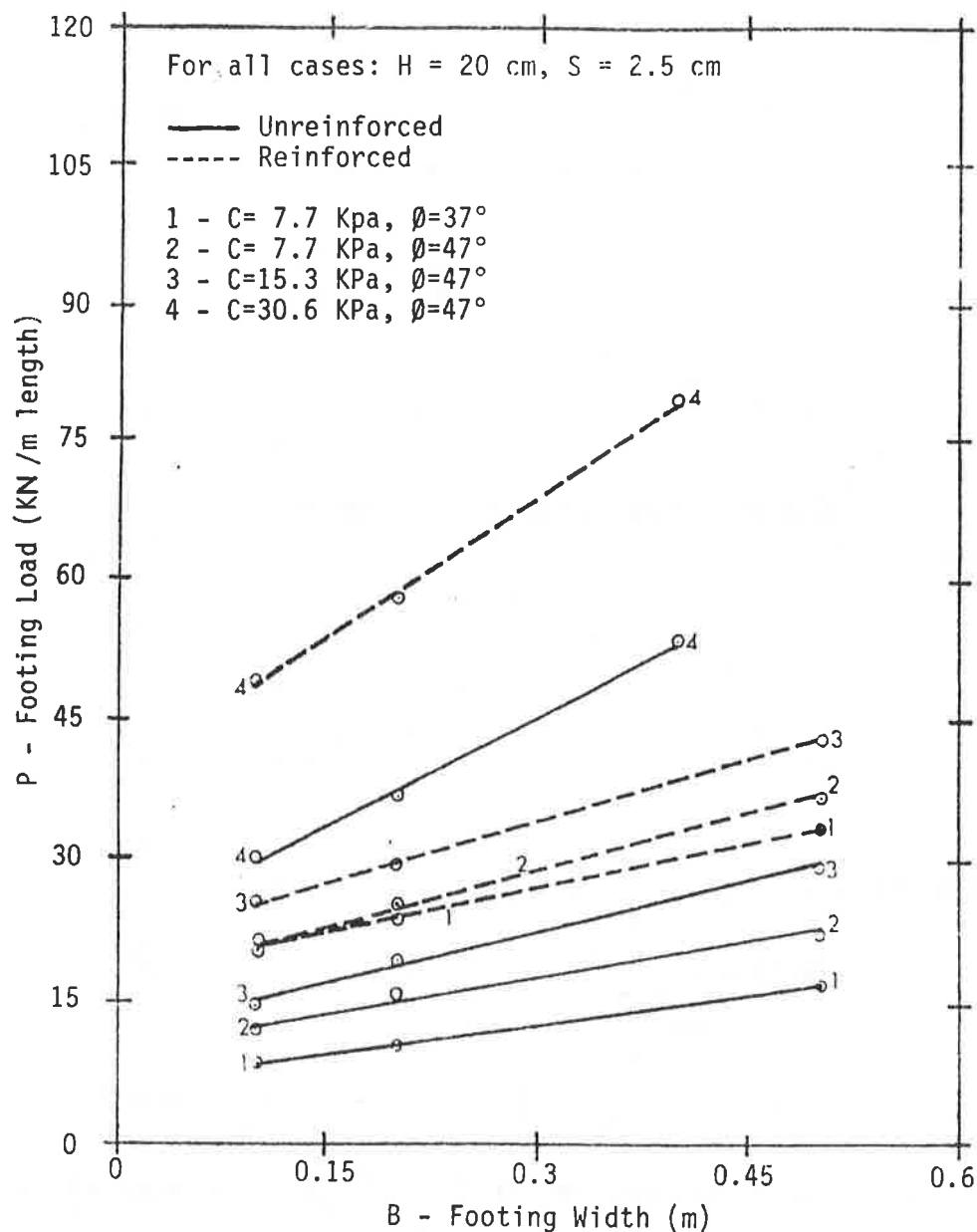


Figure 3. Footing Load Vs. Width for Strip Footing with $H=20 \text{ cm}$ and Immediate Footing Settlement of 2.5 cm .

As shown in Figure 3 (for $H=20 \text{ cm}$) a significant improvement of footing load capacity is achieved when the geogrid reinforcement is included. The improvement ranges between 50% to 100% for the stiffer and softer subgrades, respectively. However, as shown in Figure 4 (for $H=40 \text{ cm}$), the relative improvement in load capacity of the

reinforced systems is less significant. With the thicker base the geogrid reinforcement has a relatively small effect on the footing load at immediate settlement of 2.5 cm since the settlement occurs, primarily, at the top part of the base.

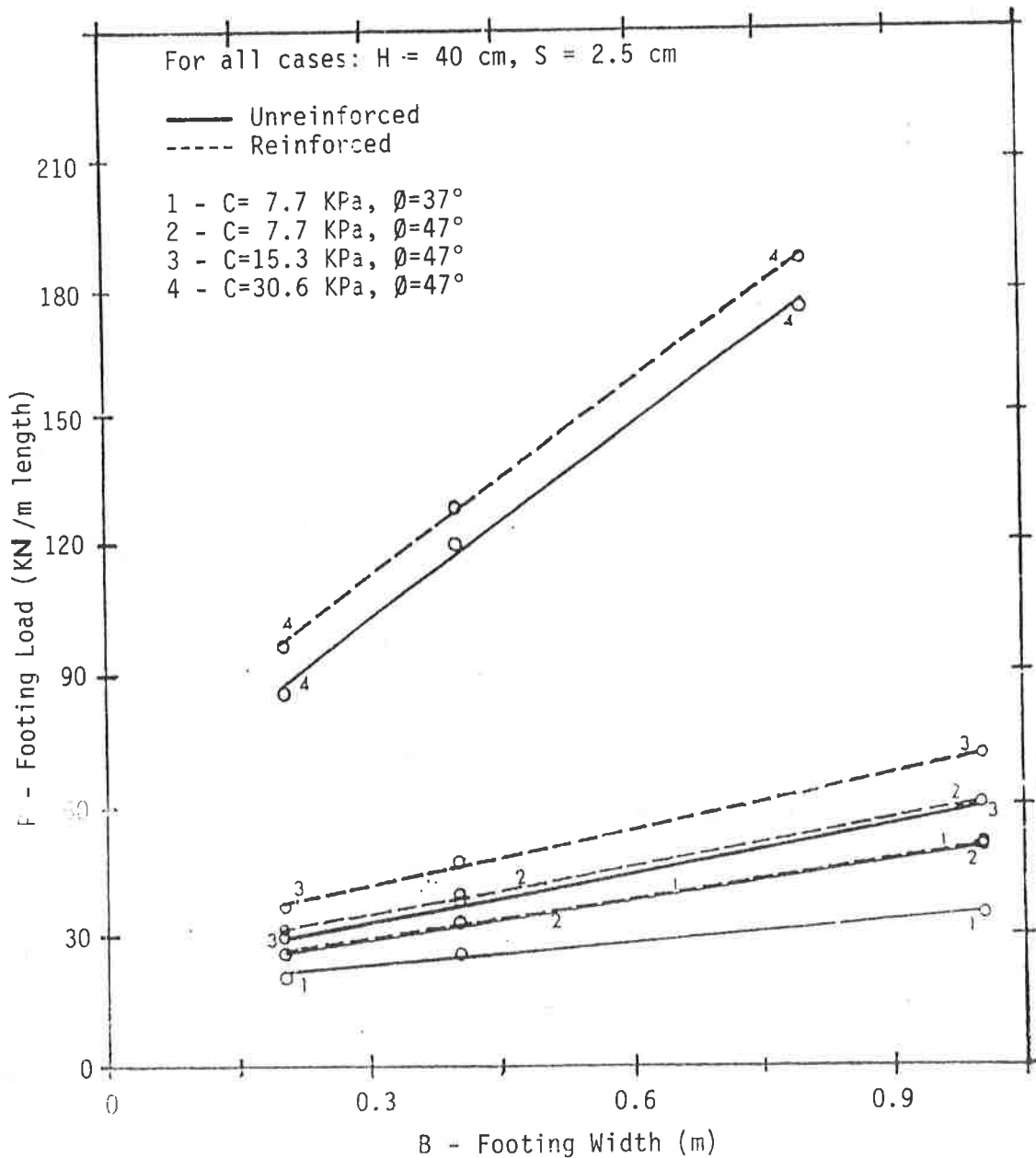


Figure 4. Footing Load Vs. Width for Strip Footing with $H=40$ cm and Immediate Footing Settlement of 2.5 cm.

The application of the SAC-2 code as demonstrated in this parametric study is the basis for the proposed design procedure for design of footing and loaded areas with limited allowable settlements as follows.

PROPOSED DESIGN PROCEDURE

A procedure is recommended for footing design using this finite element analysis according to the following steps:

I) **Design Load:** The design load should be determined with appropriate factors for live and dead loads.

II) **Granular Fill Thickness:** Based on available literature or experience the initial thickness of the granular fill should be estimated.

III) **Footing Width:** Initial footing width should be estimated based on bearing capacity using an appropriate simplified method such as proposed by Poran (1985). A safety factor may be applied as appropriate.

IV) **Material Properties:** Model parameters for the SAC-2 code should be determined for the soils and the geogrid. If no experimental data are available for the soils model parameters should be determined based on available correlations such as reported by Kaliakin (1985), Poran (1985), and Poran et al. (1986). When laboratory results, such as triaxial and consolidation tests, are available for the soils, the "bounding surface" parameters are calibrated using EVALS to match the test results. The geogrid parameters should be determined based on manufacturer specifications according to the methods previously discussed in this paper.

V) **Settlement Analysis:** Using SAC-2, with an appropriate mesh and loading rate, short and long term settlements are calculated with or without reinforcement, as needed.

VI) **Iterations:** If the footing settlement is in excess of the allowable settlement several options are available; return to step III and increase footing width; and/or, return to step II and increase thickness of granular fill. Obviously, if the settlements are much smaller than the allowable settlement the footing width and/or base thickness may be decreased. Two or three analyses should be sufficient to determine the required footing width and the corresponding thickness of the granular base layer. If appropriate it is also possible to check the effect of additional geogrid reinforcement layers within the granular fill by repeating step V for the different configurations.

VII) **Cost Analysis:** Finally, when cost data are available the feasibility of geogrid reinforcement may be decided based on the comparison.

Obviously, the proposed procedure requires a fair amount of pre and post processing for the finite element analysis which may be regarded as too complex and time consuming for applications where large settlements may be tolerated and bearing capacity may be the critical design factor. However, for large scale applications where allowable footing settlements are relatively small (such as a working pad for an oil rig) the proposed procedure may be very beneficial. Ultimately, this procedure may be available as a single compounded, interactive and user friendly code, suitable for the new generation of desk top personal computers.

CONCLUSIONS

The paper demonstrates the application of finite element analysis for the evaluation of settlement of footing placed on geogrid reinforced granular fill overlaying soft clay subgrade. The results from a parametric study indicate the effects of geogrid reinforcement for improvement of the load-deformation behavior of such system. Finally, a design procedure is proposed for cases where the allowable footing settlements are relatively small. In such cases it is impossible to estimate such settlements under working stress conditions using any of the available simplified design methods, therefore, the proposed method may be very beneficial.

ACKNOWLEDGMENT

This paper includes results from the study on "Analytical and experimental Modeling of Tensar Grids for Soil Improvement" conducted at the University of California at Davis. The authors express their appreciation to the Tensar Corporation for funding that study.

REFERENCES

Bender, A. and Barenberg, E.J. (1978) "Design and Behavior of Soil-Fabric-Aggregate Systems," Proc., TRB, Tran. Research Record 671, Washington, D.C., Jan. 18, pp. 64-75.

Dafalias, Y.F. and Herrmann, L.R. (1982) "Bounding Surface Formulation for Soil Plasticity," Chapter in Soil Mechanics - Transient and Cyclic Loads, John Wiley, eds., Zienkiewicz and Pande, New York, pp. 253-282.

Giroud, J.P., Ah-Line, C. and Bonaparte, R. (1984) "Design of Unpaved Roads and Trafficked Areas with Geogrids," Proc. Sym. on Polymer Grid Reinforcement in Civil Engineering, Paper No. 4.1, London, England, March.

Geosynthetics '89 Conference
San Diego, USA

Giroud, J.P. and Noiray, L. (1981) "Geotextile-Reinforced Unpaved Road Design," Geotechnical Division Journal, ASCE, Vol. 108, No. GT12, December, pp. 1654-1670.

Hanna, A.M. and Meyerhof, G.G., (1980) "Design Charts for Ultimate Bearing Capacity of Foundation on Sand Overlaying Soft Clay," Canadian Geotechnical Journal, Vol. 17, pp. 300-303.

Herrmann, L.R., and Kaliakin, V. (1987) "Revised User's Manual for Sac-2," a revised report for the Civil Engineering Laboratory, Naval Construction Battalion Center, Port Hueneme, CA, USN N62583/85MT176.

Herrmann, L.R., Kaliakin, V. and Shen, C.K. (1985) "Improved Numerical Implementation of the Bounding Surface Plasticity Model for Cohesive Soils," Final Report for the Civil Engineering Laboratory, Naval Construction Battalion Center, Port Hueneme, CA, USN N62583/85MT176.

Herrmann, L.R., and Mish, K.D. (1983) "Finite Element Analysis for Cohesive Soil, Stress, and Consolidation Problems Using Bounding Surface Plasticity Theory," Research Report for the Civil Engineering Laboratory, Naval Construction Battalion Center, Port Hueneme, California, USN N62583-83-M-T062, September.

Kaliakin, V.N. (1985) "Bounding Surface Elastoplasticity-Viscoplasticity for Clays," PhD Thesis, University of California, Davis, December.

Love, J.P., Burd, H.J., Milligan, G.W.E. and Houlsby, G.T. (1987) "Analytical and Model Studies of Reinforcement of a Layer of Granular Fill on a Soft Clay Subgrade," Can. Geotech. J., Vol. 24, pp 611-622.

Poran, C.J., Kaliakin, V., Herrmann, L.R., Romstad, K.M., Lee, D.-F. and Shen, C.K. (1986) "Prediction of Trial Embankment Behavior Hertfordshire County Councils - Stanstead Abbots," Proc. Intl. Sym. on Reinforced Embankment, King's College, London, September.

Poran, C.J. and Shen, C.K. (1987) "Plate Bearing Tests on Geogrid-Reinforced Granular-Base Overlaying Soft Clay," Proc. Intl. Sym. on Geotechnical Engineering of Soft Soils, Mexico City, August.

Poran, C.J. (1985) "Bearing Capacity of Geogrid-Reinforced Granular-Base Overlaying Soft Clay," PhD Thesis, University of California, Davis, December, 1985.

Tensar (1984) "Test Methods and Physical Properties of Tensar geogrids," Manual, Tensar Corp., Morrow, Georgia.

SESSION 7A
STEEP SLOPES



D. CHU

I. POORMAND

Leighton & Associates, Inc., U.S.A.

Reinforcement of an Earthen Buttress with a Polymer Geogrid

ABSTRACT

Geologic, environmental, and other constraints necessitated the design of a 1,500-foot long, up to 115-foot high earthen stabilization buttress fill at a steep slope ratio of 1h:1v (horizontal to vertical). Strength parameters of the prevailing soils were insufficient for attaining an adequate safety factor for the internal stability of the buttress. Analysis of lime treatment, welded steel mesh reinforcement, and use of Tensar geogrid resulted in selection of the latter for reinforcement of the buttress. Because of existing improvements that restricted the limits of excavation, a steep, 0.75h:1v back cut for this buttress was necessary. Approximately 180,000 cubic yards of soil was excavated, moisture-conditioned as necessary, and recompacted. Approximately 150,000 square yards of Tensar SR-3 polymer geogrid and 40,000 square yards of Tensar SS-1 geogrid were incorporated in this buttress at various designed spacings. An instrumentation program was adopted to study the performance of this geogrid-reinforced buttress. This consisted of strain gauges on both sides of the SR-3 geogrid at three different elevations within the buttress and installation of two vertical and one horizontal slope indicators. Sinco magnetic rings were installed along the slope indicators so that with Sinco's Sondex probe, relative settlements could be measured. Results of this instrumentation program are presented in this paper and are in general agreement with our design assumptions.

INTRODUCTION

The project site is located in a suburban hillside area north of San Diego, California. Mass grading was performed during 1980 and 1981 to create a series of relatively flat building pads for residential development. Improvements built after grading include paved street, installation of utilities, and some landscaping with associated irrigation system.

During 1981 grading, adverse geologic conditions were encountered in the steep natural slopes along the southerly boundary of the site. These included an ancient landslide, remolded clay seams along out-of-slope dipping beds, and a potentially active fault zone. Slope stability analysis indicated that the adverse geologic conditions affected the stability of the steep natural slope that supported the only access road to the subdivision and 21 rim lots adjacent to the road. A factor of safety of less than 1.5 was obtained from the slope stability analysis. Since city ordinance requires a minimum factor of safety of 1.5, issuance of building permits for the entire subdivision (168 lots) was denied until the slope was stabilized.

This paper presents the design and construction of a geogrid-reinforced soil buttress to increase the factor of safety of the slope to the required minimum value. Results of the instrumentation program to monitor the performance of the buttress are also included in this paper.

SITE DESCRIPTION AND GEOLOGY

The subject site is located above a prominent northwest-southeast trending hillside in La Jolla, California. The 21 rim lots generally consist of relatively level graded pads above relatively steep (0.75h:1v to 2h:1v) slopes descending from each pad to the south (see Figure 1). A very limited buildable area (generally not more than 40 feet in depth) is available for each lot. An erosional drainage channel exists at the toe of the natural slope. Site elevations range from approximately 180 to approximately 490 feet (above mean sea level).

The geology of the San Diego area is characterized by a thick sequence of relatively flat-lying sedimentary rocks, ranging in age from Cretaceous to late Quaternary, overlying Cretaceous and Jurassic formations. Localized tectonics in the Mount Soledad and southwest San Diego areas, and regional uplift or sea level lowering have caused stream erosion to create the deeply incised topography in the area. The Mount Soledad area consists of an uplifted block of complexly folded and faulted late Cretaceous and Eocene sedimentary rocks. Deformation and uplift of the area appear to have been the result of faulting within the Rose Canyon fault zone.

The subject site is underlain by strata of the late-Cretaceous Cabrillo Formation and Eocene Mount Soledad Conglomerate and Ardath Shale. These materials are overlain by colluvial material and compacted fill. The majority of the subject site is covered by Ardath Shale.

The Ardath Shale is composed of thinly bedded clayey siltstone. This formation is highly fractured and jointed with close to moderate spacing between fractures. The fractures are commonly infilled with gypsum and/or clay. At frequent intervals, remolded clays were observed along bedding planes. The clay seams are often sheared in appearance with multiple slickensides. These bedding-plane faults were most likely created during deformation (tilting, warping, and folding) of the Ardath Shale in the Mount Soledad area. These clay seams have a much lower shear strength than the relatively undisturbed siltstone above or below the seams, resulting in potential failure surfaces where adversely inclined bedding planes are present in natural or cut slopes.

Bedding inclinations measured during our subsurface investigation and those measured previously, indicate that the formational units beneath the majority of the lots dip moderately to the southeast (out of slope). Due to local faulting, the dip direction was reversed and was favorable for a short portion of the slope. An ancient landslide was mapped by the previous geotechnical consultant on six of the lots and was again identified by Leighton and Associates during the field investigation.

REMEDIAL DESIGN ALTERNATIVES

The following remedial design alternatives were considered:

1. Flattening the existing slope by removing the 21 rim lots at the top of the slope.
2. Construction of a gravity fill to abut against the existing slope.
3. Benching and excavating the existing slope, reconditioning the excavated soil and recompacting the soils back to match the existing topography.

In addition to the economic impact of loss of 21 lots, it was found that the stabilization effect of flattening the slopes (alternative 1) was insufficient to meet code requirements. Alternative 2 was found environmentally unacceptable since it proposed to fill in a canyon to be dedicated as open space. Alternative 3 was selected as a viable option.

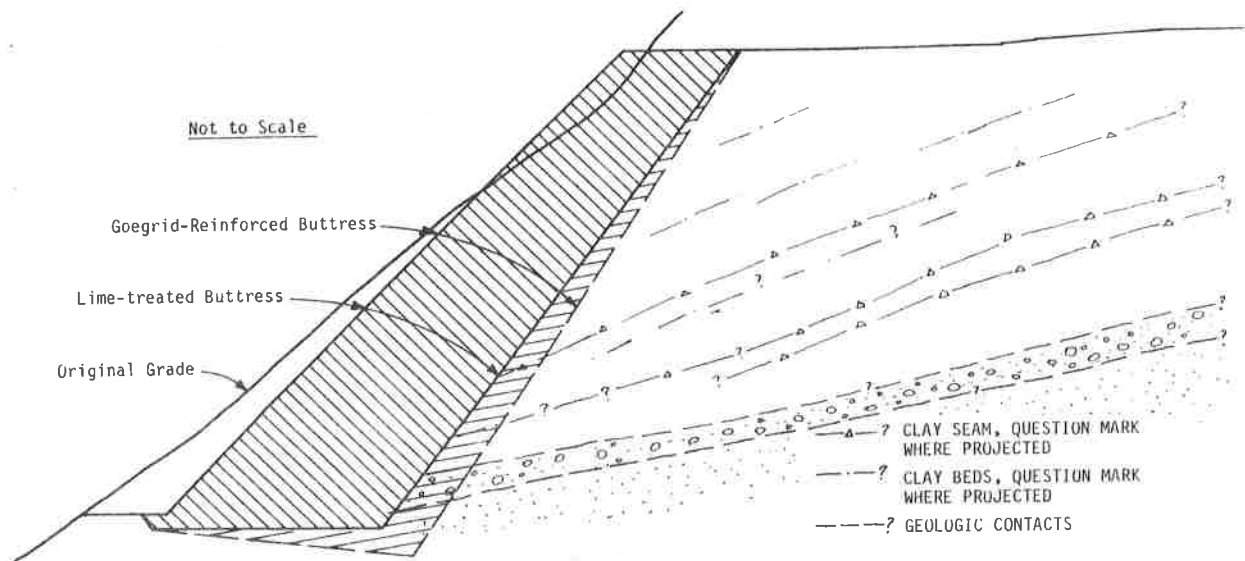


Figure 1 - Typical Profile of Buttrass

Figure 1 shows a representative profile view of the proposed buttress design. This buttress design is unique and challenging because of the height and steepness of the slope as well as the limited and narrow construction area. In order to satisfy both the external stability and the internal stability of the buttress, three designs including lime treatment of the on-site clayey soils derived from the Ardath Shale; reinforcing the fill soils with welded steel wire mesh; and reinforcing the fills with a geogrid were considered. The three design alternatives are described below.

● Lime-Treated Buttrass

Lime is one of the most common additives used in soil stabilization, particularly with clayey soils, to increase the soil strength and decrease water sensitivity and volume change during wet/dry cycles. Previous research indicates that lime reacts readily with most plastic soils containing montmorillonite clay or kaolinite clay with Plasticity Index from 10 to 50+. The only exception would be organic soils, containing more than 20 percent organic matter, which can inhibit reactions (3).

The mechanisms of lime stabilization include ion exchange and cementation. The amount of lime used (depending on soil type, stabilizer type, curing conditions, and other factors) is usually between 3 to 8 percent of the dry weight of soil. Because of dust control difficulties and other environmental hazard concerns, granular quicklime is commonly used in southern California. After extensive laboratory tests of pH value determination (ASTM C977-83) as well as the Atterberg limits test of lime-treated soils, it was determined that 4 percent of quicklime by dry weight of soils should be utilized for soil stabilization purposes.

Figure 2 shows laboratory direct shear test results of the lime-treated soil samples. These test samples have been treated with 4 percent of quicklime, initially cured overnight, processed, cured for periods of up to 28 days or more,

and then direct shear tested. As anticipated, test results indicated that the strength gain was quite sensitive to the duration of curing. Assuming a constant friction angle of 25 degrees, the increase in cohesion intercept was found to be 150, 250, and 650 percents for one, seven and 28 days of curing, respectively. With these strength improvements, a lime-stabilized buttress was designed and approved by the city subject to certain quality control measures such as dust control, frequent strength testing, and appropriate curing. It was recognized that vegetation of the buttress face would be difficult and that the curing requirement would slow down the construction progress.

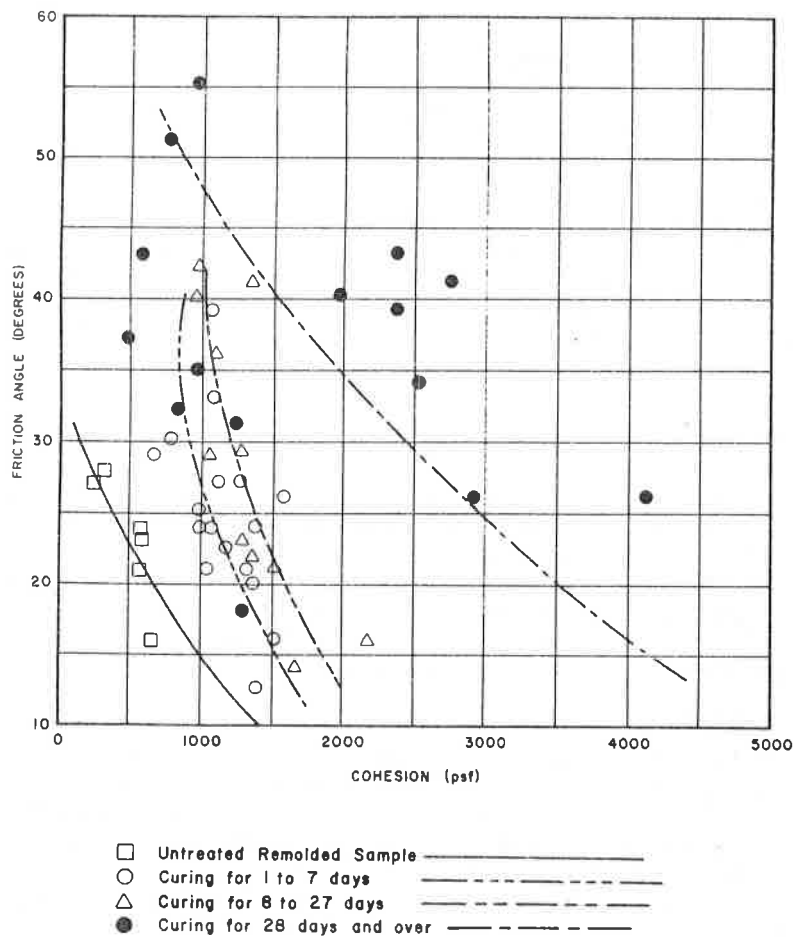


Figure 2 - Laboratory Direct Shear Test Results for 4% Quicklime Treatment of Soil Derived from Ardath Shale

● Buttress Fill, Reinforced with Welded Steel Mesh

A soil buttress reinforced with welded steel mesh was considered as another design alternative. The Gridcote Retaining Wall System consisting of L-shaped welded-wire trays, coated with fusion bounded-epoxy placed and locked into successive lifts of compacted fill was studied. With consideration of the plasticity of the on-site soils, it was determined that the native soils were too plastic (with an average plasticity of 22) to be used as backfill material. Economics of import of sandy soils for backfill rendered this design alternative unfeasible.

● Buttress Fill Reinforced with Geogrid

Consideration was then given to reinforcement of the buttress by geogrid which is not subject to corrosion in a plastic soil environment. Considering that the strength gain by using geogrid is uniaxial, the buttress designed with this concept was deeper and wider at the base than the buttress designed to utilize lime treatment (see Figure 1). However, since the excavated material could be directly used over the geogrid (as opposed to the need for lime treatment and overnight curing prior to compaction into the lime-treated buttress), this alternative proved to be more cost effective. In addition to the cost advantage, the alternative was also perceived to be environmentally preferred since the slope face planting would be easier. This alternative was selected for construction.

Buttress construction first would involve excavating the buttress key utilizing a 0.75h:1v back cut slope down to the designed buttress key elevation. The design width of the buttress key ranged from approximately 25 to 75 feet wide. Tensar SR-3 geogrid would then be placed at selected intervals between the compacted fill as transverse reinforcement perpendicular to the slope face. Tensar SS-1 (biaxial) geogrid was designed to be placed at 1-foot vertical intervals between the SR-3 layers for surficial slope stability concerns. A subdrain system consisting of gravel wrapped in filter fabric placed at the heel of the buttress and Tensar DC-1100 drainage composite used at the back cut, was also included in the design.

DESIGN SHEAR STRENGTH PARAMETERS

Table 1 presents shear strength parameters used in our slope stability analysis. The shear strength parameters of relatively undisturbed Ardath Shale and Mount Soledad Formation or Cabrillo Formation, as well as the shear strength parameters for compacted fill, were determined in accordance with ASTM D-3080 test method. Shear strengths along the clay seams and the ancient landslide slide plane were conservatively back-calculated assuming that a factor of safety of one prevailed prior to grading and that clay seams were continuous.

TABLE 1

Summary of Shear Strength Parameters Used in Buttress Design

<u>Soil Type</u>	<u>Cohesion (psf)</u>	<u>Friction Angle (degrees)</u>
Ardath Shale	800	29
Mount Soledad/Cabrillo Formation	2,500	34
Clay Seam	180	19
Slide Plane	150	20
Slide Debris	400	22
Compacted Fill derived from	400	25
Compacted Fill derived from Cabrillo Formation	600	25

REINFORCEMENT PROPERTIES

The main transverse reinforcement material (Tensar SR-3) is a uniaxially oriented, high density polyethylene geogrid. The tensile strength is approximately 7,500 lb/ft based on tests at a strain rate of 10 percent per minute at 68 degrees Fahrenheit (ASTM D-4595). The geogrid rolls delivered from the factory are 3.3 feet wide and 98.5 feet long (1 meter wide by 30 meters long).

The biaxial geogrid (Tensar SS-1) has a peak tensile strength of 840 lb/ft along the machine direction (along roll length) and a peak tensile strength of 1,400 lb/ft across the machine direction (across roll width). These values were also determined in accordance with ASTM D-4595 test method. The SS-1 geogrid roll is 9.8 feet in width and 164 feet in length (3 meters by 50 meters).

Two key parameters in the reinforcement design analysis are long-term allowable tensile strength of the reinforcement and coefficient of soil-geogrid interaction. By using the procedure published by Bonaparte and Berg in 1987 (2), a long-term allowable tensile strength of 3,000 lb/ft was utilized in the design. Due to the silty nature of Ardath Shale, a coefficient of soil-geogrid interaction of 0.7 was recommended (0.8 is conventional).

BUTTRESS DESIGN

A minimum factor of safety of 1.5 was needed for both the external and internal stability of the slope. The internal stability of the geogrid-reinforced buttress is a function of the steepness of the buttress face, height of the buttress, width at the buttress top, width of the buttress key, strength parameters of compacted fill, and amount of geogrid used. The external stability of the slope is controlled by the size of the buttress, layout and effectiveness of the drainage system, and geologic conditions behind the buttress.

● Internal Stability

The internal stability was evaluated by using an unpublished computer program (Tenslo 1) from the Tensar Corporation. This program, with some modifications, is Bishop's modified method of slices (1). Modifications include the effect of tensile strength of the geogrid layers into the overall moment equilibrium equation.

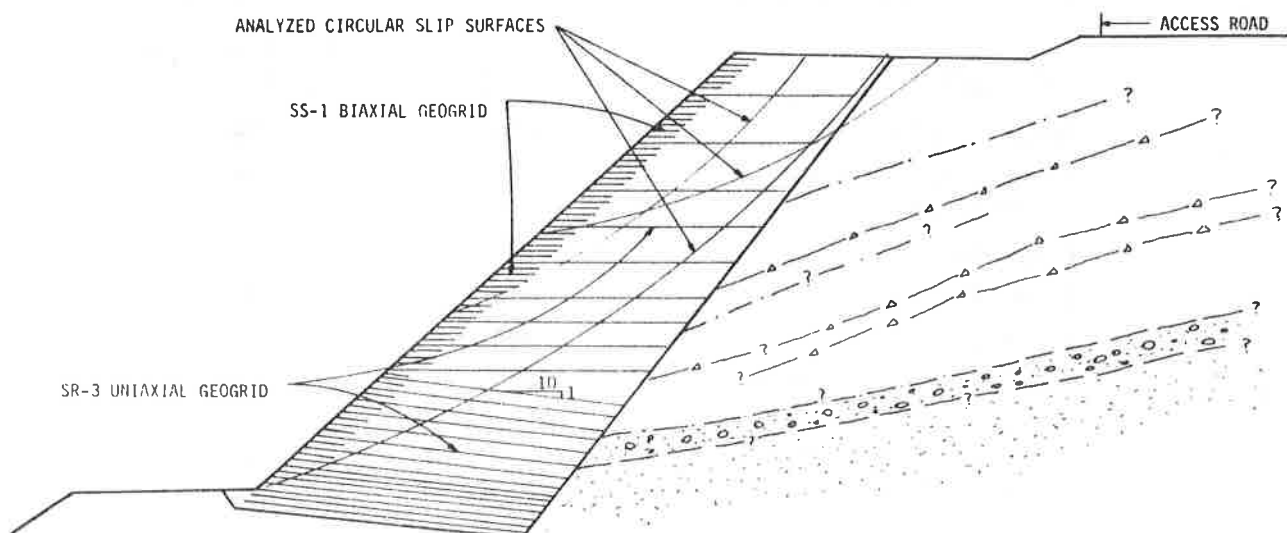


Figure 3 - Geogrid Layout of the Typical Geogrid - Reinforced Buttress

Figure 3 shows geogrid layout at a typical buttress cross section. In this cross section, the design calls for 24 layers of SR-3 geogrid placed at vertical intervals ranging from 1 foot to 8 feet with 100 percent coverage. The cross section also illustrates the use of SS-1 geogrids at the slope face to increase the surficial slope stability.

● External Stability

External stability of the buttressed slope was analyzed using Spencer's method (4). Stability analyses confirmed that the critical slip surfaces were non-circular and followed the remolded clay seam behind the buttress and soil geogrid interfaces within the buttress. Although static ground water was not encountered during the field investigation, a conservative phreatic surface was assumed in the analysis.

The bottom width of the buttress was generally governed by external stability considerations. Where the overall slope height exceeded 60 feet, it was determined that a more cost effective design would result from: (1) placing the approximately bottom one-third of the SR-3 geogrid at a 10 percent slope towards the back cut; (2) placing granular fill materials derived from the Cabrillo Formation and/or Mount Soledad Formation in the lower portion of the buttress to increase the shear strength of fills.

BUTTRESS CONSTRUCTION

Because of complex geologic conditions at the site and safety concerns, several early-warning measures were implemented prior to grading. These measures included the following: (1) installation of 5 inclinometers at selected locations and 18 crack monitors on the curb of the access road behind the proposed back cut. The instruments were monitored during grading so that impending instability could be detected. The monitoring crew was equipped with a compressed air horn and smoke bombs to provide warning to field personnel if a construction failure was about to occur. (2) All personnel were required to wear hard hats and safety vests when entering the construction site. Safety meetings were held regularly and safety awareness was promoted.

The buttress keys were designed to be approximately 3 feet into competent Mount Soledad or Cabrillo Formation. However, due to faulting in two areas, the depth to the Mount Soledad or Cabrillo Formation was discovered to differ significantly from prior interpretations. Consequently, buttress redesigns were performed in these areas.

Due to concerns for back cut failures, buttress construction was planned to proceed in segments in order to minimize the extent of open back cut. Buttress construction was carried out by excavating down to the key elevation at the eastern 1/5 of the buttress key (Phase I). Excavated soils were stockpiled in an adjacent canyon. After the key bottom, for each phase was geologically observed and subdrains and back drain were installed, fill was brought in from the excavations for the next 1/5 of the buttress key.

The fill was then placed in 6- to 8-inch lifts, moisture-conditioned to approximately 2 percent above the optimum moisture content, and recompacted to at least 90 percent of the maximum dry density as determined by ASTM D1557-78. Geogrids were then placed at designed elevations as the fill height increased. The last phase of the excavation (westernmost 1/5 of the key) was filled in with stockpiled material excavated from the first 1/5. Using this sequencing technique, only one back cut failure occurred. This failure involved a 50-foot long by 40-foot high portion of the back cut. Figure 4 photos were taken during and after construction.

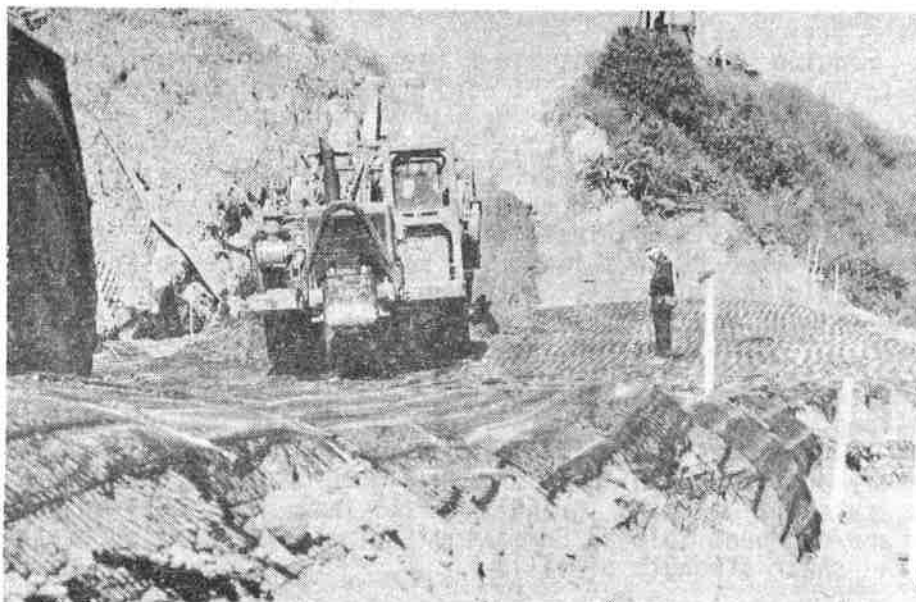


Figure 4a - Fill placement over a layer of SR-3 geogrid



Figure 4b - A portion of completed slope. Note the instrumentation station at the foreground

INSTRUMENTATION

In addition to the inclinometers and crack monitors installed for back-cut instability concerns, an instrumentation program was designed and installed to verify the performance of the completed buttress.

The instrumentation program included two vertical and one horizontal slope indicators, multiple foil-type resistance strain gauges attached to two sides (top and bottom) of the geogrid, subsurface settlement monitoring systems using a magnetic probe with sensor rings, and surface settlement monuments. The approximate layout of instrumentation is presented in Figure 5. Figures 6 and 7 present selected plots of instrumentation monitoring results.

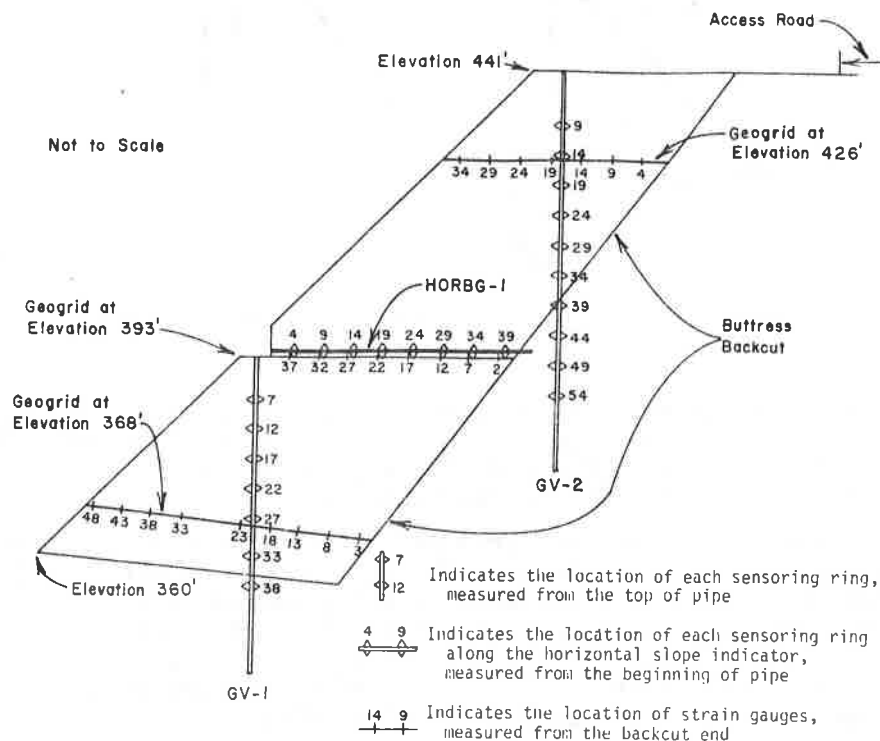


Figure 5 - Instrumentation Layout

The horizontal slope indicator was unoperational a week after installation, possibly due to a loose coupling located approximately 20 feet from the open end. Figure 6 indicates lateral deflections of the two vertical slope indicators during and after buttress construction. Slope indicator GV-1 shows a total of 1.2 inches deflection, the majority of which was caused by fill surcharging during construction. Slope indicator GV-2 indicates a total of 0.6 inch deflection. This deflection may reflect the post-grading buttress adjustment.

A total of 50 strain gauges were installed on both sides of the geogrid so that not only extension but also bending could be detected. Instrumented geogrid strips were installed at three different elevations within the buttress and gauges were monitored.

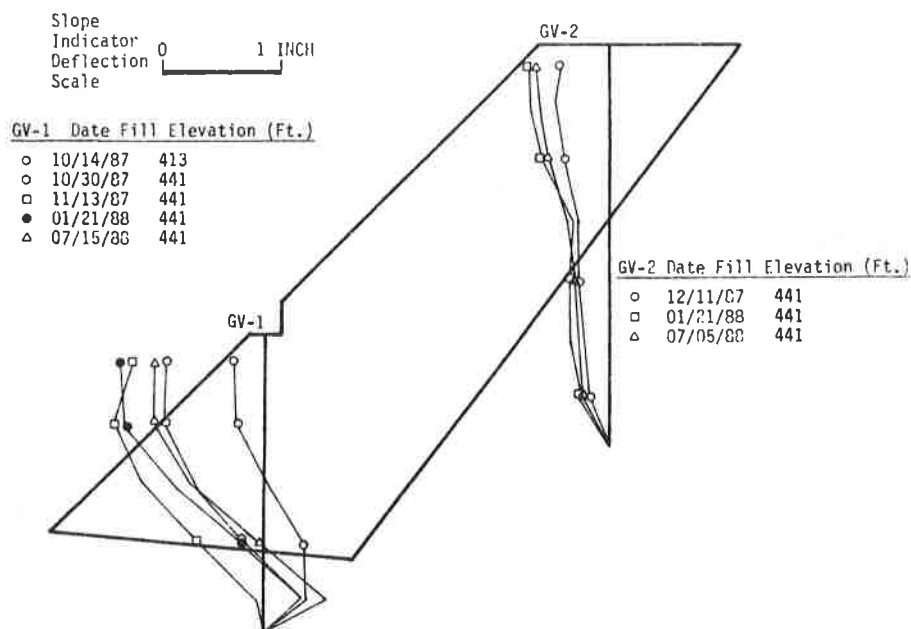


Figure 6 - Measured Lateral Deflections of the Slope Indicators GV-1 and GV-2

Results of strain gauge readings (Figure 7a, 7b and 7c) indicate a maximum strain of up to 0.4 percent and an average strain of less than 0.2 percent. These values are well within the design tolerable strain of 2 percent. The results indicate that most of the strain occurred during construction.

Figure 7d, depicting sensor data from GV-1, indicates that settlements in the order of 2 inches may have occurred between the period of December 1 to December 11, 1987. This settlement, probably associated with lateral deformations detected from slope indicator GV-1 during the same period (08/01/87 to 08/11/87), is believed to be caused by the buttress fill construction. Approximately 0.1- to 0.3-inch settlements were obtained from surveys of surface settlement monuments installed at the top of the buttress after completion of grading.

CONCLUSIONS

This paper illustrates the successful application of geogrid-reinforced soil buttress construction, enabling the stabilization of adverse geologic conditions at considerable savings and without adverse environmental effects. The total amount of fill placed was approximately 200,000 cubic yards (includes approximately 20,000 cubic yards of imported fill). The total cost for construction of the buttress was approximately \$2,100,000. The lime-stabilized buttress was cost estimated at approximately \$3,000,000.

ACKNOWLEDGMENTS

Tensar Corporation (the geogrid vendor) and Sukut Construction, Inc. (earthwork contractor), as well as the owner, participated in sponsoring instrumentation programs on this project. The authors sincerely appreciate this participation and cooperation during both design and construction.

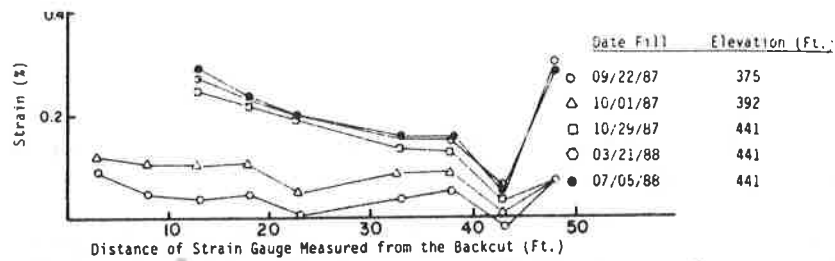


Figure 7a - Measured Strains from the Strain Gauges Placed at Elev. 369'

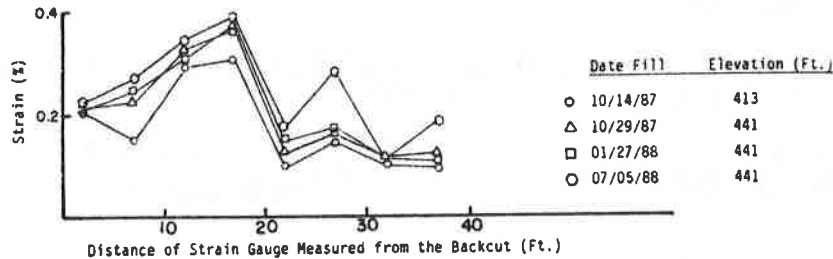


Figure 7b - Measured Strains from the Strain Gauges Placed at Elev. 393'

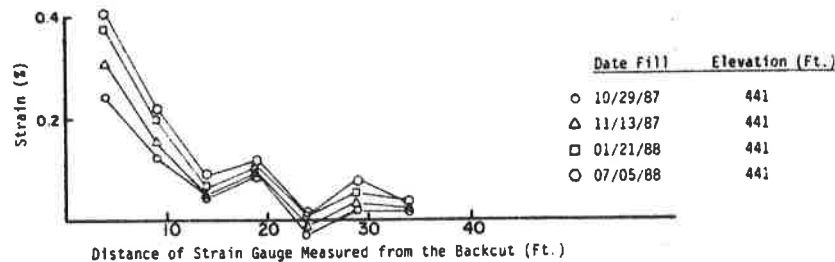


Figure 7c - Measured Strains from the Strain Gauges Placed at Elev. 426'

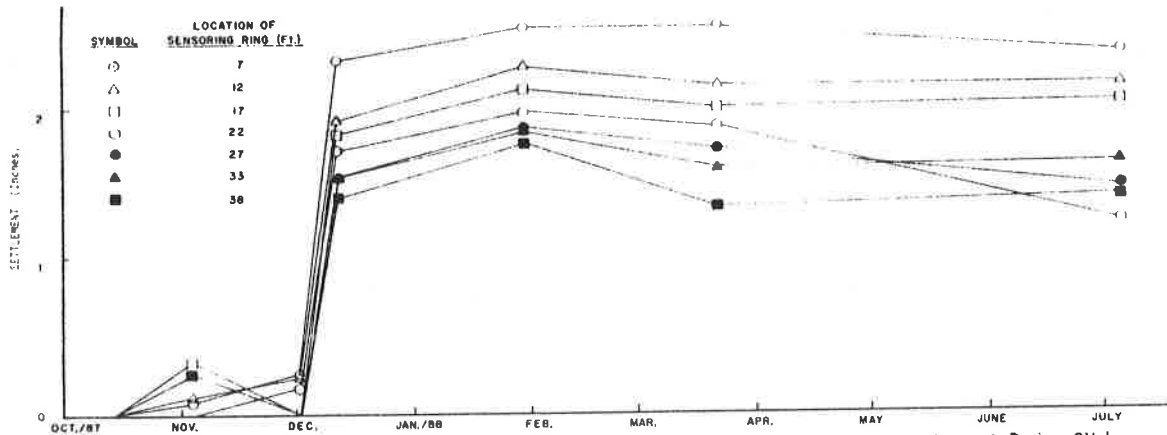


Figure 7d - Measured Subsurface Settlements of the Sensoring Rings at Boring GV-1

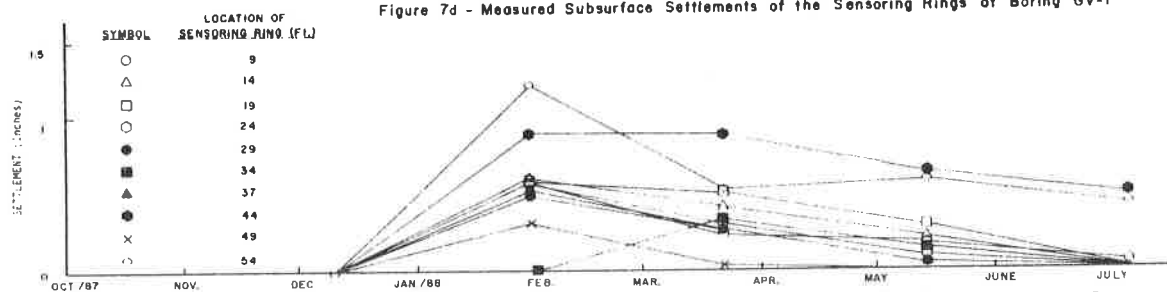


Figure 7e - Measured Subsurface Settlements of the Sensoring Rings at Boring GV-2

REFERENCES

- (1) Bishop, A.W., "The Use of the Slip Circle in the Stability Analysis of Slopes," Geotechnique, 1955, p.p. 7-17.
- (2) Bonaparte, R. and Berg, R.R., "Long-Term Allowable Tension for Geosynthetic Reinforcement," Proceedings of Geosynthetics '87, Industrial Fabrics Association International, New Orleans, USA, 1987, p.p. 181-192.
- (3) National Lime Association, Lime Stabilization Construction Manual, Bullentin 326, Sixth Edition, 1976.
- (4) Spencer, E., "A Method of Analysis of the Stability of Embankments Assuming Parallel Interslice Forces," Geotechnique, 1967, p.p. 11-26.

W.O. ENGEMOEN
P.J. HENSLEY
U.S. Bureau of Reclamation

Geogrid Steepened Slopes at Davis Creek Dam

ABSTRACT

Davis Creek Dam will be a 110-foot-high rolled earthfill embankment dam located in central Nebraska, designed by the Bureau of Reclamation. During the design of this structure, it was recognized that significant cost savings were associated with steepening the embankment slopes. Specifically, it was estimated that approximately \$1,000,000 in construction costs savings would result from steepening the approximate upper 25 feet of the dam slopes from 3.5:1 (upstream) and 2.5:1 (downstream) to 1:1 (both upstream and downstream). The upstream slope was steepened through the use of a thickened soil-cement section, while the downstream slope was steepened through the use of high-strength polymer geogrids. The design of the downstream slope consisted of 25 layers of geogrids with a vertical spacing of 1 foot between layers and two different embedment lengths of 6.5 and 16.4 feet. In addition to designing on the basis of required strengths, considerable attention during the design was focused on the constructability of the reinforced slopes. Both geogrid and earthwork dimensions were optimized, and the specifications were written to allow the contractor some freedom in selecting construction equipment and methods, rather than restricting operations to specialized equipment.

¹Civil Engineers, Bureau of Reclamation, Denver Office,
Geotechnical Engineering and Embankment Dams Branch,
Denver CO 80225-0007

INTRODUCTION

Davis Creek Dam is a feature in the Bureau of Reclamation's North Loup Division, a water project designed to provide irrigation to over 53,000 acres of land in central Nebraska. The dam will be located across Jack's Canyon, a tributary to the North Loup River, about 30 miles north of Grand Island. Davis Creek Reservoir will have a total capacity of approximately 48,000 acre-feet. Because the reservoir is primarily for irrigation storage, it will generally be filled and emptied every year.

The dam will be a compacted earthfill embankment about 3,000 feet long, with a height above creek bed of 110 feet, and an embankment volume of approximately 3,000,000 cubic yards. Waterways for the dam will include a 72-inch diameter steel-lined, reinforced concrete outlet works which will release reservoir water into Fullerton Canal for downstream distribution; and an open cut emergency spillway located in the reservoir rim and consisting of a grass and soil-cement lined channel with a reinforced concrete control sill.

SITE CONDITIONS

The damsite is located in the loessial hills of Nebraska, with the surface topography consisting of gently rolling low hills. The entire damsite and reservoir area consists of about 30 to 40 feet of loessial materials (silts and low plasticity clays) overlying fluvial deposits of generally silty sands. "Bedrock" at the site consists of the Ogallala Formation, a granular deposit comprised of compacted sands and lightly cemented sandstones. A geologic profile along the centerline of the dam is presented in Figure 1.

GENERAL DESIGN CONCEPTS

The relatively thick deposit of loessial materials had a profound influence on the design of the dam. In a dry condition, loess is a very strong foundation material with low compressibility. When wetted, however, the loess loses strength and upon loading can experience large, sudden, collapse-like settlements. Because the reservoir will eventually saturate the dam foundation, which would lead to large settlements of the loess which in turn could jeopardize the integrity of the embankment, it was decided to completely remove the loess from underneath the entire limits of the dam (upstream toe to downstream toe as shown on Fig. 2.)

Furthermore, the considerable thickness of the loessial material over the entire reservoir area made it the only economical embankment material. For that reason, an essentially homogeneous dam was designed, comprised almost entirely of compacted silts

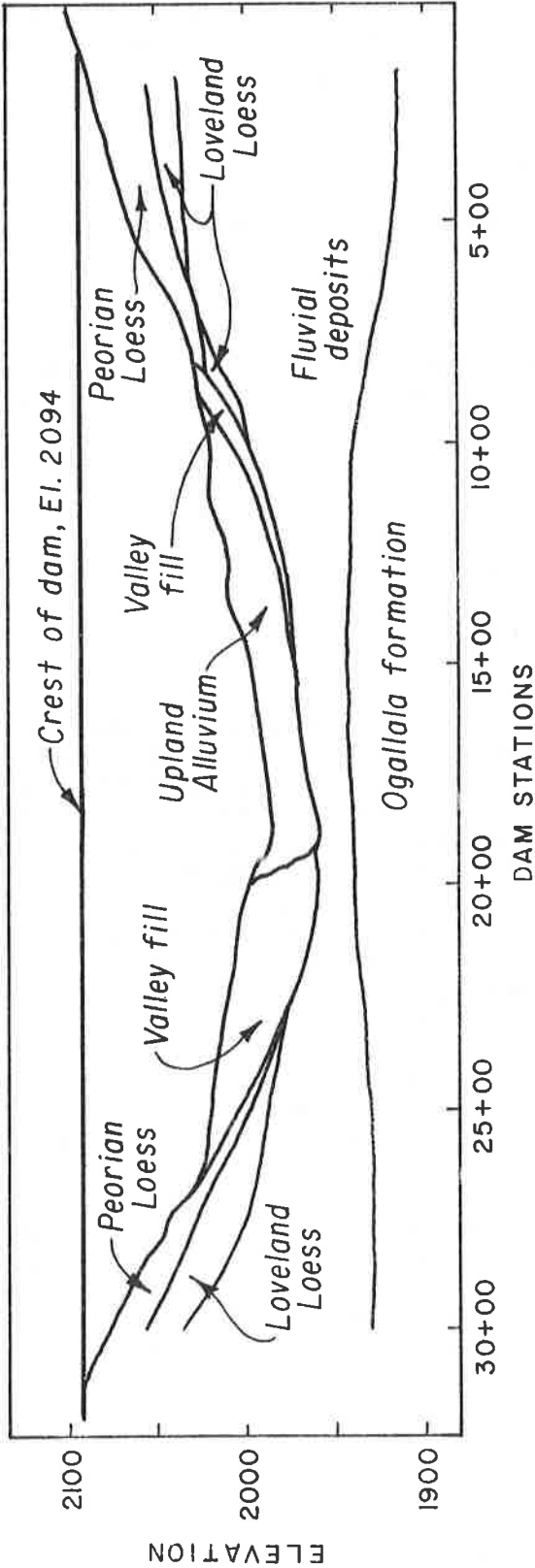


FIGURE 1. - GEOLOGIC PROFILE ALONG CENTERLINE OF DAM

and clays. In order to control any seepage and to prevent erosion, a sand and gravel embankment drainage system was included; consisting of a chimney drain, horizontal drainage blanket, and downstream foundation drain.

To protect against wave damage, the upstream face of the dam will be protected with a 2.5-foot normal thickness of soil-cement slope protection. The nearest reasonable quality riprap was over 150 miles away, which made soil-cement a much more economical choice.

The downstream slope of the dam is a fairly conventional 2.5:1. The upstream slope is a relatively flat 3.5:1, due to the fact that the yearly 70-foot reservoir fluctuation coupled with the clayey embankment's poor ability to drain creates drawdown stability concerns.

By far the most interesting aspect of the Davis Creek Dam design, however, involves the very steep slopes utilized at the very top portion of the embankment.

DECISION TO USE 1:1 SLOPES

During the early designs for the embankment, designers realized that by steepening the slopes of the dam, considerable construction cost savings could be realized. Not only would steepened slopes reduce the overall embankment volume, but they would also reduce the volume of foundation excavation, reduce the length and volume of the relatively expensive, processed sand and gravel horizontal drainage blanket, and reduce the length of the reinforced concrete outlet works conduit passing through the center of the embankment. Detailed cost estimates were then prepared to evaluate these types of savings as compared to expected increased construction costs due to additional hand labor, slower earthfill placement rates, and the use of different types of equipment. The completed cost estimates showed that an alternative to steepen the upper 25 feet of the dam utilizing a soil-cement buttress upstream and a geogrid reinforcement system downstream would result in an overall construction cost savings of \$1,000,000.

In spite of the significant cost savings, this type of design for a major embankment dam was unprecedented, and consequently required additional justification. A key selling point was the relatively "noncritical" location of the steepened slopes. As shown on Figure 2, the steepened slopes are located in the uppermost 18 to 25 feet of the dam, and above the level of the top of active conservation capacity water surface (highest normal water surface). Due to the yearly reservoir fluctuation, the reservoir elevation will be near the steep slopes for only a month or so each year, and will encroach upon the steep slopes only during a flood event. It was also recognized that the relatively simple embankment design and the type of earthfill

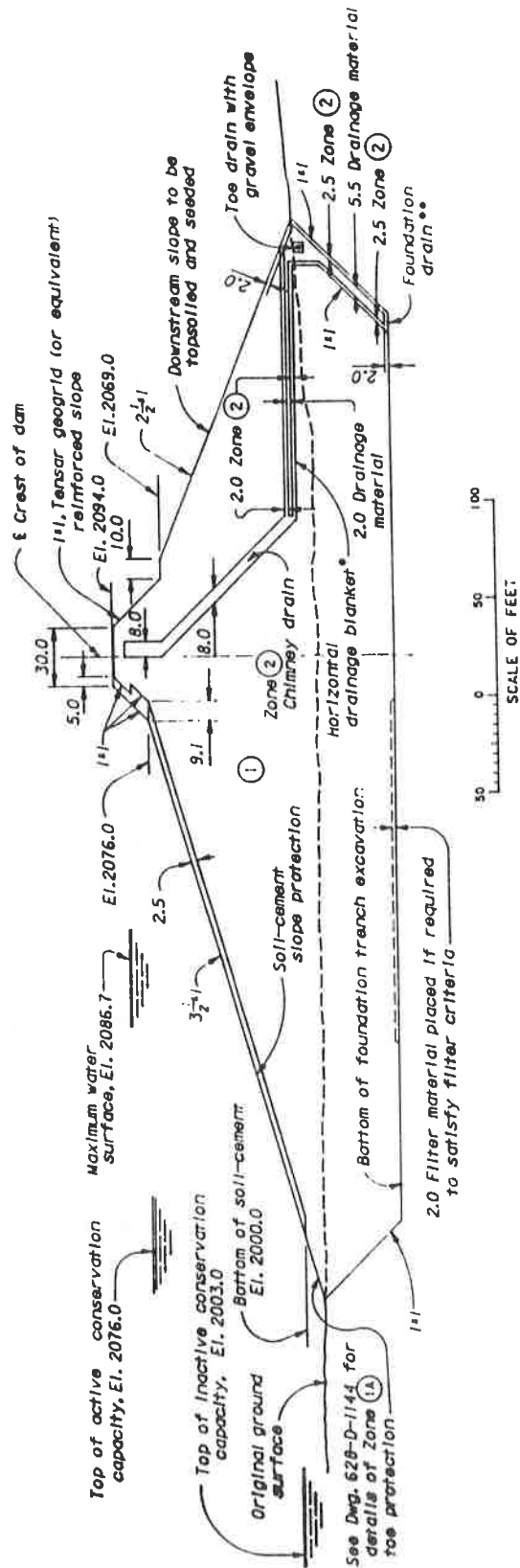


FIGURE 2 - MAXIMUM SECTION

materials utilized were each conducive to a steepened slope design because construction would be relatively simple. Finally, the designers provided extra space at the toe of the dam such that in the event of long-term problems with the slopes, sufficient space was available to flatten the downstream slope without affecting the reservoir operations.

DESCRIPTION OF 1:1 SLOPE DESIGN

Figure 3 shows the details of the selected steepened slope design. First of all, it should be pointed out that the chimney drain, which was inclined in the lower portion of the dam, was made vertical near the top to simplify construction. With the exception of the chimney drain, silts and clays (zone 1) comprise the embankment within the steepened slopes.

The upstream slope will be steepened to 1:1 for the uppermost 18 feet of the dam; from elevation 2076 (top of active conservation water surface) to elevation 2094 (crest of dam). A 1:1 upstream slope is possible due to the utilization of a thickened soil-cement section. Because soil-cement was being utilized in a 9-foot horizontal width for slope protection everywhere on the upstream face, the 9-foot width was maintained on the 1:1 slope, resulting in a thick section of relatively strong material. The uppermost 9 feet of the soil-cement will be reduced to a 5-foot horizontal width in order to obtain further cost savings.

The downstream slope will be steepened to 1:1 for the uppermost 25 feet of the dam, with a berm provided at the base of the slope for future maintenance and surveillance of the slope and to serve as an additional working surface during construction. The 1:1 slope will be stabilized through the use of synthetic geogrid reinforcement. Specifically, six layers of TENSAR[®] UX-1500 polyethylene geogrids (or an equivalent geogrid) with embedment lengths of 16.4 feet will provide the primary reinforcement of the slope. In addition, TENSAR[®] 2 BX-1200 polypropylene geogrids (or equivalent) with 6.5 feet embedment lengths will be placed at 1-foot vertical spacings to stabilize the outer edges of the slope. The completed downstream slope will have 4 inches of topsoil spread over it and will then be seeded. In order to prevent erosion before a grass stand is established, the seeded topsoil will be protected by a straw erosion control mat, which will also serve as a mulch. Long-term erosion protection will be provided by the seeded native grass stand and its root system.

[®]Registered Trademark of the Tensar Corporation.

²The information contained in this paper regarding commercial products or firms may not be used for advertising or promotional purposes and their mention is not to be construed as an endorsement of any product or firm by the authors or the Bureau of Reclamation.

DOWNSTREAM SLOPE DESIGN

General

The downstream slope would, at the moisture content present during construction, provide adequate factors of safety for all loading conditions without any soil reinforcement. However, it can be argued that the earthfill moisture content in the downstream slope could increase due to rainfall infiltration. To design for this potential worst case situation, a low embankment strength was assumed by neglecting all apparent cohesion in the earthfill from placement at the optimum moisture content or possible capillarity in the near saturated state. Synthetic reinforcement was selected as an economical method of providing the soil reinforcement necessary for reestablishing the desired level of stability for this lower strength assumption. The design of the synthetic reinforcement was based on the level of reinforcement required to obtain an internal factor of safety consistent with that available from a 2:1 slope under similar assumptions.

Synthetic Reinforcement

A product line, TENSAR[®] geogrids, manufactured by The Tensar Corporation was selected as representative of the type of synthetic reinforcement required. Their product line is manufactured by heat stretching a perforated sheet of high density polyethylene or polypropylene to form a grid-like structure. When used as embankment slope reinforcement, geogrids are generally placed in horizontal layers between lifts to distribute the loads in the embankment through tension in the geogrids.

A potential concern associated with the use of synthetic reinforcement is the potential for creep deformations in the reinforcement that could eventually lead to failure. Each geogrid product has a particular load under which creep deformations are within performance limits (10 percent) for the design life of the structure. The synthetic reinforcement is designed assuming the stress-strain characteristics of the soil and reinforcement in the slope are reasonably compatible (i.e., the required soil strength is fully mobilized without significant overstressing in the reinforcement). However, there is a significant tolerance for some degree of incompatibility due to the stress relief associated with creep deformations resulting from the applied overstress in the synthetic reinforcement. To ensure that the reinforcement is not overstressed to a condition of failure, instrumentation capable of measuring the strain of the synthetic reinforcement has been included in the design.

By monitoring the strain in the reinforcement, the degree of overstressing, if present, can be estimated and the rate of increase or decrease in the strain rate used to determine if

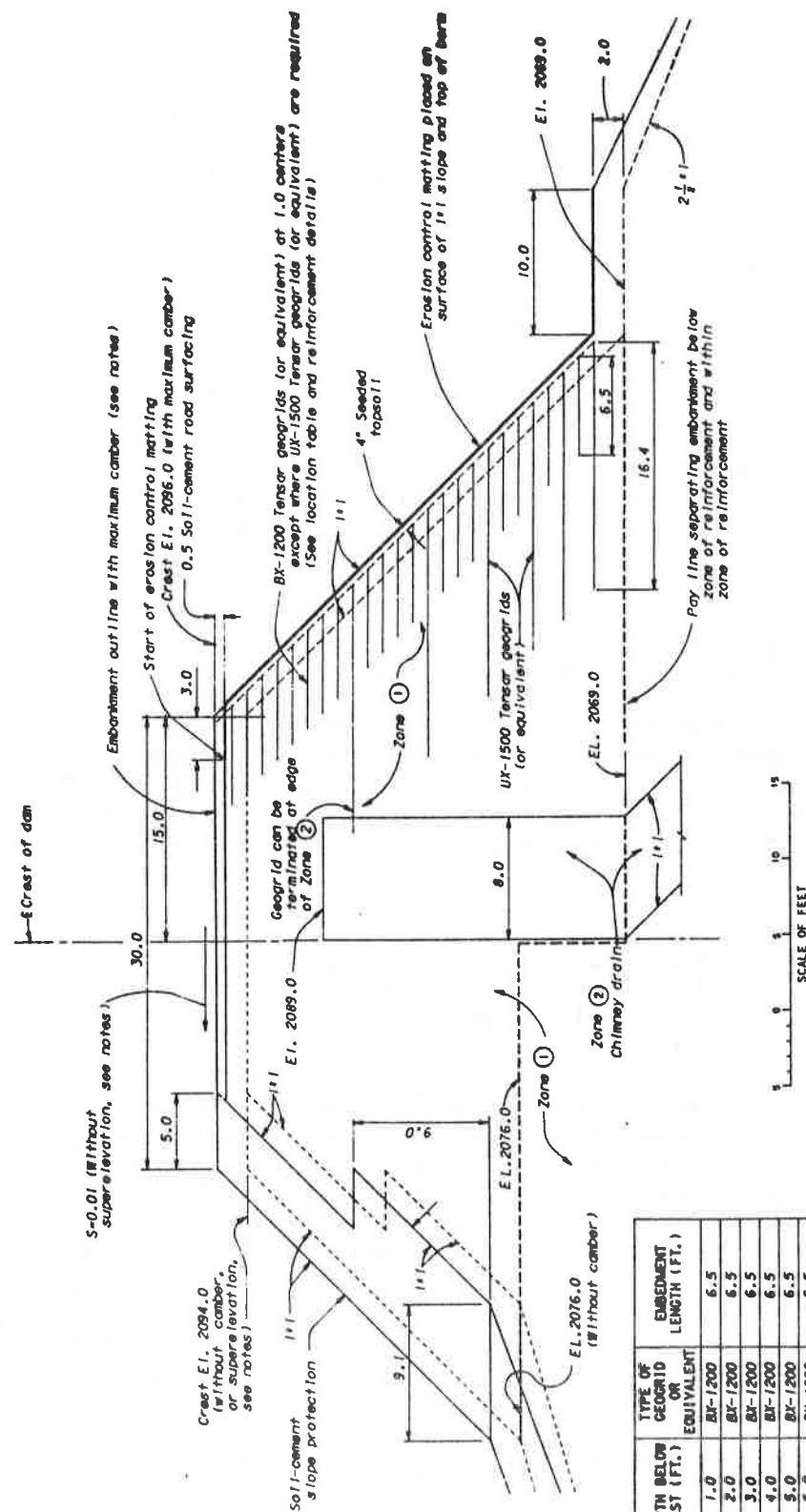


FIGURE 3. - MAXIMUM CAMBER AND CREST DETAILS

remedial measures are required. If, in fact, the embankment moisture does not increase appreciably, the actual stiffness and strength present in the earthfill constructed at near or below the optimum moisture content will make any overstressing of the reinforcement unlikely.

TENSAR® geogrids are available in a wide range of strength and configurations to suit many particular applications. At the time the dam was designed (1984-85), two types of geogrids available from The Tensar Corporation for slope reinforcement were their uniaxially-drawn SR-2 and biaxially-drawn SS-2 products. The product nomenclature used by The Tensar Corporation has recently changed. Uniaxial geogrids now have a UX prefix, i.e. SR-2 is now UX-1500, and biaxial geogrids now have a BX prefix, i.e. SS-2 is now BX-1200.

Figures 4 and 5 show the strength versus time-loading characteristics of the SR-2 and SS-2 products utilized during the design. The design strengths for the SR-2 and SS-2 products suggested by the manufacturer were 2,000 and 270 lb/ft, respectively. During the design, additional data were provided by The Tensar Corporation on their SS-2 product.

These later data indicated that the SS-2 product because of its polypropylene construction, did not appear to have a clearly definable design strength and could experience nearly continuous creep at loading much less than the design loading previously suggested. The use of the SS-2 product as slope reinforcement was, therefore, limited to the outer edges of the slope. Its use in this location was primarily to prevent localized sloughing from rain infiltration and to permit the operation of construction equipment near the edge of the slope. The SR-2 geogrids were utilized as the primary means of reinforcement.

TENSAR® geogrids were reported by the manufacturer to be completely resistant to chemical and biological attack under conditions normally occurring in soils.

Stability

The stability of the synthetically reinforced slope, like the soil-cement reinforced slope, can be separated into external and internal stability. The external stability requires that an analysis be performed to ensure that there is an adequate factor of safety against a deep-seated failure surface.

The external stability analysis of the slope was performed as part of the overall stability analysis of the dam using a conventional Spencer limit equilibrium method as incorporated in the computer program, SSTAB2 (1)³. The internal stability refers

³Numbers in brackets refer to references.

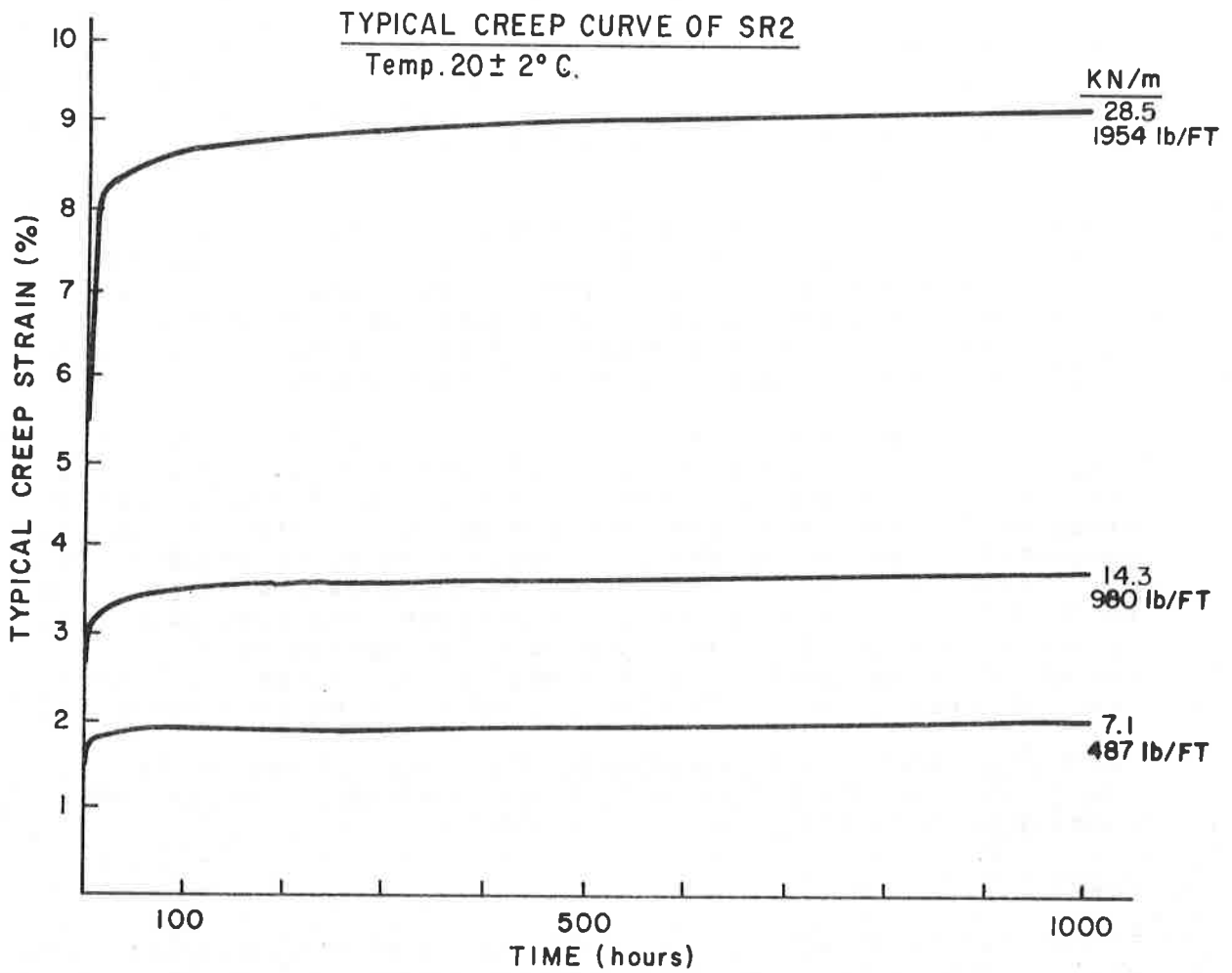


FIGURE 4.- TYPICAL STRAIN -TIME CURVES FOR SR2

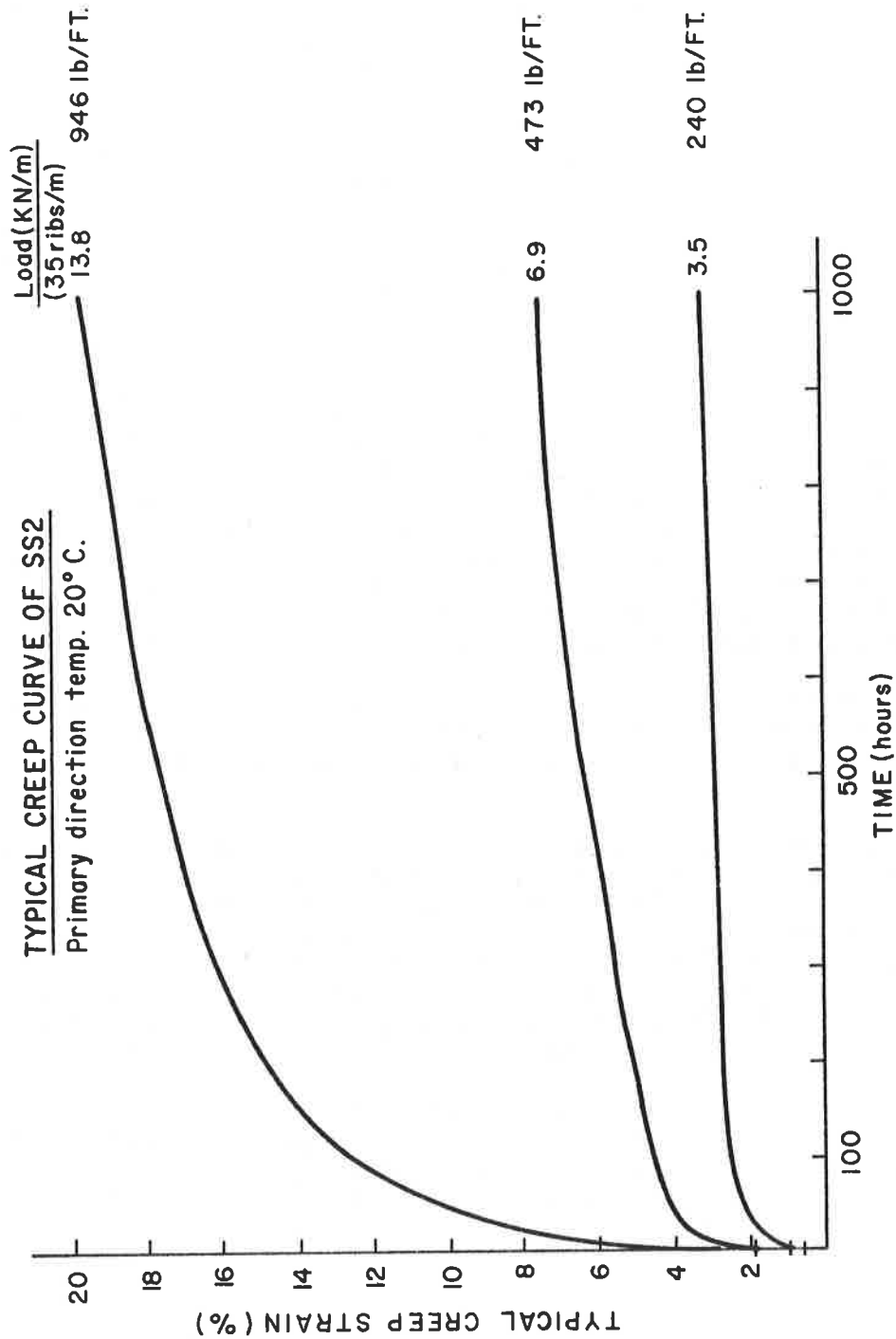


FIGURE 5. - TYPICAL STRAIN-TIME CURVES FOR SS2.

to that portion of the slope above the toe in which stability is directly affected by the synthetic reinforcement. The internal stability of the synthetically reinforced slope is controlled by the strength characteristics of the soil together with the design strength, spacing, and embedment length of the geogrids.

The selection of the initial required geogrid spacing and embedment lengths for both the SS-2 and SR-2 products was performed in accordance with the geogrid design manual (2) provided by The Tensar Corporation. The design was based on increasing the unreinforced internal stability of the slope to an overall factor of safety of 1.5 for the assumed loading conditions. For a given pore pressure coefficient (r_u), soil friction angle (ϕ) and slope angle (β), the lateral force coefficient (k) can be obtained from charts in the design manual. The lateral force coefficient (k) can then be counteracted by tension in the geogrids to obtain the desired factor of safety. Similar charts were available in the manual to obtain the required embedment length of the geogrids to ensure internal slope stability. Once the total force required by the geogrid was established, the design strength of the individual products was then used to determine the required spacing. Spacing was determined with the aid of spacing constants calculated as functions of the design strength of the products, lateral force coefficients, and lift thickness.

The initial reinforcing configuration obtained from the design manual consisted of four layers of SR-2, 15 feet long, and 21 layers of SS-2, 5 feet long provided for the control of surface sloughing.

As a check on the design manual approach, an independent slope stability analysis and reinforcement design was performed. This analysis and design was based on the use of the simplified Bishop limit equilibrium method, modified to account for the use of geogrids. The final design resulting from this detailed analysis consisted of six layers of the SR-2 geogrids with an embedment length of 16.4 feet. This design produced a 1.6 factor of safety on the critical surface passing through the crest of the dam.

For a final check, designers performed a stability analysis using the Bureau's standard computer stability program, SSTAB2, with no reinforcing, and then hand calculating the increase in factor of safety with geogrid reinforcing. This analysis verified the 1.6 minimum factor of safety on the critical surface.

CONSTRUCTION CONSIDERATIONS

The application of synthetic reinforcement in the downstream slope prevents the use of sheepsfoot roller compaction and deep disk scarification within the reinforced zone 1 material in the downstream slope. However, satisfactory densities can be obtained using "padfoot" tamping rollers or rubber-tired rollers that will not damage the geogrids.

The specifications required the use of "padfoot" tamping roller compaction within the reinforced slope area. The material is required to be placed in 6-inch lift thicknesses, with the same material, moisture content, and dry density requirements as specified for the zone 1 materials used throughout the unreinforced bulk of the dam.

Connecting or overlapping of the uniaxial (SR-2) geogrid widths was not required, but a maximum separation distance of no more than one-half inch was specified. Securing the geogrids to the fill through the use of anchors to minimize movement during fill placement was not required but allowed as a contractor option. The specifications do require, however, that the geogrids remain flat and free of wrinkles to ensure thorough interlock with the earthfill. To the extent that disturbance to the geogrids is minimized, rubber-tired equipment will be allowed to travel upon the geogrids.

The payment for the placement and compaction of the zone 1 fill material in the reinforced slope is provided as a separate bid item in the specifications. This was done to account for the more restrictive working area and conditions associated with the construction of the reinforced slope. It is expected that the earthfill placed within the reinforced zone will be more expensive than the earthfill in the rest of the embankment.

No special controls were placed on the storage and handling of the geogrids other than the requirement they be stored in a protective area where they are not exposed to extreme cold or hot temperatures or to direct sunlight. The 16.4- and 6.5-foot embedment dimensions were in part selected because they are exact fractions of a roll length or width, which ensures that no portions of a manufactured geogrid roll are wasted.

Lastly, it was recognized that topsoiling and seeding to provide downstream slope protection would be somewhat labor intensive regardless of the method selected. It was felt that a straw erosion control mat was not only quite economical but would be easy to construct, and will provide protection for the germinating grass cover by both minimizing erosion and by serving as a mulch.

SUMMARY

Cost analyses indicated significant savings could be obtained by steepening the downstream slope of Davis Creek Dam. The steepened downstream slope would in all likelihood remain stable at or near the placement water content for the life of the structure, without reinforcement. However, to ensure that the slope would remain stable under the worst case conditions, soil reinforcement was required. Synthetic reinforcement of the type manufactured by The Tensar Corporation (or equivalent) was shown to provide an economical method of ensuring the required level of stability in the steepened downstream slope under the worst case conditions.

REFERENCES

- (1) Chugh, Ashok K., "User Information Manual, Slope Stability Analysis Program, 'SSTAB2' (A Modified Version of 'SSTAB2' by Steven G. Wright)," Bureau of Reclamation, Denver, Colorado, February 1981.
- (2) Guidelines for the Design and Construction of Embankments Over Stable Foundations Using 'TENSAR' Geogrids," The TENSAR Corporation, Morrow, Georgia.
- (3) McGown, A., Andraws, K. Z., Yeo, K. C., and Dubois, D., "The Load-Strain Time Behavior of TENSAR Geogrids," Symposium on Polymer Grid Reinforcement in Civil Engineering, Netlon Ltd., Blackburn, Lancs, England.

R.R. BERG
V.E. CHOUERY-CURTIS
C.H. WATSON
Tensar Engineering, Inc., U.S.A.

Critical Failure Planes in Analysis of Reinforced Slopes

INTRODUCTION

Current limit equilibrium methods of analyzing reinforced soil slopes often incorporate an assumed critical failure plane. A common assumption is that failure planes are not affected by addition of tensile reinforcement inclusions into the soil mass. Hence, the critical failure plane located by analysis of the unreinforced soil mass is taken as the critical failure plane for the reinforced soil mass.

This assumption, that the critical failure plane determined by analyzing an unreinforced soil structure can be utilized as the critical failure plane for design of a geosynthetic reinforced soil structure, is examined within. A generic example and case histories are utilized to illustrate findings. Over-steepened slopes, which may be appropriately analyzed with circular failure planes, are the focus of this inquiry.

BACKGROUND

Types of Structures

Geosynthetics are commonly being utilized in three types of reinforced slope structures. These structures are: embankments over weak foundation soils; vertical slopes or retaining walls; and over-steepened slopes. Embankments are typically low to moderate in height, 1 m to 6 m, and are utilized as containment dikes, flood levees, and roadway structures. Geosynthetic reinforced soil retaining walls typically vary in height from 2 m to 9 m and are used as an economic alternative to cantilever concrete walls, metallic reinforced soil walls, and other gravity type of wall structures. Over-steepened slopes ranging in height from approximately 1 m to 35 m are utilized in lieu of vertical faced walls, to enable use of on-site soils in construction, and to reinstate failed slopes.

Assumed Failure Planes

Different assumptions for location and geometry of critical potential failure planes are utilized for the three types of structures. Lateral sliding and rotational slip surface failure planes, as illustrated in Figure 1.a, are typically used in design of embankments over weak foundation soils (1, 2, 3, 4). The lateral sliding wedge failure plane is located at the weak foundation soil-geosynthetic or embankment soil-geosynthetic interface. The wedge length need not be defined if reinforcement remains constant across the embankment width. A critical rotational slip surface failure plane can be defined by analyzing the embankment with conventional slope stability

techniques. Circular and non-circular failure planes are utilized. The stabilizing effect of the geosynthetic reinforcement is typically calculated by assuming that the reinforcement provides a tensile force at its intersection with the failure surface. The critical slip rotational failure plane for an embankment over weak foundation soils is typically defined by analysis of the unreinforced embankment cross section (1,3,6,7), although more detailed methods of analysis have been presented (2, 5).

Geosynthetic reinforced soil retaining walls are typically designed assuming that a state of active Rankine lateral earth pressure develops (8,9,10), as illustrated in Figure 1.b. At-rest Rankine lateral earth pressures are used by others such as the USDA Forest Service (11). Concentrated loads, line loads, and sloping fill that affect the failure plane can be accounted for by analyzing random wedges of the unreinforced section to find the critical plane (9,10,12). Thus, the critical failure planes for a geosynthetic reinforced retaining wall are defined by analysis of the unreinforced structure.

Two different methodologies for locating the critical failure plane in limit equilibrium analysis of geosynthetic reinforced over-steepened slopes have generally been utilized. The first approach assumes that the critical failure plane is the same for both the unreinforced and reinforced slope as described by Christopher and Holtz (3), Tensar (13), and Koerner (14). This plane, as illustrated in Figure 1.c, is then utilized to determine the amount of reinforcement required to maintain internal stability. A failure external to the reinforced mass is then checked by examining sliding of the reinforced mass or rotational type failure behind and under the mass (Fig. 1.c). This method lends itself to the use of existing stability computer programs and addition of tensile reinforcement moment-righting contribution by hand calculations.

The second approach, which the authors have found to be more comprehensive, does not presume a critical failure plane for the reinforced section. Critical failure planes are located by a computerized search that directly includes the reinforcement force in the analysis. Internal, external, and compound (combination of internal and external) failure modes are examined with this approach.

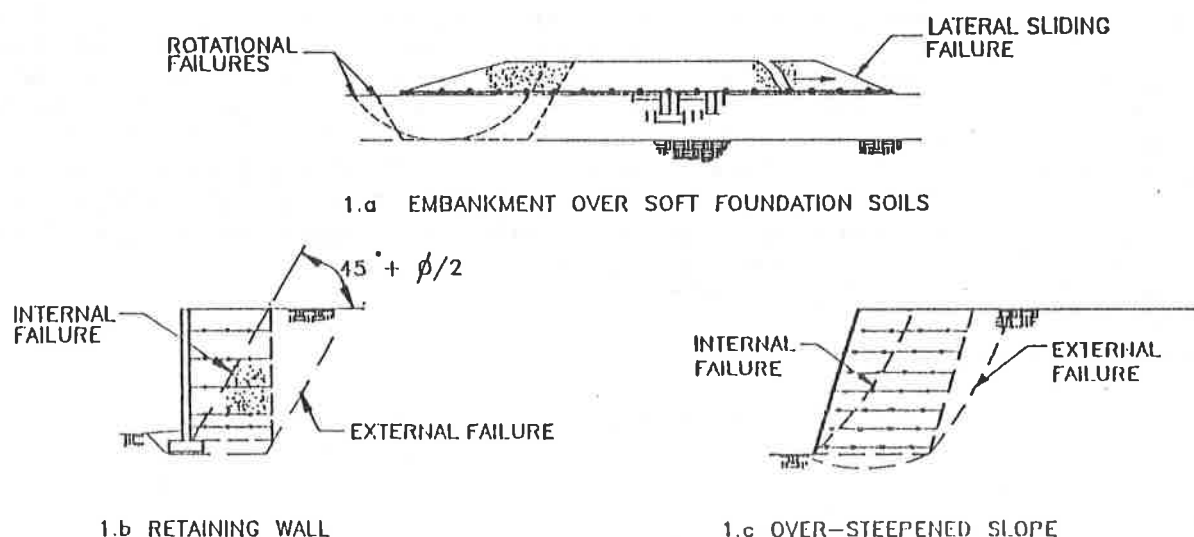


FIGURE 1: REINFORCED SLOPES & FAILURE PLANES
270

ANALYSIS OF OVER-STEEPENED SLOPES

Factors of Safety

Factors of safety utilized by geotechnical engineers in design of reinforced soil structures should vary on a project by project basis. The factor of safety should reflect: confidence in definition of soil shear strength and weight parameters; accuracy of analysis technique; breadth of geotechnical site investigation; life of structure; definition of long-term reinforcement strength; and criticalness of the structure. Potential loss of life and dollar loss usually define criticality. Factors of safety against slope instability of 1.3 to 1.5 are typical for static loading of unreinforced slopes. The same range of values is typically used for reinforced slopes, exclusive of safety factors on the long-term strength of the reinforcing material. The long-term reinforcement strength used in the analysis should account for creep, aging, and installation damage of the geosynthetic (14,15,16,17).

Failure Modes

What is the difference in potential failure mode(s) of conventional unreinforced slopes versus reinforced over-steepened soil slopes? Unreinforced slopes fail by sloughing and/or when the mass of a soil wedge exceeds the shear strength of the soil, as shown in Figure 2.a. In contrast, reinforced soil slopes have several potential failure modes. As illustrated in Figure 2, an over-steepened reinforced slope may fail by: exceeding the tensile capacity of the reinforcement elements and shearing of the reinforced soil fill (Fig. 2.b); reinforcement pullout (Fig. 2.c); exceeding the shear strength of the soils behind and beneath the reinforced mass (Fig. 2.d); exceeding the shear strength of the soils behind and within the reinforced mass (Fig. 2.e); and a combination of exceeding soil strength behind and within the reinforced mass and tensile failure of some of the reinforcement elements (Fig. 2.f).

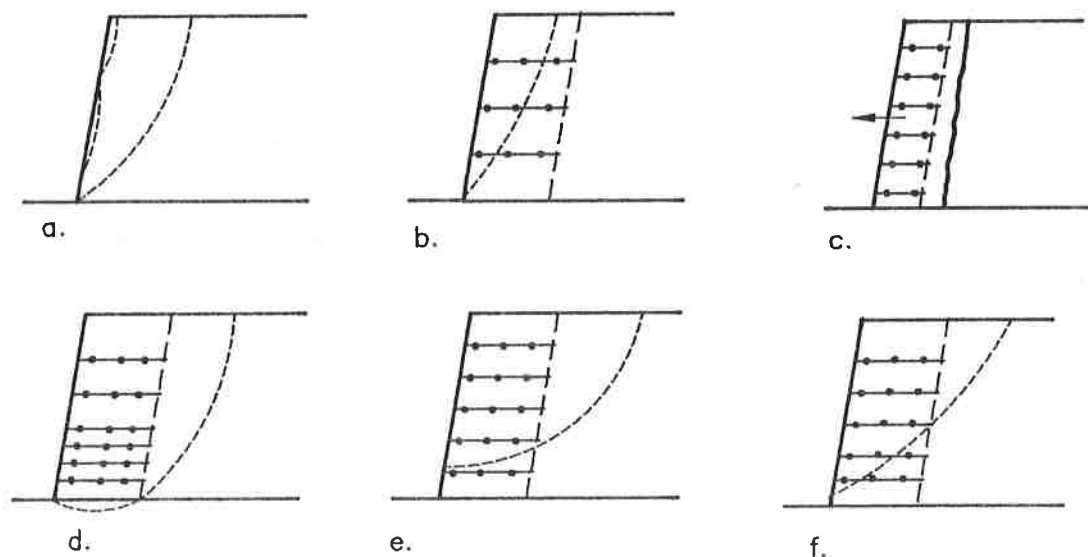


FIGURE 2 POTENTIAL FAILURE MODES OF REINFORCED SLOPES

Failure Plane Search

As described by Terzaghi and Peck (18) the critical plane in analysis of unreinforced slopes with circular failure planes may be located by plotting curves of equal values of factors of safety. These curves are drawn in the field of trial failure circle centroids. The curves, taken as contour lines of depression, identify the critical circle location as being at the bottom of the contour depression.

The necessity of plotting contours is even greater for reinforced slopes. Plotting is required whether the analysis is by hand or with a computer program that directly incorporates the effect of reinforcement. Slope stability programs typically include an option for a "random" search, beginning at one defined failure circle centroid, to locate the critical failure plane and an option to analyze an operator inputted range or area of failure circle centroids. With a "random" search pattern the program can lock onto only one of several possible critical failure planes. A specified search range may be too small to include all potential critical failure circle centroids. Also, a potential minimum within a "random" or specified search area may be overlooked if the search steps are too large. Plotting factors of safety graphically points out any areas overlooked in either option.

Two basic steps should be taken to comprehensively search for potential critical failure planes in over-steepened reinforced slopes. Firstly, computerized analysis which directly incorporates the effects of reinforcement should be used in the stability analysis. This is needed because critical failure planes differ between unreinforced and reinforced slopes, as illustrated in the following cases. Secondly, a contour plot of computed factors of safety within the field of failure circle centroids should be drawn. This plot aids in identifying additional potentially critical planes. The following generic and case history examples illustrate the need for comprehensive search in analysis of reinforced slopes.

GENERIC CASE

A generic slope, 15 m high, and at an angle of 1:1 is examined under various reinforcement schemes to illustrate changes in critical failure plane and factor of safety. Stability was analyzed using a Bishop's modified method of slices (19) adapted to account for the reinforcement (20). The adaptation involved adding an additional resisting moment into the overall moment equilibrium equation for each layer of reinforcement intersected by a considered slip surface. The resisting moment magnitude/increment depends on the reinforcing layer's elevation; orientation; percent coverage and embedment length beyond the slip surface.

The critical failure plane and contours of factors of safety for the unreinforced slope are presented in Figure 3. The reinforced case, designed for a factor of safety of approximately 1.5, with its factor of safety contours is presented in Figure 4. The final design also incorporated surficial reinforcement and erosion protection to prevent sloughing, as shown in Figure 5.a.

Varying the soil reinforcement in this example results in the following observations. An under-reinforced slope is illustrated in Figure 5.b. Halving the amount of reinforcement lowers the factor of safety from 1.49 to 1.07 and results in a different critical failure plane. Doubling the amount of reinforcement in the lower two-fifths of the slope results in an over-reinforced slope as illustrated in Figure 5.c. The critical failure plane is driven further back into the slope and the factor of safety increases from 1.49 to 1.64. A second potential critical failure plane is located in

the upper portion of the slope (Fig. 5.c). A reduction in reinforcement length of approximately 10 percent decreases the factor of safety from 1.49 to 1.34, as illustrated in Figure 5.d. An increase of reinforcement length of approximately 10 percent steepens the critical failure plane and increases the factor of safety from 1.49 to 1.53, as shown in Figure 5.e. Results from a variation in foundation soil strength are illustrated in Figure 5.f. The foundation soil strength was decreased and set equal to the slope soil strength. A deeper critical failure plane and a decrease in factor of safety from 1.49 to 1.41 were found.

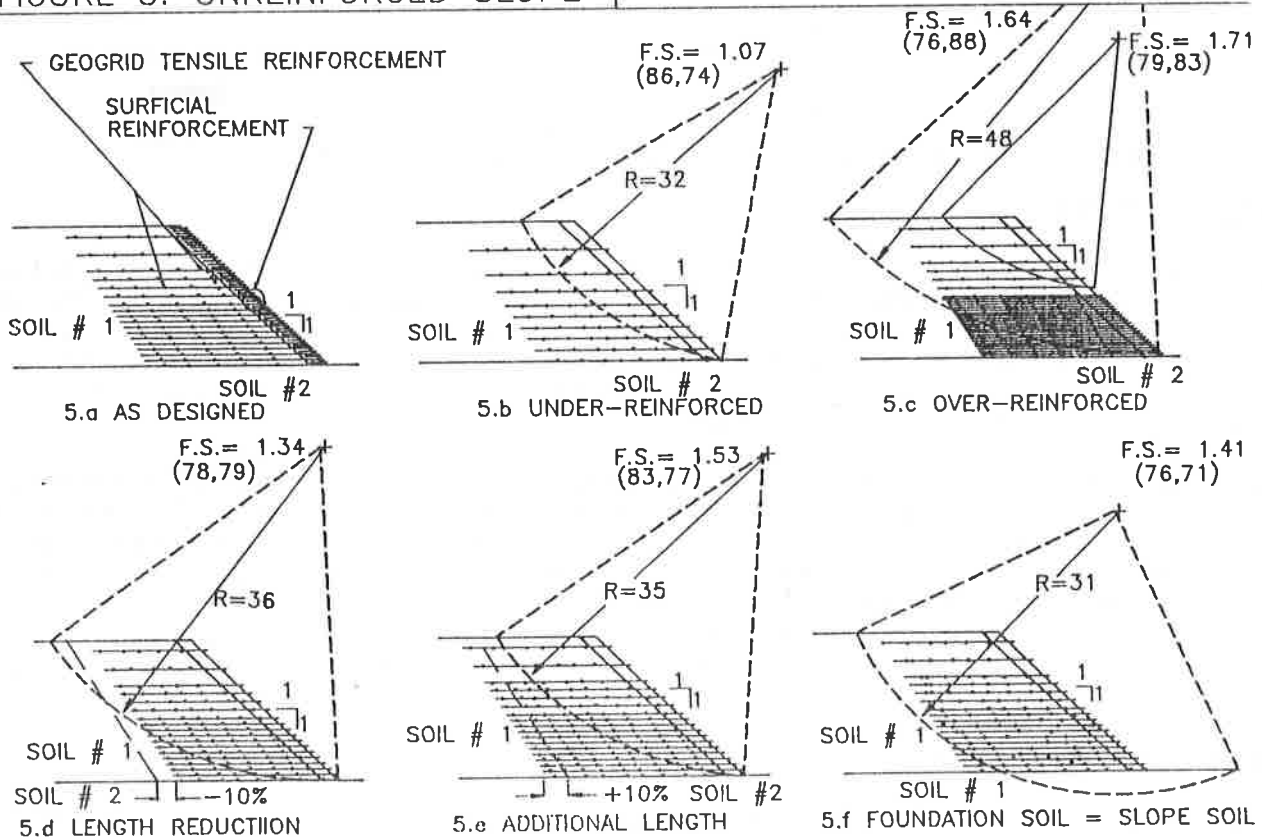
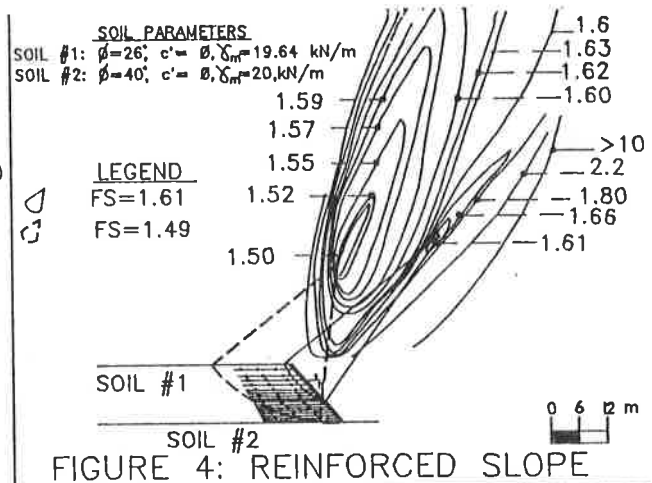
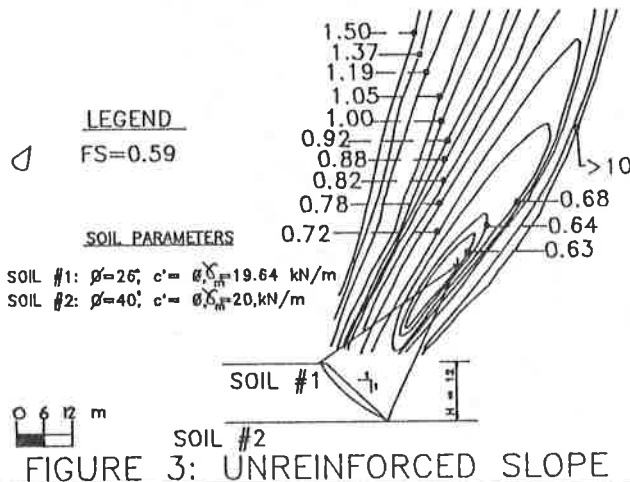


FIGURE 5: GENERIC CASE: VARIATIONS TO DESIGN

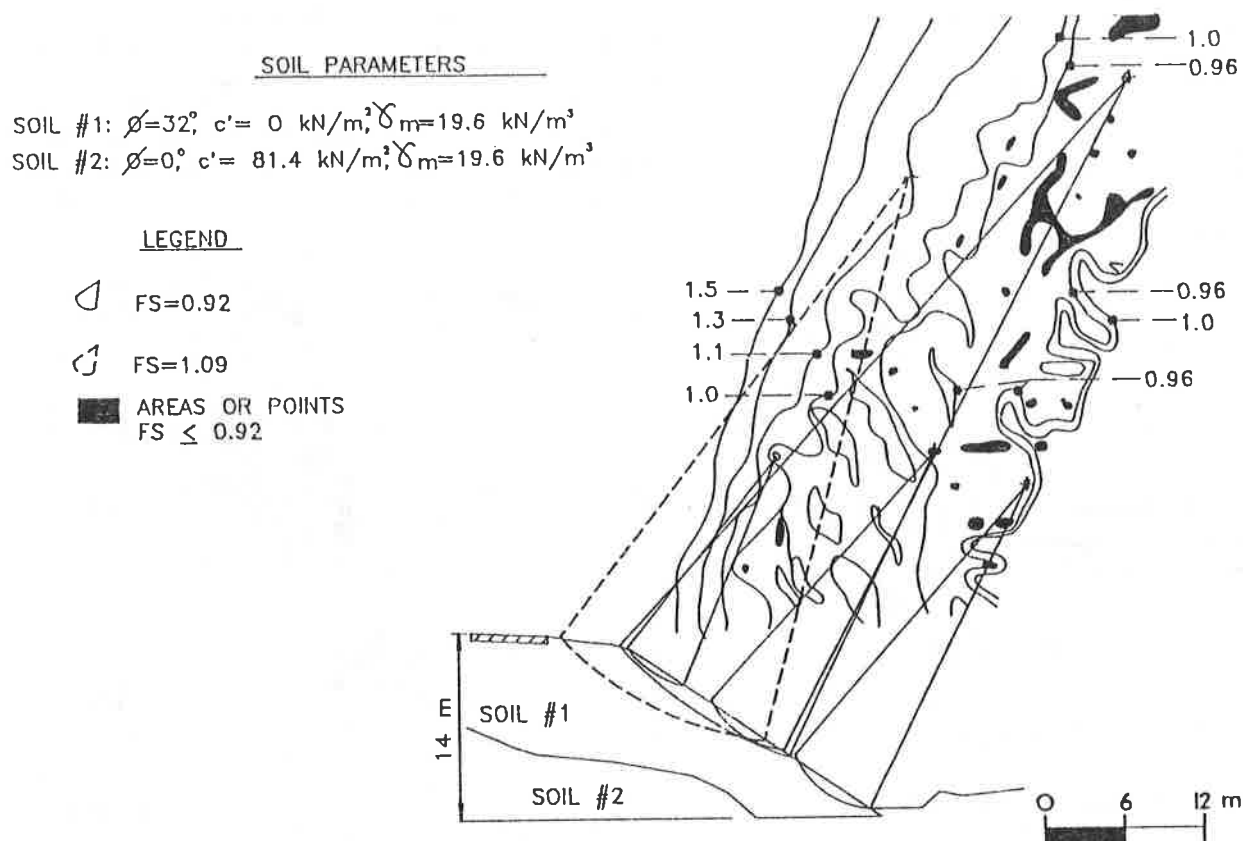


FIGURE 6: F.S. COUNTOURS FOR UNREINFORCED SLOPE

CASE HISTORIES

Two case histories are presented to illustrate the need to search for several potential minimum failure planes and the need to locate the critical failure plane by analysis of the reinforced section. A contour plot of factor of safety values and potential critical failure planes are shown for both the unreinforced and reinforced sections. A Bishop's modified method of slices adapted to incorporate the effects of reinforcement (20) was utilized in the analyses.

Uniaxial HDPE geogrids were utilized as primary reinforcing elements on these two projects. The long-term geosynthetic strength was defined on a basis of a minimum of 10,000 hour creep testing (16). Narrow, 1 to 1.5 m, widths of light-weight biaxial polypropylene geogrids were placed at the face between layers of primary reinforcement. This reinforcement facilitates soil compaction at the slope face and provides stability in the zone intermediate of primary layers. The addition of intermediate reinforcement and a thin cohesive surface soil layer to model erosion protection were used in both analyses.

Maryland Highway Slope

This project consists of approximately 152 lineal meters of 1.5H:1V over-steepened slopes ranging in height from 11 to 15 m. The reinforced embankment was more economical than retaining walls to keep the slopes within the highway right-of-way. The granular fill embankment rests upon clayey foundation soils and will carry a four-

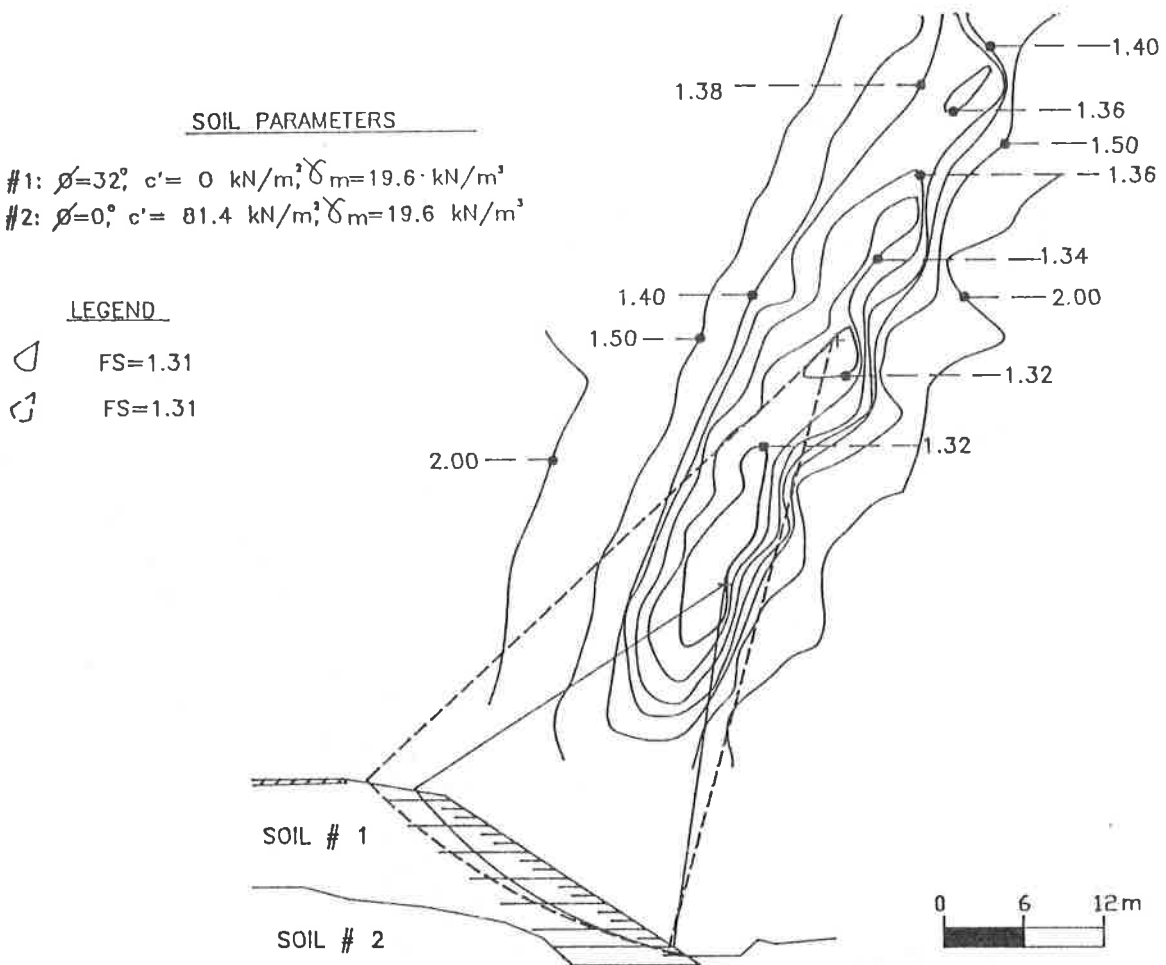


FIGURE 7: F.S. CONTOURS FOR REINFORCED SLOPE

lane highway. The soil properties used for design are noted on the figures. The water table was assumed to be at the top of the foundation soil. A surcharge of 12 kN/m² was used to model traffic loading.



The critical failure mode for the unreinforced section is surficial sloughing. This is due to the slope angle of 33.7° being slightly larger than the soil's angle of repose of 32°. Several zones of failure circle centroids with factors of safety of 0.92 or less were found, as shown in Figure 6. The addition of intermediate reinforcement at the slope face increased the minimum factor of safety to 0.94. The increase is small because the shallow cover of soil over the reinforcement does not provide a sufficient normal load to fully mobilize its long-term design strength. Addition of a cohesive layer to the face of the slope to model erosion protection results in a factor of safety of 1.09, with the critical circle passing behind the surficial reinforcement elements.

Contours obtained for the reinforced configuration used to achieve a factor of safety of 1.3 are illustrated in Figure 7. The critical circle passes through all but the uppermost of the primary reinforcing geogrids. It should be noted that the final design contours show two potential locations of the critical circle centroid. The factor of safety in the two localized minimums are both 1.31.

SOIL PARAMETERS

SOIL #1: $\phi' = 38^\circ$, $c' = 0$ kN/m², $\gamma_M = 21$ kN/m³
 SOIL #2: $\phi' = 24^\circ$, $c' = 5$ kN/m², $\gamma_M = 21$ kN/m³
 SOIL #3: $\phi' = 26^\circ$, $c' = 5$ kN/m², $\gamma_M = 21$ kN/m³

LEGEND

 FS=0.90
 FS=1.00

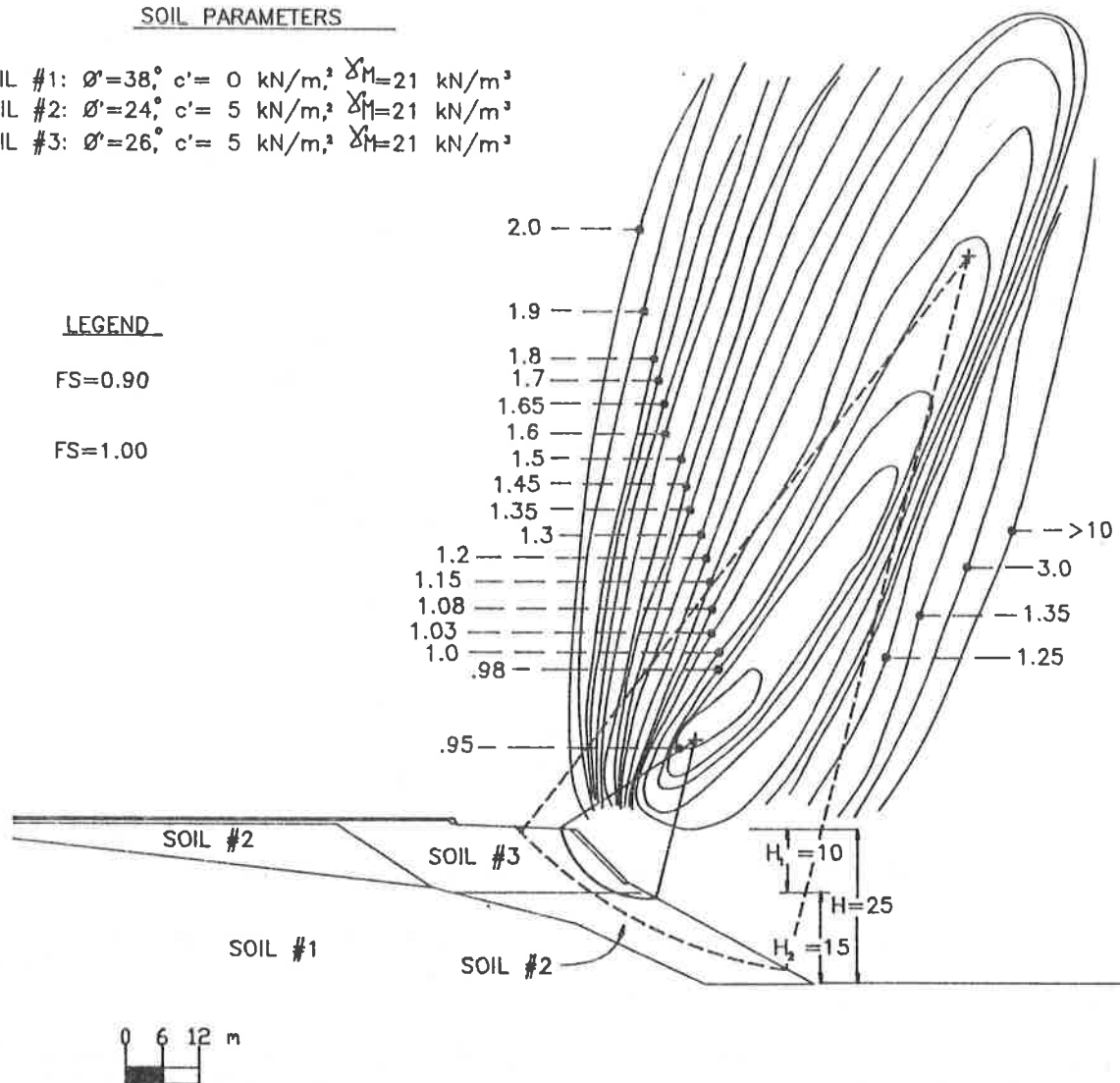


FIGURE 8: F.S. CONTOURS FOR UNREINFORCED SLOPE

Pennsylvania Commercial Site

An over-steepened reinforced slope was used to create more area on a marginal site near Pittsburgh, Pennsylvania for a retail store. The site had an existing 1.9H:1V slope that dropped 11 m from the middle of a proposed parking area. An originally proposed 20 m high retaining wall was changed to a reinforced slope because of global stability concerns created by weak foundation soils. Soil borings indicated the presence of 1 to 11 m of loose silty clay and silt fill under the proposed structure. The critical failure plane and contours of factors of safety for the unreinforced slope are presented in Figure 8. The existing weak fill that controls stability is listed

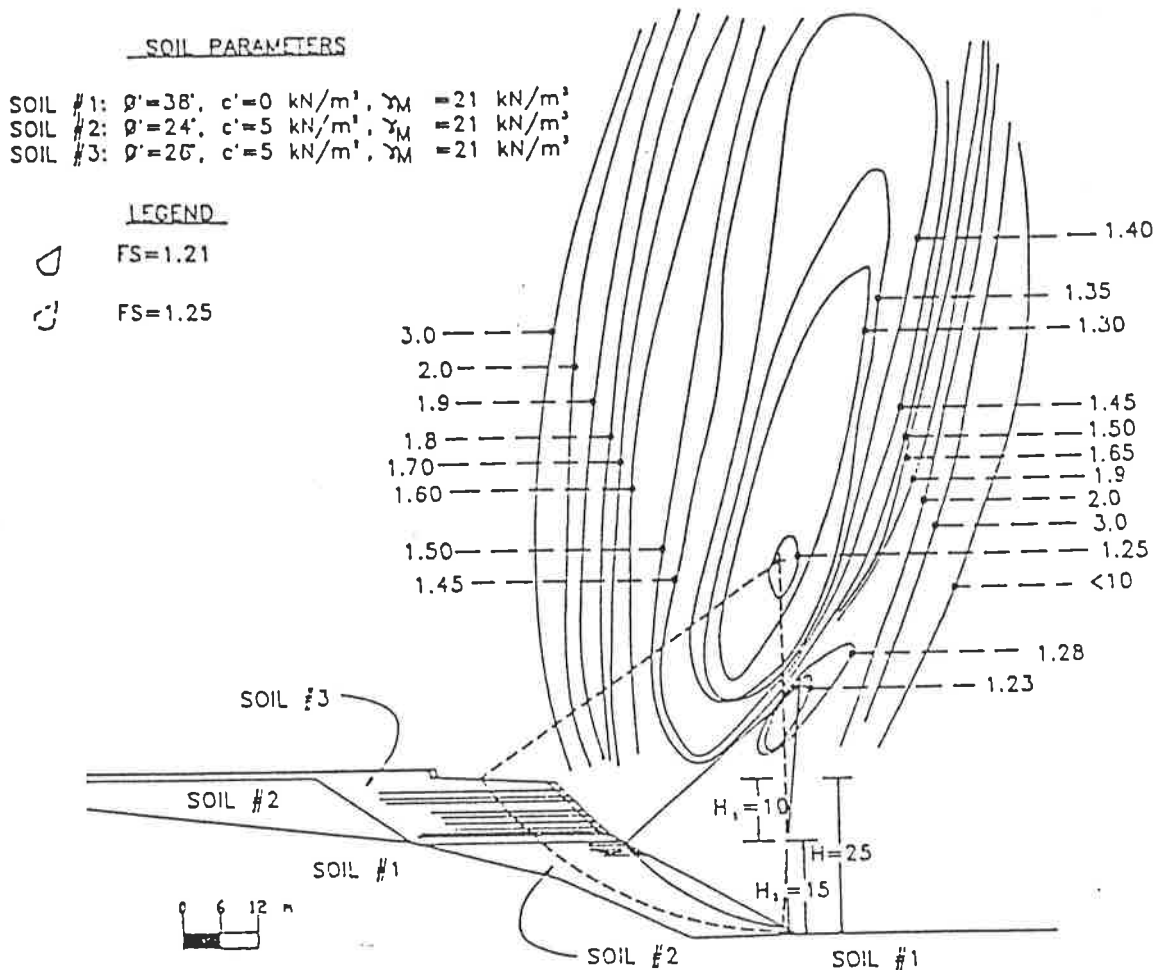


Figure 9: F.S. CONTOURS FOR REINFORCED SLOPE

as Soil #2 on the figure. Primary reinforcement, intermediate reinforcement and erosion protection were used to achieve a factor of safety of 1.25.

Analysis of the slope was carried out considering circular failure surfaces passing through, under, and behind the reinforced soil mass. The 15 m high slope beneath the 10 m 1H:1V slope complicated this analysis. Two localized factor of safety minimums were located by plotting contours, as illustrated in Figure 9. The reinforcement layout was designed to provide the minimum required factor of safety at each localized area. The critical failure planes are also shown on Figure 9.

DISCUSSION

As illustrated in Figures 3 and 4; 6 and 7; and 8 and 9, the critical failure plane for a given unreinforced slope is not necessarily the critical failure plane for a reinforced slope. In fact, the critical failure plane of the reinforced slope can change significantly as illustrated in Figure 5. No attempt was made to parametrically study the differences in failure plane locations. There are several additional items that the geotechnical design engineer should be cognizant of when designing reinforced soil structures that were not addressed within the scope of this paper. These items include: non-circular failure planes; method of incorporating reinforcement force into slope stability analysis equations; differences in critical failure planes for unreinforced and reinforced embankments over weak foundations; analysis of vertical wall/slope combinations; and definition of long-term geosynthetic strength.

CONCLUSIONS

Based upon the limited cases presented it is concluded that:

1. It can not necessarily be assumed that the critical failure plane for a reinforced slope is the same as for the unreinforced slope.
2. Stability analyses of reinforced slopes should directly account for reinforcement effects in the computations.
3. There are several more types of possible failure mechanisms for a reinforced slope than for an unreinforced slope.
4. Contours of factor of safety values should be plotted in the field of failure circle centroids to locate zones of potential critical failure plane centroids.

REFERENCES

- (1) Haliburton, T.A., Lawmaster, J.D. and McGuffey, V.C., "Use of Engineering Fabrics in Transportation Related Applications", Report to FHWA under Contract No. DTFH-80-C-0094, 1982.
- (2) Jewell, R.A., "A limit Equilibrium Design Method for Reinforced Embankments on Soft Foundations", Proceedings of the Second International Conference on Geotextile, Las Vegas, Vol. 3, 1982, pp. 671-676.
- (3) Christopher B.R. and Holtz, R.D., "Geotextile Engineering Manual, Course Text", Federal Highway Administration, Washington, D.C, 1985.
- (4) Bonaparte, R., and Christopher, B.R., "Design and Construction of Reinforced Embankments Over Weak Foundations," presented at the Symposium on Reinforced Layered Systems, Transportation Research Board Meeting, Washington D.C., January, 1987.
- (5) Bonaparte, R., Holtz, R.D. and Giroud, J.P., "Soil Reinforcement Design Using Geotextiles and Geogrids," Geotextile Testing and the Design Engineer, ASTM STP 952, J.E. Fleet, Jr., Ed., American Society for Testing and Materials, Philadelphia, 1987.

Geosynthetics '89 Conference
San Diego, USA

- (6) Broms, B.B., "Polyester Fabric as Reinforcement in Soil." Proceedings of the International Conference on the Use of Fabrics in Geotechnics, Paris, Vol. I, 1977, pp. 129-135.
- (7) Wager, O., "Building of a Site Road Over a Bog at Kilanda, Alvsborg County, Sweden, in Preparation for Erection of Three 400kv Power Lines." Report to the Swedish States Power Board, AB Fodervavnader, Boras, Sweden, 1981, pp. 16
- (8) Bell, J.R., Stilley, A.N., and Vandre, B., "Fabric Retained Earth Walls", Proceedings of the 13th Annual Engineering Geology and Soils Engineering Symposium, Moscow, Idaho, 1975.
- (9) Jones, C.J.F.P., Earth Reinforcement and Soil Structures, Butterworths Advanced Series in Geotechnical Engineering, London, 1985.
- (10) Tensar, "Tensar Technical Note: Guidelines for Design of Tensar Geogrid Reinforced Soil Retaining Walls." The Tensar Corporation, Morrow, Georgia, August, 1986.
- (11) Foundation Sciences, Inc., "Retaining Wall Design Guide," prepared for USDA Forest Service, Region 6, Contract No. 006702N, December, 1979.
- (12) Netlon, Ltd., "Guidelines for the Design & Construction of Reinforced Soil Retaining Walls Using TENSAR Geogrids," Blackburn, England, 1984.
- (13) Tensar, "Designing with TENSAR," The Tensar Corporation, Morrow, Georgia and Toronto, Canada, 1982, pp. 17.
- (14) Koerner, R.M., Designing with Geosynthetics, Prentice-Hall, Englewood Cliffs, NJ, 1986.
- (15) Bonaparte, R. and Berg, R.R., "Long-Term Allowable Tension for Geosynthetic Reinforcement," Proceedings of the Geosynthetics '87 Conference, New Orleans, February, 1987.
- (16) Wrigley, N.E., "Durability and Long-Term Performance of Polymer Grids for Soil Reinforcement," Materials Science and Technology, Vol. 3, The Institute of Metals, March, 1987.
- (17) Shelton, W., and Wrigley, N.E., "Long-Term Durability of Geosynthetic Soil Reinforcement", Proceedings of the Geosynthetics '87 Conference, New Orleans, February, 1987.
- (18) Terzaghi, K. and Peck, R.B., Soil Mechanics in Engineering Practice, 2nd Edition, John Wiley & Sons, New York, 1987.
- (19) Bishop, A.W., "The Use of the Slip Surface in the Stability Analysis of Slopes", Geotechnique, Vol. 5, 1955.
- (20) Tensar, "TENSLO1; Slope Stability Program," Internal Program, The Tensar Corporation, Morrow, Georgia, 1985.

J.R. VERDUIN

Hart-Crowser, Inc., U.S.A.

R.D. HOLTZ

University of Washington, U.S.A.

Geosynthetically Reinforced Slopes: A New Procedure

SUMMARY

The paper presents a simple but practical method for the design of slope reinforcement with geosynthetics. A circular failure surface is assumed, and surcharges and pore pressures can be taken into account. Any convenient method of analysis of the unreinforced slope can be used as long as the coordinates of the slip circle and the safety factor of the unreinforced mass are known. Conventional construction practices including site location, foundation stability, geosynthetic spacing, and project budget can be appropriately considered. Three reinforcement conditions are possible: 1) equal number and strengths of reinforcement layers in the top and bottom portions of the slope; 2) different number and strengths of reinforcement in the top and bottom of the slope, and 3) an equal number but different strength reinforcement layers in the top and bottom of the slope. Design for both sliding and pullout are considered. The design procedure can easily be programmed. An example problem is presented.

INTRODUCTION

The stability of unreinforced slopes is generally controlled by the shear strength of the soil in the slope and the slope angle. Slopes of cohesionless materials are usually stable up to slope angles of 30° to 35°, while the maximum stable slope for compacted cohesive soils is typically 26°. If designs require steeper slopes, then reinforcement is needed.

This paper describes a simple slope reinforcement design procedure, in which multiple layers of geosynthetic reinforcement are used to increase the stability of potentially unstable new construction or for the reparation of failed slopes.

Characteristics of the Procedure

- ° No complex iteration required
- ° Circular failure surfaces with a choice of design safety factor
- ° Pore pressures and surcharges considered
- ° Variable soil types
- ° Choice of lift thicknesses
- ° Design for pullout included

Scope

The procedure is based on the following construction practices and observed performance:

- ° Reinforced slopes consist of relatively homogeneous soils since they are usually remolded and compacted;
- ° Variable lift thicknesses are generally impractical;
- ° When geosynthetically reinforced slopes fail, they mainly do so in their lower third (3); and
- ° Site location and project budgets often affect the reinforcement selection as much as the slope geometry and soil conditions at the site.

It is assumed that the foundation of the slope has adequate sliding resistance and is stable with respect to bearing capacity.

The design of geosynthetic reinforcement involves determining: 1) additional tensile force required for overall stability, 2) geosynthetic tensile strength required by each layer, and 3) reinforcement length required to resist pullout.

DESIGN PROCEDURE

Unreinforced Slope Stability

The procedure is based on moment equilibrium, not force equilibrium; thus it is only applicable to circular failure surfaces. The first step of the procedure is to determine the critical slip circle of the unreinforced slope. The following information is needed: 1) centroid, 2) factor of safety, and 3) resisting moment of the critical sliding mass. The first two items can be easily obtained from common slope stability analyses, and the last item can be obtained using graphical methods.

Surcharges and pore pressures within the slope environment can also be considered, provided the procedure used for the analysis of the unreinforced slope has these capabilities. The resisting moment also needs to reflect any additional surcharge and pore pressures.

Additional Tensile Force Required for Stability

With geometric and soil characteristics of the failure surface known, the additional tensile force (ΣT) needed for stability can be calculated from:

$$FS_{wg} = \frac{M_R + R \Sigma T}{M_D} \quad \text{and} \quad FS_{wog} = \frac{M_R}{M_D}$$

So

$$\Sigma T = \frac{FS' M_R}{FS_{wog} R} \quad (1)$$

where FS_{wog} = factor of safety without geosynthetic reinforcement,
 FS' = increase in factor of safety desired ($FS_{wg} - FS_{wog}$),
 FS_{wg} = factor of safety with geosynthetic reinforcement,
 M_R = resisting moment of unreinforced mass, and
 R = radius of critical failure circle.

Equation 1 is based on conventional limiting equilibrium principles, and a detailed derivation is given in (12). This equation neglects any resistance the geosynthetic may provide normal to the slip surface. As shown in Fig. 1, the increase in normal force along the slip surface produced by the geosynthetic is $T \sin \alpha$ while the tangential force is $T \cos \alpha$, where T is the geosynthetic tensile force.

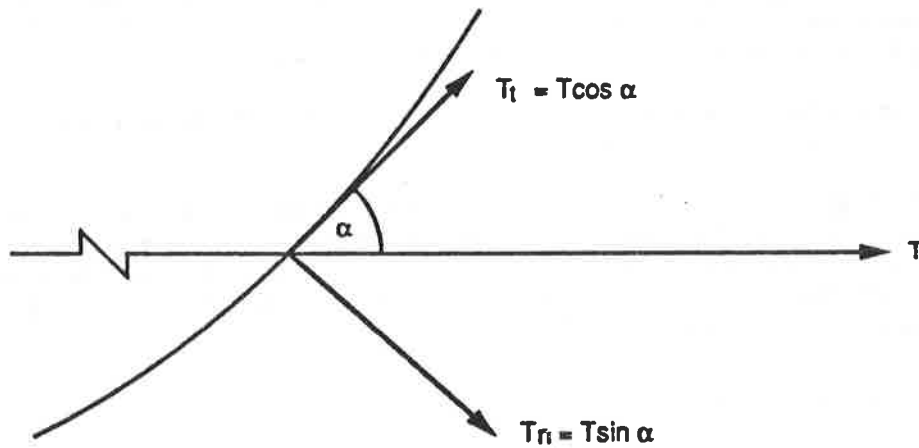


Figure 1. Components of Reinforcing Force

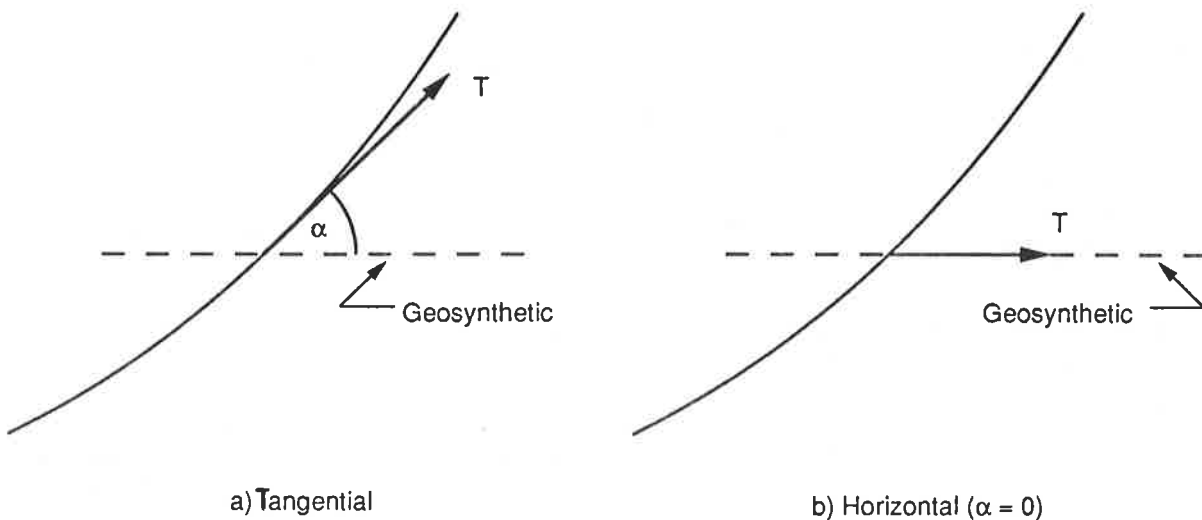


Figure 2. Reinforcing Force Orientation

To evaluate the effect of a possible increase in normal stress on the potential slip surface, two extremes of geosynthetic force orientation are shown in Fig. 2; they range from tangential to the slip surface ($\alpha > 0$) to horizontal ($\alpha = 0$). The assumption of a tangential geosynthetic force produces the lowest tensile forces required for stability, while assuming the geosynthetic force to be horizontal will produce the highest force. For example, Humphrey (5) assumed that the geosynthetic provides only a resisting moment or force and does not increase the normal stresses on the slip surface. On the other hand, Jewell (6), Murray (9), Schneider and Holtz (11), and Schmertmann, et al. (10) considered the increase in normal stress on this surface. In fact, Schmertmann, et al. (10) arbitrarily assumed that the geosynthetic force is inclined at 0.25α . Bonaparte and Christopher (2) concluded that "the orientation of the reinforcement at failure will depend on a number of factors including the load-deformation characteristics of the reinforcement, its flexural rigidity, and the stress-strain characteristics of the embankment-foundation system." Accurately determining these factors is beyond the scope of this paper. Because no information exists as to the actual inclination in the field, we have assumed the geosynthetic force to be horizontal and acting in the plane of the geosynthetic. This assumption produces the most conservative value of the force.

To account for the increase in normal stress produced by the geosynthetic, the total tensile force in Eq. 1 was modified as follows:

When α is 45° or greater, it is assumed that the normal force equals the tangential force. This assumption becomes more conservative as α increases, because $\sin \alpha > \cos \alpha$ for $\alpha > 45^\circ$. Two other ranges for α [$\alpha < 25^\circ$ and $25^\circ < \alpha < 45^\circ$] and their corresponding total tensile force modifications are similarly defined below. These ranges are arbitrary but conservative. Equation 2 gives these modifications to the total tensile force.

$$\text{For } \alpha \geq 45^\circ: \Sigma T' = \frac{\Sigma T}{1 + \tan \phi} \quad (2a)$$

$$\text{For } 25^\circ < \alpha < 45^\circ: \Sigma T' = \frac{\Sigma T}{1 + 0.5 \tan \phi} \quad (2b)$$

$$\text{For } \alpha < 25^\circ: \Sigma T' = \frac{\Sigma T}{1 + 0.35 \tan \phi} \quad (2c)$$

The actual α value depends on the location of the critical surface and slope geometry or:

$$\alpha = \cos^{-1} \left(\frac{Y_0 - H/3}{R} \right)$$

where Y_0 = the vertical distance between the centroid of the critical slip surface and the bottom of the slope (y_{ob} in Fig 3).

Geosynthetic Tensile Strength Required Per Layer

With the knowledge of the additional tensile force needed for stability, the individual geosynthetic strengths can now be determined. In order to give maximum flexibility, three different reinforcing options are available. The first allocates the same geosynthetic spacing and strength throughout the slope. Option No. 2 enables the designer to control both the geosynthetic spacing as well as the strength in the upper and lower halves of the slope. In the third option the geosynthetic spacing is constant throughout, but the designer can select different strength geosynthetics in the top and bottom portions of the slope.

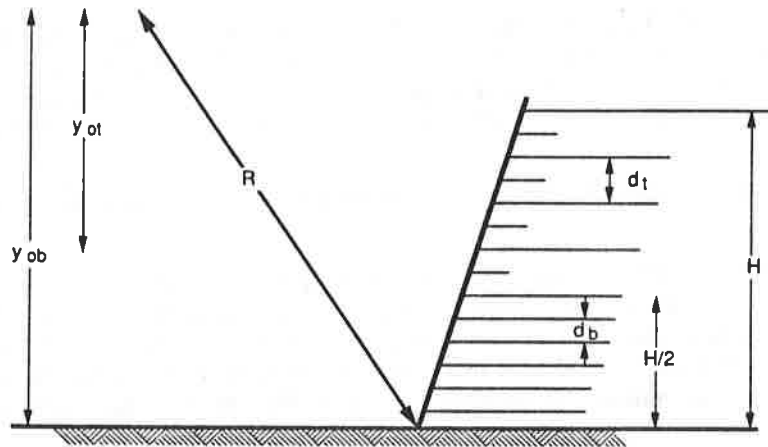


Figure 3. Reinforcement Definitions

The geosynthetic strengths required in the upper layers (T_u) and in the lower layers (T_ℓ) of the slope are determined by Eqs. 3 and 4, respectively. Each equation is modified accordingly for the three options.

$$T_u = \frac{(1 - \text{Percent})(\Sigma T')(R)}{nfl_t(y_{ot}) - d_t[\Sigma(nfl_t)]} \quad (3)$$

$$T_\ell = \frac{(\text{Percent})(\Sigma T')(R)}{nfl_b(y_{ob}) - d_b[\Sigma(nfl_b)]} \quad (4)$$

where Percent = percent of force desired in lower portion of slope;

$$y_{ot} = Y_0 - H/2$$

$$y_{ob} = Y_0$$

$$R = \text{radius of critical circle}$$

$$\Sigma T' = \text{total tensile force required for stability}$$

$$nfl = \text{number of fabric layers (t=top, b=bottom)}$$

$$d = \text{spacing between layers (t=top, b=bottom)}$$

A detailed derivation of Eqs. 3 and 4 can be found in (12)

Option One - Same Spacing and Strengths: - If the designer finds that only one geosynthetic type and spacing will be the most practical, Eq. 4 is used with the following modifications:

$$\text{Percent} = 100\% \text{ and } nfl_b = n_b - 1$$

where T_ℓ in Eq. 4 is the geosynthetic strength for all the layers, and $n_b = H/d_b$ (rounding up to next whole number).

Option Two - Different Spacings and Strengths: - If the slope is higher than 10 to 15 m, it usually is feasible to consider two different strength geosynthetics and spacings. Because studies indicate that geosynthetically reinforced slopes fail mostly in the lower third of the slope (3), it seems prudent to increase the amount of reinforcement in the lower portion of the slope.

Fig. 3 illustrates the assumed reinforcement configuration for Option Two.

There are two different lift thicknesses, one in the top half of the slope (d_t) and one in the bottom half (d_b). From a construction standpoint this is more practical than varying the geosynthetic spacing continuously throughout the embankment. It is evident that the number of geosynthetic layers in the bottom nfl_b equals the number of lifts in the bottom (n_b), while the number of geosynthetic layers in the top (nfl_t) equals one minus the number of lifts in the top (n_t). Key relations include:

$$\begin{aligned} d_t/d_b &= n_t/n_b = X \\ n_t &= \frac{H}{2(X)d_b} \\ nfl_b &= n_b; nfl_t = n_t - 1 \end{aligned}$$

where X is the ratio of the number of top layers to bottom layers.

The percent of total reinforcement force in the bottom half should range from 60% to 80%. With more than this amount, the top half may become unstable. Since cost is roughly proportional to tensile strength, it is generally cost effective to have more, lower tensile strength geosynthetic layers in the bottom, and fewer, higher tensile strength geosynthetic layers in the top. Sometimes geosynthetic selection may be limited by availability or construction costs to only one type and therefore one strength geosynthetic. For this situation, the percentage of reinforcement in the bottom giving similar T_u and T_ℓ values (Eqs. 3 and 4) should be used. The higher of the two strengths (T_u or T_ℓ) should be used for both.

Option Three - Same Spacings, Different Strengths: If the same geosynthetic spacing in both the upper and lower halves of the slope but with different strengths is desired, the same procedure as above is used with the following modifications:

$$d_t = d_b, n_t = H/(2d_b), \text{ and } n_b = n_t$$

Then Eqs. 3 and 4 are used as before.

- - - - -

Often the calculated number of geosynthetic layers (nfl_t and nfl_b) is not an integer. Then the required strength per layer is determined using these fractional values in Eqs. 3 and 4. The number of geosynthetic layers in the bottom is rounded up to the next whole number. After the geosynthetic strengths and their respective spacings are determined, the reinforcement locations can now be finalized from the foundation up, as shown in Fig. 3. The thickness of soil at the very top of the slope might be less than d_t in some cases, which is satisfactory unless it produces construction problems. Depending on d_t , short geosynthetic strips 1 to 2 m long may be needed midway in the upper lifts to help in compaction of the slope edges (see Fig. 3). The strength of these strips does not contribute to stability.

Geosynthetic Spacing Guidelines

In designing slope reinforcement, it is usually best that the reinforcement spacing be specified to be at some convenient multiple of typical compaction lift thicknesses, say 150 mm to 300 mm, which are appropriate for the backfill soil under consideration. When weaker geosynthetics are used, smaller lift thicknesses may be selected; with stronger reinforcement, thicker spacings are generally more economical, although they may require temporary support of the facing during construction. Even with temporary supports, thicker lifts may be more economical overall because of reduced construction time. The most economical designs should, of course, consider construction as well as material costs.

LENGTH OF GEOSYNTHETIC REINFORCEMENT

The length of geosynthetic in the upper and lower portions of the slope is controlled by two different conditions. The upper geosynthetic layers have to be sufficiently embedded into the slope to ensure that sufficient resistance is mobilized to develop the required individual geosynthetic forces. This is critical in the upper part of the slope, because the confining stress is less due to lower overburden stress. On the other hand, the geosynthetic layers in the bottom of the slope have to be long enough so that they produce enough resistance to prevent sliding. Schmertmann, et al. (10) use a similar concept.

Mobilized Resistance

The procedure for determining geosynthetic lengths in the upper half of the slope considers the length of geosynthetic required to mobilize the needed individual geosynthetic strengths. The traditional model (Fig. 4a) used for pullout length selection assumes that the mobilized resistance is uniform and equal to $2\tau_{\max}$ along the geosynthetic (4). This model requires either the same initial uniform displacement at every point on the geosynthetic or large geosynthetic movements at all points on the geosynthetic (approaching ultimate resistance). Because the geosynthetic is extensible and confined, the magnitude of local movements at different points along the geosynthetic will probably never be the same. Therefore, mobilized resistance will also never be the same, but will decrease with distance from the critical slip surface.

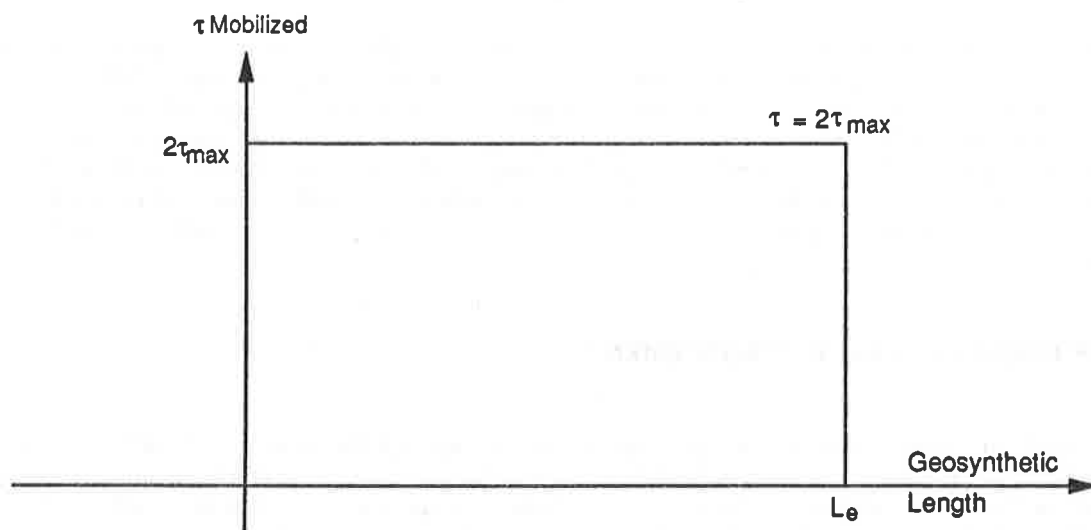
Beech (1) developed a procedure for predicting the pullout tension (which is a function of the resistance) as a function of the geosynthetic displacement. Fig. 4b shows the model we used, which is a generalization of the curves in Beech (1). It considers the mobilized shear strength to attenuate linearly from a maximum at the critical surface to zero at the end of the geosynthetic. Equation 5 is derived by setting the area under the curve equal to the required individual geosynthetic strengths (T); or

$$L_e = \frac{T}{\tau_{\max}} \cdot FS \quad (5)$$

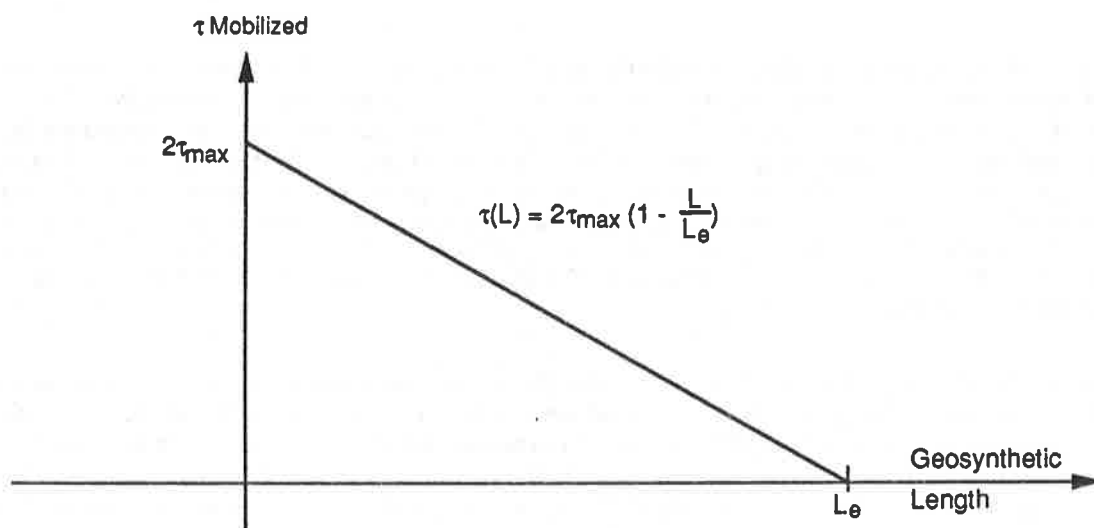
where L_e = length of geosynthetic extending beyond assumed failure surface

τ_{\max} = maximum mobilized shear strength = $\sigma_n \tan \phi_{SG}$

σ_n = overburden stress at the elevation of the geosynthetic,



a) Traditional Model



b) Proposed Model

Figure 4. Mobilized Resistance Models

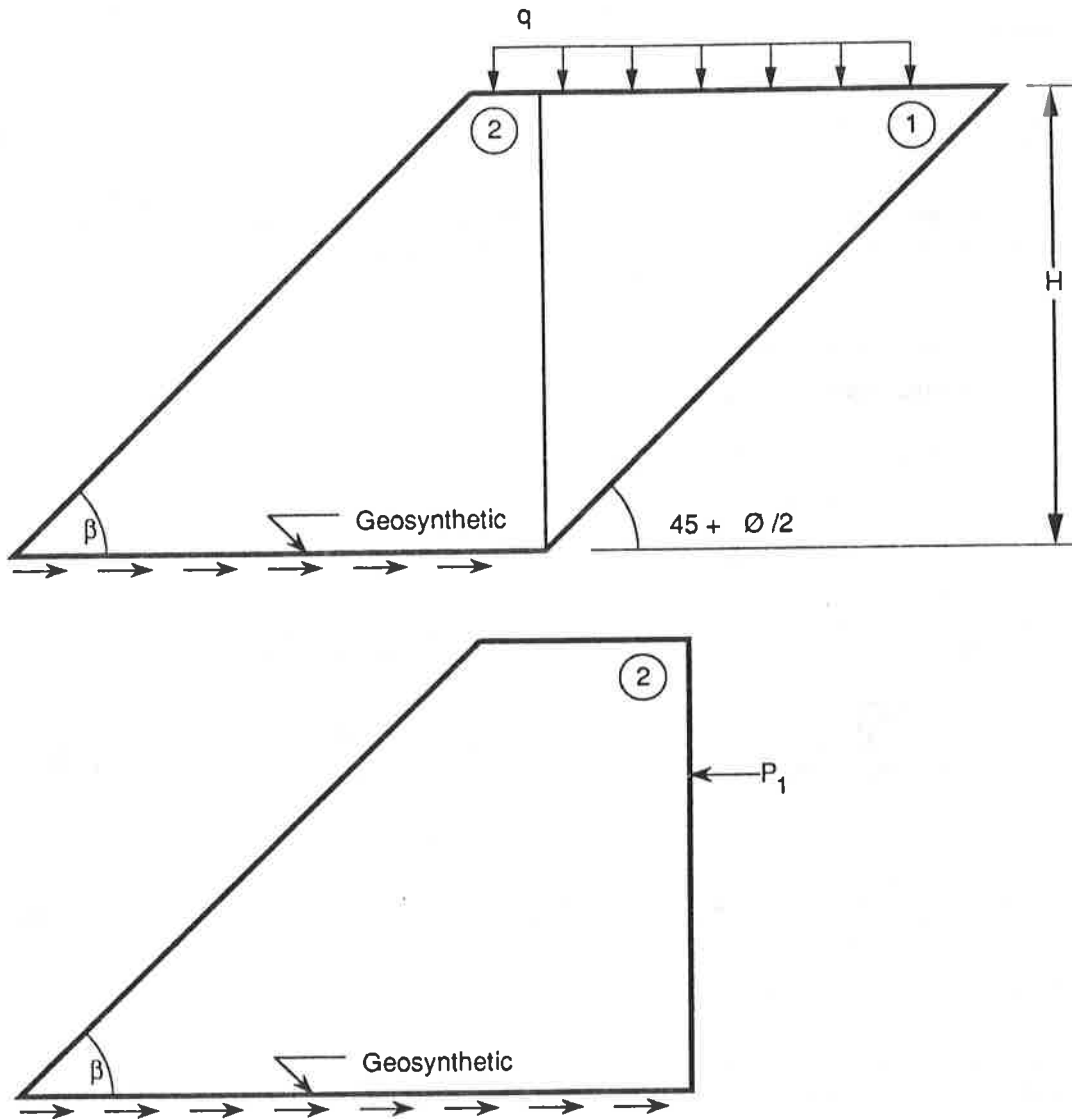


Figure 5. Sliding Block Model

ϕ_{SG} = soil-geosynthetic friction angle.

The factor of safety (FS) against pullout is required because of uncertainty in the maximum mobilized shear strength. Selection of the safety factor, therefore, depends on the designer's confidence in the value of this strength and how critical the slope is with respect to a potential failure. The soil-geosynthetic friction ϕ_{SG} is influenced by both the soil and geosynthetic, and it can be estimated from the literature (7,8). A geosynthetic with openings similar to the soil particle sizes will have higher soil-geosynthetic friction values, while geosynthetics which do not interlock well will obviously have lower friction.

Sliding Resistance

The geosynthetic layers lower in the slope should be analyzed for possible sliding. As seen in Fig. 5, the model used for this analysis divides the slope into two blocks. The first block is an active wedge, which pushes against the second wedge with a force P_1 . This force is assumed to act horizontally. The second wedge offers resistance in the form of friction at the soil-geosynthetic interface. By balancing the capacity and demand, geosynthetic length determination is computed by Eqs. 6:

$$P_1 = \frac{wt + \text{surch} - coh}{1 + \tan\phi \tan(45^\circ + \phi/2)}$$

$$\text{where } wt = [\frac{1}{2}H^2\gamma \tan(45^\circ - \phi/2)][\tan(45^\circ + \phi/2) - \tan\phi]$$

$$\text{surch} = q[H - \frac{H \tan\phi}{\tan(45^\circ + \phi/2)}]$$

$$coh = \frac{cL_1}{\cos(45^\circ + \phi/2)}$$

$$L_1 = \frac{H}{\sin(45^\circ + \phi/2)}$$

$$L = \sqrt{\frac{2P_1FS}{\gamma \tan\beta \tan\phi_{SG}}}$$

$$L_T = \frac{H}{\tan\beta} \quad (6a)$$

If $L > L_T$:

$$L = \frac{P_1FS}{H\gamma \tan\phi_{SG}} + \frac{L_T}{2} \quad (6b)$$

where the symbols are defined in Fig. 5.

The safety factor for pullout is based on the uncertainty of the resistance developed at the soil-geosynthetic interface as well as the driving force. Again, selection of the factor of safety depends on the designer's confidence in the soil-geosynthetic interface behavior and how critical the slope is.

Geosynthetic Lengths - Intermediate Layers

The lengths of intermediate geosynthetic layers are linearly interpolated between the length of the bottommost layer (designed against sliding) and the length of the top layer (designed against pullout).

CONCLUDING REMARKS

The design procedure presented herein can easily be programmed for use on microcomputers and a copy is available from the authors.

EXAMPLE PROBLEM

- o A slope stability program identified the critical failure surface:

$$(X_o, Y_o) = (-46.1, 95.1) \quad R = 105.7 \text{ ft} \quad FS = 0.73.$$

- o The resisting moment was found to be 2,534,400 lb-ft.

- o Equation 1 gives the Total Tensile Force required for stability (FS=1.5):

$$IT = \frac{(1.5 - 0.73)(2534400 \text{ lb-ft})}{(0.73)(105.7 \text{ ft})} = 25,290 \text{ lb/ft-width}$$

- o Equation 2b gives the modified Total Tensile Force:

$$IT' = \frac{(25,290 \text{ lb/ft})}{(1 + 0.5 \tan 34^\circ)} = 18910 \text{ lb/ft}$$

- o Option 1 is used to find Tensile Strength required per layer. The lift thickness will be 3.0 feet (d_b):

$$n_b = 40 \text{ ft} / 3 \text{ ft} = 14 \quad n_{f1} = 14 - 1 = 13 \quad \text{Percent} = 1.0$$

- o Equation 4 gives the Tensile Strength required per layer:

$$T_1 = \frac{(1.0)(18910 \text{ lb/ft})(105.7 \text{ ft})}{13(95.1 \text{ ft}) - 3 \text{ ft}(91)} = 167 \text{ lb/in}$$

- o Equation 5 gives the Length of the upper geosynthetic layer (FS=1.5):

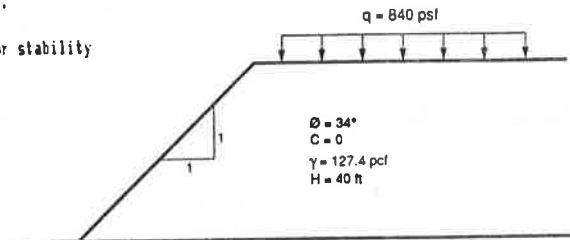
$$L_o = \frac{167 \text{ lb/in}}{162 \text{ psf}} (1.5) = 1.5 \text{ ft} \\ L = L_o + L = 1.5 \text{ ft} + 5 \text{ ft} = 6.5 \text{ ft}$$

- o Equation 6 gives the Length of the lower geosynthetic layer (FS=1.5):

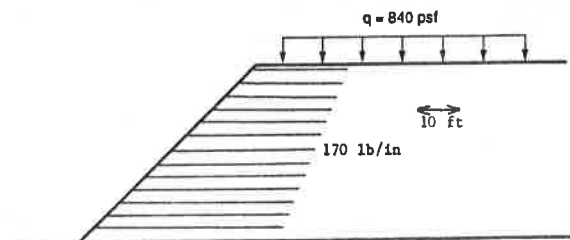
$$L = \frac{(33445 \text{ lb/ft}) 1.5}{37 \text{ ft}(127.4 \text{ psf}) \tan 23^\circ} + \frac{37 \text{ ft}}{2} = 43.5 \text{ ft}$$

- o Taper the lengths of the intermediate layers:

Layer	Height From Bottom (ft)	L (ft)
1	3.00	44.5
2	6.00	43.0
3	9.00	41.0
4	12.00	39.0
5	15.00	37.5
6	18.00	35.5
7	21.00	34.0
8	24.00	32.0
9	27.00	30.0
10	30.00	28.5
11	33.00	26.5
12	36.00	25.0
13	39.00	23.0



Example Problem



Example Problem

REFERENCES

- (1) Beech, J. F., "Importance of Stress-Strain Relationships in Reinforced Soil System Design," Proceedings of Geosynthetics '87, New Orleans, 1987, Vol. 1, pp. 133-144.
- (2) Bonaparte, R., and Christopher, B. R., "Design and Construction of Reinforced Embankments over Weak Foundations," Transportation Research Record 1153, pp. 26-39.
- (3) Christopher, B. R., Personal Communication, 1987.
- (4) Christopher, B. R., and Holtz, R. D., Geotextile Engineering Manual, FHWA, Washington D.C., 1985, 1044 pp.
- (5) Humphrey, D. N., "Design of Reinforced Embankments," Joint Highway Research Project, Purdue University, Report No. JHRP-86-16, 1986.
- (6) Jewell, R. A., "A Computer Design Method for Equilibrium Soil Structures Using Limit Equilibrium Analysis," Report prepared by Binnie and Partners, London, for Netlon, Ltd., 1981, 6 pp.
- (7) Koerner, R. M., Designing with Geosynthetics, Prentice-Hall, Englewood Cliffs, NJ, 1986, 424 pp.
- (8) Martin, J. P., Koerner, R. M., and Whitty, J. E., "Experimental Friction Evaluation of Slippage between Geomembranes, Geotextiles and Soils," Proceedings of the International Conference on Geomembranes, Denver, 1984, Vol. 1, pp. 191-196.
- (9) Murray, R. T., "Fabric Reinforcement of Embankments and Cuttings," Second International Conference on Geotextiles, Las Vegas, 1982, Vol. III, pp. 707-713.
- (10) Schmertmann, G. R., Chouery-Curtis, V. E., Johnson, D. D., and Bonaparte, R., "Design Charts for Geogrid-Reinforced Soil Slopes," Proceedings of Geosynthetics '87, New Orleans, 1987, pp. 108-120.
- (11) Scheider, H. R., and Holtz, R. D., "Design of Slopes Reinforced with Geotextiles and Geogrids," Geotextiles and Geomembranes, No. 3, 1986, pp. 29-51.
- (12) Verduin, J. R., "Geosynthetically Reinforced Slopes: A Design Procedure," Report for CE 6970 - Geotextiles and Geomembranes, Purdue University, 1987, 14 pp. + Appendices (available from the authors).

C.K. SU
N.N.S. CHOU
Colorado Department of Highways, U.S.A.

A Test Embankment Reinforced by Four Types of Geosynthetics

ABSTRACT

This paper describes the performance characteristics of four selected geosynthetic materials used in reinforcing a highway test embankment along I-76 in northwest Denver. The test embankment was constructed for the purpose of evaluating the performance properties of four geosynthetic materials over a soft homogeneous fly ash subsurface.

The test embankment was constructed within 10 days to a height of approximately 30 feet with oversteepened $1\frac{1}{4} : 1$ side slopes. The embankment was divided into four individual test cells. Each test cell with the exception of one, contained one layer of selected geosynthetic material. One test cell was not reinforced and served as a control cell. The geosynthetic materials selected for testing included one woven geofabric, one non-woven geofabric, and two bi-axial geogrids.

Geotechnical instrumentation consisting of horizontal and vertical inclinometers, strain gauges and ground water monitoring holes, were placed at strategic points along the test embankment to monitor each test cell. The test data collected and analyzed suggests that the use of geosynthetic reinforcing materials slightly or moderately reduced the amount of embankment settlement within certain test cells. In addition, lateral movement within the subsurface was also reduced. The strain gauges which were successfully attached to the non-woven geofabric and geogrids, showed tensile stress development during the construction and settlement of the embankment. Only one strain gauge out of 41 failed during the testing period.

1. INTRODUCTION

Construction of I-76 through northwest Denver has caused numerous foundation problems for highway engineers because of the

extremely poor subsurface conditions that exist along the entire alignment. Subsurface conditions consist primarily of landfill wastes and other loose backfilled foundation soils which have been discarded during the last 25 years.

Since most of the proposed I-76 alignment is elevated on embankments ranging from 10 to 55 feet in height, it was realized from preliminary studies that significant foundation modification and strengthening would be needed to reduce the effects of the high embankment loads on the soft subsurface. The conventional practice of removal and replacement was found to be too expensive for a project of this scale. Numerous alternatives that included dynamic compaction, stone columns, vibroflotation, lime and fly ash injection, staged construction with surcharge and geosynthetic reinforcements, were evaluated. It was concluded that staged construction with surcharge and geosynthetic reinforcement was the most viable and cost-effective method to deal with the problem.

Initially, the reinforcing geosynthetic consisted of bi-axial polymer geogrids of very high strength, but also at high material cost. In an attempt to reduce the material cost, it was decided that it might be possible to substitute less expensive geosynthetic materials of equal or lesser strength capabilities for areas that required less demanding loading conditions.

It was at this time that a method of comparison between the various geosynthetic materials was needed, thus, the idea for the instrumented test embankment evolved.

2. SUBSURFACE CONDITIONS AND SOIL PROPERTIES

The test embankment was constructed over a backfilled fly ash pit that was to be crossed by the I-76 alignment. The excavated pit originally contained approximately 40 feet of Clear Creek river alluvium. The alluvium was mined out and sold as aggregate for local Denver construction projects. The empty pit was then lined with clay and converted into a fly ash disposal site. Placement of the fly ash began in the early 1980's and continues as of the date of this paper. The source of the fly ash is the Public Service Company's Cherokee coal fired generating plant located in north Denver.

The fly ash was apparently end dumped either moist or as a slurry mix from large haul trucks. Methods of placement consisted of dumping the fly ash directly down a pit slope or by dumping the fly ash on the ground and shoving it into the excavation with a bulldozer. Where the fly ash was backfilled to the design elevation, the surface was covered with an approximately 2 foot thick layer of top soil to prevent dusting during times of windy weather.

Classification of the fly ash ranged from AASHTO A-4 to A-5, with a zero plastic index. Figure 1 shows the typical subsurface

profile. The top 3-5 feet of fly ash was much more dense when compared with the lower softer deposits. The hardened condition of the top crust was thought to be the result of desiccation as well as compaction from the haul trucks. The lower fly ash deposit was very loose with Standard Penetration Test (SPT) blow counts ranging from 0 to 3 throughout the area. Laboratory consolidation tests indicated a settlement potential of 18-22 inches. Hard shale bedrock was encountered at the approximate depth of 40 feet.

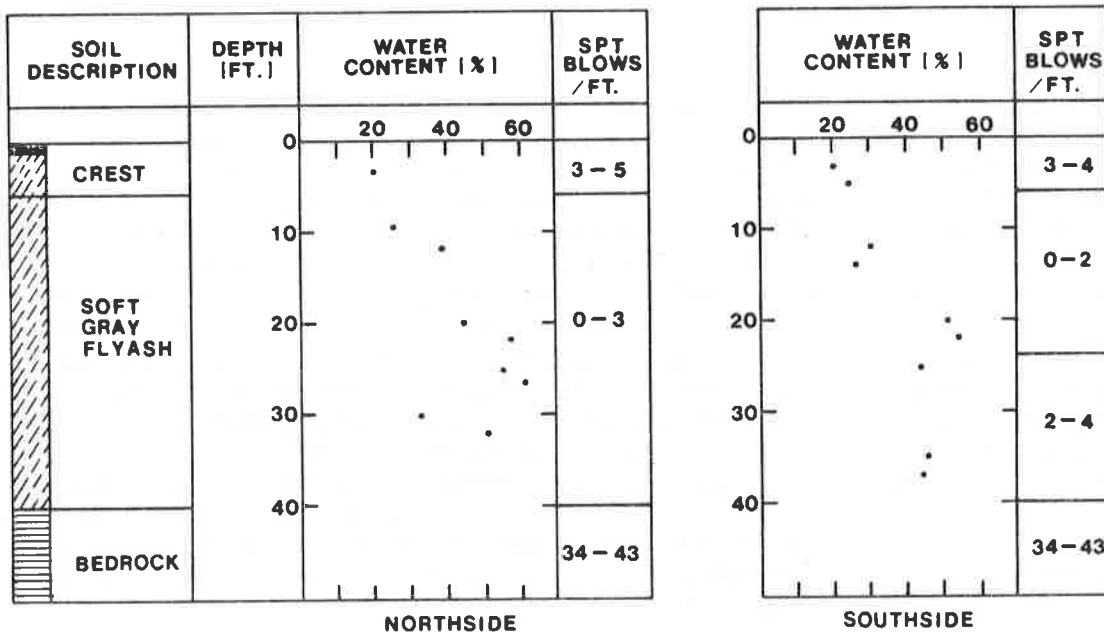


Figure 1 : Typical Subsurface Profiles

3. PROPERTIES OF THE REINFORCEMENT MATERIALS

The test embankment consisted of four instrumented sections. The geosynthetic materials selected for testing included TYPAR 3601, a non-woven heat bonded geofabric; SUPAC 4WS, a woven geofabric; TENSAR SS-2, a polymer heat-strengthened bi-axial geogrid, and MIRAFI 5T, a fibrous spun bond bi-axial geogrid. Table 1 lists pertinent physical properties of these four geosynthetic materials.

4. PERFORMANCE OF THE TEST EMBANKMENT

4.1 Test Embankment Description and Specifications

Table 1 : Material Physical Properties Along The Roll Length

Material Type	MIRAFI 5T	TENSAR SS-2	TYPAR 3601	SUPAC 4WS
Structure	Geogrid	Geogrid	Non-Woven	Woven
Grab Strength (lb/in.) (ASTM D-1682)	242 (43 kn/m)	98 (17 kn/m)	239 (42 kn/m)	85 (15 kn/m)
Grab Elongation (%, ASTM D-1682)	21	12	120	22

The geometric configuration of the test section with its four cells is shown in Figure 2. Each test cell was approximately 100 feet long by 120 feet wide. The test embankment side slopes were designed to be 1:1, but after construction and due to weathering, the slopes eventually sloughed to 1.25 to 1. The embankment height across all four test cells was constructed to a design height of 30 feet and was approximately 45 feet wide across its top. The test embankment width along its base was approximately 120 feet from toe to toe. Access ramps with 6:1 slopes were constructed on each end of the test embankment so that heavy construction equipment could access the top of the embankment. The embankment was constructed in 10 days and consisted of a decomposed clay-shale material, uncompacted, with no moisture control. The test embankment was removed in July of 1988 so that the main I-76 production embankment could be constructed. Figure 3 details the layout of the test embankment sections.

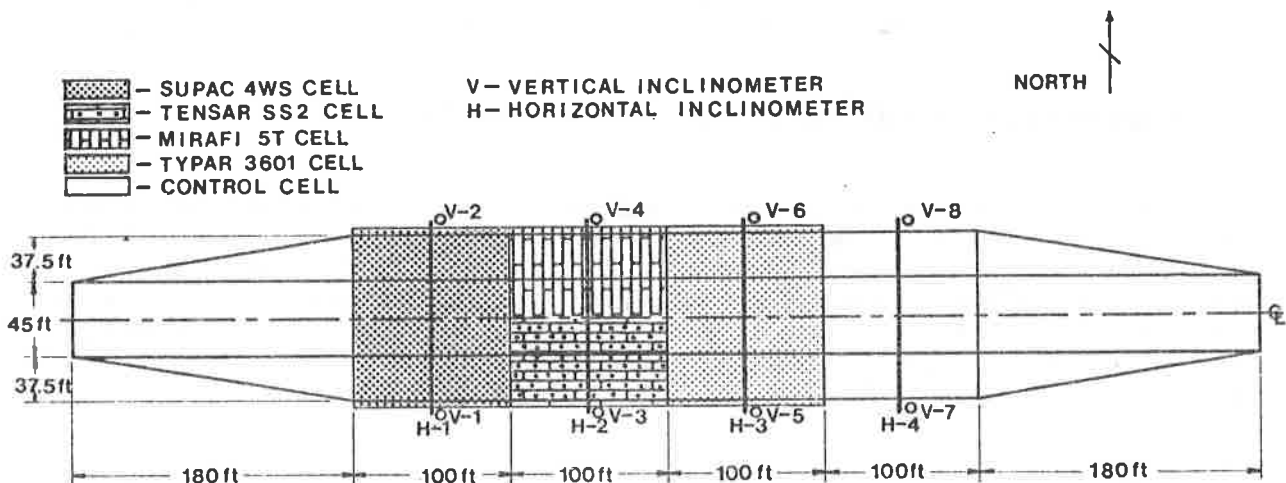


Figure 2 : Layout of Test Embankment

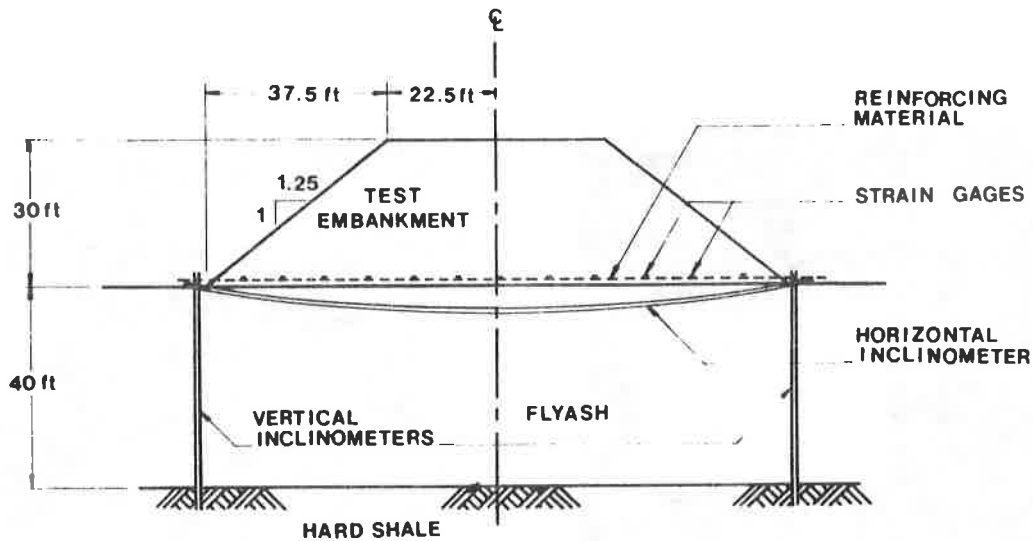


Figure 3 : Cross Section of Test Embankment

4.2 Instrumentation Installation Procedures

Prior to the site preparation, the geotechnical instrumentation for each test cell was installed. The first instruments to be placed were the vertical inclinometers. A total of 8 vertical inclinometers were used to monitor potential lateral movement within the embankment slopes. Each test cell contained 2 vertical inclinometers which were placed opposite one another along the approximate center of each test cell at each test cell's embankment toe. The vertical inclinometers were anchored in shale bedrock and grouted in place with a bentonite/cement grout. Initial data readings were then recorded following hardening of the grout.

Four horizontal inclinometers were installed following completion of the vertical inclinometer installations. Each test cell contained one horizontal inclinometer to record the amount of settlement within that test cell. Each horizontal inclinometer was installed normal to the control line of the test embankment so that a settlement profile across each test cell could be recorded. In addition, each horizontal inclinometer was located in its own trench excavated across the approximate center of each test cell.

Four strain gauge readout stations were installed with a pair of readout boxes opposite one another situated in a similar manner as the vertical inclinometers. A total of 41 strain gauges were installed on the non-woven geofabric and both geogrids for measuring the tensile stresses of the reinforcing materials (See photos 1, 2 and 3).

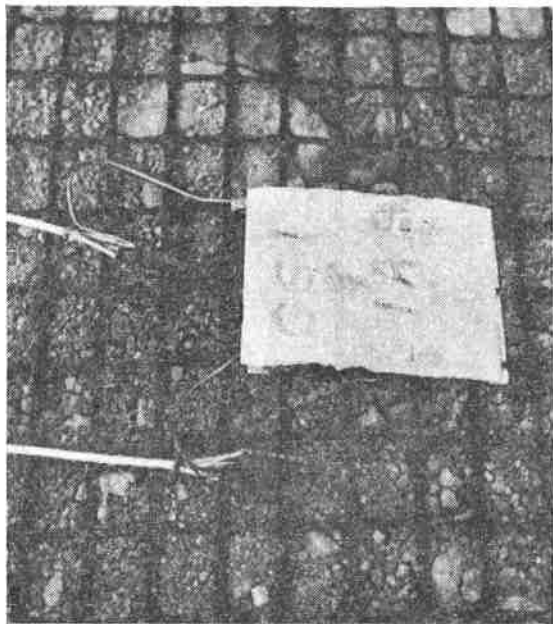


**Photo 1: Installation of Strain Gauge
for Tensar SS-2 Grids**



**Photo 2: Installation of Strain Gauge
for Typar 3601 Fabric**



Photo 3 : Alignment of Strain Gauges for Geogrids

Following installation of the instrumentation, two of the four test cell sites were then cleaned and grubbed of surface debris. Each test cell except the control cell and cell number 1 was then covered with a 6 inch thick cushion layer of ABC (aggregate base coarse) material. The purpose of the cushion layer was to smooth out and level the ground surface so that the fabrics and geogrids could be easily installed. In addition, the interlocking force (passive resistance) and friction between geogrid and surrounding soils can be increased. The test cell containing the woven fabric was not cleaned nor was a cushion layer installed so that the puncture resistance of the fabric could be assessed.

4.3 Geosynthetic Material Installation Procedures

The TYPAR 3601 installed in test cell 3 arrived at the site in rolls 150 feet long by 13 feet wide. One roll of fabric was delivered several months early to the CDOH materials laboratory so that strain gauges could be attached to the material in a clean controlled environment. This roll was to be located in the center of the test cell directly above the horizontal inclinometer. At the site, the instrumented middle roll was installed first and was located in such a way so that the strain gauges installed on the fabric were offset from the disturbed material of the horizontal inclinometer trench. The remaining fabric rolls were then laid out normal to the test embankment control line and sewed together using a double overlapped "J" seam.

Two types of geogrid supplied by different manufacturers were installed in test cell 2. The north one-half of test cell 2 contained TENSAR SS-2 geogrid with the south one-half of the test cell containing MIRAFI 5T geogrid. Both geogrids contained 10 strain gauges installed prior to their delivery to the field site. Both geogrids were oriented with their roll lengths running normal to the center line of the test embankment. The geogrid rolls were overlapped one foot and were physically connected to one another by various means of attachment such as metal hog rings, steel tie rods and plastic tie bands. Several geogrid rolls were not physically attached but simply overlapped.

The last geosynthetic material installed was SUPAC 4WS. This material was installed in test cell 1 and laid out in a similar manner to the geogrids and non-woven fabric with the exception that the woven fabric was laid directly on the ground surface with no granular cushion material shielding the fabric from potential debris puncture. The woven fabric panels were sewed together using the same stitching pattern described for the non-woven fabric. However, some of the woven panels were delivered to the job site with factory sewed seams. These seams were not sewed in the same manner as the double "J" seam and

consisted mainly of a single overlap with double stitch. These factory seams were noted and marked so that they could be examined after the test embankment was removed. The woven fabric did not contain strain gauges since the texture and weave design of the fabric would not allow attachment of the gauges by methods employed on the non-woven and geogrids.

All four geosynthetic materials contained various connection devices and movement telltales which were to be analyzed for effectiveness after removal of the test embankment.

4.4 Field Measurements

Vertical Displacement (Settlement)

Figure 4 shows settlement profiles for the various geosynthetic materials plotted against corresponding embankment heights. These profiles were obtained from the horizontal inclinometers H-1 through H-4 buried beneath the test cells. The inclinometer data suggests that the woven material (SUPAC) and the two types of geogrid (Mirafi and Tensar) appear to have more uniform settlement curves than the non-woven (Typar) and control cell. Approximately 20 to 30 percent more settlement was recorded in the control cell than in the cells that utilized geosynthetic material.

Lateral Displacement

Horizontal displacement was measured by 8 vertical inclinometers, each one anchored in shale bedrock at its respective test cell slope toe location. Figure 5 shows the measured horizontal displacement versus the depth at various inclinometer locations. Despite this discrepancy, the horizontal displacement plots still suggest that the geogrids permitted less lateral movement than the fabrics or control cell. This is probably due in part to the higher material strength of the grids as compared to the fabrics.

It should be noted, none of the inclinometer pairs, e.g. V-1 vs. V-2, showed similar lateral deformation profiles. With the control section itself, both the lateral deformation and settlement were higher on the south side of the test embankment than that of the north side. This suggested that the fly ash subsurface was not homogeneous, and in the south side the fly ash was weaker than that of the north side.

Strain Gauges

Figure 6 shows data obtained from the strain gauges installed along each cross section of the Typar, Mirafi, and Tensar test cells. The gauges were installed to measure the tension expected to develop within the confined reinforcing materials as the result of loading due to construction of the

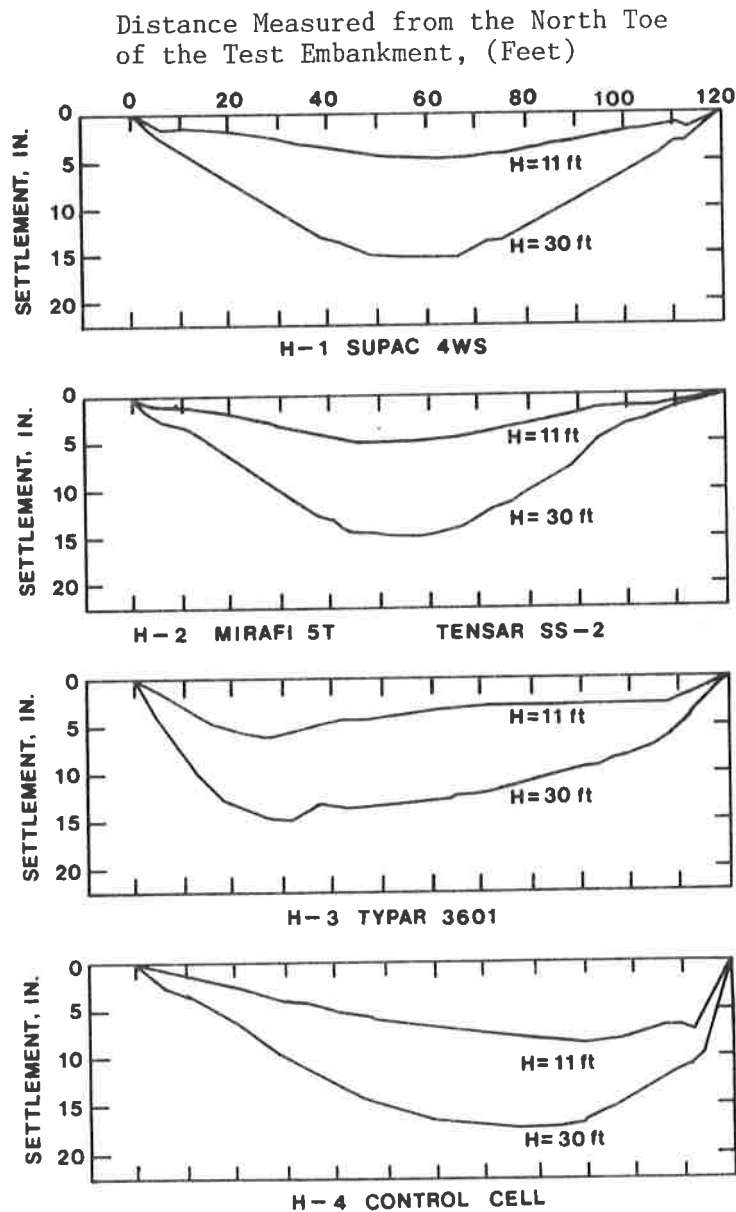


Figure 4 : Settlement Profiles Along the Cross Sections of Test Cells for Various Fill Heights

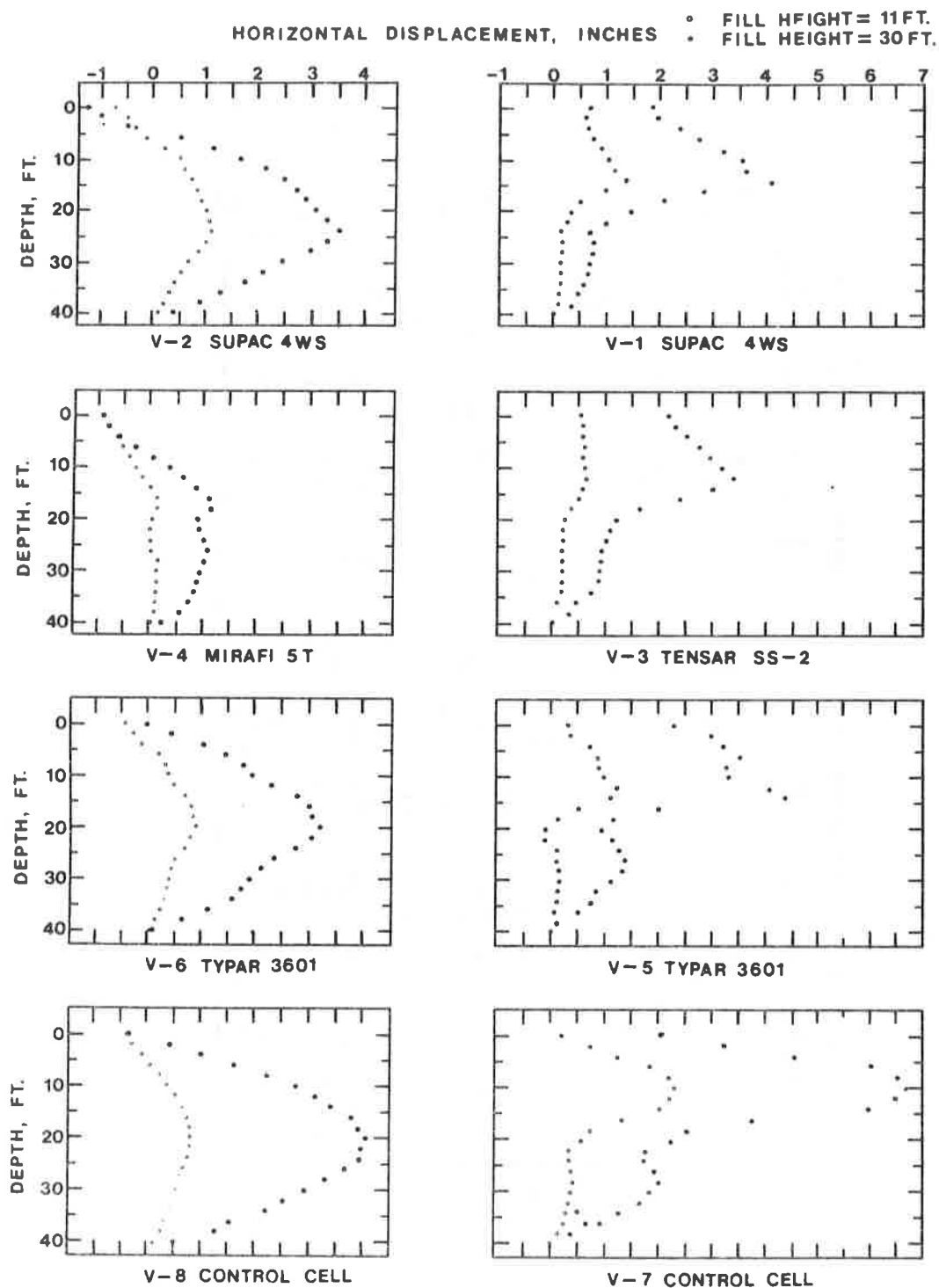


Figure 5 : Horizontal Displacements Versus Depth
at Various Embankment Heights

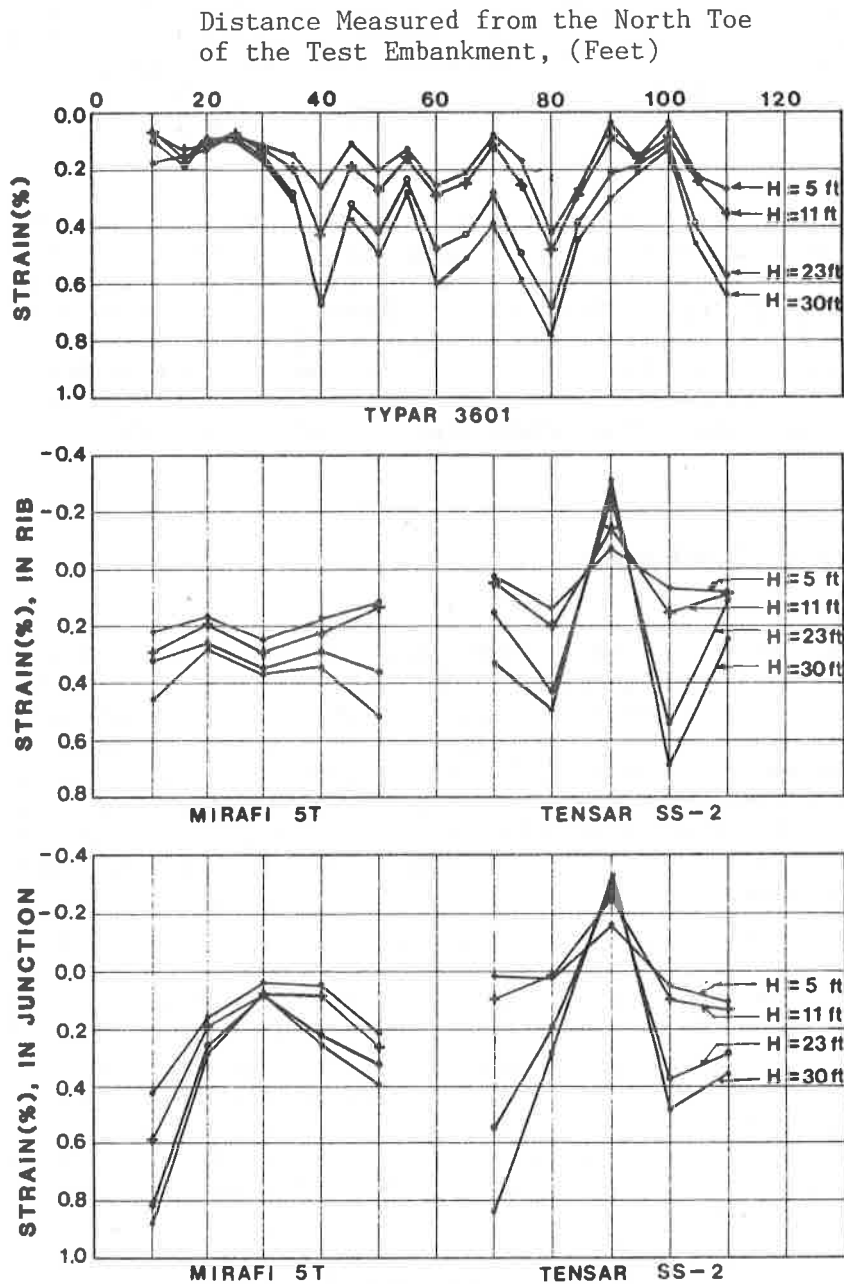


Figure 6 : Strain Gauge Readings Along the Cross
Sections at Various Embankment Heights

test embankment. The gauges were mounted on the TYPAR fabric using standard methods recommended by the gauge manufacturer and were oriented parallel with the direction of expected maximum strain, which was perpendicular to the center line of the embankment. The orientation of the gauges mounted on the Tensar and Mirafi were the same as the Typar, however, the Tensar and Mirafi gauge locations were placed on both the connecting rib and the rib junction. This was done because it was discovered in laboratory tests that the Tensar geogrid tended to fail through the junction rather than the rib.

The strains developed by the full embankment loads were found to be relatively small, ranging from -0.3 to 0.9 %. The negative strain (compression) which developed in some of the gauges was not fully understood. Disregarding the possibility that the negative readings were isolated occurrences caused in part by installation procedures of the geosynthetic materials, a detailed finite element analysis may reveal additional unknown factors that affected the embankment and geosynthetic material behavior.

5. SUMMARY AND CONCLUSIONS

The experience gained from the test embankment will be valuable for similar projects in the future. All of the instrumentation performed well. The instrumentation data indicated that the use of reinforcing materials moderately or slightly reduced the vertical and horizontal displacements of the test embankment and its foundation. In addition, the strain distribution data from the strain gauges will assist in better understanding how tensile stresses were developed during and after construction.

In general, the field performance of the four geosynthetic materials was satisfactory. The geogrids were found to be more effective in reducing lateral and vertical deformations than the geofabrics we tested. However, it does not imply that the geogrids may be more cost effective in all applications. The fly ash subsurface did not behave as a homogeneous soil mass as was originally expected. The fly ash in the south side of the test embankment appeared to be weaker than that of the north side. But apparently the general trend of settlements and lateral deformations documentations remained valid.

It was concluded that no geosynthetic material was needed to increase the slope stability for the test embankment. This was due to the fact that fly ash was highly permeable and therefore a drained condition was maintained resulting in an increase of shear strength during the embankment construction.

This paper is but one of two that will analyze the data acquired at the I-76 test site. Subsequent paper will address the finite

element analyses for embankment and geosynthetic material evaluation.

6. ACKNOWLEDGEMENT

The authors wish to acknowledge and express their appreciation to the manufacturing companies and their representatives for the donation of the test materials. Special thanks to Edwin Belknap and George Pavlick of the CDOH Materials Laboratory for their significant contribution in instrumentation and field work. The assistance and coordination from the personnel of the Geotechnical Section, Research Section and District 6 of CDOH are also appreciated.

7. REFERENCES

- (1) Barsvary, A.K., Maclean, M.D., and Cragg, C.B.H., "Instrumented Case Histories of Fabric Reinforced Embankments over Peat Deposits," Proceeding of the Second International Conference on Geotextiles, Las Vegas, Vol. III, 1982, p.p. 647-652.
- (2) Bell, J.R., Barrett, R.K., and Ruckman, A.C., "Geotextile Earth Reinforced Retaining Walls Test, Glenwood Canyon, Colorado," Presented at the Annual Meeting, Transportation Research Records, 1983.
- (3) Chou, N.S.S., Wu, T.H., and Siel, B.D., "The Effectiveness of Tensile Reinforcement in Strengthening An Embankment Over Soft Foundation," Proceedings of Geosynthetics'87 Conference, New Orleans, Vol. I, February, 1987, p.p. 332-340.
- (4) Fowler, J., Haliburton, T.A. and Langan, J.P., "Design and Construction of Fabric Reinforced Embankment Test Section at Pinto Pass, Mobile, Alabama," Transportation Research Record No. 749, 1980, p.p. 27-33.
- (5) Fowler, J., "Design, Construction and Analysis of Fabric-Reinforced Embankment Test Section at Pinto Pass, Mobile, Alabama," Technical Report E1-81-8, USAE Waterways Experiment Station, Vicksburg, Mississippi, 1981, p.p. 238

- (6) Rowe, R.K., MacLean M.D. and Barsvary, A.K., "The Observed Behavior of Geotextile-Reinforced Embankment Constructed on Peat," Canadian Geotechnical Journal, Vol. 21, No. 2, May, 1984, p.p. 289-304.
- (7) Rowe, R.K. and Soderman, K.L., "An Approximate Method for Estimating the Stability of Geotextile-Reinforced Embankments," Canadian Geotechnical Journal, Vol. 22, No. 3, August, 1985, p.p. 392-398.
- (8) Scott, J.D., Sego, D.C., and Hofmann, B.A., "Design of the Devon Geogrid Test Fill," Proceedings of Geosynthetics'87 Conference, New Orleans, Vol. 1, February, 1987, p.p. 157-168.
- (9) Siel, B.D., "An Investigation of the Effectiveness of Tensile Reinforcement in Strengthening an Embankment over Soft Foundation," Master Thesis, Department of Civil Engineering, University of Colorado at Denver, 1986.
- (10) Sluimer, G. and Risseeuw, P., "A Strain-Gauge Technique for Measuring Deformations in Geotextiles," Proceedings of the Second International Conference on Geotextiles, Las Vegas, 1982, Vol. III, p.p. 835-838.

GEOSYNTHETICS '89

FEBRUARY 21-23 TOWN & COUNTRY HOTEL, SAN DIEGO, CA

CONFERENCE PROCEEDINGS

Town & Country Hotel
San Diego, California
February 21-23, 1989

Volume 2

Sponsored by the Industrial Fabrics Association International under the auspices of the International Geotextile Society (IGS) and the North American Geosynthetics Society (NAGS) and with support of the American Society of Civil Engineers (ASCE).

GEOSYNTHETICS '89

FEBRUARY 21-23 TOWN & COUNTRY HOTEL, SAN DIEGO, CA

CONFERENCE PROCEEDINGS

Town & Country Hotel
San Diego, California
February 21-23, 1989

Volume 2

GEOSYNTHETICS '89 CONFERENCE

**NORTH AMERICAN
REGIONAL CONFERENCE**

**SPONSORED BY:
THE INDUSTRIAL FABRICS
ASSOCIATION INTERNATIONAL**

**UNDER THE AUSPICES OF:
INTERNATIONAL GEOTEXTILE SOCIETY (IGS)
NORTH AMERICAN GEOSYNTHETICS SOCIETY (NAGS)**

**WITH THE SUPPORT OF:
AMERICAN SOCIETY OF CIVIL ENGINEERS (ASCE)
(THE COMMITTEE ON PLACEMENT AND IMPROVEMENT OF
SOILS)**

VOLUME 2

GEOSYNTHETICS '89 CONFERENCE

ORGANIZING COMMITTEE

CHAIRMAN

J. E. (TED) GAILER Chairman, Geotextile Division, IFAI; Organizing Committee Member, Geosynthetics '87.

COMMITTEE MEMBERS

JAY F. BEECH, Ph.D., P.E. Member, International Geotextile Society; Member, American Society of Civil Engineers.

R.G. (BOB) CARROLL, JR., P.E. Vice President, North American Geosynthetics Society; Member, Geotextile Division, IFAI; Member, Task Force 25.

LAURIE L. HONNIGFORD Staff Director of Geomembrane and Geotextile Divisions, IFAI.

JOSEPH D. LUNA Member, International Geotextile Society; Member, North American Geosynthetics Society; Member, ASTM D35 Committee on Geotextiles, Geomembranes and Related Products.

BILL NEAL Vice Chairman, Geomembrane Division, IFAI; Former Vice President, Society of Plastic Engineers.

IRAJ NOORANY, Ph.D. Professor, Civil Engineering, San Diego State University; Visiting Professor, University of California, San Diego; Recipient, Thomas A. Middlebrooks Award.

KERRY ROWE, Ph.D., P. Eng. Member, International Geotextile Society; Vice President, North American Geosynthetics Society; Editor, IGS News.

STEPHEN M. WARNER Executive Vice President, Industrial Fabrics Association International; Former Secretary General, American Society of Geosynthetics, (currently, North American Geosynthetics Society); Former Secretary General, 2nd International Conference on Geotextiles; Organizing Committee Member, Geosynthetics '87.

NEIL WILLIAMS, Ph.D., P.E. Member, Executive Committee ASTM D35; U.S. Delegate, International Standards Organization; Member, North American Geosynthetics Society; Member, American Society of Civil Engineers.

ADVISOR

JOSEPH E. FLUET, JR. P.E. President, North American Geosynthetics Society; Former Secretary/Treasurer, International Geotextile Society; Former Chairman, Geotextile Division, IFAI; Organizing Committee Member, 2nd International Conference on Geotextiles and 1st International Conference on Geomembranes; Former Committee Member Geotechnical Fabrics Conference '85; Chairman, Geosynthetics '87 Conference.

These papers are published by:
Industrial Fabrics Association International
345 Cedar St., Suite 450
St. Paul, MN 55101
(612)222-2508
TWX: 910-563-3622
FAX: (612)222-8215

Industrial Fabrics Association International

TABLE OF CONTENTS

TABLE OF CONTENTS

VOLUME 1

OPENING ADDRESS

Opening Address	1
GAILER, J.E. (Ted), Chairman, Organizing Committee, Geosynthetics '89 Conference	

SESSION 1A: LANDFILLS & LININGS SYSTEMS

Paradise Peak Tailings Impoundment Stage II Construction	5
A.A. McCREADY Harding Lawson Associates, U.S.A.	
The Use of Geosynthetics As Drainage Media at Solid Waste Landfills	10
C.M. LUNDELL, S.D. MENOFF Waste Management of North America, Inc., U.S.A.	
Rates of Leakage Through Landfill Liners	18
J.P. GIROUD, R. BONAPARTE, B.A. GROSS GeoServices, Inc., Consulting Engineers, U.S.A.	
Lined Cut and Fill Reservoirs in Israel- Forty Years of Development	30
P.I. MARCUS Mekorot Water Co., Ltd., Israel	
Stability Of Soil Layers On Geosynthetic Lining Systems	35
J.P. GIROUD, J.F. BEECH GeoServices, Inc., Consulting Engineers, U.S.A.	

SESSION 2A: QUALITY ASSURANCE AND SPECIFICATIONS

Stringent Construction Specifications and Quality Control Assure Maximum Liner Performance	47
T.N. DOBRAS, D.G. YACKO Harza Environmental Services, Inc., U.S.A.	

Design Methods and Construction Quality Assurance For a Double Geocomposite Industrial Waste Landfill	58
M.J. MONTELEONE, G.J. DiPIPPO AWARE Incorporated, U.S.A.	

Inspection of HDPE Geomembrane Installations	70
G.R. KOERNER, Drexel University, U.S.A. J.A. BOVE, Westinghouse Environmental Engineering, U.S.A.	

The Benefits of Construction Quality Assurance of Lining Systems Installation: Real or Perceived?	84
R.B. WALLACE GeoServices, Inc., Consulting Engineers, U.S.A.	

SESSION 3A AND 2B: DRAINAGE & WALLS

Design Of Verticle Drains Using The Hydraulic Conductivity Ratio Analysis	95
S.M. LUETTICH, N.D. WILLIAMS GeoServices Inc., Consulting Engineers, U.S.A.	

Effectiveness of Tensile Reinforcement in Alleviating Bridge Approach Settlement	104
T.H. WU, University of Colorado, U.S.A. G.J. MONLEY, J.U. Lowney & Associates, U.S.A.	

Parametric Study of Geosynthetic Reinforced Retaining Walls Using the Displacement Method	112
J.P. GOURC, P.H. GOTTELAND, University of Grenoble, France P. DELMAS, Laboratoire Central des Ponts et Chaussees, France	

SESSION 5A: EMBANKMENTS

Consideration of Strain in the Design of Reinforced Embankments	124
R.K. ROWE, B.L.J. MYLLEVILLE University of Western Ontario, Canada	
Effect of Surface Crust on Reinforced Embankment	136
D.N. HUMPHREY University of Maine, Orono, U.S.A. R.D. HOLTZ University of Washington, Seattle, U.S.A.	

Design and Construction of Synthetic-Grid Reinforced Embankment over Soft Waste	148
M.F. HOULIHAN, W.K. RODGERS	
Law Environmental, U.S.A.	
G. WILLIBEY	
Nicolon Corporation, U.S.A.	
N.D. WILLIAMS	
GeoServices, Inc., Consulting Engineers, U.S.A.	

Case Study of a Geotextile Reinforced Levee on a Soft Clay Foundation	160
F.M. DUARTE, G.S. SATTERLEE	
U.S. Army Corps of Engineers, U.S.A.	

Design Methods For Reinforced Embankments On Soft Foundations	172
P.J. LANGSTON, N.D. WILLIAMS	
GeoServices, Inc., Consulting Engineers, U.S.A.	

Geotextile Assisted Soft Site Stabilization	184
J.N. PAULSON	
Exxon Chemical Co., U.S.A.	

SESSION 6A: FOUNDATIONS & RAILWAYS

A Functional Approach to the Design of Geotextiles	195
O. GICOT, Soltechnique, Fribourg, France	
J. PERFETTI, Rhone-Poulenc, Bezons, France	
J.M. RIGO, K. Smolders, University of Liege, Belgium	
C. LEGRAND, C.S.T.C. Belgium	

Foundation on Sand Underlain by Soft Clay with Geotextile at Sand-Clay Interface	203
B.M. DAS	
Southern Illinois University at Carbondale, U.S.A.	

A Comparison of Texturized and Non-Texturized GEOWEB-Reinforced Earth Slabs	215
V.A. GUIDO, J.P. SOBIECH	
The Cooper Union School of Engineering, U.S.A.	
S.N. CHRISTOU	
Kanika Construction Ltd., U.S.A.	

Finite Element Analysis of Footings on Geogrid-Reinforced Soil	231
--	-----

C.J. PORAN

University of North Carolina, Charlotte, U.S.A.

L.R. HERRMANN, K.M. ROMSTAD

University of California at Davis, U.S.A.

SESSION 7A: STEEP SLOPES

Reinforcement of an Earthen Buttress with a Polymer Geogrid	243
---	-----

D. CHU, I. POORMAND

Leighton & Associates, Inc., U.S.A.

Geogrid Steepened Slopes at Davis Creek Dam	255
---	-----

W.O. ENGEMOEN, P.J. HENSLEY

U.S. Bureau of Reclamation

Critical Failure Planes in Analysis of Reinforced Slopes	269
--	-----

R.R. BERG, V.E. CHOUERY-CURTIS, C.H. WATSON

Tensar Engineering, Inc., U.S.A.

Geosynthetically Reinforced Slopes: A New Procedure	279
---	-----

J.R. VERDUIN

Hart-Crowser, Inc., U.S.A.

R.D. HOLTZ

University of Washington, U.S.A.

A Test Embankment Reinforced by Four Types of Geosynthetics	291
---	-----

C.K. SU, N.N.S. CHOU

Colorado Department of Highways, U.S.A.

Volume 2

SESSION 1B: PAVEMENTS

The Use of Drainage Wicks for the Mitigation of Frost Effects on Existing Roadways	305
--	-----

R.A. D'ANDREA, J.D. SAGE

Worcester Polytechnic Institute, U.S.A.

A Study of Permanent Road Stabilization: Low-Cost Pavement Structures and Lightweight Geotextiles	316
---	-----

C.J. SPRAGUE, G. CICOFF

Hoechst Celanese Corporation, U.S.A.

Using Geosynthetics to Control Lateral Spreading of Pavements in Alaska--Preliminary Results	324
T.C. KINNEY, B.M. SAVAGE	
University of Alaska, Fairbanks, U.S.A.	

The Function of Geotextiles in Pavement Structures	334
J. PERFETTI, Rhone-Poulenc Fibres, France	
T. SANGSTER, Rhone-Poulenc Chemicals Ltd., United Kingdom	

The Influence of Nonwoven Geotextiles on the Compactability of the Fill Material	345
G. WERNER, S. RESL	
Polyfelt Ges.m.b.H., Linz/Austria	
R. MONTALVO	
Polyfelt Inc., U.S.A.	

Geotextiles and Geogrids: Cost Effective Alternate Materials for Pavement Design and Construction	353
P. ANDERSON, M. KILLEAVY	
Trow Geotechnical Ltd., Canada	

SESSION 3B: BEHAVIOR OF SOIL GEOSYNTHETIC SYSTEMS

Behavior of Soil-Geotextile Composites and its Application to Finite Element Analysis	365
T.H. WU	
University of Colorado at Denver, U.S.A.	

Stress-Deformation Response of Geotextile Reinforced Granular Structures	373
D.H. GRAY, M. KALDJIAN	
University of Michigan, U.S.A.	
C. WU	
Tamkang University, Taiwan	

Dynamic Behavior of Saturated Sand Reinforced with Geosynthetic Fibers	385
I. NOORANY	
San Diego State University, U.S.A.	
M. UZDAVINES	
Woodward-Clyde Consultants, U.S.A.	

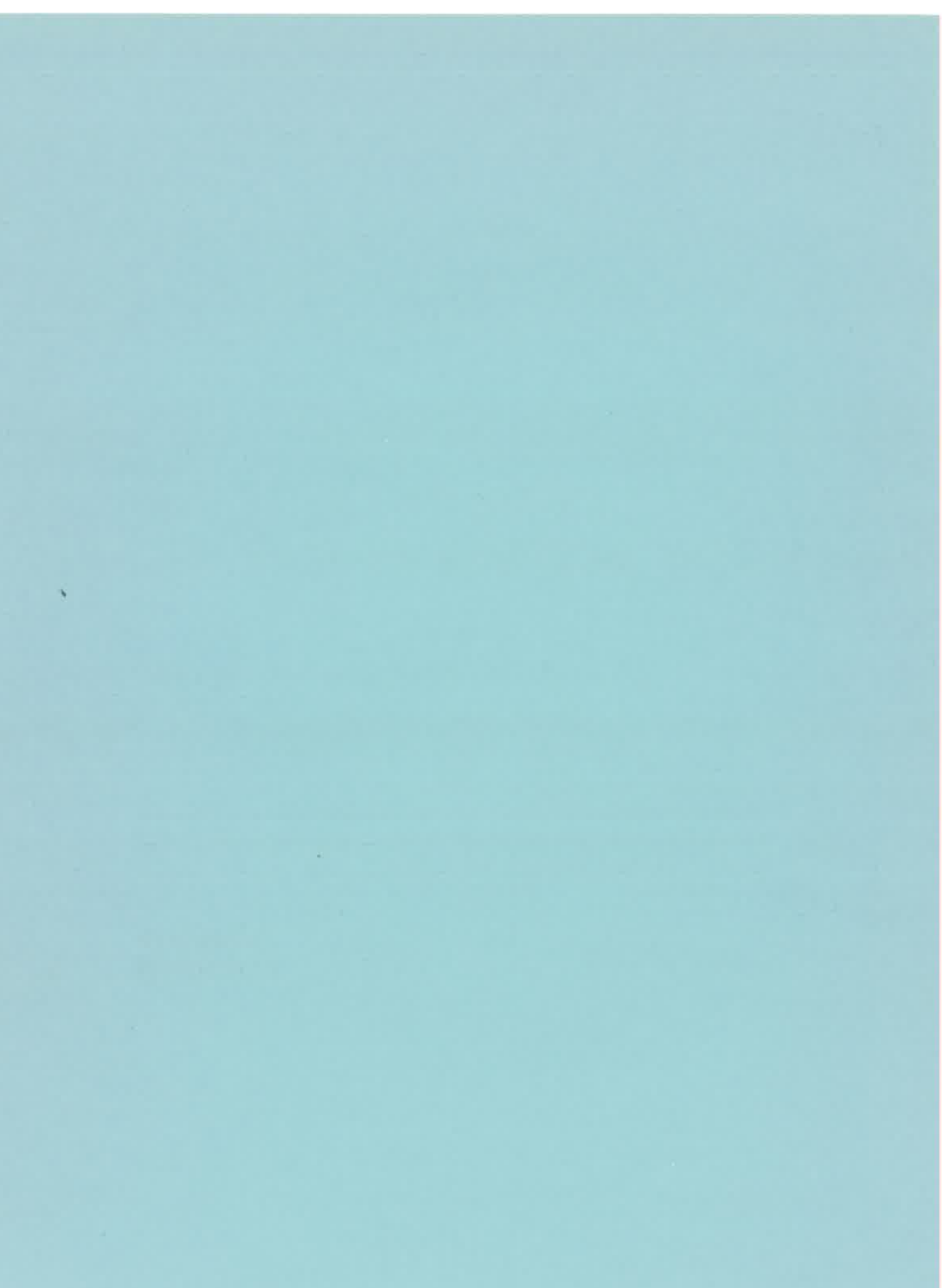
SESSION 4B: TESTING - CHEMICAL

- Flex - An Expert System to Assess
Flexible Membrane Liner Materials 397
R.E. LANDRETH
U.S. Environmental Protection Agency, U.S.A.
- Polymers for Synthetic Lining Systems: Some Molecular
Structure-Property-Application Relationships 408
R.M. CHARRON
GeoSyntec, Inc., U.S.A.
- Microtome Sections for Examining Polyethylene
Geosynthetic Microstructures and Carbon Black Dispersion 421
I.D. PEGGS, R.M. CHARRON
GeoSyntec, Inc., U.S.A.
- Evaluation of the Effects of Waste Loads on Geocomposites
In Double-Lined Landfills and Surface Impoundments 433
G. YAZDANI, J. NORBERT
Poly-America, U.S.A.
- Evaluation Of HDPE Geomembrane Field Welding Techniques,
Need To Improve Reliability Of Quality Seams 443
A.L. ROLLIN, A. VIDOVIC
Ecole Polytechnique de Montreal, Canada
R. DENIS, M. MARCOTTE
Solmers International, Canada
- The Electrical Leak Location Method for Geomembrane Liners:
Development and Applications 456
G.T. DARILEK, D.L. LAINE, J.O. PARRA
Southwest Research Institute, U.S.A.
- Locating And Repairing Leaks In Landfill/Impoundment
Flexible Membrane Liners 467
R.E. LANDRETH
U.S. Environmental Protection Agency, U.S.A.
- Loading Point Puncturability Analysis of Geosynthetic Liner Materials . . 478
D.L. LAINE, M.P. MIKLAS, C.H. PARR
Southwest Research Institute, U.S.A.

SESSION 5B: TESTING - General

Shear Resistance Between Cohesive Soil and Geogrids	489
E.A. RICHARDS, J.D. SCOTT, L.W.M. BOBEY	
University of Alberta, Canada	
V. DIYALJEE	
Alberta Transportation and Utilities, Canada	
Evaluation Of The Degradation Of Geotextiles	501
J.R. MONTALVO	
Polyfelt, Inc., U.S.A.	
Microstructural Analysis Of The Durability of a Polypropylene Geotextile	513
L.G. TISINGER	
GeoSyntec, Inc., U.S.A.	
Analytic Behavior Of Geogrid Anchorage	525
R.M. KOERNER	
M.H. WAYNE	
Drexel University, U.S.A.	
R.G. CARROLL	
Tensar Corporation, U.S.A.	

SESSION 1B
PAVEMENTS



SESSION 1B
PAVEMENTS

R.A. D'ANDREA

J.D. SAGE

Worcester Polytechnic Institute, U.S.A.

The Use of Drainage Wicks for the Mitigation of Frost Effects on Existing Roadways

SUMMARY

A laboratory study of an innovative technique of utilizing geosynthetic wick drains to reduce the frequency of repair of pavement above frost susceptible soil is described. This technique consists of installing vertical wick drains at the time of pavement repair in order to facilitate thaw consolidation. Flexible pavements constructed on frost susceptible soil and subjected to periodic cycles of freezing and thaw often fail. This failure results from a loss of shear strength and bearing capacity of the soil supporting the pavement. Laboratory evidence is presented which shows a rapid increase in the rate of dissipation of excess pore water pressures upon loading of a thaw weakened non-plastic soil after installation of a wick insert. The wick insert can also function as a vertical drain to remove a portion of the melt-water directly from the thaw plane to the permeable base course. Theory dictates that this increased rate of pore water dissipation and melt-water drainage leads to a more rapid recovery of soil shear strength and a lessening of the damage to flexible pavements. Data from a series of thaw consolidation tests from two slowly draining frost susceptible soils, a uniform silt and a clay till, regarding the above observations are presented. The presence of plastic fines in the frost susceptible soil is shown to lead to reduced effectiveness of the wick drain system.

INTRODUCTION

In geographical areas which are subject to significant seasonal freezing temperatures, the phenomena of frost heaving and subsequent thawing of roadway base soils often results in annual deterioration of the road surface. Although the mechanics of such pavement breakdown due to frost action is reasonably well understood, there remains a need for an economical method of either preventing or reducing the frequency of the resulting damage.

When a frost susceptible soil is subject to freezing temperatures and has access to an appropriate water supply, ice lenses will form within the soil. The thickness and locations of these ice lenses are random and vary with thermal history and initial crystallization site. However, the end result of such a freezing system is essentially the same in that the pavement surface above the frost susceptible soil is underlain by local zones of high void ratio. These zones, which are initially solid ice, become sites of high water content upon thaw with downward drainage prevented by frozen soil. It is well known that when all other factors (such as stress history) are equal, the ability of a frost susceptible soil to resist shear will be inversely proportional to its water content. When these sites of low shear strength are close enough to the pavement surface to coincide with the locations which are highly stressed by vehicular loading, severe engineering problems are produced. Sage and D'Andrea (4) refer to the zones of markedly lower shear strength as "thaw weakened" zones. Thaw weakening is viewed as a complex process because the soil is not only weakened by increase in water content but also upon application of

load, compressive pore water pressures are induced further decreasing the ability of the soil to withstand shear.

Sage and D'Andrea (4) have further described the thaw-weakening and strength recovery phenomenon as occurring in three stages. In the first stage, a tightly packed soil configuration in the prefreeze condition increases water content during freezing and heaving. During the second stage, which consists of soil thaw, the high water content is retained resulting in very low shear strength. Finally, as the soil consolidates under load, the water content decreases and strength regain occurs, but probably not to the extent that full recovery to the pre-freeze strength is achieved unless additional consolidating stress is applied. As the freeze-thaw cycle is repeated, the soil strength in the vicinity of ice lensing oscillates from the minimal value immediately after thaw to the recovered strength after consolidation. Since pavement failures occur during the time between thaw and strength regain, increasing the rate of recovery by increasing the rate of consolidation decreases the likelihood of failure under vehicular loading. This paper describes laboratory experiments performed to determine the effectiveness of wick drains in accelerating post-thaw consolidation.

Most pavement deterioration and subsequent pothole formation currently occurs in flexible pavements. These pavements consist of a surface course or courses of a mixture of mineral aggregates and bituminous material underlain by soil layers. The upper soil layer, designated herein as the base layer, is made of non-frost susceptible and free draining soil if properly designed. The soil below the base, known as the sub-grade, is generally the site where ice lenses are formed. Although attempts are often made to insure that the sub-grade also consists of soil which is not frost susceptible, at least to the depth of seasonal frost penetration, there appear to be many instances where this goal is not achieved. These situations are generally the result of improper construction procedures or inadequate inspection of the sub-grade soil. In addition, it is occasionally assumed that sufficient free water to develop ice lenses will be unavailable at a particular site and, therefore, little effort is expended to insure adequate gradation of the sub-grade soil. However, conventional drains, culverts, or water bearing strata often do produce localized sources of sufficient water. Regardless of the specific reason, it is readily apparent that there are many segments of flexible pavement with adequately constructed surface and base layers underlain by some localized areas where ice lensing will initiate during the freezing season. Upon thaw, these areas become sites of potential pavement deterioration.

The pavement repair method addressed in this paper would consist of inserting a wick drain (or drains depending on the size of the affected area) at the pothole site as part of the repair process. The wick would extend into the frost susceptible subgrade below the depth of seasonal frost penetration and up into the freely draining base course material. The pavement would then be patched using existing appropriate methods (2). Presumably ice lenses would again be generated in the subgrade during the next freezing season. However, upon the onset of thaw excess pore water pressures would dissipate as water flows upward through the wick drain and laterally through the base, with the filtering action of the wick preventing the migration of fines. Hopefully, pore water pressure would be reduced rapidly enough to prevent the excessive strength loss often occurring in frost susceptible soils which eventually leads to pavement failure. Figure 1 graphically portrays the anticipated action.

THEORY OF RADIAL AND VERTICAL CONSOLIDATION

Two types of tests were performed in order to evaluate the effectiveness of wick drains with respect to consolidating thaw weakened soils. The first test type was essentially a control test and was performed on a specimen which was enclosed in a circular mold and which had no wick drain. For this test the control sample undergoes one-dimensional consolidation via drainage in the vertical direction.

In the freeze-thaw-load experiments described in this paper samples were thawed to a particular depth and loaded while the soil below was still frozen. Under these conditions the length of the longest vertical drainage path, h , was assumed to be the thickness of the thawed layer. This is known as "single drainage" with the upper surface assumed free draining and the frozen lower layer assumed impermeable.

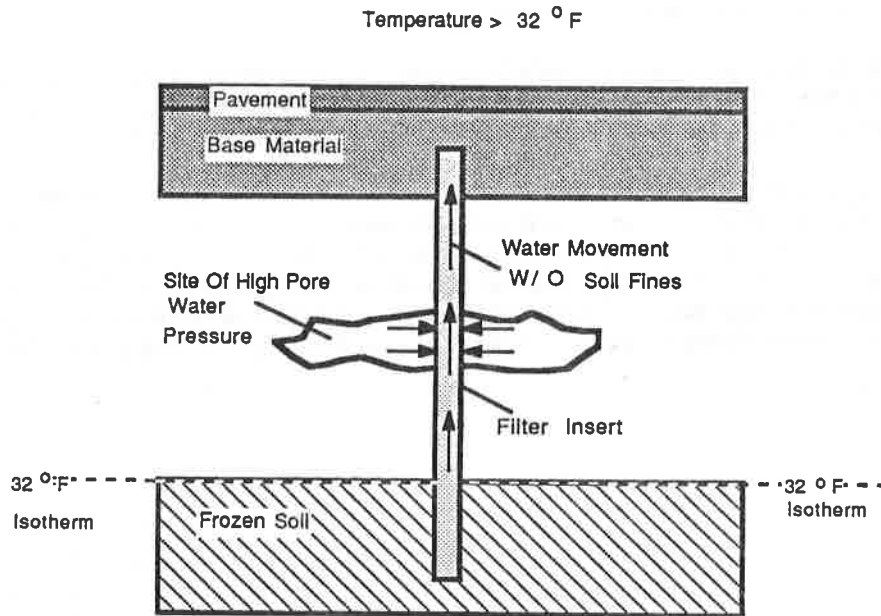


Figure 1. Schematic Of Mechanism Of Wick Enhanced Drainage.

Taylor (5) has shown that under these conditions if the soil is loaded such that it is subject to a constant uniform initial excess pore pressure, u_0 , the excess pore pressure, u_v , at depth z , is given in terms of time factor, T_v , by:

$$u_v = \sum_{m=0}^{m=\infty} \frac{2u_0}{M} \left(\sin \frac{MZ}{h} \right) \exp (-M^2 T_v) \quad (1)$$

where

Z = vertical distance downward from the free draining upper surface of the consolidating layer.

t = time, with $t = 0$ at the instant of loading.

C_{vv} = the coefficient of consolidation in the vertical direction.

T_v = time factor defined as $T_v = \frac{C_{vv}t}{h^2}$

$$M = \frac{(2m + 1) \pi}{2}$$

Equation (1) was used to produce values of "predicted excess pore water pressure" which were subsequently compared to measured values.

The second type of test which was performed consisted of loading a similar soil sample in a similar mold but differed due to the insertion of a vertical wick drain of circular cross section through the sample center. Figure 2 shows the test cylindrical sample configuration.

The sample again undergoes consolidation with a frozen base as was the case with the control sample, so that some of the excess pore water pressure dissipates in the vertical direction as described by Equation (1). However, excess pore water pressure is simultaneously dissipating radially due to the presence of the wick drain. The wick drain is assumed freely draining in the mathematical model of radial consolidation described below. The determination of whether or not the wick drain would actually act in this way after undergoing the effects of freezing and thawing, was one of the objectives of the study.

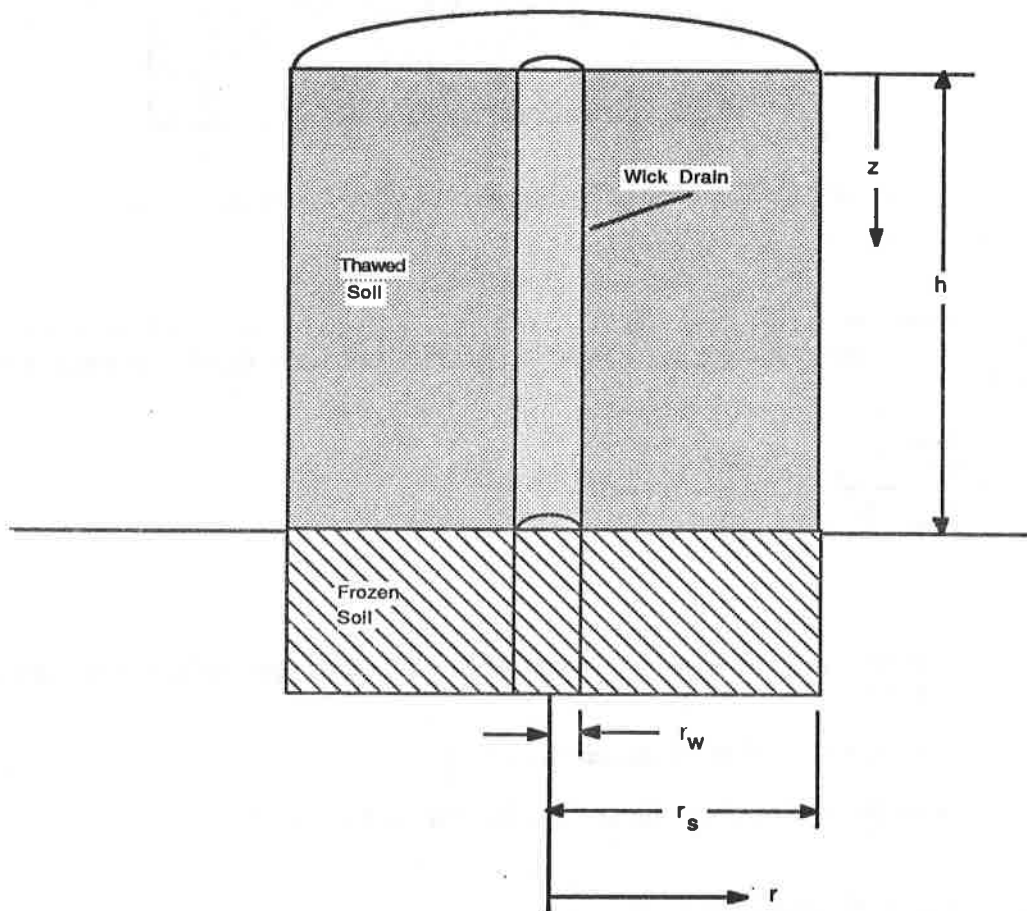


Figure 2. Geometry of Wick Drained Thawed Soil Undergoing Consolidation

The theory of radial consolidation was developed by Barron (1) and clarified by Johnson (3). Barron solved both the case of free strain and equal strain and the latter situation was utilized due to the nature of the device which applied load to the thawed specimen. For equal strain radial consolidation, Barron showed that excess pore pressure, u_r , at any time, t , and radial distance, r , as shown in Figure 2 is given by:

$$u_r = \frac{4 u_o \exp(\lambda)}{d_s^2 F(n)} \left[r_s^2 \ln\left(\frac{r}{r_w}\right) - \frac{r^2 - r_w^2}{2} \right] \quad (2)$$

where

u_o = constant uniform initial excess pore water pressure
 r_s = sample radius (as shown in Figure 2)
 d_s = sample diameter = $2r_s$
 r_w = wick radius (as shown in Figure 2)

$$n = \frac{r_s}{r_w}$$

$$F(n) = \frac{n^2}{n^2 - 1} \ln(n) - \frac{3n^2 - 1}{4n^2}$$

C_{vr} = coefficient of consolidation for radial flow at the appropriate stress level

$$T_{vr} = \text{radial time factor} = \frac{C_{vr} t}{d_s^2}$$

and

$$\lambda = \frac{-8 T_{vr}}{F(n)}$$

In these tests both vertical and radial consolidation occur simultaneously. Thus excess pore water pressure, u , at any point at depth, Z , and radial distance, r , is, according to Johnson (3), given by:

$$\frac{u}{u_o} = \left(\frac{u_v}{u_o} + \frac{u_r}{u_o} \right) \quad (3)$$

where

u_o = the constant uniform initial excess pore water pressure
 u_v = the excess pore water pressure with vertical consolidation only as given by Equation (1)

and

u_r = the excess pore water pressure with radial consolidation only as given by Equation (2)

Equation (3) was used to calculate the values of "predicted excess pore water pressure" which were subsequently compared to measured values of excess pore pressure for the wick samples.

DESCRIPTION OF SOILS TESTED

Two different soils, namely Moulton Silt and Sibley Till, were subjected to testing. Bulk samples of these soils were procured from the Massachusetts Department of Public Works Frost Research Station (MDPWFRS) in Winchendon, Massachusetts. These soils were selected since they had been shown to be frost susceptible to at least some degree both at the MDPWFRS and in the laboratory at WPI during earlier research.

Results of index and compaction tests performed on each soil in accordance with the indicated ASTM procedure are shown in Table 1. Since both soils had significantly higher than two percent of their weight comprised of particles finer than 0.02 millimeters, they were expected to be susceptible to significant ice lens formation.

Table 1
Results of Index and Compaction Testing

Soil	Sibley Till	Moulton Silt
<u>Property:</u>		
Specific (ASTM D854) Gravity	2.69	2.72
Liquid (ASTM D4318) Limit	20.0	not plastic
Plastic Limit (ASTM D4318)	15.8	not plastic
Particle Size (ASTM D422)		
% weight finer than:		
No. 4 (4.76mm)	83	100
No. 10 (2.00mm)	78	100
No. 20 (0.84mm)	71	100
No. 40 (0.42mm)	62	100
No. 60 (0.25mm)	55	100
No. 100 (0.149mm)	46	100
No. 200 (0.074mm)	35	96
0.02mm	20	78
0.005mm	12	15
0.001mm	7	4
Compaction (ASTM 698):		
Maximum Dry Density (pcf.)	128.0	98.0
Optimum Water Content (%)	9.0	21.0

TEST PROCEDURE AND APPARATUS

A comprehensive series of tests was performed in order to determine if vertical wick drains would accelerate pore water pressure dissipation within a soil which had been subjected to frost heave in the manner predicted by the previously described theory. This theory was originally developed for a soil-wick regime which was not frozen. During these tests, the soil was subjected to heave, subsequent thaw and static loading with pore water pressure measured during the static load phase of each test. These tests were performed for similar specimens with and without vertical wick drains in order that comparisons of behavior could be made. Major conclusions regarding the effectiveness of wick drains as a potential method of pothole repair were formed from the results of these tests. The precise sequence of steps performed for a typical test is described in detail below.

A 17 inch high sample was first fabricated in an acrylic cylinder 20.5 inches in height with an inner diameter of 10 inches increased by a one degree taper over the length of the cylinder that which confined the soil which would be expected to heave. The taper reduced the effects of side friction facilitating heave once ice lenses began to form. During fabrication, Type T thermocouples and pore water pressure measuring probes were placed at positions appropriate for eventual temperature and pore pressure dissipation monitoring. For wick samples, a drain constructed of filter fabric was placed in the center of the sample to a depth of 13 inches. In order to insure that the capillarity of the wick drain did not increase the frost susceptibility of the soil into which it was inserted, preliminary tests (not reported here) were performed on various wick drain fabric materials. Of the fabric samples tested, the fabric with the lowest opening size which exhibited negligible capillary rise was DuPont's Tyvar 3401. The drains eventually employed consisted of a hollow grooved perforated polyethylene core wrapped with Tyvar 3401 producing a circular cross section of one inch outer diameter.

The mold was placed in a frost cabinet capable of independently controlling temperatures at both the sample surface and base simulating frost heave in the field. The mold base was connected to a constant elevation water supply which was monitored to record moisture migration into the sample during all phases of the test. Heave measuring devices were also installed, and the sample was saturated via capillary action as required.

Insulation was packed around the mold and heave was initiated by lowering the temperature of the upper surface of the sample to a value below freezing. Once significant heave was produced, the temperature at the sample base was lowered and the sample was rapidly frozen throughout its entire length. The sample was next thawed from the top downward by increasing the upper surface temperature. Throughout this process, temperature, water migration into the sample, and sample heave were continually monitored and measured via the devices previously described. Eventually, the sample was thawed to a level slightly below the lowest pore pressure measuring device.

A static stress simulating traffic loading was applied to the leveled soil surface using a pneumatic loading device which fit into the frost cabinet. Pore water pressures were measured until satisfactory consolidation had occurred. Vertical consolidation as described by Equation (1) was assumed as if the frozen soil was impermeable, and soil temperatures were monitored during consolidation to validate the assumed thickness of thawed soil.

The sample was removed from the mold and precise locations of the pore pressure measuring devices were obtained to determine if movement had occurred during heave and thaw.

TEST RESULTS

Figure 3 portrays the results of a test series on Moulton Silt, by plotting the pore pressure as a percentage of the initial pore pressure, denoted %U, versus elapsed time measured at a point in the sample at a depth, Z, of 8.0 inches from the surface and located at a distance, r, of 3.0 inches from the center of the specimen for both the control sample and the sample in which a wick drain was installed.

To compare these results with expected results obtained from the theoretical analysis, the coefficient of consolidation of the soil was first calculated using the results of the measured pore pressure response from the control test. The value of the coefficient of consolidation calculated and used in the theoretical analysis was 1.3 sq. in./min. The theoretical variation of %U with elapsed time for the control sample and for a freely draining wick sample was calculated at a depth of 8.0 inches. In Figure 4, the measured %U and that predicted from theory are plotted against elapsed time for the control sample for a depth of 8.0 inches. In Figure 5, the measured and predicted values of %U are plotted for the wick sample at the depth of 8.0 inches. The results indicate that for the Moulton Silt, wick drains behaved in accordance with theory and therefore serve to accelerate pore pressure dissipation in a thawed soil.

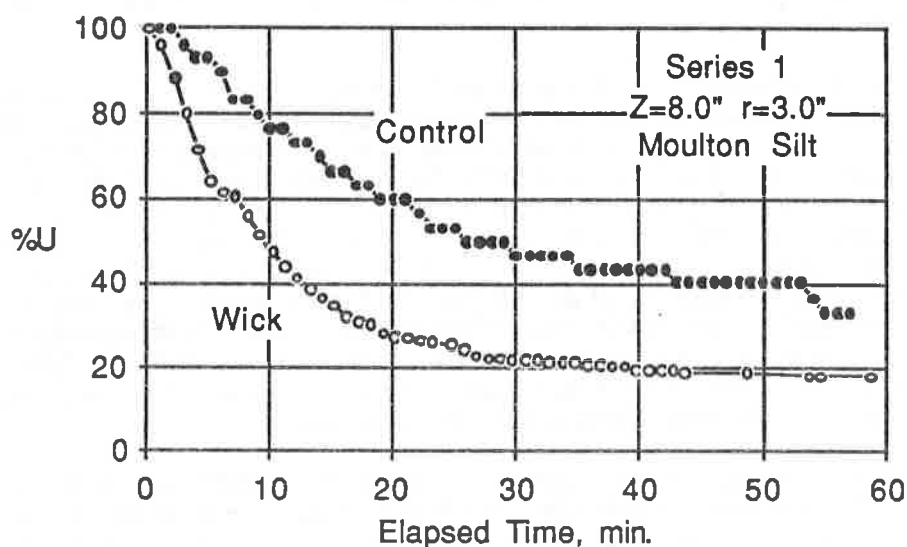


Figure 3. Measured Pore Pressure as a Percentage of Initial Pore Pressure Versus Elapsed Time.

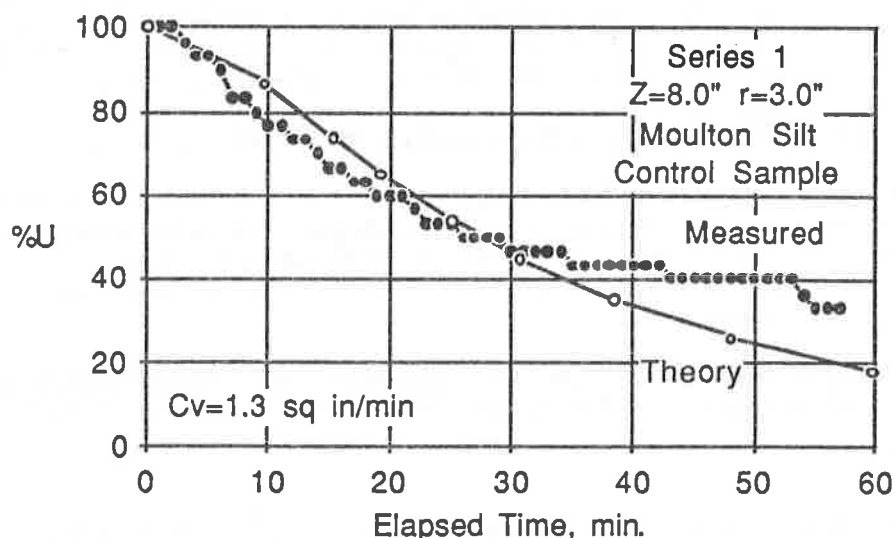


Figure 4. Measured and Theoretical Pore Pressure as Percentage of Initial Pore Pressure Versus Elapsed Time for the Control Sample of Moulton Silt.

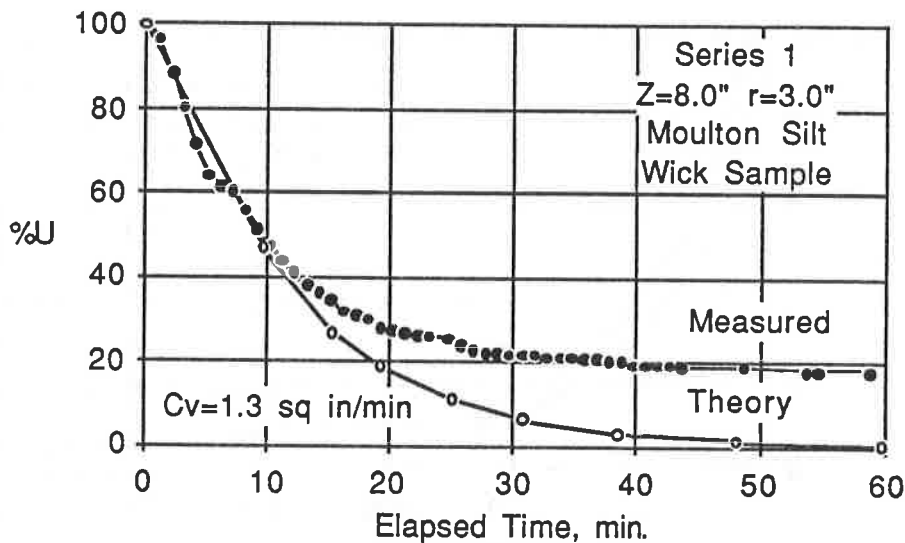


Figure 5. Measured and Theoretical Pore Pressure as Percentage of Initial Pore Pressure Versus Elapsed Time for the Wick Sample of Moulton Silt.

Figures 6 and 7 portray the results of a test series on Sibley Till, by plotting %U versus elapsed time at a point in the soil at a depth, Z, of 8.0 inches from the surface and located at distance, r, of 3.0 inches from the center of the specimen (Figure 6) and, r, of 1.0 inch (Figure 7) for both the control sample and the sample in which a wick drain was installed. These results indicate similar rates of pore pressure dissipation in both the control sample and the sample with the central wick drain.

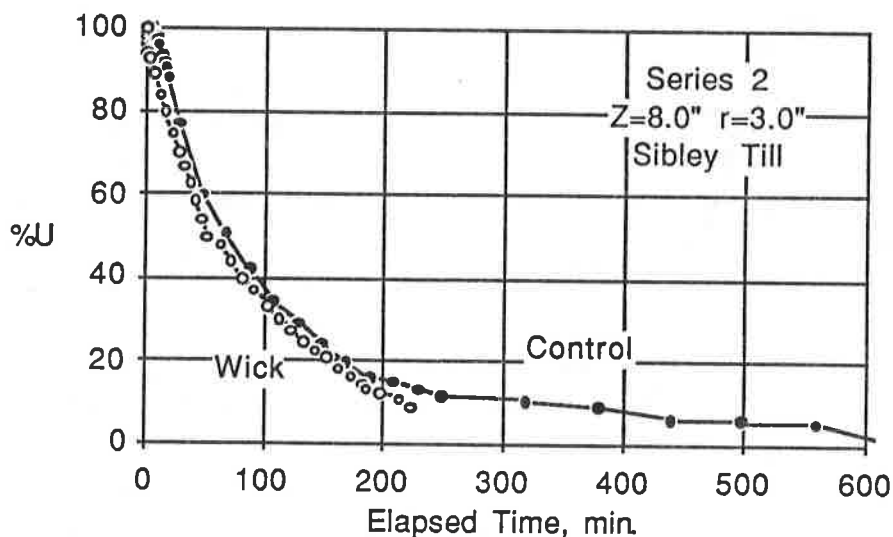


Figure 6. Measured Pore Pressures as a Percentage of Initial Pore Pressure Versus Elapsed Time for Sibley Till.

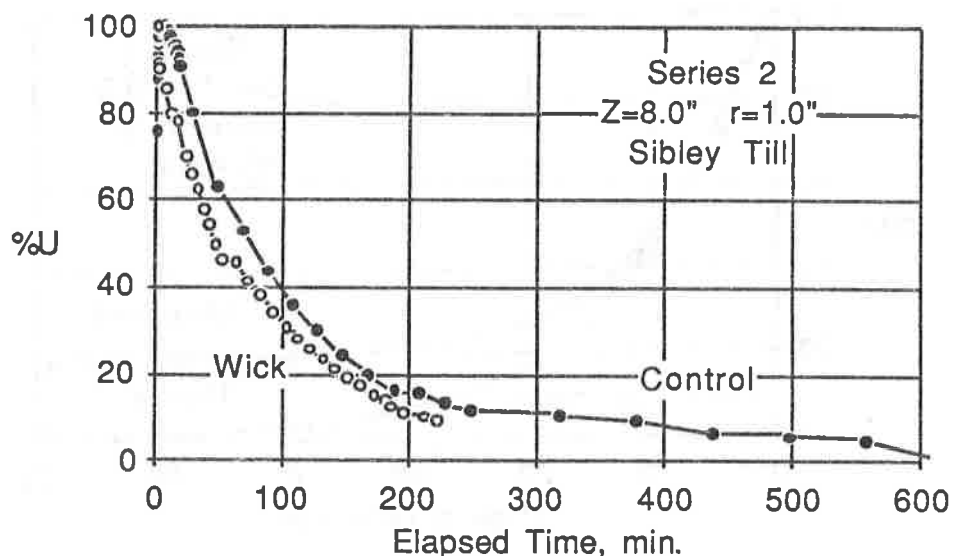


Figure 7. Measured Pore Pressures as a Percentage of Initial Pore Pressure Versus Elapsed Time for Sibley Till.

To compare these results with the expected results from the theoretical analysis, the coefficient of consolidation was calculated for the Sibley Till as was previously described for the Moulton Silt. An average coefficient of consolidation of 0.46 sq. in./min., was used in the theoretical model for Sibley Till to calculate the expected values of %U versus time for a depth, Z, of 8.0 inches for a radial distance, r, of 3.0 inches for the wick sample as shown in Figure 8. Again it is evident that the theoretical calculations, assuming a freely draining wick, predict more rapid consolidation than was actually observed.

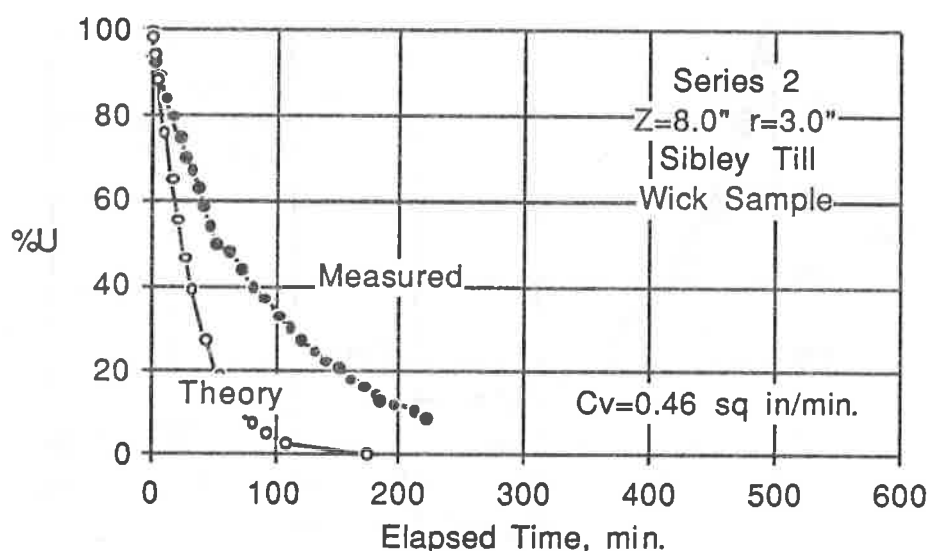


Figure 8. Measured and Theoretical Pore Pressures as a Percentage of Initial Pore Pressure Versus Elapsed Time for the Wick Sample for Sibley Till.

CLOSURE

The tests performed indicate that although the use of vertical wick drains constructed of "Typar 3401" filter fabric accelerates the dissipation of pore pressure in the Moulton Silt, it failed to perform up to expectations in the Sibley Till.

The drain utilized in this research performed as originally hypothesized in a non-plastic slowly draining frost susceptible soil. However, when that drain was tested in a plastic frost susceptible soil, the fabric of the drain appeared to clog. In light of the excellent results in the non-plastic soil, it seems premature to abandon the possibility of eventual use of wick drains. The development of geotextiles began relatively recently. Thus, it seems logical to expect that as standards governing fabric clogging criteria are developed, fabrics with smaller openings will be manufactured. Unfortunately, such fabrics may promote additional capillary rise of water and promote more frost heave. However, it is believed that this problem can be solved by designing suitable capillary draw restrictions along the longitudinal axis of the drain. Furthermore, wrapping appropriate fabrics around one another to produce a "graded" filtering effect would be feasible once finer opening fabrics are developed.

ACKNOWLEDGEMENTS

The test results presented in this paper are part of a research project on the long term mitigation of frost deterioration of existing roadways. The tests were performed by Jay Hedstrom. The material is based upon work supported by the National Science Foundation under Grant No. ECE-8518813. Any opinions, findings, and conclusions or recommendations expressed in this material are those of the authors and do not necessarily reflect the views of the National Science Foundation.

REFERENCES

- (1) Barron, R.A., "Consolidation of Fine-Grained Soils by Drain Wells", Transactions, ASCE, Vol. 113, 1948, pp. 718-754.
- (2) Eaton, R., Wright, E., & Mongeon, W., "The Engineer's Pothole Repair Guide", U.S. Army Corps of Engineers Cold Regions Research & Engineering Laboratory Technical Digest No. 84-1, March, 1984, pp. 1-12.
- (3) Johnson, S. J., "Foundation Precompression with Vertical Sand Drains", Journal of the Soil Mechanics and Foundations Division, ASCE, Vol. 96, No. SMI, January, 1970, pp. 145-175.
- (4) Sage, J.D., and D'Andrea, R.A., "Shear Strength Characteristics of Soils Subjected to Frost Action", U.S. Dept. of Transportation, Research and Special Program Administration Report No. DOT/RSPA/DMA-50/84/14 January, 1984, pp. 1-143.
- (5) Taylor, D.W., "Fundamentals of Soil Mechanics", Wiley, N.Y., 1948, pp. 208-247.

C.J. SPRAGUE

G. CICOFF

Hoechst Celanese Corporation, U.S.A.

**A Study of Permanent Road Stabilization: Low-Cost Pavement Structures
and Lightweight Geotextiles**

Phase I: Construction Survivability
Abstract

Greenville County, South Carolina, constructs permanent paved surfaces on approximately 20 miles of existing gravel roads each year. The County Engineer sought to protect his new low-cost pavements from premature degradation and more frequent maintenance by including an appropriate geotextile as a separator between the subgrade and the pavement structure.

A two-phase trial installation was made on an 8000+ foot county road. Phase I of the study looked at the construction survivability of the three fabrics used and is the focus of this paper. Phase II will be a long-term evaluation of stabilization effectiveness.

Three different pavement structures were installed over the subgrade, including:

1. 2½" full depth asphalt
2. 1½" surface asphalt and 3" stone base
3. Triple treatment surface and 3" stone base

Five hundred feet of a 4 oz/yd² needlepunched nonwoven geotextile and a 4 oz/yd² slit film woven geotextile were installed beneath each pavement type on comparable grades and subgrade conditions. Additionally, a 6 oz/yd² needlepunched nonwoven was installed under road sections encountering severe conditions such as steep grades and subgrade drainage problems. Control sections were constructed without fabric for each pavement type.

Numerous samples were exhumed from beneath the two pavement types after the stone base had been completely spread and compacted, but before the surface course was constructed. Mullen Burst (ASTM D-3786) and puncture (ASTM D-3787) tests were run on all exhumed samples. Testing indicated that, under comparable conditions, like-weight woven and nonwoven geotextiles exhibit virtually the same degree of construction survivability in terms of percent strength retained. Additionally, the grade on which the installation was made has a significant influence on geotextile survivability.

Introduction

Greenville County, South Carolina, constructs permanent paved surfaces on approximately 20 miles of existing gravel roads each year. The County Engineer sought to protect his new low-cost pavement from premature degradation and more frequent maintenance by including an appropriate geotextile as a separator between the subgrade and the pavement structure.

The physical properties required to make the geotextile an effective long-term separator include both strength properties, which resist the forces of coarse aggregate being pushed into the subgrade, and hydraulic properties, which prevent the pumping of fine soils up into the coarse base aggregate while still allowing for pore water pressure dissipation from the subgrade.

The necessary hydraulic properties will be evaluated in Phase II of this study. The required strength properties to survive construction and provide long-term separation are looked at in Phase I.

Installation Layout

Stockton Road, in southern Greenville County, South Carolina, was selected for this trial installation because it had been surfaced with aggregate twice in the preceding 18 months and was once again in need of additional surfacing. This was a clear indication that the road subgrade was unstable when saturated and could benefit from the installation of a stabilization geotextile.

The full length of the road, approximately 8100 feet, was surfaced with pavement sections as detailed in Table I. The following cross-sections were used on approximately one-third of the road each:

- 1" triple treatment surface course over 3" compacted stone base.
- 1½" asphaltic concrete surface course over 3" compacted stone base.
- 2½" full depth asphaltic concrete binder course.

Approximately 500 feet each of three different geotextiles, 4 and 6 oz/yd² needle-punched nonwoven geotextile and a 4 oz/yd² slit film woven geotextile, were installed between the subgrade and each pavement section. The remaining footage of the road will act as a control for the long-term evaluation of each pavement section.

Prior to the placement of the geotextile or pavement systems, the road subgrade was fine graded, surface saturated by water truck, and baseline cone penetration measurements were made.

Table 1
Stockton Road Pavement Installation

<u>Station</u>	<u>to</u>	<u>Station</u>	<u>Stabilization</u> <u>Geotextile</u>	<u>Pavement Section</u>
0+00		5+00	A	2½" Full Depth Asphalt
5+00		10+00	B	2½" Full Depth Asphalt
10+00		20+00	None	2½" Full Depth Asphalt
20+00		25+00	C	2½" Full Depth Asphalt
25+00		30+00	None	1½" Asphalt over 3" Stone Base
30+00		35+25	A	1½" Asphalt over 3" Stone Base
35+25		40+25	B	1½" Asphalt over 3" Stone Base
40+00		45+50	None	1½" Asphalt over 3" Stone Base
45+50		50+00	C	1½" Asphalt over 3" Stone Base
50+00		55+00	C	Triple Treatment over 3" Stone Base
55+00		61+00	None	Triple Treatment over 3" Stone Base
61+00		66+00	B	Triple Treatment over 3" Stone Base
66+00		71+00	A	Triple Treatment over 3" Stone Base
71+00		81+00	None	Triple Treatment over 3" Stone Base

Table 2
Typical Properties of Stabilization Geotextiles

<u>Construction</u>	<u>ASTM</u> <u>Method</u>	<u>A</u>	<u>B</u>	<u>C</u>
		<u>PET</u> <u>Continuous</u> <u>Filament</u> <u>Needlepunched</u> <u>Nonwoven</u>	<u>PP</u> <u>Slit Film</u> <u>Woven</u>	<u>PET</u> <u>Continuous</u> <u>Filament</u> <u>Needlepunched</u> <u>Nonwoven</u>
Weight, oz/yd ²	D3776	4.2	4.0	6.0
Grab Strength, lbs	D4632	135/110	200/200	205/175
Grab Elongation, %	D4632	70/85	20/18	75/85
Puncture, lbs	D3787	60	80	90
Trapezoid Tear, lbs	D4533	60/50	65/65	80/75
Mullen Burst, psi	D3786	210	385	315
Water Flow Rate, gpm/ft ²	D4491	140	5	130
A.O.S., sieve size	D4751	70-100	40	70-100

Site Data Collection and Evaluation

To facilitate meaningful evaluation of long-term road performance, the following information was obtained during the trial installation:

- Road centerline survey including staking of stations (50 foot intervals)
- Centerline plan and profile of roadway, including stations, fabric location and I.D., and pavement location and I.D.
- Saturated soil strength as measured using the Cone Penetrometer Index.

The survey revealed two segments of the roadway that would provide conditions significantly different than the rest of the road. These two segments involved edge drains with no outlets and steep grades, respectively. It was decided to use a heavier nonwoven geotextile in these areas and concentrate the use of the 4 oz/yd² geotextiles in the areas of more uniform conditions to facilitate more accurate performance comparisons of the like-weight materials.

Cone penetrometer data indicated that the road subgrade either varied in its stability over its length or, more likely, greater water penetration was achieved in portions of the roadway. Penetrometer readings were consistently in the 150 to 180 range ($c = 12$ to 15 psi), but from Station 0+00 to Station 57+50 they were achieved at an average penetration depth of less than one inch. From Station 58+00 to 81+00 the average penetration depth was approximately $1 \frac{3}{4}$ inches. In either case, the upper zone of the subgrade appeared affected by saturation.

Geotextile Installation and Road Base Construction

With the road and edge drains fine graded for proper cross-slope and drainage, installation of the geotextiles began. The first segment to be constructed involved the construction of the stone base in two - $1\frac{1}{2}$ " compacted lifts followed by a triple treatment surface course. The very thin lifts of base material with a substantial coarse fraction (see Table 3 for base aggregate grain size analysis) were expected to produce a "worst case condition on the geotextiles."

The second segment to be constructed involved the construction of a full 3" compacted lift of stone base followed by a 1" asphaltic concrete surface course.

The third constructed segment was a compacted $2\frac{1}{2}$ " of full depth asphaltic concrete binder course.

In all three segments, the geotextiles were unrolled and tacked in place using 16 penny nails to prevent them from being disturbed by the wind. Special caution was taken to eliminate any wrinkles in the geotextile in the full-depth segment. Since the geotextile was tacked down, only a nominal 6"-12" overlap was required on the dry, firm subgrade.

Table 3
Road Base Aggregate
Sieve Analysis

<u>50+00 to 81+00</u>		<u>25+00 to 50+00</u>	
<u>Sieve #</u>	<u>Percent Passing</u>	<u>Sieve #</u>	<u>Percent Passing</u>
1 $\frac{1}{2}$	100	1 $\frac{1}{2}$	100
1	92.5	1	96.9
3/4	79.9	3/4	90.0
1/2	69.7	1/2	76.8
3/8	63.1	3/8	69.2
4	52.7	4	56.7
8	45.7	8	47.8
16	37.9	16	39.0
30	30.0	30	30.5
50	19.5	50	19.6
100	10.7	100	10.7
200	5.7	200	5.5
PAN	--	PAN	--

Trucks dumping base aggregate were allowed to run and dump directly on the fabric. This was considered a "practical" acceptance of the typical methods of constructing these low-volume roads as well as providing a "worst case" evaluation.

A motor grader spread the aggregate to the desired depths and an 8-ton steel-wheeled roller provided the compaction of the base material. Geotextile sampling for construction damage was done after the completion of the aggregate base, but before the construction of the surface course.

The third pavement segment was full-depth asphalt binder to a compacted thickness of 2½". No sampling was done in this segment, but some field observations were made.

The only unsatisfactory observations made during the construction of the full-depth segment involved placement of the 2½" of hot asphalt on the woven slit film geotextile. Circular-arc shaped cracks appeared in the pavement as the paver progressed up a very modest (< 1%) grade and once again when paving a somewhat steeper grade. This is believed to be a result of slippage of the pavement at the geotextile/pavement interface.

Exhuming Geotextile Samples

Geotextile sampling for determination of construction damage was performed following compaction of the aggregate base. It was assumed that the most severe construction loadings occur during set-up of the base aggregate and that construction of the ensuing surface course would impose less significant stresses on the geotextiles.

Geotextile sampling was not done in the full depth asphalt pavement segment. Construction stresses in this segment only involved asphalt trucks running directly on the geotextile, which was similarly done by aggregate trucks in the other two segments, and paver wheel loads which appeared insignificant.

Samples were initially exhumed by shoveling aggregate off 30" x 30" areas every 50 feet and cutting out 18" x 18" geotextile samples. 30" x 30" patches were then "tucked in" to repair the sampled area.

After the initial sampling of the first segment, shoveling was restricted to a "doughnut" around the 18" x 18" sample. The sample was then cut and the aggregate was gently rolled off the geotextile. It was hoped that this would minimize abrasion to the fabric due to the sampling. Subsequently, the first segment was resampled using the "doughnut" approach. Laboratory results did not indicate that shoveling aggregate off the sample rather than the "doughnut" approach resulted in more abrasion to the geotextile.

All samples were marked with the station number corresponding to the sampling location and a note was made if aggregate depth above the fabric varied significantly from the desired 3 inches.

Laboratory Testing and Results

The evaluation of construction damage of the geotextile required laboratory testing of appropriate strength properties to determine the extent of degradation resulting solely from construction-related activities.

It was decided to utilize those strength properties which are often cited in stabilization geotextile specifications but which are independent of fabric orientation. This simplified the notation requirements on the exhumed fabrics.

Two non-directional tests, Mullen Burst and puncture, were chosen. These tests are quick and straight forward and each provides a useful measure of strength loss during construction.

Control samples were cut from the rolls received on site and tested in the laboratory to verify that published data was acceptable for subsequent comparisons.

Ninety-nine field samples were exhumed--twenty-two of each geotextile in segment one and eleven of each geotextile in segment two. Most field samples had puncture damage to a minor extent. To avoid extreme results, both Mullen Burst and puncture tests were set up to intentionally exclude obvious puncture holes. Five Mullen Burst and five puncture tests were run on each sample and the results were averaged.

The results, as could be expected, were widely scattered, but when averaged for each sample and for each location, when two samples were exhumed from the same location, the results appeared quite consistent.

As shown in Table 4, the 4 oz/yd² fabrics used in the low survivability conditions performed similarly in terms of percent strength retained. The slit film woven geotextile appeared to be somewhat less susceptible to reduction in puncture strength while just slightly more sensitive to Mullen Burst strength reduction than the nonwoven needlepunched geotextile. The differences seem relatively insignificant and do not appear to be grounds for differentiating between the two geotextiles for purposes of construction survivability. Four ounce per square yard geotextiles are more susceptible to puncture than to abrasion under thin base aggregate lifts. While a relatively small percentage strength reduction was apparent, puncture holes were apparent in nearly every sample.

Table 5 gives interesting insight into the need for a more durable geotextile when more demanding survivability conditions are experienced. The six ounce per square yard needlepunched nonwoven geotextile experienced approximately 20% and 40% strength loss in the two pavement segments built using aggregate base. This data points out the importance in considering road grade and drainage when assessing survivability conditions and would indicate that this geotextile may not have been durable enough for the given moderate survivability conditions.

Note that under both low and moderate survivability conditions (see Tables 4 and 5), the allowance of extraordinarily thin compacted lifts of base course, as was allowed in the triple treatment segment of Stockton Road, should elevate the applicable geotextile survivability conditions one level (i.e., from low to moderate).

Table 4
Low Survivability Conditions*
Geotextile Strength Retained

	4 oz/yd ² Continuous Filament Needle punched		4 oz/yd ² Slit Film	
	NONWOVEN		WOVEN	
	Mullen	Puncture	Mullen	Puncture
	<u>Burst %</u>	<u>%</u>	<u>Burst %</u>	<u>%</u>
Triple treatment over 3" Base	80	80	77	100
1" Asphalt Surface over 3" Base	100+	100+	93	100+

*Heavy construction equipment operating on firm, dry, well draining subgrade. Road grades are flat to slight.

Table 5
Moderate Survivability Conditions**
Geotextile Strength Retained

	6 oz/yd ² Continuous Filament Needle punched Nonwoven	
	Mullen	Puncture
	<u>Burst %</u>	<u>%</u>
Triple treatment over 3" Base	57	73
1" Asphalt Surface over 3" Base	77	79

**Heavy construction equipment operating on poorly drained subgrade. Road grades are moderate to steep.

Conclusions and Long-Term Monitoring

Geotextiles have long been used to enhance the long-term performance of low-cost roadways. Long-term performance of the roadway might well depend on the ability of the geotextile to survive construction without a significant reduction in physical properties. Phase II of this study will look at long-term performance.

Following are conclusions concerning the construction survivability of geotextiles in low-cost, low-volume pavement structures:

- Like-weight woven slit film and nonwoven needlepunched geotextiles exhibit the same degree of construction survivability, in terms of retained strength, under like conditions.
- The required level of survivability must include an assessment of lift thickness of base aggregate and roadway grade, as well as saturated subgrade strength and construction vehicle loading.
- 4 oz/yd² geotextiles of all types are too light-weight to resist localized puncturing when thin base course lifts are used.
- Table 6 summarizes survivability conditions and suggested appropriate geotextile mass per unit area.

Table 6
Geotextile Specifications for Construction Survivability
in Low Cost, Low-Volume Roads¹

<u>Level</u>	<u>Subgrade Conditions</u>	<u>Base Course Thickness²</u>	<u>Geotextile Mass/Unit Area</u>
Low	Dry, firm, flat	> 6" compacted	4 oz/yd ²
Moderate	Water sensitive, flat	> 3-4" compacted	6 oz/yd ²
High	Water sensitive, grade >2%	> 3-4" compacted	8 oz/yd ²

¹These recommendations incorporate the allowance for construction vehicles to run directly on the fabric during aggregate base construction.

²For base course lifts less than 3", required survivability should be increased one level (i.e. low to moderate).

Slit film woven geotextiles should not be used between the subgrade and a full-depth asphalt pavement.

T.C. KINNEY
B.M. SAVAGE

University of Alaska, Fairbanks, U.S.A.

Using Geosynthetics to Control Lateral Spreading of Pavements in Alaska--Preliminary Results

SUMMARY

Longitudinal cracking of pavement presents a serious safety hazard to motorists as well as a costly maintenance problem to the State of Alaska. One way to alleviate this problem is to reinforce embankment or pavement sections with a high strength, high modulus geosynthetic. This paper presents the results of a field test using a single layer of geogrid near the pavement surface. This allows the embankment section to crack without affecting the road surface. This paper presents one stage of a research project to develop a design procedure for using a geogrid in the maintenance or rehabilitation of a road section. The theory is presented along with initial results of a field test that verified the validity of the design approach.

INTRODUCTION

Lateral spreading of road embankments can cause longitudinal cracking of the pavement surface. Many mechanisms causing lateral spreading are progressive in nature, so the longitudinal cracks continually get wider with time until they are dangerous to motorists. There are many causes of progressive lateral spreading such as the embankment overstressing the soft subgrades, slope instability, and thawing permafrost. Literally hundreds of miles of roads in Alaska have progressive lateral spreading of the embankment materials, with pavement cracking rates of up to one inch per month (Photograph 1). The pavement is sometimes patched several times in a single summer, and voids large enough for wheels to drop into are commonly found in the major highways (Photograph 2).

The most commonly used repair is the "dump and run" technique, which consists of filling any visible holes with asphalt and leveling the road surface. This leaves a void under the pavement that can approach several feet across before the condition becomes intolerable and the road is rebuilt. Catastrophic failures could be averted by grouting all cracks at the time of asphalt repair, but this is not routinely done.

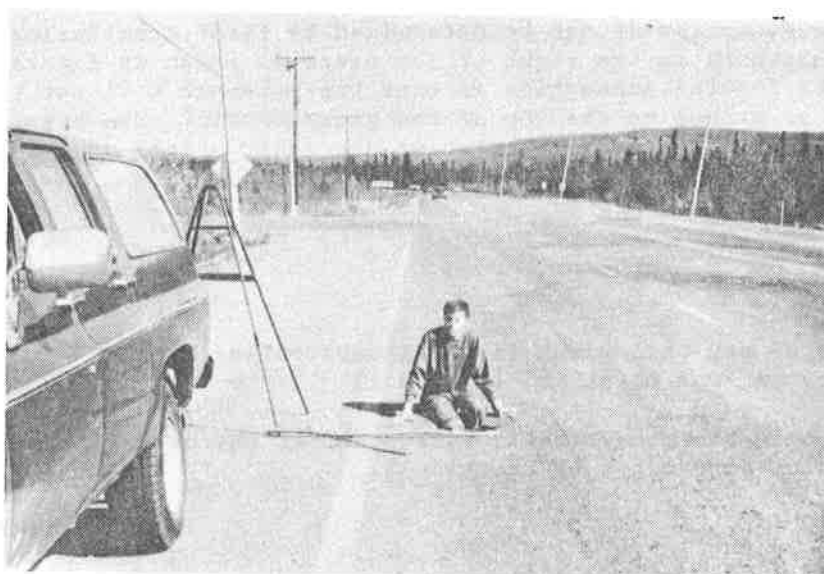
This report presents a design technique for stabilizing the road surface using a single layer of geosynthetic placed several inches below the pavement surface. We also present the initial set of field tests performed using the design concept. Additional laboratory tests, field tests, and theoretical analyses are under way.

THEORY

There are two independent parts to the theoretical design. The first deals with the



Photograph 1. Longitudinal cracks in Farmers Loop Road, Fairbanks, Alaska.



Photograph 2. Hole in Farmers Loop Road, Fairbanks, Alaska caused by thawing ice.

Geosynthetics '89 Conference
San Diego, USA

tension and strain that develop in the geosynthetic and surfacing materials during lateral spreading and cracking of the embankment without the traffic loading. The second deals with the performance of the area over the crack in the embankment with traffic loading. Each part will be treated separately. Both are equally important in design.

Performance During Lateral Spreading Without Traffic Loading

During lateral spreading, the subbase materials will slide outward along the bottom of the geosynthetic as shown in Figure 1. About 0.1 inches of relative movement between the lower embankment materials and the geosynthetic are required to develop full frictional resistance between the two. Since a small amount of relative movement will result in the maximum shear stress, it is sufficiently accurate to assume that the shear stress is zero or maximum at every point along the geosynthetic. The maximum shear stress on the bottom of the geosynthetic can be determined using Equation 1.

$$S = D * H * f \quad (\text{Eq. 1})$$

where:

S = shear stress on the geosynthetic
D = average density of material above geosynthetic
H = height of material above geosynthetic
f = coefficient of friction between geosynthetic and material below

The tension in the geosynthetic can be determined by first considering only the portion of the embankment to the right of the crack as shown in Figure 1. For simplification, the initial assumption is that the pavement will not take tension, so there is no shear stress on the top of the geosynthetic. The tension in the geosynthetic can be determined by integrating the shear stress on the geosynthetic from the free end (point "a") to the left using Equation 2.

$$t = S * x \quad (\text{Eq. 2})$$

where:

t = tension per unit width in the geosynthetic
x = distance from point "a" (Figure 1)

The maximum tension in the geosynthetic will occur at the crack in the embankment and will have a value determined by Equation 3.

$$T = S * L \quad (\text{Eq. 3})$$

where:

T = maximum tension per unit width in the geosynthetic
L = distance from the closest free end as shown in Figure 1

The maximum tension, coupled with an appropriate factor of safety, is one design criterion for the geosynthetic.

Assuming that there is minimal shear strain in the embankment material, the shear stress on the bottom of the geosynthetic to the left of the crack as shown in Figure

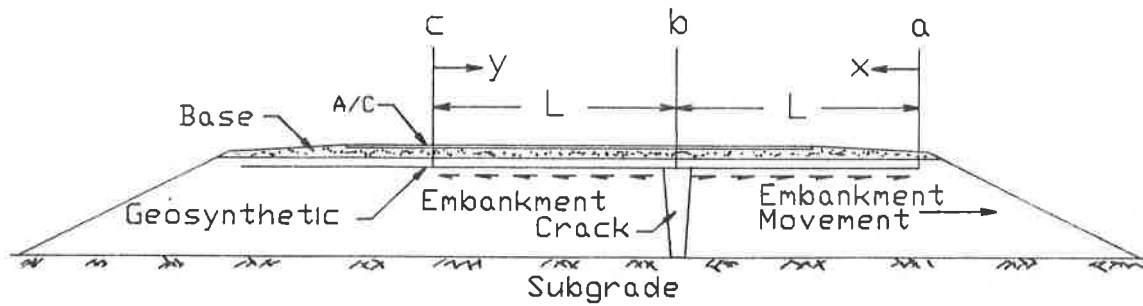


Figure 1. Typical cross section of road embankment.

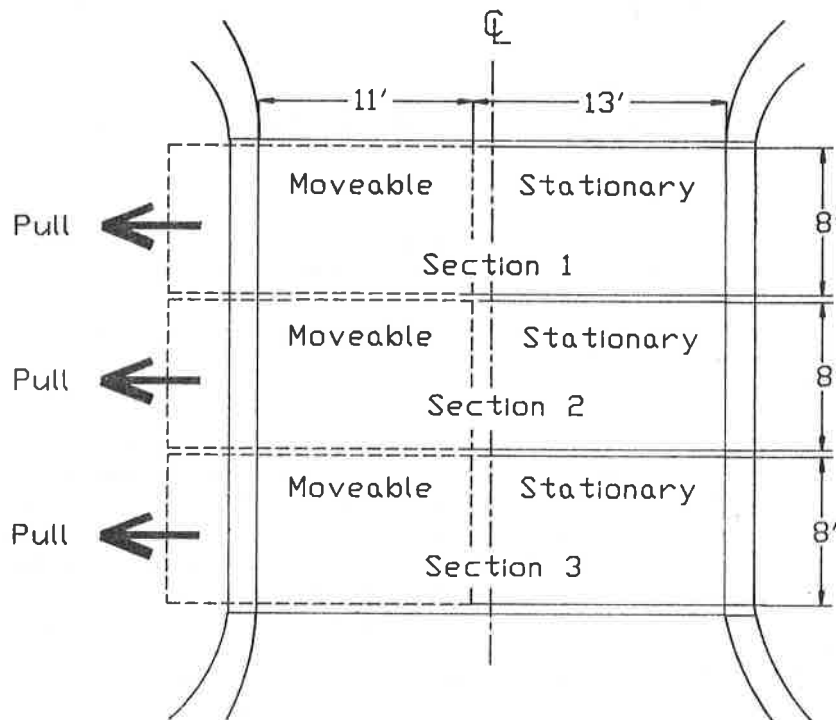


Figure 2. Plan view of test sections.

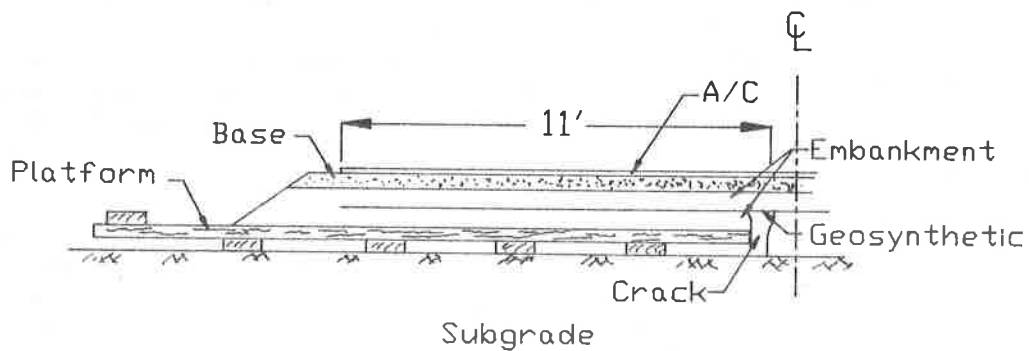


Figure 3. Typical cross section of test.

Geosynthetics '89 Conference
San Diego, USA

l must be the maximum for a distance of L away from the crack to satisfy static equilibrium. The tension in the geosynthetic to the left of the crack can be determined in the same manner that it was on the right.

The tension in the geosynthetic causes strain in the geosynthetic. This strain will be a function of the stress strain properties of the geosynthetic at the strain rate dictated by the field conditions.

The absolute displacement of any point on the geosynthetic can be determined by integrating the strain in the geosynthetic from point "c" in Figure 1 to the right over the length of the geosynthetic. If the geosynthetic is linearly elastic, the displacement of any point can be represented by Equation 4.

$$d = (1/2) * (t/E) * y \quad \text{for} \quad 0 < y < L \quad (\text{Eq. 4})$$

and

$$d = (1/2) * (T/E) * L + (1/2) * ((T+t)/E) * (y-L) \quad \text{for} \quad L < y < 2*L$$

where

d = absolute displacement of the geosynthetic
E = the effective secant modulus of the geosynthetic

The maximum stretch of the geosynthetic can be represented by Equation 5

$$d_{\max} = T/E * L \quad (\text{Eq. 5})$$

If the surface is paved and the paving material will sustain tension, the conditions are much more complex. The outward motion of the geosynthetic caused by its stretching will create tension in the paving material. This will put a shear stress on the top of the geosynthetic in the direction opposing the motion of the geosynthetic. The pavement and the geosynthetic will then act in tandem to resist the outward motion of the material under the geosynthetic. If this occurs, the pavement is placed in permanent tension, which will cause it to fatigue crack more quickly. If the paving material is creep sensitive or plastic, time and traffic loading will reduce or eliminate the tension stresses in these materials. It is conservative to neglect any effect of tension in the pavement material on the geosynthetic performance, so we have done this in the remainder of our discussion.

It would be highly desirable to construct the road section up to the point of paving and then let the embankment expand laterally until maximum tension was developed in the geosynthetic. This would force the geosynthetic to carry nearly all of the tension created by lateral spreading. There would be some additional spreading of the surfacing (and tension in the paving material) even if this is done, because the weight of the paving material adds to the shear stress on the bottom of the geosynthetic. In addition, the paving material must compensate for any creep within the geosynthetic.

The amount of lateral spreading that the designer feels should take place before paving will dictate when paving should be done. If the section is designed so that the material over the geosynthetic will spread two inches and if two inches of lateral spreading occurs in one year, then the pavement should be placed one year after the rest of the construction. A higher modulus geosynthetic will reduce the amount of lateral spreading that will occur over it and, therefore, reduce the time to completion of the project.

If paving is done immediately after construction, the pavement will be subjected to a tensile strain that is in relation to the strain in the geosynthetic. If the pavement material will not take much tension at the rate of loading experienced in the field, the pavement may develop a series of micro cracks or the pavement may become thinner. If cracks develop, they may heal under traffic loading. If the pavement will take a substantial tension, there will be fewer cracks, but each one will be larger. There will not necessarily be any relationship between the cracks that develop in the pavement and the ones that develop in the embankment materials below the geosynthetic.

Performance Over Crack With Traffic Loading

After a crack develops under the geosynthetic, the geosynthetic and the material above it must support the traffic load over the crack. This will occur through a combination of hoop tension in the geosynthetic and bridging in the materials above the geosynthetic. If properly designed, the geosynthetic will substantially increase the bridging ability of the materials above it as well as provide the hoop tension. Hoop tension theory is fairly well developed. When the width of the void is much larger than the thickness of the fill, hoop tension dominates the problem. In the application considered herein, the crack width will probably be less than the thickness of the fill over the geosynthetic, and bridging action will likely dominate.

There is a substantial body of circumstantial evidence indicating that geosynthetics can increase the bridging action, but no conclusive theory has yet been developed. The quantitative work that has been done does not fit the constraints of the design considered herein. At this point in the development of the design methodology, it appears prudent to rely heavily on empirical data. The tests reported on herein provide the only truly applicable data available to the authors.

Very little is known about the dynamic effects of traffic loading on either the geosynthetic or the cracks in the soils or pavement. One would presume that there would be little effect on the geosynthetics but that the cracks might collapse under dynamic loading, in effect making them wider.

Soil-Geogrid Friction and Required Geogrid Joint Strength

There has been a considerable amount of discussion regarding required joint strengths, methods of measuring joint strengths and methods of measuring soil-geosynthetic friction. At this writing, the preferred method of measuring soil-geosynthetic friction seems to be a pullout box. Soil is placed above and below the geosynthetic in a box, and the geosynthetic is pulled out laterally through the side of the box. Use of this technique has led some researchers to the conclusion that the maximum pullout strength (shear strength) can only be realized if the joint strength approaches the strength of the straps.

The pullout box does not model the application considered herein. In a uniform sand, each individual joint would need to carry a major portion of the shear stress over the area between that joint and the surrounding joints. At a depth of one foot, with six nodes per square foot, each node would have to carry about 20 pounds.

Geosynthetics '89 Conference
San Diego, USA

A problem arises when there is an obstruction (such as a large rock) penetrating the grid in an area where there is a large differential movement between the grid and the material below.

In isolated incidences, it would be better if the joint failed and slippage could occur. If many such protrusions are anticipated, it would be preferable to place a membrane such as a geotextile under the grid. This would reduce the stress in the grid and avoid the stress concentration problem.

FIELD TEST

Test Configuration

The field test consisted of a full-scale road embankment containing three test sections. Each test section was eight feet long parallel to the centerline of the road and 24 feet wide perpendicular to the centerline of the road as shown in Figure 2.

Each section had one lane built on a silt subgrade and the other lane built on a wooden platform as shown in Figure 3 and Photograph 3. The longitudinal crack in the road was simulated by pulling the wooden platform away from the centerline, leaving a crack. The stationary lane was 13 feet wide and the platform was 11 feet wide, positioning the crack one foot off centerline.

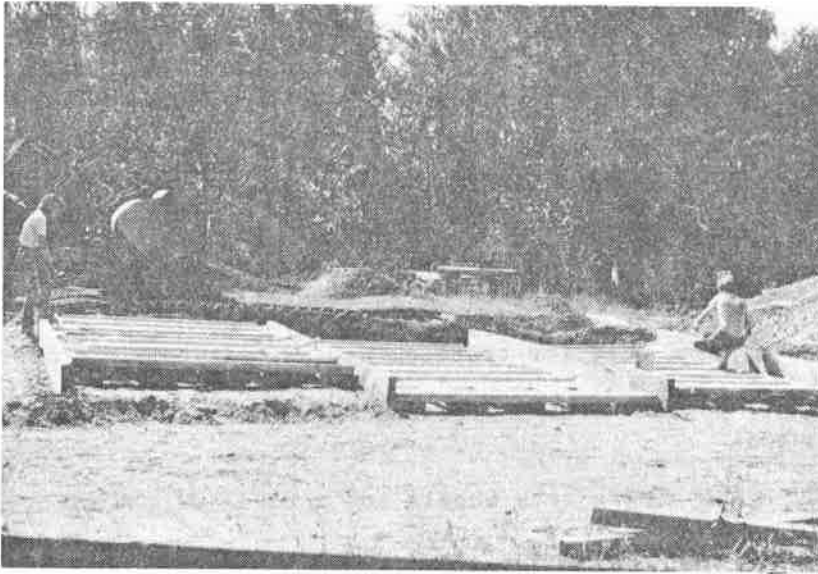
Test Section Construction

The silt subgrade was leveled, and the wooden platforms were constructed as shown in Photograph 3. Sand and gravel fill was then brought up to an elevation of six inches over the wooden platforms and compacted with several passes of a vibratory steel wheel roller. A strip of the grid was placed over test section 2, and another six inches of fill were placed and compacted on sections 1 and 2. A strip of grid was placed over test section 3, and 4.5 inches of crushed rock base course material was placed and compacted over all three sections. Test section 1 served as the control section and thus did not contain a layer of geogrid.

After the crushed rock base course material was placed, each of the wooden platforms was pulled out from the centerline a few inches to create the initial strain in the grid. In test section 1, a crack with a width equal to the length of the pull formed at the back side of the platform. In the other two test sections, hairline cracks were evident throughout the sections, but none of them was wide enough to fill. The crack in test section 1 was filled with crushed rock, and the surfaces of all three test sections were compacted again. Then 1.5 inches of asphalt were added to the surface of all three test sections.

The wooden platforms under test sections 1 and 3 were pulled again. The asphalt in test section 1 failed immediately, and the crack was filled with sand and gravel to allow completion of the test. Test section 1 was abandoned at this time.

Trafficking was done first with a light truck and then with a heavy truck. The truck was driven forward and then backed up across the test sections, keeping the wheel path directly over the crack (Photograph 4). Following trafficking, the wooden skids were pulled further and trafficking was done again. We looked for cracks, measured vertical and lateral movement of numerous points on the surface of the asphalt and measured the distance the skids were pulled.



Photograph 3. Test facility under construction.



Photograph 4. Trafficking test section.

**Geosynthetics '89 Conference
San Diego, USA**

The test sections were considered to have failed when they had three inches of vertical displacement (Photograph 5). Following failure, the areas between the test sections were excavated to assure that there was a void of the anticipated width and depth at the proper location.

Materials and Equipment

A polyester geogrid with a published short-term strength of 6,000 pounds per foot and a modulus of 156,000 pounds per foot at 2% elongation was used.

Three different trucks were used for trafficking.

1. A light duty flatbed truck with single rear wheels and a total weight of 4,960 pounds.
2. A Suburban with single rear wheels and a total weight of 5,500 pounds.
3. An empty dump truck with dual rear wheels on tandem axles and a total weight of 21,460 pounds.
4. A loaded dump truck with dual wheels on tandem axles and a total weight of 37,540 pounds.



Photograph 5. Test sections after three inches of vertical deformation.

Data

At no time did the asphalt in test sections 2 and 3 crack more than a few thousandths of an inch. Even hairline cracks did not appear until there was nearly two inches of vertical movement over the crack. Trafficking with the light trucks caused a fairly narrow depression to form. When the loaded dump truck was used, it tended to flatten out the depression, which had the net result of slightly reducing the maximum depth of the rut.

The testing sequence, including the width of the crack and the maximum rut depth after trafficking, is shown in Table 2.

Table 2. Test data.

Step	Truck Weight lb	Number of		Section 2		Section 3	
		Passes		Total	Rut	Total	Rut
		Light	Heavy	Void Width in	Depth in	Void Width in	Depth in
1	Finish construction up to the asphalt						
2	-	-	-	11.1	-	4.0	-
3	Pave						
4	4,960	300		11.1		7.6	
	21,460	150	100		1.25		1.19
5	4,960	150	100	15.0	1.31	12.1	1.69
6	5,500	60	50	21.8	1.62	15.8	1.75
7	-	-	50	29.8	2.12	23.6	2.25
8	-	-	50	36.5	2.69	29.9	3.19

CONCLUSIONS

Our test data substantially support the design concepts presented herein for the use of geosynthetics to stop the lateral spreading of pavement. The data also support the assertion that the use of the geosynthetic in the described application may significantly reduce, if not eliminate, both the associated danger to the motorists and the expense of road repairs that often occur with lateral spreading. Although our results are preliminary, it appears that cracks up to two feet wide can be spanned with an acceptable amount of vertical deformation using commercially available materials.

ACKNOWLEDGEMENTS

Funding for the research was provided by the Research Section of the Alaska Department of Transportation and Public Facilities and the ITW/Signode Corporation. The location for the test and some of the material were donated by H & H Contractors in Fairbanks, Alaska.

J. PERFETTI

Rhone-Poulenc Fibres, France

T. SANGSTER

Rhone-Poulenc Chemicals Ltd., United Kingdom

The Function of Geotextiles in Pavement Structures

(1) INTRODUCTION

Sheets of cotton were first used as reinforcement to asphalt layers in roads in North Carolina in the 1930s. Since then there have been numerous cases of textile materials being used in the upper layers of roads. Many of the results of these uses have been disappointing as the role of the textile has been misconceived and no account has been taken of the action of the composite textile/bitumen system.

The new approach which is now being taken is based essentially on the complementary properties and characteristics of the textile and the bitumen, the former acting as a reservoir for the latter. The textile has certain mechanical characteristics and the bitumen certain visco-plastic properties. The combination of these two elements enables the useful life of a road to be extended and maintains the waterproofing of the road structure.

The types of loading, levels of serviceability and functional requirements of different types of road means that the field of application for textiles may be divided into three sectors :

- Low cost roads
- Surface dressings
- Reflective crack prevention interfaces

(2) LOW COST ROADS

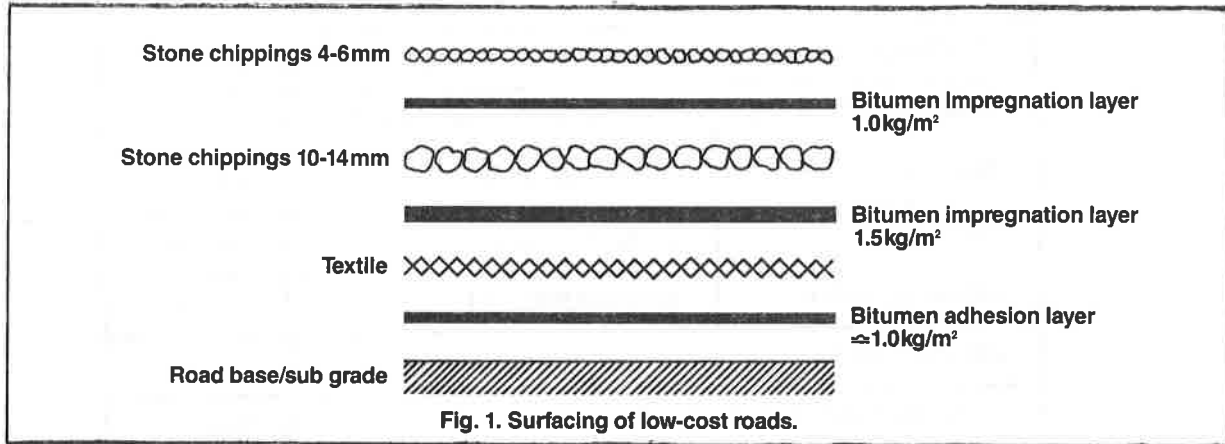
2.1. AREAS OF APPLICATION FOR TEXTILES

Low cost roads are generally constructed using locally available materials, or often re-using insitu material. They support a very wide range of traffic and their serviceability requirement is merely to be able to maintain vehicle circulation.

For surfaced roads, a textile provides a homogeneity and continuity to the surface thus enabling it to maintain water tightness even under the relatively large deflections common in this type of road.

2.2. POSITION OF TEXTILE

In general, surfacing of low cost roads is done in two layers (fig. 1).



2.3. ROLE AND FUNCTION OF TEXTILE

Surface degradations in low cost roads are generally initiated by the variability of the road structure.

A textile, being continuous, helps to overcome this problem. In addition it acts as a reservoir for the bitumen and thus :

- ensures continuity of the surface under deformation (rutting)
- maintains the waterproofness of the structure
- restrains the surfacing gravel as it punctures the textile, in effect a spider's web.

2.4. CHARACTERISITICS OF THE GEOTEXTILE

Needlepunched nonwovens are well suited to these technical requirements, especially those of deformability and of a container for bitumen. In economic terms relatively lightweight materials are preferred for their lower price and their lower consumption of bitumen. This latter can be further reduced if the geotextile is calendered. Geotextiles that meet the requirements defined in Table 1 have been found to be very suitable for this application.

2.5. CHARACTERISTICS OF BITUMEN BINDER

In low cost roads the choice of binder is often very limited. Bitumen emulsions have a number of advantages, in particular great flexibility in use. However, this type of material is not available in many countries and in those cut-back bitumens are frequently used. These can present problems with polyolefin based geotextiles.

TABLE 1. GEOTEXTILE PROPERTIES FOR SURFACING OF LOW-COST ROADS

UNIT MASS (g/m^2)		AFNOR G.38013	110-140
THICKNESS UNDER 20kPa (mm)		AFNOR G.38012	0.8-1.0
TENSILE STRENGTH AFNOR G.38014	LONGITUDINAL (kN/m)		2.75
	TRANSVERSE (kN/m)		4.50
ELONGATION AFNOR G.38014	LONGITUDINAL (%)		35-50
	TRANSVERSE (%)		35-50
MELTING POINT ($^{\circ}\text{C}$)			> 150
BITUMEN ABSORPTION (l/m^2)			0.9

2.6. PLACING OF MATERIALS ON SITE

Manual unrolling is possible with rolls that are relatively narrow (up to 2m wide) and are sufficiently flexible to be laid without folds and tucks, which must be minimised.

Mechanical placing enables much faster progress to be made together with better quality of laying than manual unrolling. However, special equipment is needed for this operation.

2.7. FIELD TRIAL

2.7.1. LOCATION - French Guiana, route N2

- Rainfall
 - annual 4.0m
 - maximum intensity 65mm/hr
- Traffic
 - 150 vehicles per day
 - 10% heavy trucks, 26 to 38T; 130kN per axle
- Trial section - 250m long (200m textile, 50m control)
6.60m wide

2.7.2. PLACING

Preparation of existing surface. This was scarified and reprofiled using a local lateritic gravel with the following grading :

d_{80}	20mm
d_{60}	5mm
d_{50}	< 2mm
L_L	34%
P_L	35%

After compaction, the modulus of the material remained very low (between 0.9 and 2.0MPa) and this gives a rutted profile to the road.

Textile reinforced coating. Initially the surface was stabilised by spraying 0.9 - 1.0kg/m² of cut-back bitumen. This was followed by spraying 1.5kg/m² of 65% bitumen emulsion after which the geotextile, with properties as in Table 1, was placed.

A further quantity of 65% bitumen emulsion was sprayed over the geotextile, giving a bitumen dosage of 1.5kg/m², then chippings, 11 l/m², 10 - 14 mm size. This is compacted by 2 passes of a roller without vibration.

Following this first compaction a further layer of 65% bitumen emulsion was applied, to give a bitumen dosage of 1.0kg/m². 9 l/m² of 4 - 6mm surface chippings was then placed and compacted with 20 passes of a rubber tyred roller.

2.7.3. RESULTS AND OBSERVATIONS

The project was carried out in October 1985 and monitoring of the road over three years shows the following :

During the first six months, apart from a certain loss of loose chippings from the surface there was no apparent difference in behaviour between the control and reinforced areas.

During the second six months the control area showed pronounced deformation, ie rutting, due to infiltration of water into the structure. The textile reinforced zone continued to perform satisfactorily. During the rest of the three year period, the control area underwent further deformation leading to accumulation of water in the ruts and then severe potholing of the surface. No problems whatsoever have been experienced with the textile reinforced section.

Another trial was carried out in the Piedamo-Morales region of Colombia, at an altitude of 1800m. The existing surface showed a deflection of 4.1mm under Benkelmann beam. Traffic was 550 vehicles per day of which 30% was heavy trucks. The installation was similar to that in French Guiana, except that both the experimental and control sections were 250m in length. Initial observations after one year in service show one pothole in the textile reinforced section and 20 potholes in the control section.

(3) SURFACE DRESSING

3.1. AREAS OF APPLICATION

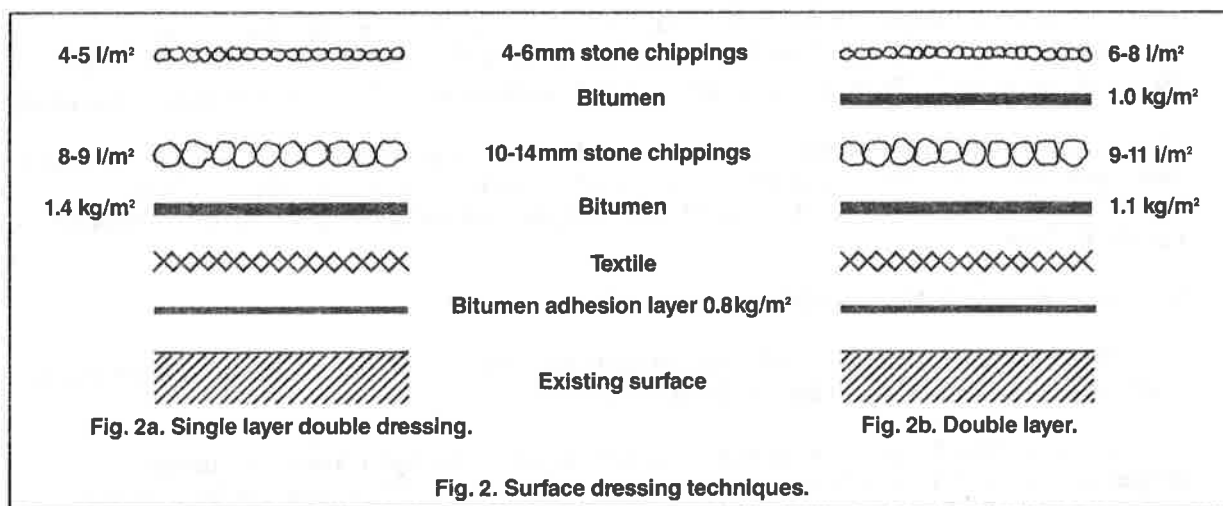
Surface dressings usually have two functions :

- to improve skid resistance
- to seal the surface to impede water infiltration

Surface dressing is essentially a maintenance operation and is applicable to roads where the underlying structure is able to sustain traffic loadings.

3.2 POSITION OF THE TEXTILE

The location of the textile is different depending on the type of surface dressing, single layer double dressing or full double layer (fig. 2).



3.3. ROLES AND FUNCTIONS OF TEXTILE

A textile used in conjunction with a modified bituminous binder having elastomeric properties acts as both a reservoir for the bitumen and as a screen against the appearance of cracks at the surface. The bitumen contained in the pores of the textile enables an auto-repair of small cracks and hence maintains the waterproofness of the structure.

3.4. CHARACTERISTICS OF THE TEXTILE

Needlepunched nonwovens calendered on one face, hence asymmetrical, are well suited to the notion of a container. Table 2 defines the required properties

TABLE 2. TEXTILE PROPERTIES FOR SURFACE DRESSING

UNIT MASS (g/m^2)	AFNOR G.38013	110
THICKNESS (mm)	AFNOR G.38012	0.3
TENSILE STRENGTH (kN/m)	AFNOR G.38014	5.0
ELONGATION AT BREAK (%)	AFNOR G.38014	25

3.5. CHARACTERISTICS OF THE BITUMEN BINDER

A polymer modified bitumen is required with the following properties :

- Cohesion
- Low sensitivity to temperature variations
- Elastic behaviour especially at low temperature

TABLE 3. BITUMEN PROPERTIES FOR SURFACE DRESSING

PENETRATION AT 25°C (1/10mm) AFNOR T.66014	83
SOFTENING POINT, BALL & RING (°C) AFNOR T.6608	57
FRAASS BRITTLINESS POINT (IP 50/53) (°C)	- 20

3.6. PLACING

The rigidity of the textile means that it cannot follow sinuous, winding roads. To place it effectively without folds at bends the textile is placed using plant that unrolls it in bands 0.5 - 1.0m in width. Adhesion of the textile to the surface is instantaneous.

3.7. FIELD TRIAL

3.7.1. LOCATION - France, Rhône-Alpes Region
State road CD51. Département du Rhône

Traffic - 7500 vehicles/day; 12% heavy trucks

Trial area - 3000m², on a curve

Existing road - deflection 40 - 60/100mm. Surface degradation; crocodile skin cracking, longitudinal joints, potholes.

3.7.3. CONSTRUCTION WORK

After cleaning of the surface, an elastomeric binder was placed at 0.8kg/m^2 as an adhesion layer. The textile was then laid in bands 0.5m wide. This was followed by a single layer double dressing as follows :

1.4kg/m^2	elastomeric binder
$8 - 9 \text{ l/m}^2$	chippings 10 - 14mm
$4 - 5 \text{ l/m}^2$	chippings 4 - 6mm

Vibrating compaction was carried out to ensure good dispersion of the binder throughout the thickness of the dressing. Excess chippings were removed by sweeping and vacuuming and traffic was allowed to pass over the surface as soon as this had been done.

3.7.3. RESULTS AND OBSERVATIONS

After 18 months, including two very severe winters (-10°C for several weeks) an initial inspection was carried out. This showed satisfactory behaviour and the performance was better than that of a conventional surface dressing. Vehicle adhesion was also improved.

After three years the textile reinforced surface dressing continued to perform its waterproofing function in spite of local deformations.

(4) REFLECTIVE CRACKING INTERFACE

4.1. AREAS OF APPLICATION

The major applications for this type of interface are in semi-rigid roads, either in new construction or an overlay forming part of a maintenance programme; and in maintenance of rigid concrete roads.

4.2. POSITION OF TEXTILE

The textile is just one component of an interface system, and is associated not only with the bitumen binder but also with the placing technique. The location of the textile is shown in fig. 3.

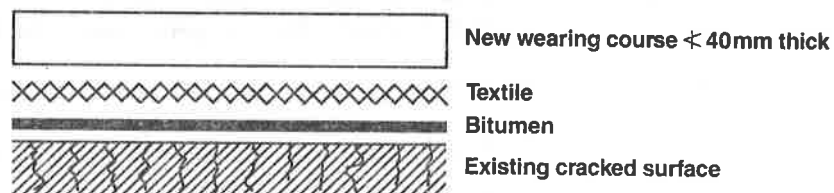


Fig. 3. Location of textile in anti-cracking interface.

4.3. ROLES AND FUNCTIONS OF TEXTILE

The textile has to perform a number of simultaneous functions :

- "Sponge" for the modified bitumen, to enhance its properties
- Debonding of the different adjacent layers under slow, thermal loadings to prevent upward transmission of cracks
- Dimensional stability in the vertical sense.

This latter is very important and is fundamental to the efficient functioning of the entire system. This is because any flexure caused by traffic loading leads to fatigue failure of the wearing course. A thick, compressible geotextile allows this to occur, as has been observed on several sites where conventional geotextiles have been used in this application.

4.4. CHARACTERISTICS OF THE SYSTEM

A specialised system, which we will describe, has been developed and patented.

4.4.1. THE TEXTILE

Nonwovens are ideal for fulfilling the function of a container for the bitumen. The cross-section of the fibres together with bonding by point calendaring gives a fabric both deformable in the plane and relatively incompressible.

Polyester is preferred to polyolefines because of its superior resistance to both high temperature and aliphatic solvents.

4.4.2. THE BITUMEN

Laboratory studies have shown that conventional pure bitumens are too susceptible to temperature variations to meet the requirements of the system.

Bitumens modified with polymers - styrene butadiene styrene, polyisoprene etc. - are very stable under temperature variations and are well suited to use in an interface system (table 4).

TABLE 4. BITUMEN PROPERTIES FOR ANTI-CRACKING INTERFACE

PENETRATION AT 25 ^o C; 5 SECONDS	(1/10mm)	ASTM D-36	180/240
SOFTENING POINT, BALL & RING	(^o C)	ASTM D-5	> 75
VISCOSITY AT 135 ^o C	(p)		> 750
FRAASS BRITTLNESS POINT	(^o C)		(approx) - 18

4.4.3. CONSTRUCTION METHOD

4.4.3.1. BINDER SPRAYER

Modified bitumens have very high viscosity, so high performance sprayers are required to give good coverage at the low quantities to be applied (around 700g/m²).

4.4.3.2. TEXTILE PLACEMENT

Specialised plant is necessary to cope with both the particular width of the rolls and the need to lay them on curves without folds.

4.5. FIELD TRIALS

Different site trials in Europe have shown that conventional geotextiles are not well suited to this particular application, especially when used with conventional bitumens.

4.5.1. LOCATION - France, Rhône-Alpes region between Grenoble and Nice. Interstate road RN85 (route Napoleon)

As part of reinstatement of a landslip, the new road construction consisted of a lightweight embankment of polystyrene blocks on which was poured a concrete slab reinforced with two steel meshes and using crack inducing compression joints.

Traffic is 5000 vehicles per day of which 5% is heavy trucks. Climate is one of very severe winters by French standards, with annual snowfall between 80 and 250cm. Altitude is 780m. Annual temperature variations are quite large; 1986/87 from +25°C to -20°C. The geometry of the trial area is as follows :

- Slope 9%
- 60m in length, 1 compression joint every 5m
- Slab width 8.4m

4.5.2. CONSTRUCTION

This took place in November 1986, at an ambient temperature of 5°C in strong winds. Initially 1.1kg/m² of bitumen emulsion was applied, giving 0.7kg/m² bitumen dosage. This was 90/140 pen. grade, ball & ring softening point 45 - 50°C and Fraass brittleness temperature -20°C.

The textile was then laid directly onto this emulsion. A conventional asphalt wearing course was then placed over the textile, 40 - 50mm in thickness, laid moving up the slope. The temperature of application ranged from 120 - 150°C. This was then compacted.

During the works, trafficability for plant on the textile was excellent as the textile was firmly affixed to the slab.

4.5.3. RESULTS AND OBSERVATIONS

After the first winter, the slab was considered to have cracked at the compression joints. In the section containing the textile interface system no surface cracks have appeared in spite of both the harshness of the first winter and the thickness of the wearing course (only 30 - 40mm in places).

Moreover, it is worth emphasising that conditions were far from ideal when the work took place. Emulsion was used with characteristics considerably at variance with Table 4. Climatic conditions were not favourable, temperature being around 5°C, and the asphalt overlay was placed by travelling uphill thus putting the textile in tension.

(5) CONCLUSION

The rôles and functions of textiles used in pavement surfacing are clearly different depending upon the particular application. Therefore the textile must be selected to suit the application, in contrast to simply using traditional geotextiles for all uses.

The only common function to all three applications is that of a container for the bitumen binder. This requirement is better served by nonwovens than by wovens by virtue of the structure of the fabrics, the fibres acting as a matrix to confine the bitumen and to prevent it from flowing.

In no way can the textile be considered as structurally reinforcing the pavement structure. In mechanical terms, however, the continuity of the textile appears to be important because it gives to the bitumen a capacity for plastic deformation compatible with the particular application.

It is clear that the most important element in the interface system is the bitumen. The specialised textiles used with it are means of enabling it to work to the full extent of its capabilities.

REFERENCES

- (1) COLOMBIER, G., ASTESAN, A. and GOUACOLOU, A. Using a geotextile to prevent shrinkage crack of rigid pavements. Proc. 2nd Int. Conf. on Geotextiles, Las Vegas (1982) 501-506.
- (2) COLOMBIER, G., LARTAUT, M. and MACHET, J.M. Reflective cracking. A new test for SAMI. Proc. 3rd Int. Conf. on Geotextiles. Vienna (1986) 105-108.
- (3) PERFETTI, J. The development of a geotextile system to retard pavement cracking. Proc. 3rd Int. Conf. on Geotextiles, Vienna (1986) 109-111.
- (4) GOUACOLOU, H., MARCHAND, J.P. and MOURATIDIS, A. La méthode des éléments finis. Application a la fissuration des chaussées et au calcul de temps de remontre des fissures. Bulletin de liaison des Laboratoires des Ponts et Chaussées No. 126 (May/June 1983) 76-91.
- (5) LEFLAIVE, E. Les géotextiles. Revue PCM No. 12 (1978) 53-57.
- (6) BROWN, S.F., BRUNTON, S.M., HUGHES, D.A.B. Polymer Grid Reinforcement of Asphalt. Annual Meeting of the Association of Asphalt Paving Technologists, San Antonio, Texas. February 1987.

G. WERNER

S. RESL

Polyfelt Ges.m.b.H., Linz/Austria

R. MONTALVO

Polyfelt Inc., U.S.A.

The Influence of Nonwoven Geotextiles on the Compactability of the Fill Material

Introduction

One indispensable prerequisite for the construction of roads over weak subsoil is a good compaction of the base layer material. It is well known from practice that the use of a geotextile as separation layer between soft subsoil and fill material can increase significantly the load bearing capacity of the subsoil and the compactability of the fill material. Nevertheless it is important to state that insufficient compaction can lead to severe rut formation, rupture of the separating geotextile and finally to the failure of the entire road. Therefore most construction guidelines for geotextile applications require "good compaction" of the fill material in order to take full advantage of the geotextile's separation effect. However, what means "good compaction" to the contractor?

To be able to give a clear answer to this question it was necessary to quantify the geotextile influence on the compactability of fill material over weak subsoils. Large scale compaction tests have been carried out for that purpose at the Geotechnical Institute/Federal Establishment for Research and Testing ARSENAL/Vienna, with a needle-punched non-woven PP geotextile as separating layer, which yielded valuable information for both consultant and contractor.

1. Test set-up

The compaction tests were carried out in an open-air test pit appr. 15 m long and 5 m wide with three separate test sections showing different water contents and shear strengths, each section being 3 x 5 m big (fig. 1). The test pit was sealed with a PE-geomembrane, then a 100 mm thick

drainage gravel layer was placed on top of the membrane, and irrigation pipes were embedded. The irrigation pipes were connected to a water supply with constant water-head. On top of the drainage layer followed a needle-punched non-woven geotextile as separation layer between gravel and soft subsoil material, which was placed in various layers up to 1 m high (fig. 2).

The subsoil material of the three test fields was placed at different water contents and densities, the water table was raised according to the fill height at construction. Prior to placing and compacting the base layer material a needle-punched non-woven geotextile was layed on top of the subgrade on one half of the test pit as separation layer. The fill material was then placed and compacted in three layers up to a total thickness of app. 450 mm.

2. Material properties

2.1. Geotextile

As separation layer, a needlepunched nonwoven PP-endlessfibre geotextile of 200 g/m² weight was used, with a tensile strength acc. ASTM D 4595 of 13 kN/m and 50 % elongation at break.

2.2. Subsoil material

For the test purposes the subsoil material had to meet certain requirements of normally consolidated clay at undrained shear strength values of app. 10 kPa, 30 kPa and 80 kPa.

However, to achieve a homogeneous soil layer in general which is in accordance with the natural soil conditions, it is necessary to consolidate

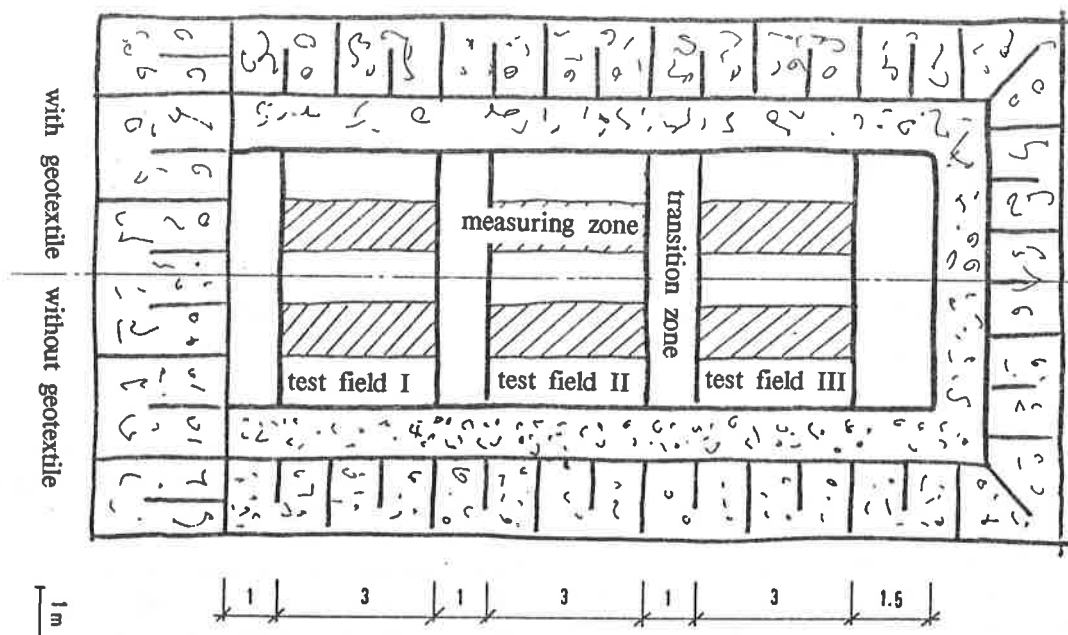


Fig. 1: Test pit layout

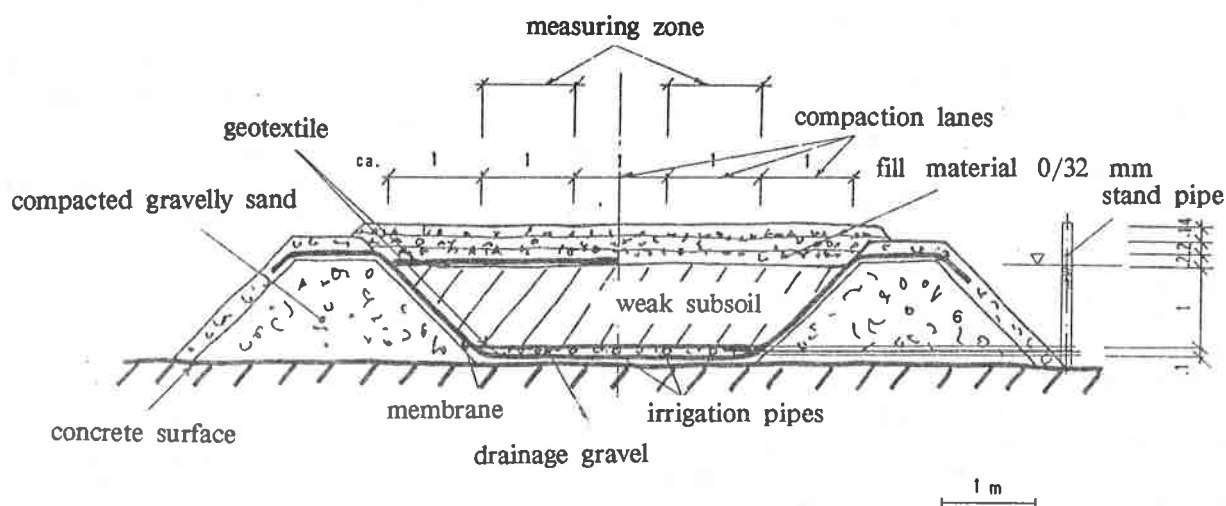


Fig. 2: Test pit cross-section

sludge material. As in our particular case it was neither possible to apply the required surcharge nor to allow for a required consolidation period of one year, it was necessary to place the soil at various water contents and densities and saturate it subsequently.

Three different types of soil were tested as to their suitability:

- Type 1: "Wiener Tegel": a clayey silt of high clay content
- Type 2: Reservoir sediment "Aschach": sediment material from the stream-power-plant Aschach/Danube - a plastic clay of high sand content and little clay content
- Type 3: Reservoir sediment "Wallsee": sediment material from the stream-power-plant Wallsee/Danube - a plastic organic clay

For reasons of special demands on placing conditions and water saturation of the subsoil, type 3) proved to be the most convenient type of soil for the compaction tests.

The well-graded sediment material contained 75 % silt, 15 % clay and 10 % sand with an organic content of 2,14 %. Its grainsize distribution is shown in fig. 3.

The undrained shear strength of the sediment material was determined at different water contents and at a constant normal stress of 10 kPa, which corresponds to a 0,5 m thick gravel layer. Test results are given in fig. 4.

2.3. Fill material

Crushed sand-gravel mix was used as fill material on top of the soft subsoil. The grainsize distribution of the fill material is shown in fig. 5. The proctor density has been determined with $\rho_{Pr} = 2,02 \text{ g/cm}^3$ at a water content of $w = 3 \%$ (fig. 6).

3. Compaction equipment

Based on results of preliminary compaction tests with the specified fill material a hand-guided vibrating roller of 1,3 kN weight was considered to be sufficient to achieve maximum compaction values.

Technical data of vibrating roller:

static linear load	f/r	5,89/8,56	kg/cm
bandage width	f/r	900	mm
velocity		1,60/2,60	km/h
frequency		55	Hz
amplitude		1	mm
centrifugal force per bandage		3000	daN

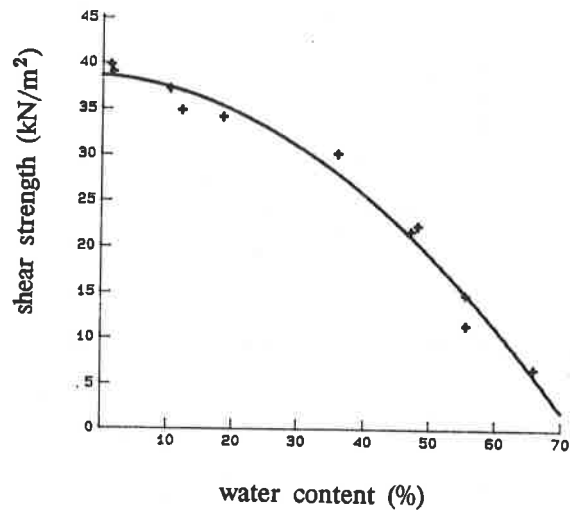


Fig. 4: Shear strength of subsoil material as a function of water content.

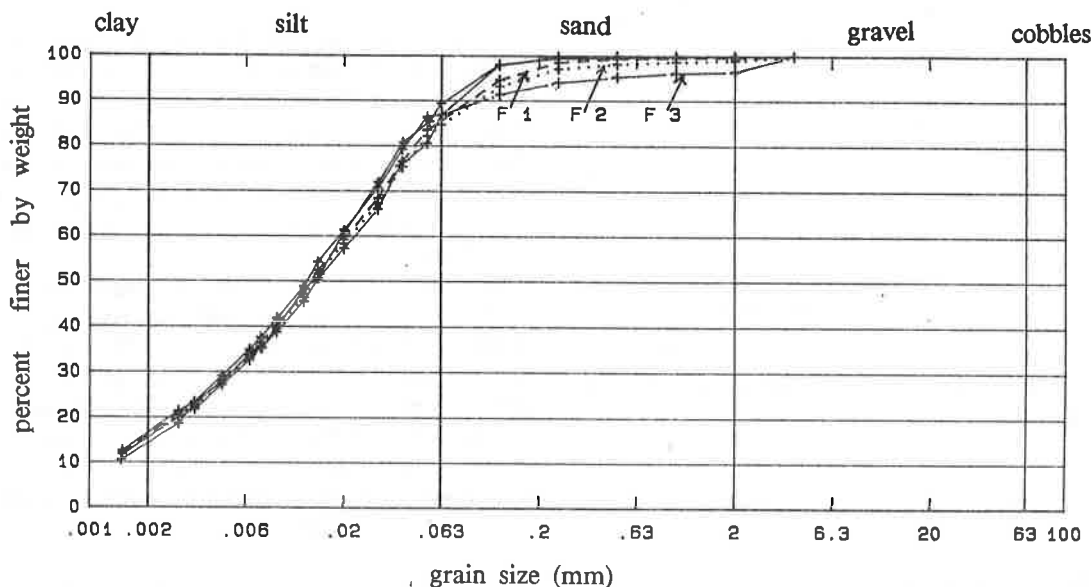


Fig. 3: Grainsize distribution of subsoil

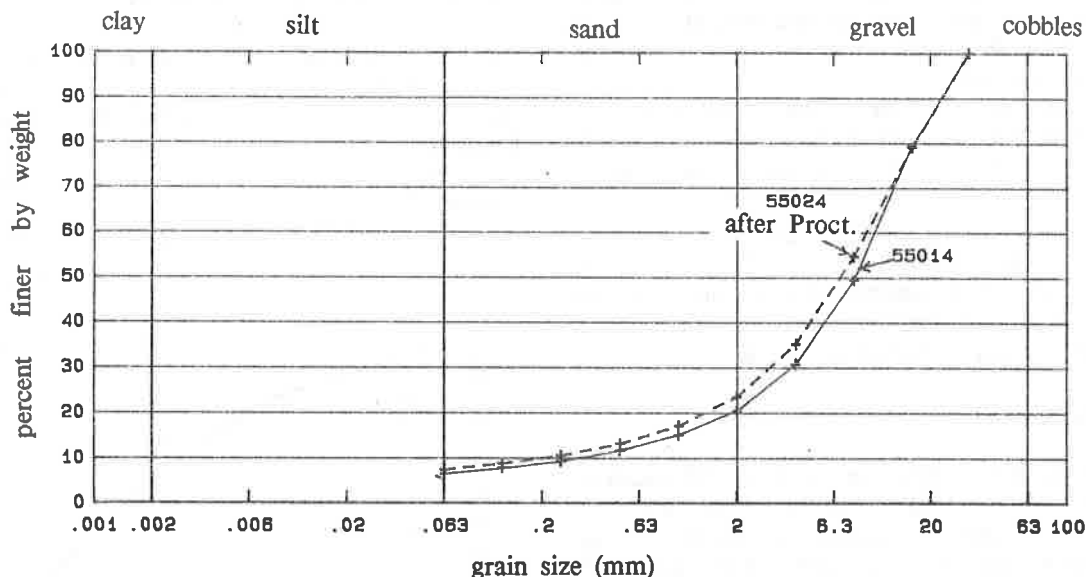


Fig. 5: Grainsize distribution of fill material

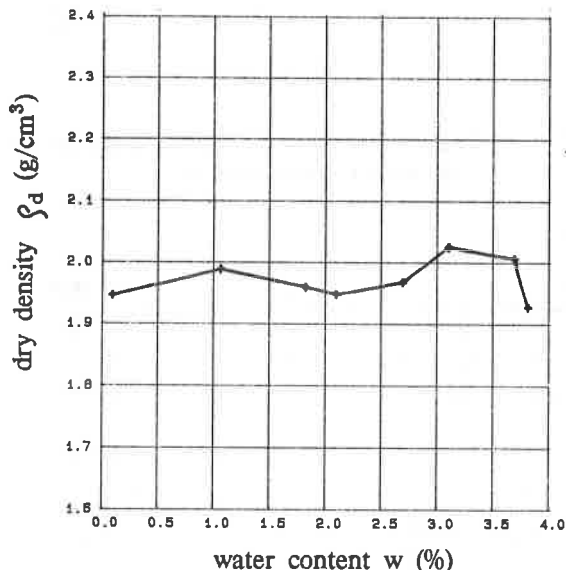


Fig. 6: Proctor density determination of fill material

4. Placing of fill material

The placing of the fill material was done manually in order to avoid any precompaction by the construction equipment. The fill was placed in 3

layers of 200 mm, 200 mm and 140 mm. Every single layer was then compacted dynamically by 20 passes of the vibration roller.

5. Measurements during testing

5.1. Subsoil

5.1.1. Shear strength

Undisturbed soil samples were taken from the surface to determine water content and density as well as uniaxial compressive strength, CBR-values and load bearing capacity were taken in-situ.

The average water content for test section 1, 2 and 3 were 60,7 %, 40,3 % and 28,9 %, and the average density 1,0 g/cm³, 1,2 g/cm³ and 1,22 g/cm³ respectively.

CBR-values for test field 1 were ranging from 0,1 % - 0,5 %, for test field 2 from 2,3 % - 2,7 % and for test field 3 from 6,8 % - 13,4 %. With an average undrained shear strength $c_u = 24$ kPa and an average CBR-value of 2,4 % in test field 2 a ratio of $c_u/\text{CBR} = 10$ was determined.

Based on that ratio of 10 the following values for the undrained shear strength could be derived out of the CBR-test results:

Test field 1 : 1-5 kPa (1,1-4,8 kPa measured)
Test field 2 : 23-27 kPa (23,7-26,5 kPa measured)
Test field 3 : 68-134 kPa

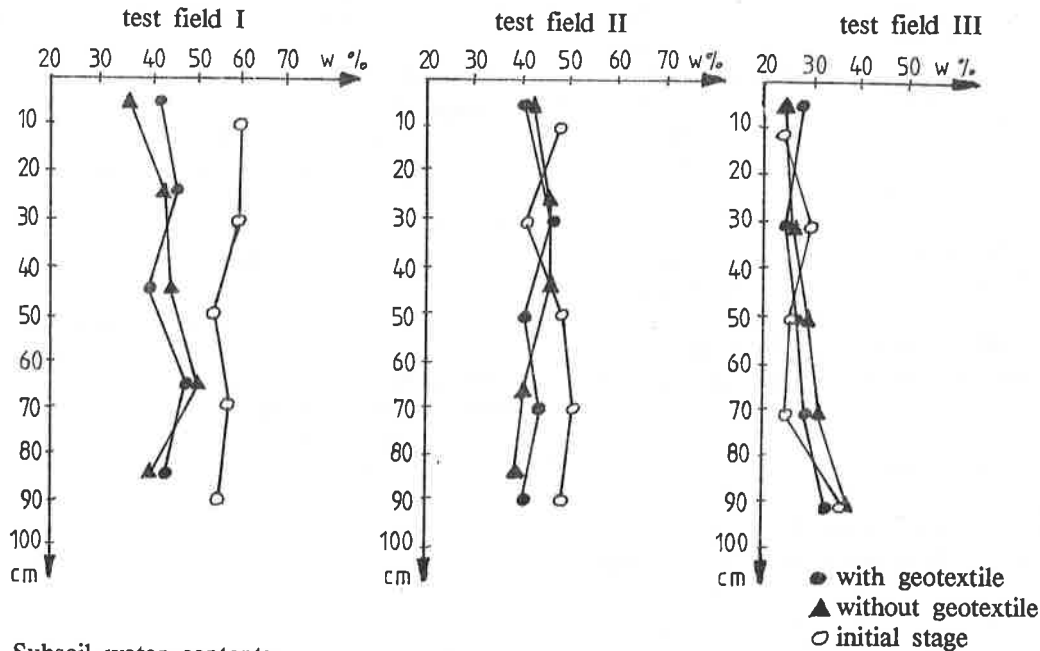


Fig. 7: Subsoil water contents

5.1.2. Water content

Soil samples were extracted from the 3 separate test sections using a soil auger in order to determine the exact water contents. Results are shown in fig. 7.

Results of test field I show that the water content decreased over the test period due to consolidation.

5.2. Fill material

5.2.1. Density determination

Measurements with the nuclear gauge tracer during compaction showed that maximum compaction was achieved after 10 passes. Differences inbetween the single test sections could not be observed, due to the inaccuracy of this test method.

Density determinations were carried out acc. to the "Rubber balloon method" for every single test field after compacting the fill material. The results show clearly that the use of a needle-punched non-woven geotextile as separating layer increases the density of the fill material and therewith the compaction degree. However, it is important to mention that the relatively high proctor density $\rho_{Pr} = 2,02 \text{ g/cm}^3$ of the sandy gravel fill material does not show that signifi-

cant difference which can be expected for gravel with $\rho_{Pr} = 1,9 \text{ g/cm}^3$ or medium coarse sand with $\rho_{Pr} = 1,8 \text{ g/cm}^3$.

5.2.2. Dynamic load bearing tests

More than 200 dynamic load bearing tests were conducted during the various stages of placing the fill layers which have not been evaluated at the time when this paper was written.

5.3. Interpretation of test results

5.3.1. Density

The results of the obtained field densities are summarized in Table 1.

Table 1: Density values of the top fill layer

	ρ_D [g/cm ³] with Polyfelt geotextile	ρ_D [g/cm ³] without Polyfelt geotextile
Test field 1	2,05	2,01
Test field 2	2,07	1,97
Test field 3	2,12	1,80

Table 2: Corresponding degrees of compaction D_{Pr}

	D_{Pr} [%] with Polyfelt- geotextile	D_{Pr} [%] without Polyfelt- geotextile
Test field 1	101	99
Test field 2	102	97
Test field 3	105	89

The results show that 100 % proctor density can be achieved and exceeded of standard type base layer fill material of approx. 450 mm fill height and subsoil CBR-values of 0,3 % - 10 % when using a needle-punched non-woven geotextile as separation layer.

5.3.2. Compaction behaviour

As interesting tendency has been observed that differences in compaction degree values became bigger with increasing strength of the subsoil. In the test sections with the non-woven geotextile as separating layer the density of the fill material increased with increasing stiffness of the subsoil, whereas in the section without geotextile the density decreased (fig. 8).

5.3.3. Mixing zones

Subsequent to the density determination and load bearing tests the total fill layer thickness plus

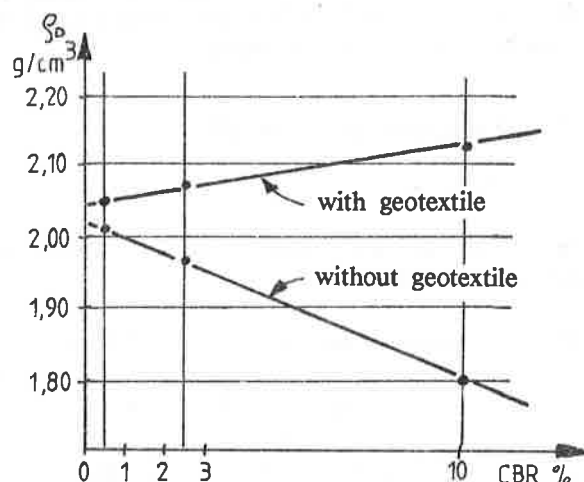


Fig. 8: Density values of fill material as a function of subsoil CBR with and without geotextile

mixzone were measured for every single test section with and without geotextile.

The investigation revealed following results:

Test field 1:

average CBR = 0,3 %:

total thickness 46 cm

mixzone 10 cm (without geotextile)

Test field 2:

average CBR = 2,5 %:

total thickness 45 cm

mixzone 6 cm (without geotextile)

Test field 3:

average CBR = 10 %:

total thickness 42 cm

no mixzone

Conclusions

The compaction tests, carried out at full scale out-door conditions, proved the influence of a needle-punched non-woven PP geotextile, used as separating layer between soft subsoil and standard road base material, on the compactability behaviour of the fill material. Following results can be deemed significant:

- The density of the compacted fill material was found superior to its proctor-density for all subsoil test conditions, when using a non-woven geotextile: $\frac{D_{Pr}}{D_{Pr}} > 100\%$ at CBR-values ranging from 0,3 %-2,5 %-10 %.
- The test sections without geotextile did not reach 100 % proctor density
- As clear tendency was observed that in the test sections with a non-woven geotextile the density of the fill material increased with increasing stiffness of the subsoil, whereas in the sections without geotextile the density decreased.
- The thickness of the mixing zone in the transition area between subsoil and fill material was found to be 10 cm for CBR = 0,3 % and 6 cm for CBR = 2,5 % in the case without a geotextile. For CBR = 10 % no mixzone was observed.

Appendix: Photos

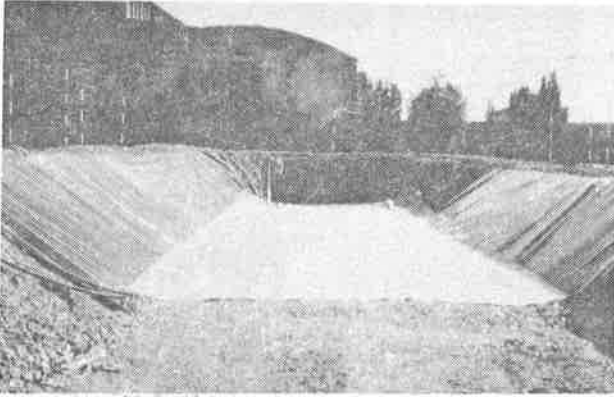


Photo 1: Test pit prior to installation of subsoil material

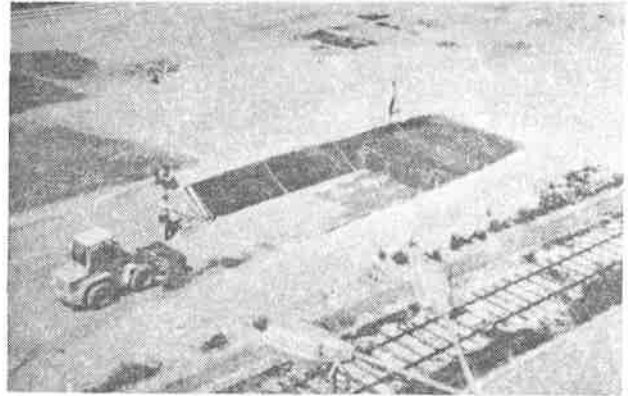


Photo 2: Installation of subsoil material



Photo 3: Installation of subsoil material, test fields 1 (front), 2 and 3



Photo 4: Surface of installed subsoil

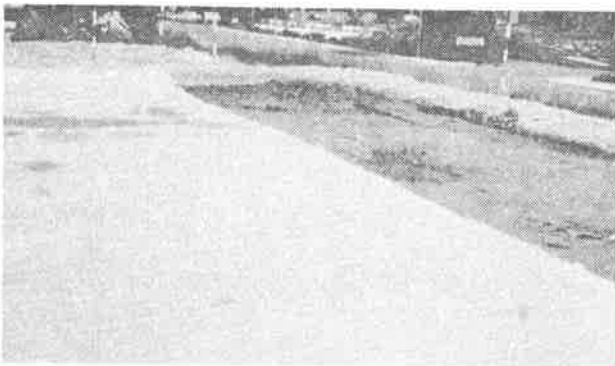


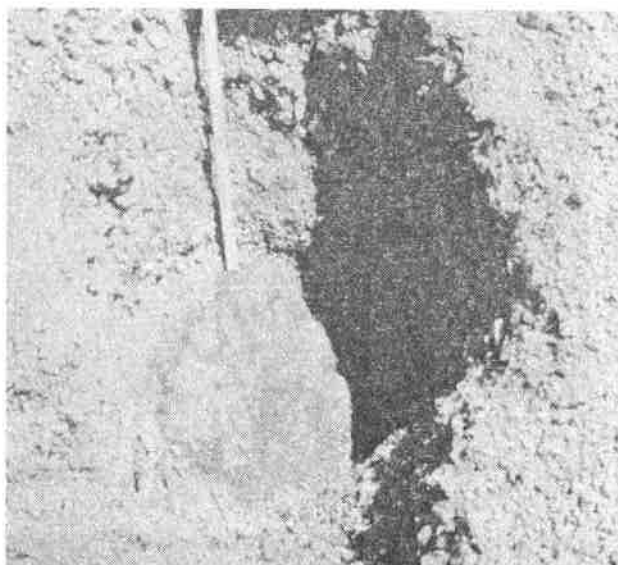
Photo 5: Test pit prior to installation of fill material



Photo 6: Deformations of the first fill layer in test field 1 with (right) and without (left) geotextile



Photo 7: Dynamic plate loading tests



**Photo 8: Excavation after end of tests in a
section with geotextile**

P. ANDERSON

M. KILLEAVY

Trow Geotechnical Ltd., Canada

**Geotextiles and Geogrids: Cost Effective Alternate Materials for Pavement
Design and Construction**

1.0 INTRODUCTION

The utilization of geosynthetic materials in flexible pavement design and construction represents a potential cost-effective alternative to achieving satisfactory pavement performance. In particular, the cost vs benefit of using geotextile separation barriers and geogrid granular base reinforcement materials should be regarded as an analysis step in the design process.

This paper presents a case study in which site subsoil properties, surface evaluation restraints, scheduling and operational considerations presented unfavourable conditions for conventional asphalt on granular pavement design and construction. An alternative design using geosynthetic materials was developed to address the objectives of achieving:

- .1 adequate structural strength to support construction traffic and accommodate the projected traffic loadings;
- .2 reduced construction problems due to unfavourable subsoil, groundwater and late season construction weather; and
- .3 satisfactory long-term performance at reasonable construction costs.

Pavement construction was completed in 1987 and the performance of the geosynthetic improved pavement structure is being monitored and assessed by means of visual condition surveys, non-destructive dynamic deflection testing using the Falling Weight Deflectometer (FWD), and elastic layer analysis of the FWD data. Additional pavement structures constructed in 1987 at the same site include an asphalt on granular structure, with a geotextile separation barrier, and a conventional asphalt on granular structure. These

pavements are being monitored to assess relative performance characteristics in terms of surface cracking, deformations, deflection response under dynamic loading, and dynamic layer moduli. The results of the 1988 spring monitoring are presented in this paper.

2.0 SITE CONDITIONS

The case study site is a trucking facility located in southern Ontario. Truck traffic in 1987 was approximately 65 to 70 vehicles per week and included liquid tanker and multi-axle tractor trailer trucks with axle loads up to approximately 130 kN. The estimated 1987 traffic loading, in equivalent 80 kN single axle loads (ESAL's) was about 12,000 ESAL's/year. The 15 year design ESAL was calculated to be 1.8×10^5 .

The site was formerly a low lying marshy area which had been filled and levelled. The traffic areas consisted of the main driveway entrance road, truck staging yard, and the truck staging yard expansion area. The yard expansion area was undeveloped land, whereas existing traffic areas had a granular structure consisting of about 0.150 m of base course quality crushed limestone over approximately 0.300 m of 50 mm clear crushed limestone. The subgrade throughout the site was generally loose to compact clayey silt to silty clay fill, with random organic pockets, which was very sensitive to loss of support properties due to excess moisture. A surficial water table was encountered at about 1.0 m depth below the gravel surface in the truck staging area and subgrade pumping through to the gravel surface was evident where concentrated truck turning movements occurred.

3.0 FACTORS INFLUENCING PAVEMENT STRUCTURE DESIGN

The pavement structure design and construction was required to address the following constraints for the truck staging yard and yard expansion:

- .1 achieve suitable pavement structural strength for the projected traffic loadings;
- .2 achieve finished pavement grades which contain and collect surface water within the pavement areas, and direct drainage away from existing buildings;
- .3 excavated material was not permitted to be hauled off site;
- .4 pavement subdrain installations were not permitted;
- .5 construction was scheduled for the late summer and fall of the year in potentially wet and inconsistent weather;
- .6 there would be no available outlet during pavement construction for storm water or ground water collection and discharge; and
- .7 truck traffic flow into and out of the site and staging yard was to be maintained during construction.

The constraints on the truck staging yard pavement design and construction indicated that the design pavement structure section thickness had to be minimized in order to reduce soil excavation and handling costs and reduce the risk of subgrade support problems. It was also apparent that the existing granular would have to be utilized in the new structure to reduce on-site disposal problems, and subgrade support and stability were critical to facilitating construction. Concrete pavement construction was not considered feasible due to the concrete curing period necessary and the requirement of maintaining traffic flow in the truck staging area.

The main access road pavement and truck yard expansion areas were not subject to the same constraints as the truck staging yard. Consequently, section thickness and finished grade height were not controlling factors in establishing the design pavement structures in these areas.

4.0 DESIGN ANALYSIS

A flexible pavement structure section was initially developed based on The Asphalt Institute design methods (1). The design was modified based on a comparative design using Ministry of Transportation of Ontario methods (2). An alternative design was developed with geogrid reinforcement using the methods developed by Haas (3), and included a geotextile separation barrier. No structural contribution was attributed to the geotextile material, as recommended by Rolin Jarrett and Wallace (4), since it was only included in the alternative design to facilitate construction by improving subgrade stability and uniformity. The alternative pavement structure design using geogrid reinforcement and geotextile fabric was considered an option which would minimize the pavement section thickness, provide adequate structural strength, and also reduce the potential construction problems associated with the soil, groundwater and weather factors.

The alternative geosynthetic design structure is illustrated in Figure 1(a). Figure 1(b) presents the pavement design for the main driveway access road which was not subject to design constraints and was considered to be structurally equivalent to the reinforced pavement section. The design for the truck staging yard expansion area was not subject to grade and section thickness constraints, but was subject to construction problems due to soil, groundwater and weather conditions. Consequently, the design pavement section provided in Figure 1(c) for the yard expansion area included a geotextile fabric separation layer.

The specifications for geotextile and geogrid placement required that the material be placed loosely with a minimum 600 mm overlap. Following the placement of the granular base layer, the reinforced area was pre-stressed by traversing loaded trucks across the area (4).

Material Properties

The pavement asphalt and granular layer materials used in construction complied with premium construction materials available in the Province of Ontario.

The geosynthetic materials used in the design were in conformance with Ontario standards (5) and were:

Biaxial Geogrid: Tensar SS-1 with a reported initial tangent modulus of 370 kN/m (2057 lb/in) and an ultimate tensile strength of 21 kN/m (119 lb/in) at a strain of 13.5 percent (5).

Non-woven Geotextile: Terrafix 270 R staple fibres, needle punched, with a grab tensile strength of 556 N and a water permeability of 2.6×10^{-1} cm/sec. (5).

5.0 COST ANALYSIS

The construction costs of the truck staging yard pavement, with geosynthetics, in comparison to the costs of a conventional asphalt on granular structure were calculated based on tender unit prices. The costs, on an average square metre basis, are presented in Table 1.

Table 1
Comparative Pavement Structure Costs

Pavement Component	Average Cost Per Square Metre	
	Geosynthetic Section	Conventional Section
Asphalt Surface Course	\$4.30	\$4.30
Asphalt Binder Course	\$7.00	\$7.00
Granular Base Course	\$0.20	\$3.10
Geogrid	\$3.93	-
Geotextile	\$1.95	-
Excavation, Stockpile, and On-Site Disposal	\$2.50	\$6.00
Total Cost	\$19.88/m ²	\$20.40/m ²

The cost analysis indicates that the geosynthetic pavement section has a marginal cost advantage over the conventional design structure. It was apparent during construction, however, that pavement construction would have been seriously jeopardized without the use of a geotextile separation barrier and geogrid reinforcement in the truck staging yard. The subgrade support conditions experienced a fairly sudden deterioration during construction due to traffic, wet weather, and the proximity of the groundwater to the subgrade surface. Within a day or so, severe subgrade distortion began to occur under traffic. There is no question that the use of the geotextile fabric in combination with the geogrid reinforced granular allowed construction to proceed with a relatively thin pavement section.

The true cost benefit of the geosynthetic pavement section can only be assessed based on long-term performance since the maintenance costs will be a function of the performance properties.

6.0 PAVEMENT PERFORMANCE ANALYSIS

The relative performance of the three pavement structure types has been assessed in terms of dynamic deflection properties, surface cracking and deformation, and calculated equivalent granular layer moduli in the pavement sections. The results of the performance analysis are presented in following sections.

Deflection Properties

The deflection properties are presented in Table 2 in terms of the mean, standard deviation, and range of FWD centre deflections in each pavement section. The deflections have been normalized to a load of 40 kN for comparative purposes between sections. The load normalization is required since the actual applied load varies with the pavement stiffness. The normalization procedure is a linear regression analysis of the FWD load and deflection plot which does not fit the line through the origin.

Table 2
Summary of FWD Centre Deflections

Pavement Section	No. of Test Points	Centre Deflection Values (mm)		
		Mean	Standard Deviation	Range
Access Road (non-reinforced, no geotextile)	19	0.74	0.18	0.61 to 1.34
Truck Staging Yard (reinforced with geotextile)	26	0.68	0.19	0.11 to 0.86
Yard Extension (non-reinforced, includes geotextile)	14	0.64	0.13	0.38 to 0.83

The FWD deflections in Table 2 indicate that the FWD means deflections and standard deviations are comparable for all three pavement types. The yard extension pavement has a somewhat lower standard deviation and this may be due to the fact that weather conditions during construction were favourable to achieving uniform subgrade support. The somewhat higher standard deviation of the Truck Staging Yard deflections compared to the Yard Extension deflections is also likely due to the deterioration in subgrade support conditions which was experienced during construction.

Typical FWD load and deflection basins are presented on Figure 2 for the three pavement types.

The deflection basin plots are representative of similar conditions of asphalt temperature (asphalt stiffness) and layer material properties. Applied dynamic load varies slightly and depends upon the actual pavement dynamic stiffness such that the magnitudes of deflection are influenced somewhat by the variation in applied load. A comparison of the deflection basin plots indicates the following:

- o the shape and magnitude of the deflection basins at the outer FWD sensors 6 and 7 are very similar in all cases; this indicates that subgrade deformations and strains are in the same range for the different pavement types;
- o the shape of the deflection basins at FWD sensors 1 (loading plate) to 5 are comparable for the access road (no geosynthetics) and the truck yard extension (geotextile only); the basin shape for the reinforced truck yard pavement has a larger radius of curvature than the other pavement sections which indicates reduced strains in the asphalt layer and improved load distribution through the pavement;
- o the truck yard extension pavement deflection basin (with the geotextile fabric) has the smallest radius of curvature; this corresponds to the highest asphalt strain condition and the weakest pavement section under equivalent dynamic loading.

Elastic Layer Analysis

The pavement layer moduli in each section were back-calculated using iterative, deflection basin matching methods. ELMOD (7) was used to analyze all deflection points and is based upon the equivalent thickness concept by Odemark. CHEVDEF (8) was used at a few test points for a comparative analysis. The layer analysis was performed to determine the effective granular layer modulus of the geogrid reinforced pavement in comparison to the other non-reinforced pavements. In the analysis, the asphalt layer modulus was confined to a pre-set range based on temperature and stiffness considerations. Subgrade moduli ranges were also used as controls in the back calculation procedures. That is, the acceptable subgrade moduli ranges were pre-set for the pavement areas on the basis of construction data on soil moisture, density, and stability. The subgrade moduli ranges were set as follows:

- o access roadway - 60 to 80 MPa
- o truck staging yard - 30 to 50 MPa
- o truck yard expansion - 50 to 80 MPa.

The ELMOD layer analysis is summarized in Table 3.

Table 3
Summary of Calculated Granular Layer Moduli in MPa

Pavement Section	Mean	Standard Deviation	Range
Truck Staging Yard (Reinforced & Geotextile)	560	190	300 to 800
Access Road (not reinforced)	170	70	160 to 270
Truck Yard Expansion (geotextile only)	400	120	280 to 590

The ELMOD analysis indicates that some improvement in the equivalent granular layer moduli has resulted in the reinforced section. CHEVDEF analyses on a random sample of test points were inconsistent with the ELMOD results. This may be due to the fact that ELMOD allows for a non-linear subgrade, and CHEVDEF models a linear subgrade response.

Pavement Surface Properties

The pavement surface properties, in terms of cracking, distortion and rutting were visually determined and the results are presented in Table 4.

The results in Table 4 indicate there is essentially no difference in pavement performance to date for the three pavement sections. The geogrid reinforced truck staging yard and the access road are subject to identical truck traffic volumes and similar repeated

truck patterns. The truck staging yard pavement is likely subjected to more severe and damaging truck turning movements than the access road.

Table 4
Summary of Pavement Surface Characteristics

Pavement Section	Surface Distortion ⁽¹⁾ in % of Total Area			Surface Cracking ⁽²⁾		
	Slight	Moderate	Severe	Slight	Moderate	Severe
Access Road (no geosynthetic)	0	0	0	Nil	Nil	Nil
Truck Staging Yard (geogrid + geotextile)	< 0.5	0	0	1 m	Nil	Nil
Yard Extension (geotextile only)	0	0	0	Nil	Nil	Nil

NOTES

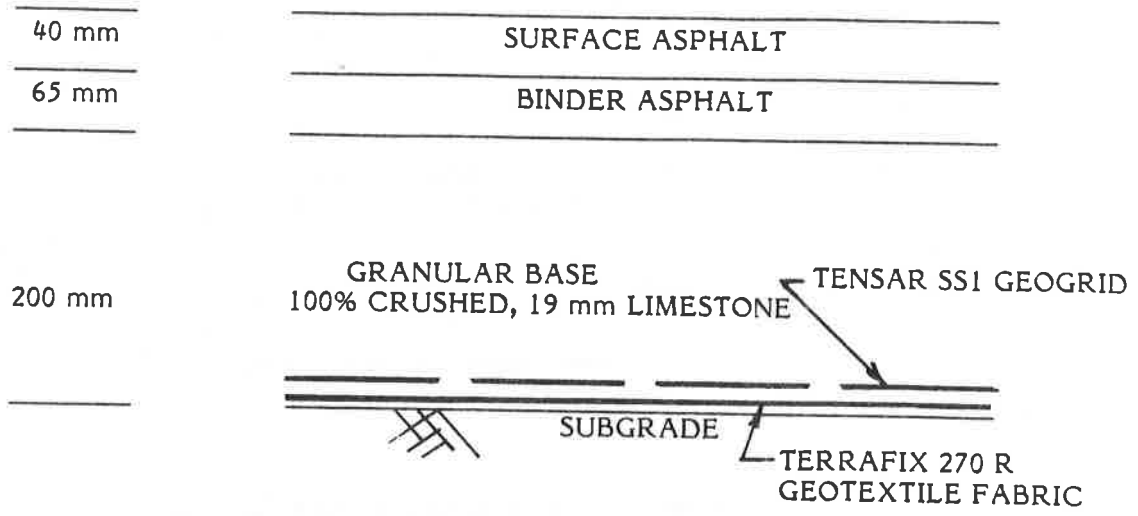
- (1) Surface Distortion relates only to apparent vehicle load related distortion after construction; roller marks and construction related distortion were not included.
- (2) Surface Cracking relates only to distinct vehicle load related cracking, edge cracking at granular shoulder were not included.

7.0 DISCUSSION

The performance of the pavement structures, after about 1100 ESAL's, indicates that the geogrid reinforcement has contributed to reduced subgrade and asphalt strain. The positive contribution of the relatively low stiffness geogrid material to date is somewhat in disagreement with findings of Barksdale and Brown (9). Their work indicates that deformations of up to 25 mm would be required to mobilize even modest forces in relatively low stiffness geogrids. However, construction of the reinforced granular base included pre-stressing the geogrid/granular layer with loaded vehicles. When subgrade support deterioration occurred due to adverse moisture conditions, the effect was also to generate deformations in excess of 25 mm in the granular and subgrade. As a result, construction conditions, either by design or by accident, successfully achieved a condition of locked-in stress in the reinforced layer.

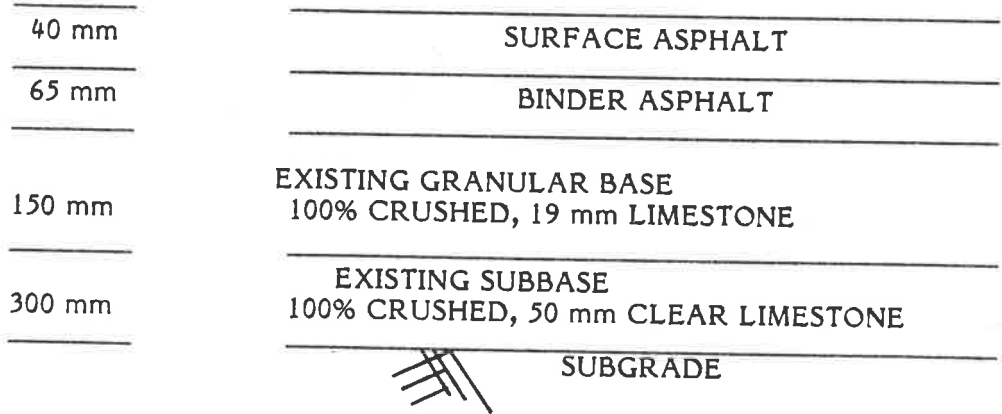
8.0 CONCLUSIONS

The findings of the site monitoring to date are regarded as preliminary, but generally indicate that pavement structural properties and performance under dynamic loading are improved with the use of geogrid reinforcement. Deflection basin and elastic layer analysis suggest that improved performance can be expected due to greater load distribution and reduced strain levels in the reinforced section. Although long term monitoring is proposed to assess and document pavement performance, the use of geosynthetics at the case study site has indicated that alternative geosynthetic pavement sections should be considered in the general pavement design process.



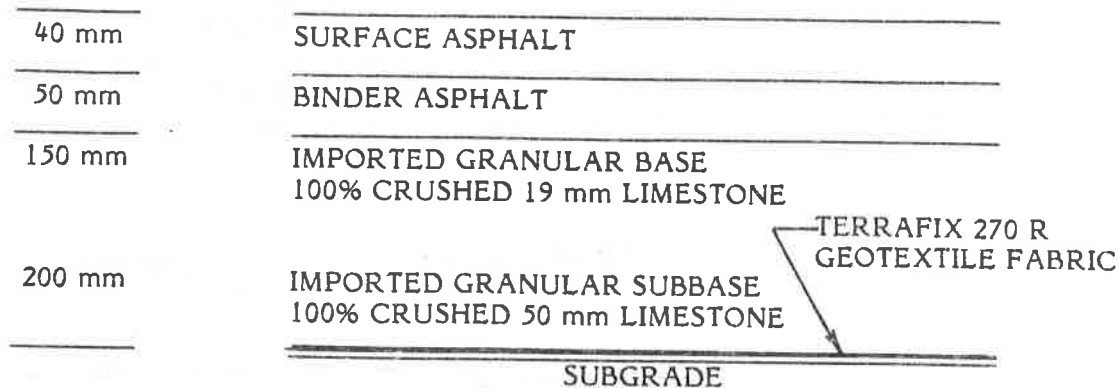
Geogrid Reinforced Design Structure With
Geotextile Fabric - Truck Staging Yard

Figure 1(a)



Non-Reinforced Pavement Section for Access Roadway

Figure 1(b)



Pavement Section with Geotextile Fabric for
Truck Staging Yard Expansion

Figure 1(c)

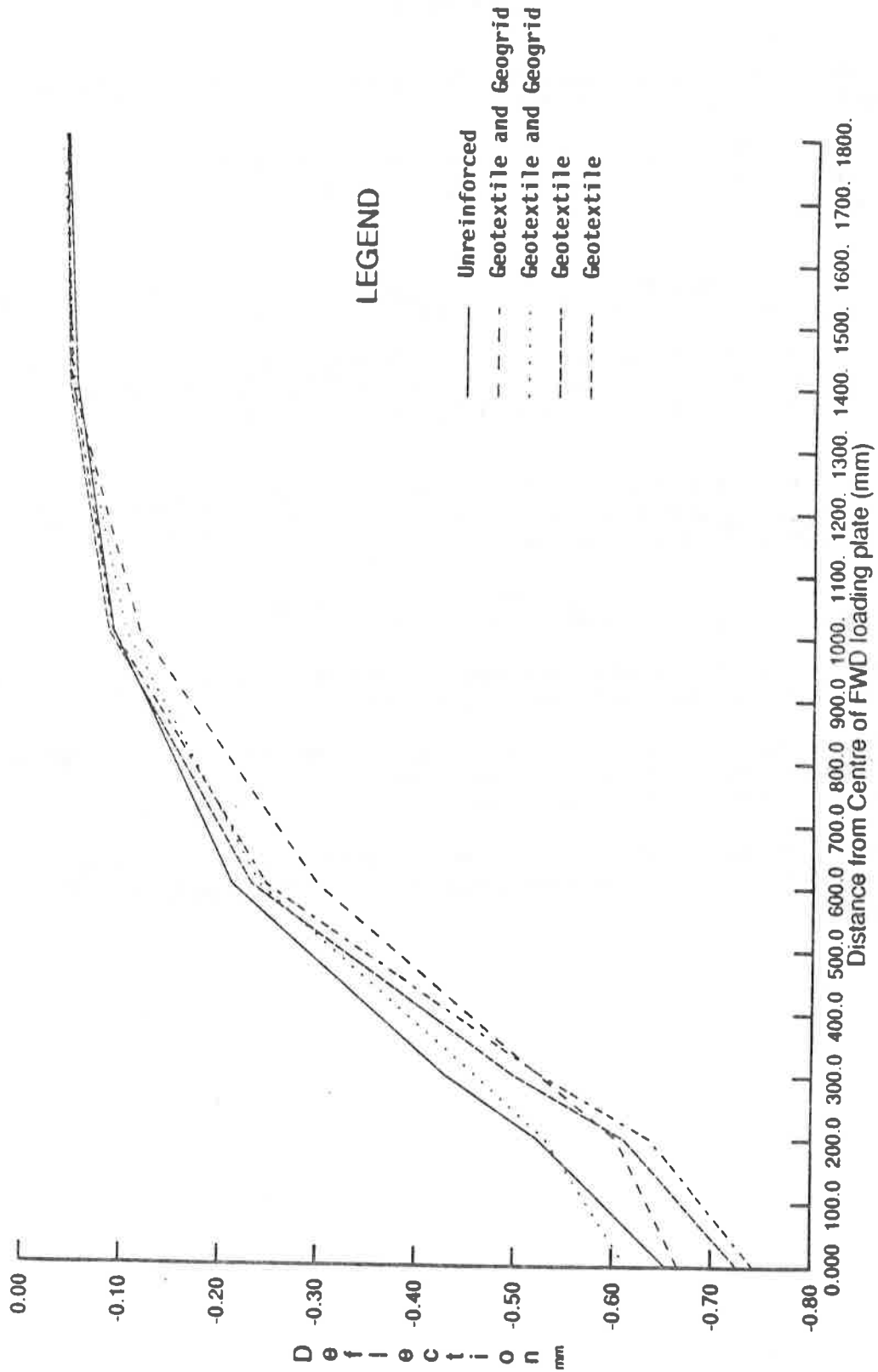


FIGURE 2

FWD LOAD/DEFLECTION BASIN PLOTS

References

- (1) "Thickness Design - Asphalt Pavements for Highways and Streets", The Asphalt Institute Manual Series No. 1, September 1981.
- (2) Jung, F.W. and Phang, W.A., "Elastic Layer Analysis Related to Performance in Flexible Pavement Design", published document by the Ontario Ministry of Transportation and Communications.
- (3) Haas, R.G., "Structural Behaviour of Tensar Reinforced Pavements and Some Field Applications", Proceedings of the Symposium on Polymer Grid Reinforcement in Civil Engineering, Institution of Civil Engineers, London, March, 1984.
- (4) Rolin, A.L., Jarrett, P.M. and Wallace, R.B., "Three Day Short Course on Geotextiles and Geomembranes", Sponsored by the Regional Geotechnical Group, Saskatoon Geotechnical Group, and the Canadian Geotechnical Society, Regina, Saskatchewan, March 19-21, 1985.
- (5) Barsvary, A.K., and Maclean, M., "Engineering Geotextiles", Research Document EM-45 prepared by the Engineering Materials Office Soils and Aggregates Section of the Ontario Ministry of Transportation and Communications, June, 1981.
- (6) Tensar Technical Note, "Design Guideline for Parking Areas With Tensar Geogrid Reinforced Base Layers", TTN:BR3, January, 1986.
- (7) ELMOD, elastic layer program developed by Dynatest and based upon the Odemark equivalent layer concept, and Boussineq's Equations.
- (8) CHEVDEF, iterative elastic layer program based on the CHEVRON N LAYER program; back calculates the layer moduli by deflection basin matching procedures, program assumes semi-infinite, homogeneous, linear elastic material properties.
- (9) Barksdale, R.D., and Brown, S.F., "Geosynthetic Reinforcement of Aggregate Bases of Surfaced Pavements", Transportation Research Board Meeting, January, 1987.

SESSION 3B
BEHAVIOR OF SOIL GEOSYNTHETIC SYSTEMS



T.H. WU

University of Colorado at Denver, U.S.A.

Behavior of Soil-Geotextile Composites and its Application to Finite Element Analysis

ABSTRACT

The stress-strain behavior of geotextile-reinforced soils is often obtained by performing triaxial compression tests with layers of geotextile specimen placed horizontally in the soil sample. In the literature, it has been shown that the triaxial compressive stiffness of reinforced soil is smaller than that of the unreinforced soil at low strains and that the loss in stiffness is more pronounced when the number of layers of the geotextile is greater, indicating an adverse effect of geotextile inclusion at low strain levels. Through this study it was learned that the "loss of compressive stiffness" was due entirely to compression of the geotextile.

It was noted that in typical geotextile-reinforced soil structures the thickness of soil lift was significantly larger than the sample height of the triaxial tests. As a result, the tests greatly exaggerated the effect of the geotextile compression. For accurate assessment of soil-geotextile composite properties in typical geotextile-reinforced soil structures, correction of geotextile compression is necessary, especially for thick geotextiles.

In addition, the application of the soil-geotextile composite properties to finite element analysis of geotextile-reinforced soil structures was addressed. The advantages and disadvantages of the composite approach for analysis of geotextile-reinforced soil structures was discussed.

INTRODUCTION

A variety of tensile reinforcements ranging from flexible geosynthetics to relatively stiff metallic materials have been used to reinforce soil structures. A considerable amount of research has been conducted to investigate the performance of reinforced soil structures using the finite element method. Two methods of simulation had been used to account for inclusion of the tensile reinforcement in finite element analysis. One method, known as the discrete approach, simulates the tensile reinforcement and the soil as separate discrete elements -- the tensile reinforcement is represented by bar (truss) elements and the soil by two-dimensional (plane) or three-dimensional (solid) elements. The constitutive relations of the bar element (i.e., the reinforcement) can be determined by conducting uniaxial tension tests on the reinforcement confined in the soil employed in the

soil structure. The other method is known as the composite approach. The method simulates the soil-reinforcement "composite" as two- or three-dimensional elements which are locally homogeneous. The constitutive relations of the composite materials can be obtained by performing triaxial compression tests on reinforced soil.

This paper addresses the stress-strain behavior of soil-geotextile composites and its application to finite element analysis of geotextile-reinforced soil structures.

STRESS-STRAIN BEHAVIOR OF SOIL-GEOTEXTILE COMPOSITES

The stress-strain relationship of soil-geotextile composites reported in the literature is obtained by performing triaxial compression tests with layers of geotextile specimen placed horizontally in the soil sample. Broms (1) conducted a series of triaxial compression tests on soil-geotextile composites. His work, shown in Figure 1, is for dense and loose sands at low and high confining pressures. The results indicated that the soil-geotextile composite was stiffened and had a higher shear strength when geotextile was properly placed in the soil. It is to be noted, however, that the stiffness of the reinforced soil is somewhat smaller than that of the unreinforced soil at low strains in most of the tests shown in Figure 1.

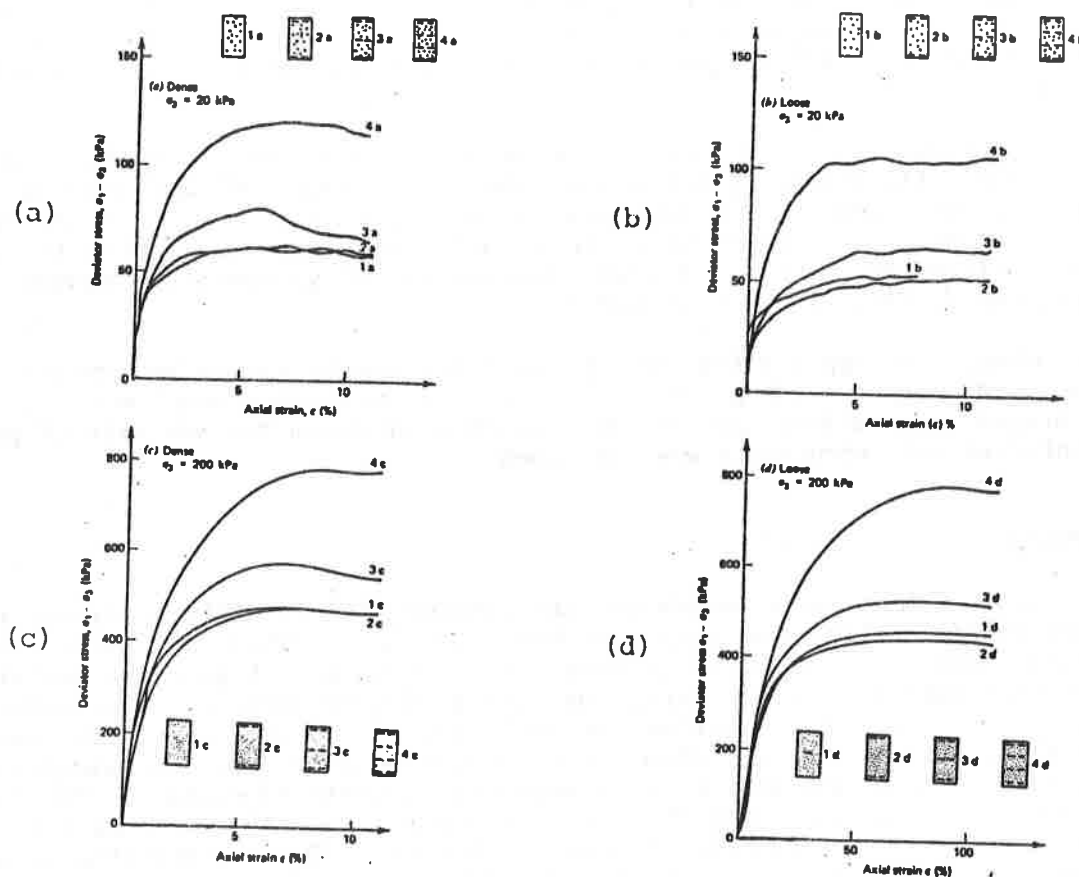


Figure 1. Results of Brom's Triaxial Tests (1)

Holtz et. al (5) performed triaxial compression tests on soil-geotextile composites with geotextile specimens placed at the upper and lower third points and on the top and bottom platens (the same as Configuration 4 in Brom's tests). Various reinforcement materials were used in the test. The stress-strain relationships for the reinforced and unreinforced specimens are shown in Figure 2. It can be seen that the geotextile inclusion markedly increased the shear strength. However, except for the low confining pressure of 35 KPa, the stiffness of the reinforced soil appears to be lower than that of the unreinforced soil at small strains.

The stress-strain relationships of geotextile-reinforced and unreinforced soil specimens shown in Figure 3 were presented by Gray and Al-Refeai (3). They concluded that greater number of geotextile layers increased the shear strength of the soil and decreased the stiffness at low strains.

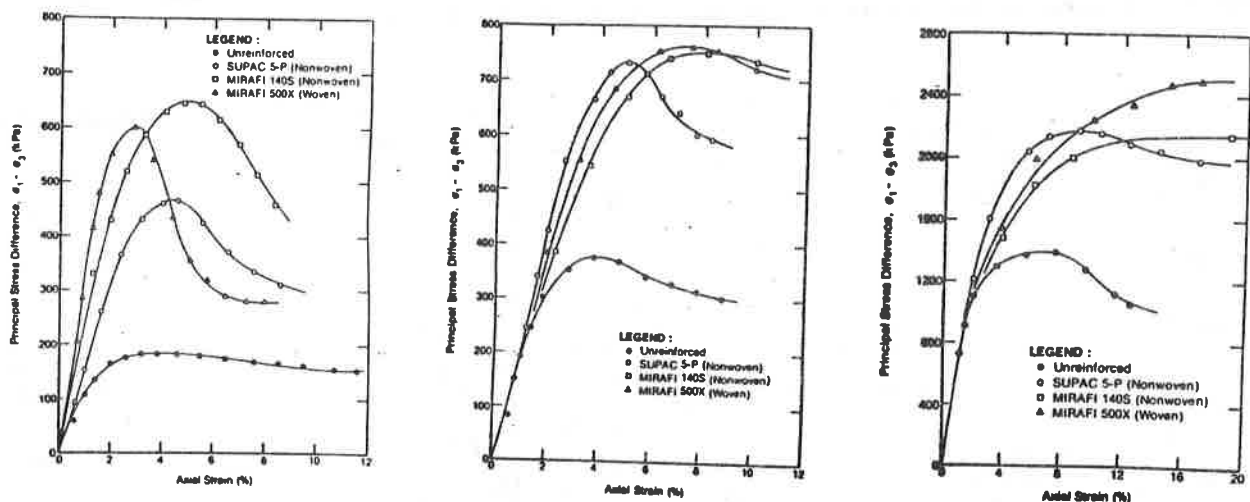


Figure 2. Results of Holtz, et al's Triaxial Tests: (a) $\sigma_3 = 35$ kPa, $D_r = 90\%$
(b) $\sigma_3 = 69$ kPa, $D_r = 90\%$ (c) $\sigma_3 = 276$ kPa, $D_r = 90\%$ (5)

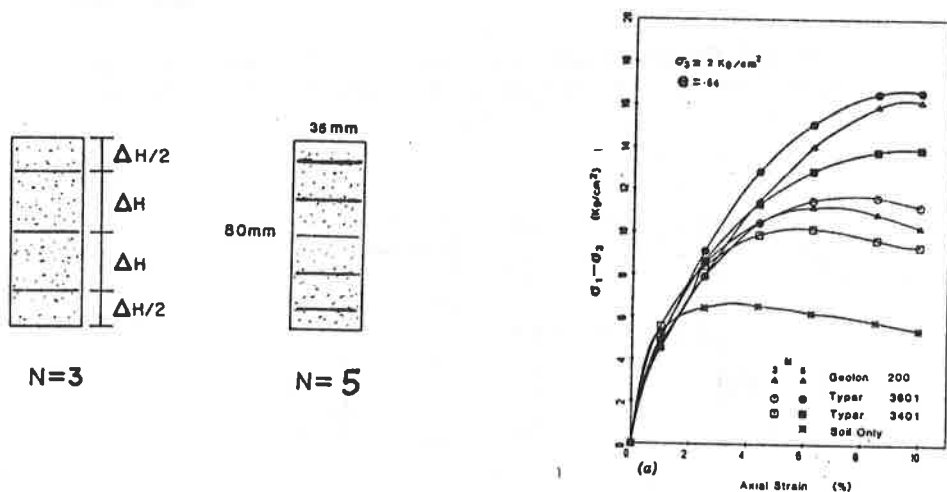


Figure 3. Results of Gray and Al-Refeai's Triaxial Tests (3)

COMPRESSIVE STIFFNESS AT LOW STRAINS

In order to gain insight into the stress-strain response of reinforced soil at low strains (2% to 5%), which could be important in some soil-reinforcement applications, a series of tests were performed. Figure 4 shows the stress-strain relationships from triaxial compression tests on fabric-reinforced Ottawa sand and non-reinforced Ottawa sand. The tests were performed on cylindrical samples of 2.0 inch in diameter and 4.25 inch in height. The positions of geotextile layers in the reinforced soil samples are illustrated in Figure 5. The sand has a uniformity coefficient of 1.43. The maximum and minimum unit weights (Earth Manual, 2nd ed., 1974) are 112.19 pcf and 97.52 pcf, respectively. The soil was prepared at 107.35 pcf ($D_r = 70\%$). The geotextile used in the test is a needle-punched nonwoven polyester, Bidim C-34. The thickness of the geotextile determined in accordance with ASTM D-1777 is 2.3 mm (0.005 bar pressure) and 1.05 mm (2.000 bar pressure). The tests were conducted at 15 psi and 45 psi confining pressures.

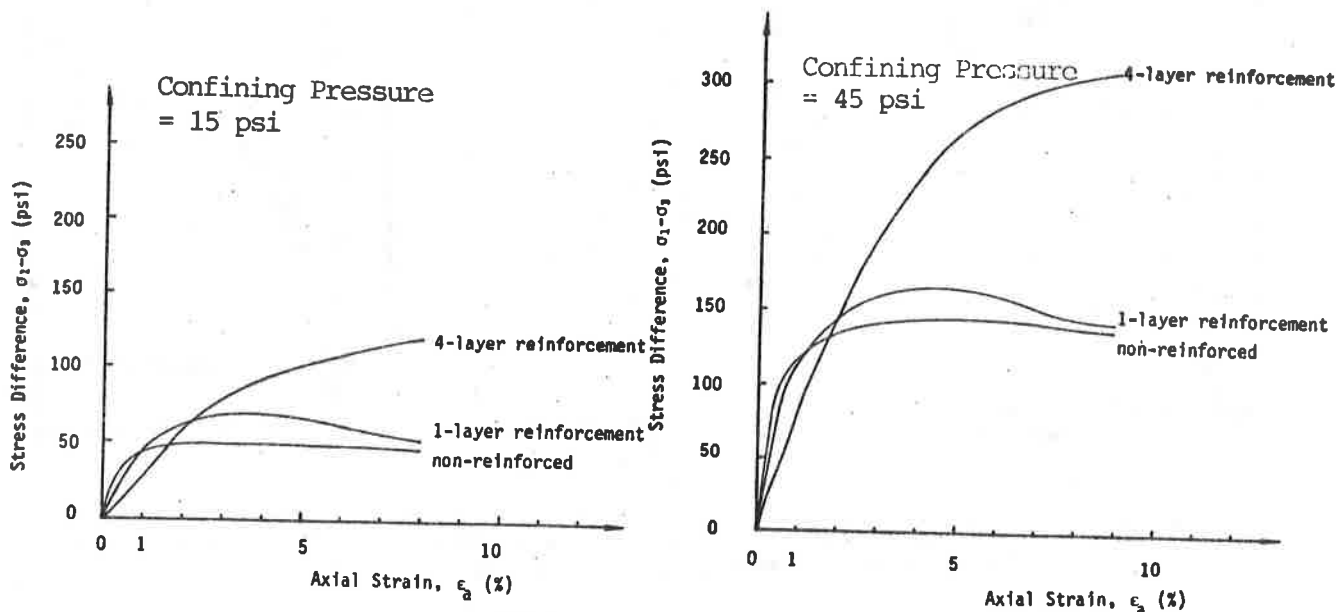


Figure 4. Triaxial Compression Test Results of Reinforced and Unreinforced Ottawa Sands at Confining Pressures of (a) 15 psi, and (b) 45 psi.

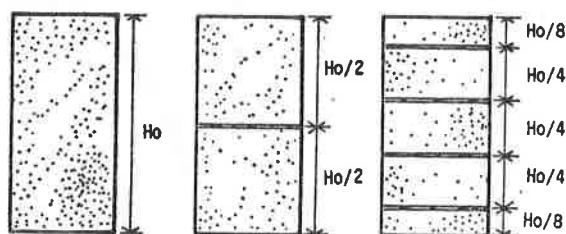


Figure 5. Positions of Geotextile Reinforcement upon Application of the Confining Pressures

The test results support other researchers' observation that the triaxial compression stiffness of the reinforced soil was smaller than that of the unreinforced soil at low strains. It was also clear that the loss of stiffness was more pronounced as the number of geotextile layers increased.

It can be demonstrated that the "loss of compressive stiffness" was due entirely to compression of the geotextile. Figure 6 depicts the geotextile thickness versus pressure relationship (6). The thickness of the geotextile was obtained by measuring the thickness of 5 and 10 layers of the geotextile and dividing it by the number of layers. From the figure it is seen that, for example, the thickness of the geotextile is reduced by approximately 0.012 inch as the pressure increases from 15 psi to 40 psi. The reduction in thickness is amount of 0.28% axial strain in the test sample which is very close to the difference in axial strain between the non-reinforced soil and the soil with one-layer reinforcement for $\sigma_1 - \sigma_3 = 25$ psi at 15 psi confining pressure, Figure 4(a). The same observation can be ascertained for the results of 45 psi confining pressure.

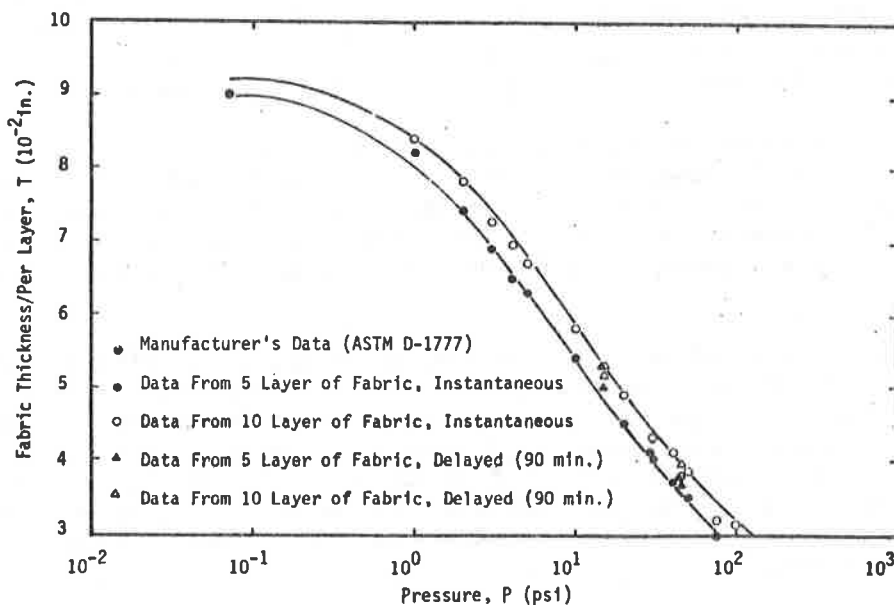


Figure 6. Thickness versus Pressure Relationship of Bidim C-34 Geotextile (6)

Figure 4 also showed that at low strains the difference in the axial strain between the samples with four-layer reinforcement and non-reinforced samples was approximately four times the corresponding difference between the samples with one-layer reinforcement and non-reinforced samples. This again demonstrated that the loss of compressive stiffness at low strains were due mostly, if not entirely, to compression of the geotextile.

As strains became larger, frictional resistance between soil and geotextile began to mobilize and increase the overall stiffness of the soil. The magnitude of the axial strain required to initiate the friction can be deduced from the stress-strain curve where the stiffness of non-reinforced soil and the stiffness of reinforced soil (after correcting for geotextile compression) began to differ.

It is to be noted that in typical geotextile-reinforced soil structures, the thickness of soil lift is significantly larger than the sample height of the triaxial tests. As a result the triaxial tests greatly exaggerated the effect of the geotextile compression. For more accurate assessment of soil-geotextile composite properties in typical geotextile-reinforced earth structures, correction of geotextile compression is necessary, especially for thick geotextiles.

APPLICATION TO FINITE ELEMENT ANALYSIS

The composite approach of finite element method (i.e., treating the soil-reinforcement composite as a locally homogeneous material) had been used to analyze performance of reinforced soil structures. Herrmann and Al-Yassin (4) compared the composite and discrete approaches in analyzing the behavior of a Reinforced Earth wall. They concluded that both approaches can be applied with equal accuracy to analysis of reinforced soil systems, and that for large two-dimensional and three-dimensional configurations, only the composite approach is economically feasible.

A recent study by Chou, et al. (2) to investigate the effectiveness of a geogrid-reinforced embankment also demonstrated that the two approaches gave similar results under the working load condition (namely, not approaching failure) and indicated that the composite approach is preferable to the discrete approach.

For analysis of earth reinforcement systems, the composite approach has the advantages of: (1) the economy of laboratory test -- achieved by not having to test the soil property, the in-soil reinforcement property, and soil-reinforcement interface behavior separately, and (2) the economy of analysis -- achieved by not having to discretely represent each and every component in the finite element analysis.

It should be pointed out that the composite approach suffers from two major disadvantages. The first disadvantage is that it does not produce information regarding potential slippage along soil-reinforcement interface nor does it give the stress and strain states (hence the forces and displacements) in the reinforcement. Since the internal stability of earth reinforcement systems is generally evaluated on the basis of pullout failure and rupture failure of reinforcement, this disadvantage prevents direct assessment of the internal stability of reinforced soil structures.

The second disadvantage is that "proper" discretization of soil-composite systems is difficult to obtain, especially when reinforcements are closed spaced. Figure 7 shows two finite element discretizations of an earth reinforcement system. While the two discretizations are bound to yield different results, and in some cases it could be very significant, it is not possible to determine which of the two meshes is better. Rational decision of the proper discretization requires the knowledge of the extent of influence of the reinforcement inclusion. As the extent of influence is very difficult to determine, so as the proper finite element discretization.

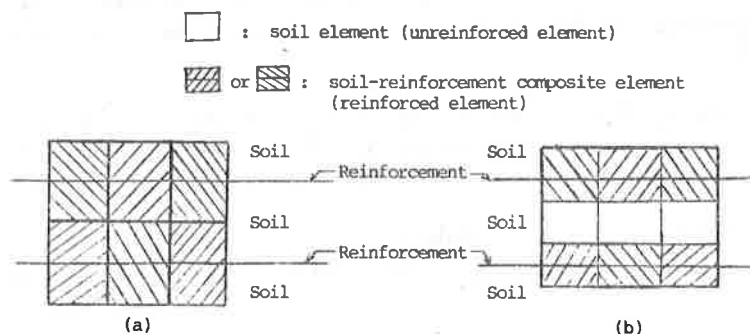


Figure 7. Two Different Finite Element Discretizations of a Soil Reinforcement system : (a) Discretizing into 6 Reinforced Elements, and (b) Discretizing into 6 Reinforced Elements and 3 Unreinforced Elements.

SUMMARY AND CONCLUSIONS

A study was undertaken to investigate the stress-strain behavior of soil-geotextile composites, particularly, the loss of compressive stiffness at low strains due to the reinforcement inclusion. In addition, the application of the composite property to finite element analysis of reinforced earth structures was addressed.

It was demonstrated that the loss of compressive stiffness observed in the tests was due entirely to compression of the reinforcement. As the soil lift in field construction is much larger than the soil thickness used in the triaxial tests, correction of geotextile compression is needed before applying to finite element analysis, especially if the strains of up to 2-5% are considered important.

The composite approach is more economical (in terms of both testing and analysis) than the discrete approach in finite element analysis. However, it suffers from two drawbacks: (1) it does not allow direct assessment of the internal stability of reinforced soil structures, and (2) discretization of soil-composite system is somewhat arbitrary.

REFERENCES

- (1) Broms, B.B., "Triaxial Tests with Fabric-Reinforced Soil," Proceedings, International Conference on Use of Fabrics in Geotechnics, L'Ecole Nationale des Ponts en Chaussees, Vol. III, Paris, France, April 1977.
- (2) Chou, N.N.S., Wu, T.H., Siel, B.D., "The Effectiveness of Tensile Reinforcement in Strengthening an Embankment Over Soft Foundation," Proceedings of Geosynthetics '87, New Orleans, LA, February 1987.
- (3) Gray, D.H. and Al-Refeai T., "Behavior of Fabric-versus Fiber-Reinforced Sand," Journal of the Geotechnical Engineering Division, ASCE, Vol. 112, No. GT8, August 1986.

Geosynthetics '89 Conference
San Diego, USA

- (4) Herrmann, L.R. and Al-Yassin Z., "Numerical Analysis of Reinforced Soil Systems, "Symposium on Earth Reinforcement, ASCE Annual Convention, Pittsburg, PA, April 1978.
- (5) Holtz, R.D., Tobin, W.R., and Burke, W.W., "Creep Characteristics and Stress-Strain Behavior of a Geotextile-Reinforced Sand," Proceedings of the Second International Conference on Geotextiles, Las Vegas, August 1982.
- (6) Liu, H.-C., "Static and Cyclic Behavior of Fabric-Reinforced Sand," M.S.Thesis, Department of Civil Engineering, University of Colorado at Denver, 1987.

D.H. GRAY

M. KALDJIAN

University of Michigan, U.S.A.

C. WU

Tamkang University, Taiwan

Stress-Deformation Response of Geotextile Reinforced Granular Structures

SUMMARY

The stress-deformation response of embedded granular structures reinforced with both woven and non-woven geotextiles was determined by a finite element analysis. The analysis procedure was used to investigate both the axisymmetric case of a fabric encapsulated stone column and the plane strain case of a granular trench reinforced with horizontal layers of fabric.

The finite element model took into account both material and geometric non linearities and allowed for possible slip at soil-inclusion interfaces. The soil matrix could be modelled as either an elasto-plastic or visco-elastic material. A special testing device was developed to determine independently the interface friction and in-situ stress strain behavior of geotextile inclusions. As a result of these experimental tests the tensile modulus of the geotextile inclusions was modelled as either a polynomial function of strain or alternatively as a function of confining stress. The former was representative on woven geotextiles, whereas the latter described better the behavior of non-woven inclusions.

The finite element model was tested and validated against the results of triaxial tests on sand specimens reinforced with layers of horizontal, geotextile inclusions. The program was then used to predict the response of a fabric reinforced granular trench or column embedded in a soft clay matrix. Results of these predictions showed that geotextile encapsulation and/or reinforcement significantly improved the bearing capacity of embedded granular structures.

INTRODUCTION

Granular structures can be introduced into a weak or soft clay in order to improve bearing capacity and reduce settlement. The granular structures are formed in-situ by backfilling a cylindrical hole (stone column method) or rectangular slot (granular trench) that is excavated in a weak soil or soft clay. Methods of estimating the lateral (confining) stress acting on a granular column embedded in a soft, plastic clay and the maximum vertical stress the column can sustain have been reviewed by Brauns (1). Results of a full scale field trial on a sand column embedded in a soft clay have been reported by Hughes *et al.* (2).

The bearing capacity of a continuous foundation or strip footing placed over a sand trench in a soft clay has been estimated by Madhav and Vitkar (3) using an upper bound, limit analysis theorem. Hamed *et al.* (4) have presented the results of laboratory model tests to determine the variation in bearing capacity of a strip footing resting on a granular trench in a soft, saturated clay. A schematic illustration of a granular trench beneath a strip footing is shown in Figure 1. The width of the trench is equal to W and the width of the foundation is equal to B . The height of the trench is H . The width of the trench W can be smaller or larger than B . The parameters of the stronger trench (or column) material and the weak clay soil are denoted as follows for bearing capacity calculations:

	Trench (column) <u>Material</u>	Weak Clay <u>Soil</u>
Angle of Friction	ϕ_1	ϕ_2
Cohesion	C_1	C_2 (or C_u)
Unit Weight	γ_1	γ_2

The increase in bearing capacity provided by these embedded granular structures depends upon the mobilization of lateral or confining stresses exerted by the surrounding clay. In order to mobilize these confining stresses it is necessary that some vertical and concurrent lateral deformation of the granular structure occur under vertical loading. Gray *et al* (5) indicated that the performance of an embedded granular structure could be enhanced by reinforcing the structure with layered geotextile inclusions or alternatively by encapsulating the structure within a fabric skin. In both cases the effect of the geotextile will be to restrict lateral deformation under vertical load

and hence induce a confining stress increase that in turn improves shear strength and bearing capacity.

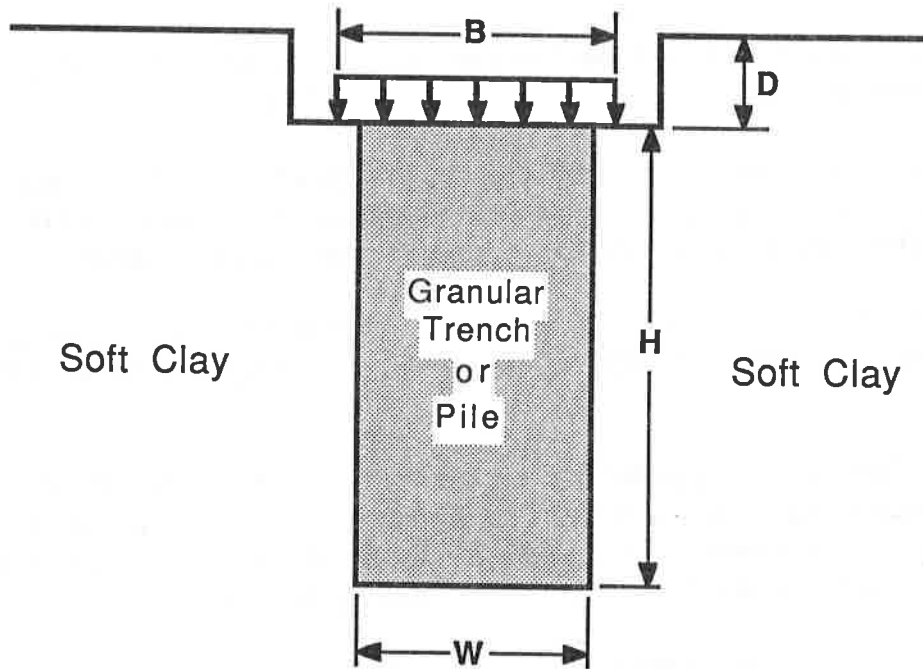


Figure 1. Schematic illustration of an embedded granular trench or pile

The analysis and prediction of bearing capacity of embedded granular structures that are encapsulated and/or reinforced in the preceding manner is the main subject of this paper. The analysis is complicated by the interactive nature of the restraint on lateral deformation (and consequent confining stress increase) provided by the fabric and surrounding clay respectively. A finite element program was developed to solve the soil-fabric composite problem. The finite element model was validated by comparing predictions against the results of triaxial compression tests on sand specimens reinforced with horizontal layers of both woven and non-woven geotextiles and against the results of quasi uniaxial compression tests on sand specimens encapsulated in a woven geotextile.

THEORETICAL MODEL

A finite element program was developed to analyze both plane strain (granular trench) and axisymmetric (stone column) type problems. Only a brief out-

line of the theoretical model is presented herein, details are provided elsewhere by Wu (6). The finite element program includes the following features and capabilities:

- 1) Higher order strain terms can be included as an option in the analysis; thus geometric nonlinearities can be taken into account.
- 2) The material properties of the soil can be modelled as either linear or nonlinear. Elasto-plastic and elasto-viscoplastic behavior modes can be invoked as alternatives to an elastic constitutive model.
- 3) The interface between dissimilar materials is modelled as either perfectly bonded or with slip/separation potential, using interface link elements.
- 4) The fabric element is modelled as an element which resists tension; it offers no resistance in compression or bending. The load-deformation relationship of the fabric is modelled as either an elastic polynomial function of strain, or as a function of confining stress.
- 5) The external loading is applied to the system incrementally. The total load can be divided into equal increments or can be applied in irregular increments. The body weight of the soil can be included in the analysis as the first loading increment.

EXPERIMENTAL PROGRAM

A series of triaxial compression tests were conducted on sand specimens reinforced with up to three layers of both woven and non-woven geotextiles. Quasi uniaxial compression tests were also conducted on sand specimens encapsulated in a woven geotextile. Properties of the sand and geotextiles are summarized in Tables 1 and 2. Results of these tests were compared against theoretical predictions from the finite element model. The in-situ constitutive behavior, both the stress-strain response and surface friction characteristics, of the geotextiles were also determined experimentally in separate tests. These results were used as input data in the finite element model. Results of these tests showed that the in-situ stress-strain response of woven fabrics was best modelled as an elastic, polynomial function of strain, whereas that of non-woven fabric was best represented by a function of confining stress as follows:

TABLE 1. PROPERTIES OF MUSKEGON DUNE SAND

Effective grain size D10 (mm)	Median grain diam D50 (mm)	Coef of Uniform Cu (mm)	Spec grav solids Gs	Max void ratio	Min void ratio	Angle of internal friction (triaxial test)
0.28	0.41	1.5	2.65	0.78	0.50	39 (Dr = 86%) 32 (Dr = 21%)

TABLE 2. PHYSICAL PROPERTIES OF GEOTEXTILES

Fabric	Manufacturer	Filament	Fabrication process	Nominal thickness (mm)	Weight (gm/sq m)
GEOLON 400	Nicolon Corp	Polypropylene multifilament	woven	0.74	220
GEOLON 200	Nicolon Corp	Polypropylene multifilament	woven	0.46	136
TYPAR 3601	Dupont	Polypropylene multifilament	nonwoven	0.38	203
TYPAR 3401	Dupont	Polypropylene multifilament	nonwoven	1.09	136

Woven fabrics: The in-situ stress-strain behavior was not significantly affected by normal compression and the response can be represented by a polynomial function of strain alone, viz.

$$\sigma_T = a_1 \epsilon + a_2 \epsilon^2 + a_3 \epsilon^3 + \dots a_n \epsilon^n \quad (1)$$

where: σ_T = axial load/unit width of fabric, ϵ = axial strain, and a_1, a_2, a_3 = polynomial constants.

The instantaneous tangent modulus (E_T) can be used directly in the finite element analysis to evaluate the stiffness of the fabric elements and is given by the following equation:

$$E_T = \frac{d\sigma_T}{d\epsilon} = a_1 + 2a_2 \epsilon + 3a_3 \epsilon^2 + \dots n a_n \epsilon^{n-1} \quad (2)$$

Non-woven fabrics: The in-situ stress strain behavior strongly depends on normal confining stress. A non-linear hyperbolic model can be used to represent the modulus response, viz.,

$$E_i = k P_a (\sigma_n/P_a)^n \quad (3)$$

where: E_i = initial tangent modulus, P_a = reference atmospheric pressure, k , n = empirical constants.

The stress-strain curves for non-woven fabrics can be represented by a general equation of the form

$$\sigma_T = \frac{\epsilon}{(m\epsilon + b)} \quad (4a)$$

$$\text{At } \epsilon = 0, \quad E_T = E_i = (1/b) \quad (4b)$$

Combining equations (3) and (4) yields an expression for the instantaneous tangent modulus for evaluating the stiffness in the fabric elements, viz.,

$$E_T = \frac{d\sigma_T}{d\epsilon} = \frac{(1/kP_a) (\sigma_n/P_a)^{-n}}{[m\epsilon + (1/kP_a) (\sigma_n/P_a)^{-n}]^2} \quad (5)$$

VALIDATION OF FINITE ELEMENT MODEL

The finite element model was first checked against exact analytical solutions for a number of relatively simple loading conditions, e.g., stress distribution beneath a circular load over an elastic, isotropic half space. The finite element model predictions were then compared with lab triaxial test results on fabric reinforced sand specimens and with results from quasi uniaxial compression tests on fabric encapsulated sand cylinders.

1. Axisymmetric Sand Cylinder with Horizontal Layers of Fabric

Specimens with 1, 2, and 3 layers of horizontal, internal fabric layers were used in the finite element model. A finite element mesh configuration for a specimen with three layers of fabric inclusions is shown in Figure 2. A comparison between predicted and experimental test results for a sand

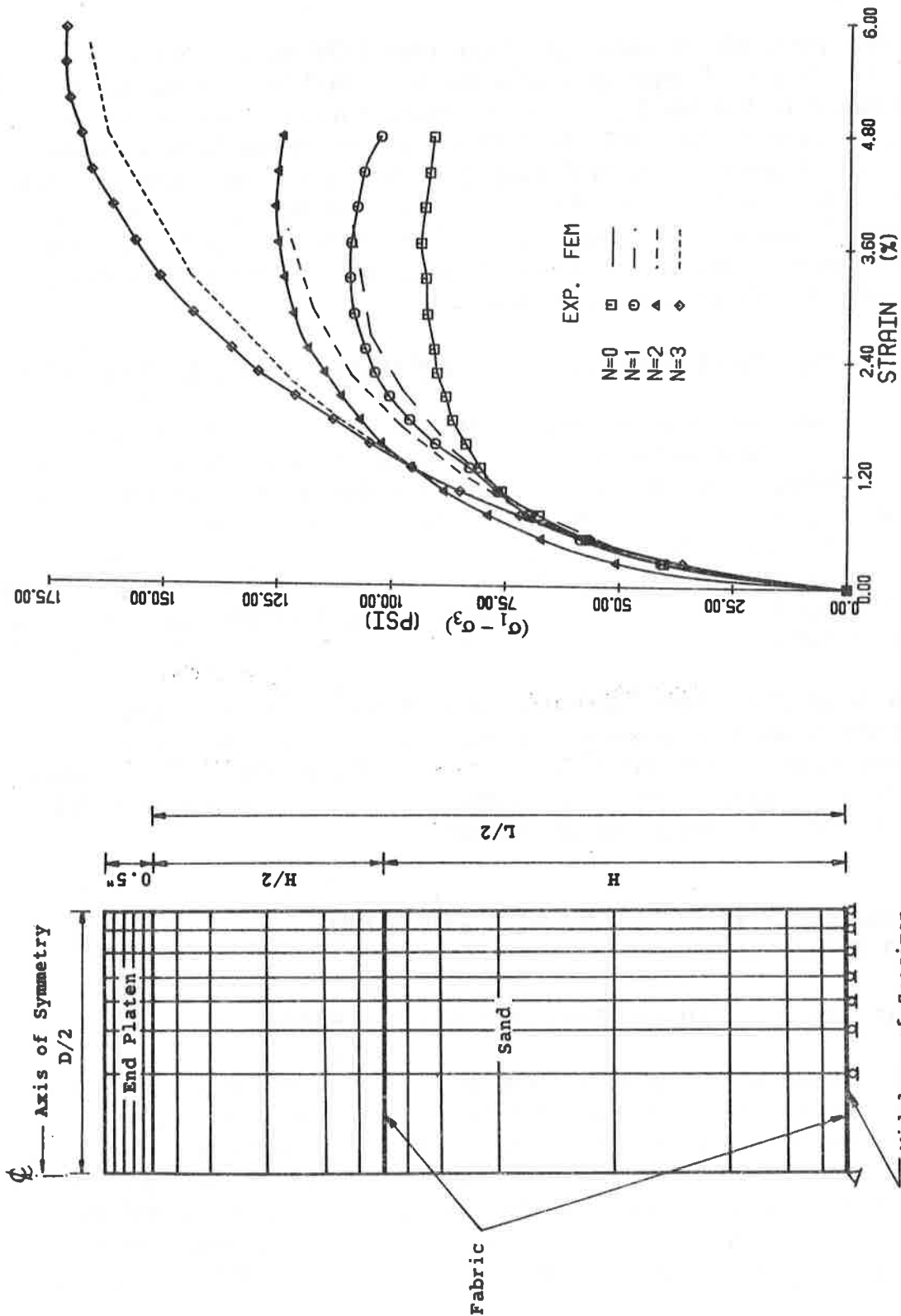


Fig. 2 Finite Element Grid for Triaxial Test Sample with 3-Layer Fabric Reinforcement

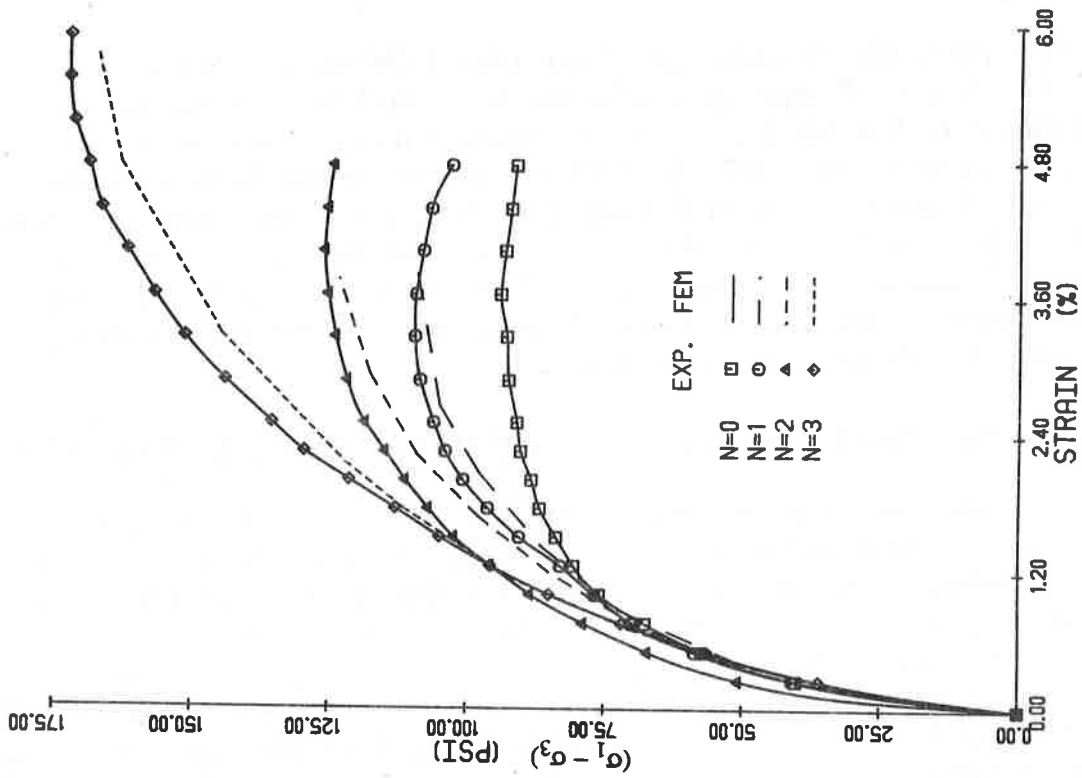


Fig. 3 Experimental vs FEM Predicted Stress-Strain Curves for Triaxial Tests on Sand with Layered Reinforcements (GEOLON 400, Poisson's ratio = 0.45, Drucker Prager Yield criterion).

specimen reinforced with a woven geotextile (GEOLON 400) is shown in Figure 3. The Drucker-Prager yield criterion was used to describe the constitutive behavior of the sand in the finite element model. Values of Poisson's ratio ranging from 0.35 to 0.45 were tried in the finite element analysis. Use of large values of Poisson's ratio cause large lateral deformations in the sand which in turn further mobilize the restraining (reinforcing) effect of fabric inclusions. Results of the finite element analysis showed that the predicted curves with a Poisson's ratio of 0.45 were in relatively close agreement with experimental results.

2. Axisymmetric Sand Cylinder with External Fabric Encapsulation

In the case of encapsulated specimen, vertical compression of the specimen induces radial or lateral deformation. This lateral deformation causes the encapsulating fabric to stretch and develop a circumferential tensile (hoop) stress. The hoop stress in turn exerts a radial confining stress on the encapsulated sand specimen which mobilizes compressive strength and resistance to further axial deformation in an interactive manner. The magnitude of the hoop stress depends on the circumferential strain and tensile modulus of the encapsulating fabric.

The experimental stress-strain response of a dense, cylindrical sand specimen encapsulated by a woven geotextile was checked against finite element predictions. Both the Drucker-Prager and Modified Critical State yield criteria were used in the finite element analysis with the latter giving better agreement with experimental results.

BEARING CAPACITY PREDICTIONS FOR EMBEDDED GRANULAR STRUCTURES

1. Granular (Stone) Column Encapsulated by Fabric

In order to investigate the effectiveness of fabric encapsulation, the load-deformation relationships of a sand column with and without encapsulation was compared with that of a circular footing (same diameter as the granular column) resting on top of clay alone. The sand column was assumed to have a friction angle of 39° and to be embedded in a soft clay with an undrained shear strength (c_u) of 5.9 psi (40.6 kN/m²). The column was also assumed to be 1-foot in diameter by 4-feet long ($H/D = 4.0$). GEOLON 200 was used as

the encapsulating fabric. The body weight of the two soils ($\gamma_{\text{sand}} = \gamma_{\text{clay}} = 110$ pcf) were applied as the first loading increment.

The encapsulating fabric provided a significant extra margin of bearing capacity (vertical stress) especially at high deformation. Encapsulation of a granular column in a geotextile provides a further benefit of separation, i.e., it prevents fines from squeezing or migrating into the granular column which would compromise the column's stabilizing/reinforcing function. The beneficial influence of fabric encapsulation around a granular column is more pronounced for embedment in a soft clay. Soft, plastic clays only provide small amounts of lateral confining stress or passive resistance; hence large lateral deformations tend to result in an embedded granular column subjected to vertical loads at the top. These large lateral deformations in turn would mobilize large hoop stress resistance or confining stress in any encapsulating fabric. Stiff clays, on the other hand, provide much greater lateral restraint or passive resistance which limits lateral deformation or expansion of the granular column. This limited deformation, in turn, would reduce the amount of hoop stress or confining stress that could be contributed by an encapsulating fabric. Test results described in the previous section of this paper on fabric encapsulated sand specimens loaded in uniaxial compression represent the extreme case of a granular column where no surrounding clay is present.

2. Granular Trench with Internal Fabric Reinforcement

The load-settlement relationship of a strip footing resting on a soft clay stabilized by a granular trench both with and without internal reinforcement was predicted by the finite element analysis. The trench was assumed to be the same width as the strip footing. The depth of the foundation (D_f) was 2.0 feet; the granular trench was assumed to be 2 feet high and 1.5 feet wide ($w/B = 1.0$, $H/B = 1.33$). The reinforced case was analyzed by inserting three layers of GEOLON 200 fabric into the hypothetical trench backfill. The FEM mesh for the fabric reinforced granular trench is shown in Figure 4. The internal angle of friction for a plane strain analysis of the granular material in a dense condition was assumed to be 43° .

The initial, lateral stress in a clay prior to placement and loading of an embedded granular structure affects the maximum vertical stress or bearing capacity of the structure. Based on pressuremeter tests Hughes and Withers (7) suggested values for the initial lateral stress in the range 0 to $2.7 c_u$, where c_u is the undrained shear strength of the clay. The initial lateral

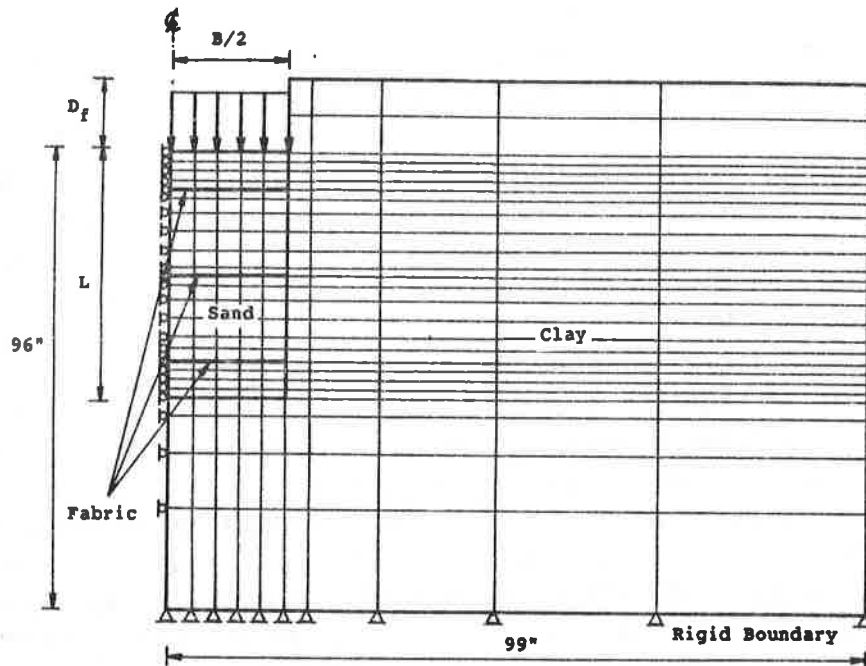


Fig. 4 Finite Element Grid for a Granular Trench Reinforced with Three Layers of Fabric Embedded in a Soft Clay

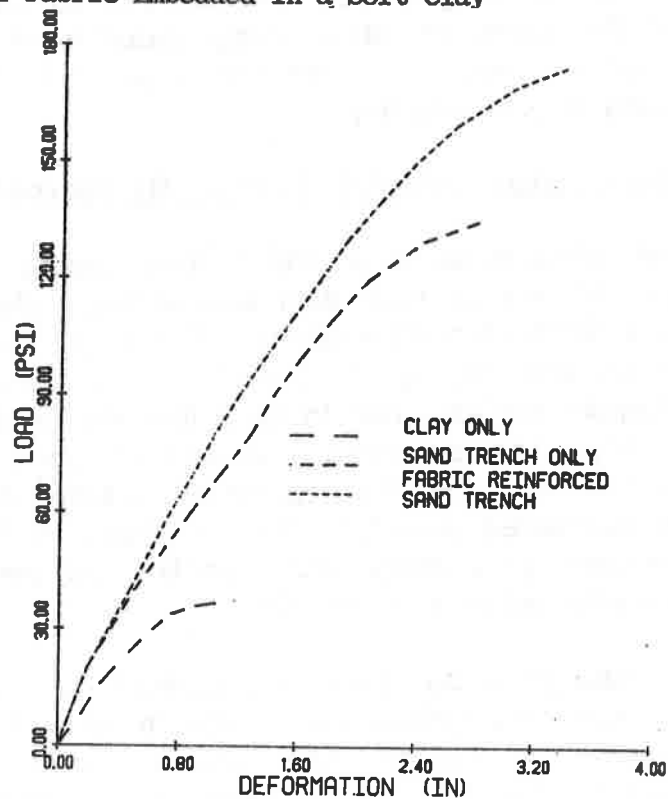


Fig. 5 Predicted FEM Load-Deformation Relationships for a Granular Trench (with and without Layered Fabric Inclusions) Embedded in a Soft Clay (GEOLON 200, $W/B = 1.0$, $H/B = 1.33$, $\phi = 43^\circ$, $c = 5.9$ psi)

stress in the clay was assumed to be 1.2 cu and the undrained strength of the clay was assumed to be 5.9 psi (40.6 kN/m²) in the FEM simulation.

Load-settlement relationships for the granular trench with and without fabric reinforcement for the preceding boundary conditions are shown in Figure 5. The FEM predictions indicate that a granular trench resulted in approximately a fourfold increase in bearing capacity (35 to 135 psi) compared to the clay alone. The presence of the trench also increased the amount of deformation required to reach the peak vertical stress. These results can be compared with the bearing capacity of a plane strain granular trench predicted by Madhav and Vitkar (3) using an upper bound limit analysis theorem. The latter theorem predicts bearing capacities of 30 and 124 psi respectively for strip footings with and without a trench ($c_u = 5.9$ psi, $\phi_1 = 43^\circ$, $\gamma_1 = \gamma_2 = 110$ pcf, $D_f = 2.0$ ft). The upper bound predictions agree reasonably well with the FEM predictions.

Hamed *et al* (4) have presented the results of laboratory model tests of bearing capacity of granular trenches embedded in a soft clay. Their tests were conducted in a much softer clay ($c_u = 1.5$ psi) than that used in the FEM simulation. They also examined the influence of the height of the granular trench by conducting tests over the range $0 < H/B < 4$. Their laboratory test results show that the height/width (H/B) ratio must equal or exceed 3 in order to mobilize the full benefit of the trench. Comparison of results shows that the upper bound estimate and FEM prediction exceed the bearing capacity determined in the laboratory model test. Additional FEM simulations over a range of (H/B) ratios and using the same undrained clay shear (c_u) strength are required in order to test the sensitivity of the predictions to these two parameters. In addition, measurement of actual horizontal (lateral) stresses in the clay would also be important in making any further comparisons between laboratory test results and theoretical predictions.

The FEM predictions in Figure 5 suggest that fabric reinforcement of a granular trench with three layers of fabric in the manner shown in Figure 4 resulted in an additional increase in bearing capacity (135 to 170 psi). Reinforcement also shifted (increased) the strain required to reach the peak vertical stress. Additional simulations with different numbers of fabric layers, placed in different positions in the trench, and with different H/B ratios should also be investigated to determine optimal trench/fabric configurations.

ACKNOWLEDGEMENT

The study described in this paper was supported by a research grant from the Air Force Office of Scientific Research, Grant No. AFOSR-84-0189.

REFERENCES

1. Brauns, J., "Initial Bearing Capacity of Stone Columns and Sand Piles," Proceedings: Symposium on Soil Reinforcing and Stabilizing Techniques, University of New South Wales, Sydney, Australia, 1978, pp. 477-496.
2. Hughes, J.M., Withers, N.J., and Greenwood, D.A., "A Field Trial of the Reinforcing Effect of a Stone Column in Soil," Geotechnique, Vol. 25, No. 1, pp. 34-44.
3. Madhav, M.R. and Vitkar, P.P., "Strip Footing on Weak Clay Stabilized with a Granular Trench or Pile," Canadian Geotechnical Journal, Vol. 15, 1978, pp. 605-609.
4. Hamed, J.T., Das, B.M., and Echelberger, W.F., "Bearing Capacity of a Strip Footing on a Granular Trench in Soft Clay," Civil Engr. Practice Design Engineers, Pergamon Press, Vol. 5, No. 5, 1986, pp. 359-376.
5. Gray, D.H., Athanasopoulos, G., and Ohashi, H., "Internal/External Fabric Reinforcement of Sand," Proceedings: 2nd International Conference on Geotextiles, Vol. 3, Las Vegas, Nevada, 1982, pp. 611-616.
6. Wu, Cho-sen, "Finite Element Analysis of Fabric Reinforced Sands," dissertation presented to the University of Michigan, Ann Arbor, Michigan, in 1986, in partial fulfillment of the requirements for the degree of Doctor of Philosophy.
7. Hughes, J.M. and Withers, N. J., "Reinforcing of Soft Cohesive Soils with Stone Columns," Ground Engineering, May 1974, pp. 42-49.

I. NOORANY

San Diego State University, U.S.A.

M. UZDAVINES

Woodward-Clyde Consultants, U.S.A.

Dynamic Behavior of Saturated Sand Reinforced with Geosynthetic Fibers

INTRODUCTION

The beneficial effects of geosynthetic inclusions on the shear strength of compacted soils is well known. Soil reinforcement in the form of sheets or strips of synthetic fabric and continuous or randomly distributed fibers has been shown to increase soil strength. However, there is little data on the effects of synthetic inclusions on the dynamic properties of saturated soils. The objective of this study was to investigate the dynamic strength of saturated sand reinforced with randomly distributed synthetic fibers. The study was undertaken to determine if geosynthetic materials can be used to increase the resistance of sand fills to earthquake and reduce their susceptibility to liquefaction.

Technical information on the strength of fiber-reinforced soils is limited. Hoare (1) investigated the effect of randomly distributed discrete fibers on the properties of dry angular sandy gravel. Two types of geosynthetic materials were used: A polypropylene/nylon fabric cut into 66 mm X 7 mm strips, and a twisted 50 mm chopped staple fiber. Specimens were prepared with reinforcement ratios (the ratio of weight of reinforcement to total specimen weight) varying from 0% to 0.46%. The results indicated that for a given compactive energy, the reinforcement resisted compaction, causing less dense packing with increasing reinforcement ratio. Consequently, higher compaction energies were required to achieve the same density in the soil. It was also found that the synthetic inclusions increased soil strength.

In another study, Gray and Al-Refeai (2) performed triaxial compression tests on a dune sand reinforced with randomly distributed fibers. The fibers consisted of basket reed and fiberglass filament, and varied from 13 mm to 38 mm in length and 0.3 mm to 1.75 mm in diameter. The percentage by weight of fibers varied from 0% to 1%. The specimens were compacted to a relative density of 57%. Test results indicated that increasing the amounts of reinforcement increased the peak strength and reduced the post-peak loss in soil strength up to a critical confining stress. Above this critical confining stress, the failure envelope for reinforced sand paralleled that for the unreinforced sand.

Leflaive (3) studied continuous synthetic threads as soil reinforcement. Triaxial tests were performed on three different sands reinforced with 0.14% to 0.2% by weight of continuous threads. These inclusions gave the compacted specimens an apparent cohesion of 150 kPa to 250 kPa. It was also noted in this study that application of cyclic loads to the thread-reinforced unsaturated sand increased peak static strength subsequent to cyclic loading. This study led to development of TEXOL, a process by which continuous synthetic threads are introduced into a soil as reinforcements during compaction.

No literature could be found documenting research into the effect of soil reinforcement on the response of saturated sand to cyclic loading.

METHOD OF INVESTIGATION

The present study investigated the effect of fiber reinforcement on the liquefaction resistance of saturated sand. Stress-controlled cyclic undrained triaxial tests were performed on saturated sand specimens reinforced with synthetic fibers. Monterey No. 0 sand (a uniform subrounded sand having a grain size distribution and index properties as shown in Figure 1) was used in this study.

All triaxial test specimens were prepared by moist tamping as described in the University of California, Berkeley Laboratory Manual (4). The sand was compacted in eight layers using a special compaction jig and tamper designed to place the weighed material for each layer into a predetermined volume (4). In order to study any effect of reinforcement on the dynamic behavior of sand, the relative density of the sand within the reinforced and nonreinforced specimens was kept constant at $Dr = 50\%$. For details regarding sample preparation and test procedures, refer to Uzdavines (5).

Two types of synthetic fibers were used as reinforcements. Table 1 lists their physical characteristics. The AMOCO fibers were 0.1 mm thick, 1.5 mm wide green threads separated from AMOCO Series A Siltstop fabric and cut 25 mm to 40 mm long. FORTA-FIBRE consisted of hairline, 20 mm-long fibers typically used as secondary reinforcement in Portland cement concrete. Fibers were mixed with sand and compacted. The weight and volume fractions in Table 1 are the ratios of fiber to sand plus fiber.

Table 1. Physical Properties of Fibers

	Chemical Composition	Elastic Modulus (10^6 psi)	Specific Gravity	Weight Fraction of Specimen (%)	Volume Fraction of Specimen (%)
AMOCO Propex Siltstop Fibers	polypropylene	0.70	0.91	0.38	0.59
FORTA-FIBRE Type A-5	polypropylene	0.70	0.91	0.39	0.65

Compacted samples were back pressure saturated as described in references (4) and (5), and were consolidated under an effective stress of 50 kPa. Cyclic load was then applied as a series of constant amplitude axial stresses under an undrained condition. The frequency of the cyclic stresses for all tests was 1 Hz, and the cyclic stress ratio varied between 0.30 and 0.54. The cyclic stress ratio is defined in equation 1. The number of cyclic stress applications, the axial deformation and the pore-pressure were recorded during cyclic loading until liquefaction occurred.

$$SR = \frac{\sigma_a}{2 \sigma'_3} \dots \dots \dots (1)$$

where: SR = cyclic stress ratio, σ_a = single amplitude cyclic stress

σ'_3 = effective confining pressure

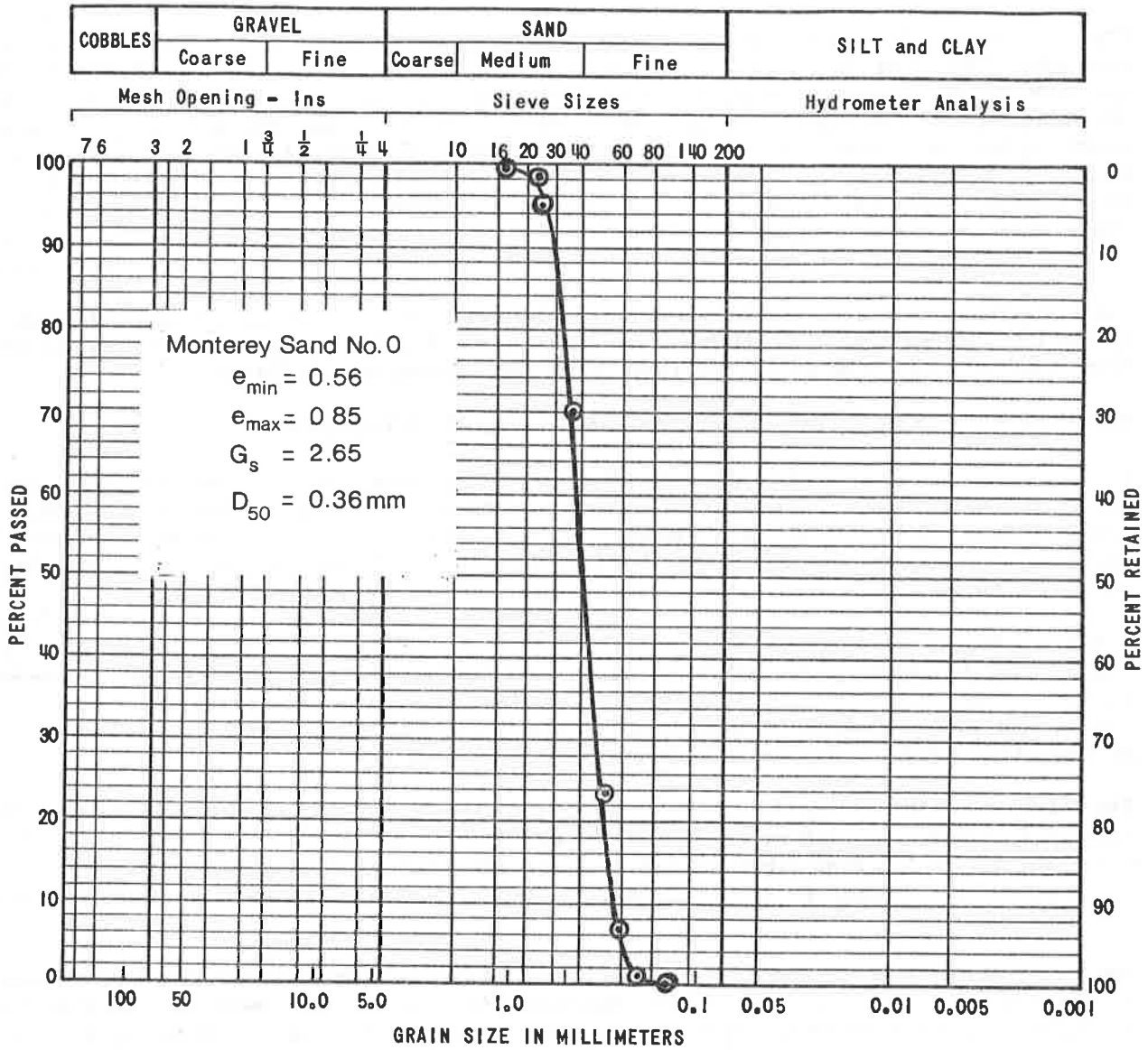


Figure 1. Physical Properties and Grain Size Distribution of Monterey No. 0 Sand.

TEST RESULTS

Figure 2 shows the typical results of an undrained cyclic triaxial test on a reinforced specimen. The test began with an effective confining pressure of 50 kPa. As the specimen pore pressure increased under repeated stress applications, the effective confining stress decreased. Initial liquefaction occurred when the effective confining stress approached zero. From the recorded axial deformations, the double-amplitude strain of the specimen at initial liquefaction and the number of cycles to induce 5% and 10% double-amplitude strain were determined. A summary of data for all tests on reinforced specimens is given in Table 2. Double-amplitude strain for a given stress cycle is the sum of compressive and tensile deformations divided by the specimen length.

For comparison, the dynamic behavior of unreinforced sand was measured in 26 undrained cyclic triaxial tests at a confining pressure of 50 kPa under cyclic stress ratios ranging from 0.26 to 0.53. The results of these tests are summarized in Table 3.

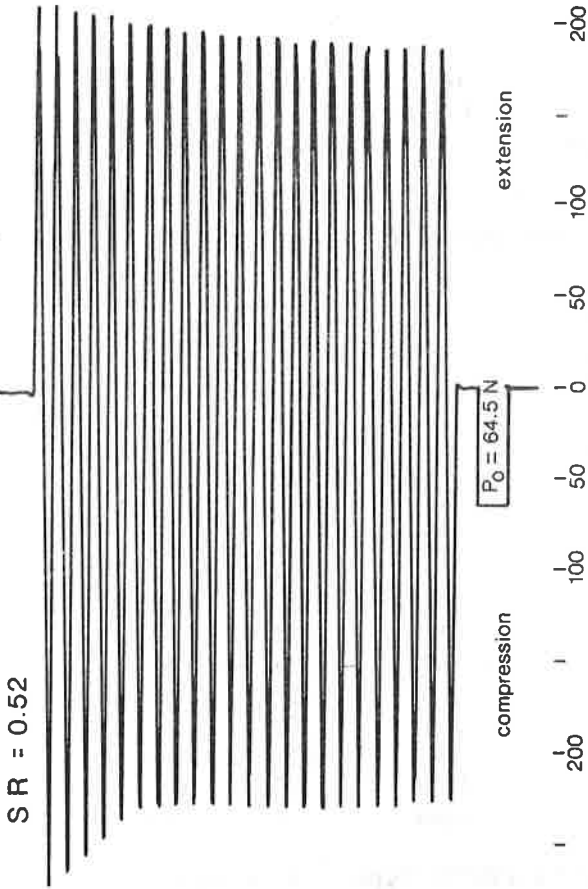
EFFECTS OF FIBER REINFORCEMENT ON DYNAMIC STRENGTH

A comparison of the dynamic strength of unreinforced saturated sand and saturated sand reinforced with fibers from AMOCO Propex Siltstop is shown in Figure 3 where cyclic stress ratio is plotted against the number of cycles required to initiate liquefaction. It can be seen that the inclusion of 0.38% by weight of polypropylene fibers increased the soil's resistance to liquefaction at all levels of stress ratios. To evaluate the effect of inclusions on the strain characteristics, the double amplitude strain at initial liquefaction was plotted (Figure 4) against the cyclic stress ratio at which each specimen was tested. Figure 4 indicates that the presence of synthetic inclusions decreased the strain at initial liquefaction. Furthermore, it was found that beyond initial liquefaction, fiber-reinforced specimens withstood several additional cycles at high stress ratios compared to unreinforced specimens.

The results of the series of tests with saturated sand reinforced with FORTA-FIBRE Type A-5 fibers are plotted on Figures 5 and 6. It can be seen from Figure 5 that 0.38% by weight of these fibers included within the sand greatly increased its resistance to liquefaction. Figure 6 indicates that the strain at which liquefaction occurred was also reduced.

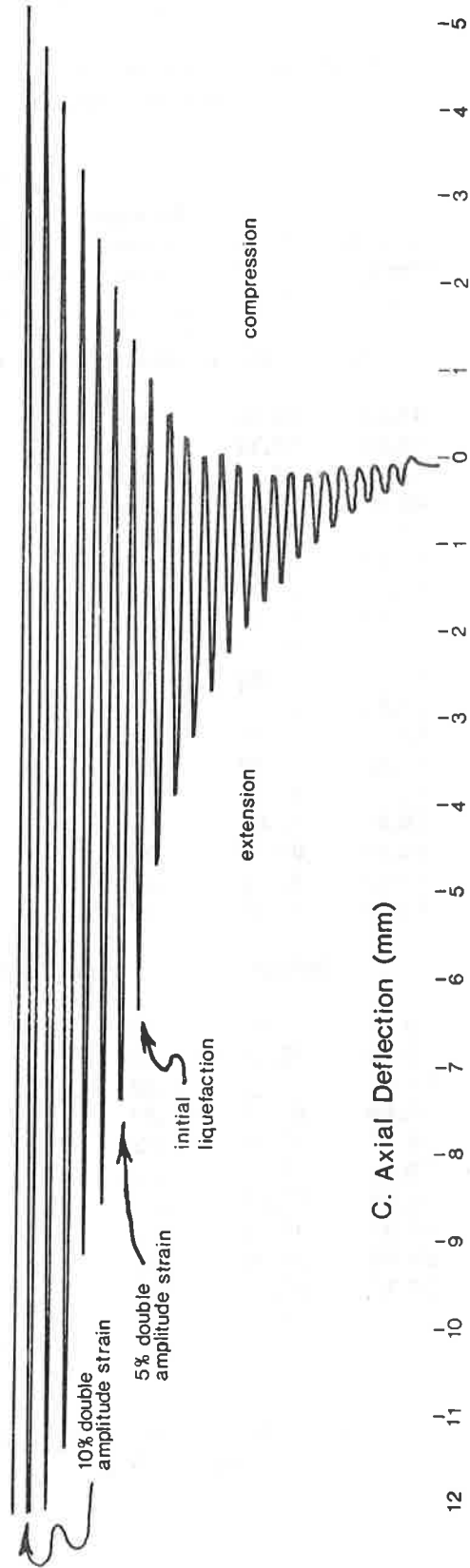
The dynamic response of the composite material (fiber-reinforced sand) is different from the unreinforced sand because of the restraining effects of the fibers in: (a) reducing strain, and (b) in recovering some of the strain after each cycle of stress application. In loose to medium dense sand, much of the induced strains in each load and unload cycle are permanent. In fiber-reinforced sand, the tensile resistance of the fibers increase the elasticity of the composite material (more rebound when load is removed) thereby lowering the rate of pore-pressure build up in the sand.

During specimen preparation, specimens with fibers required more compactive effort to compact the sand to a relative density of 50% than the unreinforced specimens. This same mechanism by which the composite material resists compaction also acts to impede particle movement in response to externally applied stresses. If those particles in contact with reinforcement are impeded from moving, the particles in contact with these will also be somewhat restrained. The influence of reinforcement will extend, in this fashion, to a region of sand particles surrounding the reinforcement. Consequentially, a small amount of fiber inclusions (0.38% by weight in these experiments) can be effective in markedly increasing the soil's resistance to liquefaction.



B. Cyclic Load (Newtons)

A. Effective Confining Pressure (kPa)



C. Axial Deflection (mm)

Figure 2. Typical Strip Chart Test Record of a Reinforced Specimen.

Table 2. Summary of Test Data From Cyclic Triaxial Tests
on Reinforced Specimens of Monterey No. 0 Sand.

Relative Density (%)	Dry Density (pcf)	Average Stress Ratio	Dbl Amp Strain at Initial Liquefaction (%)	Number of Cycles to:		
				Initial Lique- faction	5% Dbl Amp Strain	10% Dbl Amp Strain
Specimens reinforced with fibers from AMOCO Propex Siltstop						
49.09	96.99	.52	3.89	16	17	22
49.87	97.12	.53	3.78	18	19	25
49.09	96.99	.48	3.20	19	21	25
40.54	97.09	.44	3.62	22	23	27
50.72	97.26	.46	2.56	34	39	49
49.39	97.04	.41	3.62	47	49	54
50.12	97.16	.38	1.28	54	60	64
50.84	97.28	.40	1.23	153	160	166
49.87	97.12	.34	1.39	176	183	190
49.51	97.06	.36	2.24	220	224	229
50.42	97.21	.38	1.65	226	232	238
49.69	97.09	.36	1.86	231	236	241
49.03	96.98	.35	1.12	330	337	343
50.72	97.26	.33	1.17	442	450	458
49.57	97.07	.31	1.70	700	706	712
51.32	97.36	.32	1.07	833	841	848
49.69	97.09	.30	1.17	1116	1124	1132
49.15	97.00	.38	NA	>3000	NA	NA
Specimens reinforced with FORTA-FIBRE Type A-5 fibres						
49.57	97.07	.54	5.17	15	15	22
50.66	97.24	.52	3.73	19	21	28
50.42	97.21	.49	1.49	22	25	31
50.66	97.25	.40	1.44	46	51	58
50.60	97.24	.42	1.39	52	62	70
50.42	97.21	.36	3.14	128	131	144
50.66	97.25	.37	2.45	133	139	148
50.30	97.19	.32	0.96	197	209	220
50.96	97.30	.34	1.49	359	369	379
50.12	97.16	.35	1.28	512	520	531
50.90	97.29	.30	0.80	1833	1848	1857

Note: All tests were conducted under an effective confining
pressure of 50 kPa.

Table 3. Summary of Test Data from Cyclic Triaxial Tests
on Unreinforced Specimens of Monterey No. 0 sand.

Relative Density (%)	Dry Density (pcf)	Average Stress Ratio	Dbl Amp Strain at Initial Liquefaction (%)	Number of Cycles to:		
				Initial Lique- faction	5% Dbl Amp Strain	10% Dbl Amp Strain
50.66	97.25	.45	7.57	7	6	8
51.75	97.43	.49	8.36	7	6	8
50.66	97.25	.45	7.03	8	7	9
49.09	96.99	.49	5.91	8	6	9
49.51	96.07	.52	6.87	8	7	9
49.33	97.03	.49	NA	8	6	9
49.82	97.11	.53	5.33	9	9	11
51.20	97.34	.43	6.77	9	8	11
49.87	97.12	.47	7.62	11	10	12
50.54	97.23	.50	5.33	11	11	13
49.09	96.99	.39	8.35	13	11	14
50.12	97.16	.40	5.01	13	13	15
49.30	96.98	.36	7.25	17	16	18
50.60	97.24	.38	6.18	30	29	32
48.42	96.88	.36	NA	31	31	33
50.60	97.24	.38	3.73	39	37	39
50.12	97.16	.33	5.27	85	84	86
49.51	97.06	.33	5.33	94	94	96
50.18	97.17	.32	2.93	145	146	148
49.15	97.00	.34	5.97	167	168	170
49.27	97.02	.29	1.60	376	NA	NA
49.81	97.11	.31	6.23	406	405	408
50.54	97.23	.32	4.10	551	551	553
50.90	97.29	.26	1.92	946	949	952
50.90	97.29	.27	NA	>2500	NA	NA
51.44	97.38	.29	2.88	3276	3277	3279

Note: All tests were conducted under an effective confining
pressure of 50 kPa.

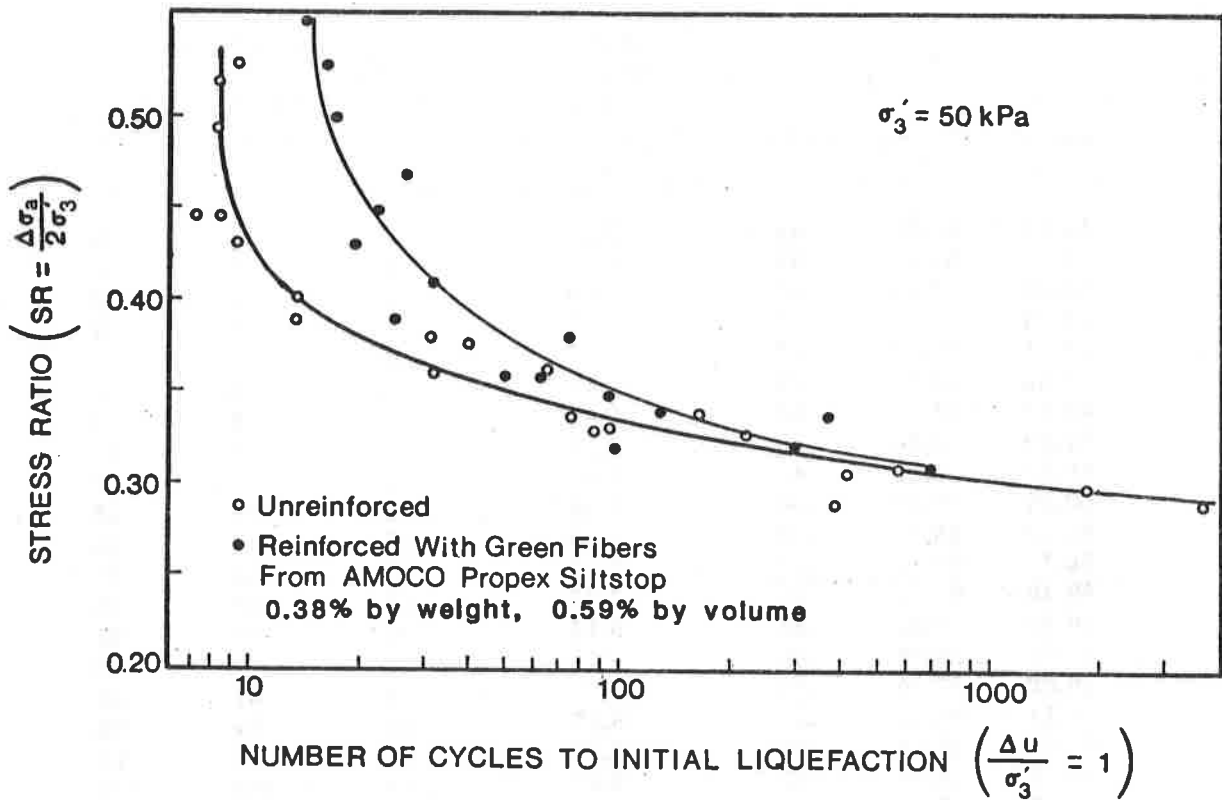


Figure 3. Dynamic Response of Unreinforced Specimens Compared to Specimens Reinforced with AMOCO Propex Siltstop Fibers.

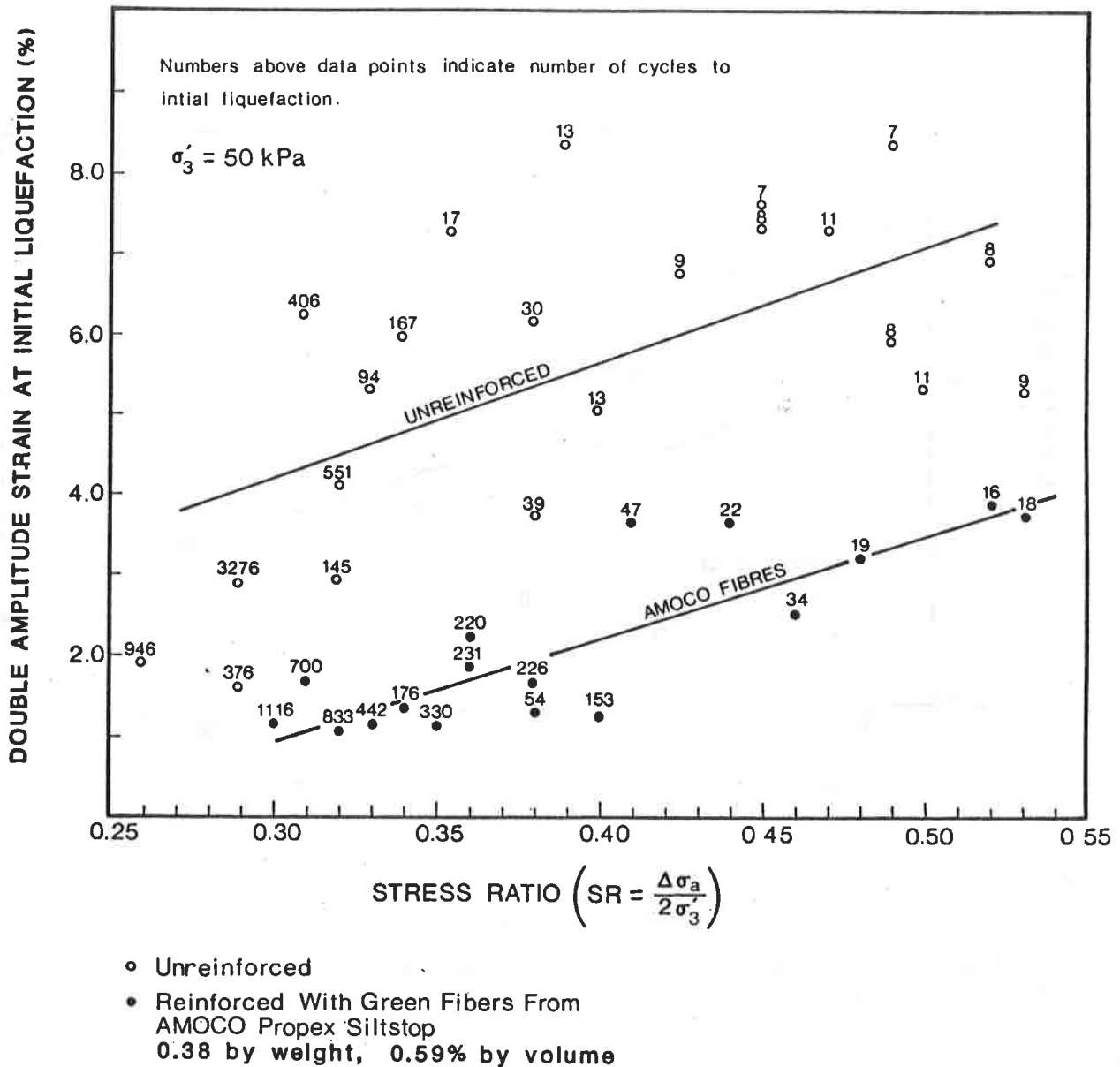


Figure 4. Double Amplitude Strain at Initial Liquefaction of Specimens Reinforced with AMOCO Propex Siltstop Fibers Compared to Unreinforced Specimens.

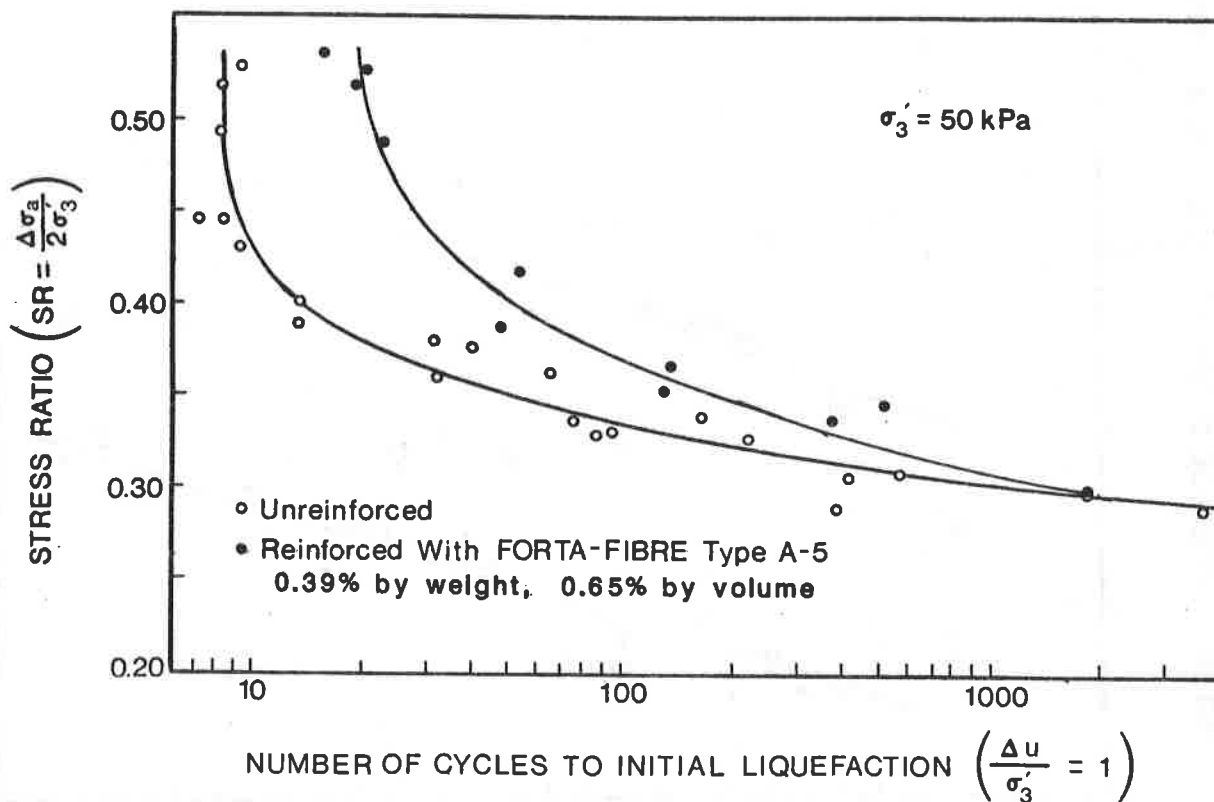
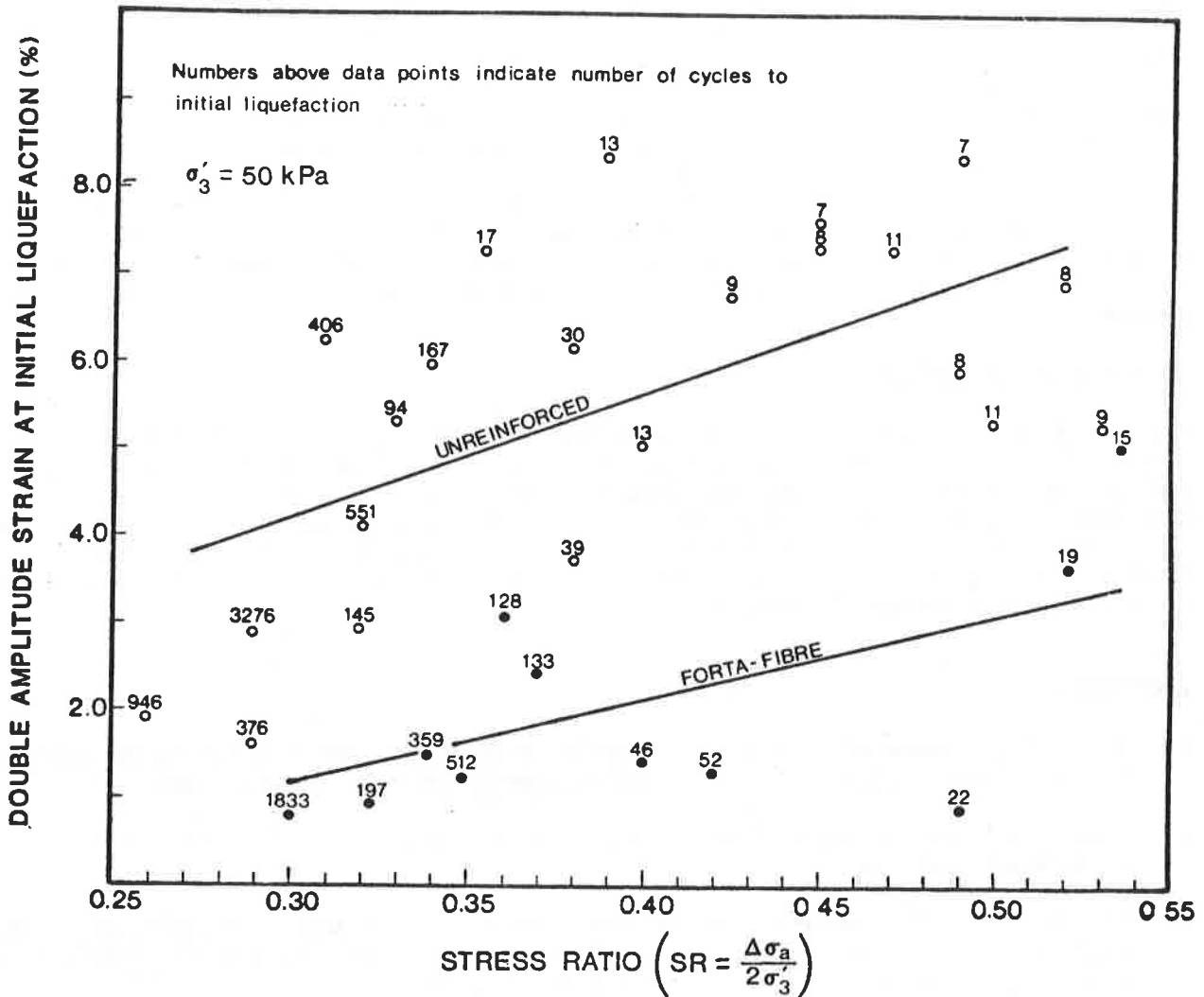


Figure 5. Dynamic Response of Unreinforced Specimens Compared to Specimens Reinforced with FORTA-FIBRE Type A-5 Fibers.



- Unreinforced
- Reinforced With FORTA-FIBRE Type A-5
0.39% by weight, 0.65% by volume

Figure 6. Double Amplitude Strain at Initial Liquefaction of Specimens Reinforced with FORTA-FIBRE Type A-5 Fibers Compared to Unreinforced Specimens.

SUMMARY AND CONCLUSIONS

The objective of this study was to investigate the effect of randomly distributed synthetic fibers on the dynamic resistance of saturated sand. Undrained cyclic triaxial tests were performed on saturated sand reinforced with two types of polypropylene fibers. On the basis of the analysis of the data from these tests, it can be concluded that randomly distributed synthetic fibers are effective in improving dynamic strength behavior of saturated sand, and increasing sand's resistance to liquefaction. For a given cyclic stress ratio and a given number of cyclic load applications, the axial strain and the increase in pore pressure in reinforced sand are lower than in unreinforced sand. These comparisons were made for equivalent sand densities in both the unreinforced and reinforced conditions. It was found that the addition of fiber reinforcement to sand increased the amount of compactive energy required to compact the sand to a given density.

ACKNOWLEDGEMENTS

This work is a result of research sponsored in part by NOAA, National Sea Grant College Program, Department of Commerce, under grant number NA80AA-D-00120, project number R/cz-72, through the California Sea Grant College Program. The U.S. Government is authorized to reproduce and distribute for governmental purposes. The tests were carried out by the authors at the Soil Mechanics Laboratory, Department of Civil Engineering, San Diego State University. Thanks are expressed to Mr. B. Rehkoph for his help with electronic instrumentation.

REFERENCES

1. Hoare, D.J. "Laboratory Study of Granular Soils Reinforced with Randomly Oriented Discrete Fibers." C.R. Coll. Inter. Renforcement des Sols. Paris, France, 1979.
2. Gray, D.H., and Al-Refeai, Talal, "Behavior of Fabric vs. Fiber Reinforced Sand." Unpublished manuscript.
3. Leflaive, E. "Sol renforce par des fils continus: le Texsol." Proceedings of the Eleventh International Conference on Soil Mechanics and Foundation Engineering, Paper No. 5/C/5, pp. 1787 -1790. San Fransisco, 1985.
4. University of California, Berkeley, 1983, Berkeley Lab Manual, Geotechnical Engineering Division.
5. Uzdavines, Michael, Effect of Soil Reinforcement on the Liquefaction Potential of Saturated Sand, Master's Thesis, San Diego State University, Spring, 1987.

SESSION 4B
TESTING-CHEMICAL

the 1990s, the number of people in the world who are undernourished has increased from 600 million to 800 million (FAO 1996). The number of people who are malnourished has increased from 1.2 billion to 1.5 billion (FAO 1996).

There is a growing awareness of the need to improve the nutritional status of the world's population. The United Nations World Food Programme (WFP) has been established to coordinate international efforts to combat hunger and malnutrition. The WFP has been successful in providing food aid to over 100 million people in over 100 countries.

One of the main reasons for the increase in malnutrition is the rapid population growth in the developing world. The world population is expected to reach 6 billion by the year 2000, and 8 billion by the year 2025. This rapid population growth is putting increasing pressure on the world's food resources.

Another major factor is the increasing incidence of chronic diseases, such as heart disease, cancer, and diabetes. These diseases are often associated with poor nutrition, and they are becoming more common in the developing world as people adopt Western diets and lifestyles.

There are a number of factors that contribute to malnutrition, including poverty, lack of access to food, and poor health care. In many developing countries, people do not have enough money to buy the food they need, and they often live in areas where food is scarce.

Malnutrition is a serious problem that affects millions of people around the world. It is a major cause of death and disability, and it can have long-term effects on a person's health and development. It is important to take steps to improve the nutritional status of the world's population.

There are a number of ways to improve the nutritional status of the world's population. One way is to increase the production of food. This can be done by improving agricultural practices, such as using fertilizers and pesticides, and by increasing the number of people working in agriculture.

Another way to improve the nutritional status of the world's population is to increase the distribution of food. This can be done by providing food aid to people who are in need, and by improving the infrastructure for food distribution.

There are also a number of ways to improve the nutritional status of the world's population that do not involve increasing the production or distribution of food. These include improving the health care system, and providing education and training to people about nutrition.

Improving the nutritional status of the world's population is a complex task that requires the cooperation of many different groups and organizations. It is important to continue to work on this issue, and to find new ways to improve the nutritional status of the world's population.

R.E. LANDRETH

U.S. Environmental Protection Agency, U.S.A.

Flex - An Expert System to Assess Flexible Membrane Liner Materials

INTRODUCTION

When a landfill or lagoon site is proposed, the U.S. Environmental Protection Agency (EPA) requires the party seeking the permit to submit evidence that the proposed site will not cause damage to the surrounding environment. To protect the soil and groundwater beneath and adjacent to the site, flexible membrane liners (FML) have been determined to meet the Agency's liquids management strategy. Since there are wide variations in the quality of leachates from waste management sites and a wide variety of candidate liners, part of the proposal package must include data that will allow the EPA or state permit reviewer to judge the suitability of the proposed FML material. Will the FML be chemically resistant to the anticipated wastes and leachates at that particular site?

To demonstrate the chemical resistance of the FML, EPA requires that its Method 9090 be used, as a minimum, to test chemical resistance. In the test, the physical properties of FML specimens that have been immersed in waste/leachate (at 25°C and 50°C) are measured after each of four successive months and compared with the original unexposed FML physical properties. These results are included in the application for a permit to install and operate the site, and the EPA or state permit reviewer employs them to assess whether the proposed FML material will be chemically resistant.

The decision of FML suitability is complex, requiring knowledge of chemistry, polymer science, waste site construction, etc. Because a less complex decision-making process was needed for chemical compatibility determinations, EPA developed a computerized expert system--one that would embody the best thinking of recognized experts in this field. Three materials were selected for inclusion in the system: polyvinyl chloride (PVC), chlorosulphonated polyethylene (CSPE), and high density polyethylene (HDPE).

To that end, FML experts at liner fabrication firms, liner material suppliers, and an independent consultant were interviewed. What measures would these experts use and what was their rationale to evaluate the chemical resistance of the proposed liner material? Their rationale became the criteria or rule base for chemical resistance measurements that were expressed in the form of IF---THEN statements of a computer program on an IBM-PC-AT employing sophisticated system shell based on the science of artificial intelligence.

The result is the Flexible Liners Expert system: The FLEX system for evaluating chemical resistance data of FML's. Unlike conventional computer software which produces numeric results, the results of an analysis by the FLEX system are presented in a written textual report generated as the system runs. This report lists problems with the data (too scattered or missing) as well as any values that indicate that the liner may be substandard or incompatible with the immersion medium. Also included in this report are explanations as to why any data are deficient. The report may therefore be useful to a Method 9090 test reviewer to confirm a decision IF the review concurs with the rationale proposed by the FLEX system.

It should be noted that the program is designed to PROVIDE ASSISTANCE to those responsible for evaluation of Method 9090 test results. Under no circumstances should the recommendations of FLEX be considered absolute; especially when the FLEX system finds no problems with the test results. FLEX is not a substitute for a review of the test results by a skilled professional. Rather, FLEX is a screening tool to be used by those familiar with flexible membrane liner testing and EPA Method 9090. The system can rapidly pinpoint inconsistencies in the test data and test results that suggest the liner is substandard or incompatible. In this capacity, FLEX can save time, reduce oversights, and enhance the consistency of Method 9090 test reviews.

THE COMPARISON TESTING

To test the validity of the FLEX advisory system, five recognized FML experts evaluated sample data sets for three types of FML's--data sets similar to those produced by EPA Method 9090 (Table 1).

The 14 different sample sets of the three types of liner materials included data measurements of properties used to judge the chemical resistance of FML liners: unexposed specimens and exposed specimens measured at 25°C and 50°C for each of 4 months. Common to all 14 samples were percent-change measurements for weight, 100% modulus, and elongation at break. Each sample set did not include data for all the properties (Table 2). This lack of submitted data was typical before Agency policy established which data were required.

At least two experts analyzed each type of FML (Table 3).

The experts were asked to review each assigned data set and conclude that

- ° the results indicate that the liner material is not resistant to the chemical/waste (not resistant), or
- ° there are no results that indicate the liner material is not resistant to the chemical/waste* (no indication not resistant), or
- ° data are insufficient to reach a conclusion (data missing), or
- ° data are inconsistent (scattered).

*This statement does not say that the liner material is resistant.

Table 1. Immersion-test data sets for three flexible membrane liners*

Sample FML	Abbreviation	No. of data sets	Temperature ⁺ of samples reviewed
High-density polyethylene	HDPE	6	25°C & 50°C
Polyvinyl chloride	PVC	4	25°C & 50°C
Chlorosulphonated polyethylene	CSPE	4	25°C & 50°C

*The data were not those of an actual Method 9090 test.

⁺The data for both 25°C and 50°C were submitted for each of the three FML's.

Table 2. Properties used to judge chemical resistance of three FML's; all properties not tested for each FML.

Property	Unit of measurement, % change	HDPE	PVC	CSPE
Weight	gram	x [*]	x ⁺	x [#]
Tensile strength at yield	psi	x [*]	-	-
Elongation at yield	%	x [*]	-	-
100% modulus	psi	x [*]	x ⁺	x [#]
Breaking strength	psi	x [*]	-	x [#]
Elongation at break	%	x [*]	x ⁺	x [#]
Length	inch	x	x	-
Width	inch	x	-	-
Puncture strength	pound	x	x	-
Tensile strength at break	psi	-	x ⁺	-
Tear strength	psi	-	x ⁺	x [#]
Hardness	B-2	-	x	-
Thickness	inch	-	x	-

* All HDPE FML samples were tested for this property.

+ All PVC FML samples were tested for this property.

All CSPE FML samples were tested for this property.

x Tests conducted.

- Tests not conducted.

Table 3. Expert and FML analyzed

Expert	HDPE	PVC	CSPE
FLEX	x	x	x
A	x	x	x
B	x	-	-
C	-	x	-
D	-	-	x
E	-	-	x

^xSample analyzed.

⁻Sample not analyzed.

For each conclusion, the expert was asked to give the reason for the conclusion, state which test results were the most or least important in reaching the conclusion, draw trend lines or graphical exhibits of data provided with the data, and state how the data at 25°C and 50°C were used. In addition, if the conclusion was that there were insufficient data, the expert was to describe what additional data would be needed to reach a conclusion, and if there were inconsistencies in the data, the expert was to identify and describe how the inconsistencies could be worked around to reach a conclusion.

RESULTS

To judge the validity and limitations of the FLEX system and to identify where it can be improved, the conclusions and reasonings of the experts were compared with those of the system. In Tables 4, 5, and 6, the areas of agreement and disagreement between the FLEX system and the FML experts are noted for the three types of FML's.

There was good agreement between FLEX and Expert A for all three liner materials; there was less agreement between FLEX and the other experts. Generally FLEX and Expert A were more apt to find the FML "not resistant" than were the other experts, although the reasoning behind FLEX and Expert A's conclusions sometimes differed. Experts B through E applied less stringent criteria to the data, were more willing to judge inconclusive data in favor of "no indication not resistant," and, in some cases, judged test results considered important by FLEX and Expert A as outliers. The experts generally agreed about which properties were the most significant in judging chemical resistance: weight change and 100% modulus (Table 7).

CONCLUSIONS

The comparison of the FLEX conclusions with those of the experts demonstrates the feasibility and practicality of FLEX. FLEX is able to advise concerning the FML chemical resistance of data submitted as part of a permit application.

The system can be characterized as conservative--more stringent in its criteria than were some of the experts. Where FLEX and the experts disagreed, the system more often found the FML not resistant whereas the experts judged the data as being missing or with no indication not resistant. The system is presently useful to guide the permit reviewer and to identify those parts of the permit application where a more in-depth investigation is needed.

WHAT NEXT?

Information gaps do exist; the dependence of the results on time, data trend analysis, and the relative importance of data stabilization need investigation. The need to test FML at two temperatures should also be investigated.

To further refine FLEX, the system should be reevaluated with the use of more data sets and with insights gained from the experts' analyses. The precision and accuracy of Method 9090 data should be examined. Should there be different criteria for different liner materials? for judging when physical properties have stabilized? Has the composition of the waste/leachate in the test cell remained constant during the exposure period? What are the consequences of the

Table 4. Agreement/disagreement among FLEX and FML experts concerning HDPE (at 25°C)

Liner	Not resistant	Data missing	Scattered/ conflicting data	No indication not resistant
80 mil				
HH.8	FLEX-A-B*	-	-	-
HI.8	FLEX-A	-	-	B
HJ.8	-	FLEX-A	FLEX	B
HK.8	FLEX-A	B	-	-
60 mil				
HL.6	FLEX-A	-	-	B
HM.6	-	FLEX-A	FLEX	FLEX-B

*FLEX is the computer system; A and B are two experts.

Table 5. Agreement/disagreement among FLEX and FML experts concerning PVC (at 25°C)

Liner	Not resistant	Data missing	Scattered/ conflicting data	No indication not resistant
PP.3	FLEX-A*	-	-	C
PQ.3	A	A	-	FLEX-A-C
PR.3	FLEX-A	A	A	C
PS.3	FLEX-A	-	-	C

*FLEX is the computer system; A and C are two experts.

Table 6. Agreement/disagreement among FLEX and FML experts concerning CSPE (at 25°C and 50°C)

Liner	C°	Not resistant	Data missing	Scattered/ conflicting data	No indication not resistant
CC.3	25°	-	-	-	FLEX-A-D-E
CC.3	50°	FLEX-A-E	-	-	D
CD.3	25°	FLEX-A	-	-	D-E
CD.3	50°	FLEX-A	-	-	D-E
CE.3	25°	FLEX-A-D	-	-	E
CE.3	50°	FLEX-A-D	-	-	E
CF.3	25°	FLEX-A-D	-	-	E
CF.3	50°	FLEX-A-D-E	-	-	-

*FLEX is the computer system; A, D, and E are three experts.

Table 7. Relative importance* of properties (test results)
to the experts judging the chemical resistance of
FML materials

Property	HDPE		PVC		CSPE	
	A	B	A	C	A	E
Weight	1	1	1	2	1	1
100% modulus	2	2	2	5	3	2
Tensile strength at break	least	4	-	3	least	-
Elongation at break	least	-	-	1	least	-
Tensile strength at yield	3	3	-	-	-	-
Elongation at yield	4	least	3	-	-	-
Puncture	5	-	-	6	-	-
Tear	-	-	3	4	-	-
Length	-	-	-	7	-	-

*1 is most important; 7 is least important.

loss of volatile solvents? Shouldn't the format of Method 9090 be the same as that of the FLEX system, with similar units used to express similar results? These questions should be resolved.

Part of the answer to these questions can be addressed in a good laboratory quality control-quality assurance program. The development of a QA/QC program will at least identify shortcomings at the laboratory level. When data are submitted from an individual laboratory, at least the Agency will have some understanding of the data quality.

AVAILABILITY

The Agency is currently reviewing the FLEX Program to determine if it is consistent with policy. The Office of Research and Development is also working with selected Regional Offices for final Beta testing and to determine the utility of the system. It is intended to make the program generally available to the EPA Regional Offices and authorized states.

R.M. CHARRON
GeoSyntec, Inc., U.S.A.

Polymers for Synthetic Lining Systems: Some Molecular Structure-Property-Application Relationships

SYNOPSIS

Currently, a variety of polymers is used in the geosynthetics industry. Among them are polyethylene, polypropylene, polyethylene terephthalate, and polyvinyl chloride. These basic materials are tailored by plastics engineering professionals into a vast number of highly specialized products to service the geotechnical engineer.

Physical, mechanical, and chemical properties all are a result of a myriad of molecular interactions that are related to the basic repeat structure of the polymer. Initially, basic intermolecular forces are considered in this paper. Subsequently, orientation, crystallinity, polymer processing, and their relationships to applications in geosynthetics are discussed.

Suggestions are made concerning the natural progression of current testing methodologies to better simulate field conditions and alleviate some of the current reservations associated with the use of certain geosynthetics. In order to establish these methodologies, some basic polymer characteristics and how these characteristics are affected by installation and field environments are considered.

INTRODUCTION

During the past 20 years, a variety of polymers has been selected for use as geomembranes (flexible membrane liners) to isolate contaminated liquids from natural aquifers. In addition to geomembranes, other geosynthetics such as geonets, geotextiles, and geogrids are being used together to establish complete synthetic lining systems.

When selecting a geosynthetic, consideration should be given to the base polymer's molecular structural characteristics to ensure the polymer's suitability for a particular application. This molecular structure-property-application approach surveys the following major polymer families used in the geosynthetics industry:

- . Polyolefins
 - .. Low density polyethylene (LDPE)
 - .. Linear medium density polyethylene (LMDPE)
 - .. High density polyethylene (HDPE)
 - .. Polypropylene (PP)
- . Polyvinyl chloride (PVC)
- . Polyethylene terephthalate (PET) polyester

Emphasis is on the olefin family due to its prevalence in the geosynthetics industry in the United States.

From a practical standpoint, polymers are very long chains of molecules called macromolecules, which are comprised of a series of basic repeat units. As the number of these basic units increases, individual molecules become large and entangled with other molecules. At this stage, the material has a characteristic free volume and an inability to be readily separated. This restricted motion is manifested in the mechanical, physical, and chemical properties associated with each polymer family.

The selection of new or existing polymers for use as geosynthetic materials is best accomplished when testing is conducted that reflects the synergistic effects of site-specific environmental conditions.

INTERMOLECULAR FORCES

Intermolecular forces play a significant role in defining the ability of polymer molecules to respond to externally applied mechanical stresses or to withstand aggressive chemical environments. Geosynthetics often are exposed to both simultaneously. These intermolecular forces include London dispersion forces, dipole attractions, hydrogen bonding, and crosslinking.

London dispersion forces hold adjacent molecules together by means of temporary polarity. These secondary attractive forces account for some strength and moderately high melting points in crystalline materials such as PE or isotactic PP.

Dipole attractions, whether induced (temporary electron displacement) or permanent (between atoms of different electronegativity), are relatively weak forces, usually accompanied by the much stronger forces of hydrogen bonding and the summation of those forces identified as crystallinity, which together render insignificant the contribution of the dipole attractions to material strength.

Hydrogen bonding is an attraction between atoms that vary in electronegativity and are located on adjacent molecules. This is a common and significant

force, the effects of which often are credited to a crystalline structure. Secondary hydrogen bonds between molecules significantly increase molecular size and enhance the capacity of a material to resist applied stresses. The basic strength properties of polymers are therefore a function of molecular weight and size.

A crosslink (Figure 1) is a primary covalent bond between molecules that results in the formation of a three-dimensional structure. Crosslinks draw polymer chains closer together, decreasing sectional chain motion and free volume and enhancing properties such as hardness, tensile strength, modulus of elasticity, and resistance to permeation. Low temperature flexibility and elongation characteristics are therefore decreased by crosslinks.

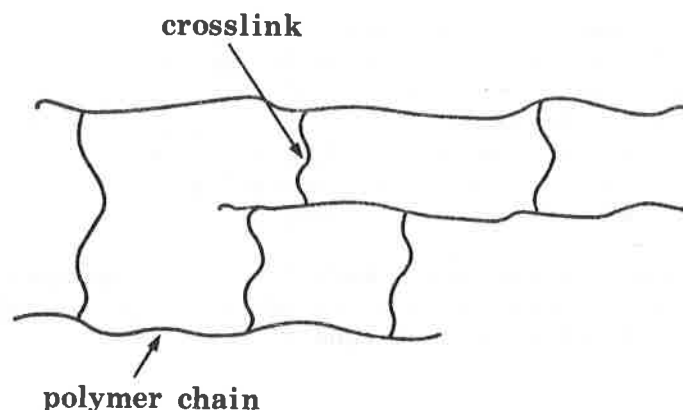


FIGURE 1. Crosslinked structure.

INTERMOLECULAR ORDER

Polymers can exist in any combination of three states: amorphous, crystalline, and oriented. The dash lines of Figure 2 define possible combinations of these three states. In the amorphous state, individual polymer molecules are randomly coiled and entangled, while in the crystalline state, they are highly ordered. Some polymers (e.g., PE, PP, PET) are semi-crystalline and form a three-dimensional molecular structure of identical, periodically repeated unit cells (see Figure 3). This ordered structure facilitates close packing of individual molecules, thereby maximizing the effects of all intermolecular forces. Crystallinity is the summation of a large number of small forces whose total effects are intermediate between those of hydrogen bonding and crosslinking. Molecular orientation occurs in polymers that have been mechanically stretched at a temperature above their glass transition temperature (T_g) and then cooled quickly below the T_g , effectively locking the aligned molecules in place. Uniaxial orientation is present in all fibers

used in geotextiles, biaxial orientation is present in PE geomembrane and pipe, and either or both forms of orientation can be present in geogrids. Orientation is responsible for the enhanced load-carrying capacity of fibers and geogrids, however, other geosynthetic features such as geomembrane seams can be adversely affected by orientation as described later.

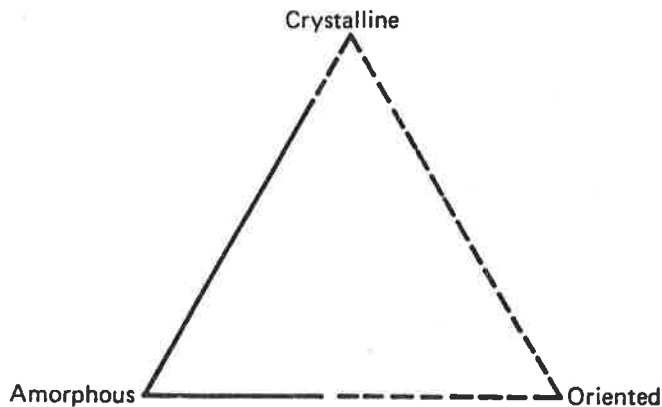


FIGURE 2. States of molecular order.

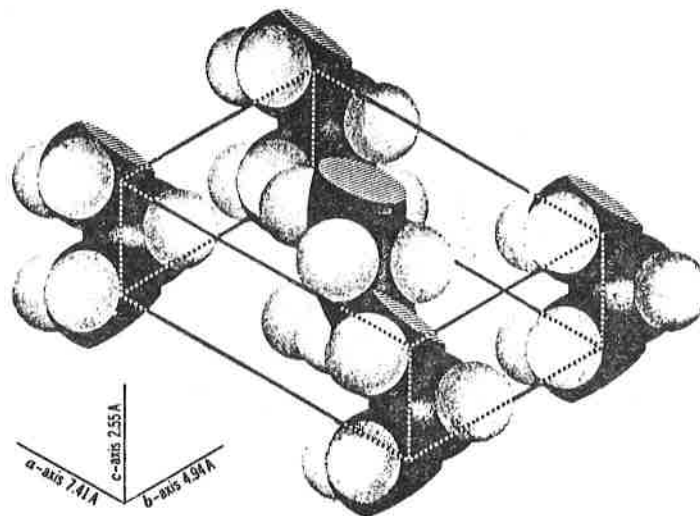


FIGURE 3. Unit cell of polyethylene.

AGING AND DEGRADATION

Degradation is a term commonly used to describe seemingly detrimental changes in material properties that result from a change in chemical structure. Photo-oxidation, thermal oxidation, and chemical attack are the three most prevalent forms of molecular degradation in polymers. Photo-oxidation is a

process in which ultraviolet radiation excites certain molecules, causing chain scission along the polymer structure and, after prolonged exposure, material embrittlement and eventual failure. The most effective stabilizer used to hinder photo-oxidation is carbon black. Thermal oxidation is a result of excessive time/temperature exposure. There is a wide variety of stabilizers used to combat this process with varying degrees of success. Chemical attack can occur at any reactive sites along the polymer chain, resulting in material changes such as swelling, softening, crosslinking, and chain scission, all of which have varying degrees of severity in terms of material property loss.

Long-term aging and durability characteristics of geosynthetics are of extreme importance, especially for outdoor applications where resistance to ultraviolet radiation is essential. Such effects are manifested in changes of molecular weight that can be counter opposing. Both chain scission (a reduction in molecular weight) and crosslinking (an increase in molecular weight) can occur simultaneously during degradation. The former will tend to diminish properties while the latter, in small amounts, will enhance properties. Excessive amounts of either crosslinking or chain scission will embrittle ductile materials. A recent study on the durability of two non-woven PP geotextiles isolated the onset of degradative processes at a stage where mechanical property changes associated with degradation could not be identified (1). Extensive degradation has also been observed in PP fibers using scanning electron microscopy, thermal gravimetric analysis, and infrared spectroscopy, where significant mechanical property loss was also present (2).

MOLECULAR STRUCTURE

Polymer end-product properties are influenced by a vast number of polymerization and processing variables. Polymer molecular structure is described by some important post-polymerization material characteristics including:

- . Average molecular weight (MW, size of chains)
- . Molecular weight distribution (MWD, distribution of chain sizes)
- . Type and extent of chain branching (polyolefins)
- . Percent crystallinity

Polyethylene

LDPE (Figure 4) contains a significant number of side chains that hinder crystallization and create free volume, making the material very flexible and generally producing inferior physical and mechanical properties when compared with higher density materials.

$$-(\text{CH}_2\text{CH}_2)-$$

A log-log plot showing the relationship between zero-shear viscosity (η_0) and molecular weight (M.W.). The y-axis is labeled $\text{LOG } \eta_0$ and the x-axis is labeled LOG M.W. . The curve consists of two segments: a lower-slope segment at lower molecular weights and a steeper segment at higher molecular weights. A vertical dashed line marks the transition point at M_c on the x-axis. The equation $\eta_0 = K(M.W.)^{3.4}$ is shown next to the steeper segment of the curve.

413

Table 1 shows some typical property trends in PE as a function of density, melt index, molecular weight, and molecular weight distribution.

TABLE 1
PROPERTY TRENDS FOR POLYETHYLENE

Typical Properties	As Density Increases	As MI Decreases or avg MW Increases	As MW Distribution Narrows
Thermal:			
Softening Point	Large Increase	Slight Increase	Slight Increase
Viscosity at Melt Temperature	Increase	Increase	Slight Increase
Mechanical:			
Stiffness	Increase	Increase	Slight Increase
Tensile Strength	Increase	Increase	Slight Increase
Torsional Strength	Increase	Increase	Slight Increase
Impact Strength	Decrease	Slight Increase	Difficult to Define
Low-Temperature Flexibility	Decrease	Increase	Increase
Chemical:			
Environmental Stress Cracking Resistance	Decrease	Decrease	Increase
Permeability	Decrease	Slight Increase	Decrease
General Resistance to Chemicals at Room Temperature	Increase	Increase	No Effect

MI = melt index
MW = molecular weight

Chemical Properties

In the non-stressed state, PE generally has excellent chemical resistance to a wide variety of solvents except oxy acids (e.g., nitric, sulfuric). When exposed to a combination of mechanical and chemical stresses, environmental stress cracking may produce brittle fracture failure at lower stresses than in the absence of a chemical environment (3). Some chemicals that appear to cause a problem are alcohols, liquid hydrocarbons, organic esters, metallic soaps, sulphated and sulphonated alcohols, polyglycol ethers, and silicone fluids (4).

Polypropylene

PP (Figure 7) is commonly used in the manufacture of woven and non-woven geotextiles and geogrids and is generally superior to PE in all mechanical and physical properties. PP geotextiles and geogrids acquire enhanced strength characteristics as a result of molecular orientation during processing.

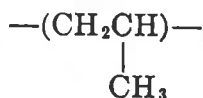


FIGURE 7. Basic repeat unit for PP.

Mechanical Properties

PP, like PE, is also a linear molecule. However, due to the methyl group (CH_3), it can exist in three forms of different tacticity (i.e., the CH_3 group is in different spacial arrangements): isotactic, syndiotactic, and atactic. Most commercial polymers are approximately 90 percent isotactic and crystallize in a helix form as shown in Figure 8. Most fibers used in geotextiles exist in this formation, while the atactic formation is amorphous and is used primarily for adhesives.

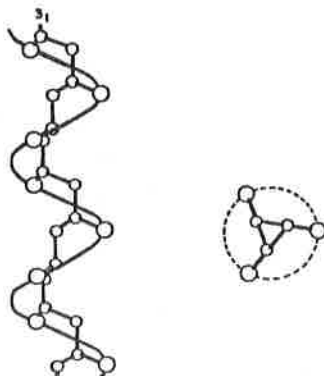


FIGURE 8. Helical structure of polypropylene.

Chemical Properties

The methyl (CH_3) side group on the repeat unit of PP creates reactive sites along the polymer backbone by the formation of a tertiary carbon. A tertiary carbon is one that is bonded to three other carbon atoms and one hydrogen. This carbon-hydrogen bond is weak in comparison to other carbon-hydrogen or carbon-carbon bonds along the polymer chain and is subject to chemical attack, making PP more susceptible to chemical degradation than PE.

Polyester

PET (Figure 9) is a base polymer used in fibers for woven and non-woven geotextiles and geogrids. Similarly to PP, it is often highly oriented for enhanced strength characteristics.

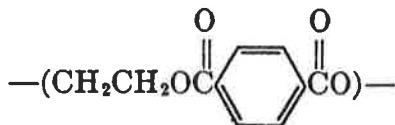


FIGURE 9. Basic repeat structure for PET.

Mechanical Properties

The cyclic ring structure and adjacent ester linkage supply rigidity to the polymer through resonance stabilization. (Chemical bonds move to spread equal bond strength over a larger area of the molecule.) This structure is planar and promotes crystalline formation, resulting in a highly ordered crystalline material with tensile strengths two to three times that of PE.

Chemical Properties

Polyesters in general possess reasonable chemical resistance but are subject to hydrolysis. Hydrolysis is a process in which water-based solvents, or water alone, cause the polymer chains to break, thereby producing a reduction in the basic mechanical properties of the polymer. Hydrolysis can occur at any temperature or pH but is most damaging to the polymer at elevated temperatures and in basic solutions (i.e., $\text{pH} > 7.0$).

Polyvinyl Chloride

PVC (Figure 10) requires a number of additives to facilitate being processed into useful products. These additives include: primary and secondary plasticizers, stabilizers, lubricants, and pigments. This extensive list of

additives makes PVC an extremely versatile material that can be very stiff and rigid with low plasticizer content (e.g., pipe) or extremely flexible with plasticizer content approaching 50 parts per hundred (e.g., geomembranes). This versatility allows for PVC to be tailored for mechanical properties to suit the application.

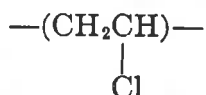


FIGURE 10. Basic repeat structure for PVC.

Mechanical Properties

If the repeat unit of PVC is compared with that of HDPE, the only difference is the presence of the highly electronegative chlorine atom, which draws polymer chains closer together, making the material harder and stiffer than PE. The mechanical properties of PVC in general can vary significantly and are most affected by plasticizer content. Rigid PVC with very low plasticizer or processing aid content exhibits excellent stiffness, hardness, and abrasion resistance. Plasticized or flexible PVC exhibits excellent flexibility and extensibility while maintaining moderate tensile strength.

Chemical Properties

PVC has good chemical resistance when compared with rubbers and only fair chemical resistance when compared with polyolefins. Many of the additives used in PVC formulations are relatively large polar molecules that are reactive in polar solvents, leading to generally inferior chemical resistance in these media.

Polyethylene Geomembrane Seams

PE geomembranes exist in a state of biaxial orientation as a result of the extrusion process. During seaming, an additional heating/cooling cycle may drastically alter the morphology of both geomembranes directly adjacent to the seam by forming new molecular orientation parallel to the seam. During cooling, molecular contractions draw moderate temperature material from areas adjacent to the weld and, in cases of severe overheating, cause both the geomembrane and the seam itself to warp (see Figure 11).

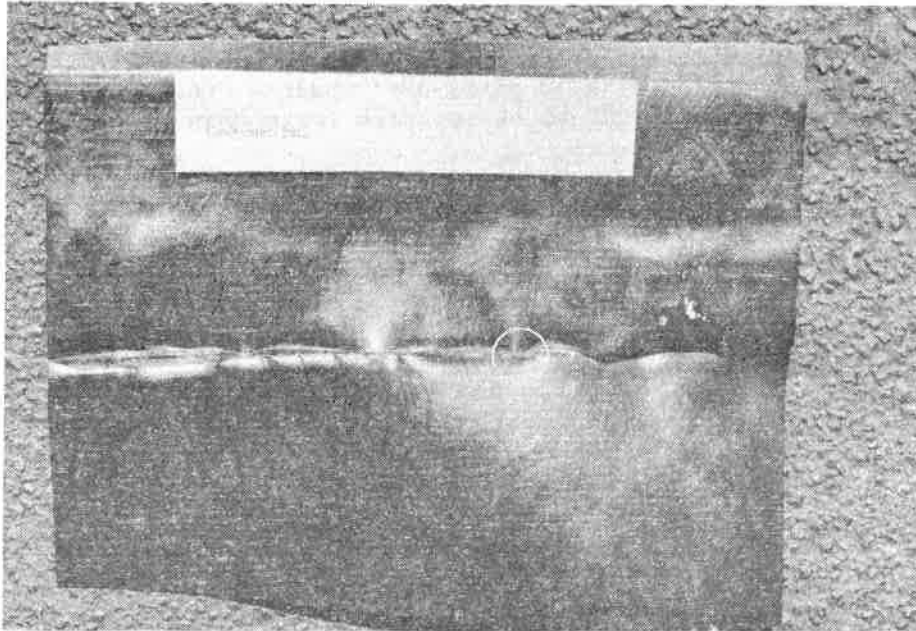


FIGURE 11. Underside of severely overheated extruded fillet seam.
Circled area indicates area of cracks and crazes.

When geomembrane seams are distorted to the extent of that in Figure 11, crazes or cracks, the precursors to brittle fracture failure, can occur (5). Microtome sections taken from the geomembrane seam in Figure 11 show cracks that extend up into the bottom geomembrane from directly beneath the weld zone (see Figure 12). Under tensile loading, these cracks can propagate up through the weld.



fillet weld
extrudate

severely warped
bottom geomembrane

FIGURE 12. Arrow indicates cracks and crazes extending up from
a crease in the bottom geomembrane. (x 65)

NEW MATERIALS AND TESTING METHODOLOGIES

Currently, most polymeric materials used as geosynthetics are "commodity resins," which are relatively low cost (less than \$1.00/lb), low strength materials when compared to engineering resins. Polyesters are the only "engineering resins" currently used.

One polymer family that offers excellent characteristics for use in geosynthetic applications is the fluoropolymer family, which includes: ethylene tetrafluoroethylene copolymer, fluorinated ethylene propylene copolymer, perfluoro alkoxy, polytetrafluoroethylene, polyvinylidene fluoride, and polyvinyl fluoride. These materials offer excellent thermal stability, chemical resistance, and mechanical properties. Although they are expensive materials, creative new product development will likely result in the utilization of these polymers in the geosynthetics industry.

Another material suitable for some applications in the geosynthetics industry is very low density polyethylene. It is characterized by excellent low temperature flexibility and environmental stress cracking resistance.

Material performance testing methodologies are only as good as their relationship to actual end-use conditions. To date, engineers who design with geosynthetics have taken great care to have adequate laboratory testing conducted to support new design ideas. The author of this paper believes that the one area that has been lacking is adequate testing of geomembranes and geomembrane seams to evaluate the synergistic effects of orientation, mechanical loading associated with thermal expansion and contraction, and the presence of "chemically active" liquids. This could be accomplished by expanding chemical compatibility testing programs to include constant load environmental stress cracking and low frequency cyclic tensile tests.

CONCLUSIONS

Polymer end-use properties are directly related to the basic molecular structure and processing techniques used during manufacturing and installation. Factors to be considered in determining compatible relationships between molecular structure, property, and application should include the following:

- . Careful material selection, sound manufacturing quality control, and onsite quality assurance are essential for long-term serviceability.
- . Testing methodologies should be established to evaluate the synergistic effects of the chemical environment, types of mechanical loading during service, and thermal expansion and contraction cycles should be evaluated prior to installation of the material(s).

REFERENCES

Text References

- (1) Bonaparte, R., Ah-Line, C., Charron, R., and Tisinger, L., "Survivability and Durability of a Nonwoven Geotextile," Proceedings of the ASCE Symposium on Geosynthetics for Soil Improvement, Nashville, Tenn., 1988.
- (2) Peggs, I.D., and Tisinger, L.G., Proprietary Report, GeoSyntec, Inc., 1988.
- (3) Tisinger, L.G., Proprietary Report, GeoSyntec, Inc., 1988.
- (4) Brydson, J.A., Plastics Materials, 4th Ed., Butterworth Scientific, 1982.
- (5) Peggs, I.D., "Evaluating Polyethylene Geomembrane Seams," Geosynthetics '87 Conference Proceedings, New Orleans, La., February 1987, Vol. 2, pp. 505-518.

General References

Modern Plastics Encyclopedia 88, McGraw-Hill, Inc., New York, N.Y.

Shah, V., Handbook of Plastics Testing Technology, John Wiley & Sons, Inc., New York, N.Y., 1984.

Billmeyer Jr., F.W., Textbook of Polymer Science, 3rd Ed., John Wiley & Sons, Inc., New York, N.Y., 1984.

Handbook of Plastics and Elastomers, Ed. by C.A. Harper, McGraw-Hill Book Company, 1975.

Deanin, R.D., Polymer Structure, Properties and Applications, Cahners Books, Boston, Mass., 1972.

Tisinger, L.G., Peggs, I.D., and Kimmet, J., "Differential Scanning Calorimetry Interpretation of Results Obtained on Polyethylene Geosynthetics," Proceedings of the 10th Annual Madison Waste Conference, Madison, Wis., September 1987.

I.D. PEGGS
R.M. CHARRON
GeoSyntec, Inc., U.S.A.

Microtome Sections for Examining Polyethylene Geosynthetic Microstructures and Carbon Black Dispersion

SYNOPSIS

The method of preparing very thin, translucent slices of geosynthetics with a sharp microtome knife is described. The microtome sections produced permit the examination of microstructural characteristics within the basic geosynthetic and within features such as geomembrane seams and surface roughening of friction sheets.

Microtome sections of polyethylene (PE) geomembranes facilitate the upgrading of carbon black dispersion measurements so that dispersion may be evaluated as it is in the geomembrane itself rather than in a modified melted and resolidified form. Typical microstructural features are presented that may form the basis of a new standard test for defining carbon black dispersion.

INTRODUCTION

For many years, microtomes and ultramicrotomes have been used to prepare very thin slices of biological materials that are translucent when observed through a light transmission microscope. Such microtome sections reveal the internal microstructure and defect distribution within the materials.

The technique is equally applicable to polymers (1) and hence to geosynthetic components, particularly those manufactured from semi-crystalline materials such as high density polyethylene (HDPE).

SPECIMEN PREPARATION

The basic microtome consists simply of a clamp capable of rigidly holding the sample of material. The sample can be raised controllably in increments of approximately 0.1 μm so that a very sharp, rigid knife may cut slices in the range of 8 to 20 μm thick. Figure 1 shows a section being prepared from a double hot wedge seam in a PE geomembrane. Figure 2 shows the final translucent section of the seam.

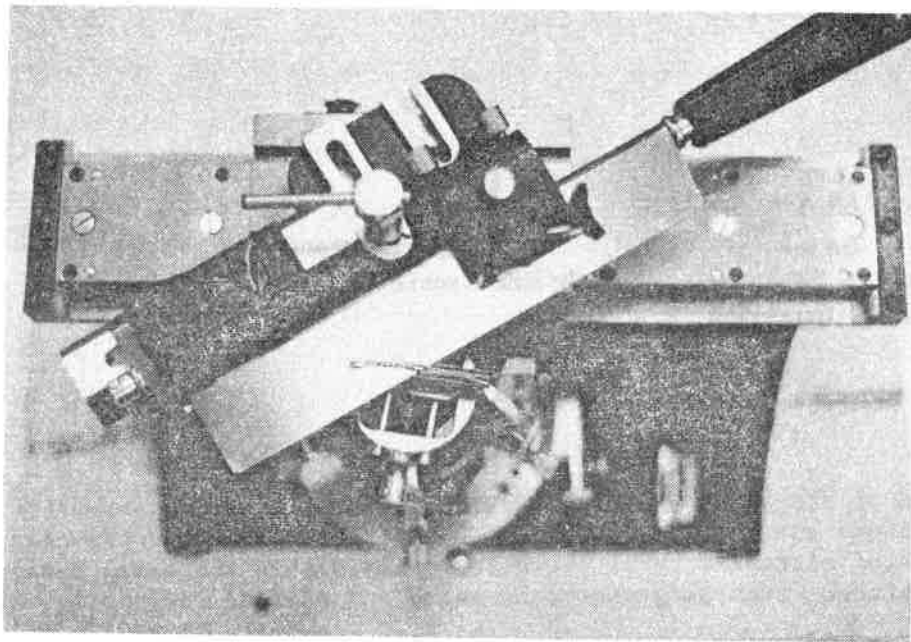


FIGURE 1. Cutting a geomembrane seam section.

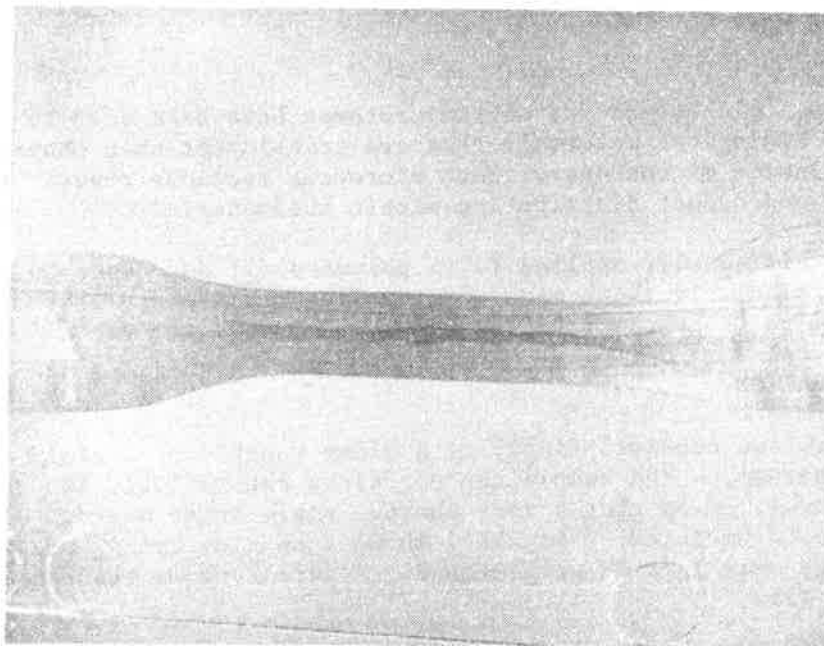


FIGURE 2. Microtome section of a geomembrane seam.

It is still much of an art to prepare a large, thin section since each grade of PE requires fine tuning adjustments to the knife angle. As a general guide, we have found that the knife should be at a vertical angle of approximately 15 degrees to the horizontal plane of the surface being cut. The longitudinal axis of the sample itself should be held at an angle of approximately 8 degrees to the direction of motion of the microtome knife. In this way, the markings caused by the roughness of the knife will not be oriented in the same direction as the extrusion pattern of the geomembrane. The knife, in turn, is best held at an angle of approximately 55 degrees from normal to the direction of motion. Figure 3 illustrates the orientation of the knife with respect to the specimen.

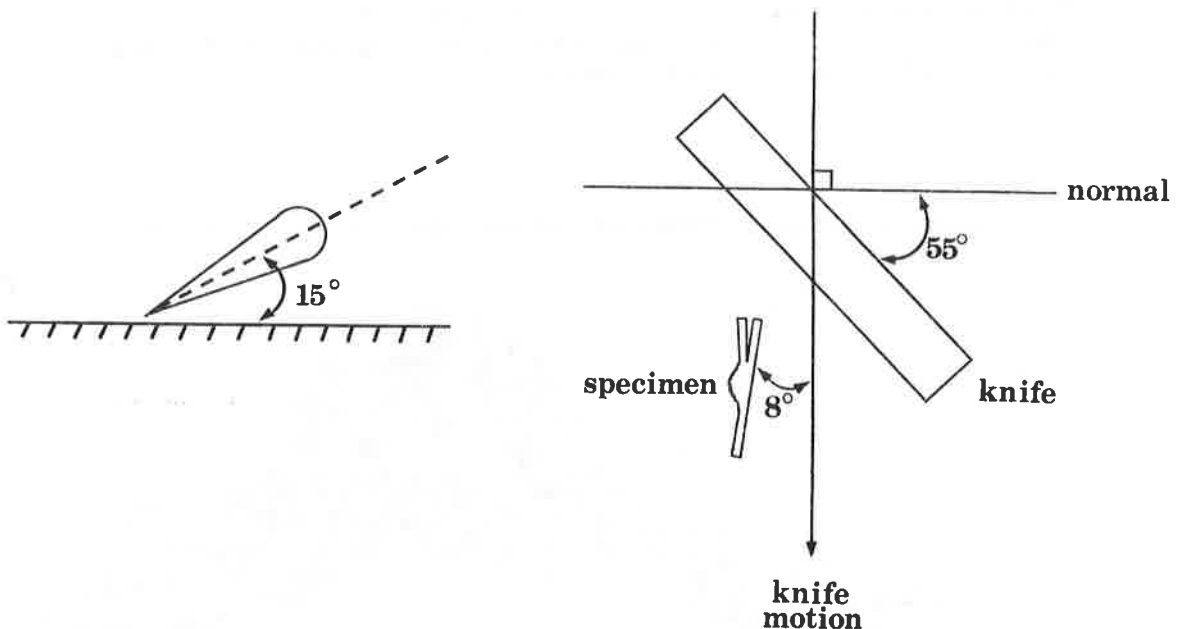


FIGURE 3. Microtome knife orientation.

When the section is first cut, it will probably curl. It can be gently uncurled into a layer of balsa cement that is spread on the surface of a glass slide. The section should be completely covered with cement before a transparent glass cover slide is placed on top of it. The two slides are gently compressed to flatten the microtome section and to expel air bubbles from the balsa cement. An alternative to balsa cement is nail varnish.

SECTION MICROSCOPY

The slide assembly is placed on the stage of a light transmission (biological) microscope or a metallograph so that rotating polarizing filters may be placed on each side of the section. It is advisable to use at least one thin cover slide so that high magnification objectives may be used.

When the microtome section is viewed, the processing flow patterns within the material are highlighted by the distributions of additives such as carbon black in PE. Therefore, the uniformity and symmetry of post-manufacturing processes such as seaming can also be identified. Figure 4 shows a cross section of an extruded fillet seam, which gives an indication that the following features may be identified on this and other types of sections:

- . The density matching of extrudate and parent resin,
- . The effectiveness of extrudate and parent geomembrane mixing,
- . The elimination of distinct interfaces,
- . The width, symmetry, and uniformity of the weld and heat-affected zones,
- . The presence of lack of fusion, voids, and dirt,
- . The distribution of carbon agglomerates and degraded resin, and
- . Crazes (precursors of cracks) and cracks.

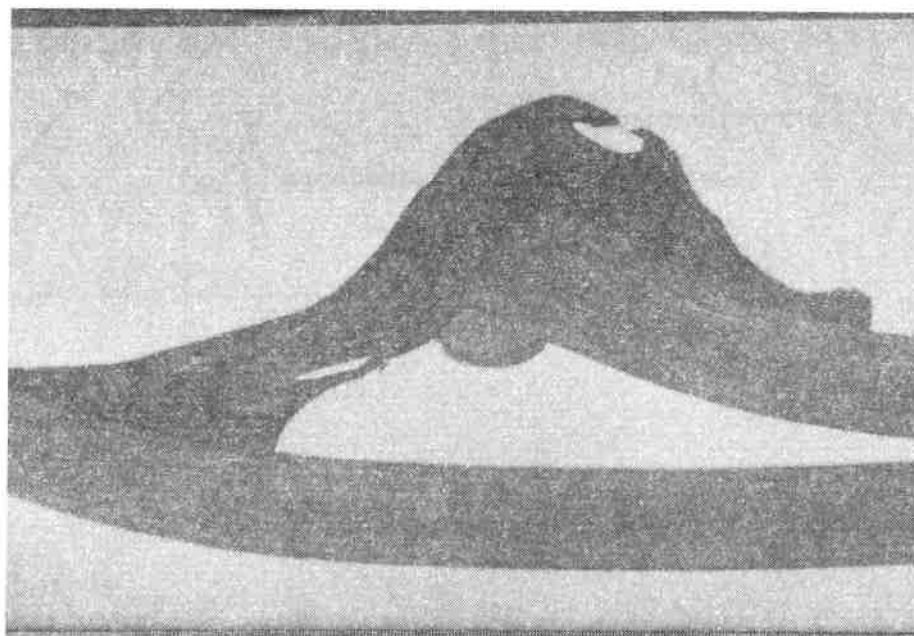


FIGURE 4. Cross section of extruded fillet seam. (x 5)

When crossed or partially crossed polarizing filters are placed on each side of the section, the contrast between many of the above features is improved, and most significantly, the distribution and relative magnitude of residual stresses are identified.

Some of the features listed above as they are observed in PE geomembrane seams are shown in Figures 5 through 10.

It is apparent that if dirt and voids (Figure 5) occur on the geomembrane/extrudate interface, poor bonding will result. Similarly, if there is a distinct interface between the heated geomembrane surfaces (Figure 6), there will be poor bonding. The distribution of such defects across a seam can be determined in the microtome section and is of particular interest in those seam peel specimens that appear to perform satisfactorily because only the part of the seam that is initially stressed is adequately bonded.



FIGURE 5. Dirt and lack of fusion on extrudate/geomembrane interfaces.
(x 130)

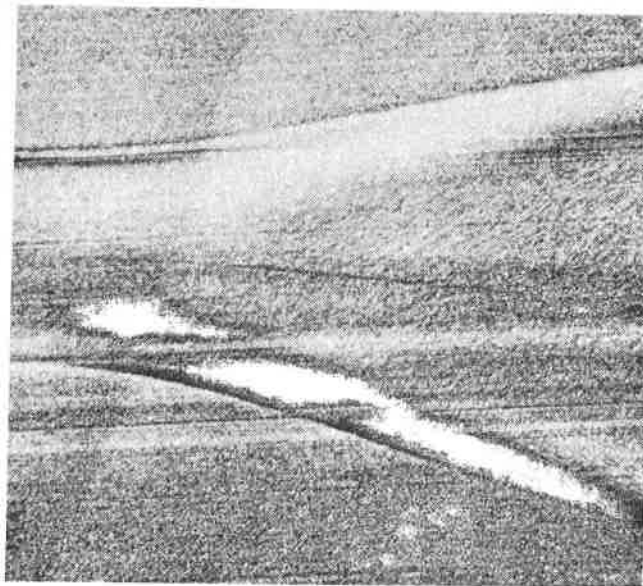


FIGURE 6. Distinct interface along the center of a fused seam weld zone.
Wide bands are residual stress at edge of weld zone. (x 65)

When a seam peel test is performed, some peel separation may occur before the geomembrane itself breaks. The significance of such separation in the acceptance or rejection of a peel test (2) is indicated in Figure 7 by the appearance of crazes that penetrate through 30% of the thickness of the geomembrane after separation has occurred. Since peel stresses can occur in the field, a seam which can be made to peel may be subject to crazing and ultimate premature failure as such crazes open up into cracks. Depending on the local stress situation, these cracks may propagate completely through the liner.

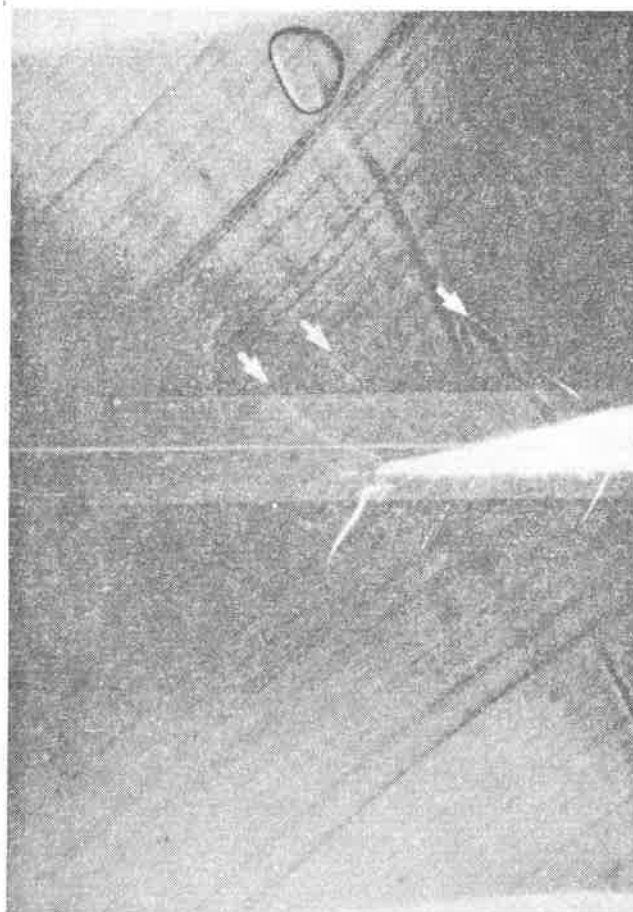


FIGURE 7. Crazes initiated in partially bonded surfaces separated by peeling. (x 50)

The appearance and effect of residual stresses are shown in Figures 8 and 9. Residual stresses are shown by brilliant blue, yellow, and orange colors (birefringence) which, in this case, can be observed at the root of the small extruded bead at the edge of a fused seam (Figure 8). When service stresses are applied to such a seam, crazes (Figure 9) are initiated at the residual stress area. These crazes eventually propagate upward through the geomembrane to form a brittle crack along the edge of the seam.



FIGURE 8. Residual stress (arrowed)
in hot wedge seam. (x 65)

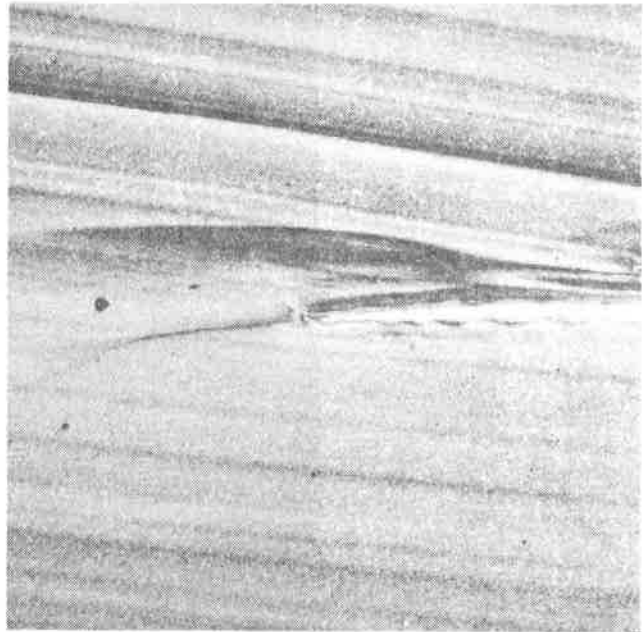


FIGURE 9. Crazing initiated by residual
stress shown in Figure 8.
(x 65)

Figure 10 shows part of a microtome section through an extruded fillet seam at the bottom of the edge of the top sheet over which the extrudate has been deposited. There is an area of residual stress on the edge of the top sheet which, in service, subsequently initiated a crack up the edge of the top sheet. At the tip of the crack (not shown), crazes were initiated in the extrudate that ultimately caused fracture up through the extrudate. Figure 10 also shows some crazing that has been initiated at the notch stress concentrator where some of the extrudate has separated from the top of the bottom geomembrane.

Other interesting features that may be observed by examining microtome sections are the corners of the conical protuberances, the distribution of voids, and the nature of the surface geometry in the various friction sheets. Other interesting features include the junctions of geogrids.

Microtome sections of geotextile fibers may be prepared, and if yarns and geotextiles are impregnated with a resin, the geotextiles themselves, even if previously impregnated with dirt (3), may be sectioned and examined.

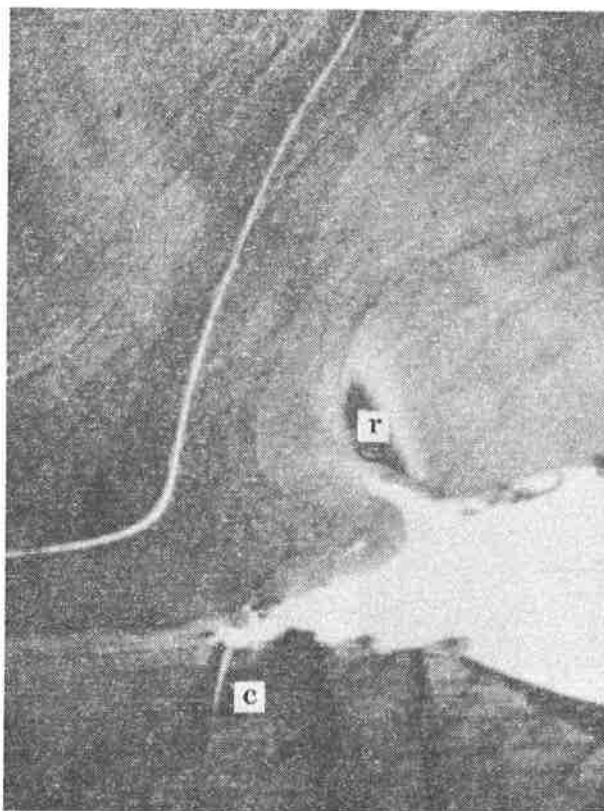


FIGURE 10. Residual stress (r) and crazing (c) in extruded fillet seam.
(x 100)

CARBON BLACK DISPERSION

The microtome technique offers a very simple way of being able to determine the actual dispersion of carbon black in as-manufactured PE geosynthetics.

Carbon black is added to PE geomembrane to provide resistance to ultraviolet degradation. To achieve this, the carbon black should be uniformly dispersed. Not only is the resistance to ultraviolet degradation affected by poorly dispersed carbon black, but environmental stress cracking resistance and tensile properties are also affected and can be significantly reduced (4).

Two ASTM standards are currently being used for the classification of carbon black dispersion in PE geomembrane. The standards are: ASTM D3015 (Standard Practice for the Microscopical Examination of Pigment Dispersion in Plastic Compounds) and ASTM D2663 (Standard Methods of Testing Rubber Compounds -- Dispersion of Carbon Black).

ASTM D3015, the standard normally specified in manufacturers' literature and design specifications, contains neither a set of observational standards nor a numerical rating system to classify carbon black dispersed in PE. In essence, this is a standard that defines a methodology for specimen preparation but only recommends the development of buyer/seller criteria via observational standards to classify dispersion characteristics.

In accordance with ASTM D3015, specimens are to be prepared by heating the polymer (a piece of geomembrane) between microscope slides and applying pressure at a temperature of 175 - 225°C. Under these conditions, the morphology of the as-extruded geomembrane, including the spatial arrangement of carbon black and any internal residual stresses, is altered due to melting and recrystallization of the polymer.

This change in morphology often disperses large agglomerates and thermally degraded material into a haze, possibly blanketing areas of unpigmented resin and making classification of the true features of the geomembrane difficult. A false impression that the carbon black is uniformly dispersed could therefore be obtained.

Figures 11 and 12 are photomicrographs that were taken of specimens prepared by the melting and pressing technique of ASTM D3015. Figure 11 shows the remnants of a spherical carbon agglomerate, similar to those in Figure 13, whose nucleus is readily discernible.



FIGURE 11. Cloudy carbon-rich area.
(x 100)

An example of how the morphology can change is shown in Figure 12 where a well-defined carbon streak located at the left side of the photo gradually becomes partially dispersed to the right of the photo.

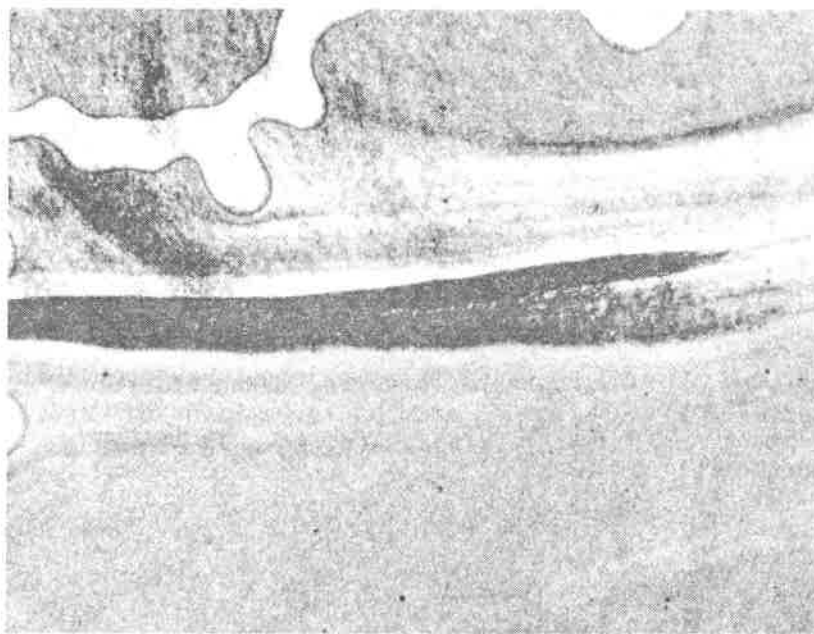


FIGURE 12. A partially dispersed carbon streak.
(x 100)

Although the standard used for classification, ASTM D2663, has both a numerical rating system and a set of observational standards, it was developed for rubber containing 18% carbon black by volume. Interestingly, the microtome technique is a recommended method of specimen preparation in this standard. The agglomerate count method, which is the basis of the alphanumeric rating system, evaluates the average size of a large number of moderately sized agglomerates, a situation that is seldom, if ever, present in PE geomembrane. PE geomembrane contains between 2 and 3% carbon black, and its dispersion characteristics do not coincide with those in rubbers manufactured by different techniques. Only one or two agglomerates may be seen in a microscope field of view.

PE geomembrane usually contains a fine background dispersion of carbon black with a small number of odd-shaped agglomerates and, in some instances, contains long streaks of non-dispersed carbon black or long streaks of totally unpigmented resin or both. We have analyzed some large agglomerates and found them not to be carbon. Such agglomerates and streaks may be either thermally degraded material or partially cross-linked clumps of regrind that were not uniformly dispersed with virgin material during the extrusion process. The latter is the most likely scenario since thermal gravimetric analysis on geomembrane samples removed from positions directly adjacent to the location of microtome sections containing fairly high concentrations of agglomerates shows two distinct molecular weight fractions (5).

Figure 13 is a chart of photomicrographs showing the carbon black and other agglomerate dispersion characteristics in as-extruded PE geomembrane. These are photos of specimens prepared using the microtome section technique. This chart represents both ends of the range of typically observed dispersion characteristics and is only a portion of a chart recently proposed to ASTM as the basis of acceptance criteria for a new carbon dispersion classification standard for PE geosynthetics.

The chart consists of four rows exhibiting different dispersion characteristics of increasing severity or size from left to right. Row 1 ranges from completely dispersed uniform particle size distribution to moderate-size agglomerates up to approximately 60 μm in diameter. Row 2 contains the next larger range of semi-spherical agglomerates ranging from approximately 95 to 300 μm in diameter. Row 3 contains streak agglomerates with areas of nondispersed carbon surrounding the agglomerates. The thicknesses range from approximately 30 to 120 μm . Row 4 contains streaks of unpigmented resin varying in width from approximately 20 to 70 μm in thickness.

CONCLUSIONS

The microtome technique of geosynthetic microstructural examination can make a significant contribution to the development of new materials, modified materials, and subsequent processing (e.g., seaming) methods. It is also invaluable in determining the characteristics of fracture phenomena during failure analyses.

Microtome sections permit the microstructural evaluation of the basic geomembrane, which facilitates the upgrading of the standard method of determining the dispersion of carbon black in PE geomembranes. As a result, the geosynthetics industry is provided with a standard means of evaluating and classifying the carbon black dispersion in the actual as-extruded geomembrane, which is the product that is exposed to the ultraviolet radiation while in service.

REFERENCES

- (1) Bell, G.R. and Cook, D.C., "Microtoming: An Emerging Tool for Analyzing Polymer Structures," Plastics Engineering, Aug. 1979, pp. 18-22.
- (2) Peggs, I.D., "Evaluating Polyethylene Geomembrane Seams," Proceedings of Geosynthetics '87, Vol. 2, New Orleans, La., Feb. 1987, pp. 505-518.
- (3) Sotton, M., "Durability of Geotextiles," 23rd International Man-made Fibres Conference, Dornbirn, Austria, Sept. 1984, pp. 9-10.
- (4) Gilroy, H.M., "Polyolefin Longevity for Telephone Service," Proceedings of the 43rd Annual Technical Conference (ANTEC '85), Society of Plastics Engineers, Inc., Washington, D.C., Apr.-May 1985, pp. 258-260.
- (5) Tisinger, L.G., Proprietary Reports, GeoSyntec, Inc., 1987-1988.

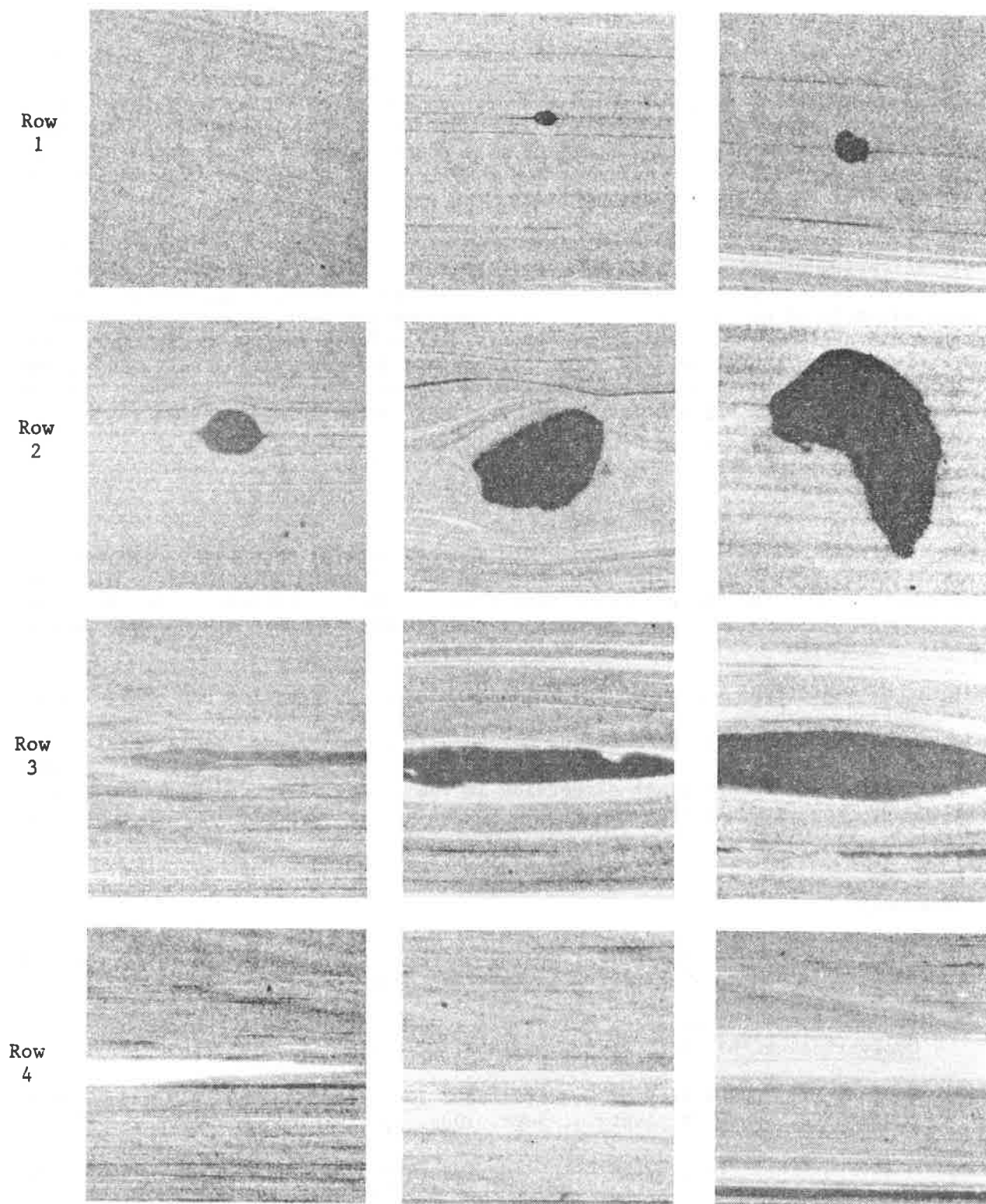


FIGURE 13. Photomicrographs of dispersion characteristics of as-extruded PE geomembrane taken from microtome sections. (x 100)

G. YAZDANI
J. NORBERT
Poly-America, U.S.A.

**Evaluation of the Effects of Waste Loads on Geocomposites In Double-Lined
Landfills and Surface Impoundments**

ABSTRACT

In an effort to meet the regulatory requirements of leak detection and collection systems, products combining geomembranes, geonets and geotextiles are being used with increased frequency.

A load placed on the liner system above a geonet may cause stress deformation and in time reduce the transmissivity of leachate to the collection points. The use of composites with a geotextile on top of the grid and the liner on top of the geotextile may also result in reduced flow.

This paper addresses these situations using a large-scale hydrostatic tester to simulate actual field conditions of a geomembrane/geonet and geomembrane/geotextile/geonet system. Stress was introduced by applying incrementally increasing overburden pressure over a period of time. The diameter of the test vessel is 22 in. (550 mm.), which allows for any elongation and intrusion of the membrane or geotextile that would occur in the field.

Various thicknesses of HDPE membranes were evaluated and were post tested for physical properties after exposure.

Such composite systems can be underdesigned, whereby thinner membranes may intrude into the system and reduce transmissivity. In addition, roll-over of the geonets under pressure reduces flow and should be taken into account.

INTRODUCTION

Clay has been the conventional lining material for land waste containments for many years. Where suitable clays with the required permeabilities were inobtainable, other materials have been used as barriers in groundwater and soil conservation projects. Fly ash, bentonite, cement, asphalt, hydrated lime or combinations of these have been used as stabilizers to improve mechanical properties of on-site soils and to reduce hydraulic conductivity to desirable levels.

As the need for waste containment increased, alternate methods of achieving "impermeable barriers" were explored. The majority of recently constructed waste containments have used

geosynthetics for drainage systems and seepage barriers. Geomembrane has replaced clays and stabilized soils as the barrier of choice, and the latter are now used as backings beneath secondary liners where available. Conventional leachate collection systems, consisting of sand and gravel layers, are being increasingly replaced by geosynthetics such as geonet and geotextile. This paper briefly discusses selected topics regarding the stability of composite synthetic liner systems under static loading and reviews the effects of overburden loads on the performance of the liner system. These topics are as follows:

1. Effects of Waste Loads on the Hydraulic Transmissivity of Drainage Systems and Geomembrane Performance
2. Effects of Subgrade Condition on a Composite Liner System when Subjected to Increasing Work Loads

EFFECTS OF WASTE LOADS ON HYDRAULIC TRANSMISSIVITY OF DRAINAGE SYSTEMS AND GEOMEMBRANE PERFORMANCE

A sound geocomposite system design is achieved through the careful evaluation of long-term tensile and tear strength, and the puncture resistance of its proposed components. The hydraulic transmissivity of synthetic drainage materials under compressive loads should also be considered. The hydraulic transmissivity of a leachate collection and removal system depends on the following variables:

1. The Density, Viscosity and Temperature of Contained Fluids
2. Types of Drainage System Components and the Characteristics of their Strength and compressibility
3. Hydraulic Gradient
4. Boundary Conditions
5. Time Dependent Creep

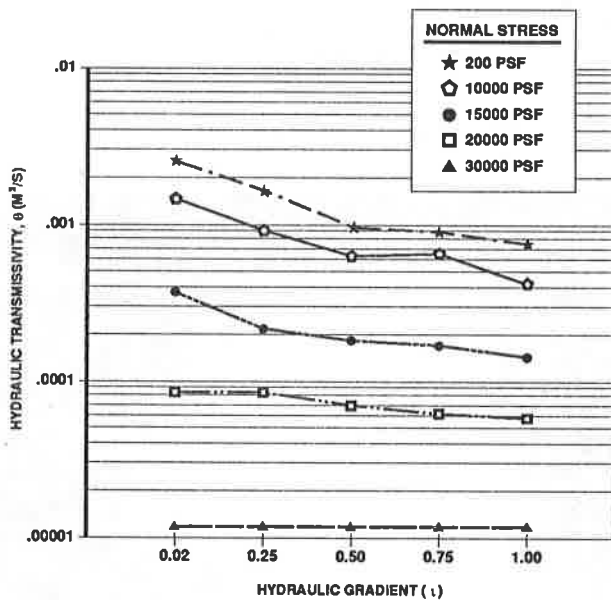
The *Minimum Technology Guidance Document* of the Resources Conservation Recovery Act (RCRA) sets minimum requirements for leachate collection and removal systems. A minimum 2% slope, and a hydraulic conductivity value of not less than 1×10^{-2} cm/sec. for a drainage layer that is 12 inches thick is required. This translates to a transmissivity value of 3×10^{-5} m²/sec. Currently, these specifications can be met by using a drainage net with a geotextile upper layer.

A drainage net is composed of two parallel arrays of plastic strands. The arrays intersect, as in a grid, but at an angle that is not perpendicular. Unlike the weave pattern of a fabric, individual drainage net strands keep to one side of the strands they intersect. The resulting two-tiered mesh is designed to efficiently channel waste liquids (leachate) to desired locations in the cell for disposal. The geotextile between the containment and the drainage net prevents waste and soil particles from entering into and potentially obstructing the drainage net channels.

A nonwoven, needlepunched geotextile or a mat (400 to 800 mil) is often used to allow for

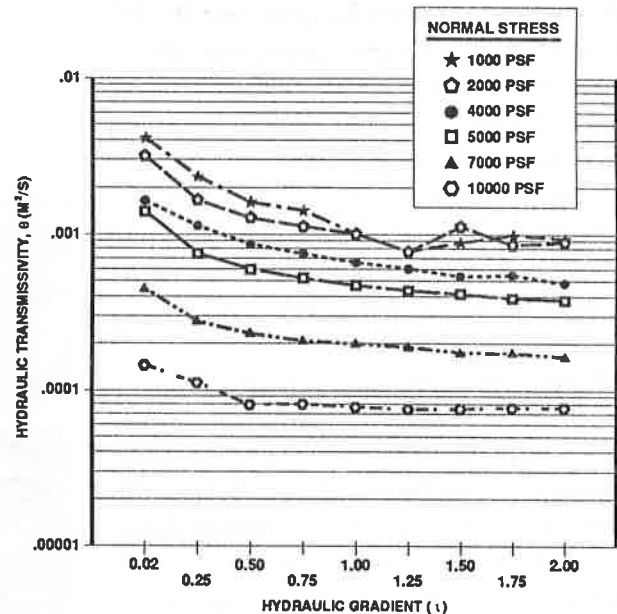
transmission of fluids and gases. Several factors are important in the consideration of particular geotextiles or mats for this application. One is the fabric's ability to act as a filter without clogging. Another is permittivity (hydraulic conductivity of a fabric when the flow is perpendicular to its plane, divided by the fabric's thickness). Tests for these parameters should be conducted under simulated field loading and boundary conditions.

Hydraulic transmissivity also depends on the cross-sectional area (between the supporting strands) of the flow channels or nets. Any reduction in this cross-sectional area will result in reduced flow. The intrusion by the geomembrane and geotextile into this area of the net will constrict flow, as will the deflection of the geonet strands that can occur when overburdened with compressive loads. Figures 1 and 2 demonstrate the hydraulic transmissivity findings of two tests, in which boundary conditions were variable. Water at room temperature was used as the leachate.



Boundary Conditions: Plate/HDPE/Drainage Net/HDPE/Plate

Fig. 1. Transmissivity Test Data



Boundary Conditions: Plate/Soil/Geotextile/Drainage Net/HDPE

Fig. 2. Transmissivity Test Data

The first test (Figure 1) simulates a typical secondary leachate detection and removal in a geosynthetic liner system. A 150 mil polyethylene drainage net was placed between two 60 mil High Density Polyethylene liners. Different overburden pressures were applied at several hydraulic gradients (hydraulic head divided by length of flow).

The second test (Figure 2) simulates a primary leachate collection and removal system. A mixture of sand and clay forming a layer approximately one inch thick was compacted at optimum moisture content to about 95% of standard proctor and placed over a 4 oz. nonwoven geotextile over a 250 mil polyethylene geonet. Underneath this layer was a 60 mil HDPE membrane. This system was tested under different overburden pressures and gradients.

The results of these tests indicate that significant reductions in hydraulic transmissivity oc-

cur at higher overburden pressures. So that values more closely approximating field conditions could be obtained, long-term transmissivity tests should be carried out. Such a long-term evaluation would be able to measure time-dependent creep, which is not accurately measurable in short-term tests.

Additional tests were performed using a hydrostatic pressure vessel (Figure 3) to evaluate the magnitude of geomembrane intrusion into the open spaces of drainage nets, the reduction in the thickness of nets, and the physical integrity of each component under hydrostatic compressive loads. Two tests were performed using 40 mil and 60 mil HDPE liners and 150 mil (junction thickness) drainage nets. The net was initially sandwiched between two 40 mil liners and laid across a tightly packed, smooth sandy soil surface. The final applied pressure was 75 psi, maintained for a period of two days. Through the vessel's viewing window one may note a considerable amount of liner intrusion into the open spaces of the net (Figure 4). The net's thickness was measured prior to and immediately following the test. Results indicate an average reduction of about 7 mils (4.7%) throughout the net's area under the applied pressures. These effects result in a reduced flow area and consequently, reduced flow.

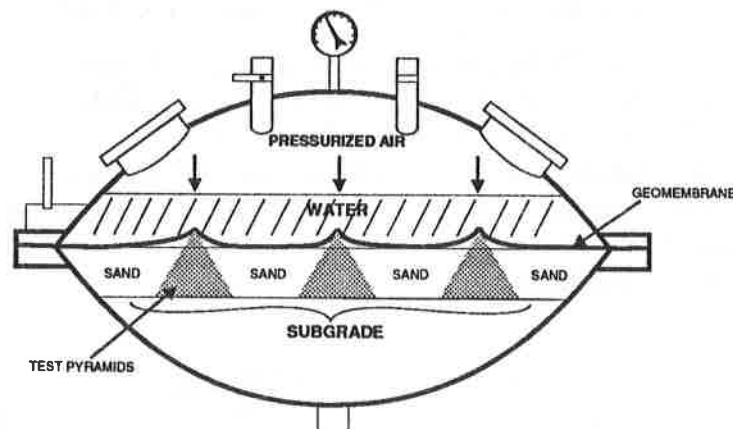


Fig. 3. Hydrostatic pressure test vessel

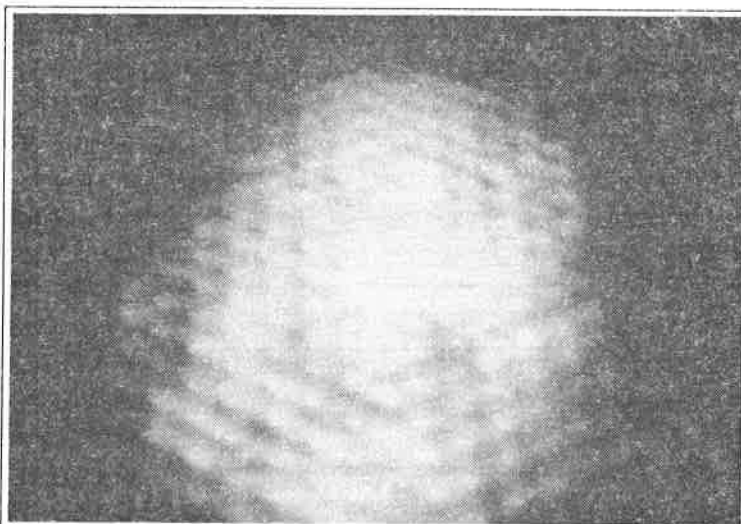


Fig. 4. Intrusion of a 40 mil HDPE liner into the open spaces of a 150 mil LDPE drainage net under 75 psi pressure

These test conditions were recreated with a 60 mil HDPE liner. The final pressure was 100 psi. The liner intrusion into the net was not as noticeable as with the 40 mil liner, even under this higher pressure, but the average reduction in the net's thickness was about 10 mils (6.7%). Results from subsequent tests appear in the latter part of this paper.

The selection of a liner in a composite system must be made with careful regard to physical and mechanical properties (Table 1). Tensile and tear strengths are usually determined by standard ASTM tests. Figure 5 represents the stress-strain diagram for HDPE, VLDPE, and PVC membranes. As indicated, the HDPE membrane yields at about 2500 psi, while VLDPE and PVC do not exhibit yield points. Energy absorption of a material at failure is defined as the total area under a complete stress-strain diagram. This is more commonly defined as

Table 1. Physical property comparison: 30 mil HDPE, VLDPE, and PVC

Property	Test Method	HDPE	VLDPE	PVC
Gauge (nominal) mils $\pm 10\%$	—	30	30	30
Density (gm/cc)	ASTM D1505	0.950	0.920	1.2 – 1.4
Tensile Strength @ Yield (lb/in)	ASTM D638	75	*	*
Elongation @ Yield (%)	ASTM D638	10	*	*
Tensile Strength @ Break (lb/in)	ASTM D638	125	120	90
Elongation @ Break (%)	ASTM D638	800	1200	300
Secant Modulus 1% Elong. (psi)	ASTM D638	100,000	8,000	5 – 10,000
Tear Strength (lb)	ASTM 1004	22	14	8
Puncture Resistance (lb)	FTMS 101 2065	57	52	46

* VLDPE and PVC do not exhibit true yield points.

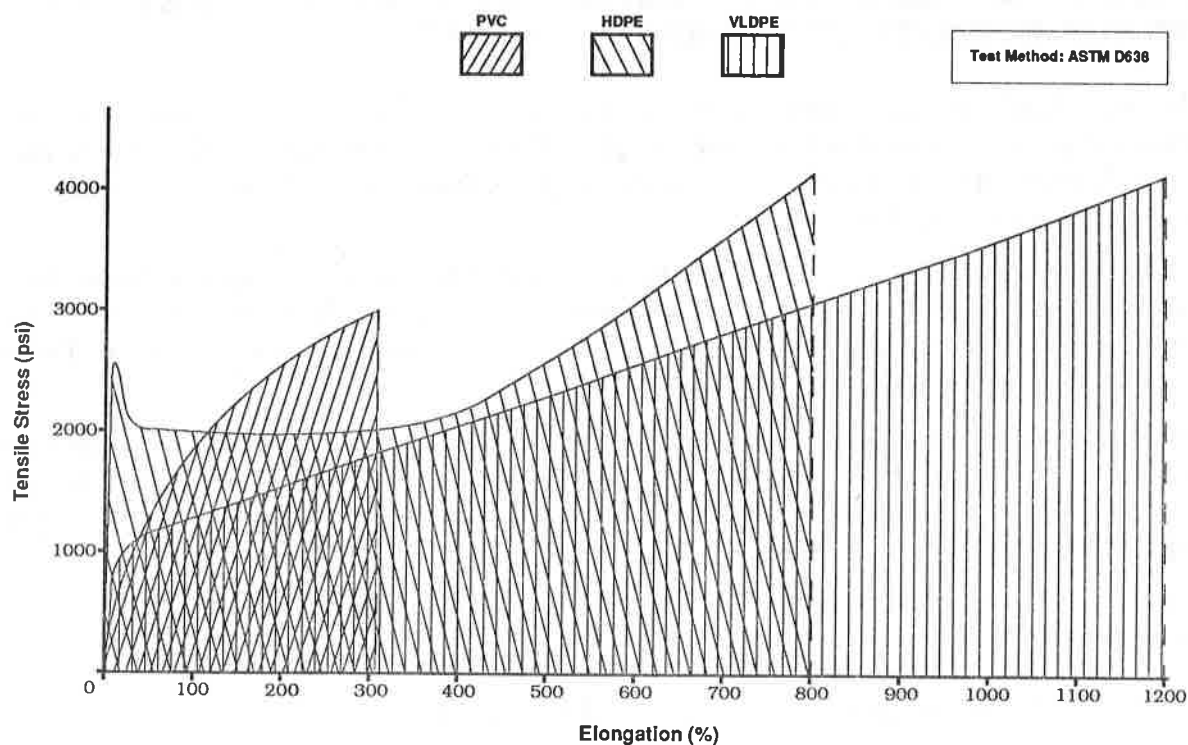


Fig. 5. Energy Absorbed During Tensile Rupture: HDPE, VLDPE, and PVC

"toughness." Puncture resistance is evaluated under Federal Test Methods, where the resistance is measured by the force required to puncture a restrained sample liner by a standard probe. The results of these tests (Figure 6) indicate that VLDPE elongates twice as much as HDPE or PVC before it punctures. This is a good indication of VLDPE's ability to maintain flexibility and absorb greater punishment before failure, a desirable geomembrane characteristic to have available when designing for subgrades susceptible to differential settlement or when the soils are composed of large or angular particles. A hydrostatic pressure vessel was developed to evaluate the puncture resistance of these liners under simulated field conditions. In the author's opinion, this test evaluates this parameter more accurately than the standard laboratory probe puncture test, and it can be used to guide the selection of a membrane. Another series of tests in this study will compare the adaptability of these liners in different settings.

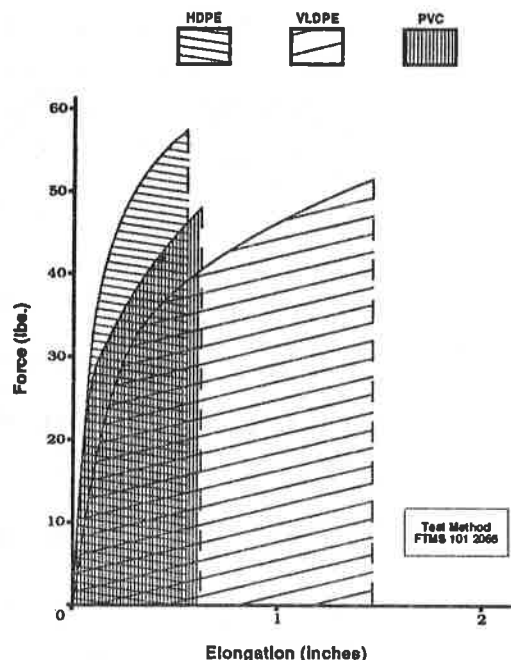


Fig. 6. Energy Absorbed During Puncture Resistance:
30 Mil HDPE, VLDPE, PVC

EFFECTS OF SUBGRADE CONDITION ON A COMPOSITE LINER SYSTEM WHEN SUBJECTED TO INCREASING WORK LOADS

The intent behind the development of the hydrostatic tester (Figure 3) was to evaluate the performance of geomembranes when they are placed on various subgrades under overburden waste loads replicating field conditions. In this way, a reliable recommendation could be made regarding the selection of a liner.

The lower chamber of the hydrostatic tester is designed to hold the subgrade materials. The test area allows for 280 in² of subgrade to be exposed to the liner. The liner is clamped between the upper and lower chambers of the hydrostatic tester and a tight seal is created. The liner cannot slip during the test.

Water is introduced into the upper chamber through ports. A line is added to the upper chamber, through which compressed air passes to increase pressure to 100 psi. Because the lower chamber is vented to the atmosphere, any rupture to the liner will allow water to escape through the vent.

The hydrostatic tester has been used to study four problems related to the interaction of liners and subgrades:

1. Liner Integrity Against a Specific Subgrade
2. Integrity and Transmissivity of a Composite Liner System Against a Subgrade

3. Liner Integrity Where the Liner Spans Voids in the Subgrade
4. Liner Integrity Over Protrusions in the Subgrade

Liners on Soils—The criterion governing the selection of a liner by an engineer is whether it will “hold up” under actual field conditions. Many standard index tests, such as puncture resistance, tear strength, and tensile strength, were developed in the laboratory to determine this. However, results from these tests can be misleading. Results should index similarities between materials in the same lineage of liners (i.e., varieties of HDPE).

Three subgrade types have been evaluated: sand, a sand and gravel mixture (with subangular particle size ranging up to 2”), and gravel (angular particles ranging up to 1”). The liners tested were HDPE, VLDPE, and PVC. Table 2 records the test results.

Table 2. Hydrostatic test for liner performance on subgrades

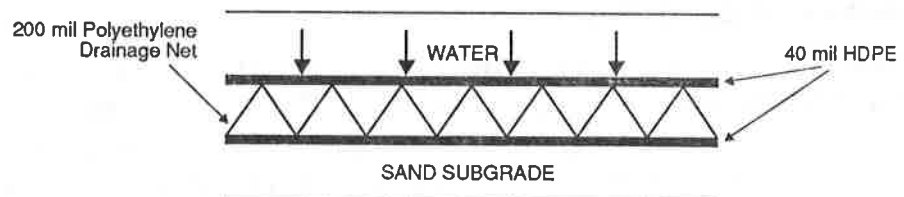
Liner	Sand (SP)	Sand & Gravel (GP)	Gravel (GP)
30 mil PVC	passed @ 100 psi	failed @ 90 psi	—
60 mil HDPE	passed @ 100 psi	passed @ 100 psi*	failed @ 80 psi
30 mil VLDPE	passed @ 100 psi	passed @ 100 psi	passed @ 100 psi

* Severe thinning occurred in several locations where the liner had to conform to the shape of gravel. Pressure was applied hydrostatically at a rate of 5 psi (34.5 kpa) per hour. The final pressure was 100 psi (690 kpa), maintained for 4 days.

As will be noted, all materials performed well against sand. However, subgrades containing gravel (such as is typical around mining operations) require a more durable liner, such as VLDPE. It is noteworthy that VLDPE outperforms HDPE at half its thickness.

Composite Systems—The hydrostatic tester can evaluate the performance of composite systems, as well as single liners.

The bottom liner in a composite system was evaluated (Figure 7). The test was designed to measure the additional stress transmitted to the bottom liner by the geonet. At 100 psi, the total load on 280 in² of test area is 28,000 lbs. The drainage net magnifies this load upon the bottom liner. Because the total area of the strands that make contact with the bottom liner is significantly less than 280



Pressure was applied hydrostatically at a rate of 5 psi (34.5 kpa) per hour. The final pressure was 100 psi (690 kpa), maintained for 4 days.

Fig. 7. Hydrostatic Test (Composite Section)

in², the transmitted pressure would be significantly greater than 100 psi. Table 3 indicates that under this extreme load HDPE retains its structural integrity.

Table 3. Physical property comparison for bottom liner, (Fig. 7)

Property	Test Method	Units	Value (before test)	Value (after test)
Gauge	ASTM D1593	mils	37	38
Tensile Properties	ASTM D638			
Yield		lb/in	110	100
Elongation @ Yield		%	9	9
Break		lb/in	180	160
Elongation @ Break		%	870	790
Tear Strength	ASTM D1004	lb	29	30
Puncture Resistance	FTMS 101-2065	lb	60	59

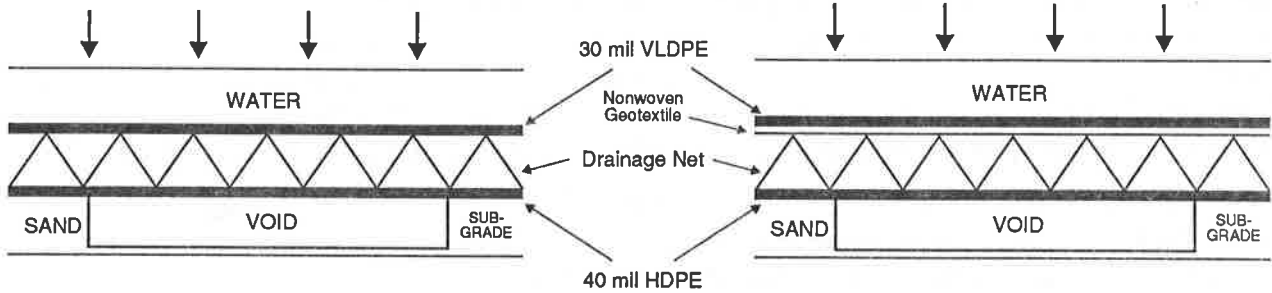
A composite system was also evaluated to determine susceptibility to deformation across an abrupt change in grade, or a void in the subgrade. The primary objective was to discover whether transmissivity would decrease if the geonet stretched or flattened over the void. In these experiments, a round pan 9" across and 1.5" deep was imposed into the subgrade. Pressure on the composite system was gradually increased to 100 psi. Since transmissivity would be directly affected by any reduction in the cross-sectional area of the net (at the junction of upper and lower strands), the net's thickness was measured before and after the test. No difference was found.

The results indicate that the net permanently yielded and deformed to the shape of the depression in the subgrade, but did not flatten or show signs of collapse, even at points of maximum stress.

Voids in Subgrade—Although subgrades are intended to be smooth and unyielding, this condition is not always achieved. It is possible that voids will form underneath the liner at some point during the life of the system. In areas where the subgrade does not support the liner, the liner will have to support the load itself by flexurally conforming to the spatial contours of the void area.

The next test evaluated the performance of the liner over two rectangular void areas (Figures 8 and 9). One void measured 5.5" x 9.5" x 2.5", the other, square shaped, measured 7.75" x 7.75" x 2". In each case, a single liner was placed in the hydrostatic tester across the void. Pressure was increased at the rate of 5 psi/hour until failure or 100 psi was reached.

The 30 mil VLDPE easily conformed to the void contour without rupturing, although some localized permanent deformations occurred. These deformations were isolated to areas directly over a void, and did not extend into areas with subgrade support. The liner thinned excessively at the corners of its depression over the deeper pan, but this was expected.



Pressure was applied hydrostatically at a rate of 5 psi (34.5 kpa) per hour. Final pressures were 80 psi (552 kpa), maintained for 1 day.

Fig. 8.

Fig. 9.

30 and 60 mil HDPE were also tested over the rectangular pans. These liners did not stretch as dramatically as VLDPE into the corner contours of the square pan. Instead, a gradual, rounded contour was formed, which was maintained throughout the gradual increase to 100 psi. 30 mil HDPE ruptured over the rectangular pan, but 60 mil HDPE did not, though excessive thinning in one area suggested that failure would have occurred had the test pressure or duration been increased.

Although this information is not quantitative as such, it does determine that voids in the subgrade can contribute to the failure of a liner under stress.

Artificial Protrusions in the Subgrade—Subgrades are prepared to be free of sharp and potentially damaging objects, however, any rock or sharp object that makes incidental contact with a liner may cause it to puncture or tear.

Three pyramidal blocks were placed in a sand subgrade at the bottom of the hydrostatic tester (Figure 3). The blocks were set around the center of the test area, equidistant from each other, and at about the same distance from its perimeter. A single liner was laid across the blocks and firmly clamped between the tester's upper and lower chambers. The sharp tips of the pyramids projected 1" above the subgrade. Pressure was increased at a rate of 2.5 psi per half hour.

30 mil PVC and VLDPE were tested against these subgrade protrusions at pressures up to 100 psi. Both 30 and 60 mil HDPE failed this test at less than 10 psi. The 30 mil VLDPE and PVC did not fail.

It may be concluded that while HDPE is strong, it is not as tough as VLDPE or PVC. VLDPE and PVC were elastic enough to accommodate the sharp tips of the pyramidal blocks without failing. VLDPE and PVC are better suited, therefore, to accept rough or irregular subgrade surface conditions. Aside from evaluating the adaptability of different varieties of geomembrane, this test asserts the preeminence of the hydrostatic tester over standard laboratory puncture test devices.

SUMMARY

Results of the hydrostatic pressure tests indicate that the 40 mil HDPE liner intruded into the

open spaces of the net to a degree significantly greater than did the 60 mil HDPE liner, even at lower pressures. These effects are more profoundly exaggerated when test periods are longer. It is necessary to consider these parameters when designing the composite liner system, especially when a liner 40 mil or less is to be used. VLDPE and PVC liners tend to magnify this effect, due to their characteristically lower modulus and higher flexibility.

The hydrostatic test apparatus proved to be a valuable tool for evaluating both single and composite liner systems next to various subgrades or conditions within a subgrade. VLDPE liners are easily the most durable and adaptable of the three liners evaluated.

A sound synthetic composite liner system will perform and function effectively in soil and ground water conservation projects. It is the responsibility of the designer to gather all necessary information regarding all design parameters to achieve this goal.

WORKS CONSULTED

1. Bonaparte, R., Williams, N., and Giroud, J.P. "Innovative Leachate Collection Systems for Hazardous Waste Containment Facilities," Tensar Technical Note (The Tensar Corporation), Morrow, Georgia, March 1987, pp. 1-26.
2. The Tensar Corporation. "Tensar Drainage Nets," (undated and unpaginated documentation), Morrow, Georgia.

A.L. ROLLIN

A. VIDOVIC

Ecole Polytechnique de Montreal, Canada

R. DENIS

M. MARCOTTE

Solmers International, Canada

Evaluation Of HDPE Geomembrane Field Welding Techniques; Need To Improve Reliability Of Quality Seams

SUMMARY

An investigation of polyethylene geomembrane field seams has been conducted to identify the main influential welding parameters which need to be controlled and properly monitored in order to insure consistent field seam quality. Different existing welding techniques were either studied or reviewed including such methods as both extruded fillet and overlap seaming, thermal fusion seaming and ultrasonic seaming. Welding speeds, ambient temperatures, sheet thicknesses, moisture and dirt contents were among the parameters retained for this study. Seam quality assessments were made through industry standard quality control test methods such as both shear and peel testing. In addition, innovative microscopic analyses of seam cross sections were performed in order to directly observe inadequately fused seam specimens and to reveal structural modifications as previously undetected from traditional indirect methods. This paper outlines the major observations along with the authors' recommendations pertaining to the enhancement of seam quality and reliability.

INTRODUCTION

Materials such as compacted clays, asphaltic compounds and composites, and concrete have all been extensively used to provide hydraulic barriers in earth structures such as canals, landfills, dams, sewage lagoons and storage ponds of all sorts. Synthetic materials still commonly referred to as "synthetic liners" or adequately termed as "geomembranes" have on the other hand, rather recently been successfully used to perform similar duties under specific conditions. Within this latter category of products, High Density Polyethylene (HDPE) geomembranes constitute a frequently preferred material largely on account of the polymer's high chemical resistance to a wide variety of corrosive agents.

All geomembranes provide extremely low permeabilities as long as their continuously linked molecular structure remains intact. Material integrity is thus subsequently insured by strict adherence to proper field installation methods. In particular, the protocol associated with field seaming of geomembrane panels requires extensive quality control procedures since this single operation inevitably yields artificially induced molecular discontinuities in the welded area at which point material deficiencies are liable to be concentrated.

On account of HDPE's remarkable chemical inertia, geomembrane panels may only be effectively assembled through polymer fusion where basically a quantity of energy (heat) is supplied at the panels' interface, enabling new molecular links between adjacent panels. This quantity of energy may be provided by any heat transfer mechanism (conduction, convection and/or radiation) from different originating sources such as heating elements, melted extrudate and tuned prongs. Additionally, in order to insure continuous bonding, pressure is also often applied following heat treatment.

The quality of geomembrane seams depends on numerous parameters as induced from the type of equipment used. In summary, most parameters are related to the effective rate of transferred energy. The polymer's physical properties, the sheets' thickness, the welding speed, the welding temperature and pressure (if applicable) all constitute governing parameters. Field constraints such as climatic conditions, condition and geometry of subgrade only add to the complexity of achieving consistent quality seams.

Field seams must be verified by destructive quality control methods to constantly corroborate the welding equipment's calibration and performance. As long as specific geomembrane testing procedures remain to be developed and instituted, governing agencies are endorsing the utilization of existing but somehow remote testing procedures on account of the urgent need to assess seam quality. Geomembrane seam quality is thus evaluated through customary plastic and rubber industry-standard shear and peel test procedures. As it shall be demonstrated in this paper, the data yielded from these test methods should be used with caution as in many cases, supplemental microscopic analyses will reveal previously undetected flaws such as structural modifications, unbonded areas within the seam, failure modes and slow crack growth, which are all liable to restrict the anticipated long term performance of the seams.

EVALUATION OF THE INFLUENCE OF SOME IMPORTANT WELDING PARAMETERS

Foreword

As previously mentioned, geomembrane welding parameters are usually identified from the type of equipment and welding method used, although some generally apply to all techniques regardless of their operating modes. All of the data and ensuing inductions presented herein were mainly obtained from existing literature and from two proprietary research project reports;

- Evaluation of a specific ultrasonic field welding prototype and,
- Evaluation of a specific factory overlap extrusion process.

Conclusions and recommendations are nevertheless generalized considering the broad applicability of the findings. One last opening comment concerns the data as originally gathered during the evaluations, requiring the use of peculiar americanocentric units. For the sake of publication all units were approximated to SI units. Since the overall objective is to indicate tendencies for generalization purposes, rounded approximations were deemed appropriate.

Raw Materials; Identification and Quality

The energy required for the fusion of the material is linked to the physical properties of the compounded mixture. Very often HDPE is falsely interpreted as a very specific product, where in truth the abbreviation stands for a surprisingly broad range of polyethylene based geomembranes. Physical properties such as density, melt index, carbon black and dispersing agent content, will influence welding performances although their respective property values are all within the tolerances of the generic requirements.

Sheet Thickness

Generally, thicker HDPE geomembranes facilitate their welding simply from the fact that more material is available thus offering a wider window of welding parameter variances. As an example, thinner gauges are much more vulnerable to overheating largely responsible for such problems as material ondulation and frequent burn throughs. On the other hand, the amount of energy required for thicker gauges becomes so large that the resulting welding speed is greatly affected. Most of the welding techniques used are then limited to a workable range of sheet thicknesses in order to weld efficiently at a reasonable speed.

For example, the maximum welding speed of the ultrasonic prototype is plotted versus HDPE sheet thicknesses in Figure 1. It can be observed that acceptable (1) peel strength were obtained at a maximum welding speed of 1.35 m/min for sheets of 1.2 mm gauge. This maximum value decreases as the sheet's thickness both increases or decreases.

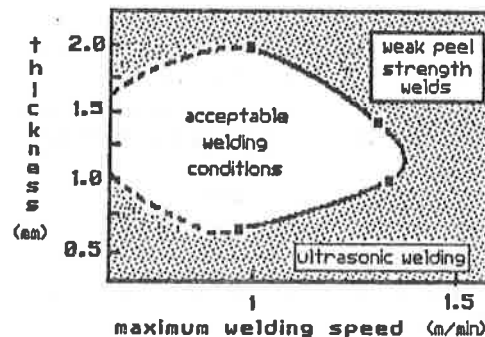


FIGURE 1. INFLUENCE OF SHEET THICKNESS ON WELDING SPEED.

Surface Neatness

The surface of the sheets should always be cleaned of any foreign substances including greases, oily compounds, moisture and dirt. As shown by Peggs (2) and as presented on Figures 2, 3 and 4, the presence of contaminants contributes in lowering the bonding strengths of seams. Cleansing of the sheet's surface by way of a forced air pre-heating procedure for example, is certainly recommended in an effort to vaporize both organic solutions and moisture, and to blow away dirt, immediately preceding the actual welding operation.

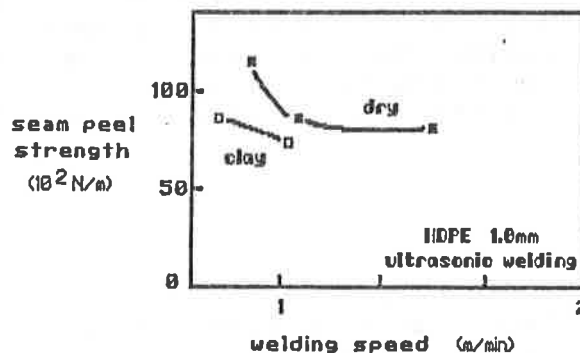


FIGURE 2. INFLUENCE OF CLAY PARTICLES ON SEAM QUALITY.

(1) "acceptable" as defined by the authors, must meet or exceed 70 % of the parent material's tensile strength at yield point.

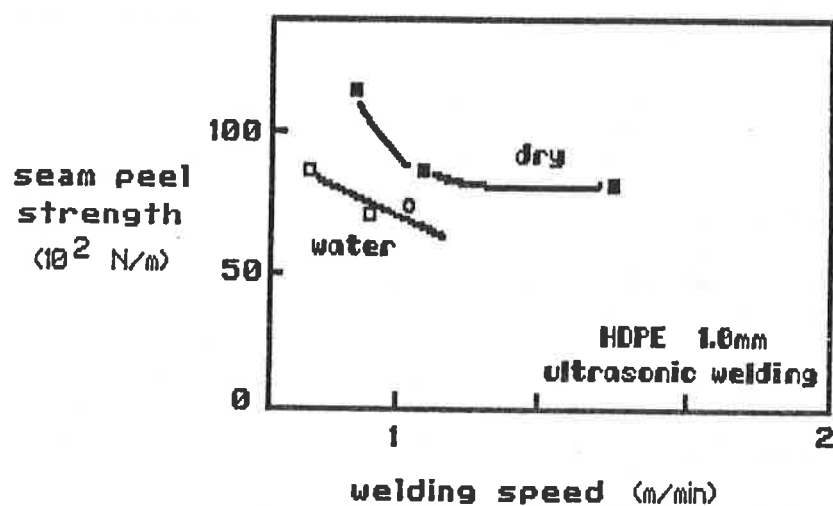


FIGURE 3. INFLUENCE OF MOISTURE ON SEAM QUALITY.

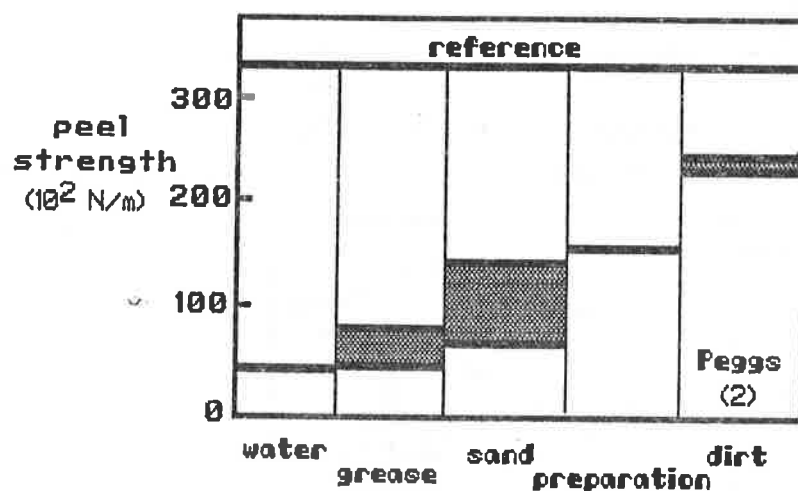


FIGURE 4. INFLUENCE OF SURFACE CONTAMINANTS ON SEAM QUALITY.

Ambient Temperature

On account of the varying ambient temperature and solar exposure, the HDPE sheet temperature fluctuates constantly during installation, hovering often as high as 20 °C above the indicated ambient temperature. At the other end of the spectrum, geomembranes installed in nordic climates may have been placed on a cold if not frozen subgrade at which point ambient temperature might contrastingly even be higher than that of the geomembrane sheets. As an example of the influence of the ambient temperature, experimental results for 20 °C and 8 °C as obtained during the evaluation of the ultrasonic prototype are presented in Figure 5. Field welds performed at 20 °C showed greater peel strength than the ones performed at 8 °C. The influence of ambient temperature may also be observed on Figure 6, whereby reported data is added onto previously published information by Peggs (2). It is then highly recommended to monitor the sheet's temperature in addition to the ambient conditions, and that welding parameters be adjusted consequently.

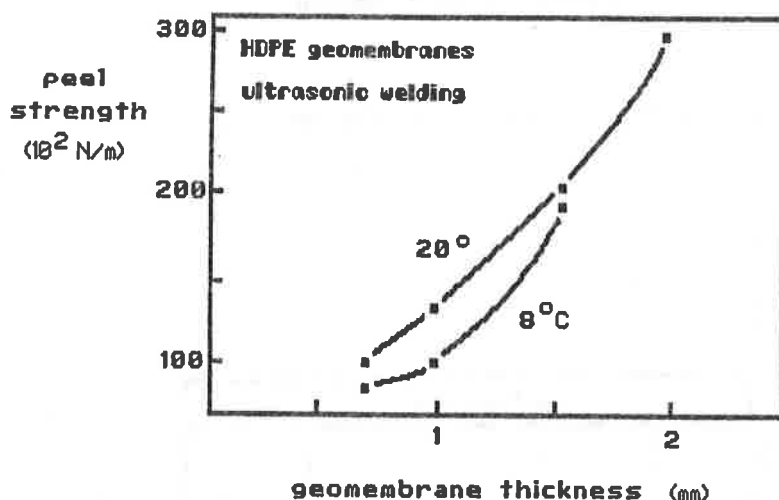


FIGURE 5. INFLUENCE OF AMBIENT TEMPERATURE ON SEAM QUALITY.

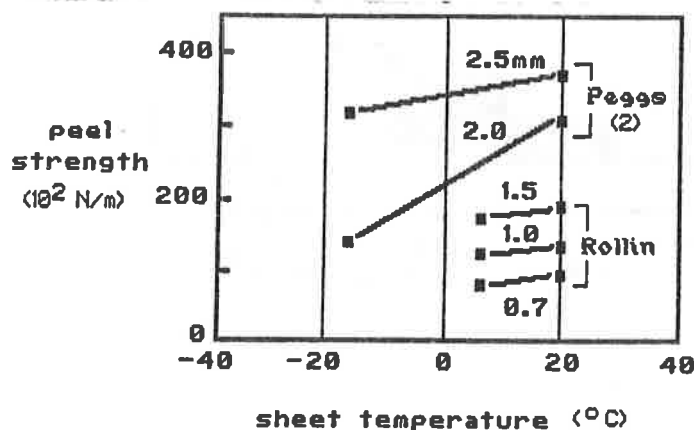


FIGURE 6. INFLUENCE OF SHEET'S TEMPERATURE ON SEAM QUALITY.

Welding Speed

Maximum welding speed is defined as the highest speed attained while yielding acceptable peel strengths without any visual material deformation. Regardless of the type of welding equipment used, this maximum speed may only be reached following optimal equipment calibration and rarely exceeds 3 m/min for HDPE geomembranes. As a comparison, factory seaming under controlled and ideal conditions was monitored for a process known as overlap extrusion. The thickness of the material was 1 mm, corresponding to a thin gauge HDPE geomembrane by standards which theoretically requires minimal energy while enabling high welding speeds. As shown on Figure 7, the corresponding maximum welding speed was determined at 2.5 m/min, all higher speeds deemed unacceptable. This data is presented in order to perceive the relatively low speeds of existing welding equipments.

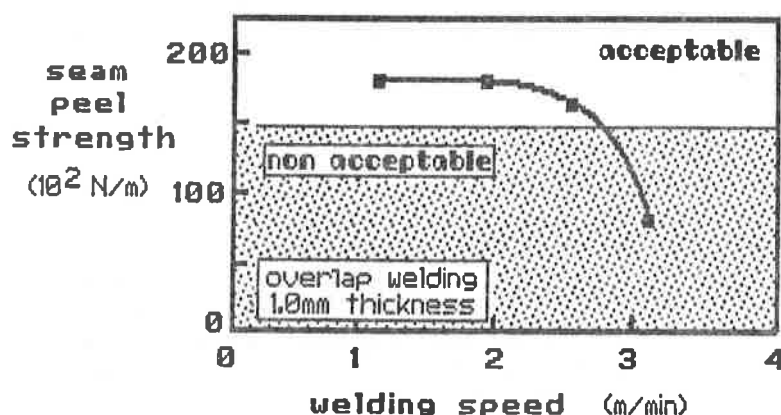


FIGURE 7. INFLUENCE OF WELDING SPEED ON SEAM QUALITY.

Preheating

Preheating certainly constitutes a beneficial procedure since it raises the sheet's temperature in order to minimize the sudden thermal gradient, when for example the hot extruded polymer comes in contact with the ambient sheets. A typical preheated overlap extrusion welding process is presented in Figure 8. It can be observed that acceptable peel strengths were obtained for preheating temperatures ranging from 80 C to 120 C while weaker seams were produced at both higher and lower pre-heating temperatures.

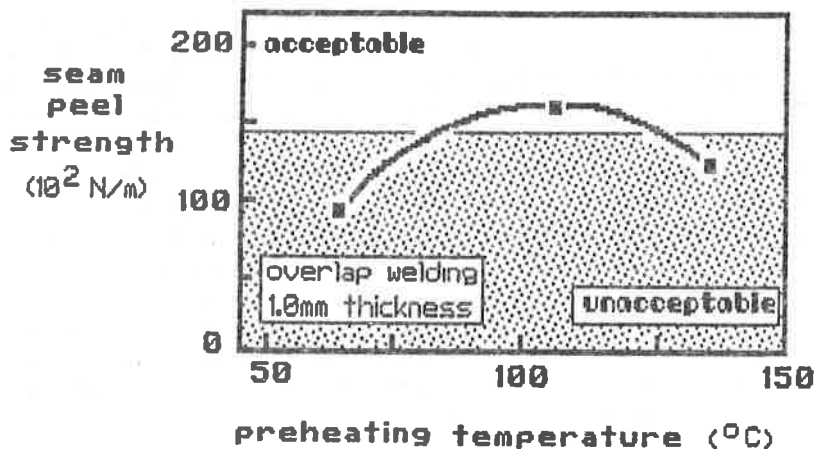


FIGURE 8. INFLUENCE OF PREHEATING ON SEAM QUALITY.

Die Temperature

Temperature of the extruded polymer must also be closely and adequately monitored when using an extrusion process. As all other welding parameters studied, an optimal value is also reached for each specific HDPE formulation. As illustrated in Figure 9, die temperatures lower than 230°C did not transfer the required amount of energy whereas higher temperatures rendered the extruded polymer unworkable from its loss of consistency.

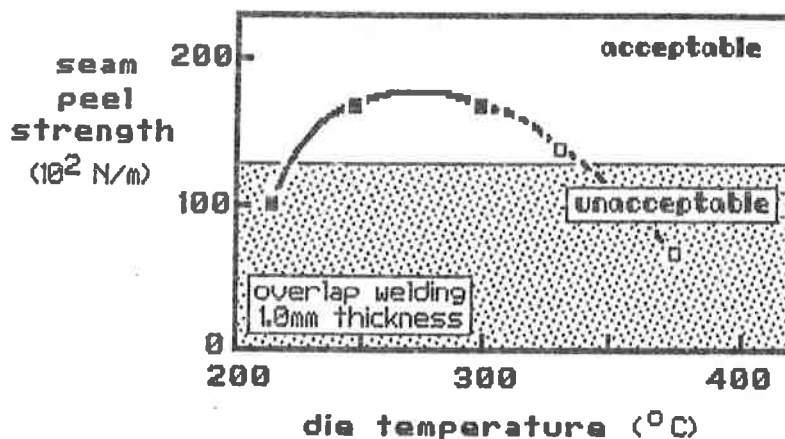
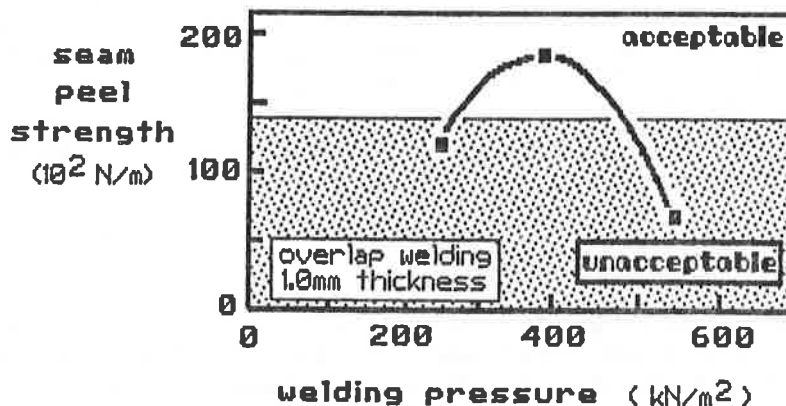


FIGURE 9. INFLUENCE OF DIE TEMPERATURE ON SEAM QUALITY.

Pressure

Many welding techniques require the application of pressure onto the molten polymer immediately following the heating process. This procedure is usually performed using parallel pressure rollers. The value of this applied pressure varies in accordance with the seam's thickness, polymer properties and prevalent field conditions. As an example, experimental results are presented on Figure 10, where peel strengths are plotted against welding pressures during a factory overlap extrusion process. Once again an optimal welding pressure was identified, whereby unacceptable seams were obtained for both higher and lower pressure ratings. Subsequent microanalysis of cross sections revealed high stress structural modifications for samples welded at high pressures. It is also believed that both the rate of cooling and the duration of the applied pressure are important parameters. Furthermore, experimental data indicated that proper pressure roller alignment is required in order to avoid unbonded areas.



Typical welding curve
for HDPE 40 mils

FIGURE 10. INFLUENCE OF WELDING PRESSURE ON SEAM QUALITY.

COMMENTS ON THE CUSTOMARY DESTRUCTIVE TEST METHODS

Shear

The customary industry-standard HDPE seam shear requirement, designated as "Bonded Seam Strength", is referenced to the National Sanitation Foundation's Standard Number 54 "Flexible Membrane Liners". This dynamic destructive requirement is actually a modified version of the ASTM D3083 standard specification, specifically designated as "Standard Specification for Flexible Poly (Vinyl Chloride) Plastic Sheeting for Pond, Canal and Reservoir Lining", and specifically addressed for thicknesses between 0.20 mm and 0.76 mm (8 to 30 mil). This requirement is associated with the simulation of field performance under tensile stresses induced by mechanical agents and thermal contractions, and requires an acceptable sample to fail beyond the seam area, under a specified minimum tension value. This minimum value varies between 75 and 90% of the specified tensile strength value at yield of the base material as determined by the ASTM D638 standard test method "Tensile Properties of Plastics". It is worthy of comments to underline that obviously, both of those ASTM references were not specifically developed for this intended use. Closer examination also reveals discrepancies between sample preparation and overall testing methodology which again triggers cautionary advice while interpreting test results for design or quality control purposes, see Peggs (1) and Rollin (4).

Peel Test

The customary industry-standard HDPE seam peel requirement, designated as "Bonded Seam Strength", is also referenced to the National Sanitation Foundation's Standard Number 54 "Flexible Membrane Liners". This dynamic destructive requirement is actually a modified version of the ASTM D413 standard test method specifically designated as "Standard Test Methods for Rubber Property - Adhesion to Flexible Substrate". Its only requirement for an acceptable sample is to fail beyond the seam area, commonly referred to as the "Film Tear Bond" criterion. But as suggested by Peggs (3), the additional use of a peel strength acceptance requirement coefficient as defined by the ratio of the peel strength at break point to the tensile strength at yield of the base material certainly constitutes a welcomed improvement. This coefficient's minimal requirement is usually set at 0.70. Nevertheless, and for previously mentioned reasons, caution is still advised when interpreting test results.

Recent studies on the determination of seam resistance to both shear and peel stresses have indicated that peel testing evaluates seam quality more adequately than shear test methods (Peggs (1) and Rollin (4)). These methods nevertheless constitute indirect methods of assessing seam quality. In addition, minimal information is obtained concerning the actual mechanisms of failure which is obviously required in order to prevent recurrences. Unless scientific analyses are performed and utilized, quality assurance boils down to a hit and miss solitaire, abysmally unreliable statistically.

MICROSCOPIC ANALYSIS

Microscopic analysis of seam cross sections constitutes a direct observational method as opposed to customary indirect test procedures. It is used to characterize structural anomalies such as micro cracks and unbonded areas unheard of from traditional dynamic test methods, in an effort to recommend proper welding guidelines and insure long term performance of the seams. It may be performed using optical or scanning microscopes.

Optical Microscopic Analysis

The examination of cross sections of welded HDPE geomembranes using an optical microscope may be performed on microtome specimen slices. A more innovative method of sample preparation obviates to the precision and time required for traditional microtome specimen, whereby samples obtained from simple die cuts are directly put under observation. Optical fibers are then used to carry light unto the black HDPE specimen. Using minimum resolution (100-200 nm) and magnifications of up to 2000X, cross sections may be observed and photographed. As shown in Figure 11, a cross section of a seam performed by ultrasonic field welding equipment, reveals unbonded areas, flow patterns of molten polymer, micro cracks and air channels. What is utterly surprising about this particular example, is the fact that this sample actually met both peel and shear requirements namely on account of the thin properly bonded area located at the very edge of the seam. The amount of observations gathered from this single photograph, enabled the researchers to present pragmatic recommendations to the grateful welding operator.

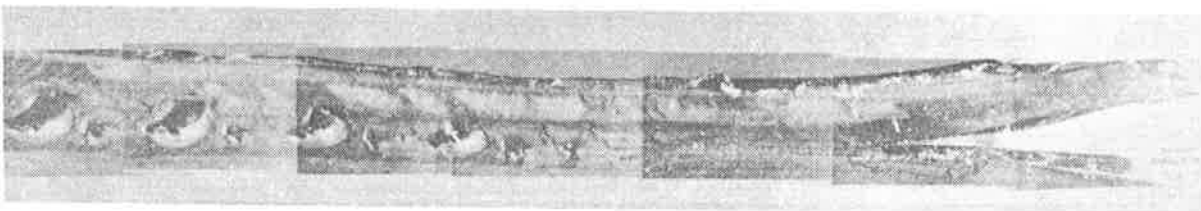


FIGURE 11. OPTICAL MICROPHOTOGRAPH OF AN HDPE WELD.

Although both macrographic and micrographic examinations may easily be performed with optical magnification, it is less applicable to microfractography on account of limited resolution and depth of field. A scanning electron microscope is thus recommended for such analyses.

Scanning Electron Microscopic Analysis

The scanning electron microscope certainly constitutes one of the most powerful and versatile instrument for analysing microstructures. Its minimum resolution ranges between 4 nm and 5 nm, and its useful magnification reaches up to 60000X. In order to demonstrate the usefulness and applicability of the technique to HDPE seam analysis, Figure 12 is presented where microcracks have developed following a clearly identifiable pattern. Amazingly this specimen was once again declared acceptable following customary test methods. Analysis of the cracks' characteristics and particularly their propagation mode provided information on the originating factors and enabled the issuance of preventive procedures.

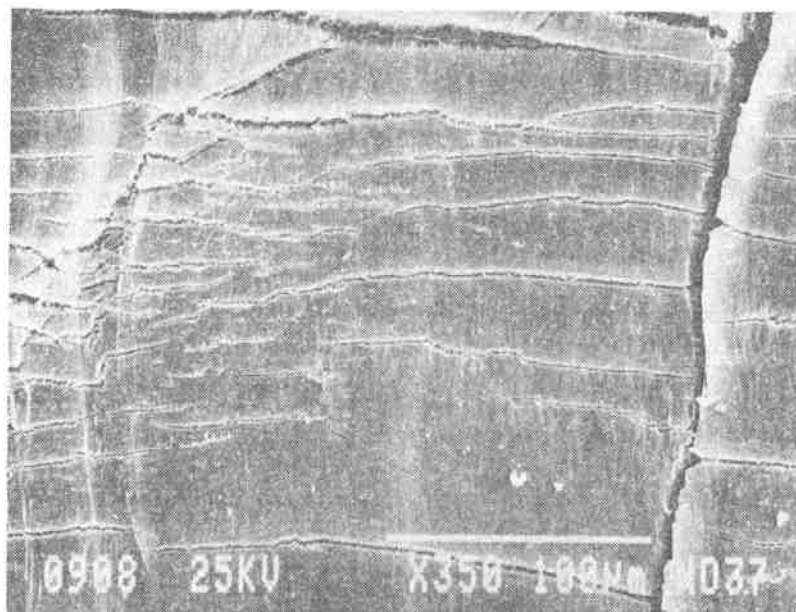


FIGURE 12. SCANNING ELECTRON MICROPHOTOGRAPH OF AN HDPE WELD.

CONCLUSION

All reviewed welding methods can successfully perform acceptable seams under both normal accomodating field conditions and customary testing procedures. The reliability of seam quality is directly proportional to the accuracy and efficiency of the methods used to calibrate the welding equipments and to enable rapid adjustments as required by the varying influential welding parameters. To this effect, significant improvements are needed from an execution and quality control point of view. This recommendation is furthermore corroborated by the evident reality of the narrowness of most welding equipment's operating windows whereby slight welding parameter deviations often induce unacceptable seams.

Data obtained from customary industry-standard shear and peel test methods should be used with caution since in many cases supplemental microscopic analyses will reveal previously undetected structural deficiencies liable to shorten the life expectancy of welds. Furthermore, on account on the direct observational nature of microscopic analyses, pragmatic recommendations may be formulated in order to prevent the recurrence of identified structural flaws. It thus becomes highly advisable to consider enhancing quality assurance programs with such microscopic analyses.

REFERENCES

- (1) Peggs, I.D. and Little, D., "The effectiveness of Peel and Shear Tests in Evaluating HDPE Geomembrane Seams", Proceedings of the Second Canadian Symposium on Geotextiles and Geomembranes, Edmonton, Canada, 1985, p.p. 141-146.
- (2) Peggs, I.D. and Rose, S., "Practical Aspects of Polyethylene Geomembrane Seam Welding", Geotechnical Fabrics Report, January 1987, p.p. 12-16.
- (3) Peggs, I.D., "Evaluating Polyethylene Geomembrane Seams", Proceedings of the Geosynthetics '87 Conference, New Orleans, USA, February 1987, p.p. 505-518.
- (4) Rollin, A.L., "Evaluating Field Polyethylene Geomembrane Seams", RILEM, Montréal, Qc, Canada, June 1988.

G.T. DARILEK

D.L. LAINE

J.O. PARRA

Southwest Research Institute, U.S.A.

The Electrical Leak Location Method for Geomembrane Liners: Development and Applications

SUMMARY

A new electrical technique has been developed to accurately locate leaks in geomembrane liners. The electrical technique takes advantage of the insulating properties of the geomembrane liner material. When no leaks are present, a voltage impressed between electrically conductive media above and below the liner produces a relatively uniform electrical potential distribution in the material above the liner. If the liner is physically punctured or separated, an electrical current path is established. Leaks in the geomembrane are located by measuring potential gradients near the surface of the liner to detect areas of high current density caused by current flowing through leaks in the liner.

A mathematical analysis of conductive media above and below an insulating liner with a leak was developed to characterize the three-dimensional response of single and multiple leaks. A computer simulation model was developed to evaluate the technique and to efficiently predict the effect of a wide range of parameters on the leak signature.

Tests on a double-lined physical model demonstrated the applicability of the method to a variety of drainage layers with various test parameters such as leak size, electrode depth, and protective cover soil. Leaks with a diameter of 0.8 mm and greater in the primary liner were reliably located to within 10 mm. When the top liner is in place, leaks in the bottom liner can be detected, but not located.

The electrical leak location method was adapted for locating leaks in geomembrane liners with protective soil covers. Scale model tests demonstrated the applicability of the method under a wide range of cover soil thicknesses and leak sizes. Non-polarizing electrodes were used to locate leaks with diameters of 3 mm and greater under 600 mm of cover soil.

Leak location instrumentation and techniques were developed to perform geomembrane leak location surveys for preservice inspection of water-filled impoundments and landfills and non-hazardous liquid-filled impoundments. The manual survey system consists of a lightweight man-portable electrical probe and associated instrumentation. Horizontal traverse lines are scanned with a coverage of 2 m on each side of the traverse line. Surveys of the side slopes are accomplished using a probe with a long handle and small wheels to support the electrodes. Leaks are accurately located to within 10 mm or less and marked with lead sinkers and floats.

These techniques have proven to be very effective for finding leaks, including many leaks that had not been previously found with conventional methods. Twenty-eight new or in-service geomembrane lined waste storage facilities were surveyed for leaks using this equipment. On average, 26 leaks per 10,000 square meters of surveyed area were found. Although most of the leaks were located in field seams, a significant number occurred in the parent material.

The electrical leak location method was used to locate leaks in a geomembrane liner with a 250-mm-thick soil protective cover. Three leaks were found. Two of these leaks were located in seams and were too small to be visually detected when the soil cover was removed. The third leak was a 40-mm tear in the liner material.

INTRODUCTION

The most common method of solid and hazardous waste disposal is in landfills and surface impoundments. To prevent contamination, geomembrane liner systems are installed beneath the landfill or impoundment to form an impermeable barrier that prevents the migration of contaminant liquids. Installation practices and operational factors can result in puncture leaks and separated seam leaks. The electrical leak location method was developed to effectively locate leaks in geomembrane liners to ensure that liners have been installed and seamed properly and that no damage has occurred.

TECHNICAL DISCUSSION

Method

Figure 1 shows the basic electrical leak location method for locating leaks in a geomembrane liner. The leak location method makes use of the high electrical resistivity of the geomembrane liner material. When no leaks are present, a voltage impressed across the liner produces a relatively uniform voltage potential distribution in the material above the liner. If the liner is physically punctured or separated, conductive fluid flows through the leak establishing a conductive path for current flow, which produces an anomaly in the measured potential in the vicinity of the leak. Therefore, leaks can be located by measuring the potential distribution patterns in the material covering the liner.

Computer Simulation Model

A computer model was developed to investigate the performance capabilities of the electrical leak location method. The model accommodated various electrical and dimensional parameters in the three layers comprising a lined impoundment or landfill. The electrical anomaly of a circular hole in a thin, highly resistive layer was used to model the response of a geomembrane lined impoundment or landfill containing a damaged geomembrane liner. The excellent agreement between experimental and synthetic model data verified the accuracy of the general solution for predicting leak signatures.

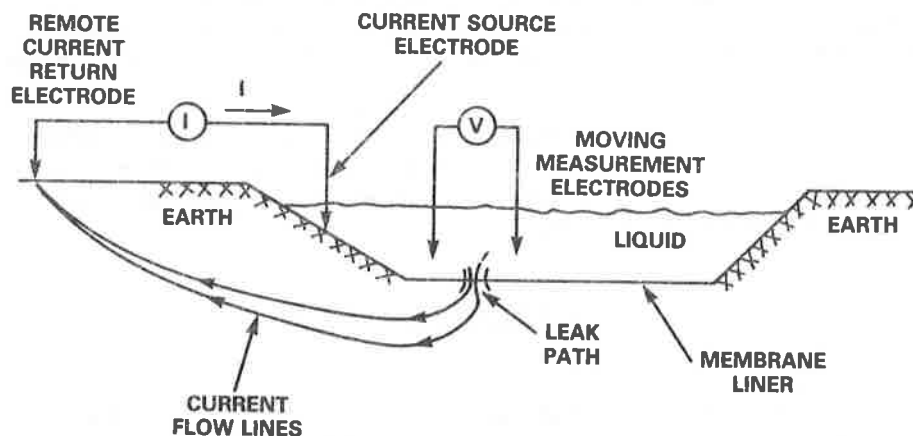


FIGURE 1. DIAGRAM OF THE ELECTRICAL LEAK LOCATION METHOD

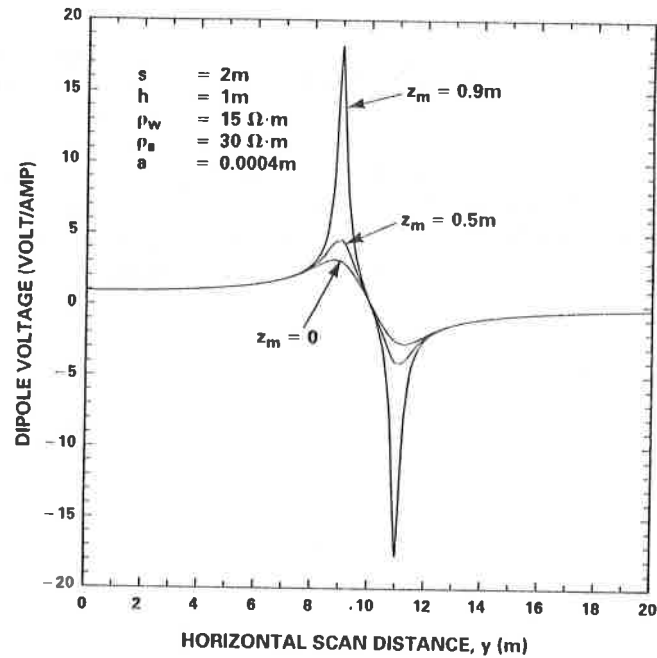
Model studies of the electrical leak location survey technique were conducted to characterize the performance of the method with various electrical parameters of the waste materials, the measurement electrode array geometry, the measurement dipole depth and proximity to the leak, and the size and number of leaks. Figure 2 shows a typical family of leak anomaly responses illustrating the effects of various measurement depths for a single leak. The leak position is indicated at the midpoint between the positive and negative peaks. A substantial improvement in detection sensitivity is obtained when the potential array is scanned closer to the leak.

Figure 3 shows the vertical dipole anomaly response of a leak. The leak is located at the position indicated by the maximum response. For practical reasons, leaks can be more easily and accurately located with a vertical dipole because the leak is located at the peak of the unipolar response rather than the bipolar anomaly with the horizontal dipole. Multiple leaks can be resolved with less ambiguity when a vertical dipole is used.

The derived geomembrane leak location model can be used to aid in planning surveys and in analyzing leak survey data acquired in lined impoundments or landfills. The computed leak responses point out the practical importance of performing survey measurements near the geomembrane liner. The injected current must be increased to offset the effect of lower measured leak anomaly attributed to lower resistivity of the liquid.

Double Liner Model Tests

By placing the current return electrode in electrical contact with the liquid-saturated drainage layer located between the two liners, the electrical leak location method can be used to locate leaks in the upper liner. Simple electrical continuity tests between the drainage layer and the earth also can determine the existence of leaks in the bottom liner but not their location.



Key: s = electrode spacing s = underlying soil resistivity x = offset distance
 h = depth of the water a = leak radius y = distance along scan line
 w = liquid resistivity z_m = electrode depth

FIGURE 2. PLOT OF THE LEAK ANOMALY VERSUS HORIZONTAL ELECTRODE DEPTH

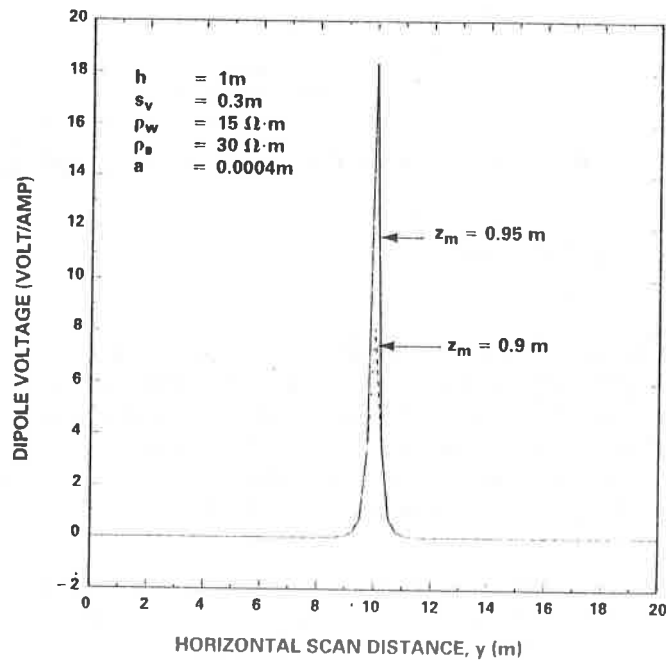


FIGURE 3. LEAK ANOMALY CHARACTERISTIC FOR VERTICAL DIPOLE ELECTRODES

A scale model with dimensions of 3 m x 3 m was used to evaluate the electrical leak location method for locating leaks in double liner installations. Physical model studies were conducted to evaluate the effects of various impoundment and landfill configurations, including different types of drainage layers, various types of leaks, and a protective soil cover over the primary liner. Figure 4 is a contour plot of the data for a leak with a diameter of 5 mm and a drainage layer consisting of a sandy loam soil layer placed over geotextile mat, which is then placed over the geonet material. The location of the leak is clearly indicated by the dipolar contour pattern. The potential gradient pattern caused by the current injection electrode is also evident in the data. Similar potential gradient patterns were obtained for the other conditions evaluated. The larger leaks required less voltage to produce the same anomaly amplitude.

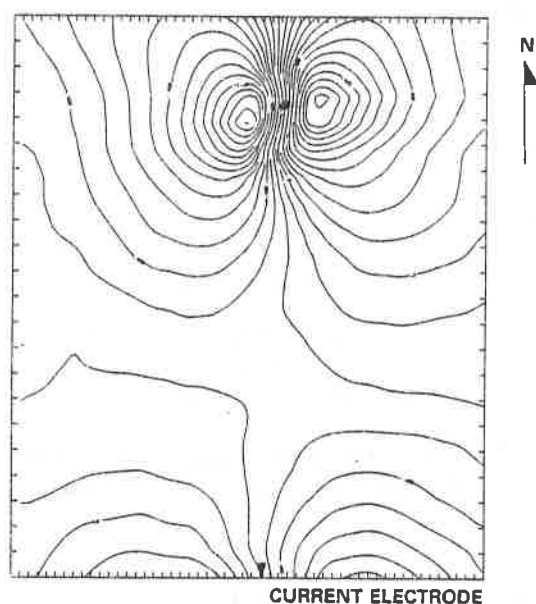


FIGURE 4. CONTOUR PLOT OF TYPICAL DOUBLE LINER MODEL DATA

Locating Leaks in Soil-Covered Geomembranes

The electrical leak location method was modified to make surface soil potential measurements to locate leaks in geomembranes covered by a protective or cap soil layer. Potential measurements were made using half-cell electrodes to reduce the polarization noise caused by electrochemical reactions at the interface between the soil and metal electrodes. A half-cell electrode typically consists of a plastic tube with a porous ceramic tip. Electrical contact is made through a metal electrode in a saturated salt solution in the half-cell.

Experiments were conducted using a physical model with dimensions of 5 m x 5 m to evaluate the method for locating leaks in geomembrane liners covered with soil. Figure 5 is a plot of the measured leak anomaly for several soil cover thicknesses. Although the peak-to-peak amplitude of the anomaly decreases rapidly with increasing soil cover, the leak was detected easily for all of the soil cover depths tested. Tests were performed to show that electrode contact noise is

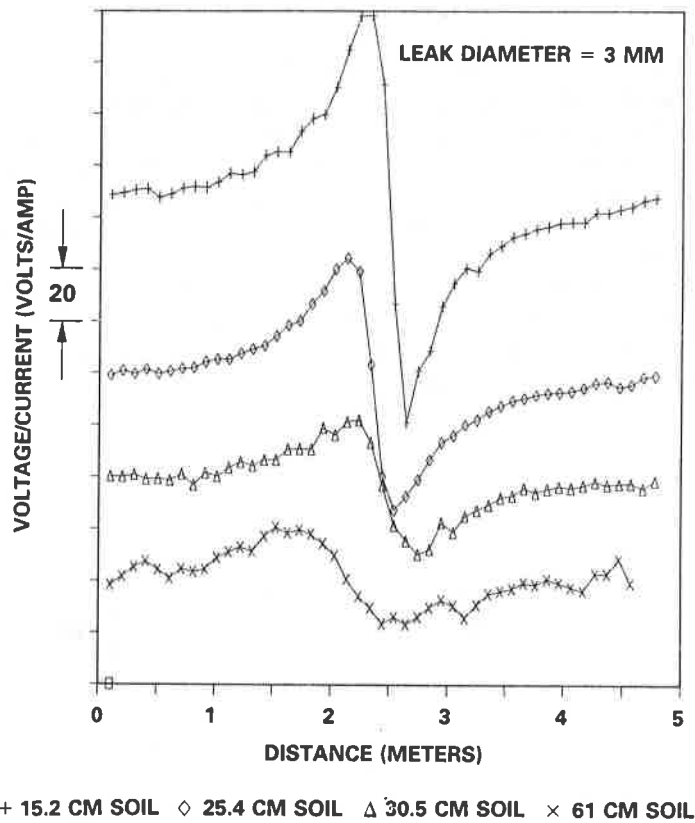


FIGURE 5. MEASURED LEAK ANOMALY FOR VARIOUS SOIL COVER THICKNESSES

reduced significantly when the electrodes are inserted in the ground to a depth of approximately 25 mm or when the dry ground surface is scraped off prior to the measurements.

Field Verification Survey

A full-scale survey at the Southwest Research Institute test impoundment was performed to locate four small circular leaks, each 0.8 mm in diameter. The impoundment was filled with water to a depth of approximately 450 mm, and the measurement electrodes were immersed at a depth of 300 mm. The contour plot of the data, shown in Figure 6, graphically indicates the locations of the four leaks.

Instrumentation and Survey Procedures

Several practical advances in the leak location instrumentation and techniques were made to make them much easier to apply for geomembrane leak location surveys. The manual survey



FIGURE 7. MANUAL LEAK LOCATION EQUIPMENT CONSISTING OF AN ELECTRODE PROBE AND ELECTRONICS UNIT

Because the electrical leak location method detects electrical conduction paths, other conduction paths caused by piping, piers, fasteners, and battens must be isolated for best results. With certain preparations, such as using rubber packers in the inlet and discharge pipes, most geomembrane-lined impoundments and landfills can be surveyed for leaks using the electrical method. The electrical leak location method can be applied most effectively and economically if the impoundment or landfill is designed such that electrical conduction paths between the liquid and the earth ground are eliminated or can be insulated.

Results of Leak Location Surveys

Twenty-eight geomembrane lined storage facilities have been surveyed for leaks using the manual leak location equipment. The total liner area surveyed was more than 200,000 square meters. The size of these installations ranged from less than 100 square meters to more than 50,000 square meters and included both double- and single-lined impoundments and landfills. Four of the liners were in steel tanks. Six of the liners were in concrete tanks, two of which had covers. The remainder of the liners were in earthen excavations. All of the liners except two were in new installations. One liner was constructed of chlorosulfonated polyethylene (CSPE), four were of polyvinyl chloride (PVC), and the remainder were of high density polyethylene (HDPE). Leak location surveys were initiated in response to a known leakage problem at four-teen of the installations. The other fourteen liners were surveyed as a construction quality assurance measure.

Geosynthetics '89 Conference
San Diego, USA

Table 1 lists the leak statistics for the surveys. Leaks were found at all of the sites except for two with small liners. The average density of leaks was 26 leaks per 10,000 square meters. Although most of the leaks occurred in field seams, a significant number were found in the parent material. At the facilities where documentation was possible, 18 percent of the leaks were in the parent material.

TABLE 1. RESULTS OF LEAK LOCATION SURVEYS

Liner Number	Size (Sq. M)	Total Leaks	Seam Leaks	Material Leaks	Bottom Leaks	Side Leaks	Leaks/10K Sq. M	QA or Problem
1	54330	79	61	18	54	25	14.5	Q
2	33695	51	37	14			15.1	Q
3	6073	6	6	0			9.9	Q
4	6073	5	3	2			8.2	Q
5	6073	7	5	2			11.5	Q
6	14008	64	46	18			45.7	Q
7	14640	12	10	2			8.2	P
8	3904	14			7	7	35.9	P
9	15244	18					11.8	P
10	651	4	4	0			61.4	P
11	2536	8	6	2			31.5	Q
12	5112	12	12	0			23.5	Q
13	2417	4	4	0			16.5	Q
14	2417	7	7	0			29.0	Q
15	460	17	17	0			369.6	P
16	460	0	0	0			0.0	P
17	460	2	2	0			43.5	P
18	9202	18					19.6	P
19	167	0					0.0	P
20	89	2					224.7	P
21	89	3					337.1	P
22	89	3					337.1	P
23	3067	63	60	3			205.4	Q
24	5051	58	45	13			114.8	Q
25	5051	11	11	0			21.8	Q
26	6883	20	19	1			29.1	P
27	6000	29	21	8			48.3	P
28	3000	25					83.3	P
TOTALS	207241	542	376	83	61	32		

Leaks per 10,000 Square Meters - 26.2

Leaks per 10,000 Square Meters for Liners Larger than 500 Square Meters - 25.1

For the installations where the sidewalls were surveyed, 34 percent of the leaks were in the sidewalls. For these installations, the density of the leaks was approximately 16 leaks per 10,000 square meters for the bottom, and approximately 12 leaks per 10,000 square meters for the sidewalls.

Figure 8 is a histogram of the distribution of the number of leaks found in liners that were larger than 500 square meters. Because of the small area involved, liners smaller than 500 square meters typically had either zero leaks or more than 200 leaks per 10,000 square meters. Therefore, the small liners were not included in the histogram. The least number of leaks found in the liners greater than 500 square meters was 8.2 per 10,000 square meters. From this data, typical installations had from 10 to 30 leaks per 10,000 square meters. Installation and field seaming problems were experienced on the liners with greater than 45 leaks per 10,000 square meters.

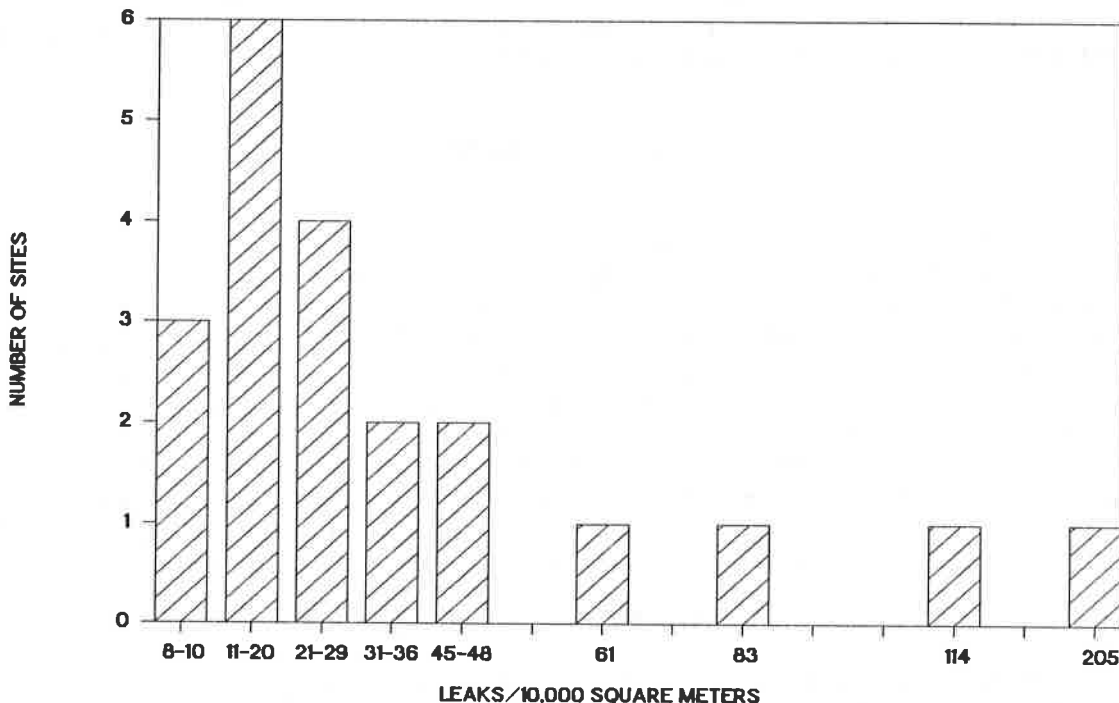


FIGURE 8. HISTOGRAM OF THE NUMBER OF LEAKS FOUND

Because some leak location surveys were initiated in response to a known leakage problem, a significantly higher number of leaks might be expected for these installations. However, this has not proven to be the case. The density of leaks at the 14 installations with a known leak problem had 27.2 leaks per 10,000 square meters. The density of leaks in the installations where the leak location surveys were performed for construction quality assurance was 25.7 leaks per 10,000 square meters. The comparable leak densities are particularly surprising considering that the installer might be expected to be particularly careful and thorough when a third party leak location survey will be performed.

These techniques have proven to be very effective in finding leaks, including many leaks that had not been previously found with conventional inspection techniques. Many of the leaks were not detectable using visual inspection.

Leak Location Surveys with Protective Soil Cover

Because of the possibility of damaging the geomembrane liner in the process of emplacing a protective soil cover over the liner, a leak location survey of the soil-covered liner is an effective method of ensuring that such leaks are found. A geomembrane liner with a 250-mm-thick soil protective cover at a landfill with an area of approximately 1500 square meters was surveyed using the special adaptations to the electrical leak location method. Three leaks were found. Two of these leaks were located in seams and were too small to be visually detected when the soil cover was removed. The presence of these leaks was verified using an electrical continuity test. The third leak was a 40-mm tear in the liner material.

CONCLUSIONS

An electrical method for locating leaks in geomembrane liners for hazardous waste impoundments and landfills has been developed and demonstrated successfully in a wide variety of applications. The validity and usefulness of the electrical leak location method has been demonstrated for testing the integrity of the geomembrane for single and double liners with and without protective soil cover systems. The technique is used for construction quality assurance and in-service performance monitoring. The electrical leak location method can be used in liquid impoundments, as a preservice inspection of solid waste landfills, and to locate leaks in the final cover for landfills or impoundments. The method will not damage the liner. The results of the surveys on full-scale installations lead to the speculation that all geomembrane-lined impoundments and landfills have leaks and should be subjected to an effective preservice electrical leak location survey before the installation is considered complete and ready for use.

ACKNOWLEDGMENT

This work has been funded in part by the United States Environmental Protection Agency under assistance agreement CR-811771 to Southwest Research Institute.

R.E. LANDRETH

U.S. Environmental Protection Agency, U.S.A.

Locating And Repairing Leaks In Landfill/Impoundment Flexible Membrane Liners

INTRODUCTION

In the United States, the large quantities of solid and hazardous wastes generated each year are commonly disposed of in landfills and surface impoundments. Because the liquids (leachates) in surface impoundments and landfills are frequently toxic, nearby surface water, groundwater, and soil must be protected.

Geomembrane liners (flexible membrane liners, FML's) are often used to form an impermeable barrier to prevent migration of contaminant liquids to nearby soil and water. The factory-fabricated sheets of polymeric materials are seamed together at a field site to form a continuous barrier between the landfill/impoundment (L/I) waste and the surrounding environment. As a pollution barrier this FML must be sound and without defect. While the FML is being installed or while the L/I is being operated, however, the FML can be punctured or seams can separate.

An effective method was needed not only to locate leaks in FML's before waste materials are introduced but to isolate leaks for subsequent repair in operating L/I's. The United States Environmental Protection Agency (EPA), recognizing the enormity and the implications of this problem, undertook a research program to determine where the leaks were, how to get to the leak, and how to repair the leak.

LOCATING THE LEAKS

The Agency established three major objectives to identify where, within a landfill or surface impoundment, the leak was actually occurring. The objectives were (1) to develop a nondestructive technique capable of locating the leak within a 1-square-foot area, and (2) develop the ability to detect leaks at existing facilities and in planned facilities. Two research projects were selected to pursue these objectives.

The first project¹ surveyed 28 geophysical techniques; 20 of these were identified as having potential as leak detection techniques. As expected, no single technique proved applicable to all situations. From this study, two techniques were thought to have sufficient potential for additional study: the time-domain reflectometry (TDR) and acoustic emission monitoring. The subject of the second project was an electrical resistivity technique believed to hold high promise to meet the stated objectives.

Acoustic Emission Monitoring

Acoustic emission monitoring techniques have been used for over 50 years to evaluate stresses in rocks and metals. Its application has more recently been extended to monitor fluid flow through soils. Normally, fluid passing through soils is not turbulent, but it can be if there is a sufficient head or potential, as might be expected in a surface impoundment.

Laboratory experiments were conducted² to determine characteristics of the sounds that are produced when liquids flow through soils at different rates, the spectral characteristics of the equipment, and the attenuation of these sounds over the frequency spectrum observed for the laboratory experiments.

The acoustic emission monitoring techniques showed that acoustic sounds, at frequencies up to 500 Hz, are emitted at turbulent flow rates of 0.3 to 1 cm/sec through sand and pea gravel. The amplitude of the acoustic sounds is 100 times greater than that of the ambient background noise level that may exist at a surface impoundment. It was also determined that at a frequency of 450 Hz, the acoustic sounds have an attenuation of 0.5 dB/m at a depth of 1 meter in an impoundment. These data suggested the potential of locating a leak with a flow rate of 1 cm/sec at a range of 3 meters from the leak.

Field tests were performed in a 1-acre impoundment that had known man-made leaks. However, the field results were less encouraging. The sound attenuation within the impoundment was found to be greater than that reported in the literature, and there were insufficient background-to-water-flowing-noise ratios to efficiently determine leak location. Although recommendations for improvement were made, it was decided not to develop this technique further.

Time-Domain Reflectometry

TDR is less well known and a more recent technique than is acoustic emission. TDR combines a wide-frequency band with a short-pulse-length measurement technique that is sensitive to the high frequency (10^6 to 10^9 Hz) electrical properties of the materials in and around the conductors of a parallel transmission line.

This potential technique requires that parallel wires be placed under the liner. The technique then detects moisture between the wires, unlike other systems where the wires have to corrode. TDR laboratory experiments showed that a leak with dimensions equal to or greater than half the spacing between the parallel transmission line conductors can be detected. Only 2-m conductor spacing was tested, but larger spacings were thought feasible.

Field testing of the TDR techniques was also made on a 1-acre impoundment (the same impoundment as the acoustical emission technique). For the type of equipment used, the length of the transmission lines, the spacing of the lines, and the soil used, the system worked as predicted.

Although recommendations were made on how to improve the electrical instrumentation and build a total system, it was decided not to pursue additional development of this technique, because (1) this system required the installation of transmission lines before placement of the FML, (2) the long-term durability of the system was questionable, and (3) excellent results were being obtained using the electrical leak location method.

Electrical Leak Location

A third technique,^{3,4} undertaken by separate contract, was the electrical leak location (ELL) method. This method adapts electrical geophysical analysis techniques to leak location and assessment of damaged FML's. The ELL method makes use of the high electrical resistivity of FML material. In a lined L/I, the current flows through the waste material, the liner, and the leaks to return to the current electrode in the soil layer (Figure 1). When no leaks are present, a voltage impressed across the liner produces a very low current flow. The low current density produces a relatively uniform voltage potential distribution in the material above the liner. A leak in the FML provides a conductive path for current flow, which produces an increase in the current density at the leak point. Because the localized current density causes an electrical anomaly in the measured potential in the vicinity of the leak, leaks can be located by measuring the potential distribution patterns in the material covering the liner. The ELL method can be used in liquid impoundments or as a pre-service inspection of solid waste landfills. To locate leaks in the final L/I cover, a modified sensor has to be used.

Computer Simulation Model--

Because evaluating electrical survey techniques under a wide range of parameters (such as liquid depth, liquid conductivity, liner resistance, and earth resistivity) is impractical, formulating a computer simulation model to obtain numerical computations that correspond to field installations is a practical alternative. Obtaining these numerical computations before making measurements at in-service L/I's also increases confidence in the measured results.

A theoretical model was developed to include the electrical and dimensional parameters in the three layers comprising a lined L/I as well as the number of leaks and locations of the current source and potential measurement electrodes. To simplify the model, the L/I, the liner, and the soil under the liner were represented as infinite horizontal layers and the liner thickness and the leak size were assumed to be much smaller than the other liner dimensions.

A model was also developed to simulate a landfill cover system. In a landfill cover system, the current flows through the cover material, the liner, and the leaks to return to the current electrode in the soil layer. Because cover systems are generally a few feet deep and many have surface areas of several acres, lateral current flowing across the perimeter of the cover is much smaller than current flowing through the lined bottom and the leaks. Therefore, the total current distribution that returns to the sink current electrode may be assumed to be equal to the currents flowing across the lined bottom of the cover system plus the currents flowing through the leaks.

To demonstrate the validity of the ELL method to predict leak signatures, synthetic signatures were compared with pole-dipole measurements taken at a 1-acre, lined, impoundment test site. The tests were made before the site's use to demonstrate the electrical techniques and to develop field procedures for conducting such tests.

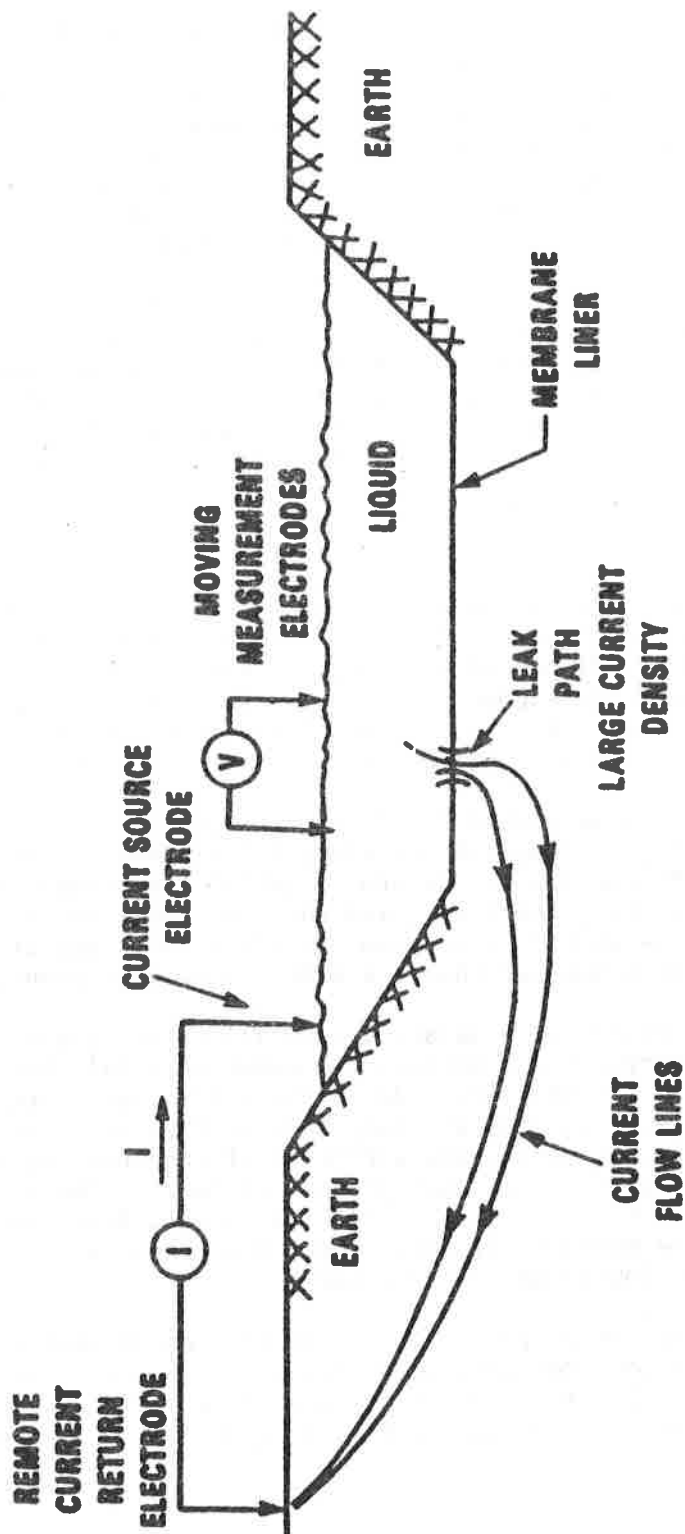


Figure 1. The electrical leak location method locates leaks by detecting the electrical potential anomaly associated with electrical current flowing through a leak.

Experimental results indicated that:

- ° the pole-dipole electrode array is more sensitive to small leaks than is the pole-pole array;
- ° A DC power supply is preferable to an AC supply since the current flow through the capacitive reactance of the liner is eliminated;
- ° the pole-dipole anomaly of a leak in an FML has a characteristic bipolar potential gradient and that detecting such anomalies depends on impoundment depth, leak size, waste material resistivity, underlying soil resistivity, measurement dipole depth and proximity to the leak, source excitation current, etc.;
- ° either horizontal or vertical dipole detectors can be used to acquire field data, but the horizontal dipole response is stronger because of the proximity of the two electrodes to the plane of the liner;
- ° multiple leaks located far apart are more easily detected than are multiple leaks located close together.

With the aid of the present computer model, the subsurface depth as well as the dipole spacing (for resolving the presence and location of multiple leaks) can be specified.

The computed parametric curves can be used to plan optimum electrical surveys for a range of field conditions, depending on FML depth and resistivity of the waste material. The computed leak responses show the importance of taking measurement near the bottom of the L/I to enhance the anomaly.

The excellent agreement between the calculated and the experimental model data establishes the ability of the model to predict leak signatures (Figure 2).

Double-Liner Model Tests--

To meet EPA minimum standards, hazardous waste L/I's must be double lined with FML. The applicability of the ELL method to detect and locate leaks in the upper liner was tested.

With the current return electrode placed in electrical contact with the liquid-saturated drainage layer between the two liners, the double-liner model studies tested:

- ° drainage layers composed of different combinations of geotextile, geonet, and soil;
- ° various sizes of leaks;
- ° a protective soil cover;
- ° various electrode materials;
- ° various electrode shapes.

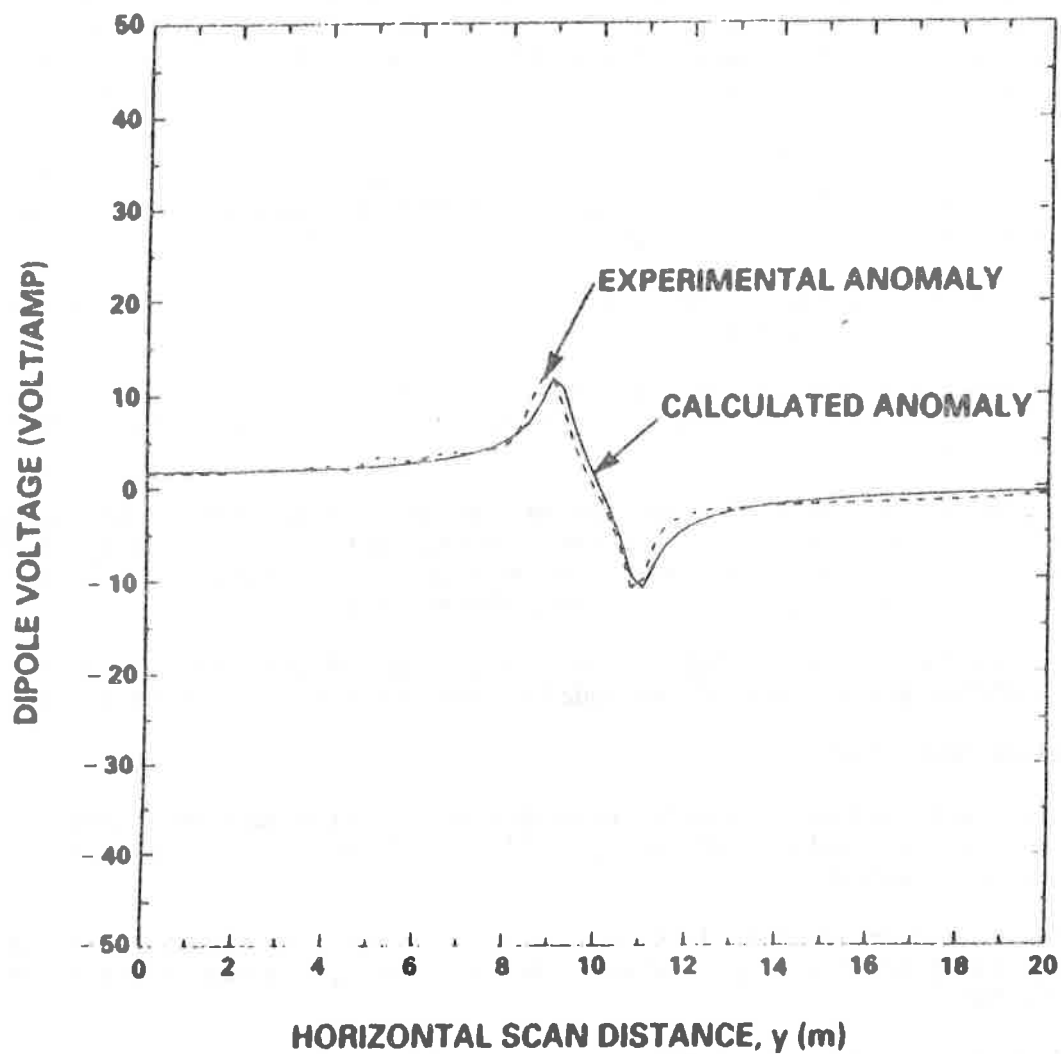


Figure 2. Comparison of experimental leak response and theoretical response predicted for the same field conditions.

To optimally apply the ELL method, there should be an electrically conductive layer between the liners (saturated conditions) that is not grounded to the earth except through the leak and the design of the drainage layer should provide access to place a current return electrode (e.g., through leachate removal system).

The double-lined model experiments successfully demonstrated the usefulness of the ELL method to detect and locate small leaks in L/I's with a wide variety of drainage layer types, leak sizes, and geometries. The method was less sensitive for locating leaks under a protective soil cover immersed in water. Simple electrical continuity tests determined the presence of, but not the location of, leaks in the bottom liner of a double-lined L/I.

The electrode material and geometry affected the sensitivity and probability of locating leaks. Polarization noise was greatly decreased with the use of carbon electrodes; this, in turn, allowed higher gain to be used in the measurement amplifier and, hence, permitted higher sensitivity. Linear electrodes scanning perpendicular to the scan direction were less likely to miss a leak than were localized electrodes.

Locating Leaks in Cover Systems--

FMLs are widely used as part of the final cover system for landfills to prevent rainwater from percolating through the waste and leaching chemicals into groundwater or surface water. A typical cover system consists of a low permeability bottom layer (e.g., a plastic liner over a layer of clay placed over the waste); a middle drainage layer of sand and gravel; and a top layer of soil and vegetation. Because such cover systems are intended for long-term storage of hazardous waste, there is the need to ensure that the cover system performs as intended. The ELL method and several alternatives were investigated to determine their applicability for this purpose.

The accuracy of surface earth potential measurements to locate leaks depends on several factors. The presence of instrument noise, poor electrical contact between the ground and the electrodes (measurement noise), localized inhomogeneities of the surface resistivity (geological noise), electrode polarization noise, and the presence of interfering signals such as electrical power line interference (electrical noise) all serve to decrease accuracy. A half-cell electrode, which reduces polarization noise significantly, was used in the tests.

The ELL method, adapted to make surface soil potential measurements with the use of half-cell electrodes, was well suited for locating leaks in L/I FML's with protective soil covers. Small leaks were located in an FML covered with soil without the need for an overlaying conductive layer of liquid. To reduce electrode contact noise, the electrodes were inserted into the soil to penetrate the dry surface soil. It was determined that surveys can be performed after the protective soil is put in place so that leaks caused by placing the soil can be located.

Liner Resistivity Tests--

The success of the ELL method is influenced by the electrical resistivity of the liner. The liner material must have a substantially greater resistivity than does the soil beneath the liner and the liquid above the liner. Does the

electrical resistance of FML's change after exposure to waste liquids and thereby reduce the usefulness of the survey technique for in-service L/I's?

A series of tests measured electrical resistance changes in selected liner materials over a period of time. Several FML materials were tested: polyvinyl chloride (PVC); high-density polyethylene (HDPE); 0.91-mm chlorosulfonated polyethylene (CSPE); 1.14-mm chlorosulfonated polyethylene (CSPE); and chlorinated polyethylene (CPE). In the tests, four liquids used: alkaline (sodium hydroxide solution, pH 10); acidic (sulfuric acid solution, pH 1); brine (sodium chloride solution 10% by weight NaCl dissolved in deionized water); and deionized water.

The test results indicated the measured resistance values of the FML's were at least two orders of magnitude greater than the resistance needed to use the ELL method. The relatively minor changes in electrical resistivity did not affect use of the method; the trend was for the materials to have a slightly enhanced applicability to the technique.

Throughout the United States, liner materials are exposed to a variety of wastes far exceeding those used in the tests. After long-term exposure to given waste liquids, the specific liner material should be tested to understand how different wastes alter the chemical and electrical properties of liner materials.

Field Demonstration Surveys--

Although previous field tests at a demonstration site had demonstrated the usefulness of the ELL method under full-scale conditions, additional investigations were needed to demonstrate the ELL method at a pre-service facility and at an in-service facility. The EPA Land Treatment Research Demonstration Facility near Ada, Oklahoma, was selected as one site. It includes two 0.6-hectare (1.5 acre) HDPE-lined liquid impoundments. The second site was a full-scale, double-lined impoundment, constructed but not yet placed in service, near San Antonio, Texas.

The equipment measured potential gradients, logged the data, and plotted the results. The system detected the presence of 0.8-mm (0.031 in.) leaks 1.5 m (5 feet) away from the leak. These leaks can be located with an accuracy of less than 15 cm (6 in.) when electrodes pass 15 cm (6 in.) above the leaks.

The field demonstration of the ELL method at a facility near San Antonio was also successful. Because the impoundment had been tested using the vacuum box method and because subsequent follow-up tests revealed no additional leaks, the one leak found was most likely the only leak. No false indications were obtained.

The ELL method proved successful in acquiring high-quality data, but the survey was time consuming. A faster data acquisition rate is needed to make the ELL method more cost effective.

REACHING THE LEAK AREA

After the leak is located in a landfill, the landfill must be excavated to reach the leak area for repair and sealing. Because each landfill is different -- there is no typical landfill -- many factors must be considered before determining how to excavate.

- How dense is the waste? Estimates can vary between 800 and 1,500 lb/yd³. Density influences both the rate at which the fill settles and the bearing capacity of the completed fill.
- How well has the fill settled? Decomposition, accelerated by water, is the prime factor influencing settlement. What kind of wastes? How well composted?
- What is the landfill's bearing capacity? How well will the landfill support heavy equipment?
- What is the landfill's decomposition rate? Decomposition varies with the kind of waste. Under anaerobic conditions, decomposition of organic material forms highly corrosive acids and also explosive and toxic gases.

All these factors differ from landfill to landfill, and all must be known to determine if the area can be excavated and how to go about doing it. Several techniques have been identified that would allow access to the leak area. It should be pointed out that these have not been field tested at landfills, but the technologies have been successfully demonstrated at other engineering sites.

REPAIRING THE LEAK

The next phase of this program was to develop techniques to effect the repair⁶. But can temporary, and possibly permanent, in situ repairs be made on FML's? Can repairs be made during installation? After in-service use?

A number of different polymers have been used as FML's. They may be either unreinforced or fabric reinforced and either cross-linked or thermoplastic.

Most of the polymeric FML's that have been or are being manufactured are of the thermoplastic type and, generally, are not cross-linked. Although cross-linked liners are more chemically resistant, thermoplastic liners are easier to seam and to repair in the field.

The methods used to seam and test the seam quality of a particular FML are the same ones used to repair that FML. FML's can be seamed with the use of:

- thermal methods (heat gun, extrusion welding, hot-wedge method, heat sealing, dielectric seaming);
- solvent methods (solvent welding, bodied solvents);
- adhesives (vulcanizing adhesives, contact adhesives); and
- tape adhesives (pressure-sensitive adhesive tapes).

The quality of seams can be tested by:

- immersing the FML seam in the waste medium to determine chemical compatibility and then measuring the effect on adhesion;
- nondestructive testing where seams are tested without being disturbed (e.g., visually; or testing coupons prepared with the same equipment and procedures used during actual seaming operations); and

- destructive testing in which samples of the seam are cut from the actual liner.

The need to repair an FML may occur at any of three major phases in the service life of the FML:

- at the time of and immediately after installation (e.g., repair damage that took place during installation or repair defective seams that show up during inspection and quality assurance testing);
- shortly after installation when the FML may have been partially covered with soil or may have undergone performance-type inspection; or
- after the facility has been placed in service and the FML has been in contact with wastes and covered with soil.

At the time of installation, the FML is generally only a few weeks old and has aged little. At this time repairs can be made employing the same preparations and methods that are used to seam the panels.

Shortly after installation, the FML is somewhat older, and although not exposed to weathering to the degree that aging has become an important factor, the sheeting may have become dirty. A successful repair now depends on having the FML clean and free from contamination.

After the L/I has been placed in use, the in-service life of the FML can range from a few weeks until the site is closed, and beyond. Even when the changes in FML composition are slight and do not affect overall performance of the liner, they can reduce repairability. To achieve a good bond, the composition of an exposed liner must match, on a molecular scale, that of the patching material and the surface must be clean and free of moisture and other contamination--conditions difficult, if not impossible, to meet. FML's exposed to waste liquids may have absorbed even small amounts of water and organic constituents from the waste liquids or have lost components, (e.g., plasticizers and anti-degradants) to the waste liquids.

Repairs to FML's at any aging stage may also be made with liquids that will harden on curing, such as epoxies if (1) good mechanical bond can be made between the liner and the plug, (2) the plugging material is deliverable to the repair location, and (3) the plugging material is compatible with the FML and the waste liquid during the curing process and the subsequent exposure.

Both of these techniques, patching with the same material⁷ and temporary seals⁸ have been attempted with limited success. The limited success stresses the need for additional research for repair of in service liners. Although mechanical seals were not investigated, they may have some application.

SUMMARY

Research has developed techniques to pinpoint the location of leaks in FML's within a very small area. Construction techniques are available to physically get to the leak. However, the ability to repair that leak on more than a temporary basis is questionable. The implications of this situation are obvious: permanent repair techniques for damaged membranes must be developed,

additional controls need to be employed at waste management facilities, or alternative methods of disposal must be found. The Agency has taken the leadership role of requiring additional controls, i.e., double-liner systems, while continuing to reevaluate other alternatives.

REFERENCES

1. Davis, J. L., Singh, R., Stegman, B. G., and Waller, M. J., Final Report: Innovative Concepts for Detecting and Locating Leaks in Waste Impoundments Liner Systems, U.S. Environmental Protection Agency, (Cincinnati, Ohio, 1984), NTIS No. PB 84-161819.
2. Davis, J. L., Singh, R., Waller, M. J., Gower, P., Time-Domain Reflectometry and Acoustic-Emission Monitoring Techniques for Locating Liner Failures, U.S. Environmental Protection Agency (Cincinnati, Ohio, 1983), Unpublished.
3. Shultz, D. W., Duff, B. M., Peters, W. R., Final Report: Electrical Resistivity Technique to Assess the Integrity of Geomembrane Liners, U.S. Environmental Protection Agency (Cincinnati, Ohio, 1984), NTIS No. PB 85-122414.
4. Darilek, G. T., Parra, J. O., Final Report: The Electrical Leak Location Method, U.S. Environmental Protection Agency (Cincinnati, Ohio, in press).
5. Ware, S. A., Jackson, G. S., Final Report: Liners for Sanitary Landfills and Chemical and Hazardous Waste Disposal Sites, U.S. Environmental Protection Agency, (Cincinnati, Ohio, 1978), NTIS No. PB 293-335/6.
6. Haxo, H. E., Final Report: Assessment of Techniques for In Situ Repair of Flexible Membrane Liners, U. S. Environmental Protection Agency (Cincinnati, Ohio,), NTIS No. PB 87-191813.
7. Haxo, H. E., White, R. M., Haxo, P. D., Fong, M. A., Final Report: Evaluation of Liner Materials Exposed to Municipal Solid Waste Leachate, U.S. Environmental Protection Agency, (Cincinnati, Ohio, 1982), NTIS No. PB 83-147801.
8. Mitchell, R. C., Hamermash, C. L., Lecce, J. V., Final Report: Feasibility of Plastic Foam Plugs for Sealing Leaking Chemical Containers, U.S. Environmental Protection Agency (Cincinnati, Ohio, 1973), NTIS No. PB 222 627/2BA.

D.L. LAINE
M.P. MIKLAS
C.H. PARR

Southwest Research Institute, U.S.A.

Loading Point Puncturability Analysis of Geosynthetic Liner Materials

SUMMARY

Geomembrane liner performance was examined in laboratory tests subjecting polyvinyl chloride (PVC), chlorosulfonated polyethylene (CSPE), and high density polyethylene (HDPE) materials, in two thicknesses each, to varying pressures, temperatures, and point loads. Loads were induced by placing the geomembrane material over truncated rigid epoxy cones used as loading points for 9.5, 19.0, and 24.5 mm heights above a sand subgrade while arranged in three-cone clusters and applying a hydrostatic load to the top side of the liner. Constant hydrostatic loads of 17.93 kPa at 23°C and 50°C were applied during a one-year test. HDPE material measuring 1.5 mm thick failed for the loading point height of 25.4 mm above the subgrade. After 365 days, the loading pressure was increased to 60.03 kPa for an additional 30 days. Failures were induced in 1.5-mm HDPE for loading point heights of 19.0 and 25.4 mm and in 2.5-mm HDPE for loading point heights of 25.4 mm. HDPE with a thickness of 1.5-mm failed for a loading point height of 19.0 mm with a 1.5-mm geotextile placed between the HDPE and the loading point at 17.94-kPa pressure and ambient temperature. HDPE with a thickness of 2.5 mm overlaying a 3.8-mm geotextile failed under 60.03-kPa pressure for a 25.4-mm loading height at the high temperature test condition. No materials failed when overlaid upon a 5.3-mm geotextile. Transient pressure loading tests without geotextile support exhibited failures caused by the maximum pressure load attained.

INTRODUCTION

One of the most important factors controlling liner performance is the quality and stability of the supporting subgrade over which the geomembrane is installed. Because geomembranes are not designed to directly support the overburden load caused by water, soil, or solid-waste material placed on the liner, the nature of the liner subgrade becomes extremely critical. Knowledge of the interactions between the geomembrane and the subgrade is vital to the design of waste storage installations. The results of this testing program provide valuable data for specifying geomembrane installations for solid- and liquid-waste disposal facilities and suggest economic guidelines for geomembranes, geocomposites, and subgrade preparation. The U.S. EPA, Hazardous Waste Engineering Research Laboratory provided the funding for this study.

RESEARCH APPROACH AND PROCEDURES

Objective

The objective of this study was to develop an understanding of the interactions between geosynthetic materials and the supporting subgrade. The relative puncturability of differing thicknesses and types of geomembrane materials and the use of geotextiles to lessen puncturability was evaluated.

Test Equipment

Long-term hydrostatic puncture-resistance tests were conducted on PVC, CSPE, and HDPE geomembrane materials, using two different thicknesses for each type of material. These tests were conducted in 36 round plastic pressure test vessels capable of withstanding pressures of up to 103.5 kPa (15 psig) and temperatures of 50°C (123°F). Figure 1 shows the design detail of the pressure test vessel. A pressure-regulated nitrogen-over-water system was used to force the geomembrane material onto a supporting sand subgrade. Eighteen of the pressure test vessels were connected to a closed-loop hot water circulating system for elevated temperature testing. Three artificial load points were placed in each test vessel to simulate an irregular subgrade surface. Figure 2 shows a detailed cross-section design of the load point that was used in this testing program. Tested load point heights above the subgrade surface were 9.5, 19.0, and 25.4 mm, respectively. Each vessel was monitored for temperature, pressure, and geomembrane failure. If a leak occurred in the geomembrane, water flowed through the puncture and accumulated in the base, activating a float switch and indicator light. The test set-up was monitored daily.

To ensure that the materials tested in this program met or exceeded the physical property specifications stated by their manufacturers, ASTM physical property tests including specific gravity, tear strength, tensile properties, hydrostatic, and puncture resistance were conducted on each of the subject geomembrane materials.

RESULTS AND DISCUSSIONS

One Year Low Pressure Tests

Laboratory tests were conducted to determine the failure mechanisms of geomembrane materials placed over an irregular subgrade and subjected to a constant hydrostatic load of 17.93 kPa for 365 days. The failures during the low-pressure tests are shown in Table 1. Figure 3 shows Sample 13, 1.5-mm HDPE, which failed. For verification purposes, another specimen of 1.5-mm HDPE was tested and failed after 60 days at ambient temperature, 17.94 kPa, and 25.4-mm load height. The failed verification sample is shown in Figure 4. Note the concentric shape which was impressed into the material.

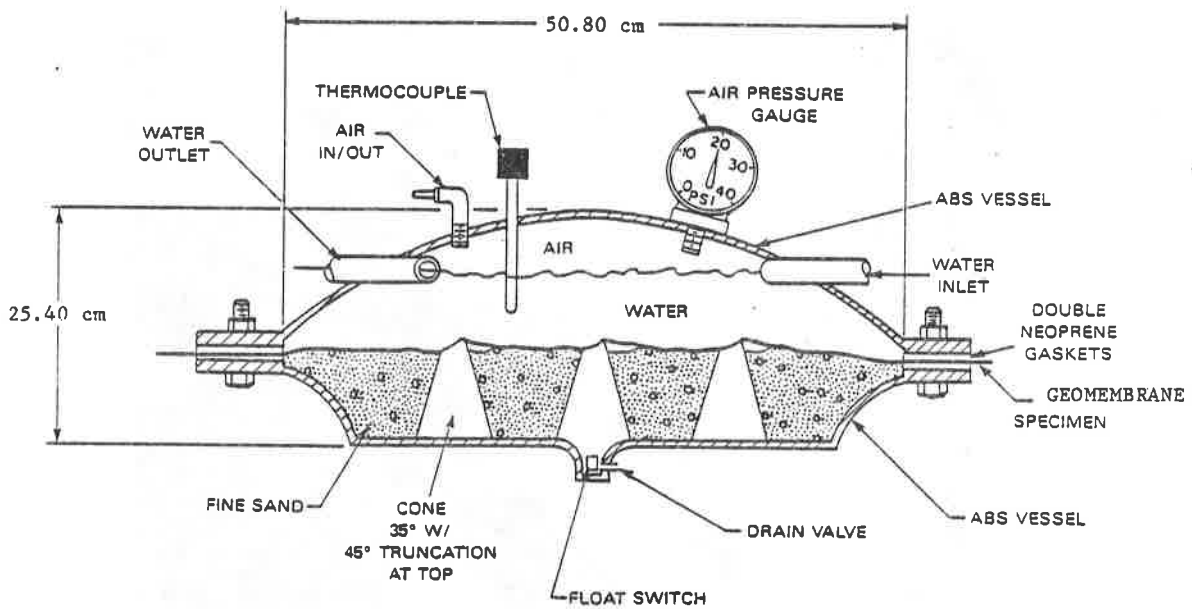


Figure 1. Cross-section drawing of the hydrostatic pressure vessel.

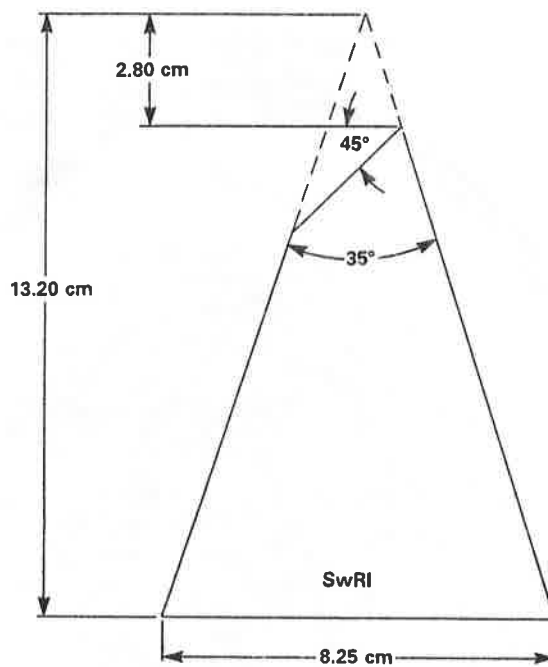


Figure 2. Cross-section of the conical loading point.

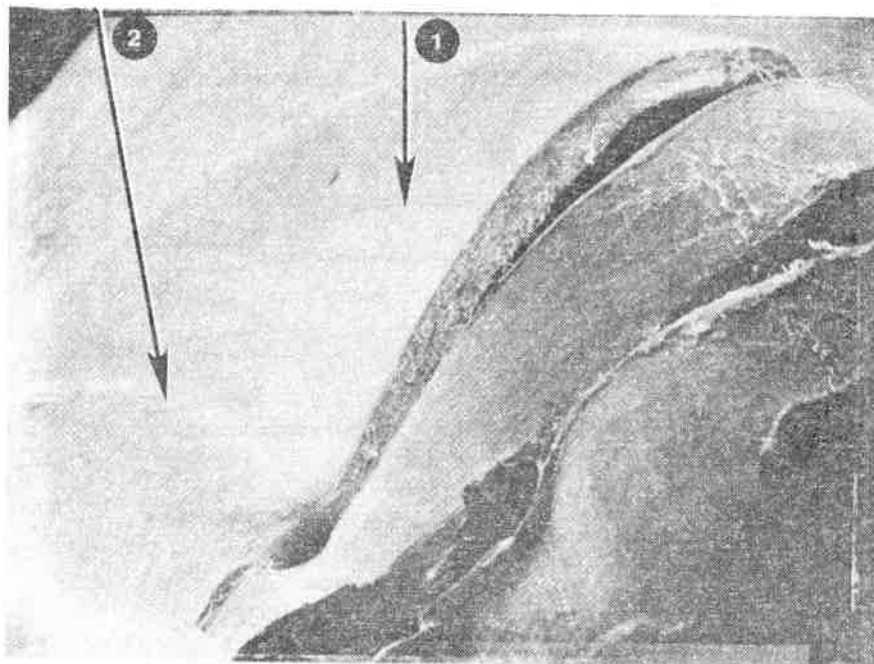


Figure 3. SEM of failure (21X); Sample No. 13 1.5-mm HDPE.
NOTE: Striations (1) and edge of drawn region (2).

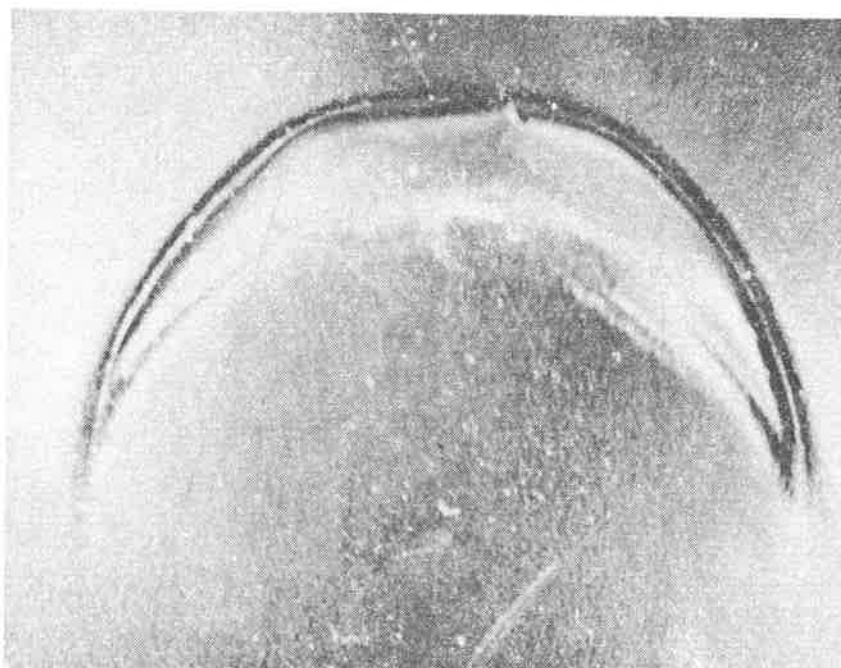


Figure 4. View of verification test failure on HDPE 1.5-mm Sample No. 24.

TABLE 1. ONE YEAR REGIMEN LOW PRESSURE FAILURE DATA

Material Type	mm	Sample No.	Geotextile mm	Temp. °C	Press. kPa	Time days	Load Height mm
HDPE	1.5	24	----	23	17.94	60	25.40
HDPE	1.5	15	----	23	17.94	148	25.40
HDPE	1.5	13	----	50	17.94	148	25.40

Polyethylene is one of several plastics which exhibit a marked plastic flow and necking at high load levels. Under some conditions, the failure elongation is more than ten times (1000 percent strain) (1). In the prominent failure of 1.5-mm HDPE, Sample No. 13, the following interpreted sequence of events occurred:

- (1) As the sheet was pressed down on the cone, a general stretching of the material occurred within a radial distance of approximately 50.8 mm around the cone.
- (2) Near the apex, a localized stress concentration caused elongation of the polyethylene into the necking region of behavior in the direction of the line of symmetry of the cone.
- (3) At this stage, the elongation in the direction perpendicular to the line of symmetry remained small.
- (4) The elongation continued until necking ended. At this point, the wall had thinned to about 0.25 mm. This corresponds with a strain of about 550 percent if the lateral strains are still small.
- (5) Because of the flow during necking, considerable alignment of polymer chains caused stiffening, which strengthened the polymer in the flow direction but reduced the polymer strength in the transverse direction.
- (6) Continued downward tension over the cone increased the elongation and stress in the transverse direction. Because the strength in this direction was compromised, fractures occurred.

This failure mode is a complex process involving a nonlinear thermoviscoelastic material with an intricate loading history. Loading conditions changed from stress-type to displacement-type loading during the test. The stress and displacement fields are two-dimensional and vary with time in each direction. The failure of the 1.5-mm HDPE appears to be a normal failure in that the loading simply extended the material beyond its capability. Characteristically, materials which are biaxially stressed fail at strain levels considerably lower than the failure strain limit in uniaxial tests. SEM examination confirmed that the 1.5-mm HDPE experienced a simple overload failure caused by the stress concentration at the apex of the point loading cone.

The thickness of the unstressed portions of the HDPE test specimens were found to vary significantly. Six thickness readings on Sample No. 13 varied from 1.40 mm to 1.62 mm, with

an average thickness of 1.47 mm. The thickness of Sample No. 15 varied from 1.47 mm to 1.70 mm, with an average of 1.65 mm. Commercial sheeting of the type tested has a specified thickness tolerance of 10 percent or, in this case, 0.15 mm, so that, except for one point, the sheets were within tolerance. Based upon the measured average thicknesses, Sample No. 15 is 40 percent stiffer than Sample No. 13 because the bending stiffness of the sheet varies with the cube of the thickness (2). This relative increase in stiffness may explain why Sample No. 15 failed to a lesser extent than Sample No. 13, even though the test temperature was higher. Obviously, this thickness variation is a real-world effect and must be considered when assessing the behavior of geomembrane liners.

In addition to the failures displayed by the HDPE material, severe delamination and scrim breakage were noted in the 0.9-mm and 1.1-mm CSPE tested at 17.94 kPa for 155 days with load point heights of 25.4 mm. After the problems were noted in the CSPE, the hydrostatic pressure tests were continued for an additional 210 days. At the end of this testing period, the pressure was increased to 60.03 kPa for an additional 30 days of testing. Neither CSPE sample failed completely.

High Pressure Accelerated Test at Conclusion of Low Pressure Test

At the completion of 365 days of low-pressure testing, the hydrostatic pressure was increased at a rate of 13.8 kPa per hour until a pressure of 60.03 kPa was achieved. This test pressure was maintained constant for an additional 30 days. The materials that failed the high-pressure testing are listed in Table 2. During this test, CSPE of 1.1 mm was damaged severely but did not leak. As previously discussed for other field samples, these failures are normal events in which the material was stressed beyond its elastic limit until failure occurred.

TABLE 2. HIGH PRESSURE FAILURE DATA ON PRESTRESSED GEOMEMBRANE

Material Type	mm	Sample No.	Geotextile mm	Temp. °C	Press. kPa	Time days	Load Height mm
HDPE	1.5	6	----	23	60.03	30	19.00
HDPE	1.5	17	----	50	60.03	30	19.00
HDPE	2.5	39	----	50	60.03	30	19.00
HDPE	2.5	32	----	23	60.03	30	25.40

A microscopic study was made of the disturbed area of the 1.1-mm CSPE material with scrim reinforcement which was damaged but did not fail. The scrim is made from 10 × 10 1000 denier polyester yarn. The delamination and breakage were directly over one of the load points that was 25.4 mm above the subgrade. The material had been stressed to a maximum pressure of 60.03 kPa for 30 days, resulting in tearing of the lower side of the sheet and scrim breakage in two places. The breakage is shown in Figure 5. Note the buckled shape of the entire area, indicating that the CSPE and/or scrim had been stretched beyond its elastic limit. Figure 6 shows a close-up view of the broken fiber shown on the right in Figure 5. The fiber break itself is unremarkable, but the striated area above it, which appears to be almost fibrous in nature, is a lineation which commonly occurs in plastic flow areas of polymers. A photograph of the scrim pattern is shown in Figure 7. A roughened appearance of the CSPE surface directly above the fibers may indicate that the CSPE and scrim were stretched beyond the elastic limit of the CSPE material. After removal of the load, the fibers snapped back, putting the

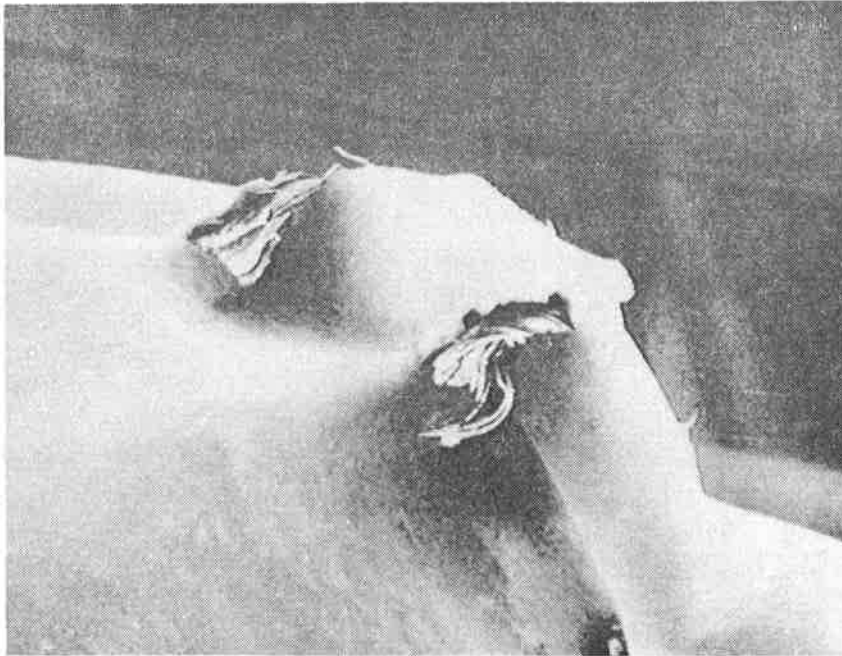


Figure 5. Scrim breakage on 1.1-mm CSPE after loading at 25.4 mm (102X).

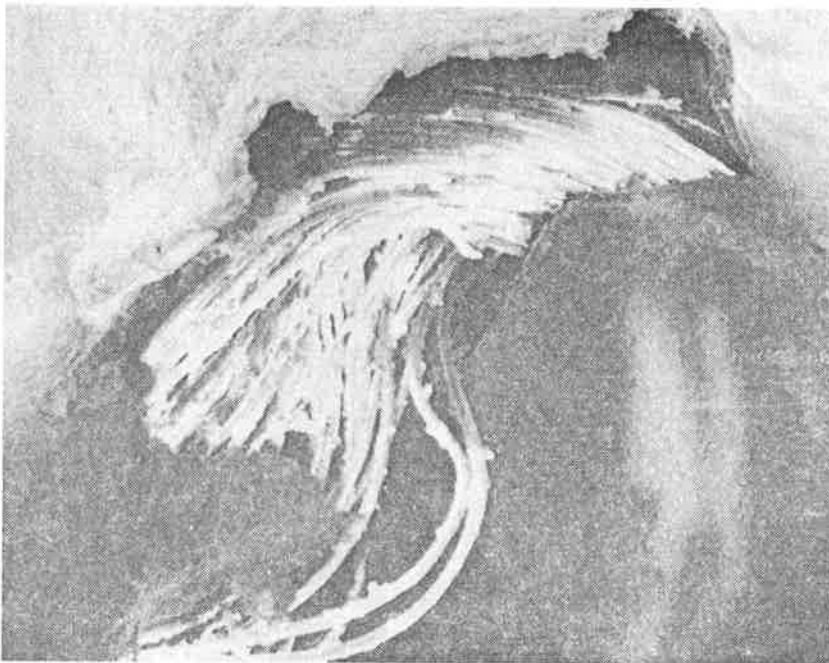


Figure 6. Close-up of broken scrim fibers 1.5 mm CSPE (50X).



Figure 7. Close-up of scrim pattern; 1.1-mm CSPE (11.5X).



Figure 8. Failed CSPE 1.1-mm for 25.4-mm loading point.

plastically deformed CSPE into compression. This compression resulted in local buckling of the CSPE. Even though severely damaged, the CSPE did not leak water.

Transient Pressure Loading Test

Transient pressure loading tests were conducted by placing new samples of geomembrane material into the test vessels and applying pressure at a rate of 55.2 kPa per hour until the final test pressure of 60.03 kPa was achieved. The final pressure of 60.03 kPa was held constant for 24 hours. Load point heights of 25.4 mm, 19.0 mm, and 9.5 mm were used at ambient- and high-temperature exposures.

The results of these transient pressure loading tests are presented in Table 3. Figure 8 shows the failure of the 1.1-mm CSPE material, and Figure 9 shows the failure of the 1.5-mm HDPE material.

TABLE 3. TRANSIENT PRESSURE LOADING FAILURE DATA

Material Type	mm	Sample No.	Geotextile mm	Temp. °C	Press. kPa	Time days	Load Height mm
CSPE	1.1	91	----	50	60.03	1	25.40
HDPE	1.5	12	----	50	60.03	1	25.40
HDPE	2.5	25	----	23	60.03	1	25.40

The HDPE 2.5-mm material failed the transient test at a temperature of 23°C at the final pressure of 60.03 kPa and a loading point height of 25.4 mm and is shown in Figure 10. Examination of the failure areas in all three materials with an optical microscope indicated that the failures were normal, resulting from overstressing the geomembrane material in the region of the point load.

Pressure Test Utilizing Geotextile Underlayment

Tests using geotextile materials were conducted to evaluate the mechanical advantages of a composite liner configuration versus a geomembrane liner material without a protective underlining of geotextile material. A typical composite liner was modeled by placing the geotextile material between the load points and the geomembrane material. All those geomembranes which failed one of the short-term tests, accelerated tests, or the transient load tests were used in this test sequence. Continuous-filament polyester nonwoven needle-punched geotextiles having thicknesses of 1.5 mm (60 mil), 3.8 mm (150 mil), and 5.8 mm (230 mil) were tested. The geomembrane materials tested were HDPE 1.5-mm, HDPE 2.5-mm, CSPE 1.1-mm, and CSPE 0.9-mm. Testing was conducted at 23°C and 50°C for a cone height of 25.4 mm.

The results of the composite material tests are presented in Table 4. Tests at ambient and high temperature resulted in failure of both 1.5-mm and 2.5-mm HDPE with 1.5-mm and 3.8-mm geotextile. The failure mode of the HDPE, in both cases, was a normal failure caused by

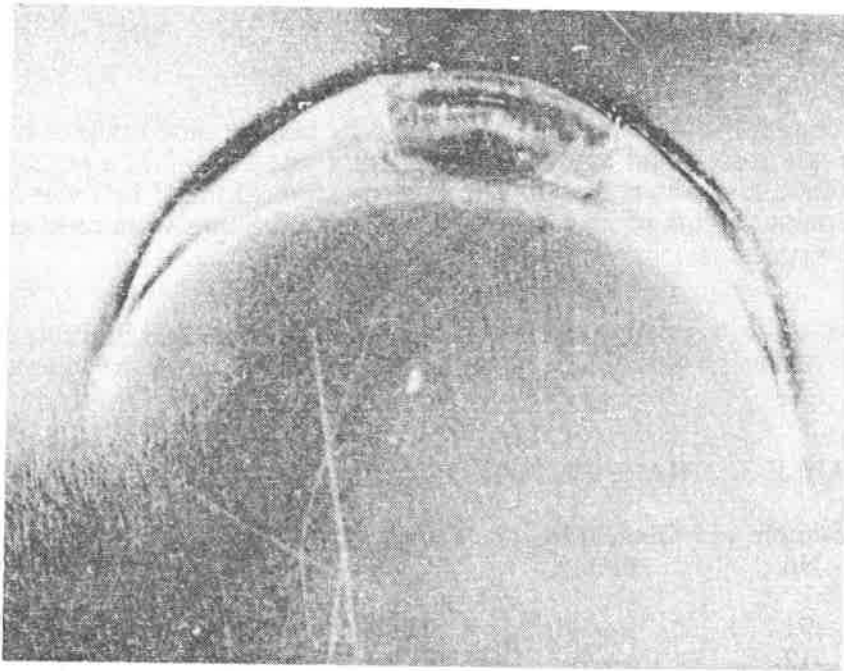


Figure 9. Failed 1.5-mm HDPE for 25.4-mm loading point.

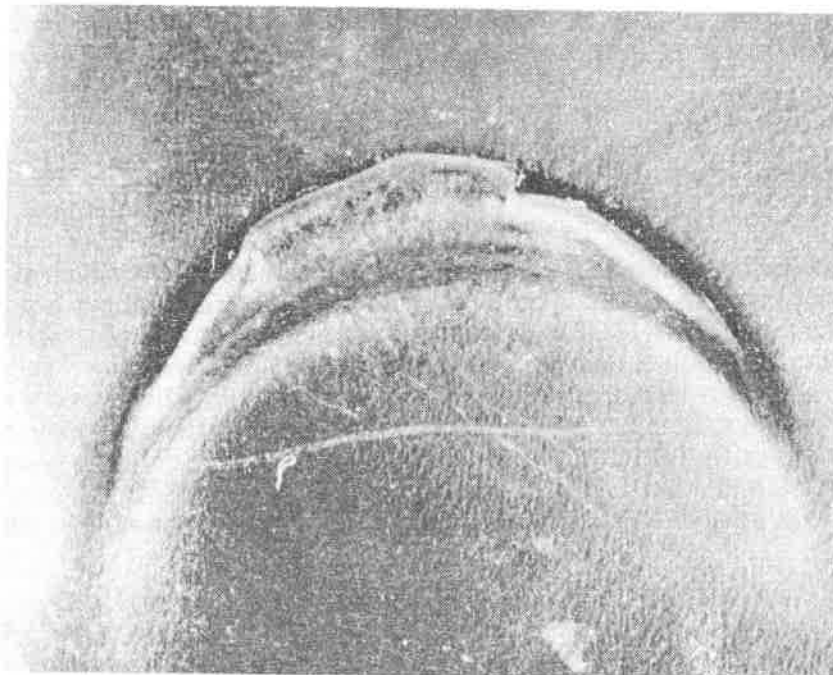


Figure 10. Failed HDPE 2.5-mm for 25.4-mm loading point.

over-stress on the liner material at the loading point. No failures were recorded when a 5.8-mm geotextile was used.

TABLE 4. COMPOSITE MEMBRANE FAILURE DATA

Material Type	mm	Sample No.	Geotextile mm	Temp. °C	Press. kPa	Time days	Load Height mm
HDPE	1.5	4	1.5	23	60.03	210	25.40
HDPE	2.5	40A	3.8	50	60.03	60	25.40

The CSPE material did not fail when a geotextile was placed between the membrane and the load points, and there was no evidence of scrim separation such as that observed in samples tested without a protective geotextile material.

CONCLUSIONS

It is recommended that a liner installation option be utilized based on a combination of factors and not based solely on cost considerations. A given site may "require" only a 0.5-mm PVC material thickness over a 25.4-mm or less irregular subgrade, based on the test results; however, an economically astute owner might elect to use a 5.8-mm geotextile at a given facility and/or a finer finish of the subgrade. The geotextile would make the liner system more secure and safe from larger particle penetration by pieces which, though absent from the initially prepared surface, might work their way upwards through the subgrade. Similarly, a finer finish than 25.4-mm particle projection would reduce the ultimate potential for penetration and subsequent failure during the anticipated lengthy (usually 20 years or more) life of the facility. Of course, mechanical properties are not the only factors which should be considered in the design. Chemical, ultraviolet, and temperature resistance are some of the other critical factors which must be a part of design considerations.

Geocomposites (geomembrane plus geotextile) have a mechanical advantage in improved performance over geomembranes alone. The economic advantage of using a composite system is associated with the improved performance (lessening of puncturability) of the geomembrane, thus preventing a costly waste clean-up operation.

REFERENCES

- (1) Zapas, L.J. and J.M. Cressman. Stress-Strain-Time Diagrams, Including Failure Envelopes, for High Density Polyethylene of Different Molecular Weight. Polymer Preprints. Vol. 19, No. 2. American Chemical Society. 1978.
- (2) Seely, F.D and J.O. Smith. Advanced Mechanics of Materials. John Wiley & Sons. New York, New York. 1957.

SESSION 5B
TESTING-GENERAL

E.A. RICHARDS

J.D. SCOTT

L.W.M. BOBEY

University of Alberta, Canada

V. DIYALJEE

Alberta Transportation and Utilities, Canada

Shear Resistance Between Cohesive Soil and Geogrids

ABSTRACT

The use of high strength geogrids and geotextiles in soil-reinforcement applications requires that the shear resistance between the soil and geosynthetics be known. A laboratory research program was undertaken to determine the influence of the geometry of four geogrids and a geotextile on interfacial shear strength.

A large capacity direct shear machine 305 mm by 305 mm was used to measure interfacial friction under normal stresses of up to 250 kPa. A silty clay used in the testing program was compacted at a water content of 23.0% to a dry density of 1.63 g/cm³. A total of forty-six consolidated undrained shear tests showed that both the reinforced and unreinforced clay exhibited similar stress-deformation relationships. The typical relationship showed a rapid rise in shear strength with increasing displacement before it leveled off to achieve a peak value at horizontal displacements of 15 to 25 mm.

The influence of geometry of the reinforcements was analyzed in terms of an efficiency value defined as the soil shear strength divided by the interfacial shear strength. Values of efficiency ranged between 0.76 and 0.96. For reinforcement purposes, therefore, these materials do not present a weak failure plane in the soil mass.

INTRODUCTION

High tensile strength geotextiles and geogrids were developed to be used as reinforcement in the design of slopes, embankments, and retaining structures. As reinforcement, the role of geotextiles is to improve the stability of the structures against shear failure.

One mechanism for failure of a reinforced slope is the direct sliding of a soil mass along a reinforcement surface (Figure 1). To prevent this type of failure, a sufficient amount of interfacial friction must be present along the surface of the reinforcement. The magnitude of this friction is primarily a function of the properties of the soil, the normal stress acting on the reinforcement, and the geometry and surface texture of the reinforcement. This interfacial friction can be determined experimentally using the direct shear test.

The objective of this paper is to show how the values of the interfacial shear strength between a silty clay and geogrids is influenced by the geometry of the geogrids. For comparative purposes, a high tensile strength geotextile was also tested. The interfacial shear strength and deformation properties between the geosynthetics and a cohesive soil were measured in a 305 mm square shear box. The efficiencies ($\tau_{\text{reinforced soil}}/\tau_{\text{soil}}$) of the reinforced soil were determined. The interfacial shear strength between the polymeric surfaces of the geogrids and the cohesive soil also were estimated from the test results.

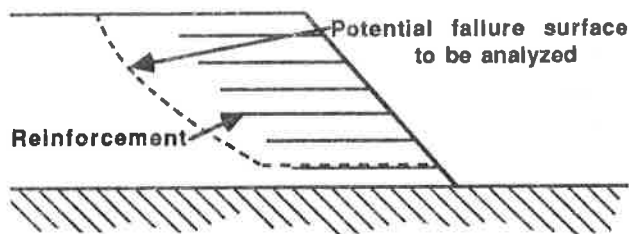


Figure 1. Potential Failure Plane Along Surface of Geogrid

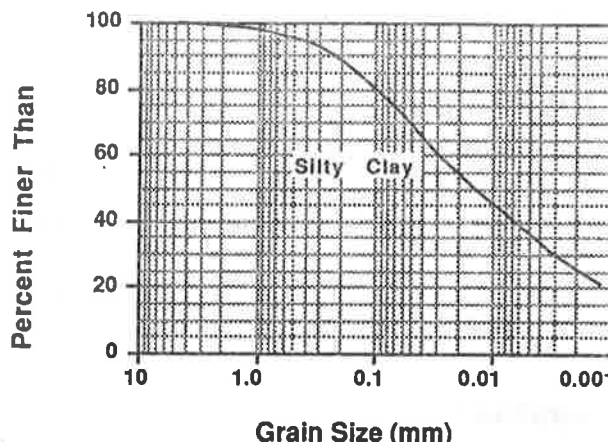


Figure 2. Grain Size Distribution of Silty Clay

TEST PROCEDURE

The geogrids tested were SR2, SS2, TNX-5001, and ParaGrid 50S and the geotextile was P600. The construction method and the geometry of the geosynthetics are summarized in Table 1. A well graded silty clay soil with 23.5% of the grain size finer than $2\ \mu\text{m}$ and with liquid and plastic limits of 40.8% and 20.6% was used (Figure 2). The standard compaction maximum dry density of the soil is $1.68\ \text{g/cm}^3$ and the optimum water content is 20.1%.

A direct shear machine with a 305 mm square box was used to measure the interfacial shear strength using consolidated undrained shear tests. Normal stresses from 5 kPa to 250 kPa were used as confining stresses. These pressures represent the vertical stresses occurring on reinforcement layers in embankments at approximate depths from 0.25 m to 12.5 m. A total of 46 consolidated undrained shear tests were performed.

The consolidated undrained direct shear test models a critical design situation which occurs when an additional stress is rapidly applied to a cohesive soil in an embankment. This rapid rate of loading may induce an undrained shear failure of the structure. In this test program, a shear displacement rate of 3.05 mm/min was chosen to model an undrained rate of loading.

A 4.54 kg hammer with a 10.2 cm square steel foot was used to apply 64 blows per layer to three layers of soil. The geogrid was placed inside the second layer of soil, such that after compaction and consolidation, the upper surface of the geogrid would coincide with the intended shear surface. All samples were compacted at a water content of 23.0% and to a dry density of $1.63\ \text{g/cm}^3$. The compacted density represented 97% of the maximum dry density, and the compacted water content was 3% greater than optimum.

Geogrid/ Geotextile Tradename	Type of Polymer	Mass (g/m ²)	Geometry					Peak Tensile* Strength (kN/m)
			Structure	Junction Method	Open Area (%)	Aperture Size (mm)	Thickness (mm)	
Paragrid 50S	polyester polypropylene	530	square grid	welded	78	* MD= 66.2 CD= 66.2	*T 2.50 A 3.75	50.0
P600	polypropylene	220	woven split film	woven	0	1.5X10 ⁻³ 5.0X10 ⁻³	0.75	32.8
TNX-5001	polyester	544	rectangular grid	welded	58	MD= 89.7 CD= 26.2	T 0.75 Junction 1.50	87.5
SR2	high density polyethylene	930	unlaxial grid	planar	55	MD= 99.1 CD= 15.2	T 1.27 A 4.57	78.8
SS2	polypropylene	345	blaxial grid	planar	77	MD= 25.4 CD= 33.0	T 1.02 Junction 3.81	17.1

*MD = Machine direction
CD = Cross machine direction

*T = Tension member
A = Anchor member

* 200 mm wide width tensile test

Table 1. Properties of Reinforcement Materials

TEST RESULTS

Soil Shear Strength

The consolidated undrained shear strength of the silty clay was determined using both 305 mm square and 60 mm square direct shear box tests. The samples for the smaller shear box were prepared by a kneading compaction method which gave a dry density of 1.58 g/cm³ and a water content of 23.5%. A higher shear strength and non-linear failure envelope were obtained with the large shear box (Figure 3). This variation in shear strength may be due to the difference in initial density and the different compaction methods that were used to prepare the 305 mm and 60 mm square specimens. In addition, the influence of wall friction between the side of the box and the specimen was greater in the smaller box.

For comparison with the direct shear tests, the total (undrained) and the effective stress shear strengths of the silty clay were determined with consolidated undrained triaxial tests with pore pressure measurements. Samples were prepared by kneading compaction. The average dry density was 1.59 g/cm³, and the water content was 24.0%. The failure envelopes for the total and effective stresses from the triaxial tests are plotted in Figure 4. The undrained strengths from the two tests are similar. The effective angle of internal friction and the effective cohesion intercept for the soil are 30.1° and 6.7 kPa.

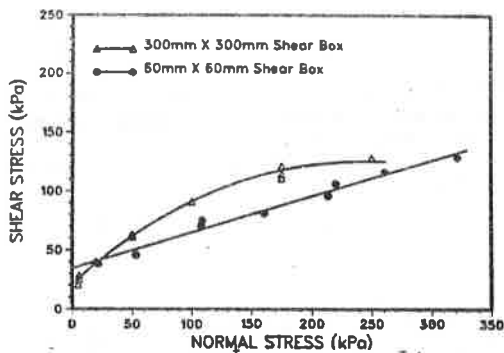


Figure 3. Failure Envelopes of Direct Shear Tests on Silty Clay

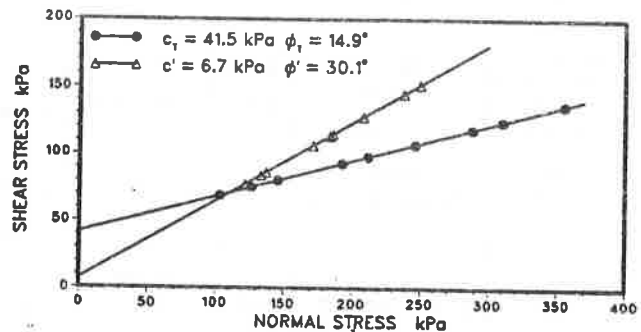


Figure 4. Total and Effective Mohr-Coulomb Failure Envelopes of Triaxial Tests on Silty Clay

Shear Stress and Deformation

A series of twelve consolidated undrained direct shear tests were carried out on the unreinforced silty clay in the 305 mm square shear box. The shear stress and displacement curves are summarized in Figure 5. The stress-deformation behavior of the dynamically compacted clay is like that of a strain-hardening soil at higher confining stresses. The shear strength rises rapidly with increasing displacement before it levels off to achieve a peak value. Normal stresses less than 50 kPa displayed strain-softening behavior. This behavior may occur because the applied normal pressure was significantly smaller than the preconsolidation stress induced by compaction forces (140 to 175 kPa). The preconsolidation stresses were determined from consolidation tests on the compacted soil.

Typical shear stress-deformation plots of a reinforced silty clay are shown in Figure 6. Strain-hardening and strain-softening behavior occurred in the tests are similar to the behavior of the unreinforced clay. The shear displacements required to mobilize the peak undrained strength (8 to 17 mm) are similar to those of the unreinforced clay (8 to 15 mm). The deformation to peak increases with increasing normal stress. The presence of the reinforcement, therefore, does not appear to have a significant effect on the shear displacement to peak.

ANALYSIS OF TEST RESULTS

The failure envelopes of two geogrids, a geotextile and the reinforced soil are compared in Figure 7. The interfacial shear strength of the reinforced clay for all materials is less than the shear strength of the unreinforced clay. All failure envelopes are gently curved indicating that the interfacial strength is non-linearly normal stress dependent for these consolidated undrained shear tests.

The geogrid TNX-5001 mobilizes slightly higher shear strength compared to SR2. Since the mechanism of interaction is the same for the geogrids, the slightly higher strength may be attributed to a difference in geometry. For the SR2 and TNX-5001 geogrids, the percent open area is similar, but the aperture dimensions differ. Possibly, the slightly higher interfacial strength of TNX-5001 is attributable to the geometry of this geogrid. The smooth, hard surface of TNX-5001 does not seem to have a deleterious effect on the shearing strength.

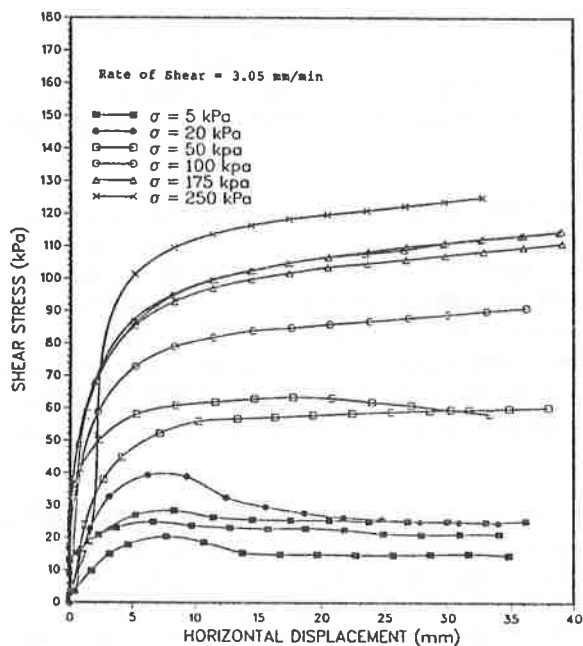


Figure 5. Direct Shear Test Results for Unreinforced Silty Clay

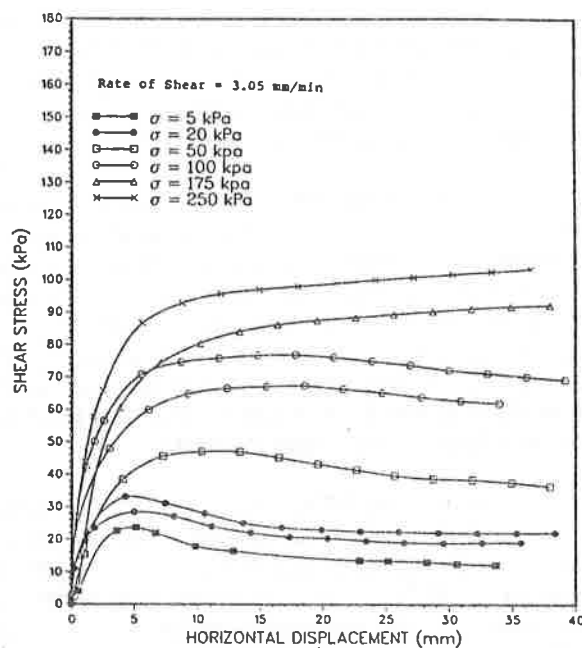


Figure 6. Direct Shear Test Results for Silty Clay Reinforced with Geogrid SR2

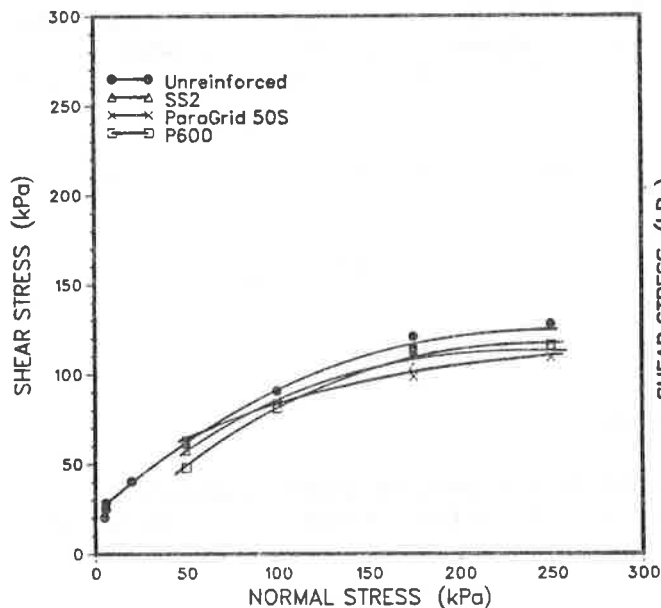


Figure 7. Undrained Shear Strength Envelopes of Reinforced Silty Clay

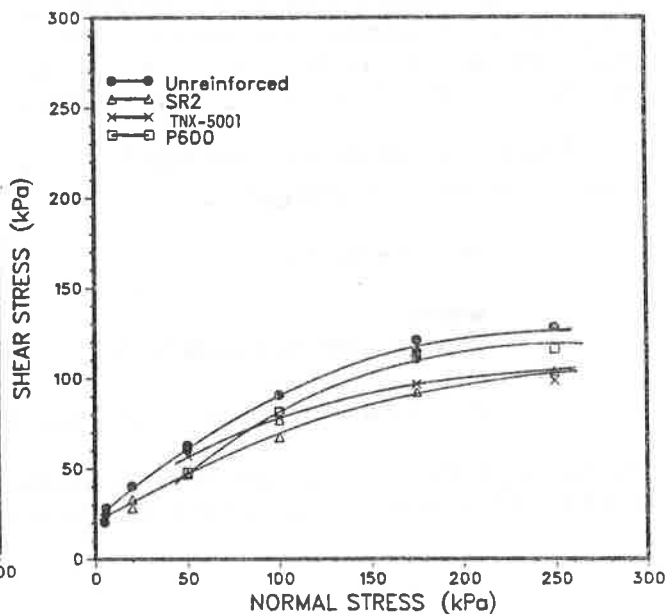


Figure 8. Undrained Shear Strength Envelopes of Reinforced Silty Clay

In Figure 8, a comparison is made of the interfacial shear envelopes of the unreinforced clay with those reinforced with SS2, ParaGrid 50S, and P600. The response of the reinforced clay is similar to that previously noted for TNX-5001 and SR2. The peak shear strength envelope for the unreinforced clay is greater than that for reinforced clay for all materials. SS2 has a slightly higher interfacial strength than ParaGrid 50S.

For ParaGrid 50S and SS2 the aperture dimension does not appear to influence the interfacial shear strength. Even though the area of an aperture in ParaGrid 50S is 5.23 times larger than SS2, the interfacial strength of ParaGrid 50S is less than SS2. Also, the embossed surface of ParaGrid 50S does not appear to increase the shear strength over that of the smooth surface of SS2. When the majority of the reinforcement consists of openings, the interfacial strength results primarily from the shearing of soil particles in the apertures. A relatively small portion of the total area of ParaGrid 50S and SS2 is solid and the contribution of the shear resistance generated from soil sliding on the solid surface is small. For this reason, the solid surface of the geogrid, whether smooth or embossed, has little effect on the shear strength.

For the woven P600, shear strength results primarily from the shearing of soil over the entire rough surface as well as penetration and lodging of soil particles in the openings between the yarns. Figures 7 and 8 indicate that this mode of shear resistance is superior to that of the geogrids. As discussed by Williams and Houlihan (1987), the interlocking of soil within the openings and the rough surface of the geotextile may be sufficient to cause the shear stress to be transferred from the interface into the adjacent soil layer. They found the shear surface developed at a distance of between 0.4 to 3.2 mm above the interface. Thus, the strength of the soil-geotextile surface can approach the strength of the unreinforced soil.

Comparison of the five shear strength envelopes demonstrates that for a grid type of reinforcement, the percent open area of the reinforcement governs the interfacial interaction. When there is an extensive amount of soil to soil interaction through the apertures as in the ParaGrid 50S and SS2, the interfacial strength is independent of the aperture dimensions and surface texture. When the soil to soil interaction is limited, the interfacial strength appears dependent on the surface characteristics of the reinforcement. Thus, it appears that the type of reinforcement and its geometry influences the interfacial shear strength behavior.

The total interfacial shear strength (τ_T) of a reinforced clay can be divided into cohesive strength and frictional strength.

$$\tau_T = c_T + \sigma_n \tan \delta \quad (1)$$

where,

c_T = total stress interfacial cohesion intercept

σ_n = normal stress

δ_T = total stress angle of interfacial friction

The interfacial shear strength can be further divided into components; the shearing between the soil and the reinforcement surface and the shearing of soil over soil in the openings of the reinforcement.

The total interfacial shear strength, therefore, can be written as the sum of the contributing components and equation 1 becomes

$$\tau_T = \alpha(c_G + \sigma_n \tan \delta_G) + (1-\alpha)(c_u + \sigma_n \tan \phi_u) \quad (2)$$

where,

α = the ratio of the solid area of the reinforcement to the total area of the reinforcement

c_G = interfacial adhesion intercept of the solid reinforcement

δ_G = angle of interfacial friction of the solid reinforcement

c_u = undrained cohesion intercept of soil

ϕ_u = undrained angle of internal friction of soil

c_u and ϕ_u can be measured in a conventional direct shear test while c_G and δ_G of a single member can be determined from the shear box test. Assuming the contribution made by each component is known, τ_T of any type of reinforcement may be estimated from equation 2. As an alternative, the influence of each component may be studied.

Collis et al. (1984), Koerner, Martin and Koerner (1986), and Milligan (1987) define efficiencies for both shear strength parameters.

$$E_\phi = \frac{\tan \delta_T}{\tan \phi_u} \quad (3)$$

and

$$E_c = \frac{c_T}{c_u} \quad (4)$$

For the test results shown here, the curvature of the failure envelope indicates that both shear strength parameters vary with applied normal stress. For this reason, efficiency is expressed in terms of total interfacial shear strength.

$$E = \frac{\tau_T}{\tau} \quad (5)$$

Equation 5 can also be written as

$$E = \frac{\tau_T}{\tau} = \alpha \frac{c_G + \sigma_n \tan \delta_G}{c_u + \sigma_n \tan \phi_u} + (1-\alpha) \quad (6)$$

where,

τ = shear strength of the unreinforced soil

and

$$\tau_G = [E + (\alpha - 1)] \frac{\tau}{\alpha} \quad (7)$$

where,

τ_G = interfacial shear strength between a cohesive soil and a polymeric surface.

Therefore, the efficiency of the polymeric surface of the reinforcement (E_G) can be calculated from

$$E_G = \frac{\tau_G}{\tau} \quad (8)$$

Discussion

Interfacial Shear Strength Efficiency

The interfacial shear strength efficiency for each test is calculated and presented in Figure 9. The efficiency values range from 0.76 to 0.96. Although the calculated E values are slightly scattered, efficiency appears to decrease with increasing normal stress.

As discussed previously α seems to have some influence on the interfacial shear strength. Figure 10 shows that when the open area ratio of the reinforcement is small, the interfacial shear strength approaches that of the unreinforced soil and the efficiency is high. As α increases, the soil to soil contact decreases and the soil to polymer surface interaction increases. A low efficiency value results. As α approaches unity, that is, a solid sheet of reinforcement, the contact surface texture becomes important. For a reinforcement with a rough contact surface, exemplified by P600, the interfacial shear strength can approach that of the soil, and the efficiency can be high.

A previous study reported that the efficiency of SR2 varied from 0.71 to 0.85 (Table 2). In this study the average efficiency of the silty clay reinforced with SR2 was 0.78 although the properties of the clay soils differ. Thus, the efficiency of SR2 in clay is approximately 0.80.

The efficiency of a very thin, but stiff, woven geotextile ranged from 0.48 to 0.61 (Table 2). In contrast, the average efficiency of the P600 was approximately 0.92. The thickness of P600 is twice that of MP500 and the surface may be rougher than MP500. The differences in thickness and the surface characteristics have considerable effects on efficiency.

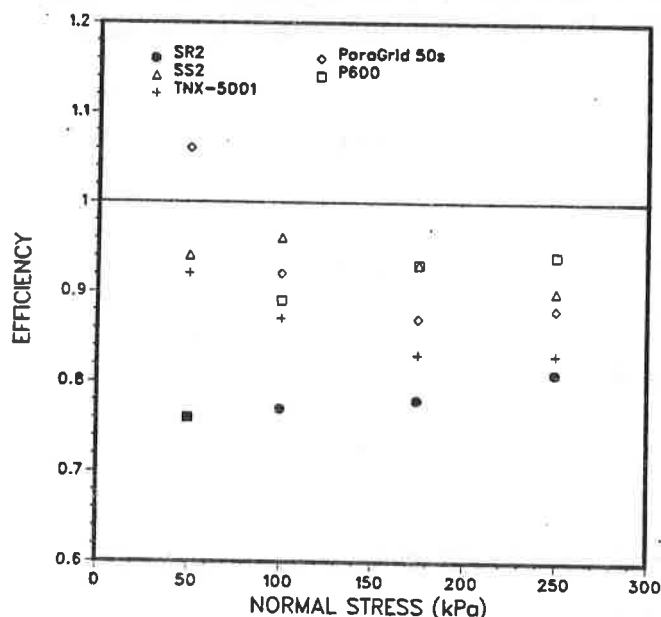


Figure 9. Interfacial Shear Strength Efficiencies of Silty Clay Reinforced by Geogrids and a Geotextile

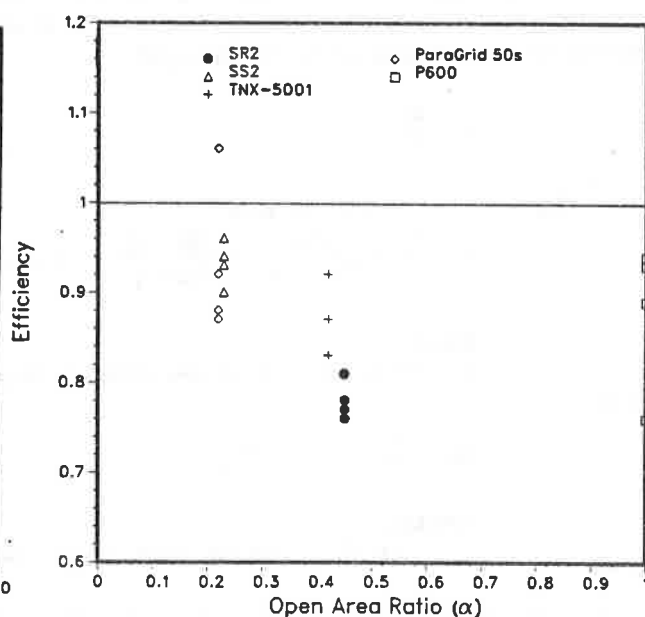


Figure 10. Influence of the Open Area Ratio on Shear Efficiency

Author	Shear Test	Soil	Reinforcement	E
Lafleur, Sall and Ducharme (1987)	50mm X 50mm rate = 0.024 mm/mln normal stress = 50 to 150 kPa	plastic clay $w_L = 56\%$ $I_P = 30\%$ $w = 25\%$ $w = 40\%$ $w = 60\%$	woven MP500 stiff, 0.4mm thick	0.58 0.61 0.48
Southern Water Authority (1982)	305 mm X 305 mm rate = 3.0 mm/mln	brown plastic clay $w_L = 82\%$ $I_P = 42.9\%$ $w = 37.2\%$ brown sandy clay $w_L = 40.5\%$ $I_P = 1.9\%$ $w = 37.4\%$	Tensar SR2 Tensar SR2	0.71 0.85

Table 2. Interfacial Shear Strength Efficiency

Efficiency of the Polymeric Surface of a Reinforcement

Equation 7 was used to calculate the interfacial shear strength between the polymeric surface and the cohesive soil. The normal stress was assumed to be uniformly distributed across the apertures and the polymeric surfaces. Efficiency of the polymeric surface (E_G) was calculated as defined in equation 8. The efficiencies range from 0.41 to 0.83 (Figure 11). There appears to be a tendency for the efficiency to decrease with an increase in normal stress. The calculation of E_G is highly dependent on the value of E used in the equation and these back calculations of E_G may vary in accuracy. At a high normal stress however, the value of E_G for all the geogrid materials varies between 0.5 and 0.6. The results indicate that the embossed surface of ParaGrid 50S did not affect the efficiency of its surface.

Ingold (1980), carried out undrained pull-out tests on kaolin clay reinforced with Netlon 1168 and Terram RF/12 among other reinforcements. The undrained shear strength of the kaolin clay was 34 kPa for $w = 35\%$, $S = 95\%$ and $\gamma_t = 1.80$ g/cm³. Netlon 1168 is a diamond mesh manufactured from polypropylene, while Terram RF/12 is a composite, 67% polypropylene and 33% polyethylene. Ingold used $E_G = 0.5$ to formulate the undrained pull-out resistance equation. A very good agreement was found between calculated and measured pull-out results using this value.

Results reported in Table 3 indicate that efficiencies of polymeric surfaces with cohesive soils range from 0.53 to 1.0. Most efficiency values for these smooth surfaced geomembranes however, lie in the range of 0.5 to 0.7. The average efficiency for the HDPE (high density polyethylene) geomembrane is 0.65 ± 0.12 . The polymer of SR2 is also HDPE which was found to have a surface efficiency of 0.52. It appears, therefore, that the efficiency of HDPE is about 0.6 and varies slightly with the clay soil properties.

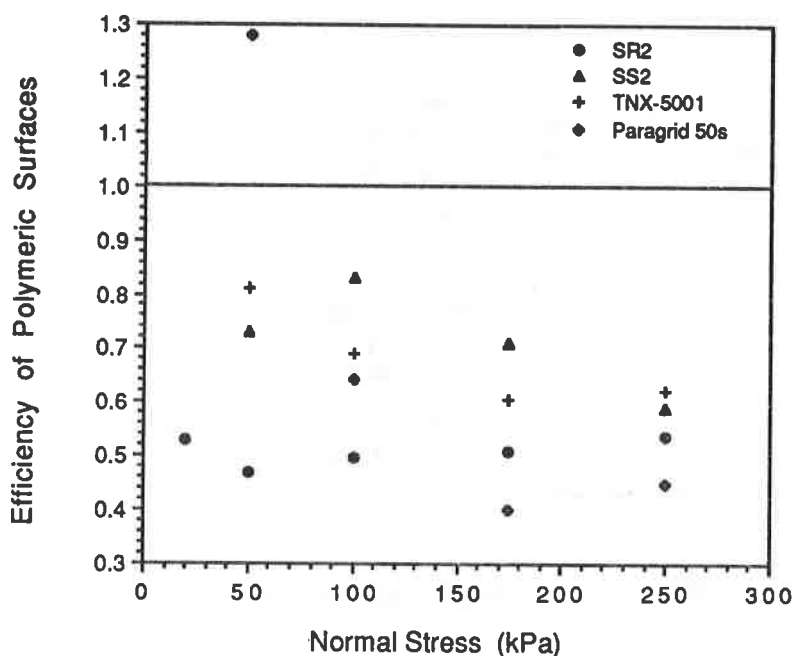


Figure 11. Influence of the Polymeric Surface on Shear Efficiency

Summary

This paper has reported on a research program which measured the interfacial shear strength between a silty clay and four geogrids and a woven geotextile. The consolidated undrained interfacial shear tests were conducted with a large shear box under normal stresses up to 250 kPa. The presence of the reinforcement had little effect on the stress-deformation behavior of the compacted silty clay.

Comparison of the shear strength envelopes demonstrates that for a grid type of reinforcement, the percent open area of the reinforcement has a strong influence on the interfacial interaction. For geotextiles, a rough surface can generate an interfacial shearing strength approaching that of the clay shear strength. Thus, the construction method and the geometry of the reinforcement strongly influences the shear strength behaviour. The interfacial shear strength efficiency values were generally found to be quite high, ranging from 0.76 to 0.96. For reinforcement purposes, therefore, these materials do not present a weak failure plane in the soil mass.

Author	Shear Test	Soil	Reinforcement	E _G
Koerner, Martin and Koerner (1986)	102 mm ² rate = 0.06 mm/min	Delaware River clayey silt w _L = 28% I _p = 8% w = 13.5%	PVC	1.03
			CPE	1.06
			EPDM	0.81
			HDPE	0.62
			Embossed HDPE	0.90
		sandy silty clay w _L = 46% I _p = 29% w = 11.8%	PVC	0.60
			CPE	0.62
			EPDM	0.61
			HDPE	0.59
			Embossed HDPE	0.83
		Kaolinite clay w _L = 57% I _p = 27% w = 30.8%	PVC	0.53
			CPE	0.55
			EPDM	0.68
			HDPE	0.50
			Embossed HDPE	0.89
		sandy clay w _L = 87% I _p = 72% w = 18.2%	PVC	0.66
			CPE	0.71
			EPDM	0.77
			HDPE	0.62
			Embossed HDPE	0.99
Williams and Houlihan (1987)	305 mm partially fixed or free shear test rate = 0.3 mm/min Normal stress 0 to 100kPa	Gulf Coast clay w _L = 42% I _p = 14% w = 15.5%	HDPE	0.68
			PVC	0.63

Table 3. Efficiency of Polymeric Surfaces

ACKNOWLEDGEMENT

This research was funded by Alberta Transportation and Utilities, Research and Development Branch. We would like to thank our colleagues in the Geotechnical Services Materials Engineering Branch and Edmonton District 7 of Alberta Transportation and Utilities and our colleagues in the Departments of Clothing and Textiles and Civil Engineering, University of Alberta.

REFERENCES

- Bobey, L.W.M., Soil-Geogrid Interfacial Shear Strength, M.Sc. Thesis, Department of Civil Engineering, University of Alberta, Spring 1988, 176p.
- Ingold, T.S., Reinforced Clay, Ph.D. Thesis, Department of Civil Engineering, University of Surrey, 1980, 252p.
- Koerner, R.M., Martin, J.P., and Koerner, G.R., Shear Strength Parameters Between Geomembranes and Cohesive Soils, Geotextiles and Geomembranes, 1986, Vol. 4, No. 1, pp. 21-30.
- Lafleur, J., Sall, M.S., and Ducharme, A., Frictional Characteristics of Geotextiles with Compacted Lateritic Gravels and Clays, Proceedings, Geosynthetics '87 Conference, New Orleans, Feb. 1987, Vol. 1, pp. 205-215.
- Southern Waterway Authority, Kent River and Water Division, Shear Box Tests on Tensar SR2 Embedded in London Clay, Bolton Institute of Technology, 1982, 15p.
- Williams, N.D., and Houlihan, M.F., Evaluation of Interface Friction Properties Between Geosynthetics and Soils, Proceedings, Geosynthetic '87 Conference, New Orleans, Feb. 1987, Vol. 2, pp. 616-627.

J.R. MONTALVO
Polyfelt, Inc., U.S.A.

Evaluation Of The Degradation Of Geotextiles

ABSTRACT

This paper presents experimental investigations into the influence of chemical solutions and ultraviolet radiation on the mechanical strength of polyester and polypropylene geotextiles. The influence of ammonia solutions, pH=10 and pH=12, cement and lime leachate solutions, Jet A-1 and diesel fuels, and sea water were studied.

Polypropylene and polyester fabrics appear to be very resistant to degradation from chemicals present in a natural soil environment. However, tensile strength retention results after immersion indicated a significant strength reduction for the polyester geotextile in ammonia with pH=12 and cement and lime leachate solutions. The polypropylene geotextile showed some strength reduction in Jet A-1 and Diesel fuels after 7 days. No effects were shown in sea water on either geotextile. Accelerated and natural sunlight condition test results indicated that chemically U.V. stabilized polypropylene fabrics have the highest U.V. resistance values.

INTRODUCTION

The degradation of geotextiles still concerns the designing engineer. The short and long-term performance of the geotextile is a question commonly asked by those considering the use of a fabric.

The durability of the geotextile depends not only on the quality of the fabric shortly after manufacture but also on its ability to maintain the original design function characteristics for a long period of time. It is a well known fact that polymers are affected by chemicals, U.V. radiation, temperature, and humidity(1, 2, 3).

Most geotextiles are primarily made from polypropylene and polyester polymer fibers. These polymers appear to be highly resistant to degradation in common chemical environments found in a

natural soil (2, 4, 5). But, when the geotextile is buried in soils having a very low or high pH or where they may be exposed to solvents such as jet and diesel fuel, special consideration may be required.

Untreated polypropylene is the polymer most quickly degraded by UV radiation while polyester is the least degraded (5, 6). However, many geotextiles with low UV resistance can be chemically treated by adding carbon black or other special chemical additives to increase their UV resistance.

The geotextile industry and researcher have put tremendous effort into the development of suitable stabilizer systems and in the quantification and evaluation of chemical comparability test methods. The majority of test results available are from accelerated tests requested by the user for a particular job application.

As fabric materials are being used more and more in critical applications, it is important to have a better understanding of the process of degradation of these fabrics during installation and throughout the life of the project. A good working knowledge of the expected degradation when the geotextile is in contact with adverse chemicals and exposed to sunlight would enable the user to assess the potential short and long-term performance of a geotextile in a particular project.

Objectives

The specific objectives of this study were:

- 1) to quantify the short and long-term performance effect of chemicals and UV radiation on continuous filament, needlepunched, polypropylene and polyester geotextiles.
- 2) to conclude on the mechanical properties' reduction that should be expected from the geotextiles under experiment when exposed to chemicals and UV radiation.

Study Approach

This paper presents the results of a study to quantify the chemical and UV resistance of two types of geotextile polymers, polypropylene and polyester. The undertaken study approach is shown in Figure 1 and discussed below.

A complete literature review on the subject was conducted to select the geotextiles to be tested and the chemicals. Polyester and polypropylene geotextiles with a weight range of 8-10 oz/sq.yd and with similar manufacturing process, i.e. continuous filament, needlepunched, were selected.

Commonly encountered leachate solutions at highway and airport facilities (cement, lime, jet and diesel fuels spillage), hazardous waste landfill projects (ammonia from decaying organic

matter), coastal protection projects (sea water), and other construction projects, were used. The leachate solutions used in the study are: ammonia, pH = 1.0 and pH = 12, cement, lime, sea water, and jet and diesel fuels.

The testing program undertaken is shown in Figure 1 and is discussed below. The test equipment and procedure for the evaluation of the tensile strength, before and after conditioning, is the ASTM D 4632, Grab tensile Strength of Geotextiles.

Upon completion of the testing program, test results were summarized and analyzed. Comparison charts of the results were prepared and conclusions and recommendations for future research programs were indicated.

TESTING PROGRAM

The test program undertaken in this research to quantify the chemical and UV resistance of polypropylene and polyester geotextiles is presented in Figure 1. The program consisted of four major phases as follows:

- 1) Test specimen preparation,
- 2) Testing of original geotextile specimens, control samples
- 3) Testing of conditioned specimens, and
- 4) Summary of test results.

Specimens used for the evaluation of the leachate chemical compatibility, were tested before and after exposure using the Grab Tensile Strength and Elongation of Geotextiles Method, ASTM D 4632. All tests were conducted wet after 7, 14, 28, and 56 days. Original specimens were tested immediately after sampling preparation to be used as control samples. Pre-cut specimens from each geotextile were conditioned by placing them into each selected leachate solution at room temperature ($23^{\circ}\text{C} \pm 2^{\circ}\text{C}$). After immersion, excess liquid was drained from each specimen, and then samples were immediately tested for tensile strength.

To quantify the UV resistance of polyester and UV chemically stabilized polypropylene geotextiles, past accelerated and on-site UV test conducted, as requested by the user for a particular project, were compiled and evaluated. Accelerated UV tests using a mercury-tungsten-phosphor incandescent (M.B.T.F.) light source and on site UV test (natural light) exposure for a period from June to September were conducted in Australia (7). In addition, accelerated UV tests were conducted in south Florida using ASTM D 4355-84 test method and procedure (8).

A summary of the test results was prepared and is discussed in detail below.

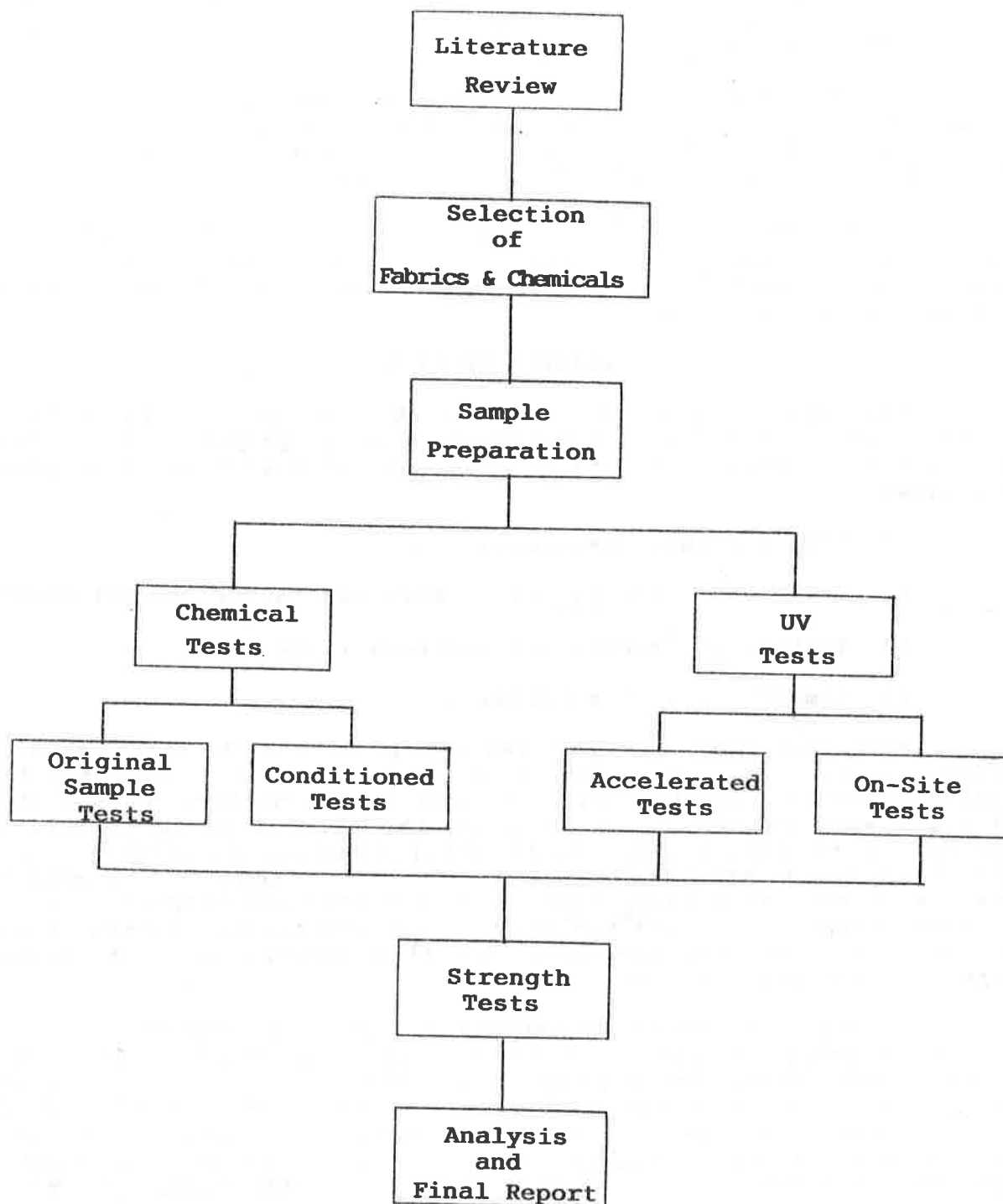


Figure 1 - Study Approach Flow Diagram

TEST RESULTS AND DISCUSSION

Chemical Test

The percent strength retained from the original geotextiles after exposure to the selected chemicals are shown in Figures 2 to 7. The original tensile strength which was used to compute the percent of strength retained, is the average of eighteen (18) tests and the conditioned tensile strength was the average of six (6) tests.

Figure 2 presents the effect of ammonia solutions, pH = 10 and 12. For the pH = 10, both geotextiles show a percent strength retention above 90 percent. A particular trend is not obvious; however, in the pH = 12 ammonia solutions the polyester geotextile shows a high strength loss with a uniform downward trend. The polyester fabric shows a 70 percent strength loss after 28 days immersion in ammonia solution, pH = 12 and turns to slush in about 35 days. The polypropylene geotextile appears to be unaffected after 56 days immersion with a percent strength retention above 92.1 percent.

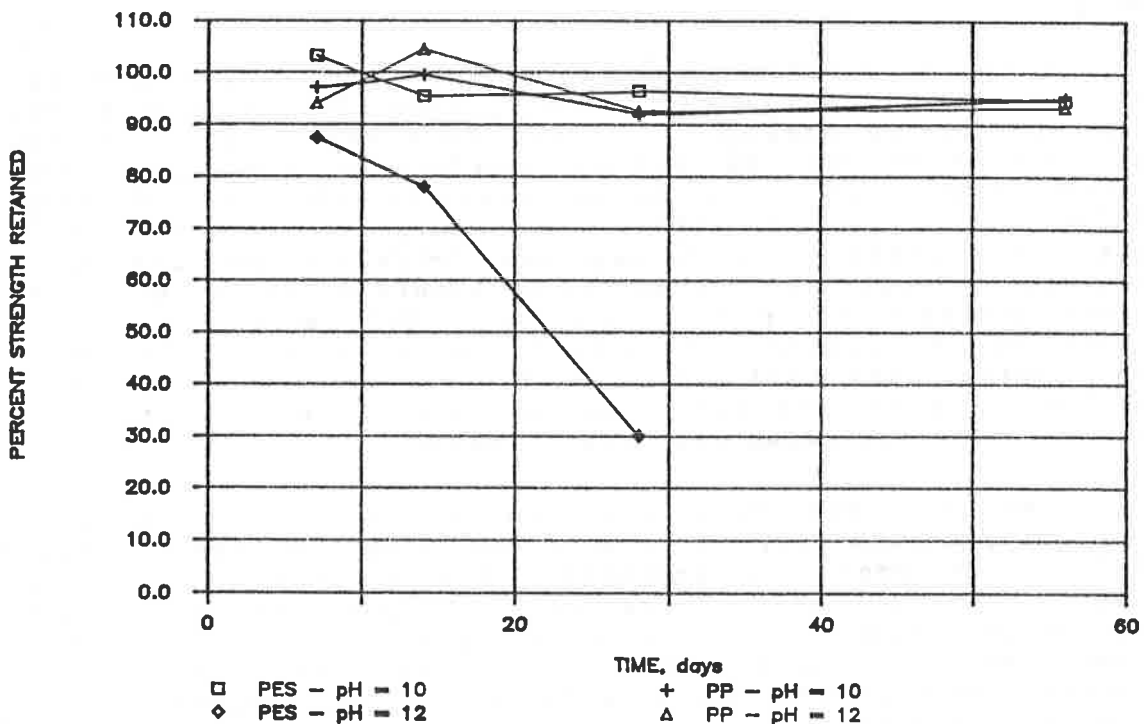


Figure 2 - After Exposure to Ammonia Solutions, pH=10 and 12.

Halse, Y., et al (1) in their research project concluded that polyester geotextiles in pH = 10 solutions did not show a marked strength decrease after 4 months of testing; however, it is possible that a decreasing trend will appear within the expected geotextile life. An increase in the temperature of the leachate solutions might increase the degradation reaction rate.

The cement and lime leachate solutions data, Figure 3 and 4, indicates that polypropylene geotextiles are not affected by these solutions. After 56 days immersion in both solutions, polypropylene showed a strength retention above 92.5 percent. On the other hand, a clear trend can be seen with the polyester geotextile. After 28 and 56 days immersion in the cement leachate solutions, the polyester geotextile retained 72.8 and 56.9 percent of its original strength, respectively. In the lime solutions, the polyester fabric showed a 69.5 and 40.3 percent strength retention after 28 and 56 days immersion, respectively.

The jet and diesel fuel solutions data, Figure 5 and 6, indicates a strong chemical resistance of the polyester geotextile to these environments. After 56 days immersion, polyester appears to be unchanged. However, the polypropylene geotextile shows approximately an initial 20 percent strength loss after 7 days immersion and does not appear to change beyond the 7 days immersion.

Both geotextiles appear to be unaffected when immersed in sea water (Figure 7).

UV Test

Table 1 presents the results of the accelerated testing program in Australia (7) and South Florida (8). Figure 8 presents the percentage of strength retained from the original geotextile properties after the Australian accelerated continuous sunlight exposure tests using a mercury-tungsten-phosphor incandescent (M.B.T.F.) light source (7). Upon averaging the strength test results (ten tests at each exposure interval) the chemically UV stabilized polypropylene geotextile retained 93 percent of its original strength after four (4) weeks (672 hours) of continuous exposure and 84 percent strength retention after eight (8) weeks (1344 hours). The polyester geotextile presented a strength retention of 88 percent and 74 percent after four (4) and eight (8) weeks of continuous exposure, respectively.

The South Florida accelerated testing program (8) using the Xenon-Arc apparatus, ASTM D 4355-84 indicated that the UV chemically stabilized polypropylene geotextile has a 99.5 percent strength retention after 500 hours of exposure. Comparative test results for the polyester geotextile produced in a similar way, i.e., continuous filament, nonwoven, needlepunched indicated a 69.0 percent strength retention. Both geotextiles were tested at the same time by the same laboratory facility.

The loss of strength for the UV chemically stabilized polypropylene geotextile after 6 months of actual on-site exposure to sunlight and weather was minimal. After 17 and 48 weeks on-site exposure to sunlight and weather, the polypropylene geotextile retained 82 and 67 percent strength, respectively. This on-site test was conducted in Australia (7).

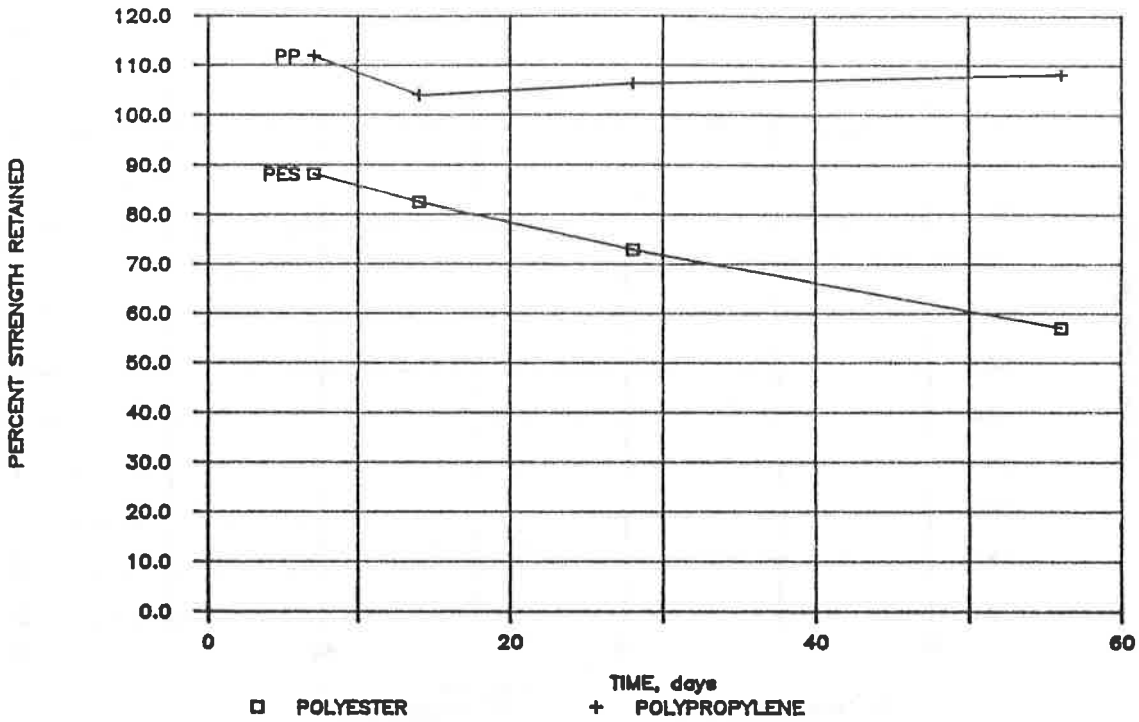


Figure 3 - After Exposure to Cement Leachate Solution.

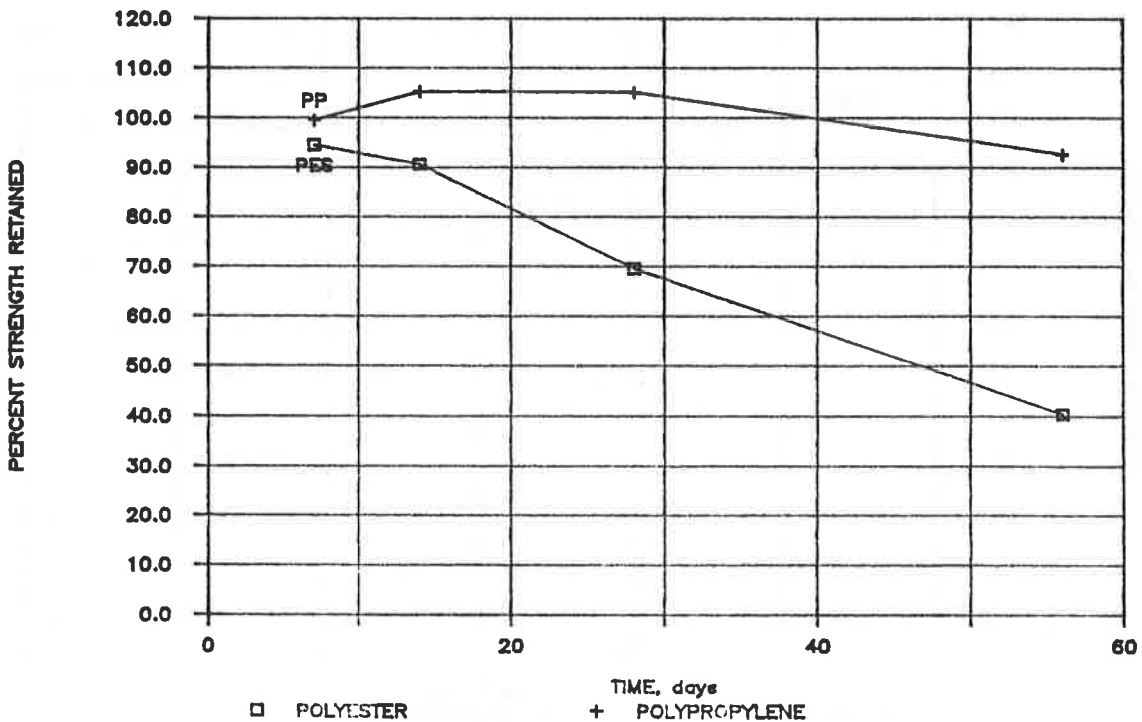


Figure 4 - After Exposure to Lime Leachate Solution.

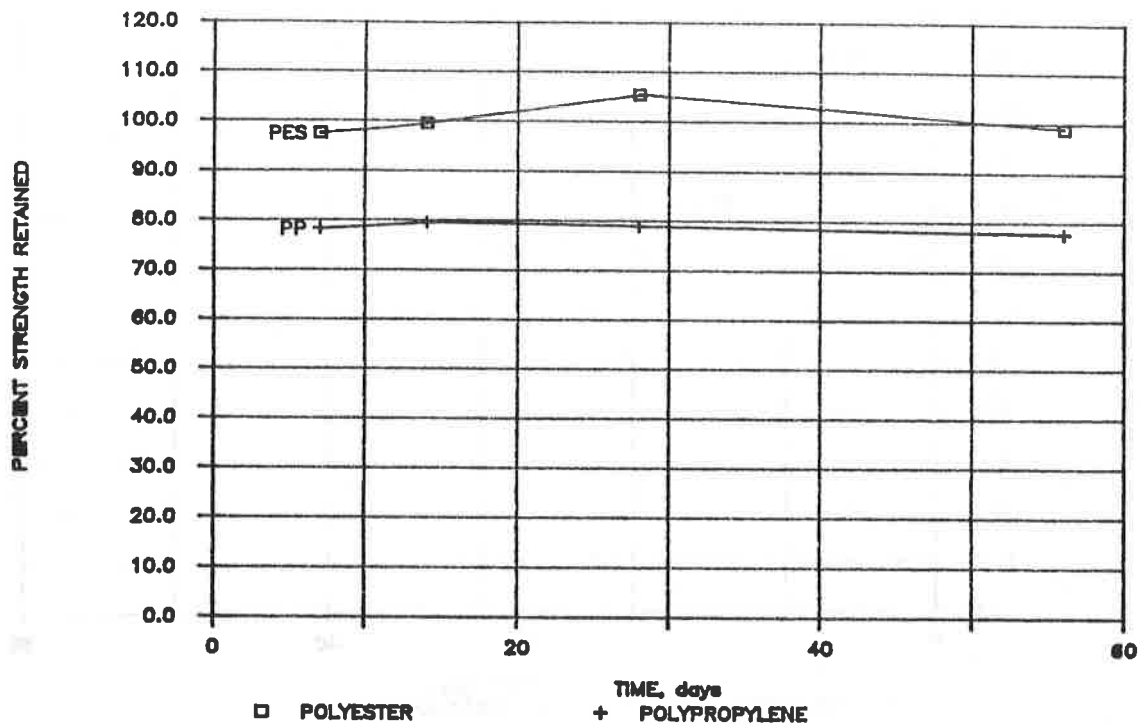


Figure 5 - After Exposure to Jet A-1 Fuel.

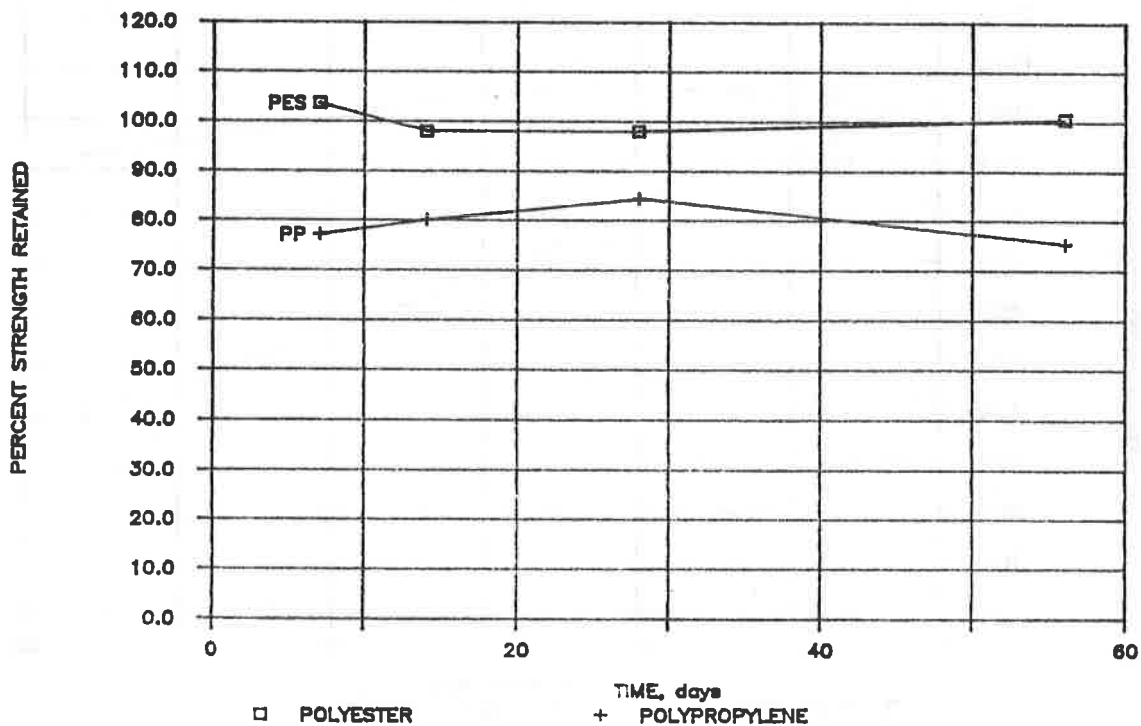


Figure 6 - After Exposure to Diesel Fuel.

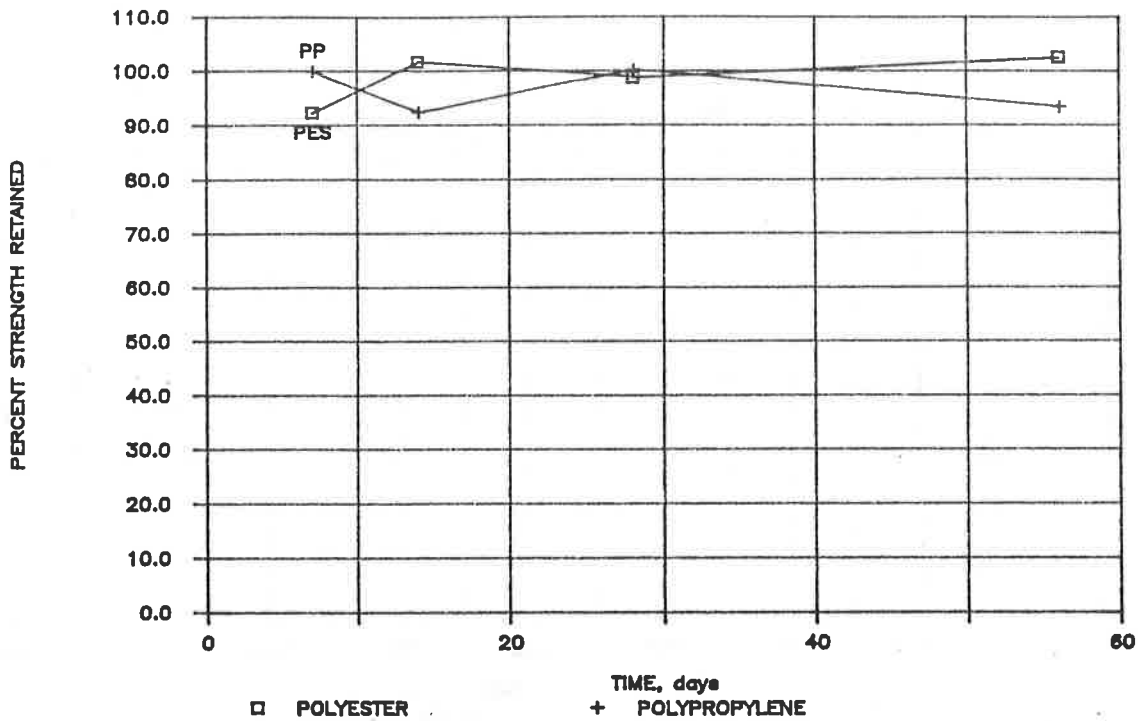


Figure 7 - After Exposure to Sea Water.

TABLE 1: PERCENT STRENGTH RETENTION vs UV EXPOSURE
(UV Stablized Geotextiles)

PERIOD OF CONTINUOUS UV EXPOSURE	*AUSTRALIA TESTS (M.B.T.F. Light Source) NONWOVEN		**SOUTH FLORIDA TEST (ASTM D4355 - 84) NONWOVEN	
	PP	PES	PP	PES
500 hours			99.5%	69.0%
672 hours (4 weeks)	93%	88%		
1344 hours (8 weeks)	84%	74%		
17 weeks (site - Natural Sunlight)	82%			
48 weeks (site - Natural Sunlight)	67%			

*After Reference 7.

**After Reference 8.

PP = Polypropylene
PES = Polyester

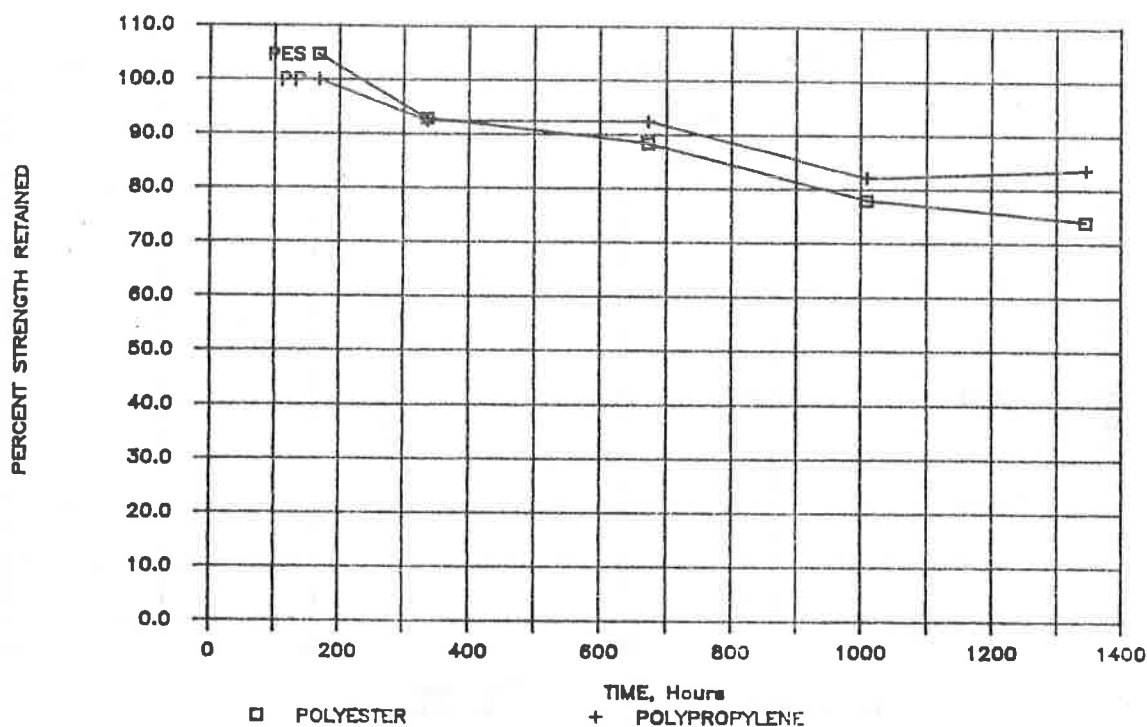


Figure 8 - After Accelerated U.V. Radiation Exposure (M.B.T.F.)(7).

CONCLUSIONS

The influence of chemical leachate solutions and ultraviolet (UV) radiation on the mechanical strength of polyester and UV chemically stabilized polypropylene geotextiles have been investigated, and compared to the original properties of the fabric. The following are the conclusions of this investigation:

- 1) There was not an obvious trend in either fabric when exposed to ammonia solution, pH = 10 after 56 days immersion.
- 2) In the ammonia solution, pH = 12, the strength of the polyester nonwoven geotextile after 28 days dropped to 30 percent of its original property and completely desintegrated after 35 days. The polypropylene geotextile appeared to be unaffected.
- 3) Cement and lime leachate solutions after 56 days immersion, appeared not to damage the polypropylene geotextile. However, a clear trend can be seen with the polyester fabric. After 28 and 56 days immersion in cement, a 27.2 and 43.1 percent strength loss was experienced. After 28 and 56 days immersion in lime, a 30.5 and 59.7 percent strength loss was also evident in the polyester geotextile.

- 4) Jet and diesel fuels test results are indicating a strong chemical resistance of the polyester fabric. The polypropylene geotextile experienced an initial strength loss of 20 percent after 7 days and remain unchanged thereafter.
- 5) Both geotextiles appear to be unaffected when exposed to sea water.
- 6) Test results indicated that U.V. chemically stabilized polypropylene geotextiles have the highest U.V. resistance values.
- 7) Temperature, humidity, global U.V. radiation, type of chemicals and concentrations, etc. to which a fabric is exposed affects the degradation reaction rate. Therefore, the results of this study are only valid for the study conditions.
- 8) Further study is warranted to include other fabrics and additional influence parameters. However, the data presented provides the designer and user with initial values for the experimental conditions which can help in evaluating or projecting the expected degradation of a geotextile.

REFERENCES

1. Halse, Y., Robert M. Koerner, and Arthur E. Lord, Jr., "Effect of Alkalinity of Geotextiles". Geosynthetic Research Institute, Drexel University, 1987.
2. Giroud, J.P., "Behavior of Geotextiles". Presented at NATO Advanced Study Institute on Mechanics of Flexible Fiber Assemblies, Kilini, Greece, 1979.
3. Schneider, H., M. Groh, "An Analysis of the Durability Problems of Geotextiles". Geosynthetics' 87 Conference Proceedings, Volume 2, page 434, New Orleans, USA, 1987.
4. Calhoun, C.C., Jr., "Development of Design Criteria and Acceptance Specifications for Plastic Filter Cloth". Technical Report F-72-7, U.S. Army Engineer Waterways Experiment Station, Vicksburg, MS., 1972.
5. Bell, J.R., R.G. Hicks, et. al., "Evaluation of Test Methods and Use Criteria for Geotechnical Fabrics in Highway Applications". Interim Report No. FHWA/RD-80/021, FHWA, Offices of Research and Development, Structures and Applied Mechanics Division, Washington, D.C., 1980-82.

Geosynthetics '89 Conference
San Diego, USA

6. "Geotextile Engineering Manual". Prepared for Federal Highway Administration by STS Consultants LTD, Northbrook, IL National Highway Institute, FHWA-TS-86-203, U.S. Department of Commerce, National Technical Information Service, 1985.
7. Kinhill Rope PTY LTD, Consulting Engineers, "Accelerated and Outdoors U.V. Technical Laboratory Report". Prepared for Chemie Linz, Australia, 1983.
8. South Florida Test Service, "Accelerated Xeno-Arc U.V. Laboratory Test Report". Prepared for Polyfelt, Inc., 1987.

L.G. TISINGER
GeoSyntec, Inc., U.S.A.

Microstructural Analysis Of The Durability of a Polypropylene Geotextile

SYNOPSIS

This paper addresses a methodology for analyzing the durability of geotextiles after exposure to the environment or aggressive chemicals, as in a compatibility test program. Data are presented that were generated from measurements of composition, oxidative stability, and morphology and chemical structure, using thermal gravimetric analysis, differential scanning calorimetry, and infrared spectrometry, respectively. The geotextile tested was a non-woven polypropylene that was buried for 11 years. Reference samples were taken from material that was manufactured at the same time. The data that were generated indicated minimal change in the microstructure of the material.

INTRODUCTION

Typically, the extent of degradation and the durability of geotextiles have been evaluated solely on the basis of mechanical property test results. Although such tests are ultimately important in assessing the actual performance of the geotextile, information on the microstructure of the base polymer is essential since mechanical properties of the fibers reflect the characteristics of the microstructure of the base polymer.

BACKGROUND

The geotextile examined in the program was a continuous filament, thermally bonded nonwoven polypropylene material. The geotextile was buried for up to 11 years and was used in a separation function in an unpaved road. The geotextile would only have encountered a significant amount of ultraviolet radiation during installation. During service, ultraviolet exposure would have been minimal since the geotextile was buried. Reference samples were obtained from archive samples manufactured at the same time (1975) as the test material.

ULTRAVIOLET AND THERMAL DEGRADATION

Sunlight is composed of ultraviolet and visible light of wavelengths equal to or greater than 290 nm. The susceptibility of polymers to damage by sunlight

varies greatly. Pure polypropylene should be very resistant to ultraviolet and visible light since it does not possess chromophoric sites in its polymeric chain. Chromophores are groups of atoms that can absorb ultraviolet radiation. However, several types of impurities may be present in polypropylene due to processing that can absorb ultraviolet radiation, making polypropylene very sensitive to ultraviolet exposure. These impurities include carbonyl groups and hydroperoxides which absorb ultraviolet radiation at wavelengths beyond 290 nm. Polypropylene typically degrades to lower molecular weight products upon thermal or ultraviolet induced oxidation. This degradation can, however, be minimized with optimum use of antioxidants and other additives (1). Polypropylene is also fairly susceptible to oxidation at elevated temperatures due to its tertiary carbon atom, which is a reactive site on the polypropylene molecule.

LABORATORY EXAMINATION

After retrieval from the site, the geotextile samples were delivered to the laboratory in tightly sealed polyethylene bags. After removal from the bags, the samples were shaken to remove loose dirt. The samples were subsequently washed with deionized water and were dried in a standard laboratory atmosphere (temperature $21 \pm 2^\circ\text{C}$, relative humidity 45-65%). The reference and exposed samples were then subjected to a series of tests as described below.

Chemical Structural Analyses

The samples were subjected to three types of analytical tests: differential scanning calorimetry (DSC), infrared spectroscopy (IR), and thermal gravimetric analysis (TGA). Reference data were generated by performing the same tests on the 1975 reference samples.

The analytical tests were used to assess the effects of environmental exposure on the microstructure of the geotextile. The degrees of crystallinity and oxidative induction temperatures were measured using DSC. Structural characteristics were evaluated using IR. Composition and the temperatures of decomposition were assessed using TGA.

Differential Scanning Calorimetry

In a DSC analysis, the thermal energy required to maintain a test specimen at the same temperature as a reference specimen heated at a constant rate of increasing temperature is monitored. This energy is exhibited as a function of the reference temperature in a thermogram. The thermogram may display endotherms (as typified in Figure 1), corresponding to energy absorbed in the specimen, and exotherms (as typified in Figure 2), corresponding to energy emitted. From endotherms, melting point ranges and degree of crystallinity may be derived. Exotherms provide data for assessing the oxidative stability of the material based on either the oxidative induction time or oxidative induction temperature.

Polypropylene is a semi-crystalline polymer. By comparing the area within the melting endotherm (the heat of fusion) to the heat of fusion of a fully crystalline material such as indium, the degree of crystallinity of the microstructure can be determined.

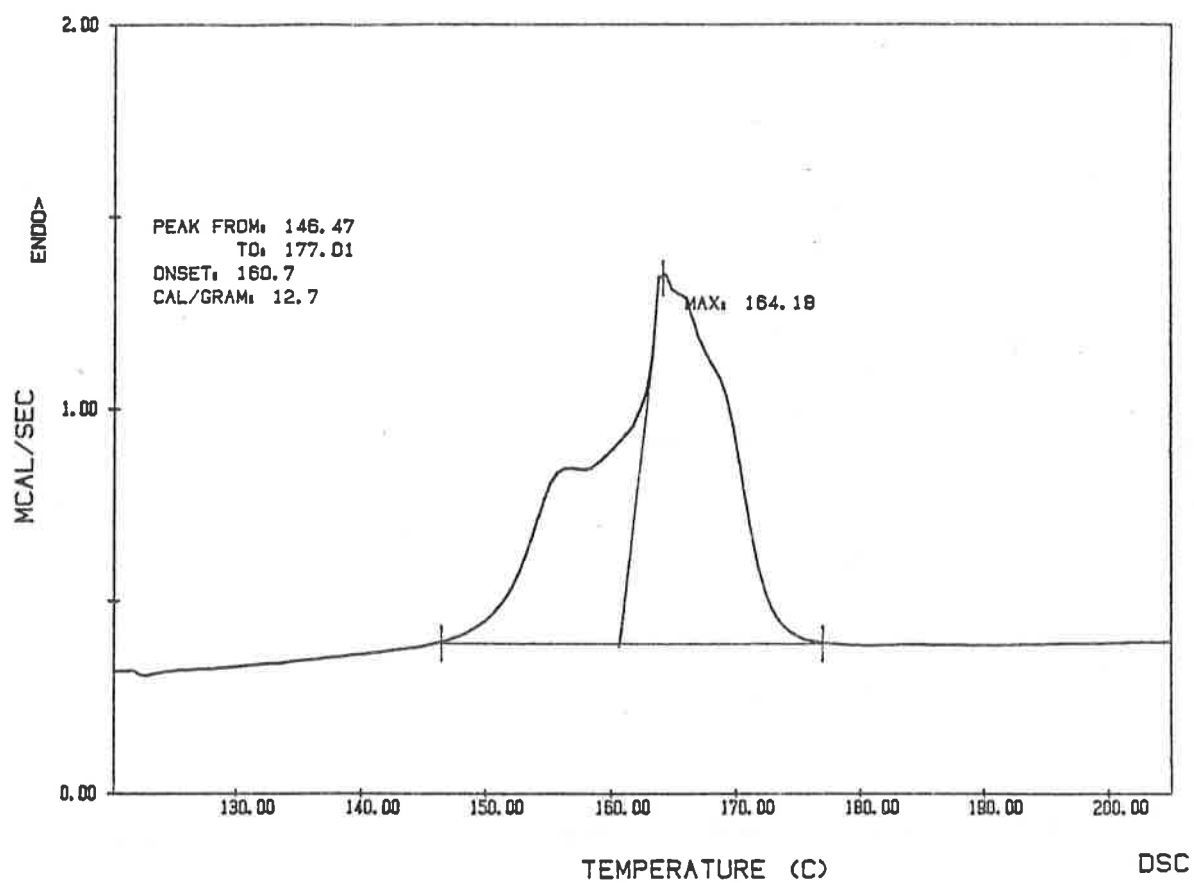


FIGURE 1. Typical endotherm for polypropylene geotextile.

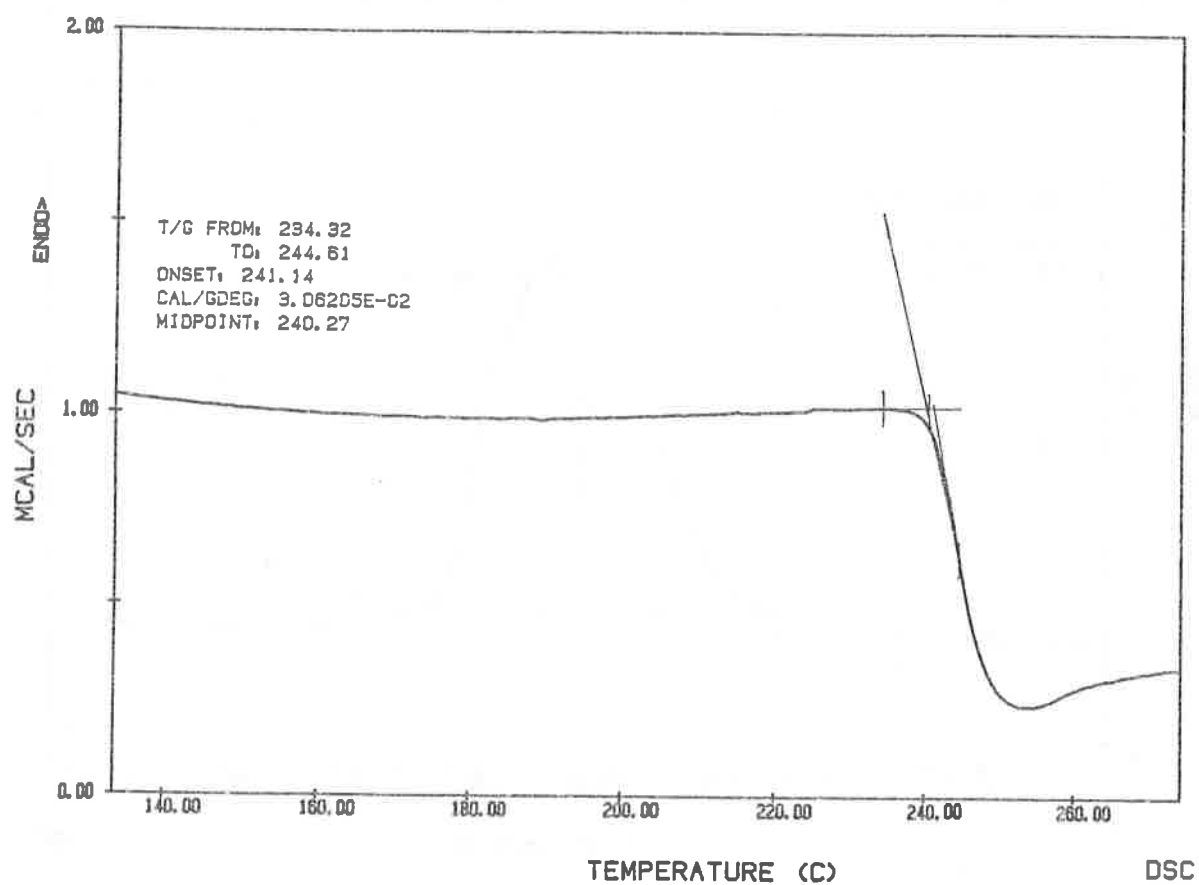


FIGURE 2. Typical exotherm for polypropylene geotextile.

The oxidative induction temperature is the temperature at which reaction of a material with oxygen occurs. The DSC analysis is conducted with the specimen in a reactive atmosphere (air or oxygen), and the oxidative induction temperature value is the temperature at the onset of the exotherm, approximately 232°C in Figure 2. This parameter indicates the oxidative stability of a material (i.e., the effectiveness of the antioxidant package).

Infrared Spectrometry

IR spectra provide information on the structural characteristics of a material. This analytical technique involves exposing the material to infrared radiation at decreasing frequencies. This radiation scan generates a spectrum of bands, each corresponding to a particular frequency or range of frequencies where infrared radiation is absorbed by the specimen. The molecular components of any given material display a characteristic "spectrum of bands," thus allowing correlations or comparisons with spectra from other materials.

IR can be used to identify a specific degradative process in a geotextile through the identification of new spectral bands generated by the products of the degradative process.

Thermal Gravimetric Analysis

TGA provides information regarding the composition of the material through thermal degradation. This technique consists of progressively heating the material in an inert atmosphere, to around 600°C, and measuring the weight loss as a function of temperature (as depicted in Figure 3). The weight loss at any given temperature corresponds to volatilization of a component from the specimen. The data commonly derived from this analysis may include the concentrations of additives, polymer, carbon black, ash, and onset of decomposition temperatures. In order to determine ash content, the carbon black is burned off in an air atmosphere.

PROCEDURE

Small specimens (approximately 1 mg) were taken from the exposed and reference samples for thermal analysis.

Degree of Crystallinity and Oxidative Induction Temperature

Degree of crystallinity and oxidative induction temperature values were obtained using a Perkin-Elmer DSC-4 Differential Scanning Calorimeter with a System 4 microprocessor controller and Model 3700 data station. Oxidative induction temperature tests were conducted in an air atmosphere using a scan rate of 20°C per minute, and degree of crystallinity tests were carried out in a nitrogen atmosphere also using a scan rate of 20°C per minute.

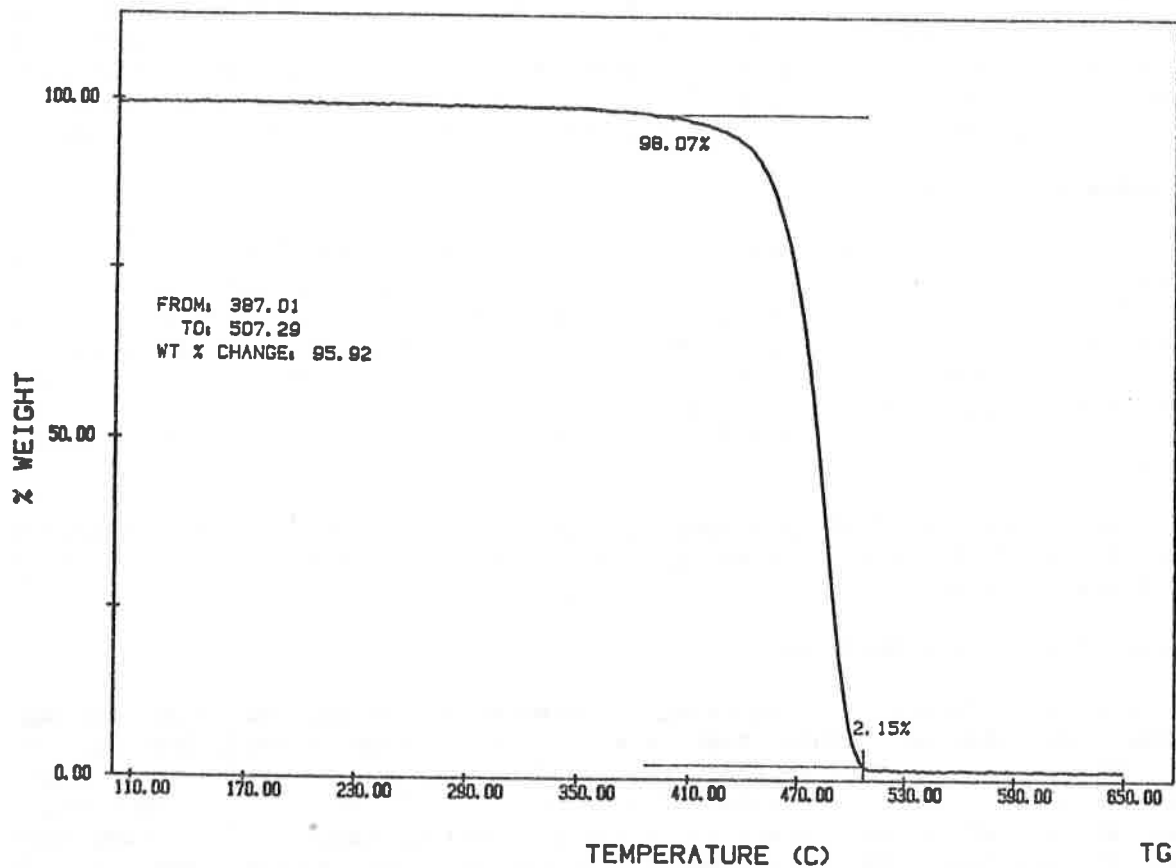


FIGURE 3. Typical weight loss diagram obtained by means of TGA.

Infrared Spectroscopy

Structural characteristics were obtained using a Perkin-Elmer 283B Infrared Spectrophotometer with a Model 3500 data station. The fibers were analyzed using potassium bromide pellets.

Thermal Gravimetric Analysis

TGA was conducted using a Perkin-Elmer TGS-2 with a System 4 microprocessor controller and Model 3700 data station. The measurements were carried out in a nitrogen atmosphere using a scan rate of 20°C per minute.

RESULTS

The results of the DSC, TGA, and IR tests conducted on the reference and exposed geotextile samples are presented in both tabular and graphical forms.

Degree of Crystallinity and Oxidative Induction Temperature

The results of the DSC scans for determinations of degree of crystallinity and melting range are presented in Table 1. The results of oxidative induction temperature tests are presented in Table 2.

TABLE 1
DEGREE OF CRYSTALLINITY AND MELTING RANGE
FOR POLYPROPYLENE GEOTEXTILES

Sample Number	Reference Sample		Exposed Sample	
	Crystallinity (%)	Melting Range (°C)	Crystallinity (%)	Melting Range (°C)
1	28.58	127.30-180.81	22.99	119.13-182.89
2	24.31	119.12-179.96	29.27	119.50-190.67
3	25.71	122.83-182.33	20.48	128.48-180.81
4	27.22	133.95-178.29	33.00	129.82-181.59
5	26.06	125.35-176.91	21.82	119.50-186.97
Average	26.38	125.71-179.66	23.51	123.29-184.59
σ_{n-1}^*	1.61	5.53- 2.12	5.37	5.38- 4.15

* σ_{n-1} = Standard Deviation

TABLE 2

OXIDATIVE INDUCTION TEMPERATURE
FOR POLYPROPYLENE GEOTEXTILES

Sample Number	Reference Sample	Exposed Sample
1	240.97°C	228.87°C
2	238.84°C	202.86°C
3	238.97°C	227.94°C
4	237.09°C	208.42°C
5	239.52°C	231.29°C
Average	239.10°C	219.88°C
σ_{n-1}^*	1.40°C	13.20°C

* σ_{n-1} = Standard Deviation

The degree of crystallinity values show relatively small changes in the crystalline structure after environmental exposure. The range of values, plus or minus one standard deviation, of the reference material still falls within the same parameters for the exposed material. The melting ranges are wider in the exposed samples. This indicates the presence of impurities in the sample, which may reduce cohesive forces between polymer chains composing the fibers.

The oxidative induction temperature values for the exposed samples show a significant reduction, which indicates that partial consumption of the antioxidants has occurred due to environmental exposure.

Structural Characteristics

Infrared spectra for the reference and exposed samples are shown in Figures 4 and 5, respectively.

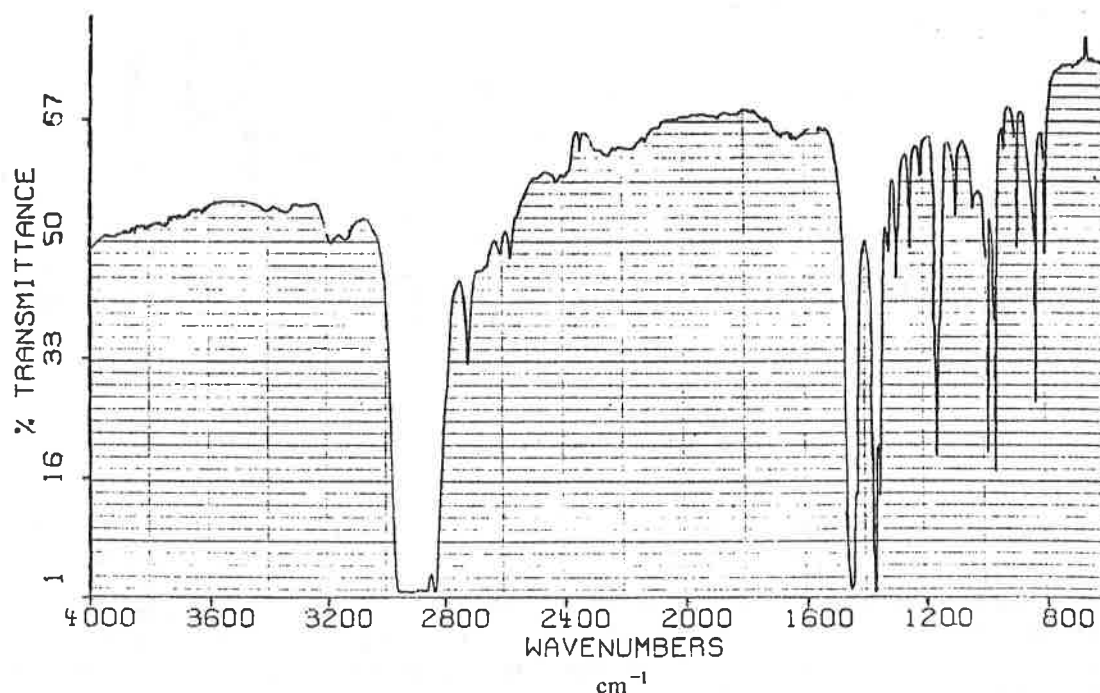


FIGURE 4. Infrared spectrum for reference polypropylene geotextile.

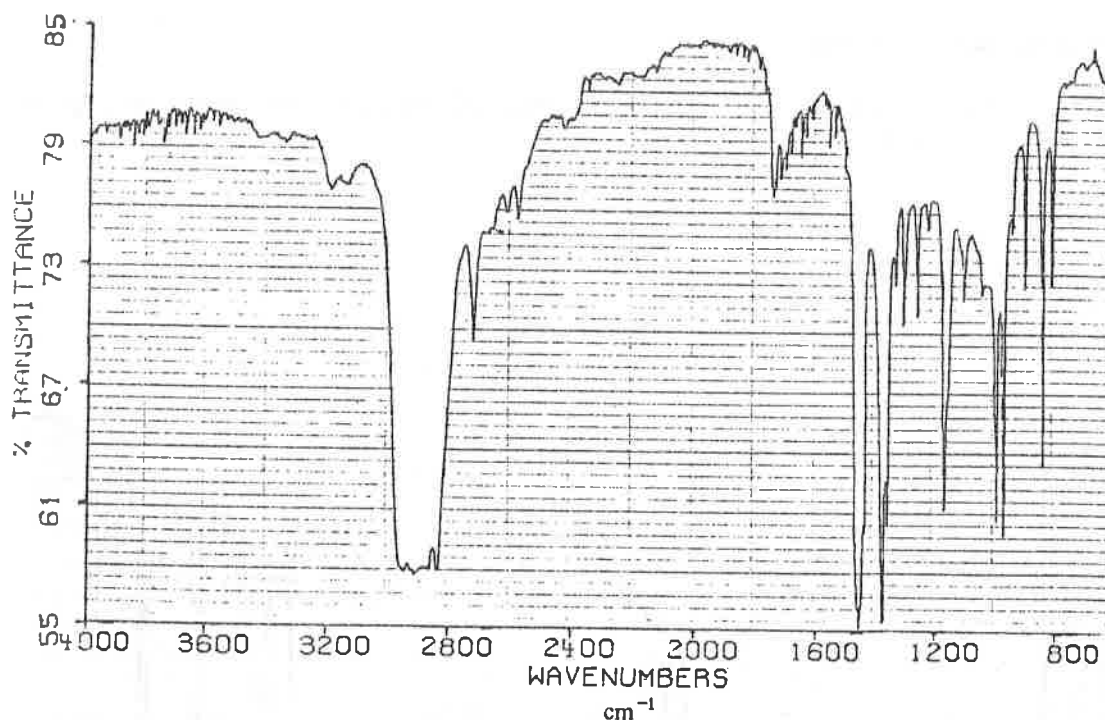


FIGURE 5. Infrared spectrum for exposed polypropylene geotextile.

The infrared spectrum for the exposed geotextile has the same features as the reference IR spectrum. The spectral bands occurring around 3400 cm^{-1} and 1750 to 1850 cm^{-1} are those bands that are consistent with oxidation on the base polymer chain. Some development of bands in the 1750 to 1850 region was observed.

Thermal Gravimetric Analysis

Table 3 lists weight loss temperatures and composition for the reference and the exposed geotextiles.

TABLE 3
COMPOSITION AND WEIGHT LOSS TEMPERATURES

Property	Unit	Reference	Exposed
Polymer	%	96.43	72.70
Ash	%	3.08	26.51
Temperature at 5% Weight Loss	°C	276.54	310.30
Temperature at 50% Weight Loss	°C	336.40	389.40

Table 3 shows one weight loss fraction (i.e., the presence of one polymer in both the exposed and reference geotextiles), indicating the homogeneity of the polypropylene fibers. Weight loss decomposition temperatures at 5% and 50% weight loss are higher for the exposed geotextile, which indicates that greater energy is required to decompose the exposed sample. This appears consistent with ultraviolet crosslinking of the base polymer. The exposed sample displays a higher residue percentage, probably due to soil particles embedded in the geotextile.

DISCUSSION

The exposed geotextiles would have encountered ultraviolet radiation in significant quantities only during installation and exhumation. Grassie and Leeming (2) found that short-term exposure of commercial polypropylene fibers to ultraviolet radiation at ambient temperatures (around 20°C) can result in increased molecular weight of the base polymer. Indeed, the relatively short exposure of the geotextile to ultraviolet radiation appears to have affected its various characteristics. Specifically, crosslinking was indicated through increased weight loss temperatures observed in the TGA scans, however, it was not indicated by the crystallinity values. This is consistent with a high proportion of crosslinking occurring in the amorphous region of the fibers. A higher proportion of oxidation would also likely occur in the amorphous regions (3) at the surface, since permeation of oxygen through crystalline regions is limited. Oxidative induction temperatures were reduced by 20°C for the exposed material, which indicates partial consumption or a lower initial concentration of the stabilizer package. If oxidation had occurred to the extent of depletion of the antioxidant package, oxidation during the test would have occurred at significantly lower temperatures (4).

The IR test results did not indicate a significant change in the molecular structure of the base polymer since the spectral features of the reference and exposed materials appeared consistent with each other. The exception is a slight development of bands in the 1750 to 1800 cm^{-1} region of the spectrum of the exposed geotextile, which is consistent with an oxidative process.

CONCLUSION

The polypropylene fibers appear to have been affected, albeit insignificantly, by short-term exposure to ultraviolet radiation. Lower oxidative induction temperatures and apparent crosslinking of the individual fibers were observed. The tests on the bulk geotextiles have confirmed the minimal effect of environmental exposure on these materials (5). Further work will involve measuring bulk properties, as well as more extensive IR studies and average molecular weight measurements on the fibers.

REFERENCES

- (1) Carlsson, D.J. and Wiles, D.M., "Effects of UV Light on the Mechanical Properties of Fiber Forming Polymers," Ultraviolet Light Induced Reaction in Polymers, American Chemical Society, Washington, D.C., 1976.
- (2) Grassie, N. and Leeming, W.B.H., "Influence of UV Irradiation on the Stability of Polypropylene and Blends of Polypropylene with Polymethyl Methacrylate," American Chemical Society Symposium Series, Washington, D.C., 1976, pp. 367-390.
- (3) Tisinger, L.G., Peggs, I.D., and Kimmet, J., "Differential Scanning Calorimetry Interpretation of Results Obtained on Polyethylene Geosynthetics," Proceedings of the 10th Annual Madison Waste Conference, Madison, Wisconsin, September 29-30, 1987.
- (4) Brydson, J.A., Plastics Materials, 4th Ed., Butterworth Scientific, London, 1982, p. 234.
- (5) Bonaparte, R., Ah-Line, C., Charron R., and Tisinger, L., "Survivability and Durability of a Nonwoven Geotextile," Proceedings of the ASCE Conference, Nashville, Tennessee, 1988.

R.M. KOERNER

M.H. WAYNE

Drexel University, U.S.A.

R.G. CARROLL

Tensar Corporation, U.S.A.

Analytic Behavior Of Geogrid Anchorage

ABSTRACT

Of the various reinforcement functions that geogrids can provide, anchorage (or pullout resistance) under sustained load conditions is most significant. Past approaches toward assessing this type of behavior have been attempted using large scale pullout boxes and rapid testing. But with the wide variety of geogrid products currently available, and with the endless types of soils, densities, moisture contents, surcharge pressures, etc., the results to date are varied and few. Additionally, the time required for testing under sustained loading conditions further limits available information. As a result it is felt that the framework for an analytic investigation is appropriate.

Presented in this paper is an analytic study on the hypothetical behavior of geogrids in an anchorage mode. It uses geotechnical engineering principles in that the geogrid's resistance is offered by (a) shear stress against the top and bottom of longitudinal ribs, (b) shear stress against the top and bottom of transverse ribs and (c) bearing capacity against the front of the transverse ribs. After setting up the mathematical formulation, a number of variations are assessed. These include the effect of estimated rib stiffness and junction strength along with estimates of anchorage capability at varying amounts of strain. The analysis does not try to integrate a time factor into the process but assumes ultimate anchorage capacity for the design life of the reinforced structure. Results are presented in a graphic format.

INTRODUCTION

While their use in North America is relatively recent, geogrids have been developed and used in Europe for over a decade. A 1984 Conference sponsored by the British Institute of Civil Engineers in London helped to bring focus on geogrids to the worldwide Civil Engineering community.⁽¹⁾ Their introduction to North America was via Canada in 1982 and shortly thereafter into the USA.

In the broadest sense, geogrids can be defined as being intersecting polymeric strips (called "ribs") formed or joined together at their intersections (called "junctions"). Depending on the orientation of the sheets, the ribs are further characterized as being either longitudinal (i.e. in the fabricated or manufactured direction) or transverse. Resulting from the relatively narrow width of the ribs with respect to their center-to-center spacing, geogrids are left

Geosynthetics '89 Conference
San Diego, USA

with rather large open spaces between sets of ribs which are called "apertures". Apertures are typically 1 to 15 cm in dimension and are either square, oval, or rectangular in shape. The longitudinal and transverse ribs are at right angles to one another at their junctions by design to enhance their interaction and reinforcement capability in soils.

Today, there are a number of commercially available products in North America, an even wider range worldwide, and probably more to become available in the future, see Table 1 for details of the products available as of this writing. They vary in polymer type; strength, size and stiffness of ribs; type, manner and methods of joining ribs at junctions; type and size of apertures; mass per unit area and general overall appearance. With such variability of the current geogrid products, it was felt that a geotechnical engineering assessment of their behavior in a major reinforcement mode, i.e. that of anchorage, would be of value. It is toward this end that this analytic study is directed. It should be emphasized at the outset that this is not a laboratory nor a field study, but one that is based solely on hypothesized behavior of the various geogrids within a soil mass. It is hoped that the study will form a framework from which full, or large, scale test results can be compared and contrasted. If so, such relevant items as rib size, stiffness and junction strength capacity can be quantified and appropriately designed.

Table 1 - Physical and Mechanical Properties of Currently Available Geogrids

PRODUCT	STRUCTURE	POLYMER	JUNCTION METHOD	Aperture Size	Thickness-mm	w-md	w-xmd	Ult. Wide Width Tensile (KN/m)	
				MD/XMD (cm)	rib/junction	(cm)	(cm)	MD	XMD
R-UX	punched sht drawn	polyethylene	united	10/1.5	1.4/4.6	0.64	1.3	78.7	-
R-BX	punched sht drawn	polypropylene	united	2.5/3.3	1/3.8	0.32	0.32	17.1	30.6
X-UX	punched sht drawn	polyethylene	united	12/1.5	1.6/1.6	0.48	1.3	60	-
X-BX	punched sht drawn	polypropylene	united	6.4/6.1	.79/.79	0.08	0.08	16	10.2
S-UX	intersecting strips	polyester	ultrasonic	6.4/6.4	.76/1.5	1.1	1.1	43.7	43.7
S-BX	intersecting strips	polyester	ultrasonic	2.5/9	.76/1.5	1.1	1.1	87.5	32.8
M-BX	woven and knit	polyester-latex coated	knit stitch	3/3.3	2/2.2	0.8	0.32	38.9	23.5
I-UX	intersecting strips	polyester-PP coated	melt bonded	14/6.4	2.5/4.3	1.3	0.95	100	24.8

FUNCTION AND MECHANISMS

Unlike other geosynthetic materials which can function in a number of mechanisms, geogrids are designed for soil reinforcement. Some of the major application areas include the following;

- to reinforce steepened soil slopes,
- to reinforce soil backfill behind retaining walls,
- to reinforce soil embankments, dikes, berms and dams,
- to provide enhanced bearing capacity for foundations,
- to reinforce stone base, aggregate and ballast subbase materials, and
- to reinforce asphalt and concrete pavement materials.

The various mechanisms involved in the above reinforcement applications are either tensile strength, shear strength or anchorage strength. Regarding each of these items the following comments apply. Determination of tensile strength is seemingly straightforward in that the geogrid is evaluated by single or multiple

rib tests thereby obtaining the desired stress versus strain curve⁽²⁾. It should be noted, however, that the long term conditions are often not included in such tests and should always be considered vis-a-vis the lifetime of the intended structure. Shear strength is evaluated by an adaptation of the direct shear test common to geotechnical engineering testing⁽³⁾. Lastly, anchorage strength is evaluated in a large soil filled box.^(4,5) Such anchorage behavior is clearly seen in the rupture patterns shown in Figure 1. The photograph was made by pulling a geogrid out of a container filled with sintered glass particles. Glycerine was used to fill the void spaces and then the system was viewed under polarized light, after Dyer⁽⁶⁾. Note the passive wedges formed against the transverse ribs as the geogrid is pulled toward the right.

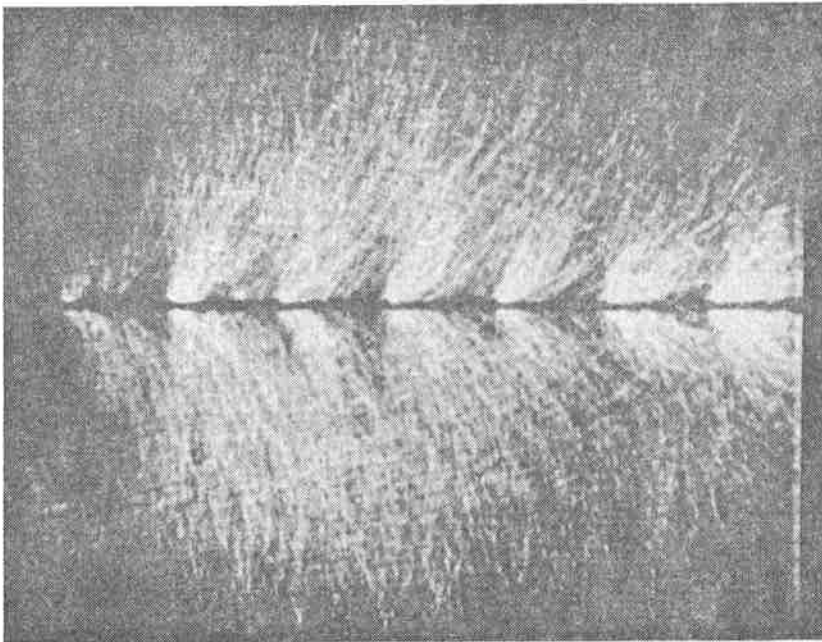


Figure 1 - Geogrid pulled from sintered glass particles as viewed under polarized light, after Dyer ⁽⁶⁾

It is this last test concerning anchorage, or pullout, where major difficulties arise. The size of the box must be large, typically 1 m wide by 1 m deep by 2 m length, requiring large quantities of carefully placed soil, with the geogrid gripped internally, and the soil surface properly loaded to the anticipated normal stresses. For every geogrid to be evaluated, with all possible soils, under a variety of loading conditions is a horrendous task, particularly in the absence of an analytic framework. Additionally, the pullout tests commonly used are rapid tests and do not account for the effects of creep strain in the grid structure.

ANCHORAGE FUNDAMENTALS

A geogrid's aperture size versus the particle size of the soil backfill is important in the development of a geogrid's anchorage strength. Clearly, the soil must be capable of striking-through the apertures resulting in continuity of the backfill soil above and below the plane of the geogrid. Sarsby⁽⁷⁾ has proposed

the following relationship in this regard:

$$B_{GG}/d_{50} \approx 3.5 \quad (1)$$

where

B_{GG} = minimum width of geogrid aperture

d_{50} = average particle size of backfill soil

Once the above requirement is satisfied, a geogrid's anchorage ability to resist pullout stress can be hypothesized. In short, when pullout stress begins to be mobilized in the plane of the geogrid it is simultaneously resisted by three components;

- shear resistance along the top and bottom of the longitudinal ribs,
- shear resistance along the top and bottom the transverse ribs, and
- bearing capacity resistance in front of the transverse ribs.

These three components are illustrated in Figure 2. As the pullout stress is further mobilized, however, a number of features interact to complicate this idealized picture. Concerning the soil's behavior; shear strength and bearing capacity strength are mobilized at different strains for different soil types, densities, water contents and normal stresses. Concerning the geogrid's behavior; varying rib stiffness (primarily the transverse ribs) will mobilize shear and bearing differently, and the ability to transfer these strength components through the junction can be a limiting factor. To complicate the picture further one must consider long term sustained stress since most of the applications noted earlier were of a permanent nature involving a certain degree of criticality.⁽⁸⁾ Thus creep strength of the geogrid's structure, which involves interaction of both ribs and junctions, must be kept in mind.

ANALYTIC HYPOTHESIS AND RESULTS

Using Figure 2 as our design model and bearing in mind the behavior just described, we have separated the three anchorage components which results in the following formulation

$$A = LR_S + TR_S + TR_B \quad (2)$$

where

A = cumulative anchorage capability

LR_S = shear stress in longitudinal ribs

$$= 2\tau (L \times w_l) N_w \quad (3)$$

TR_S = shear stress in transverse ribs

$$= 2\tau [(W \times w_t) - (w_l \times w_t) N_w] N_L \quad (4)$$

TR_B = bearing stress on transverse ribs

$$= q_o [(W \times t_t) - (w_l \times t_t) N_w] N_L \quad (5)$$

and

τ = shear strength of soil to geogrid rib material

q_o = bearing capacity of the backfill soil

N_w = number of ribs per $W = W/(a_t + w_l)$

N_l = number of ribs per $L = L/(a_l + w_t)$

a_t = aperture opening in transverse direction
 a_l = aperture opening in longitudinal direction
 W = unit width in transverse direction
 L = anchorage length in the longitudinal direction
 w_l = width of ribs in longitudinal direction
 w_t = width of ribs in transverse direction
 t_t = thickness of ribs in transverse direction

Using the above formulation, a series of curves were generated at different values of normal stress corresponding to 1, 2 and 3 m of soil fill depth. The soil's unit weight was taken as 17.2 kN/m³ and the anchorage length of the geogrid in each case was assumed to be 1 m. No pore water pressures were included in the analysis. The bearing capacity term utilized a friction angle of 35° in the " $q N_q$ " term which is common to geotechnical engineering bearing capacity analysis of shallow foundations. The soil-to-geogrid friction angle was assumed to be 30° irrespective of the type of geogrid. Resulting curves corresponded to the following conditions:

- Figure 3 represents the full mobilization of all three anchorage components described in equation #2. Table 2 lists the pullout strength calculated for these three components with respect to each grid type. Note the large contribution of the transverse ribs in both shear and bearing toward the total geogrid anchorage strength.
- Figure 4 represents mobilization based on estimated values of rib stiffness and junction strength (see ref. 9) as outlined in Table 3. (Table 2 gives numeric results for each component as discussed above where again transverse rib contribution in both shear and bearing is significant). It is felt to be representative of the particular geogrids involved but awaits further substantiation via laboratory or field data.

Table 2 - Breakdown of Geogrid Mobilization Components

PRODUCT	Depth of Soil (m)	TOTAL MOBILIZATION (Figure 3)				ESTIMATED MOBILIZATION (Figure 4)			
		LRs [(KN/m)/%]	TRs [(KN/m)/%]	TRb [(KN/m)/%]	TOTAL [(KN/m)/%]	LRs [(KN/m)/%]	TRs [(KN/m)/%]	TRb [(KN/m)/%]	TOTAL [(KN/m)/%]
R-UX	1	8.0/33	2.0/8	14.0/59	24.0/100	8.0/33	2.0/8	14.0/59	24.0/100
	2	16.0/33	3.0/6	29.0/61	48.0/100	16.0/33	3.0/6	29.0/61	48.0/100
	3	24.0/33	5.0/7	43.0/60	72.0/100	24.0/33	5.0/7	43.0/60	72.0/100
R-BX	1	2.0/7	3.0/11	23.0/82	28.0/100	2.0/13	1.0/7	12.0/80	15.0/100
	2	4.0/7	5.0/9	46.0/84	55.0/100	4.0/13	3.0/10	23.0/77	30.0/100
	3	6.0/7	8.0/10	69.0/83	83.0/100	6.0/13	4.0/9	35.0/78	45.0/100
X-UX	1	6.0/46	2.0/15	5.0/39	13.0/100	6.0/46	2.0/15	5.0/39	13.0/100
	2	12.0/50	3.0/13	9.0/37	24.0/100	12.0/50	3.0/13	9.0/37	24.0/100
	3	18.0/49	5.0/14	14.0/37	37.0/100	18.0/49	5.0/14	14.0/37	37.0/100
X-BX	1	2/3	2/3	6.0/94	6.4/100	2/100	0/0	0/0	2/100
	2	1.0/8	0/0	12.0/92	13.0/100	1.0/100	0/0	0/0	1.0/100
	3	1.0/5	1.0/5	18.0/90	20.0/100	1.0/100	0/0	0/0	1.0/100
S-UX	1	2.0/11	5.0/28	11.0/61	18.0/100	2.0/13	5.0/31	9.0/56	16.0/100
	2	4.0/11	11.0/31	21.0/58	36.0/100	4.0/12	11.0/33	18.0/55	33.0/100
	3	7.0/13	16.0/29	32.0/58	55.0/100	7.0/14	16.0/32	27.0/54	50.0/100
S-BX	1	3.0/27	3.0/27	5.0/46	11.0/100	3.0/30	3.0/30	4.0/40	10.0/100
	2	6.0/29	5.0/24	10.0/47	21.0/100	6.0/32	5.0/26	8.0/42	19.0/100
	3	9.0/28	8.0/25	15.0/47	32.0/100	9.0/30	8.0/27	13.0/43	30.0/100
M-BX	1	4.0/12	2.0/6	28.0/82	34.0/100	4.0/36	0/0	7.0/64	11.0/100
	2	8.0/12	3.0/5	55.0/83	66.0/100	8.0/35	1.0/4	14.0/61	23.0/100
	3	12.0/12	5.0/5	83.0/83	100.0/100	12.0/35	1.0/3	21.0/62	34.0/100
I-UX	1	3.0/25	1.0/8	8.0/67	12.0/100	3.0/60	0/0	2.0/40	5.0/100
	2	7.0/28	2.0/8	16.0/64	25.0/100	7.0/58	1.0/8	4.0/34	12.0/100
	3	10.0/27	3.0/8	24.0/65	37.0/100	10.0/59	1.0/6	6.0/35	17.0/100

Table 3 - Assumptions Used to Develop the Curves in Figure 3

Product	Percent of LR _s	Percent of TR _s	Percent of TR _b
	Longitudinal Rib Shear	Transverse Rib Shear	Transverse Rib Bearing
R-UX	100	100	100
R-BX	100	50	50
X-UX	100	100	100
X-BX	100	0	0
S-UX	100	100	85
S-BX	100	100	85
M-BX	100	25	25
I-UX	100	25	25

- Figure 5 represents a variation of Figure 4 but now at less than the failure state, e.g., at approximately 5% strain. Here it is arbitrarily assumed that the shear on both longitudinal and transverse ribs are fully acting, but the bearing capacity is only at 50% of full mobilization.
- Figure 6 represents the situation at still a lower strain level, e.g., at approximately 2% strain. Here it is arbitrarily assumed that the shear on both longitudinal and transverse ribs is at 50% of ultimate and the bearing capacity is only at 25% of full mobilization.
- Figure 7 represents a variation of Figure 4 again at a value less than the failure state, e.g., at approximately 5% strain, but now in a cohesive backfill soil. Here the mobilized proportions of strength are arbitrarily assumed to be 50% of longitudinal and transverse rib shear and 25% of transverse rib bearing. Thus the results should be contrasted against those of Figure 5 for granular soils.
- Figure 8 represents the situation at a lower strain level than that of Figure 7, e.g., at approximately 2% strain, and again in a cohesive backfill soil. Here the mobilized proportion of strength were arbitrarily further reduced to 25% of longitudinal and transverse rib shear and 12.5% of transverse rib bearing. These results should be contrasted against those of Figure 6 for granular soil.

DISCUSSION OF ANALYTIC RESULTS

Utilizing the curves just presented as background information a series of comments can be offered. They are as follows:

- Full mobilization of all three anchorage terms (as presented in Figure 3) is felt to be quite unrealistic due to (a) nonuniform strain mobilization of shear and bearing stresses (b) transverse rib flexibility in mobilizing its shear and bearing stresses, and (c) inadequate junction strength to transfer both shear and bearing stress from transverse ribs to longitudinal ribs.
- The latter two items are felt to be eliminated in the data of Figure 4. The adjustment factors for the various products are found in Table 3. Please note that they are arbitrary and based on observed flexibility and measured unconfined junction strengths (9). The response of the curves is seen to be very different from the comparable curves of Figure 3. Clearly, different geogrid products behave differently from one another in this type of analysis.

- At working strain levels of approximately 5% and 2%, the pullout capacities are obviously lower than at failure strain levels as was seen in Figures 3 and 4. The response curves are shown in Figure 5 for granular soil at 5% and Figure 6 for granular soil at 2%. Used in the analysis were estimated values of geogrid strength mobilization in typical sand/gravel soils for both shear and bearing.
- The complement to the above curves of Figures 5 and 6 in granular soil are the curves of Figures 7 and 8 for cohesive backfill soils. At both strain levels (5% and 2%) the pullout capacities fall noticeably lower due to reduced friction strength and bearing capacity of cohesive versus granular soils. This signifies the necessity of longer embedment lengths of geogrids when placed in cohesive soil.

SUMMARY AND CONCLUSIONS

Presented in this paper was an analytic modeling of the anchorage behavior of geogrids. The theory was based on separate components of longitudinal rib shear, transverse rib shear and transverse rib bearing capacity. Using dimensions and properties of commercially available geogrids a set of anchorage capacity response curves was generated.

These curves disclosed that maximum geogrid performance was obtained using;

- large rib surface areas
- high friction rib surfaces
- rigid rib structures
- high junction strengths
- granular, versus cohesive, soils
- high normal stresses

Most importantly, however, is that a generalized design model of geogrid behavior is now available for which field and laboratory tests can be compared. The results should now be compared to large scale laboratory tests of geogrid pullout behavior and the theory that was developed on the basis of these results, see Bonczkiewicz, et al. (5).

REFERENCES

1. -----, "Symposium on Polymer Grid Reinforcement in Civil Engineering," Institute of Civil Engineers, London, England, March 22-23, 1984.
2. McGown, A., Andrawes, K. Z., Yeo, K. C. and DuBois, D., "The Load-Strain-Time Behavior of Tensar Geogrids," Proc. Symp. on Polymer Grid Reinforcement in Civil Engineering," ICE, London, 1984 Paper #1.2.
3. Ingold, T. S., "Laboratory Pull-Out Testing of Grid Reinforcements in Sand," Geotech. Testing Jour., ASTM, Vol. 6, No. 3, Sept. 1983.
4. Jarrett, P. M. and McGown, A., Eds., "Application of Polymeric Reinforcement in Soil Retaining Structures," Royal Military College of Canada, Kingston, Ontario, Canada, NATO ASI Series, Vol. 147, Kluiver Academic Publs., Dordrecht, The Netherlands.
5. Bonczkiewicz, C., Christopher, B. R. and Atmatzidis, D. K., "Evaluation of Soil Reinforcement Interaction by Large Scale Pullout Tests," Proc. Symp. on

Geosynthetics '89 Conference
San Diego, USA

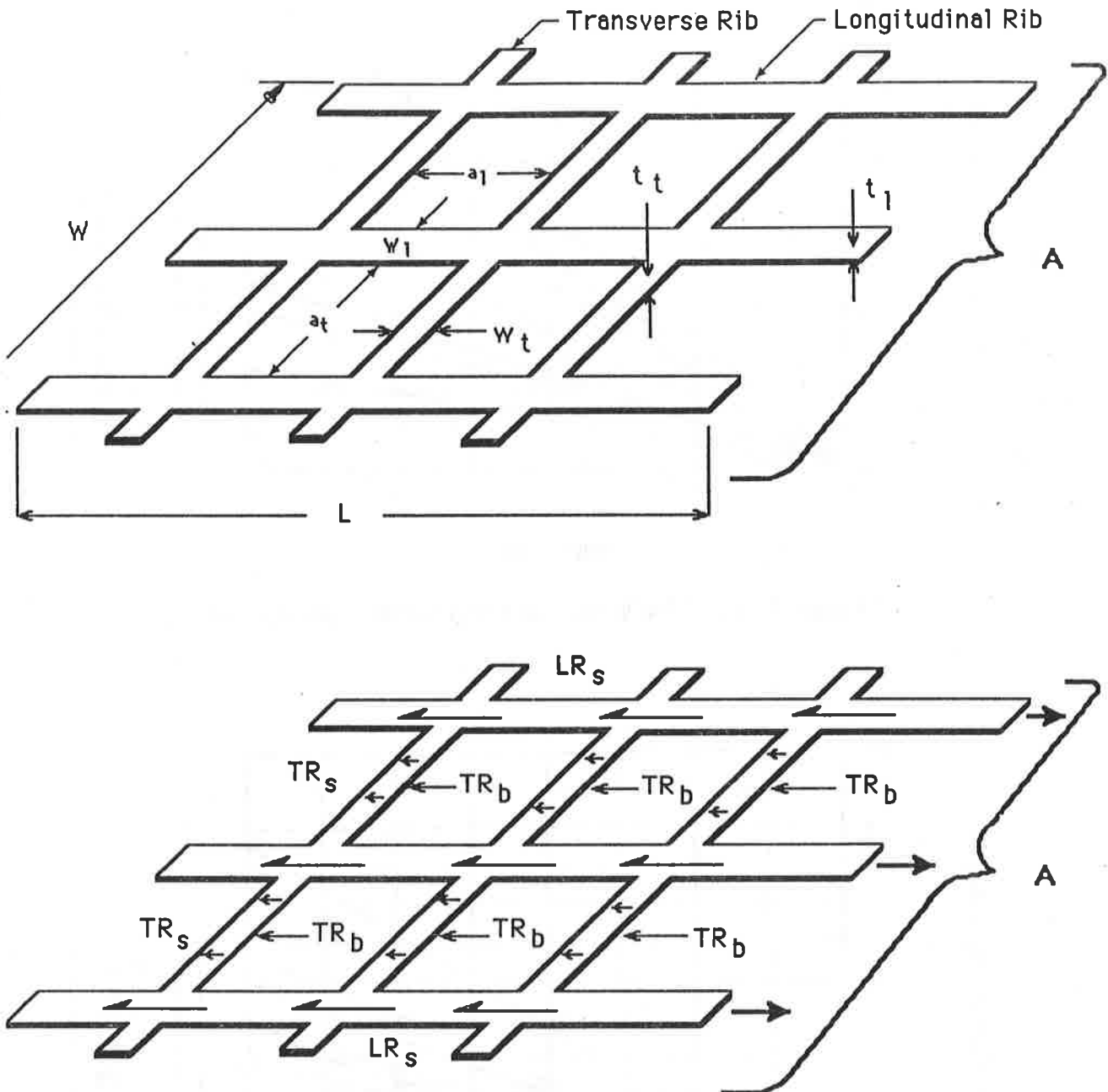
Soil Reinforcement Interaction, Jan., 1988, TRB Report to appear.

6. Dyer, M. R., "Observations of the Stress Distribution in Crushed Glass with Applications to Soil Reinforcement", Dr. Phil. Thesis, University of Oxford, 1985.
7. Sarsby, R. W., "The Influence of Aperture Size/Particle Size on the Efficiency of Grid Reinforcement," Proc. 2nd Canadian Symp. on Geotextiles and Geomembranes, Edmonton, Alberta, Canada, 1985, pp. 7-12.
8. Bonaparte, R. and Berg, R., "Long Term Allowable Tension for Geosynthetic Reinforcement," Proc. Geosynthetics '87, New Orleans, LA, IFAI, pp. 181-192.
9. Swan, R. H., "Anchorage and Shear Behavior of Various Geosynthetics," Master Thesis, Drexel University, Philadelphia, PA, June, 1987.

ACKNOWLEDGEMENTS

Work going into this paper was sponsored by the Geosynthetic Research Institute member organizations for which we extend our sincere appreciation. Currently these are as follows:

Gundle Lining Systems, Inc.
Soil & Materials Engineers, Inc.
U.S. Environmental Protection Agency
Polyfelt, Inc.
Waste Management Inc.
Hoechst Celanese Corp.
Browning-Ferris Industries
Monsanto Company
E.I. Du Pont de Nemours & Co. Inc.
Federal Highway Administration
Golder Associates, Inc.
Mirafi, Inc.
The Tensar Corporation
Fluid Systems Inc./National Seal Co
Poly-America, Inc.
Union Carbide Corp.
Stevens Elastomerics
Akzo Industrial Systems b.v.
Phillips Petroleum Co.
SLT North America, Inc.



* Note that LR_s and TR_s act on top and bottom of surfaces shown. TR_b acts on the front of each transverse rib.

Figure 2 - Geogrid Anchorage Components and Force Diagram

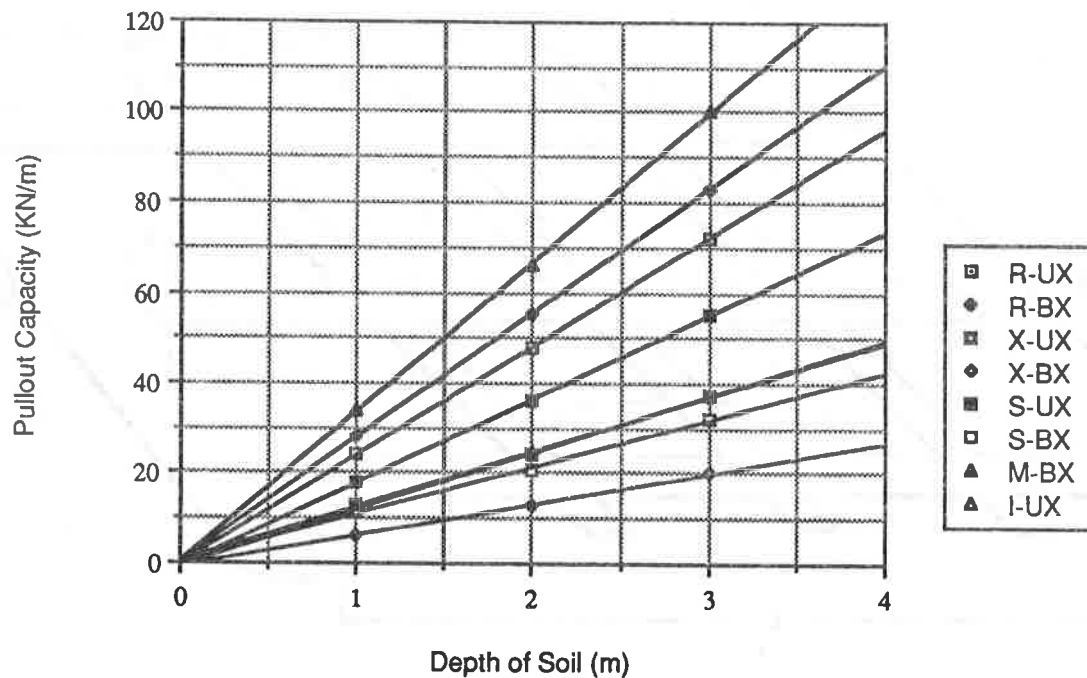


Figure 3 - Full Mobilization of Each Component (L=1m)

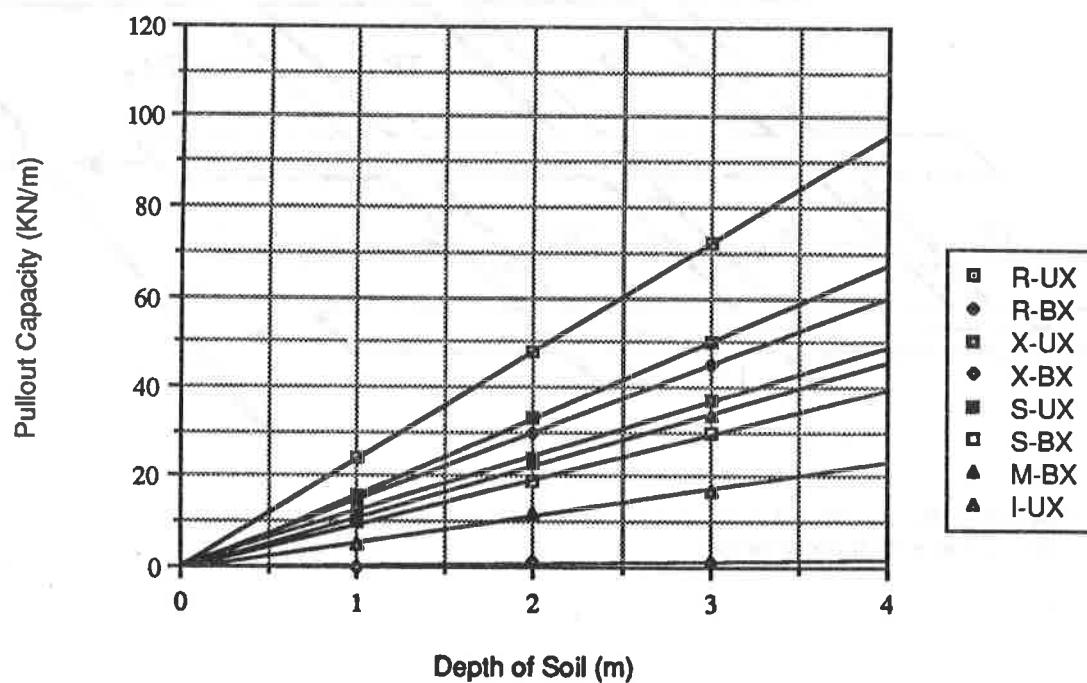


Figure 4 - Mobilization Based on Transverse Rib Stiffness and Junction Strength (L=1m)

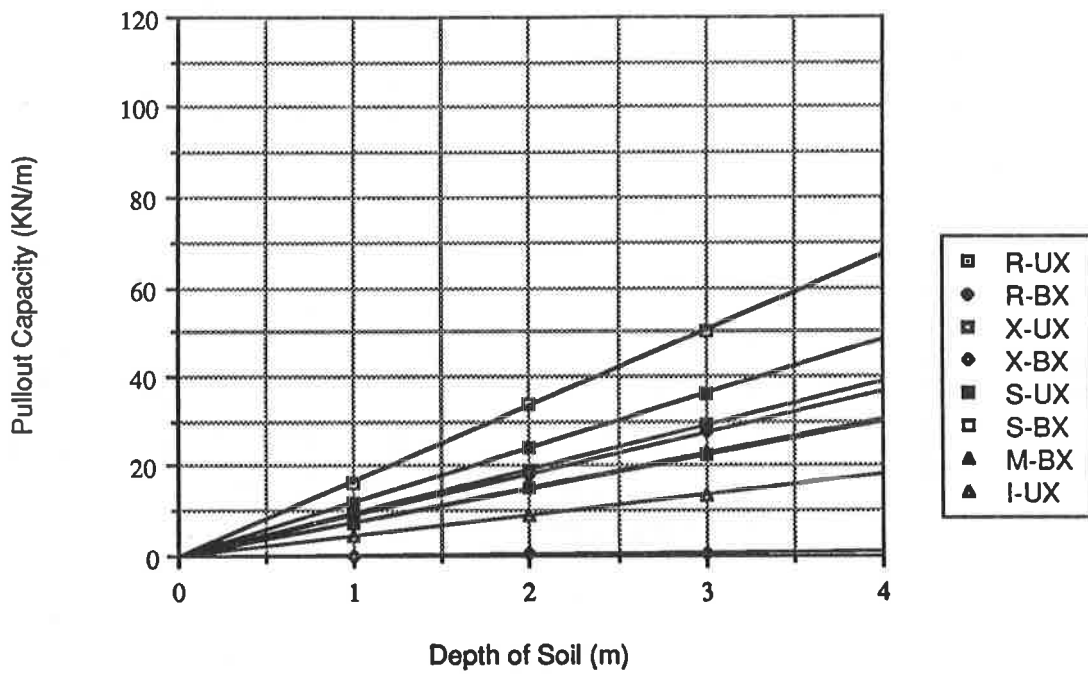


Figure 5 - Mobilization Based on 5% Strain-Granular Soil (L=1m)

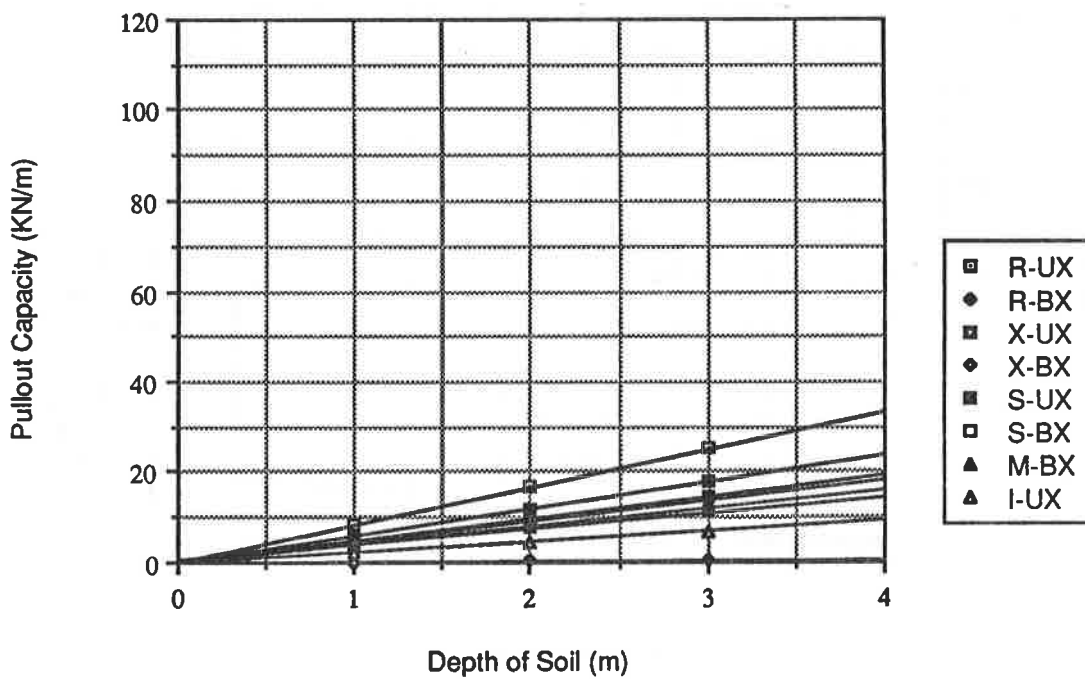


Figure 6 - Mobilization Based on 2% Strain-Granular Soil (L=1m)

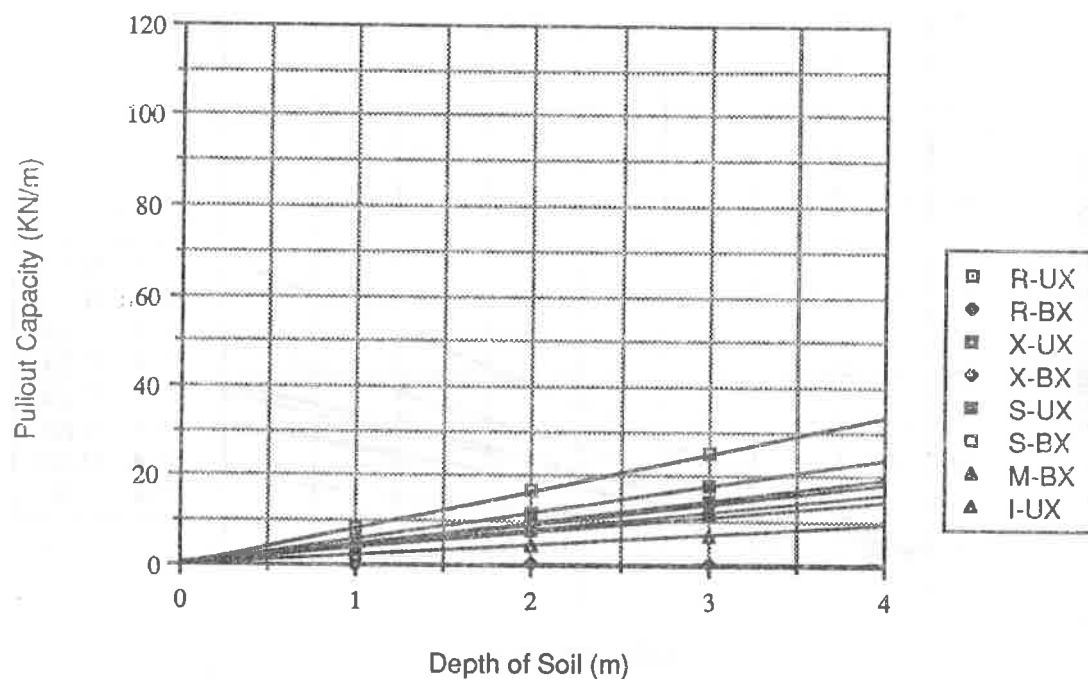


Figure 7 - Mobilization Based on 5% Strain-Cohesive Soil (L=1m)

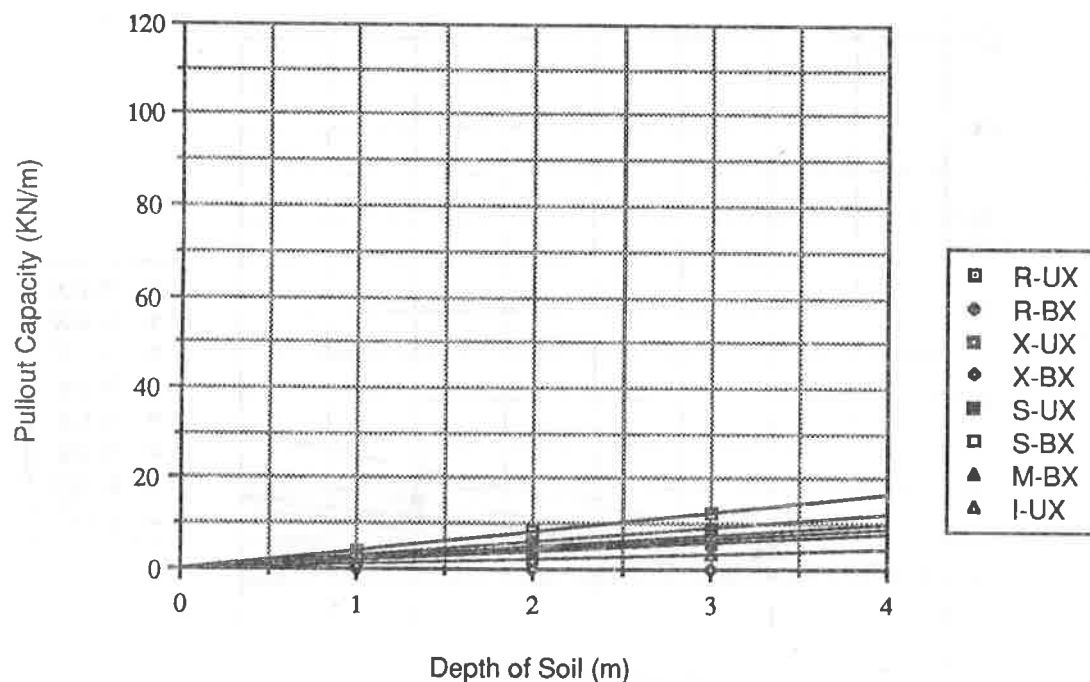


Figure 8 - Mobilization Based on 2% Strain-Cohesive Soil (L=1m)

TO ORDER EXTRA PROCEEDINGS

A GEOSYNTHETICS DATA BANK

Update your geosynthetics reference library with the latest information on the use of geotextiles, geomembranes, geogrids and geocomposites in civil engineering projects. Complete proceedings from the Geosynthetics '89 Conference, held February 21 - 23, 1989 in San Diego, California, are now available from the Industrial Fabrics Association International, conference sponsor.

A total of 49 papers are included in this two volume set. Subjects covered include: Landfills and Linings; Quality Assurance and Specifications; Drainage, Filtration and Erosions; Slope Stability and Safety; Embankments; Foundations and Railways; Steep Slopes; Pavements; Walls; Behavior of Soil Geosynthetic Systems; Testing.

PRICE: \$55.00 per two volume set, plus postage
POSTAGE RATES: \$3.00 U.S. and Mexico, \$7.00 Canada, \$13.00 Central America,
\$22.00 Europe and South America, \$30.00 all other countries
(all foreign orders are shipped air mail)

Order this valuable reference source now and stay informed!

Yes! Help me keep my geosynthetics library up-to-date with the Proceedings of Geosynthetics '89, now available from the Industrial Fabrics Association International.

NAME _____
COMPANY _____
ADDRESS _____
CITY, STATE/PROVINCE _____
ZIP/POSTAL CODE _____ PHONE () _____

Please send me _____ sets of proceedings (\$55.00 each set) Cost _____
Add Postage _____
(see prices above)
Total Cost _____

PAYMENT: ☐ Check enclosed
Please charge my ☐ VISA ☐ MasterCard ☐ American Express

Card # _____
Expiration Date _____
Signature _____

MAIL TO: IFAI, 345 Cedar St., Suite 450, St. Paul, MN 55101.

TO FAX YOUR ORDER: (612) 222-8215 QUESTIONS: (612) 222-2508

